Terahertz sources using relativistic electrons

N. A. Vinokurov[1,2]

1- Budker Institute of Nuclear Physics, Siberian Branch of the Russian Academy of Sciences, Novosibirsk, Russia
2- Novosibirsk State University, Novosibirsk, Russia

11 Lavrentyev Prospect, 630090, Novosibirsk, Russia

Carrying high peak and average power, relativistic electron beams are used for generation of electromagnetic waves in the wavelength range from 0.1 nm to 1 m. In particular, in the submillimeter (terahertz) range they can produce both narrow-band (gyrotrons and free electron lasers) and short-pulse (transition, Cherenkov, and diffraction radiation generators) radiation with extremely high power. The good examples of such devices are Novosibirsk free electron laser (FEL) [1] and multifoil radiator [2], developed at Korea Atomic Energy Research Institute.

The Novosibirsk FEL facility [3] is based on energy recovery linac and contains three FELs. It provides radiation in the wavelength range 6 – 240 micron with average power up to 0.5 kW. The radiation consists of periodic pulses with repetition frequency few MHz and duration less than 0.1 ns. The peak power exceeds 1 MW. The bandwidth is less than 1 % and is close to the Fourier-transform limit. Radiation is totally transverse coherent and the longitudinal coherence length is about 100 m. For more than ten years, the Novosibirsk FEL facility routinely provides radiation for users. They perform research in biology, chemistry and physics.

In the multifoil radiator subpicosecond electron bunch crosses the conic foil stack. The device may be considered as Cherenkov radiator with highly anisotropic media and provides subpicosecond radially-polarized radiation pulse. The resulting radiation power exceeds the power of coherent transition radiation several times. The first experiments with new radiator were performed at Korea Atomic Energy Research Institute [4].

This work was supported by the Russian Science Foundation (project No. 14-50-00080).

[1] G. N. Kulipanov et al., Novosibirsk Free Electron Laser - Facility Description and Recent Experiments, IEEE Trans. on Terahertz Science and Technology, 5(5), 798–809, (2015).

[2] N. A.Vinokurov, Y. U. Jeong, Generating High-Power Short Terahertz Electromagnetic Pulses with a Multifoil Radiator, Phys. Rev. Lett., 110, 064805-1 - 064805-5, (2013).

[3] O. A. Shevchenko et al., The Novosibirsk Free Electron Laser – unique source of terahertz and infrared coherent radiation, Phys. Procedia, 84, 13-18,(2016).

[4] J. Jo, Y. U. Jeong et al., High-power ultrashort terahertz pulses generated by a multi-foil radiator with laser-accelerated electron pulses, Proc. of FEL2015, Daejeon, Korea, 739-740, (2016). http://accelconf.web.cern.ch/AccelConf/FEL2015/papers/wep082.pdf

Multichannel subTHz-THz-IR spectroscopy with using quantum-cascade lasers for analytical applications

V.Vaks

1- IPM RAS, 7, Akademicheskaya str., Afonino village, Nizhny Novgorod region, 603087 Russia
2- Lobachevsky State University, 23, Gagarina av., Nizhny Novgorod, 603950Russia
3-ITMO University, St.-Petersburg, 197101 Russia
vax@ipmras.ru

Nowadays the development of novel methods of analytical research of multicomponent gas mixtures and its various applications is the actual problems in the gas analysis field. These methods must provide the high sensitivity at a 30-100 ppt level for precision quantifying of substance in trace concentrations in a multicomponent gas mixtures. Nowdays, the spectroscopic investigations in -infrared range are widely used for detection of various gases (CO, NO, ammonia, methane) in the infrared (IR) range (near-infrared range (NIR) and mid-infrared range (MIR)) with detection limit of about 1 ppm - 500ppb in two-component gas mixtures, e.g. However there are difficulties at detection of component content of complicated gas mixture because of vibrational bands overlapping, which worsens selectivity and hinders gas identification in multicomponent mixtures. The promising approach is using the multichannel spectroscopic method of three ranges (subterahertz (subTHz), terahertz (THz) and infrared). Among the spectroscopic methods, the only approach to date that ensures a near-theoretical-limit sensitivity along with a good spectral resolution limited just by the Doppler effect is the nonstationary spectroscopy based on free dumping polarization effect. Other advantages of the spectrometers include easy-to-use configuration and measurement time of several microseconds that provide registration of unstable gases. Application of this method will also benefits in registration of gas-markers absorption lines at one shot without overlapping effect and performing minimal measuring time of few microseconds. Development of a combined subTHz-THz-MIR gas spectroscopy method allows increasing the number of gases that can be identified and the reliability of the detection by confirming the signature in all subTHz, Hz and MIR ranges. The subTHz radiation source is based on backward-wave oscillator (BWO) or solid state harmonics generator (with Gunn generator as reference radiation source). The THz and MIR radiation sources of the spectrometer based on solid state harmonics generator and QCL are developed. The THz radiation source can be realized on the solid state generator or BWO with frequency multiplying. The harmonics generators with using the multipliers on the base of Schottky diode or quantum semiconductor superlattice (SL) were developed. It has a number of advantages comparing with other well-known microwave generators. Also for THz and MIR ranges the QCLs can be used. They have a high output power and can generate radiation in pulse and continuous modes together with fast tuning of frequency. The cornerstone of the QCL-based radiation source design is a phase-lock loop (PLL) and modulation system. The PLL systems for THz DFB QCL (3.4 and 4.7 THz) were elaborated. Detection of the radiation in all frequency ranges (subTHz, THz and MIR) are realized by the unique receiver block based on SL.The multichannel subTHz-THz-MIR gas spectroscopy method can be used for quantifying of substance in trace concentrations in a multicomponent gas mixtures of various origin. One of important application is medical diagnostics of social important diseases (diabetes, lung or gastrointestinal tract cancer) based on analysis of human exhaled breath or odors of biological liquids (urine, saliva etc.), which can be carried out simultaneously. Other actual application is using this method for safety for remote detection of markers of explosives (e.g., 2,4,6- trinitrotoluene (TNT), 1,2,3-trinitroxypropane (Nitroglycerin), cyclotetramethylenetrinitramine (HMX) etc.) and poisonous substances. There is another developing line of possible use of subTHz-THz-MIR gas spectroscopy method such as agriculture application (veterinary medicine diagnostics based on analysis of animal exhaled breath or odors of its biological liquids; determination of degree of corn mycosis based on analysis of corn odors; monitoring the quality of foodstuff (meat, poultry) based on analysis of its odors).

The authors acknowledge for partial support from of the Russian Science Foundation (project N 15-12-10035) and the Russian Foundation for Basic Research (grant N 16-52-76011 ERA_a), The Ministry of Education and Science of the Russian Federation (Grant No 074-U01).

Bioelectronic Nose:
Integration of Biotechnology and Nanotechnology

Tai Hyun Park

School of Chemical and Biological Engineering,

Seoul National University, Seoul 151-744, Republic of Korea

Human has five senses. Among the five senses, three of them are physical senses, which are vision, hearing, and touch. The other two senses are chemical senses, which are smell and taste. The science and technology for the physical senses have been advanced enormously, and electronic devices have been developed for these senses, e.g. camera, audio recorder, and tablet PC. However, we do not have any device which can capture smell or taste. In order to mimic the function of human nose and tongue a novel concept for sensor devices functionalized with odor and tastant-recognizing biomolecules was suggested. They are the bioelectronic nose and tongue. A bioelectronic nose consists of primary and secondary transducers. The primary transducer is a biological recognition element such as olfactory receptors. The secondary transducer is a highly sensitive nanodevices that convert biological events into measurable signals. In this presentation, the basic concept and principles of bioelectronic nose will be presented. In addition, applications of bioelectronic nose and the current issues will be discussed.

Millimeter-wave and Terahertz Applications Accelerated by Photonics

Tadao Nagatsuma

Graduate School of Engineering Science, Osaka University
1-3 Machikaneyama, Toyonaka 560-8531, Japan
nagatuma@ee.es.osaka-u.ac.jp

An active research and development of millimeter-wave (MMW) and terahertz (THz) technologies were initiated with use of photonics technologies in 1990's. Photonics technologies have been implemented in generation, detection and transmission of pulsed/continuous MMW and THz waves, and employed in industrial applications. In the last 10 years, with the advance of semiconductor devices and integrated circuits, electronics-based MMW/THz technologies have also gained a great attention to make MMW/THz systems and subsystems more compact and cost-effective. In this talk, we review photonics-based approaches for accelerating practical applications such as communications, sensing and measurements, clarify merit, role and issue of photonics in MMW/THz technologies, and discuss their future directions to compete and/or coexist with electronics.

[1] T. Nagatsuma et al., "Millimeter-Wave and Terahertz-Wave Applications Enabled by Photonics," IEEE J. Quantum Electronics, Vol. 52, No. 1, 0600912, Jan. (2016).
[2] T. Nagatsuma, and G. Carpintero, "Recent Progress and Future Prospect of Photonics-Enabled Terahertz Communications Research," IEICE Trans. Electron., Vol. E98–C, No. 12, pp. 1060-1079, Dec. (2015).
[3] T. Nagatsuma et al., "Advances in Terahertz Communications Accelerated by Photonics," Nature Photonics, Vol. 10, No. 6, pp.371-379, June (2016).
[4] T. Nagatsuma et al., "Photonics for Millimeter-Wave and Terahertz Sensing and Measurement," IEICE Trans. Electron., Vol. E99–C, No. 2, pp.173-180, Feb. (2016).
[5] H.-J. Song and T. Nagatsuma, eds., "Handbook of Terahertz Technologies: Devices and Applications," Pan Stanford, ISBN 9789814613088, April 15 (2015).

Laser spectroscopy and nanomaterial in biomedical applications

Chia-Liang Cheng*

Department of Physics, National Dong Hwa University, Hualien 97401, Taiwan

**Email:* clcheng@gms.ndhu.edu.tw

Various nanometer-sized materials and manipulation techniques have been developed that allows controlling of molecules for bio/medical applications in a new dimension. With the advanced laser technology and detecting apparatus, spectroscopy has become a powerful technique to visualize the trace of nanomaterials. For its non-invasive nature, *in vitro*/*in vivo* observation in the bio/medical systems is possible; therefore spectroscopy plays important roles in bridging nanotechnology and biotechnology. Characterization, visualization and dynamics of the interaction of molecules (or nanoparticles) with bio objects can be realized using spectroscopic methods, such as spectral imaging and dynamics measurements. Among these, Raman spectroscopy is a powerful non-invasive tool. It gives unique and label-free molecular signatures of a specific biological state without invading the specimen itself, allowing *in vitro*/*in vivo* observation of certain interaction in the bio/medical systems. In these applications, each Raman sepectral line represents a finger print of certain molecular configuration; this allows identifying specific molecular state and its interaction with bio-molecule/or object. Recently Raman mapping provides rapidly 2-D or 3-D visualization of the distribution of the molecular states; and hence the interaction of the investigated system, making studies possible in the molecular level. In this talk, we will show examples of how spectroscopy (IR, Raman, fluorescence, etc.) can be applied in bio systems studies.

With the help of nanoparticle labeling and imaging, nanoparticles are expected to be ideal vehicle to traffic drug molecule to the target place for more efficient delivery. Nanodiamond has been proposed to be one of the most biocompatible nanomaterials for drug delivery. We have devoted our efforts on using nanodiamond (ND) for drug loading and for more efficient anticancer drug delivery while ND's Raman and fluorescence properties are used for bio imaging. Several successful cases have been demonstrated in both cellular and animal models. The interaction of surface growth hormone receptor of A549 human lung epithelial cells with growth hormone was observed via confocal Raman mapping for cancer cell detection. ND conjugated with clinically used anti-cancer drug doxorubicin (Dox) and Paclitaxel (Taxol) have been successfully conjugated to ND. Drug loading and efficiency of nanodiamond-anticancer drug complexes and the effect of autophagy modulation on drug delivery in cancer treatment are estimated. The efficiency of the ND-drug as compared to pure drug in the cellular model was assessed. The latest development and outlook on using ND as bio imaging and drug delivery will be discussed.

Introduction into nonlinear THz photonics: basis and their potential applications

Alexey Balakin, Peter Solyankin, Alexander Shkurinov

Department of Physics and International Laser Center, M.V.Lomonosov Moscow State University, Russia.

The bright THz source is essential for exploring nonlinear THz field-matter interaction and spectroscopy. Recent advances in high peak-power pulsed THz sources with intensity greater than 1 MV/cm provided unique opportunities to study transient dynamics of non-perturbative states of matter and to investigate strong light-matter interactions. The records of pulsed THz field strength are in the range of 10 to 10 MV/cm from laser-induced gas plasma with two-color laser excitation in dry nitrogen, or up to about 80 MV/cm from organic crystals with the optical rectification. Extremely intense sub-cycle pulses pulse at THz/far-IR region will enable strong field-matter interaction and investigation of a wide range of scientific phenomena.

The present paper studies the generation mechanism of terahertz (THz) radiation from tightly focused femtosecond laser pulses in a gas medium. We measured the angular radiation pattern under different focusing conditions and observed that with the deepening of focus, the angular radiation pattern changes and optical-to-THz conversion efficiency increases. The analysis of the observed phenomena led to the assumption that the dipole radiation prevails in most cases despite the existing conception regarding the dominating role of the quadrupole mechanism of radiation. Based on these assumptions, the transient photocurrent theory of the phenomenon presented in this paper was developed by us and used for the numerical fit of the experimental data.

Conventional methods used to obtain the highly synchronized pulses necessary for the pump-probe measurements rely on an optical parametric oscillator (OPO) or optical parametric amplifier (OPA), which generates synchronized signal and idler pulses at different wavelengths. In the paper we will discuss the generation of two synchronized ultrafast radiations, THz and high harmonic radiation (XUV to soft X-ray), using an intense laser pulse in visible or near-infrared ranges with selected media such as gases and nano-structured metals.We studied THz and X-ray radiation from gas clusters while irradiating them with high-intensity femtosecond optical pulses. Clusters were produced by partial condensation of the pure Ar gas and the mixtures in the process of their expansion through a conical nozzle into evacuated chamber. Simultaneous measurements of THz and X-ray radiation properties were carried out with various durations and total energies of optical pulses, in single-color and two-color schemes of clusters jet irradiation. In the two-color scheme, optical pulse bears both the fundamental and second harmonics of Ti-Sapphire laser, we observed a significant increase of THz radiation field without any change of X-ray radiation properties. We observed a non-monotonic dependency of THz radiation power upon the pulse duration at given total energy of the optical pulse. To interpret this effect we developed a theoretical model of cluster ionization which self-consistently predicts level of ionization and electron temperature in the clusters.

These instruments, as synchronized THz, X-ray and XUV ultra-short pulses for jitter-free time-resolved pump/probe measurement, may be a unique platform for multi-dimensional ultrafast spectroscopy, nonlinear phenomena, and high-resolution (spatial and temporal) imaging. The tabletop nature of the instrument allows us to perform our research beyond previously limited national advanced light facilities.

Control of terahertz yield and field vector orientation in a two-colour femtosecond filament

O.G. Kosareva[1], N.A. Panov[1], V.A. Andreeva[1], D.E. Shipilo[1], M.N. Esaulkov[1], P.M. Solyankin[1], A.P. Shkurinov[1], Y. Chen[2], S.L. Chin[3], V.A. Makarov[1], A.B. Savel'ev[1]

1. *Faculty of Physics and International Laser Center, Lomonosov Moscow State University, 1/62 Leninskiye gori, 119991 Moscow, Russia*
2. *Key Laboratory for Laser Plasmas (Ministry of Education), Department of Physics and Astronomy, Shanghai Jiao Tong University, Shanghai 200240, China*
3. *Département de Physique, Centre d'Optique, Photonique et Laser (COPL), Université Laval, Québec, QC G1V 0A6, Canada*

kosareva@physics.msu.ru

Simultaneous focusing of the first and the second harmonic of Ti:Sapphire laser pulse into atmospheric density gas is a unique source of terahertz (THz) radiation, which provides a wideband spectrum together with the possibilities to govern THz field vector orientation and to increase the pump pulse energy without destroying the material. The polarization properties of air-based terahertz radiation attain growing interest [1,2] in view of molecular alignment by the terahertz field [3] as well as terahertz spectroscopy of macroscopic biomolecules [4]. Thus, the terahertz molecular spectroscopy requires a high-peak-intensity terahertz source with the controlled polarization properties. The purpose of this work is to reveal the THz field vector orientation and its rotation in a two-color filament and then obtain the maximum THz yield by adjustment the pulse duration by tuning the initial pulse chirp.

THz field vector orientation experimental measurements were performed at *Lomonosov MSU* using the Ti:sapphire regenerative amplifier (SpectraPhysics Spitfire Pro, 800nm, up to 3 mJ/pulse, 120 fs) separated into two beams to produce the 1st and 2nd harmonic radiation. The initial linear polarization direction of which was varied and measured independently. We have shown (left panel in Fig. 1) in excellent agreement between the numerical (based on vectorial 3D UPPE [5]) and experimental results that the polarization of THz emission remains linear and directed along the 1st harmonic polarization for the wide range of angles between the initial field vector direction of the 1st and 2nd harmonics up to 80°; increase of the such angle closer to 90° leads to the significant elliptization of THz radiation and polarization ellipse rotation following the 2nd harmonic, which itself becomes elliptical in the high-intensity filament. Note that for the large initial angle between the 1st and the 2nd harmonic the THz yield decreases and the output THz signal fluctuates essentially.

Control of THz yield using the initial 800 nm pulse chirp was performed in *Shanghai Jiao Tong University* with 800-nm 35-fs laser pulses chirped both negatively and positively up to 400 fs. In this experiment the initial 800-nm beam was not split and produced its 2nd harmonic using the BBO crystal inserted in its propagation path. Both experiment and numerical simulation show (right panel in Fig. 1) that THz yield dependence has a local minimum when the Fourier-transform limited pulse is used. Notable is that THz emission produced with positively chirped pump pulse was much stronger compared to the produced with Fourier transform-limited pulse and negatively chirped ones.

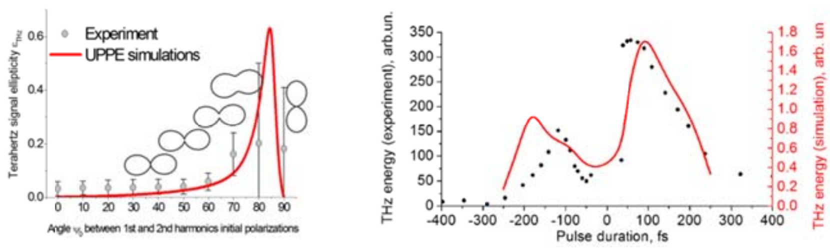

Fig. 1 (**Left panel**) the dependence of terahertz signal ellipticity on the angle between initial polarizations of 800-nm pump and 400-nm seed. Grey curves indicate the simulated polarization ellipses at different initial angles. (**Right panel**) The dependence of terahertz yield on the initial chirped pulse duration for 4.5-mJ pulse (negative values correspond to negative chirp; region from −35 to +35 fs corresponds to Fourier-transform limited pulse).

References

[1] X. Lu and X.-C. Zhang *Phys. Rev. Lett.* **108**, 123903 (2012).
[2] C. Sabah and H. G. Roskos *Progress In Electromagnetics Research*, **124**, 301 (2012).
[3] M. Shalaby and C. P. Hauri *Appl. Phys. Lett.* **106**, 181108 (2015).
[4] T.R. Globus, D.L. Woolard, T. Khromova, *et al. J. of Biological Physics* **29**, 89 (2003).
[5] V.A. Andreeva, O.G. Kosareva, N.A. Panov, *et al. Phys. Rev. Lett.* **116**, 063902 (2016).

Development and application of powerful and stable THz gyrotrons

M. Glyavin

Institute of Applied Physics RAS, 46 Ul'yanov str., Nizhny Novgorod, Russia

glyavin@appl.sci-nnov.ru

The last decade has contributed to the rapid progress in the development of THz sources in particular gyrotrons. Although in comparison with the classical microwave tubes the gyrotrons are characterized by greater volume and weight due to the presence of bulky parts (such as superconducting magnets and massive collectors where the energy of the spent electron beam is dissipated) they are much more compact and can easily be embedded in a sophisticated laboratory equipment (e.g. spectrometers, technological systems, etc.) than other devices with a comparable value of Pf^2 such as free–electron lasers (FEL) and radiation sources based on electron accelerators. All these advantageous features have opened the road to many novel and prospective applications of gyrotrons as radiation sources in a great number of high–power THz technologies, advanced spectroscopic techniques, plasma science and materials processing, fusion research as well as in many other scientific and technological fields. The CW gyrotron developed at IAP RAS provides radiation with a power up to 1 kW in the frequency range 0.26-0.52 THz [1,2]. The gyrotrons with pulsed magnetic fields operates with 100 kW power level at 0.7THz and 1 kW at 1 THz frequency. The second harmonic CW gyrotron with improved mode selection based on double electron beam [3] has been tested. The wide step tunig of frequency by excitation of different modes was demonstrated in the range 0.4-0.75 THz. The stable operation at the frequency 0.76 GHz on the second harmonic with power level about few Watts has been obtained, which useful for modern NMR/DNP spectroscopy application. The projects of "cold" (field emmision) cathode [4] and low voltage (at the level 1.5-2 kV) are under development.

The pulsed gyrotron has been used successfully for initiation of localized gas discharges. Such plasma is promising for development of both a point source of multi–charged ions and a source of high–energy ultraviolet (extreme ultraviolet EUV or XUV) [5]. The gas discharge has been successfully obtained also with 0.26 THz/CW IAP RAS gyrotron mentioned above [6]. The same gyrotron has been used also for the high-resolution molecular spectroscopy in a gas mixture. A significant improvement of spectrum quality due to power growth in contrast with traditional BWO, has allowed observing the theoretically predicted earlier transitions in SO_2 molecule [7]. The frequency stability of the gyrotron for spectroscopy application $df/f \sim 10^{-12}$ is demonstrated [8]. The sensitivity of the radio-acoustic detector was increased about three orders due to high power. The last interesting feature is high speed production of pure nanopowders by material evaporation and condensation. In the case of evaporation by 1kW/CW/0.26THz radiation, the evaporation rate was increased approximately in order in comparison with traditional heating methods.

Acknowledgements. The work supported in part by the Russian Scientific Foundation under the project 14-12-00887.

[1] V.L.Bratman, A.A.Bogdashov, G.G.Denisov, M.Yu.Glyavin, Yu.K.Kalynov, A.G.Luchinin, V.N.Manuilov, V.E.Zapevalov, N.A.Zavolsky, V.G.Zorin Gyrotron development for high power THz technologies in IAP RAS Int. J. IRMM&THz Waves, 33, 7, 715-723 (2012)

[2] M.Yu. Glyavin, A.V.Chirkov, G.G.Denisov et al. Experimental tests of 263 GHz gyrotron for spectroscopy applications and diagnostic of various media, Rev. Sci. Instr., 86(5), 054705 (2015)

[3] V.N.Manuilov, M.Yu.Glyavin, A.S.Sedov, V.Yu.Zaslavsky, T. Idehara Design of a Second Harmonic Double-Beam Continuous Wave Gyrotron with Operating Frequency of 0.79 THz. Journal of Infrared, Millimeter, and Terahertz Waves, 36, 12, 1164-1175 (2015)

[4] M.Yu.Glyavin, V.N.Manuilov, G.G.Sominski, E.P.Taradaev, T.A.Tumareva The concept of an electron-optical system with field emitter for a spectroscopic gyrotron. Infrared Physics & Technology, 78, 185-189 (2016)

[5] M.Yu.Glyavin, S.V.Golubev, I.V.Izotov et al. A point-like source of extreme ultraviolet radiation based on a discharge in a non-uniform gas flow, sustained by powerful gyrotron radiation of terahertz frequency band, Applied Physics Letters 105, 174101 (2014)

[6] A.V.Vodopyanov, A.V.Sidorov, S.V.Razin, A.I.Tsvetkov, A.P.Fokin, A.P.Veselov, S.V.Golubev, M.Yu.Glyavin Gas breakdown by a focused CW 263 GHz beam. 41st Int. Conf. IRMMW-THz 2016, 25-30 September 2016, Copenhagen, Denmark

[7] M.A.Koshelev, A.I.Tsvetkov, M.V.Morozkin, M.Yu.Glyavin, M.Yu.Tretyakov. Molecular gas spectroscopy using radioacoustic detection and high-power coherent subterahertz radiation sources. Journal of Molecular Spectroscopy, 331, 9–16 (2017)

[8] G.Denisov, A.Fokin, M.Glyavin, G.Golubiatnikov et al. High precision frequency stabilization of a 100W/263 GHz continiuos wave gyrotron 18th International Vacuum Electronics Conference 24 - 26 April 2017, London

Off-axis THz Parametric Oscillator

Yu-Chung Chiu and Yen-Chieh Huang*

Institute of Photonics Technologies, National Tsing Hua University, Hsinchu 30013, Taiwan

**email address: ychuang@ee.nthu.edu.tw*

Since a THz wave is diffractive and often absorbed in a nonlinear optical material, a THz parametric oscillator (TPO) resonating a THz wave has never been realized in the past. Here, we demonstrate an off-axis THz parametric oscillator (OTPO) resonating the THz component in a $LiNbO_3$ slab waveguide, as shown in Fig. 1(a). In the phase matching diagram, k_p, k_{signal}, and k_{THz} are the wave vectors of the pump, signal, and idler (THz) waves, respectively. When a pump laser fills up the aperture of a $LiNbO_3$ waveguide, the pump laser supplies parametric gain to the growth of the THz wave, even though the lithium niobate crystal absorbs a THz wave. The generated THz wave is incident on the *y* surface of crystal with a 25^o angle and reflected back to the pump region via total internal reflection (TIR). The zigzagging THz wave oscillates in the gain crystal similar to a wave resonating in a cavity.

In the experiment, we used a thin $LiNbO_3$ plate with 1-mm thickness as a THz nonlinear waveguide. To study the performance of an OTPO, we first carry out a side-by-side comparison for the output signal energy between *y*-cut and *z*-cut $LiNbO_3$ crystal plates of the same dimensions under the same pump conditions. The *y*-cut crystal, when pumped by a laser along *x*, is an OTPO. The z-cut crystal, when pumped by a laser along *x*, is an THz parametric generator (TPG) with its signal and THz waves walking away from the pump beam in the *y* direction. The pump is a passively Q-switched 1064-nm laser followed by a double-pass diode-pumped Nd:YAG laser amplifier. The pump polarization is along the crystallographic z-axis of the crystal. Figure 1(b) shows the measured signal energy versus pump energy from the (a) z-cut (TPG) and (b) y-cut (OTPO) crystals with a length of 40 mm. It is seen from the comparison that the output signal from the OTPO is twice stronger than that from the TPG of the same length at ~1 mJ pump energy.

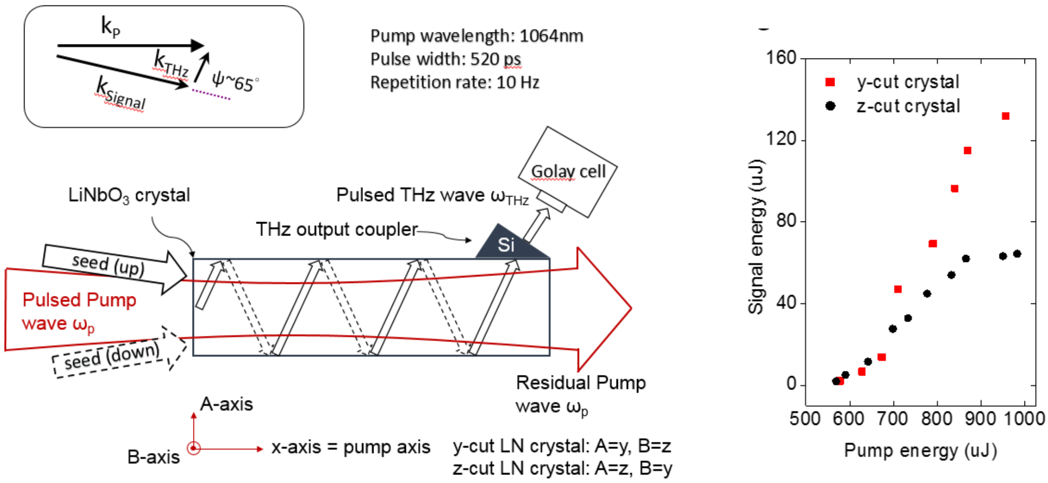

(a) (b)

Fig. 1. (a) The experimental setup of the OTPO, wherein the pump laser is an amplified passively Q-switched Nd:YAG laser. The generated THz wave zigzags in the crystal upon reflections from the two *y* surfaces of the crystal. It is also possible to see the OTPO with one or two signal waves. (c) Comparison of measured signal versus pump energy from 40 mm long *z*-cut (TPG) and *y*-cut (OTPO) crystals, indicating a doubled THz conversion efficiency from the OTPO at ~1-mJ pump energy.

It is also possible to seed an OTPO with one or two signal waves, as shown in Fig. 1(a). We will report in the conference a doubly seeded OTPO with more than 50% pump depletion. This work is supported by Ministry of Science and Technology under Contract MOST 105-2112-M-007 -021 -MY3.

Magnetophotonics with Mie Resonances in Nanoantennas

Barsukova M.G.[1], Shorokhov A.S.[1], Musorin A.I.[1] , Neshev D.N.[2], Kivshar Y.S.[2], Fedyanin A.A.[1]

[1] Faculty of Physics, Lomonosov Moscow State University, Moscow 199991, Russia

[2] Nonlinear Physics Centre, The Australian National University, Canberra, ACT 2601, Australia

fedyanin@nanolab.phys.msu.ru

The concept of metamaterials allows design of artificial subwavelength meta-atoms that support a strong magnetic response, usually termed as optical magnetism, even when they are made of nonmagnetic materials. Recent developments in the nanoscale optical physics gave a birth to a new branch of nanophotonics aiming at the manipulation of optically-induced Mie type resonances in dielectric nanoparticles made of materials with high refractive indices [1,2]. It has been shown recently that resonant dielectric structures offer unique opportunities for reduced dissipative losses and large resonant enhancement of both electric and magnetic fields. High-index dielectric structures can be employed as new building blocks to realize unique functionalities such as magnetic Fano resonances, highly transmittable metasurfaces, and novel metadevices. Here we extend the concept of high-index resonant nanophotonics to the case of magnetically active materials and study the magneto-optical response of a dielectric metasurface covered with a thin magnetic film. We have reported on the demonstration of the magneto-optical effects enhanced by optically-induced magnetic dipole Mie resonances manifesting a strong interaction of magnetic properties with induced "optical magnetism". We believe our findings will allow novel approaches in a magnetic control of recently reported strong nonlinear effects in nanoparticles as well as in the realization of the time-reversal symmetry breaking at the nanoscale for photonic topological insulators topology. In addition, our results could pave a way towards a new platform for active and nonreciprocal photonic nanostructures and metadevices, which could be tuned by the external magnetic field.

[1]. I. Staude, et al., Tailoring Directional Scattering through Magnetic and Electric Resonances in Subwavelength Silicon Nanodisks, ACS Nano **7**, 7824 (2013).

[2]. A.S. Shorokhov, et al. Multifold enhancement of thirdharmonic generation in dielectric nanoparticles driven by magnetic Fano resonances, Nano Lettets **16**, 4857 (2016).

A 2 kW single-mode fiber laser using bidirectional-pump scheme

*Fan Zhang, Wenyou Zheng, Pengyang Shi, and Xinhai Zhang**

Department of Electrical and Electronic Engineering, Southern University of Science and Technology,1088 Xueyuan Road, Nanshan District, Shenzhen, Guangdong, 518055, China

**zhangxh@sustc.edu.cn*

Abstract

A 2kW single-mode fiber laser with two cascade home-made cladding light strippers (CLSs) by employing bidirectional-pump scheme has been demonstrated. An output power of 2.009 kW is achieved at a pump power of 2.63 kW. The slope efficiency is 76.6%.The power of the Raman Stokes light is less than -47 dB at 2 kW even with a 10-m delivery fiber with core/inner cladding diameter of 20/400um. Nearly diffraction-limited beam quality is also confirmed (M2≤1.2) and the FWHM bandwidth of optical spectra is 4.34nm. No transverse mode instability (TMI) is found and the output power stability of ±0.14% is achieved by special thermal management for a more uniform temperature distribution on the Yb-doped gain fiber.

Tailored Femtosecond Bessel Beam for High Aspect-Ratio Through Hole Drilling

Koji Sugioka[1], Fei He[1,2], and Ya Cheng[2]

1- RIKEN Center for Advanced Photonics, Wako, Saitama 351-0198, Japan
2- State Key Laboratory of High Field Laser Physics, Shanghai Institute of Optics and Fine Mechanics, Chinese Academy of Sciences, P.O. Box 800-211, Shanghai 201800, China
ksugioka@riken.jp

The steady pursuit of high-performance, low-power-consumption, and small-footprint microelectronic devices has made three-dimensional integrated circuits (3D ICs) an attractive replacement for conventional 2D ICs. One of the major challenges to realize 3D ICs is the fabrication of high-aspect-ratio through Si vias (TSVs), which is a key technology for the 3D assembly of Si ICs [2]. Here, we propose to employ femtosecond (fs) 1.5-μm Bessel beams for high-speed fabrication of high-quality, high-aspect-ratio through Si holes for the TSV application. By performing laser ablation in air using conventional Bessel beams, nearly taper-free through Si holes with diameters of ~5 μm in 50-μm-thick Si substrates, which corresponds to aspect ratios of ~10, can be produced. To suppress the severe damage caused by the sidelobes of the conventional Bessel beam, a fs Bessel beam is tailored by using specially designed binary phase plates (BPPs) for the first time. We theoretically and experimentally demonstrate that this method can create a fs laser beam with a ~6-μm lateral spot size and ~400-μm focal depth, while reducing the sidelobe ratio (SLR, the ratio of the peak intensity of the maximum sidelobe to that of the central lobe) to ~0.6%, which is much smaller than the ~15.8% SLR for a conventional Bessel beam. The developed technique successfully eliminates sidelobe-induced damage to ensure high-quality fabrication of through Si holes with a high aspect ratio (Fig. 1) [1]. Our technique is potentially applicable for 3D assembly in the manufacturing of 3D Si ICs.

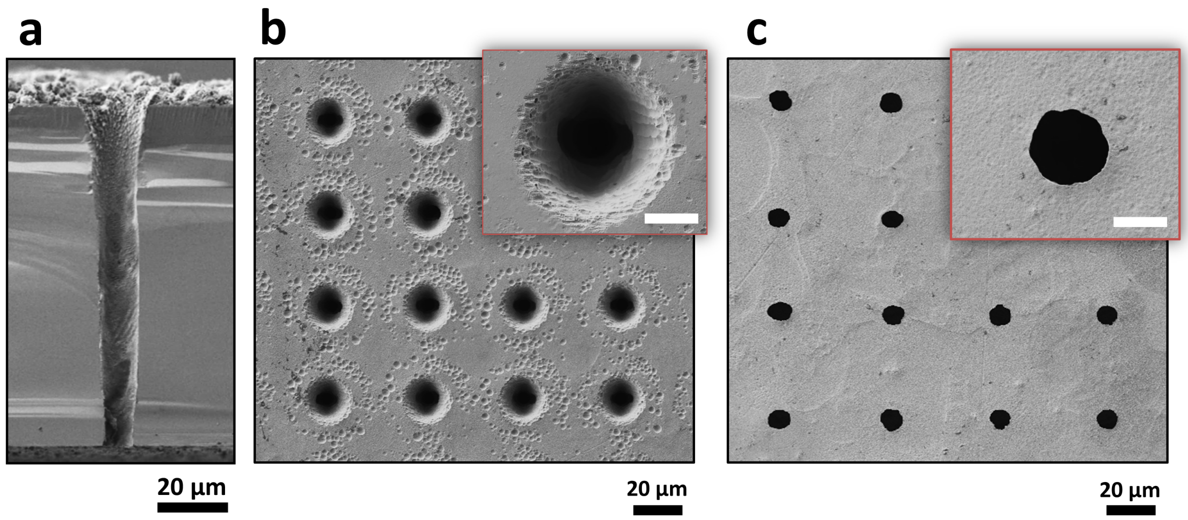

Fig.1 SEM images of (a) cross-section, (b) front surface, and (c) rear surface of TSVs fabricated in 100-μm thick Si substrates by Bessel beam tailored with a BPP. The scalar bars in the inset are 5 μm.

[1] M. Motoyoshi, Through-silicon via (TSV). Proc. IEEE **97**, 43–48 (2009).
[2] F. He, J. Yu, Y. Tan, W. Chu, C. Zhou, Y. Cheng, and Koji Sugioka, Tailoring femtosecond 1.5-μm Bessel beams for manufacturing high-aspect-ratio through-silicon vias, Sci. Rep. **7**, 40485 (2017).

Periodic nano-texturing by interference femtosecond laser processing technique

<u>Y. Nakata</u>[1], M. Yoshida[1], K. Osawa[1], N. Miyanaga[1]
1- Osaka University, 2-6 Yamadaoka, Suita, Osaka, 565-0871Japan
nakata-y@ile.osaka-u.ac.jp

Nanostructures in lattice can be fabricated in a single process by an interfering femtosecond laser processing technique. In the past papers, we have shown nanowhisker [1], nanodrop and nanobump [2–4], MHA (metallic-hole array) [2,5]. In addition, control of unit pattern of an interference pattern has been shown in experiment and simulation [3,6,7]. In the presentation, recent progress and representative results will be shown.

Short-limit of lattice constant is limited by wavelength. Here, SH (second-harmonic) wave of a femtosecond laser was used to shorten it [4]. Fig. 1 is representative nanostructures as a function of fluence fabricated by interference pattern of four beams, where the wavelength $\lambda = 392.5$ $[nm]$, the pulse width of the fundamental wavelength $\Delta t = 194$ [fs], and the correlation angle between the countering beams $2\theta = 47.0°$. The target was 100 $[nm]$ thick gold thin film deposited on silica glass substrate. The lattice constant was $a_0 = 760$ $[nm]$. The tendency of the structure to the fluence is similar to the case with longer lattice constant [2]. Here, the structure shown in the inset was fabricated by fundamental wavelength with $a_0 = 1.7$ $[\mu m]$ on 50 $[nm]$ thick gold film [2]. The radius of nanodrop was minimized from $r = 140$ $[nm]$ to 76 [nm] with shorter lattice constant because the amount of gold inside the spot was decreased from 0.037 [pg] to 0.017 [pg].

For uniform nanostructures in lattice inside a spot, a top-flat beam is required. Fig. 2 shows the beam shaping by using spatial frequency filter [8]. The beam was transferred by $4f$ system, and spatially filtered at the Fourier plane. The best spatial frequency filtering diameter was 2.0 [mm], and the standard deviation within 0.92 [mm] along the horizontal center line s = 3.7 [%].

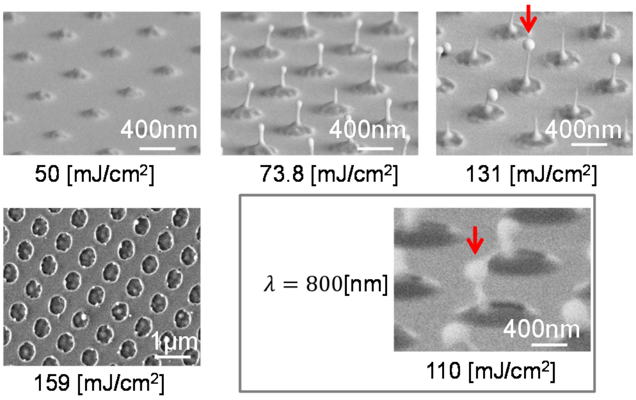

Fig.1 interference ultra-violet fs laser processing.

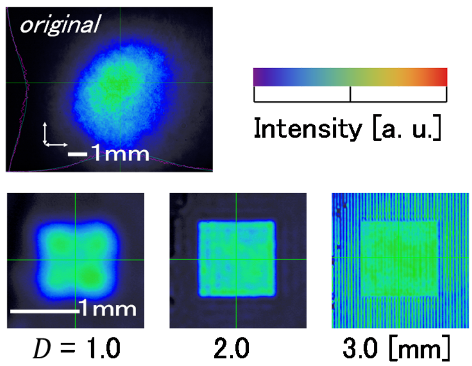

Fig. 2 beam shaping to square-topflat

References:

[1] Y. Nakata, N. Miyanaga, K. Momoo, T. Hiromoto, Solid-liquid-solid process for forming free-standing gold nanowhisker superlattice by interfering femtosecond laser irradiation, Appl. Surf. Sci. 274 (2013) 27–32. doi:10.1016/j.apsusc.2013.02.042.

[2] Y. Nakata, T. Okada, M. Maeda, Nano-sized hollow bump array generated by single femtosecond laser pulse, Japanese J. Appl. Physics, Part 2 Lett. 42 (2003) L1452–L1454.

[3] Y. Nakata, T. Hiromoto, N. Miyanaga, Mesoscopic nanomaterials generated by interfering femtosecond laser processing, Appl. Phys. A Mater. Sci. Process. 101 (2010) 471–474. doi:10.1007/s00339-010-5960-1.

[4] Y. Nakata, Y. Matsuba, N. Miyanaga, Sub-micron period metal lattices fabricated by interfering ultraviolet femtosecond laser processing, Appl. Phys. A. 122 (2016) 532. doi:10.1007/s00339-016-0061-4.

[5] Y. Nakata, T. Okada, M. Maeda, Lines of periodic hole structures produced by laser ablation using interfering femtosecond lasers split by a transmission grating, Appl. Phys. A Mater. Sci. Process. 77 (2003) 399–401. doi:10.1007/s00339-003-2078-8.

[6] Y. Nakata, K. Murakawa, K. Sonoda, K. Momoo, N. Miyanaga, Design of interference using coherent beams configured as a six-sided pyramid, Appl. Opt. 51 (2012) 5004.

[7] Y. Nakata, K. Murakawa, K. Sonoda, K. Momoo, N. Miyanaga, T. Hiromoto, Designing of interference pattern in ultra-short pulse laser processing, Appl. Phys. A. 112 (2012) 191–196. doi:10.1007/s00339-012-7239-1.

[8] K. Osawa, M. Yoshida, Y. Nakata, N. Miyanaga, A. Narazaki, T. Shoji, Y. Tsuboi, Beam shaping by spatial light modulator and 4 f system to square and top-flat for interference laser processing, Proc. SPIE. 10091 (2017) 100911C. doi:10.1117/12.2253983.

Processing of Materials with Shaped Femtosecond Laser Pulses

W. Chu[1], Y. Tan[1], Y. Cheng[1,2]

1- State Key Laboratory of High Field Laser Physics, Chinese Academy of Sciences, Shanghai 201800, China
2- State Key Laboratory of Precision Spectroscopy, East China Normal University, Shanghai 200062, China

Main author email address: ya.cheng@siom.ac.cn

Femtosecond lasers have been proven to be a powerfultool for advanced materials processing on both the microand nanoscale thanks to their unique characteristics of ultrashort pulsewidths and extremely high peak intensities.The advantages of femtosecond laser processing include suppression of heat-affected zone formationaround the irradiated area, high spatial resolution beyond thediffraction limit, and versatility in terms of the materials thatcan be processed. In particular, femtosecond laser direct writing has been employed for 2D/3D micromachining of various transparent materials (glass, crystals, semiconductors) in which the control of the longitudinal fabrication resolution becomes a major issue. Here, we show that by spatiotemporally shaping the femtosecond laser pulses, one can achieve an isotropic spatial resolution in all three dimensions of space, and improve the fabrication yield by almost 6 orders of magnitude [1]. For instance, a 3D structure of China Pavilion at the site of EXPO 2008, which is of a size of 3.5 mm × 3.5 mm × 0.5 mm, can be inscribed in glass in a few minutes, as shown in Fig. 1 below.

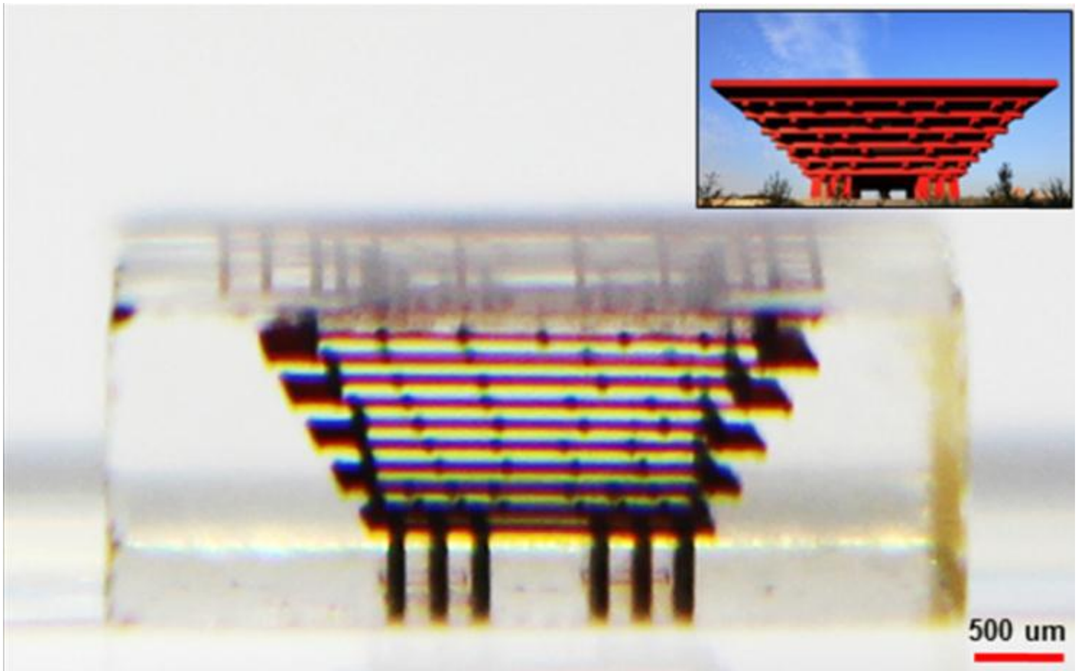

Fig. 1 Digital-camera-captured picture of a 3D model of China Pavilion inscribed in glass using spatiotemporally focused femtosecond laser pulses. Note the isotropic resolution in both transverse and longitudinal directions.

[1] Y. Tan, Z. Wang, W. Chu, Y. Liao, L.Qiao, and Y. Cheng, “High-throughput in-volume processing in glass with isotropic spatial resolutions in three dimensions“, Opt. Mater. Express 6, 3787 (2016)

Multiscale Laser Sintering Technology for Various Applications

D. Kim[1]

1 - Department of Mechanical Engineering, POSTECH, Pohang 790-784, Republic of Korea

dskim87@postech.ac.kr

This talkpresentsvarious laser sintering processes we recently developed.First, processes to fabricate/modifytransparent conductive thin films/patterns on various substrates, including flexible polymers, have been developed using nanosecond and femtosecond pulsed lasers. Use of short laser pulses enables effective sintering of indium tin oxide (ITO) nanoparticles without thermally damagingthe flexible substrate. Furthermore, it is demonstrated that pulsed-laser treatment of sputtered ITO thin film can substantially improve their bendingand adhesion characteristics as well as enhancing the electrical conductivity. Secondly, a femtosecond laser joining process to produce a welded silver (Ag) nanowire network has also been developed for transparent conductive electrodes. Thirdly, precise fabricationof metal thin films/patterns on flexible substrates by sintering metal nanoparticles with femtosecond laser pulses is demonstrated. The laser sintering process can produce flexible silverelectrodes that can be completely folded without losing their electrical conductivity. Finally, a hybrid 3D printing process combining femtosecond laser micromachining and powder injection molding (PIM) are introduced. Fabrication of stainless steel and zirconia parts with microscale structures is demonstrated.

The Multi-functional high power laser platform in NLHPLP

Jianqiang Zhu, Jian Zhu, Xuechun Li, Baoqiang Zhu, Weixin Ma, Dean Liu, Cheng Liu, Xingqiang Lu, Wei Fan, Zhigang Liu, Dongfeng Zhao, Shenlei Zhou, Yanli Zhang, Li Wang, Mingying Sun, Bingyan Wang, Zhaoyang Jiao,Lei Ren, Guowen Zhang, Jie Miao, Zunqi Lin

National Laboratory on High Power Laser and Physics
Shanghai Institute of Optics and Fine Mechanics, CAS

As fs and ps PW laser systems had been established, combined with ns SGII and SGII-Up laser facility, we had constructed unique multi-functionexperiment platform to meet the different experiment requirement.
For ns, several MJ output, some trade off analysis factors are given.
The key techniquesfor PW systems, such as pulse contrast, image delay and system auto-alinement were analyzed also.

High intensity (>10^{22} W/cm^2), high contrast (<10^{-11}), repetitive (0.1 Hz) J-KAREN-P laser facility at QST

H. Kiriyama, M. Nishiuchi, A. S. Pirozhkov, Y. Fukuda, H. Sakaki, A Sagisaka, N. P. Dover, K. Kondo, K. Nishitani, K. Ogura, M. Mori, Y. Miyasaka, M. Kando and K. Kondo

Kansai Photon Science Institute, National Institutes for Quantum and Radiological Science and Technology, 8-1-7 Umemidai, Kizugawa, Kyoto 619-0215, Japan

Main author email address: kiriyama.hiromitsu@qst.go.jp

The J-KAREN-P laser facility [1] can provide PW peak power at 0.1 Hz. It is based on the generation of short pulses of 30 fs and energy of 30 J after compression. The contrast of the generated pulses is better than 10^{12} and the final focused intensity is higher than 10^{22} W/cm^2. Such performance in high field science will give rise to the birth of new applications and breakthroughs, which include relativistic particle acceleration, bright x-ray source generation, and nuclear activation.
The schematic setup of the J-KAREN-P laser system is shown in Fig. 1. The key points of the J-KAREN-P laser system architecture are: 1) the high contrast front-end source based on a combination of some saturable absorbers and low gain OPCPA configuration, 2) the main amplification composed of four moderate gain Ti:sapphire amplifiers, employing simple off-axis mirror-based beam expanders with low aberration, 3) the adaptive control of the residual spectral phase based on a high dynamic range Dazzler and the active wavefront correction based on a deformable mirror, 4) the main compressor stage based on four high quality large sized gold gratings.
We have measured dependence of output broadband energy from the final amplifier, which uses a 120 mm diameterTi :sapphire crystal, on the total pump energy at a 0.1 Hz repetition rate. The maximum output energy of 63 J is achieved with an incident energy of 92 J. The amplified pulses are up-collimated to ~250 mm diameter and finally compressed in the compressor consisting of four 1480 grooves/mm gold coated gratings of 565 x 360 mm^2. The measured spectrum has a bandwidth of ~50 nm (FWHM). The obtained recompressed pulse duration is less than 30 fs. The peak power is expected to be over PW at 0.1 Hz on target, because the beam-line throughput from the laser room to the target chamber including the compressor is ~60 %. The contrast at less than 200 ps before the main pulse is 3 x 10^{-12} (detection limited). The contrast at 100, 50, 10 and 5 ps before the main pulse are about ~10^{-11}, ~6 x 10^{-10}, and ~8 x 10^{-9}, respectively. With an f/1.4 off-axis parabolic mirror, according to measurements of the focal spot and energy contained within it, a peak intensity of 10^{22} W/cm^2 on target is achieved at the 0.3 PW power level.
The J-KAREN-P laser system is one of the leading facilities in the provision and application of ultra-high intensity lasers for the broad scientific community. The J-KAREN laser has been used in a variety of pioneering and cutting-edge research, which have resulted in high impact discoveries for high field science [1]. As a first step, the J-KAREN-P laser system will be used for >100 MeV proton generation and ~keV ultra-short x-ray generation.

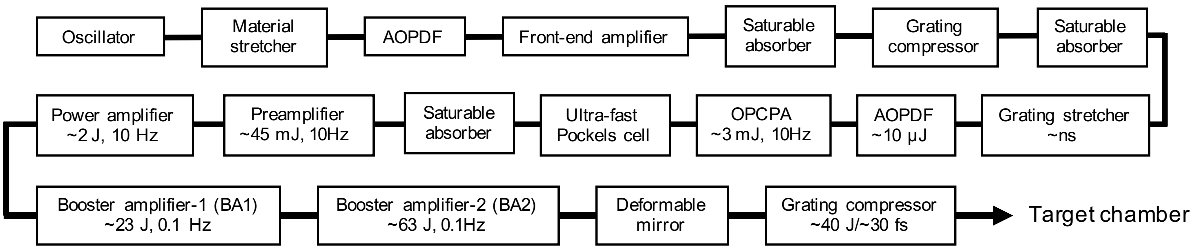

Fig. 1. Schematic of the J-KAREN-P laser system.

[1] H. Kiriyama, M. Mori, A. S. Pirozhkov, K. Ogura, A. Sagisaka, A. Kon, T. Zh. Esirkepov, Y. Hayashi, H. Kotaki, M. Kanasaki, H. Sakaki, Y. Fukuda, J. Koga, M. Nishiuchi, M. Kando, S. V. Bulanov, K. Kondo, P. R. Bolton, O. Slezak, D. Vojna, M. Sawicka-Chyla, V. Jambunathan, A. Lucianetti, and T. Mocek, "High-contrast, high-intensity petawatt-class laser and applications," *Invited Paper,* IEEE J. Quantum. Electron., vol. **21**, pp.1601118 (2015).

Efficient Coupling of Sub-PW Laser Pulse with Solid Target at PEARL Facility

A. Soloviev[1], K. Burdonov[1], S. N. Chen[1,2], A. Eremeev[1], S. Pikuz[3], G.V. Pokrovskiy[3], T.A. Pikuz[3], G. Revet[1,2], A. Sladkov[1], V. Ginzburg[1], E. Khazanov[1], A. Kuzmin[1], D.K. Batheja[4], S. Mironov[1], R. Osmanov[1], I. Shaykin[1], A. Shaykin[1], I. Yakovlev[1], M. Starodubtsev[1], and J. Fuchs1,2

[1]Institute of Applied Physics of the Russian Academy of Sciences, Nizhny Novgorod, Russia,
[2]LULI - CNRS, Ecole Polytechnique, CEA: Université Paris-Saclay; UPMC Univ Paris 06: Sorbonne Universities - F-91128 Palaiseau cedex, France
[3]Joint Institute for High Temperatures Russian Academy of Science (RAS), Moscow 125412, Russia
[4]Institute of Physics of the Czech Academy of Sciences, 252 41 Dolní Břežany, Czech Republic

7oloviev@gmail.com

The report represents experimental investigation of interaction between femtosecond sub-PW laser pulse from PEARL laser facility and plasmas. The experimentally realized conditions are close to the optimal in terms of effective laser energy deposition into the solid target leading to NTSA proton beams accelerated up to 43 MeV cut-off energy. The characterization of the interaction parameters is achieved by combining of X-ray spectrometry and proton spectra measurements, complimented by detailed laser prepulse characterization. The ways to improve the cut-off energy for the laser driven protons are considered as well as application perspectives.

The experiments were conducted at the PEARL laser facility (IAP RAS, Nizhny Novgorod, Russia). PEARL is an OPCPA laser system [1] with wavelength 910 nm and the record reported power of 0.56 PW [2]. The temporal contrast of the laser systems after compression and over a 1 ns frame before the main pulse was estimated to be 1/(2×108) [3]. By means of an off-axis parabolic f /4 mirror the laser pulse was focused on the target surface (aluminium foil 10 mm thick) making an angle of 45° with the direction of incident radiation.

Using two complementary diagnostics, we have been able to characterize the interaction of an ultra-high intensity, and ultra-high contrast laser with a thin Al solid slab. We have shown that at the time of the main laser pulse interaction, the target front and rear surfaces are gradient-free. This ensures a very efficient coupling between the laser energy and the target, and the generation of a very dense population of hot electrons at high temperature (as diagnosed by the accelerated protons). These couple very efficiently to the bulk electrons and ions, heating those (as diagnosed by x-ray spectrometry) to ~300 eV, which is in good agreement with a 1D modeling of such coupling using the hot electrons parameters as an input.

Such efficient, gradient-free, heating to high temperatures opens possibilities for probing various materials, using a much smaller-scale and relatively low-cost facility compared to a FEL. We note that for such mid-scale laser, the employed technology is key to allow high-contrast interactions without the need to resort to contrast enhancement techniques. The work is considered in the aspect of possible applications in laboratory astrophysics, medicine and homeland security.

This work was supported by the Ministry of Education and Science of the Russian Federation under Contract No.14.Z50.31.0007. The work has been supported by Russian Foundation for Basic Research under the project 16-32-60183.

[1] Ross, I. ., Matousek, P., Towrie, M., Langley, A. . & Collier, J. . The prospects for ultrashort pulse duration and ultrahigh intensity using optical parametric chirped pulse amplifiers. Optics Communications 144, 125–133 (1997).
[2] Lozhkarev, V. V. et al. Compact 0.56 Petawatt laser system based on optical parametric chirped pulse amplification in KD*P crystals. Laser Physics Letters 4, 421–427 (2007).
[3] Ginzburg, V. N. et al. Third-order correlator for measuring the time profile of petawatt laser pulses. Quantum Electronics 38, 1027–1032 (2008)

Particle acceleration by the High intensity (<10^{22} W/cm^2), high contrast (<10^{-11}), repetitive (0.1 Hz) J-KAREN- P laser

M. Nishiuchi[1], **H. Kiriyama[1], H. Sakaki[1], N.P. Dover[1], A. S. Pirozhkov[1], Y. Fukuda[1], K. Kondo[1], T. Miyahara[1,2], A. Sagisaka[1], M. A. Alkhimova[3], T. A. Pikuz[3,4], A. Ya. Faenov[5], K. Ogura[1], T. Zh. Esirkepov[1], Y. Watanabe[2], J. Koga[1], S. V. Bulanov[1], M. Kando[1], and K. Kondo[1]**

[1]*Kansai Photon Science Institute, National Institutes for Quantum and Radiological Science and Technology (QST), Kizugawa, Kyoto, Japan*

[2]*Department of .Advanced Energy Engineering Scienmve, Kyushu University, 6-1 Kasuga-kouen kasuga Fukuoka*

[3] *Joint Institute for High Temperatures, Russian Academy of Sciences, Moscow, 125412*

[4] *Graduate School of Engineering, Osaka University, Suita, Osaka, Japan Osaka, Japan*

[5] *Institute for Academic Initiatives, Osaka University, Suita, Osaka, Japan*

Main author email address:nishiuchi.mamiko@qst.go.jp

Based on the remarkable achievements in the laser technology in the resent years, many PW-class laser facilities were constructed in all over the world. J-KAREN-P laser facility is one of such laser facilities at Kansai Photon Science Institute, National Institutes for Quantum and Radiological Science and Technology (QST) [1]. Before the upgrade project of the laser system began in 2014, the previous J-KAREN system enabled us to perform the high field physics experiments with a laser intensity of 1021 Wcm^{-2}, where we successfully obtained energetic hadron beams [2,3]. For exploring further the high-intensity physics, the system has been under the upgrade project since then and it reaches at almost the final stage of the project.

We present the recent achievements in the ion acceleration experiment during the commissioning periods of the J-KAREN-P laser system. The J-KAREN-P laser is a Ti:sapphire system with double chirped-pulse amplification (CPA) providing a laser pulse with high-contrast ratio of better than10^{-11} at -500 ps. The laser system has successfully amplified a pulse with an energy of 63 J at 0.1 Hz. A deformable mirror corrects the wavefront before the compressor. The laser has been successfully compressed down to a duration of ~30 fs at full width at half maximum (FWHM) on target. These laser pulses are fed into one of the target chambers with a short-focal length (f/1.4) off-axis parabola. The focus spot is measured under full amplification condition.

The focal spot of 1.32 μm x 1.37 μm at FWHM includes 32 % of the energy. This results in the world highest intensity on target of 10^{22} W/cm^2 with 0.3 PW power level. Full system commissioning tests are continuously carried out by gradually increasing the energy on the target. Currently we carried ~9 J energy laser pulse with 5x10^{21}Wcm^{-2} on 2-μm Al target to accelerate the proton up to 50 MeV of maximum energies. By using the 5-μm Stainless steel tape target provides us an energetic proton beams with typical maximum energies of > 40 MeV with good reproducibility, which is suitable for many applications including as an injector for medical use, which is one of our objectives. Further details on the experimental results including the results of sub-μm targets shots with different laser contrast conditions will be presented.

[1] H. Kiriyama, M. Mori, A. S. Pirozhkov, K. Ogura, A. Sagisaka, A. Kon, T. Zh. Esirkepov, Y. Hayashi, H. Kotaki, M. Kanasaki, H. Sakaki, Y. Fukuda, J. Koga, M. Nishiuchi, M. Kando, S. V. Bulanov, K. Kondo, P. R. Bolton, O. Slezak, D. Vojna, M. Sawicka-Chyla, V. Jambunathan, A. Lucianetti, and T. Mocek, "High-contrast, high-intensity petawatt-class laser and applications," *Invited Paper,* IEEE J. Quantum. Electron., vol. **21**, 1601118 (2015).

[2] K. Ogura, M. Nishiuchi, A. Pirozhkov, T. Tanimoto, A. Sagisaka, T. Zh. Esirkepov, M. Kando, T. Shizuma, T. Hayakawa, H. Kiriyama, T. Shimomura, S. Kondo, S. Kanazawa, Y. Nakai, H. Sasao,. F. Sasao, Y. Fukuda, H. Sakaki, M. Kanasaki, A. Yogo, S. V Bulanov, P. Bolton, K. Kondo. *Opt. Lett.* **37**, 2868 (2012).

[3] M. Nishiuchi, H. Sakaki, T. Zh. Esirkepov, K. Nishio. T.A.Pikuz, A.YaFaenov, I Yu Skobelev, R. Orlandi, H. Sako. A. S. Pirozhkov, K. Matsukawa, A. Sagisaka, K. Ogura, M. Kanasaki. H. Kiriyama, Y. Fukuda, H. Koura, M. Kando, T. Yamauchi, Y. Watanabe, S. V. Bulanov, K. Kondo, K. Imai, S. Nagamiya, *Physics of Plasmas* **22,** 033107 (2015).

Laser pulses interaction with solid and liquid materials: Applications to biomedical, mechanical and chemical top technologies

Ion N. Mihailescu and Carmen Ristoscu
National Institute for Lasers, Plasma and Radiation Physics, POB MG-36, Magurele, Ilfov, Romania
e-mail: ion.mihailescu@inflpr.ro

Basic principles of laser pulses interaction with solid and liquid materials using advanced pulsed laser technologies are introduced and new recent results in synthesis of biomaterial layers are reviewed. The layers are optimized based upon the results of physical-chemical investigations, while biocompatibility, bioactivity and biodegradation were assessed by dedicated *in-vitro* tests.

The coating of metallic implants with composite alendronate (AL)-HA by MAPLE was demonstrated to enhance human osteoblasts proliferation and differentiation, while inhibiting osteoclasts growth, with benefic effects for the treatment of bone diseases. MAPLE thin films of calcium alendronate monohydrate, octacalcium phosphate, as well as $CaAL^{\bullet}H_2O$ / OCP composite on Titanium substrates proved that the presence of calcium alendronate in the coatings dramatically inhibits proliferation, differentiation and activity of osteoporotic osteoclast. On the contrary, the bisphosphonate does not affect osteoblast viability, and it promotes their activity. Ostoblast differentiation is further enhanced when the coating is a composite of $CaAL^{\bullet}H_2O$ and OCP, most likely due to the good bioactivity of OCP.

We showed that the composite PMMA-bioglass films deposited by MAPLE efficiently protects metal implants against the action of human fluids.

Human plasma proteins (fibronectine, vitronectine) applied by MAPLE on pulsed laser deposited HA coated metallic implants significantly increased cell adhesion and activated osteointegration.

Structures with compositional gradient are obtained by Combinatorial-MAPLE (C-MAPLE) by the simultaneous laser vaporization of two targets. Synchronized MAPLE of levan and oxidized levan cryogenic targets is applied in order to transfer under protection and assemble a two-compound biopolymer film structure. FTIR micro-spectroscopy confirmed the existence of a composition gradient along the length of the sample. I*n-vitro* cell culture assays illustrate characteristic responses of cells to specific surface locations. Cells attached along the gradient are in direct proportion with oxidized levan concentration.

C-MAPLE is applied to synthesize crystalline gradient thin films with variable composition of Sr-substituted hydroxyapatite (Sr-HA) and Zolendronate modified hydroxyapatite (ZOL-HA). The inhibitory action of ZOL on osteoclast viability and activity is more efficient than that of Sr, which plays a greater beneficial role on osteoblast proliferation and viability. C-MAPLE allows to modulate the composition of the thin films and hence the promotion of bone growth and the inhibition of bone resorption.

Our conclusion is that the thin films prepared by pulsed laser techniques are identical in chemical composition, structure, morphology, and most likely functionality resembling the base material, as proved by physical-chemical characterization and *in-vitro* testing. C-MAPLE opens the possibility to combine and immobilize two or more organic materials on a substrate in a well defined manner by laser evaporation under protection.

[1] E. Axente, F. Sima, C. Ristoscu, N. Mihailescu, I. N. Mihailescu, “Biopolymer thin films synthesized by advanced pulsed laser techniques”, Chapter 4, in "Recent Advances in Biopolymers", Ed. F. Parveen, InTech ISBN 978-953-51-4613-1, 2016

[2] F. Sima, E. Axente, C. Ristoscu, O. Gallet, K. Anselme, I.N. Mihailescu, “Bioresponsive surfaces and interfaces fabricated by innovative laser approaches”, Chapter 12, in “Advanced Materials Interfaces" Advanced Materials Book Series, Eds. Ashutosh Tiwari, Hirak K. Patra and Xuemei Wang, WILEY-Scrivener Publishing, USA, ISBN 9781119242451, 2016

[3] F. Sima, C. Ristoscu, L. Duta, O. Gallet, K. Anselme, I.N. Mihailescu, “Laser thin films deposition and characterization for biomedical applications”, Chapter 3 in “Laser Surface Modification of Biomaterials, Techniques and Applications”; 1st Edition; Editor: R Vilar, Release Date: 15 Apr 2016, Imprint: Woodhead Publishing, Print Book ISBN: 9780081008836, pp.77-125, DOI: 10.1016/B978-0-08-100883-6.00003-4

[4] Ion N. Mihailescu, Adriana Bigi, Eniko Gyorgy, Carmen Ristoscu, Felix Sima, Ebru Toksoy Oner, “Biomaterial thin films by soft pulsed laser technologies for biomedical applications”, Chapter 11 in “Lasers in Materials Science” (SLIMS 2012 Proceedings), Spinger Series Materials in Science, vol. 191, Eds. P.M. Ossi, M. Castillejo, L. Zhigilei, ISBN 978-3-319-02897-2 (2014) pp. 271-291

On-Chip Picosecond Pulses in 2DEG and Graphene

A. S. Mayorov[1], J. B. Wu[2], N. Hunter[2], O. Sydoruk[3], C. Russell[2], C. D. Wood[2], D. Mistry[2], L. H. Li[2], W. Muchenje[2], M. C. Rosamond[2], L. Chen[2], E. H. Linfield[2], A. G. Davies[2], and J. E. Cunningham[2]

[1]*Physics Department, National University of Singapore, Singapore*

[2]*School of Electronic and Electrical Engineering, University of Leeds, Leeds, United Kingdom*

[3]*Department of Electrical and Electronic Engineering, Imperial College London, London, United Kingdom*
mayorov@gmail.com

The energy scale which corresponds to the terahertz (THz) frequency range until recently has been difficult to access. Many low-dimensional semiconductor structures, graphene, and other 2D materials can support plasma excitation of ~meV range. Here we demonstrate on-chip transmission lines in which low-temperature-grown GaAs photoconductive switches (LT-GaAs) are used to provide excitation and detection of picosecond pulses which are coupled to a two-dimensional system (2DS).

In the first approach, a coplanar waveguide connected by an Ohmic contact to a channel with high-mobility 2DS allows to inject an ultra-broadband pulse (up to ~0.4 THz) into the 2DS formed on the GaAs/AlGaAs interface and create a plasmon signal which is detected on the other end of the waveguide using standard time-domain on-chip spectroscopy. This on-chip THz plasmonic circuit with a top gate is capable to manipulate plasmons electrostatically at low temperatures. Our work paves the way to detection of the broadband THz plasmon response of individual nanoscale low-dimensional electronic systems. [1]

However, this geometry is limited to very low temperatures, therefore, in the second approach 2DS is replaced with graphene and the ps pulses were excited and detected in a Goubau transmission line configuration fabricated on a quartz substrate which allows a slightly larger bandwidth at room temperature. [2] It was shown that graphene can be used as a detector in both space and time. Our findings pave the way to full THz field imaging in 2D space and time. [3]

[1] J. Wu, A. S. Mayorov, C. D. Wood, D. Mistry, L. Li, W. Muchenje, M. C. Rosamond, L. Chen, E. H. Linfield, A. G. Davies, J. E. Cunningham, Excitation, detection, and electrostatic manipulation of terahertz-frequency range plasmons in a two-dimensional electron system, Scientific Reports, vol. 5, pp. 15420, (2015).
[2] N. Hunter, A. S. Mayorov, C. D. Wood, C. Russell, L. Li, E. H. Linfield, A. G. Davies, and J. E. Cunningham, On-Chip Picosecond Pulse Detection and Generation Using Graphene Photoconductive Switches, Nano Letters, vol. 15, pp. 1591–1596, (2015).
[3] N. Hunter, A. S. Mayorov, C. D. Wood, C. Russell, M. C. Rosamond, L. H. Li, E. H. Linfield, A. G. Davies, J. E. Cunningham, Spatially resolved on-chip picosecond pulse detection using graphene, Infrared, Millimeter, and Terahertz waves, (2015).

Tunable continuous wave terahertz generation using Monolithic Integrated Dual-Mode DFB Laser

Hyun-Soo Kim, Eui Su Lee, Donghun Lee, Kiwon Moon, Sang-Pil Han, Il-Min Lee, and Kyung Hyun Park*

Terahertz Basic Research section, ETRI, Daejeon 305-700, Republic of Korea

*kimhyunsoo@etri.re.kr

Terahertz (THz) technology has received enormous interest for application in spectroscopy, imaging, security, and wireless communication [1]. Monolithically integrated semiconductor laser diode as optical beat source is a key component to achieve compact and low cost for CW THz system. In this work, we improved the wavelength tunability and mode stability of dual mode laser (DML) using asymmetric multiple quantum well (AMQW) and modified grating structure.

The wavelength tunable DML was fabricated as shown in Fig. 1. The DML consisted of two $\lambda/4$ phase-shifted DFB sections, one phase section and spot-size converter. The lengths of DFB sections and phase section are 400 μm and 50 μm, respectively. The initial wavelength spacing was set to 4 nm. A buried heterostructure with a p/n/p current blocking layer was used. The active layer consisted of asymmetric multiple quantum well (AMQW). The AMQW was composed of four 7 nm-thick InGaAsP wells (λ=1.61 μm, ε=+0.8%,) and four 5 nm-thick InGaAsP wells (λ=1.61 μm, ε=+0.8%) alternately. The conventional MQW (CMQW) consisted of seven 7 nm-thick InGaAsP wells (λ=1.61 μm, ε=+0.8%) and the same barriers of AMQW. In photoluminescence (PL) at room temperature, full width at half maximum (FWHM) of AMQW and CMQW are 26.6 meV and 49 meV, respectively. The active layer was butt-jointed to 0.33 μm-thick InGaAsP (λ=1.3 μm). In order to tune the operating wavelength independently, μ-heaters were integrated on top of each DFB sections Figure 2 shows the superimposed tuning spectra of AMQW DML and CMQW DML. The front DFB (DFB1) was only biased at 50mA. The maximum heat power was injected up to 0.62 W. As μ-heater power increases, the degradation of output power appears due to the increased difference between gain peak and Bragg wavelength. The degradation of output power in case of DFB LD with AMQW was 3 dB at a 4nm wavelength tuning, which is a 6 dB improvement to the case of CMQW. As shown in Fig. 3, the side mode suppression ratio (SMSR) of DML is maintained over above 50 dB through the whole tuning range using modified grating structure. In order to measure the CW THz radiation, a typical homodyne configuration was set up using low temperature grown (LTG) a log-spiral antenna integrated InGaAs photmixers as THz emitter and detector. We successfully measured CW THz radiation from 191 GHz to 926 GHz. The inset shows the CW THz waveform at a frequency of 191 GHz and 926 GHz.

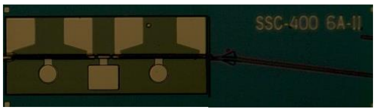

Fig. 1. Monolithically integrated DML

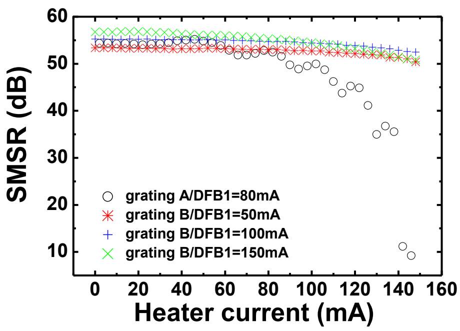

Fig. 3. SMSR of DML vs heater current

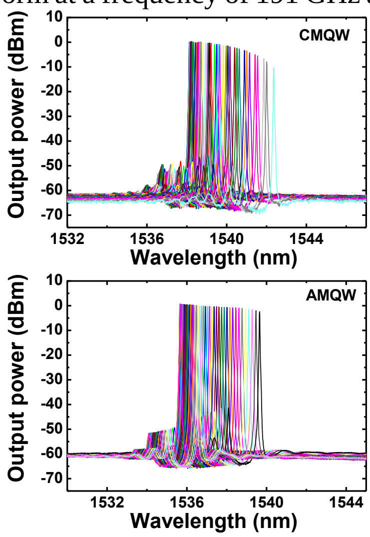

Fig. 2. Superimposed tuning spectra

[1] M. Tonouchi., “Cutting-edge terahertz technology,” Nat. Photonics **1,** 97-105 (2007).

Nano-electrode photonic devices for the generation and detection of pulse and continuous-wave THz radiation

Kiwon Moon, **Il-Min Lee, Eui Su Lee, Dong Woo Park, Hyun Soo Kim, Jeong-Woo Park, Sang-Pil Han, Kyeong Sun Choi and Kyung Hyun Park***

THz Photonics Creative Research Section, Electronics and Telecommunications Research Institute, Daejeon, 34129, Republic of Korea

Main author email address: khp@etri.re.kr

Nano-electrode provides various pathways to manipulate local ultrafast carrier collection dynamics, can be used for the generation and detection of continuous-wave and pulse THz radiation [1,2]. In conventional pulse and continuous-wave THz emitter and detectors, defect-engineered, low-temperature-grown photo-absorbing materials have been used to utilize sub-picosecond carrier lifetime [3]. But the control of defects in the semiconductor crystal has been very difficult and hardly reproduced. In this work, we present pulse and continuous-wave THz emitters and detectors, free from low-temperature-grown materials. We used various nano-electrodes and nano-structures with ordinary compound semiconductors to manipulate and control the nano-scale carrier dynamics in the device. Since the local environment around photoelectrons varies according to the operating mode of the device, it should be properly considered in the design.

[1] K. Moon, et al., Bias field tailored plasmonic nano-electrode for high-power terahertz photonics devices, Sci. Rep. 5:13817 (2015).
[2] K. Moon, et al., A comparative study of the plasmon effect in nanoelectrode THz emitters: Pulse vs. continuous-wave radiation, Appl. Phys. Lett. 109, 071105 (2016).
[3] M. R. Melloch, et al., Low-temperature grown III-V materials, Annu. Rev. Mater. Sci. 25, 547-600 (1995)..

Resonant Tunneling Diodes for THz Applications

Jaeyoung Kim[1], Toshikazu Mukai[1], Sebastian Diebold[2], Masayuki Fujita[2], and Tadao Nagatsuma[2]

1- ROHM Co., Ltd., Fundamental R&D Division, 21 Saiin Mizosaki, Ukyo, Kyoto 615-8585, Japan
2- Osaka University, 1-3 Machikaneyama, Toyonaka, Osaka 560-8531, Japan

jaeyoung.kim@dsn.rohm.co.jp

The terahertz wave, located between the radio and light wave frequency regions from 0.1 to 10 THz, has attracted considerable interests owing to its ultra-wide frequency bandwidth and spectral fingerprint. These properties offer many possibilities for high-speed wireless communication, spectroscopic sensing, and non-destructive imaging [1-2]. The development of terahertz sources and detectors started using photonic technologies which remain bulky and expensive. But recent progress in photonic integration and semiconductor electronic device technology has enabled low-cost and compact solutions for commercial applications [3-4].

The resonant tunneling diode (RTD) is an interesting device due to its negative differential resistance (NDR). The RTD can provide fundamental oscillation over 1THz at room temperature with a simple resonator and directly attached antenna [5]. Moreover, the nonlinearity close the NDR region enables compact terahertz detector using the same device. For terahertz communication, we had demonstrated 9-Gbps error-free wireless communication and uncompressed 4K video transmission using the RTD as both of transmitter and detector, and 17-Gbps data transmission using the RTD as detector [6-7]. The compact terahertz emitter and detector also can be used for non-destructive imaging and sensing [8]. The combination of RTD-based sensor devices with terahertz photonic crystal resonator can offer improved sensitivity and usability compared to the stand-alone device [9].

In this paper, we present the recent advance of RTD-based terahertz transmitter and detector technology. Based on a well-defined equivalent circuit model of the RTD, terahertz circuits such as mixers and oscillators have been integrated into a single chip [10]. Impedance matching of the antenna to the RTD oscillator enhanced the radiation and detection efficiencies of the transmitter and detector, respectively.

This work was partly supported by Core Research for Evolutional Science and Technology (CREST) program of Japan Science and Technology Agency (JST) (#JPMJCR1534).

[1] M. Tonouchi, Cutting-edge terahertz technology, Nat. Photon. 1, pp. 97–105, 2007.
[2] H.-J. Song and T. Nagatsuma, Present and future of terahertz communications, IEEE Trans. Terahertz Sci. Tech. 1, pp. 256–263, 2011.
[3] T. Nagatsuma, Terahertz technologies: present and future, IEICE Electron. Exp. 8, 1127–1142, 2011.
[4] H.-J. Song, J.-Y. Kim, K. Ajito, N. Kukutsu, and M. Yaita, 50-Gb/s Direct Conversion QPSK Modulator and Demodulator MMICs for Terahertz Communications at 300 GHz, IEEE Trans. Microw. Theory and Tech. 62, pp. 600-609, 2014.
[5] S. Suzuki, M. Asada, A. Teranishi, H. Sugiyama, and H. Yokoyama, "Fundamental oscillation of resonant tunneling diodes above 1THz at room temperature," App. Phys. Lett. 97(24), 2010.
[6] S. Diebold, K. Nishio, Y. Nishida, J. Kim, K. Tsuruda, T. Mukai, M. Fujita, and T. Nagatsuma, High-speed error-free wireless data transmission using a terahertz resonant tunneling diode transmitter and receiver, Electron. Lett. 52, pp. 1999–2001, 2016.
[7] K. Nishio, S. Diebold, S. Nakai, K. Tsuruda, T. Mukai, J.-Y. Kim, M. Fujita, and T. Nagatsuma, Resonant tunneling diode receivers for 300-GHz-band wireless communications, URSI-Japan Radio Science Meeting, Sep 2015.
[8] T. Miyamoto, A. Yamaguchi, and T. Mukai, Terahertz imaging system with resonant tunneling diodes, Jpn. J. Appl. Phys. 55, 032201, 2016.
[9] K. Okamoto, K. Tsuruda, S. Diebold, S. Hisatake, M. Fujita, and T. Nagatsuma, Terahertz Sensor Using Photonic Crystal Cavity and Resonant Tunneling Diodes, J. Infrared Milli. Terahz. Waves, 2017. doi:10.1007/s10762-017-0391-0
[10] S. Diebold, K. Tsuruda, J.-Y Kim, T. Mukai, M Fujita, and T Nagatsuma, A Terahertz Monolithic Integrated Resonant Tunneling Diode Oscillator and Mixer Circuit, Proc. SPIE proceedings 9856, 98560U, 2016.

Next generation high harmonic sources

E. J. Takahashi, N. Kanda, Y. Fu, B. Xue, K. Midorikawa

RIKEN Center for Advanced Photonics, RIKEN, 2-1 Hirosawa, Wako, Saitama 351-0198, Japan

kmidori@riken.jp

High-order harmonic generation (HHG) is now established as a high-output coherent light source in the XUV region and the sole source of attosecond pulses. Here, I present recent efforts on HHG in RIKEN by using novel pump laser technology for intense isolated attosecond pulses (IAP) and MHz repetition rated pulses.

For generating intense IAP in the soft x-ray region, we are expanding the two-color pumping scheme developed in RIKEN [1] to high-energy three-color one. Since our method has the advantage that high harmonic output yield can be linearly scaled up by increasing the HH emission volume, we can estimate exactly a scaled-up configuration in the soft-X-ray region. By straightforwardly increasing a three-color synthesizer output to 50 mJ and adopting a focusing length of 5 m with a 5-cm-long Ne medium, we expect to achieve an IAP energy greater than 0.2 μJ at 80 to 110 eV, which is almost 1000-fold higher than the energies previously reported. A pulse duration of 80 as is also estimated by our simulation. This source is attractive for research on nonlinear optics in the attosecond region.

On the other hand, the increase of the repetition rate of high-harmonic pulses up to multi-MHz is also desired to explore the wide range of applications in particular photoemission spectroscopy. However, the repetition rate of the high harmonic pulse is restricted in a range of multi kHz in accordance with a repetition rate of the fundamental laser amplifier. We propose a promising method of high repetition HHG inside the laser cavity of a high-power mode-locked oscillator, which does not need a precise control of cavity length. Energy-scalability and system flexibility of the intra-cavity HHG is expected to be better than the external enhancement cavity. For realizing our concept, we have designed and developed a high-pulse-energy Yb:YAG thin disk mode-locked oscillator with a ring cavity. In order to achieve high pulse energy at an ultrahigh repetition rate, the cavity length of 100 m which corresponds to the repetition rate of 3 MHz is employed. Intra-cavity pulse energy reaches to about 0.7 mJ which is the highest to the best of our knowledge, in mode-locked oscillators ever reported [2].

In this work, we demonstrate the operation of this high-pulse-energy Yb:YAG thin disk oscillator with the addition of multiple intra-cavity HHG ports. To obtain HHG, noble gas jets are placed at two focal points in the mode-locked oscillator cavity. Assuming a focal radius of around 30 μm, the intra-cavity peak intensity is estimated to be 8.4×10^{13} W/cm^2, sufficient for HHG. Two HHG ports are simultaneously operated, and it is shown that the harmonic order in each port can be independently controlled by choosing an appropriate gas for each port. Our method paves the way to MHz repetition-rated high-power XUV sources for multi-user or multi-color experiments.

[1] E. J. Takahashi, P. F. Lan, O. D. Mücke, Y. Nabekawa, and K. Midorikawa, Nat. Commun. **4**, 2691 (2013).
[2] N. Kanda *et al.*, Advanced Solid-State Lasers Congress 2013 **AF3A.8** (2013).

Atmospheric Applications of Ultrashort-Pulse Lasers

Pavel Polynkin[1]

1- College of Optical Sciences, University of Arizona, 1630 East University Blvd., Tucson, Arizona 85721, USA

Email: ppolynkin@optics.arizona.edu

Extreme nonlinear optics of gaseous media is an interdisciplinary branch of modern applied physics that is motivated by numerous exciting potential applications. I will discuss two such applications: air lasing and channeling the electrical breakdown of air. In the air lasing concept [1], powerful laser beams, propagating from the ground into the atmosphere, remotely pump optical gain in the constituents of air. The goal is to produce an impulsive, backward propagating laser-like radiation emanating from a remote location in the sky. Such a remote laser source will revolutionize the field of remote atmospheric sensing, as it will enable efficient single-ended remote sensing schemes [2]. Various schemes of air lasing are currently being investigated. I will discuss two schemes, one based on the dissociation of molecular oxygen and nitrogen in the air and subsequent two-photon pumping of atomic fragments [3] and the other scheme based on strong-field ionization of atmospheric molecular nitrogen [4]. In both schemes, scientific questions remain on the mechanisms of stimulated emission and on the ways towards enhancing these emissions. The second broad application I will discuss is channeling the electrical breakdown of air by powerful laser beams. This problem has been investigated for several decades, motivated by the search for a flexible solution for channeling natural lightning. The guidance range in the schemes based on the application of a single laser pulse or few laser pulses with either nanosecond [5] or femtosecond [6] duration is fundamentally limited by about ten meters. I will discuss a new approach based the application of a train of multiple (~one thousand) laser pulses that potentially can alleviate the range limitations of the single-pulse schemes.

[1] Q. Liu, W. Liu, S. L. Chin, “Lasing action in air induced by ultra-fast laser filamentation,” Appl. Phys. B **76**, 337 (2003).
[2] P. N. Malevich, D. Kartashov, Z. Pu, S. Alisauskas, A. Pugzlys, A. Baltuska, L. Giniunas, R. Danielius, A. A. Lanin, A. M. Zheltikov, M. Marangoni, G. Cerullo, “Ultrafast-laser-induced backward stimulated Raman scattering for tracing atmospheric gases,” Opt. Express **20**, 18784 (2012).
[3] A. Dogariu, J. B. Michael, M. O. Scully, R. B. Miles, “High-gain backward lasing in air,” Science **331**, 442 (2011).
[4] J. Yao, B. Zeng, H. Xu, G. Li, W. Chu, J. Ni, H. Zhang, S. L. Chin, Y. Cheng, Z. Xu, “High-brightness switchable multiwavelength remote laser in air,” Phys. Rev. A **84**, 051802(R) (2011).
[5] D. W. Koopman, T. D. Wilkerson, “Channeling of an ionizing electrical streamer by a laser beam,” J. Appl. Phys. **42**, 1883 (1971).
[6] S. Tzortzakis, B. Prade, M. Franco, A. Mysyrowicz, “Femtosecond laser-guided electrical discharge in air,” Phys. Rev. E **64**, 057401 (2001).

High Order Harmonic Generation by Tunable Laser Mid-Infrared Pulsed in Solids: New Opportunities for Spectroscopy of Electron Band Structure

***A.B. Fedotov*[1,2], *A.A. Lanin*[1,2], *E.A. Stepanov*[1,2], *A.M. Zheltikov*[1,2,3]**

1. Physics Department, International Laser Center, M. V. Lomonosov Moscow State University, Leninskie gory, Moscow 119992, Russia

2. Russian Quantum Center, 143025 Skolkovo, Moscow Region, Russia

3. Department of Physics and Astronomy, Texas A&M University, 77843 College Station TX, USA

a.b.fedotov@physics.msu.ru

One of the main streams of modern laser optics is shifting laser sources toward longer wavelengths. Motivation is dictated by numerous applications and long-standing challenges in strong-field physics, molecular spectroscopy and semiconductor electronics. Generation of few- and even single-cycle mid-infrared field waveforms has been demonstrated within a broad range of peak powers and central wavelengths [1,2]. Below-the-bandgap high-order harmonics generated (HHG) by ultrashort mid-infrared laser pulses are shown to be ideally suited to probe the nonlinearities of electron bands, enabling an all-optical mapping of the electron band structure in bulk solids [3-5].

In our present work, we used mid-IR ultrashort pulses tuning within the wavelength range of 5.0 to 6.7 μm to excite high order nonlinear processes in ZnSe thin plate (Fig.1a). High-order harmonics are generated through the interband polarization involving electron-hole recombination, as well as through the modulation of the intraband current due to the nonlinearity of electron bands. Under the conditions of pump radiation, a generation of below-the-bandgap high-order harmonics distinctly reflects an ultrafast dynamics of electron wave packets within the conduction and valence bands. We have demonstrated that these harmonics directly relate to the nonlinearities of electron bands, providing a tool for electron band structure analysis in bulk solids [6]. The intensities of individual optical harmonics as functions of the driver intensity were used to retrieve the energy dispersion profile for one of the electron conduction bands of ZnSe (Fig. 1b). For better understanding the physics behind we proposed the first-principle analysis and additional polarization sensitive experiments on HHG in monocrystal thin ZnSe plate. The work was supported by RFBR grants 16-29-11799 and 16-52-53129.

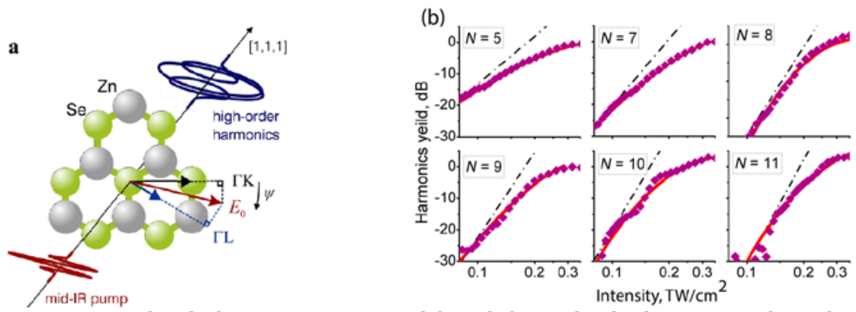

Fig. 1 (a) High-order harmonics are generated through the interband polarization involving electron-hole recombination in ZnSe as well as through the modulation of the intraband current due to the nonlinearity of electron bands. (b) The power of the Nth-order optical harmonic generated by a 85- fs driver pulse with a central wavelength of 5.0 μm in a 2-mm-thick ZnSe film as a function of the driver intensity I_0 (the experimental and the best fit data).

[1] E.A. Stepanov, A.A. Lanin, A.A. Voronin, A.B. Fedotov, A.M. Zheltikov, "Solid-State Source of Subcycle Pulses in the Midinfrared," Phys. Rev. Lett., 117, 043901 (2016).

[2] A.A. Lanin, A.A. Voronin, E.A. Stepanov, A.B. Fedotov, and A.M. Zheltikov, "Multioctave, 3–18 μm sub-two-cycle supercontinua from self-compressing, self-focusing soliton transients in a solid," Opt. Lett., 40, 974 (2015).

[3] S. Ghimire, A.D. DiChiara, E. Sistrunk, P. Agostini, L.F. DiMauro, and D.A. Reis, "Observation of high-order harmonic generation in a bulk crystal," Nature Phys., **7**, 138 (2011).

[4] G. Vampa, T.J. Hammong, N. Thiré, B.E Schmidt, F. Légaré, C.R. McDonald, T. Brabec, and P.B. Corkum, "Linking high harmonics from gases and solids," Nature, 25, 462 (2015).

[5] M. Hohenleutner, F. Langer, O. Schubert, M. Knorr, U. Huttner, S.W. Koch, M. Kira, and R. Huber, "Real-time observation of interfering crystal electrons in high-harmonic generation," Nature, 523, 572 (2015).

[6] A.A. Lanin, E.A.Stepanov, A.B. Fedotov, A.M. Zheltikov, Mapping the electron band structure by intraband high-harmonic generation in solids, Optica. 4(5), 516–519 (2017).

Anomalous Broadening and Shift of Emission Lines in Femtosecond Laser Induced Plasma Filament

A. Ilyin[1,2], S. Golik[1,2], K. Shmirko[1,2], A. Mayor[1,2], D. Proschenko[2,3]

1-Institute of Automation and Control Processes, FEB RAS, 5, Radio Street, Vladivostok, 690041 Russia
2-Far Eastern Federal University, 8, Sukhanova Street, Vladivostok, 690950 Russia
3-Maritime State University, 50a, Verkhneportovaya St., Vladivostok, Russia

kunashir@gmail.com

In this work, temporal behavior of emission lines width and shift is investigated with subnanosecond resolution. Filament was induced by femtosecond pulses (800 nm, 1 mJ, 48 fs, 1 kHz) in air. Emission of N I (3p $^4S^o$-3s ^4P) and O I (3p ^5P-3s $^5S^o$) lines were detected. Spectra are presented in our previous work [1]. Current investigations are continuation of that work. Fig. 1 shows temporal behavior of line shift and width.

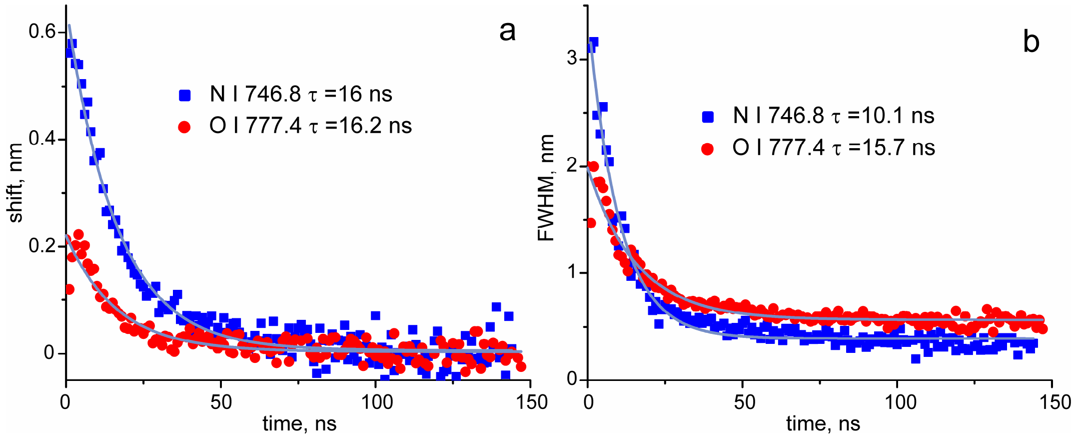

Fig. 1. Line shift and width. The solid cyan line is an approximation by exponential function with decay time τ.

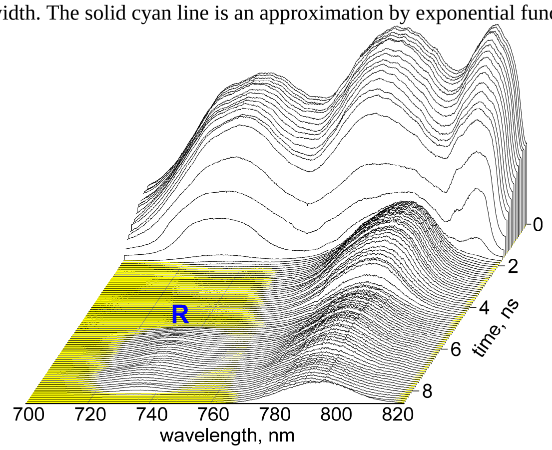

Fig. 2. Spectrum of the laser pulse passed through filament. “R” is Rabi sideband.

Briefly, main conclusions of our study can be described as follows. Filamentation of the tightly focused femtosecond laser pulse results in powerful emission of 1^+ system of N_2. Stimulated character of the emission is related to the Rabi sideband generation (Fig. 2) by electric field of amplified spontaneous emission from regenerative amplifier and post-pulses [2] on transition O I 3p ^5P-3s $^5S^o$. Strong laser field leads to break of 3p ^5P *LS* coupling. Nitrogen line shift and width are determined by joint action of electron impact shift and far-off resonance AC Stark effect. This study was supported by the Russian Science Foundation (project no. 14-50-00034).

[1] A. Ilyin, S. Golik, K. Shmirko, Absorption and emission characteristics of femtosecond laser plasma filaments in the air, Spectrochim. Acta Part B, 112, 16-22 (2015).
[2] T. Labutin, V. Lednev, A. Ilyin, A. Popov, Femtosecond laser-induced breakdown spectroscopy, J. Anal. At. Spectrom., 31, 90-118 (2016)

Novel array detectors for overcoming the dosimetry challenges of measuring laser accelerated short pulse charged particle beams – overview of the ELIDOSE project

R. A. Vasilache[1,*], M. A. Popovici[2,*], M. Straticiuc[3], D. C. Dumitras[4], C. E. Matei[4], M. Petrus[4]

1- Canberra Packard Ltd., 18 Clejani St., Bucharest 051036, Romania
2- Politechnica University of Bucharest, Faculty of Applied Sciences, Splaiul Independentei, nr. 313, BN-108, 060042, Bucharest, Romania
3- IFIN-HH, 30 Reactorului Str., P.O.BOX MG-6, 077125 Bucharest – Magurele, Romania
4- INFLPR, 409 Atomistilor Str., P.O.BOX MG-36, 077125 Bucharest – Magurele, Romania

Main author email address: r.vasilache@cpce.net, popovici@physics.pub.ro

In-beam dose measurements are paramount for any application seeking to harness the effects of the radiation beam, so all the future applications of the laser accelerated beams (as generated in the ELI and CETAL projects) will need such measurements. With a very long history in measuring doses in charged particle beams, the medical and industrial applications set up a number of methods that could be also used for the dosimetry of the beams generated by laser pulses. Dose measurements rely heavily on what is seen as the gold standard in dose measurement: the ion chambers. Ion chambers have both limitations and advantages, and in our case the disadvantage could be the large number of corrections to be applied in order to calculate a correct dose from the measured charge. The ELIDOSE project tries to address these problems by proposing an array detector that would allow the simultaneous measurement of the recombination and polarity corrections, and of the dose.

The detector consists of 4 identical ion chambers mounted together in a PMMA frame and the project will analyse its response to various charged particle beams and the reciprocal influences of the chambers on each other.

The ELIDOSE project is developed in the frame of the Romanian national program PN III 5/5.1/ELI-RO, project no. 20-ELI/2016, under the financial support of Institute for Atomic Physics - IFA.

High intensity x-ray laser - matter interactions

Byoung-ick Cho

Department of Physics and Photon Science, GIST, Korea
Center for Relativistic Laser Science, IBS, Korea

bicho@gist.ac.kr

The recent advent of x-ray free electron lasers (XFEL) has shed light on the new regime of intense light-matter interaction. The most brilliant x-ray source (ex. LCLS delivers up to 4 mJ of hard x-rays in 5-60 fs pulses) can be focused to less than 1 um. Thus, now light intensity of $10^{17} \sim 10^{20}$ W/cm^2, which had been accessible previously only with optical lasers, becomes available in hard x-ray regime. In this talk, I will present a series of work to investigate XFEL-matter, in particular aluminum, interactions at this regime. Detailed ionization processes, nonlinear absorption and emission of x-ray photons, and properties of highly excited state of matters and/or plasmas created throughout such interactions will be presented. I will also discuss similarities and differences with optical laser experiments, and possible research utilizing both optical and x-ray lasers.

This is work was supported by the Institute for Basic Science (IBS-R012-D1) and the National Research Foundation (NRF-2016R1A2B4009631 and NRF-2015R1A5A1009962).

Laser-induced damage thresholds of metals: Comparison of air and water environments

A.V. Bulgakov, S.V. Starinskiy, Yu.G. Shukhov

S.S. Kutateladze Institute of Thermophysics SB RAS, 1 Lavrentyev ave., 630090 Novosibirsk, Russia

E-mail: bulgakov@itp.nsc.ru

Pulsed laser ablation in liquids (PLAL) has proven to be an efficient and flexible technique for synthesis of colloidal nanoparticles of metals and alloys. However, controllable synthesis remains a challenge due to mainly poor knowledge of the PLAL process. The laser-induced damage threshold (DT) is an important parameter for process understanding which provides a well determined reference for modelling. The available data on DTs in liquids are rather contradictory. In most cases, higher DTs than the corresponding values in air are obtained and it is conventionally believed that the heat transfer to the liquid is an important involved process [1].

In this work, the nanosecond-laser-induced DTs of gold, silver and gold-silver alloys of various compositions in air and water have been measured for single-shot irradiation conditions. The experimental results are analysed theoretically by solving the heat flow equation for the samples irradiated in air and in water taking into account vapor nucleation at the solid-liquid interface. In order to investigate the water nucleation dynamics and to evaluate the water vaporization effect on the PLAL process, optical pump-probe measurements have been performed and the reflectance dynamics of the surfaces irradiated in air and water has been studied.

The DT fluences measured in air agree well with the calculated melting thresholds for all samples (Fig. 1) implying that metal melting is responsible for the observed surface damage. The DTs of the Au-Ag alloy systems are found to be substantially lower than those for pure metals, both in air and water, explained by lower thermal conductivities of the alloys (Fig. 1). For all the investigated metals, the thresholds obtained in water are considerably, by a factor of ~ 1.5, higher than the corresponding values for air. Based on the model calculations, it is demonstrated that this difference cannot be explained neither by the conductive heat transfer to water nor by the vapor pressure effect. Scattering of the incident laser light by the vapor-liquid interface is suggested as a possible mechanism responsible for the high damage thresholds in water. Another scattering mechanism, due to the critical opalescence in the superheated water, is also considered to occur at early laser-heating stages. Based on optical reflectance measurements performed in both air and water, direct evidence for the important role of the suggested scattering mechanisms under PLAL is obtained.

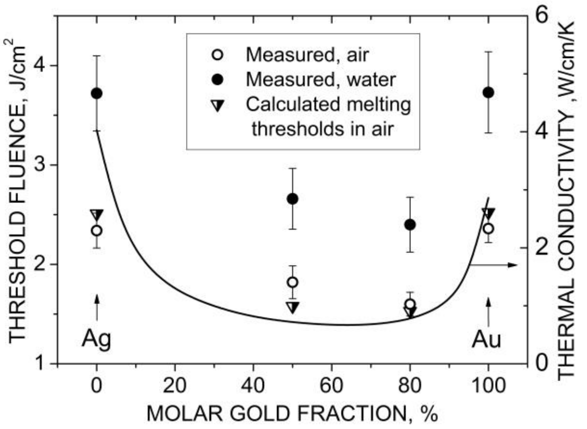

Fig. 1. The threshold peak fluences measured in air and water and calculated for air ambient conditions for the studied samples as a function of gold fraction in the sample. The line shows the data [2] for the thermal conductivity of the gold-silver alloy system.

This work was supported by the Russian Science Foundation (project No. 16-19-10506).

[1] S.V. Starinskiy, Yu.G. Shukhov, A.V. Bulgakov, Laser-induced damage thresholds of gold, silver and their alloys in air and water, Appl. Surf. Sci. **296**, 1765- 1774 (2017).

[2] C.Y. Ho, M.W. Ackerman, K.Y. Wu, S.G. Oh, T.N. Havill, Thermal conductivity of ten selected binary alloy systems, J. Phys. Chem. Ref. Data **7**, 959-1177 (1978).

High Power THz Radiation from Laser-Plasma Interaction

Min Sup Hur[1]

1- Department of Physics, UNIST, Ulsan 44910, Korea

mshur@unist.ac.kr

Identifying mechanisms of radiation emission has been a matter of great interest in science of diverse scales. While big and costly facilities based on relativistic electron beams have been successful in generating coherent, highly bright radiations, simultaneously, more compact and portable radiation sources are under intensive progress. As one of the novel radiation sources, plasma that is involved in laser-matter interactions are getting broad interest. The plasma has indeed numerous useful characteristics as an ideal radiation source; the plasma oscillation, which depends only on the plasma density, can be readily tuned, and monochromatic. Moreover, the plasma can sustain very strong electric field beyond GV/cm without material damage, thereby giving an opportunity for a very high field electromagnetic radiation. In space, most of the visible matter is in plasma state, the plasma has been considered as a source of diverse radiation bursts, e.g. solar radio bursts or fast radio burst (FRB).

While the plasma oscillation has numerous useful characteristics as a potential source of radiation, the coupling of the plasma oscillation and the electromagnetic radiation is not trivial. As the plasma oscillation usually occurs as a part of a traveling Langmuir wave, it cannot be directly converted to an electromagnetic radiation under homogeneous plasmas, since their dispersion curves do not cross each other for meaningful energy exchange. It is generally accepted that the plasma wave in inhomogeneous plasmas can emit the radiation, which is inevitably broadband due to the density variation. Whereas, there are many experimental observations of narrowband electromagnetic radiations at the plasma frequency [1,2], which is not well explained by the coupling mechanism in inhomogeneous plasmas. One common misleading argument regarding the non-radiating plasma oscillation is that the plasma oscillation is surrounded by the plasma itself in homogeneous plasma, which cuts off or absorb the radiation near the plasma frequency.

In this presentation, I show a very unique type of plasma oscillation; the oscillation of a local plasma dipole. This plasma dipole oscillation (PDO) is generated by two slightly detuned, colliding laser pulses in a locally uniform plasma. I show that actually the electromagnetic energy can be transported over a very long range of uniform density, which is much larger than the vacuum wavelength of the oscillation. The mechanism of the field transport is related with the recently-found diffusion-growing field at general cut-off condition [3]. One interesting result of the diffusion-growth analysis at cut-off is the frequency drift, from 1.5 times of the plasma frequency, asymptotically approaching to the plasma frequency. Appearance of the frequency drift while the source is oscillating with a monochromatic single frequency is a very interesting property of the field transport in homogeneous plasmas. When the plasma is properly tapered near the dipole oscillation, the radiation amplitude increases significantly, beyond several GV/m in a few or a few tens of THz spectral region, which is very useful for the currently popular FIR or MIR spectroscopy. This work has been collaborated by Prof. D.A. Jaroszynski and Dr. B. Ersfeld at University of Strathclyde, UK. This work was also funded by SRC project (Grant number NRF-2016R1A5A1013277).

[1] H. Hamster et al., Subpicosecond, Electromagnetic Pulses from Intense Laser-Plasma Interaction, Phys. Rev. Lett. vol. 71, pp. 2725-2728, (1993).
[2] U. Teubner et al., Observation of VUV radiation at wavelengths in the wp- and 2p-wavelength range emitted from femtosecond laser-plasmas, Opt. Comm. vol. 144, pp. 217-221, (1997).
[3] M.S. Hur et al., Increased Impedance near Cut-off in Plasma-like Media Leading to Emission of High-power, Narrow-bandwidth Radiation, Sci. Rep. 7:40034, (2017).

Investigating optical properties of metals and alloys in solid and liquid state with high temperature ellipsometry.

M. Schmid[1], S. Zehnder[1], P. Cam[1], P. Schwaller[1], B. Neuenschwander[1]

1- Bern University of Applied Science, Institute of Advances in Laser, Photonics and Surface Technology, Pestalozzistrasse 20, CH-3400 Burgdorf, Switzerland

marc.schmid@bfh.ch

One of the key factors for understanding laser material interaction is the complex refractive index. Especially in the case of laser processing of metals and alloys the energy is absorbed in the heated metal, in the case of cutting and welding it is actually absorbed in the liquid phase. Therefore knowing the temperature dependency of the complex refractive index of metal and alloys – not just in the solid but in the liquid phase as well - is crucial for simulating laser processing of these materials.
On the other hand calculating the temperature dependency of the complex refractive index still cannot be done satisfactory for metals and alloys of interest for the industry. In the past decades, since the beginning of laser material processing several approaches based on the well know Drude model have been discussed [1-4]. As we have reported in previous works [5-7] these models cannot be generalized and especially in the case of the liquid phase they are not reliable.
Additionally the above mentioned theoretical approaches as well as most of the experimental data published [8, 9] only deal with pure metals whereas for industrial applications alloys are of greater interest. But in what way the refractive index of alloys, including its temperature dependency can be deduced from their components is not fully understood. Therefore measuring the refractive index does not only help to verify the different theories of the optical properties of metals but increases the accuracy of simulating laser ablation processes of metals and especially alloys.
In this paper we will report on our own experimental data of measuring the complex refractive index of more metals like Al and Cu (see figure 1) as well as alloys like steel and how they fit with the different theoretical models. Further we will look into the relationship of the optical properties of alloy and their pure metal components.

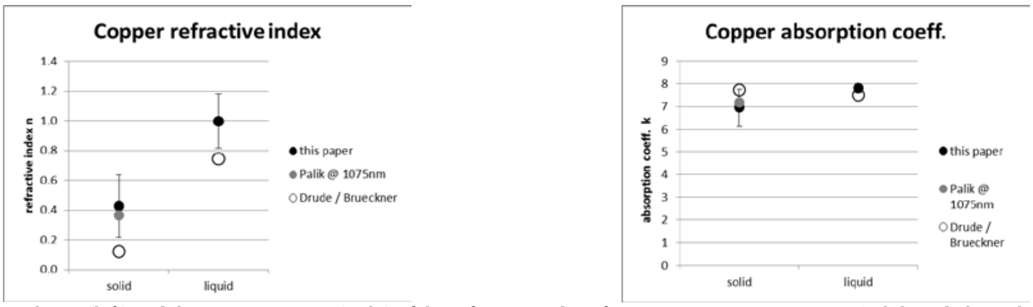

Figure 1: real part (left) and the imaginary part (right) of the refractive index of copper at room temperature (solid) and above the melting point (approx.. 1'500°K). The black dots are our measurements whereas the other are from calculations

[1] V. I. Konov, V. N. Tokarev, Temperature dependence of the absorptivity of aluminum targets at the 10.6µm wavelength, Sov. J. Quantum Electron., 13(2) Feb. (1983), 177-180.
[2] M. Brückner, J. H. Schäfer, J. Uhlenbusch, Ellipsometric Measurement of the Optical Constants of Solid and Molten Aluminum and Copper at λ=10.6µm, J. Appl. Phys. 66(3) Aug., 1326-1332 (1989)
[3] A. D. Rakic, A. B. Djurisic, J. M. Elazar, M. L. Majewski, Optical properties of metallic films for vertical-cavity optoelectronic devices, Appl. Opt. 37(22) August, 5271-5283(1998)
[4] H. Fujiwara, Spectroscopic Ellipsometry, John Wiley & Sons Ltd. (2009), ISBN 978-0-470-01608-4,
[5] M. Schmid, S. Zehnder, P. Schwaller, B. Neuenschwander, M. Held, U. Hunziker, J. Zürcher, Measuring optical properties on rough and liquid metal surfaces, ALT 12 Proceeding, TH-2A-1-IN (2012), DOI: 10.12684/alt.1.78
[6] M. Schmid, S. Zehnder, P. Schwaller, B. Neuenschwander, J. Zürcher, U. Hunziker, Measuring the complex refractive index of metals in the solid and liquid state and its influence on the laser machining, Photonic West 2013, Proc. 8607-53 (2013)
[7] P. Schwaller, S. Zehnder, M. Schmid, B. Neuenschwander, Measuring the dielectric constants of metals in the liquid state by high-temperature ellipsometry, Swiss Physical Society annual meeting 2014, poster 221 (2014)
[8]M. A: Ordal, R. J. Bell, R. W. Alexander, L.L. Long and M. R. Querry, "Optical properties of metals Al, Co, Cu, Fe, Pb, Ni, Pd, Pt, Ag, Ti and W in the infrared and far infrared", Applied Optics, Vol. 22, No. 7, pp. 1099-1119 (1983)
[9] E. T. Arakawa, T. Inagaki and M. W. Williams, "Optical properties of metals by spectroscopic ellipsometry" Surface Science, v 96, pp. 248-274 (1980)

The role and characteristics of intra-band absorption in ablation of optical crystals by ultra-short laser pulses: dominating mechanisms

Sergey Klimentov[1,2], Stéphane Guizard[3], Nikita Fedorov[4], Allan Bildé[3], Alexandros Mouskeftraras[2]

1 General Physics Institute of the Russian Academy of Sciences, Moscow, Russia
2 National Research Nuclear University "MEPhI", Moscow, Russia
3 Laboratoire des Solides Irradiés, Ecole Polytechnique, Palaiseau, France,
3 Centre Lasers Intenses et Applications, Université Bordeaux I, Talence, France

kliment@kapella.gpi.ru

Characterization of mechanisms of laser ablation and modification in optical crystals and glasses, ability to predict the optical strength of elements of laser systems is important for today laser technologies and for high power laser engineering. In many cases, namely intraband transient absorption plays the clue role in the chain of processes launched by exposure to intense pico- and femtosecond pulses involving complex and ultra-fast photo-electron kinetics resulting in optical breakdown. Experimental characterization of those calls for combination of adequate techniques in terms of time resolution, sensitivity to the created free electron concentrations, monitoring of their energy and ability to absorb the incident light.

We report the results of an extensive research aiming to determine dominating mechanisms of optical energy deposition and relaxation resulting in laser ablation, breakdown and modification in wide-band gap crystals (MgO, sapphire, quartz and alkali halides). *In situ* monitoring of electron concentrations and of the induced optical absorption near the damage threshold was performed via fast interferometry and transmission imaging techniques. Free electron energy was measured by means of photo-electron spectroscopy experiments. In some cases, the surface was exposed to a couple of laser pulses with variable time delay (UV and IR), to treat separately the stage of multiphoton transitions across the band-gap and the following heating of free electrons, keeping in mind possibility of impact ionization. Thresholds of ablation were measured under the same two-pulse irradiation conditions. This way, the complete set of direct measurements was performed for quantitative simultaneous characterization of all stages ending up at optical breakdown in these materials: the electron excitation, the induced absorption, relaxation and multiplication dynamics.

Intraband absorption and the following electron-phonon relaxation was shown to play the clue role in laser damage and ablation of optical crystals known for long lifetime of free electrons (sapphire, MgO). Multistage intraband absorption and transmission of energy to the lattice results finally in thermal instability. In spite of high energies acquired by the electrons (> 20-30 eV) no multiplication effect was observed here. Impact ionization was only revealed in crystals known for binding of free electrons within self-trapped excitons (SiO_2, NaCl).

COMBINED OPTOACOUSTIC AND NEAR-INFRARED OPTICAL TOMOGRAPHY FOR QUANTITATIVE BLOOD OXYGENATION MEASUREMENTS

L. Ulrich[1]. L. Ahnen[2], K.G. Held[1], M. Jaeger[1], S. Sanchez Majos[2], M. Wolf[2], H.G. Akarcay[1] and M. Frenz[1],

[1] Institute of Applied Physics, University of Bern, Sidlerstrasse 5, CH-3012 Bern, Switzerland, frenz@iap.unibe.ch

[2] Department of Neonatology, University Hospital Zurich, Frauenklinikstrasse 10, CH-8091 Zurich, Switzerland

Periventricular diffuse white matter injury (WMI) has become the dominant brain pathology and is the major reason for persisting spastic motor deficits and cognitive abnormalities in preterm infants. Cerebral ischemia is a key initiating factor for WMI. Such brain lesions are localized events and are characterized by drops in oxygen saturation levels (StO2). A safe bedside imaging method that can detect low local StO2 levels and monitor the effects of preventive and neuroprotective interventions and brain development is urgently needed. One promising approach is quantitative OA imaging, which exploits the wavelength-dependent optical absorption properties of oxy- and deoxyhemoglobin in the near-infrared range to provide quantitative estimates of their spatially varying concentration allowing to image local StO2 levels. Wavelength-dependent optical attenuation in the bulk tissue, however, causes spectral disruption and thus renders absolute oxygenation measurements challenging. We show that correction of the spectral disruption is possible without requiring a-priori knowledge of the tissue optical properties. For this purpose we used a combined, handheld optoacoustics/near-infrared optical tomography (NIROT) setup in reflection mode, which provides 3D reconstructions of the probed tissue volume's optical properties. To solve the NIROT inverse problem we used a modified NIRFAST software package. This Matlab-based code solves the light diffusion equation on a tetrahedral mesh by the finite element (FEM) approach, and relies on Tikhonov regularization to constrain the space of solutions. NIRFAST was also used to calculate the fluence distribution, based on the reconstructed optical properties. Our results indicate that the presented methods of combining OA imaging with NIROT is of benefit for achieving spectral correction in highly scattering non-homogeneous media.

1 Presentation Title

Listening to Light and Seeing Through:In Vivo Multiscale PhotoacousticImaging

2 Presenter

Chulhong Kim, Ph.D.

Director of Medical Device Innovation Center, Strong 20 Projects at POSTECH
Director of Bio Optics and Acoustics Laboratory
Associate Professor of Creative IT Engineering (Primary), Mechanical Engineering, Electrical Engineering, Interdisciplinary Bioscience and Bioengineering
Pohang University of Science and Technology (POSTECH)
208C5, POSTECH, Pohang, Gyeongbuk, Republic of Korea
Tel: +82-54-279-8805
Email: chulhong@postech.edu

3 ABSTRACT

High-resolution volumetric optical imaging modalities, such as confocal microscopy, two-photon microscopy, and optical coherence tomography, have become increasing important in biomedical imaging fields. However, due to strong light scattering, the penetration depths of these imaging modalities are limited to the optical transport mean free path (~1 mm) in biological tissues. Photoacoustic imaging, an emerging hybrid modalitythat can provide strong endogenous and exogenous optical absorption contrasts with high ultrasonic spatial resolution, has overcome the fundamental depth limitation while keeping the spatial resolution. The image resolution, as well as the maximum imaging depth, is scalable with ultrasonic frequency within the reach of diffuse photons. In biological tissues the imaging depth can be up to a few centimeters deep.

In this presentation, the following topics of photoacoustic imaging will be discussed; (1) multi-scale photoacoustic imaging systems (i.e., Photoacoustic Nanoscopy, Optical-Resolution Photoacoustic Microscopy, Fast 2-Axis MEMS based Optical-Resolution Photoacoustic Microscopy, Intravascular Photoacoustic/Ultrasound Catheter, Virtual Intraoperative Surgical Photoacoustic Microscopy, Acoustic-Resolution

Photoacoustic Microscopy, Clinical Photoacoustic/Ultrasound Scanner), (2) morphological, functional, and molecular photoacoustic imaging, (3)potential clinical applications, and (4) contrast agents for photoacoustic imaging.

4 BRIEF BIOGRAPHY

Dr. Chulhong Kim studied for his Ph.D. degree and postdoctoral training at Washington University in St. Louis, St. Louis, Missouri under the supervision of Dr. Lihong V. Wang, Gene K. Beare Distinguished Professor (main advisor; currently, Bren Professor of Medical Engineering and Electrical Engineering at California Institute of Technology), Dr. Younan Xia, and Dr. Samuel Achilefu. He is currently an associate professor ofCreative IT Engineering, Mechanical Engineering, Electrical Engineering, and Interdisciplinary Bioscience and Bioengineeringat Pohang University of Science and Technology (***POSTECH, #1 in the world: The 100/50 Young University rankings for three consecutive years 2012-2014, #3in the world: The world's best small universities 2017***) in Republic of Korea. Before he joined the department, he was an assistant professor of Biomedical Engineering at the University at Buffalo, the State University of New York from Aug 2010 to Jan 2013.He was the recipient of **the 2017 IEEE Engineering Medicine and Biology Society (EMBS) Academic Early Career Achievement Award** "Contributions to multi-scale photoacoustic imaging from super-resolution atomic force photoactivated microscopy for research to systems for clinical applications." He has published **95 peer-reviewed articles** in journals including***Nature Nanotechnology, Nature Materials, Chemical Reviews, Light Science & Applications,*** *Nano Letters, AngewandtChemie, Journal of American Chemical Society, ACSNano, Radiology, Biomaterials,Scientific Reports, Optics Letters, Applied Physics Letters,* *Journal of Biomedical Optics, etc*. **His Google Scholar h-index and citations have reached 37 and over 5,500, respectively.**His group's works have been selected for **the 2016 and 2017 Seno Medical Best Paper Award Finalists** in Photons Plus Ultrasound Conference (the largest conference in the field), Photonics West, SPIE.He also co-authored sixbook chapters.He has currently served as an **Editorial Board Member of Scientific Reports (Nature Publishing Group)**,Photoacoustics Journal, and American Journal of Nuclear Medicine and Molecular Imaging, and a Guest Editor of Journal of Biomedical Optics, BioMed Research International, and IEEE Pulse Magazine.He has served as an Organizing Committee for the conference on "Photons plus Ultrasound: Imaging and Sensing" and "High-Speed Biomedical Imaging and Spectroscopy: Toward Big Data Instrumentation and Management"held annually under auspices of SPIE (Photonics West) and as a Theme Co-Chair for the 39th Annual International Conference of the IEEE EMBS. He has served as a journal reviewer >80, including for*Nature Photonics, Nature Communication, Light Science & Applications, Nano Letters, ACS Nano, Scientific Reports, Optics Letters, Optics Express, Journal of Biomedical Optics, IEEE Transactions, and etc*. He has delivered a numerous invited presentations (>120) in technical conferences and seminars in universities. His research interests are the development of novel biomedical imaging techniques including photoacoustic tomography, ultrasound-modulated optical tomography, fluorescence imaging, ultrasound imaging, and laser speckle contrast imaging. Particularly, his lab developed photoacoustic gastro-intestinal tract imaging using organic agents, photoacoustic cystography, **clinical photoacoustic/ultrasound imaging scanner (clinically translated and commercialized with Alpinion Medical)**, **fast optical-resolution photoacoustic microscopy based on a 2-axis water-proof MEMS scanner (licensed to MGB;spin-off company, PAMsTECH)**, virtual intraoperative photoacoustic surgical microscopy, raster scanning based photoacoustic whole body imaging of small animals, combined photoacoustic and optical coherence tomography using a single pulsed broadband laser source, acoustic-radiation force induced ultrasound-modulated optical tomography, etc.

Principal Spectrum Decomposition in Photoacoustic Imaging

B. Wang, C. Ma

Department of Electronic Engineering, Tsinghua University, Beijing 100084, China

Main author email address: cheng_ma@tsinghua.edu.cn

In photoacoustic imaging (PAI), quantitative assessment of analyte concentration, for example, saturation of oxygen, is hindered by wavelength-dependent light attenuation in biological tissues. In essence, due to the complicated spatial distributions of scatterers and absorbers, light fluence in tissue varies with both depth and wavelength. Despite the progress in fully characterizing tissue optical property, the approach is till premature for *in vivo* applications [1]. Tzoumas *et al*. argued and demonstrated that the optical fluence in deep tissue could be decomposed into a few eigenspectra [2], potentially paving the way for quantitative PAI. Unfortunately, the originally devised decomposition was performed on a more or less empirical basis, lacking a theoretical framework and thus suffering from limited physical insight. Here, we provide a theory to support the eigenspectra decomposition method. Our theory not only attains solid and deep physical insights, but also leads to extensions of the original approach with improved accuracy and working depth.

[1] B. Cox, J. G. Laufer, S. R. Arridge, P. C. Beard, Quantitative spectroscopic photoacoustic imaging: a review, J. Biomed. Opt., vol. 17, pp. 61202, (2012).
[2] S. Tzoumas, A. Nunes, I. Olefir, S. Stangl, P. Symvoulidis, S. Glasl, C. Bayer, G. Multhoff, M. Ntziachristos, Eigenspectra optoacoustic tomography achieves quantitative blood oxygenation imaging deep in tissues, Nat. Commun., vol. 7, (2016)

Molecular photoacoustic imaging

Changho Lee

Department of NuclearMedicine, Chonnam National UniversityMedicalSchool& Hwasun Hospital, Gwangju,Republic of Korea

ch31037@jnu.ac.kr

Over the past few decades, molecular imaging has played a critical role as a diagnostic tool for early cancer detection, and its intensive researches haveled to high patient survival rate and excellent treatment outcomes.However, tissue biopsy, which is currently considered a clinical standard, is invasive and has a high false negative rate due to initial sampling errors.Most cancers are developed with molecular and structural changes before being metastasized for many years.High-resolution molecular imaging technology, which can provide non-invasive accurate in vivo diagnostic imaging information, can greatly enhance the clinical ability tocapture early-stage cancers.Photoacoustic imaging (PAI) is considered a promising hybrid imaging platform capable of visualizing cross-sectional images of tissue microstructures in vivo in real time without tissue removal. PAI imaging contrast is based on photoacoustic effect that produce acoustic signals through light absorption and thermal conversion [1].PA images are generated by illuminating nanosecond laser pulses on living tissues for mapping of the initial sound pressure distribution or absorbed energy density.With this technique, the concentration of a specific contrast agent that can adhere to a pathological site can be quantified.Therefore, there have been various studies to increase the sensitivity of PAI contrast agents and to increase the specificity of molecular PAI images [2].This presentation introduces various PAI contrast agents and their applications.

This work was supported by the National Research Foundation of Korea (NRF) grant funded by the Korea government (MSIP; Ministry of Science, ICT & Future Planning) (No. 2017R1C1B5018181)

[1] C. Kim, C. Favazza, L. V. Wang, “In vivo photoacoustictomography of chemicals: high-resolutionfunctional and molecularopticalimaging at new depths”, Chemical Reviews 110, 2756-2782 (2010).
[2] J. Kim, S. Park, C. Lee, J. Y. Kim, C. Kim, “Organic Nanostructures for Photoacoustic Imaging”, ChemNanoMat, 2, 156-166 (2016).

Optical multiplexing of off-axis digital holograms and its applications

Natan T. Shaked

Department of Biomedical Engineering, Tel Aviv University, Israel
nshaked@tau.ac.il

Off-axis digital holography is a quantitative method for capturing an interference pattern between the light interacting with a sample and a reference beam, and processing it into the sample complex wave front. This wave front contains both the amplitude modulation and the quantitative phase delays induced by the sample. Off-axis holography allows reconstruction from a single exposure, by inducing a small angle between the sample and reference beams. This is true since in the spatial frequency domain, there is a full separation between the dc order and each of the cross-correlation orders, each of which contains the complex wave front of the sample. This separation is typically across a single axis, which allows compressing more information on the other axes as well, enabling optical multiplexing of several holograms within a single multiplexed hologram and full reconstruction of the data. For example, we have lately developed a new approach for extending the recorded field of view in off-axis holography without loss in the imaging parameters, such as magnification or spatial resolution and without reducing the temporal resolution (since only a single exposure is needed). This approach, called interferometry with doubled-imaging area (IDIA) [1], is able to optically compress two off-axis interferometric fields of view taken from different areas on the sample onto a single camera sensor. This is done by optically multiplexing two orthogonally rotated off-axis holograms on the same camera field of view. Depending on the optical alignment, these fields of view can be continuous or located in far places on the sample. We implemented this technique using a compact interferometric module located at the output of the imaging system, just in front of the digital camera. These approaches can be further improved to multiplexing more than two fields of view, or other types of data, such as images of different wavelengths, polarizations, etc. Various experimental results and applications will be reviewed in this lecture.

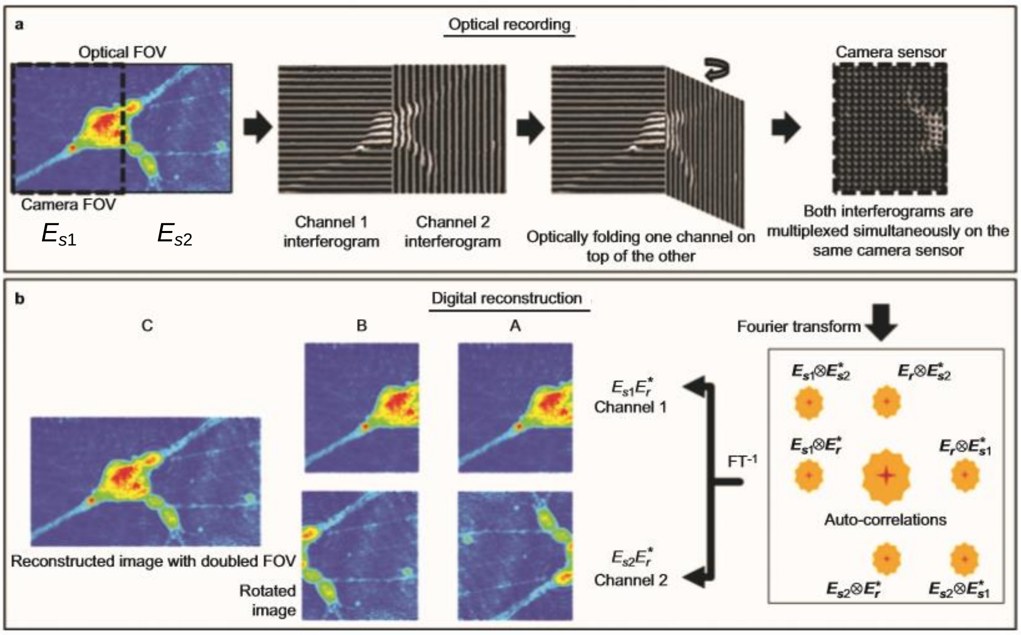

Figure 1. The IDIA principle (from Ref. [1]). (a) Optical recording: dual-image off-axis holographic multiplexing implemented optically. The digital camera records the multiplexed hologram in a single exposure. (b) Digital reconstruction: the doubled-field of view quantitative phase profile of the sample, extracted digitally using spatial filtering, applied twice. The bolded *E*s represent the spatial Fourier transforms of the coinciding *E*s, which represent the complex wave fronts of the sample and reference beams, and the sign between two *E*s represents spatial convolution. FOV, field of view; FT^{-1}, inverse Fourier transform.

[1] P. Girshovitz and N. T. Shaked, "Doubling the field of view in off-axis low-coherence interferometric imaging," *Nature – Light: Science and Applications* (*Nature LSA*), Vol. 3, e151, pp. 1-9, 2014.

Comprehensive label-free intracoronary optical imaging

H. Yoo[1]

1- Department of Biomedical Engineering, Hanyang University, Seoul, Korea

hyoo@hanyang.ac.kr

Intravascular optical coherence tomography (IV-OCT) is an imaging method that can visualize three-dimensional microstructure of arterial walls [1]. With unprecedented high-resolution, about 10 μm, IV-OCT enables clinicians to identify key features associated with high-risk lesions within the blood vessels. While grayscale IV-OCT allows a clear visualization of high-risk lesions, it can not provide comprehensive information on atherosclerotic plaques, such as biochemical compositiosn or inflammation [2]. Thus, we have developed a multimodal intra-vascular optical imaging technology that combines OCT with multichannel fluorescence lifetime imaging (FLIM). By providing multichannel fluorescence intensity as well as lifetime of the autofluorescence of the tissue, the multichannel FLIM provides quantitative analysis of the biochemical composition of the plaque [3]. In particular, the FLIM signal can be obtained from the autofluorescence of the tissue itself, thus no exogenous contrast agent is needed to acquire additional information. By providing comprehensive information of the arteries, these new imaging technologies can provide new opportunities to investigate vascular biology and stent pathobiology and to idetnfiy high-risk plaques.

[1] G. Tearney, et al., Three-Dimensional Coronary Artery Microscopy by Intracoronary Optical Frequency Domain Imaging, J. Am. Coll. Cardiol. Img., vol.1, pp. 752-761, (2008).
[2] S. Kim, et al., Intracoronary dual-modal optical coherence tomography-near-infrared fluorescence structural-molecular imaging with a clinical dose of indocyanine green for the assessment of high-risk plaques and stent-associated inflammation in a beating coronary artery, European Heart Journal, vol. 37, pp. 2833-2844, (2016).
[3] H. Fatakdawala, Fluorescence Lifetime Imaging Combined with Conventional Intravascular Ultrasound for Enhanced Assessment of Atherosclerotic Plaques: an Ex Vivo Study in Human Coronary Artereis, J. of Cardiovasc. Trans. Res. Vol. 8, pp. 253-263, (2015).

Intraoperative optical coherence tomography probe with augmented reality for surgical applications

Muhammad Faizan Shirazi and Jeehyun Kim

School of Electronics Engineering, College of IT Engineering, Kyungpook National University, 80 Daehak-ro, Buk-gu, Daegu 41566, Korea

E-mail: jeehk@knu.ac.kr

An intraoperative surgical microscope is widely used tool for ophthalmic surgery. The surgical microscope can provide the surface image of specimen but, the sub surface information is unable to achieve. Since, optical coherence tomography can give the sub surface information of specimen. Therefore, intraoperative probe is developed with augmented reality using spectral-domain optical coherence tomography (SD-OCT) for different surgical applications [1-3]. In this system, a common optical path is utilized for surgical microscope and SD-OCT setup. A projector is employed for augmented reality to project the cross-sectional OCT image on the sample image such that the simultaneous visualization of surgical microscope and OCT images is achieved in real-time. The incorporation of virtual reality enables the surgeon to visualize the real time sub surface information of specimen during surgery to focus on the operation without distraction to view OCT images on other display. Additionally, the depth perception during surgery is helpful to avoid any damage to the biological specimen. The real-time cross-sectional and volumetric images of different samples such as in vitro porcine eye, in vivo rabbit eye, mice and guinea pig inner and middle ear, were acquired to demonstrate the capability of the proposed probe for surgical procedures. A graphics processing unit (GPU) based fast signal processing is also incorporated to increase the frame rate and to minimize motion artifacts during surgery [4,5]. As a result, the efficient utilization of surgical probe is possible for real-time surgical operations. This system can reduce the surgical accidents and improve the surgical operating condition.

Reference

[1] Lee, C.; Kim, K.; Han, S.; Kim, S.; Lee, J.H.; Kim, H.k.; Kim, C.; Jung, W.; Kim, J. Stimulated penetrating keratoplasty using real-time virtual intraoperative surgical optical coherence tomography. Journal of Biomedical Optics 2014, 19, 030502-030502.

[2] Boppart, S.; Brezinski, M.; Pitris, C; Fujimoto, J.; Optical coherence tomography for neurosurgical imaging of human intracortical melanoma. Neurosurgery. 1998;43(4):834-841.

[3] Hahn, P.; Migacz, J.; O'Connell, R.; Maldonado, R.; Izatt, J.; & Toth, A.; The use of optical coherence tomography in intraoperative ophthalmic imaging. Ophthalmic Surgery, Lasers and Imaging Retina 2011, 42(4), S85-S94.

[4] Jeong, H.; Cho, N.H.; Jung, U.; Lee, C.; Kim, J.-Y.; Kim, J. Ultra-fast displaying spectral domain optical doppler tomography system using a graphics processing unit. Sensors 2012, 12, 6920.

[5] Shirazi, M.; Jeon, M.; and Kim, J.; "Structural Analysis of Polymer Composites Using Spectral Domain Optical Coherence Tomography," Sensors, vol. 17, p. 1155, 2017.

Subtractive and Additive Processing of Biocompatible Materials using Femtosecond Laser

Mitsuhiro Terakawa[1, 2], **Akimichi Shibata**[2], **Manan Machida**[2], **Yasutaka Nakajima**[2]

1- Department of Electronics and Electrical Engineering, Keio University
3-14-1 Hiyoshi, Kohoku-ku, Yokohama, Kanagawa, Japan 223-8522

2- School of Integrated Design Engineering, Keio University
3-14-1 Hiyoshi, Kohoku-ku, Yokohama, Kanagawa, Japan 223-8522

terakawa@elec.keio.ac.jp

Lasers have been widely used for processing of biomaterials because of their abilities to process complex-shaped surfaces even after molding without using a toxic chemical component. With bio- and soft materials, precise structures are able to be fabricated without significant thermal modification by using femtosecond laser. Tissue scaffolds, for example, require microprocessing technology for forming tailored structures depending on its applications. Sub-micro- or nanoprocessing of a material surface is effective for controlling cell adhesion and growth as well. In this presentation, our study on laser processing of biocompatible materials, in particular biodegradable polymers [1], will be described in detail. Biodegradable polymers are attracting considerable interest in the field of biomedicine including tissue engineering. Biodegradation is a key property for biodegradable polymer-based tissue implants because it can provide suitable space for cell growth as well as tailored sustainability depending on their role. We demonstrated the change in biodegradation rate of the polymer following irradiation with femtosecond laser pulses at different wavelengths [2]. Microscopic observation as well as water absorption and mass change measurement revealed that the biodegradation of the biodegradable polymer varied significantly depending on the laser wavelength. Significant acceleration of the degradation rate was observed upon 400-nm laser irradiation, whereas 800-nm laser irradiation did not induce a comparable degree of change. We also compared the change in biodegradability by deep-ultraviolet laser irradiation with different pulse durations [3]. Femtosecond laser irradiation significantly accelerated the degradation rate of the biodegradable polymer films, whereas the nanosecond laser irradiation did not induce such a significant acceleration. By considering XPS, FTIR, and GPC results, the significant acceleration of the biodegradation could be attributed to the decrease in molecular weight induced by the chemical bond dissociation. Our study not only shows the potential of femtosecond laser processing to control the degradation and sustainability of a scaffold structure following its fabrication but also provides scientific background for study on laser-based drug release [4]. Recent study on additive processing of biocompatible materials by using femtosecond laser [5] will also be described in the presentation.

[1] S. Yada, M. Terakawa, Optics Express, vol. 23, pp. 5694-5703, (2015).
[2] A. Shibata, M. Machida, N. Kondo, M. Terakawa, Applied Physics A, vol. 123, pp. 438/1-7, (2017).
[3] A. Shibata, S. Yada, M. Terakawa, Scientific Reports, vol. 6, pp. 27884/1-9, (2016).
[4] K. Ariyasu, A. Ishii, T. Umemoto, M. Terakawa, Journal of Biomedical Optics, vol. 21, pp. 085003/1-7, (2016).
[5] M. Terakawa, M. L. Torres-Mapa, A. Takami, D. Heinemann, N. N. Nedyalkov, Y. Nakajima, A. Hördt, T. Ripken, A. Heisterkamp, Optics Letters, vol. 41, pp. 1392-1395, (2016).

Highly Efficient Top Emission OLED Devices for Display Application

Mi Jin Park and Jang Hyuk Kwon*

Department of Information Display, Kyung Hee University, Hoegi-dong, Dongdaemoon-gu, Seoul 130-701, Republic of Korea

Main author email address: jhkwon@khu.ac.kr

Top-emitting organic light emitting diodes (TEOLEDs) have been utilized for active matrix display productions. A strong reflective anode and a semi-transparent cathode of TEOLEDs generate strong micro-cavity effect. This effect could generate good color purity of organic emitters by changing the broad spectral width. Hence, TEOLEDs could satisfy national television system committee color coordinates. In addition, such strong micro-cavity effect amplifies the light out-coupling efficiency toward the surface normal. It is very useful to apply these top emission performances for display applications. On the other hands, TEOLEDs with micro-cavity effect show the sensitive spectral peak (or color coordinates) variation and big efficiency variation along the emissive layer (EML) position and the cavity length. In our previous research, the structure design method with the calculation of EML positions and their expected performances has been presented [1]. We also reported about the highly efficient TEOLEDs for display applications by our optical design method [2,3].

In this work, we describe the optical property of TEOLEDs optimized by our optical design method. Figure 1(a) shows narrow spectra of optimized red, green and blue TEOLEDs compared with the broad spectra of bottom emissive OLEDs (BEOLEDs). The full width half mediums are 30 nm, 32 nm and 23 nm are observed, which is the half values of BEOLEDs. With these narrow spectral width, the CIE 1931 color coordinates are (0.65, 0.35), (0.21, 0.73) and (0.14, 0.08) for red, green and blue, respectively. Fabricated TEOLEDs show narrower emission pattern along the viewing angle to 90 degree than Lambertian emission pattern as shown in Figure 1 (b). It indicates that the strong micro-cavity effect amplifies the emitted light within cavity space toward surface normal. Detailed analysis about the fabricated TEOLEDs with strong micro-cavity effect will be discussed in the presentation.

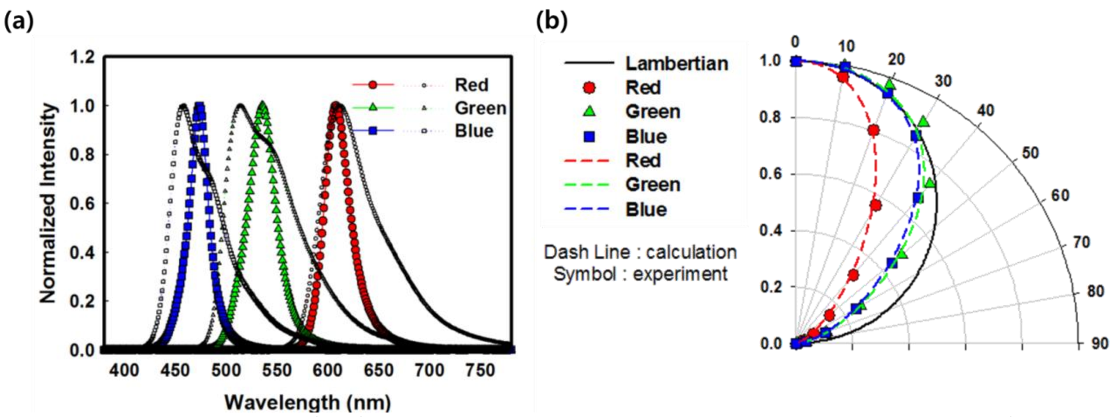

Figure 1. (a) Narrow emission spectra of the fabricated red, green and blue TEOLEDs compared with the broad spectra of bottom emitting OLEDs. (b) Emission pattern of TEOLEDs.

[1] M. J. Park, G. H. Kim, H. W. Bae, J. H. Kong and J. H. Kwon, SID Symposium Digest of Technical Papers 45, 648 (2014).
[2] M. J. Park, G. H. Kim, Y. H. Son, H. W. Bae, J. H. Kong and J. H. Kwon, Optics Express 22, 19919 (2014).
[3] M. J. Park, Y. H. Son, G. H. Kim, R. Lampande, H. W. Bae, R. Pode, Y. K. Lee, W. J. Song, J. H. Kwon, Organic Electronics 26, 458–463 (2015).

Recent researches on three-dimensional screen for projection-type three-dimensional display

Sung-Wook Min and Young Min Kim

Department of Information Display, Kyung Hee University, 26, Kyungheedae-ro, Dongdaemun-gu, Seoul, 02447, South Korea
mins@khu.ac.kr

The projection-type three-dimensional (3D) display can be one of the efficient ways to realize large-sized 3D displays. Basically, this system could be comprised of a compact 3D image device, which generates 3D source images, and a projection lens, which projects and magnifies the images onto a screen. Typical projection system necessarily uses a diffusing screen to make viewers see the entire area of images. This is due to the small exit pupil of the projection lens which makes viewers unable to see the entire images through the pupil at once. Unfortunately, this general diffusing screen cannot be used in the 3D projection system, because it causes the off-screen image blurs and loss of 3D parallax. The diffusion occurs randomly in almost all directions, which leads to loss of directional information of light rays. Consequently, it can be said that the projection-type 3D display requires a special screen to avoid these 3D information losses.

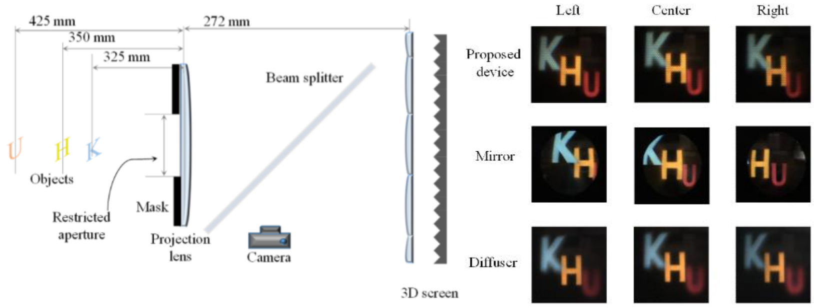

Fig. 1. Experiment and its results of three-dimensional screen

We proposed one special equipment before, which is named 3D screen [1]. The 3D screen is composed of a lens array and a retroreflector film. It has some working ranges of making off-screen images to be relatively well focused, which leads to maintain the parallax of 3D images as well. As shown in Fig. 1, when three characters are projected back and forth on the screen at different depth planes from each other, it is shown that the screen preserves the 3D scenes properly.

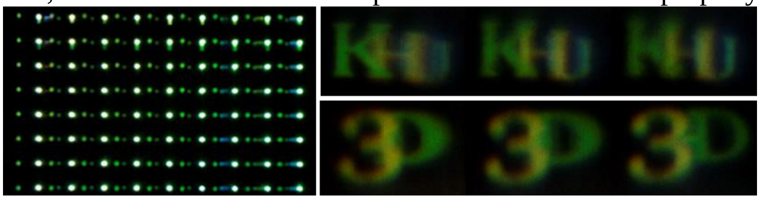

Fig. 2. Experimental results of projection-type integral imaging system using three-dimensional screen

A light field projection system was also reported as an example of the use of 3D screen, which is the projection-type integral imaging system using the 3D screen [2]. The elemental images are directly projected onto a lens array from the projector, and then the light beam from each lens goes towards a 3D screen. The experimental results show that 3D information is properly maintained by means of the screen, while only multiple exit pupil array can be observed without screen. As a results, we can find that the potential of the 3D screen as a promising device to realize large-sized 3D displays.

This work was supported by the National Research Foundation of Korea(NRF) Grant funded by the Korean Government(MSIP) (No.2011-0030079)

[1] B. Song, S. Choi, H. Sung, and S.-W. Min, "Reflection-type three-dimensional screen using retroreflector," J. Opt. Soc. Korea 18, 225-229 (2014).
[2] Y. M. Kim, B. Song, and S.-W. Min, "Projection-type integral imaging system using a three-dimensional screen composed of a lens array and a retroreflector film," Appl. Opt. 56, F105-F111 (2017).

Multi-Modal Aerial Information Display for Next Generation Digital Signage

H. Yamamoto, T. Okamoto, R. Kujime

Dept. of Optical Engineering, Utsunomiya University and JST, ACCEL,
Yoto 7-1-2 Utsunomiya City, Tochigi 321-0904, Japan

hirotsugu@yamamotolab.science

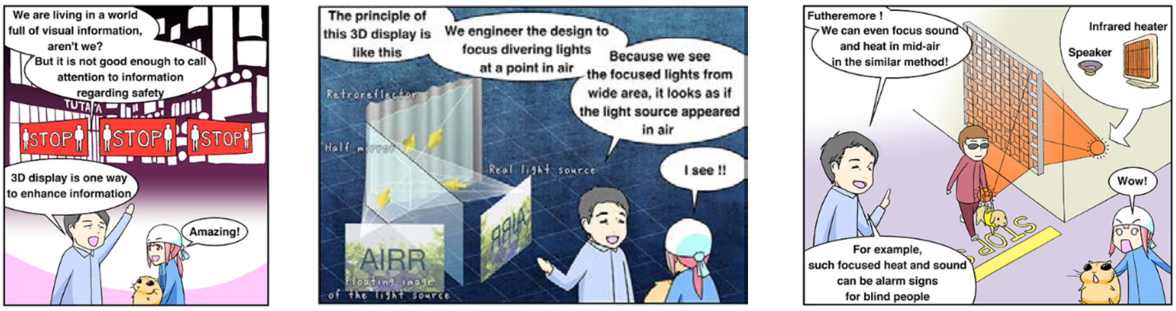

(a) (b) (c)

Figure 1. (a) Issues for next-generation digital signage. (b) Aerial imaging by retro-reflection (AIRR) to form a large aerial signage with a wide viewing angle by use of mass-productive optical components. (c) Aerial heater and aerial speaker formed by use of crossed-mirror array (CMA).

Digital signage is a new field of signage that shows information suitable for the time, the place, and the occasion. After the development of the GaN light-emitting diode (LED), large LED screens have been installed instead of outdoor large static advertisements. Moreover, state-of-art large flat panel displays changes indoor signage. Thus, digital signage becomes pervasive in our life, as illustrated in Fig. 1 (a). Furthermore, measurements of audiences have been partially performed to evaluate the impact of a digital signage. Thus, the digital signage in the next generation is expected to attract more attention of its audience as long as possible.

In order attract people's attention, showing 3D information is one of the promising techniques. For use of the public signage, such as traffic signs and exit signs, it is important to show information at the exactly right position with a wide viewing angle. In order to form a floating LED sign with a wide viewing angle, shown in Fig. 1 (b), we have realized aerial imaging by retro-reflection (AIRR) [1]. In combination of polarization-processing display that composed of stacked liquid-crystal display (LCD) panels, multi-view aerial display and secure aerial display have been realized [2]. These multiple expressions increase sensations on aerial displays.

In order to enhance sensations on digital signage, a thermal aerial display has been realized by use of a crossed-mirror array (CMA) [3]. The CMA is composed of hollow apertures and can converge infrared radiations of a heat source as well as a light source [4]. Furthermore, a scaled-up CMA can converge sound waves and forms an aerial speaker [5]. In order to increase efficiency of heating, we have specially designed and fabricated a double-layered arrays of rectangular mirrors (WARM) and combined WARM with AIRR [6]. These multi-modal aerial display techniques are expected not only to attract people's attention, as shown in Fig. 1 (c), but also to provide signs for blind people.

A part of this work has been supported by JST, JPMJAC1601.

[1] H. Yamamoto, Y. Tomiyama, and S. Suyama, Floating aerial LED signage based on aerial imaging by retro-reflection (AIRR), Optics Express, vol. 22, pp. 26919-26924 (2014).
[2] K. Uchida, S. Ito, and H. Yamamoto, Multi-Functional Aerial Display by Use of Polarization-Processing Display, Optical Review, vol. 24, pp. 72-79 (2017).
[3] R. Kujime, S. Suyama, and H. Yamamoto, Thermal and visual 3D display by use of crossed-mirror array, Proc. IDW, vol. 19, pp. 1243-1246 (2012).
[4] R. Kujime, S. Suyama, and H. Yamamoto, Different aerial image formation into two directions by crossed-mirror array, Optical Review, vol. 22, pp. 862-867 (2015).
[5] R. Kujime, K. Miyamoto, S. Suyama, and H. Yamamoto, Crossed-Mirror Array (CMA) converges sound wave in 3D space, Proc. IDW, vol. 21, pp. 906-909 (2014).
[6] T. Okamoto, S. Ito, K. Onuki, S. Onose, T. Itoigawa, and H. Yamamoto, Visual and Thermal Floating Display with AIRR and WARM, Proc. IDW, vol. 23, pp. 823-826 (2016).

Ultra Wide Vision for Emmersive Live Broadcasting

Jeongil Seo, Joo Myoung Seok, Yongju Cho, Hyun Cheol Kim and Sangwoo Ahn

Electrics and Telecommunications Research Institute (ETRI), 218 Gajeong-ro, Yuseong-gu, Daejeon, Korea

Author email: seoji@etri.re.kr

Abstract

Introduction of lager TVs and 3D service lead user to experience realistic media in broadcasting and telecommunications environment and increase user's desire for more realistic and higher quality of media. In keeping with this trend, we are developing UWV technology. The characteristics of UWV, such as wide field of view (more than 120 degree) and ultra high resolution, provide different interest and sense of reality from 3D and UHD; that is, rendering immersive viewing. The UWV technology aims to realize "The Ultra-Realistic ICT Olympics" through the high immersive UWV live broadcast service at the 2018 Pyeongchang Winter Olympics. It can satisfy the user's demand on realistic broadcasting and result in boom in future media market.

In this talk, the overview of UWV live broadcasting system and the plan for upcoming Olympic Game event will be presented.

Switchable micro-lens array for 3D displays and 3D imaging

M.-K. Park, K.-I. Joo, H. Park, S.-D. Lee, H.-R. Kim*

School of Electronics Engineering, Kyungpook National University, 80 Daehak-ro Buk-gu, Daegu 41566, South Korea

**Main author email address:rineey@knu.ac.kr*

Switchable micro-lens arrays have received much attention recently in various three-dimentional (3D) applications such as auto-stereoscopic 3D displays, integral photography, holography, and light-field cameras [1-3]. Most of these applications require micro-lens arrays with short focal lengths, small pitches, and switching capabilities to improve viewing conditions and image qualities in 3D application. In auto-stereoscopic 3D displays and integral photography, for example, the resolution of 3D image is inevitably lowered compared to a conventional two-dimensional (2D) display. The resolution of 3D image is determined by several system parameters such as the pitch of elemental lens and the pixel size of the display panel. To increase the resolution of 3D image on the same display panel, the pitch of the elemental lens should be reduced. However, as the pitch of the elemental micro-lens is reduced, the angular resolution of the 3D display is decreased. In order to overcome this trade-off relationship, a movable micro-lens array is required [4].

For years, several types of liquid crystal (LC) lens have been introduced to obtain electrically switchable micro-lens array. One method of fabricating the LC lens array is to make a gradient refractive index (GRIN) lens profile in which the LC director is controlled by fringe-fields generated by finger-patterned electrodes. This technique has an advangate of compatibility with the conventional LC display process. However, in order to get a short focal length, the cell-gap of the LC device must be enlarged, there by increasing the driving voltage and slowing the response time. In addition, it is very difficult to realize an ideal lens profile, and the fill-factor is reduced due to the dead-zone formed on the patterned electrode, which makes it difficult to apply to a high-resolution 3D applications.

In this paper, we demonstrate a well-aligned polarization-dependent reactive mesogen (RM) lens array by using top-down and conventional bottom-up alignment methods[5]. The fabricated RM lens array had a high fill factor, a short focal length, and a small *f*-number compared to those of the previous GRIN LC lens. The lens function can be switched according to the polarization direction of the incident light, which can be electrically controlled by a polarization switching layer. Using the polarization-dependent RM lens array with 1D or 2D micro-lens array type, we made 2D/3D switchable 3D display and imaging systems, which are shown in Fig. 1. Additionally, using a virtually moving micro-lens array with a stacked structure of the RM lens arrays, we broke the trade-off relationship between the 3D image resolution and the angular resolution of the 3D display.

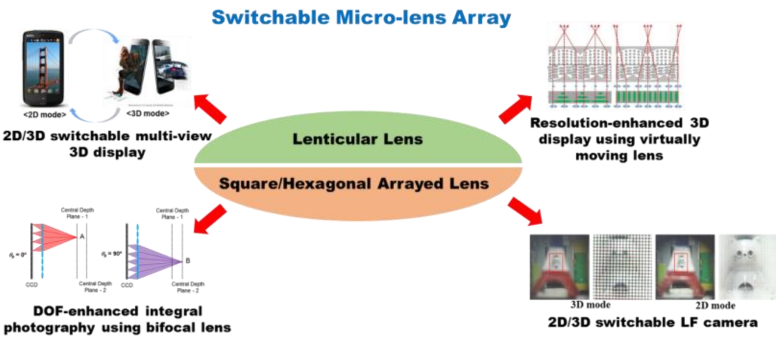

Fig. 1. Applications of the switchable micro-lens array for 3D display and imaging system.

[1] Y.-P. Huang, C.-W. Chen, Y.-C. Huang, Superzone Fresnel liquid crystal lens for temporal scanning auto-stereoscopic display, J. Disp. Tec, vol. 8, pp. 650-655, (2012).

[2] J. Kim, S.-U. Kim, B.-Y. Lee, J.-H. Suh, S.-D. Lee, Lenticular lens array based on liquid crystal with a polarization-dependent focusing effect for 2D–3D image applications, J. Inf. Disp., vol. 16, pp. 11-15, (2015).

[3] J.-S. Jang, B. Javidi, Improved viewing resolution of three-dimensional integral imaging by use of nonstationary micro-optics. Opt. Lett., vol. 27, pp. 324-326, (2002).

[4] K.-B. Son, M. Kim, M.-K. Park, H.-R. Kim, Polarization-dependent microlens array using reactive mesogen aligned by top-down nanogrooves for switchable three-dimensional applications. J. Opt. Soc. Korea, vol. 19, pp. 265-271, (2015).

THz Near-Field Microscopy

Haewook Han

Department of Electrical Engineering, POSTECH, Korea
hhan@postech.ac.kr

Combined with terahertz (THz) time-domain spectroscopy, THz near-field microscopy (THz-NFM) based on an atomic force microscope is a technique that, while challenging to implement, is invaluable for probing low-energy light-matter interactions. Nanoscale near-field imaging in the THz spectral range is of great importance for studying intriguing phenomena such as biomolecular vibrations and carrier dynamics in quantum-confined nanostructures. Conventional THz time-domain spectroscopy (TDS) can provide macroscopic imaging averaged over an ensemble of such nanostructures. Their spatial resolutions are, however, limited to ~λ/2 by diffraction. Therefore, several types of THz-NFMs have been developed to achieve sub-wavelength resolutions. In contrast to visible or IR scanning near-field optical microscopes (SNOMs), most THz NFMs have been based on THz pulse TDS systems, making it possible to perform ultra-broadband THz spectroscopy. Solid-state and biomolecular nanostructures are usually embedded in background media, and we have recently demonstrated a broadband THz pulse NFM that provides subsurface nanoimaging of a metallic grating embedded in a dielectric film. The THz near-field microscope can obtain broadband nanoimaging of the subsurface grating with a nearly frequency-independent lateral resolution of 90 nm, corresponding to ∼λ/3300, at 1 THz, while the AFM only provides a flat surface topography. In this talk, we present our recent progress on quantitative THz-NFM using a self-consistent line dipole image method (LDIM) based on an exact quasi-electrostatic image theory for the analysis of THz s-SNOMs, which are in excellent agreement with experiments.

Graphene in strong electromagnetic fields

Yu.A. Sergeev, I.V. Oladyshkin, S.B. Bodrov, A.I.Korytin, M.D Tokman, and A.N. Stepanov

Institute of Applied Physics of the Russian Academy of Sciences
46 Ul'yanov Street, 603950, Nizhny Novgorod, Russia
step@ufp.appl.sci-nnov.ru

Since the synthesis of graphene in 2004, its investigations have been attracting tremendous interest due to its unique physical properties and numerous potential applications. Hundreds of publications devoted to graphene appeared, including numerous reviews. In our presentation, we will discuss some specific nonlinear properties of graphene revealed in strong electromagnetic fields.

The first part of the presentation will be devoted to the discussion of the experimental and theoretical results on optical emission from graphene irradiated by a strong (up to 300 kV/cm) short terahertz pulse. The appearance of emission from graphene was observed in experiment in the 350-600 nm spectral range at high THz fields (Fig.1). We detected the increase of the optical emission by nearly 3 orders of magnitude, while the THz field increased by a factor of 2 only. The spectrum of the optical emission corresponded to Planck's law for the spectral radiance of a black body. We attribute the optical emission to bias-induced spontaneous emission from energetic charge carriers in the graphene. On the basis of the theoretical analysis, we revealed the importance of the dynamic (ballistic) mechanism of electron-hole pair generation induced by an intense terahertz pulse with subsequent spontaneous radiative re-combination.

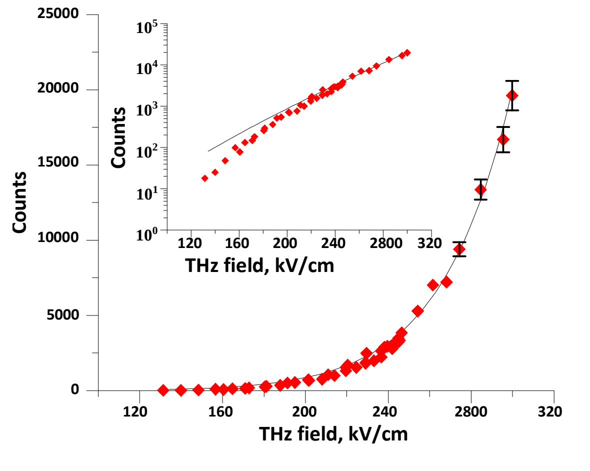

Fig.1. Optical emission from graphene vs THz field. The solid line is a theoretical fit.

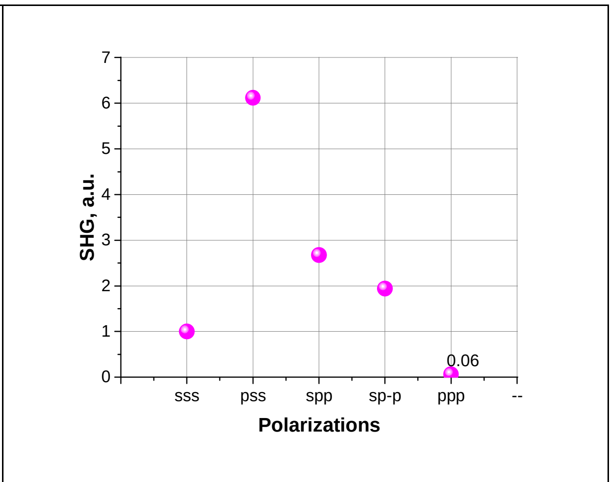

Fig.2. Polarization dependence of SHG from graphene in presence of THz field, normalized to sss polarization.

In the second part of the presentation we will discuss our results on the generation of the second optical harmonic (SHG) of laser radiation from graphene in the presence of a high power terahertz pulse. We demonstrated essential amplification of SHG under the action of THz field. Polarization characteristics of SHG specific for graphene will be presented (Fig. 2) together with the dependence of SHG efficiency on optical and THz fields. Detailed theoretical analysis of von Neumann equation allowed us to propose a new mechanism for SHG in graphene under the combined action of optical and THz fields. This mechanism is caused by broadening of the interband resonance due to quasi-particle acceleration by an intense THz field in the process of interband transition. As a result of the "field" interband resonance broadening, the region of electron-hole generation in k-space becomes asymmetric, which leads to the appearance of necessary anisotropy allowing for SHG in the dipole approximation.

Extreme Nonlinear Optics in the THz Regime

T. Ozaki[1]

1- INRS-EMT, Varennes, Québec, Canada, J3X 1S2

email address: ozaki@emt.inrs.ca

High-field carrier transport dynamics at terahertz (THz) frequencies in semiconductors can lead to numerous ultrafast phenomena, such as THz pulse self-phase modulation, intense THz field induced impact ionization, as well as dynamic Bloch oscillations driven by ultra-high THz frequencies [1-3]. In the nonresonant regime, carriers can be efficiently accelerated by the intense THz field, resulting in high ponderomotive energy that is proportional to the square of the peak field and inversely proportional to the square of the THz frequency [4]. In this work, we perform nonlinear THz-TDS measurement of InGaAs thin film using an intense THz source generated from an interdigitated ZnSe large-aperture photoconductive antenna (LAPCA), which can generate intense, asymmetric quasi-half-cycle THz pulses with low median frequency of approximately 0.2 THz. With the same peak field, the ponderomotive potential is thus much higher than other higher frequency THz sources via, for example, optical rectification [1,4]. At high fields, we observe strong THz transmission bleaching, THz phase modulation as well as the generation of high frequency components and high-order harmonics.

The interdigitated ZnSe LAPCA is composed of 35 identical electrodes (37 mm long and 0.7 mm wide) for a total area of 12.25 cm^2. The LAPCA is photoexcited by a 15 mJ, 400 nm pump pulse with a repetition rate of 10 Hz. The radiated THz electric field is controlled by varying the bias field of the LAPCA. Our InGaAs sample consists of a 500-nm-thick n-type $In_{0.53}Ga_{0.47}As$ epilayer with a doping concentration of approximately 2×10^{18} cm^{-3}. The InGaAs thin film is grown by metal-oxide chemical vapor deposition on a lattice-matched, 0.35-mm-thick semi-insulating InP substrate. Nonlinear effects are not observed with the bare InP substrate.

Experiments reveal that at high fields of 185 kV/cm, the sample shows huge transparency. In addition, we observe clear THz waveform modulations combined with compression of the half-cycle pulse. Compared with the incident THz spectrum, the transmitted THz pulse has higher spectral intensity at higher frequencies, demonstrating high-frequency THz generation.

We studied the carrier dynamics in the conduction band of InGaAs using the ensemble Monte-Carlo method to solve the Boltzmann transport equation and performing the simulations in the time domain [6,7]. At low fields, the carriers follow linearly the THz electric field in the conduction band, while the carrier dynamics become extremely nonlinear at high fields, showing an abrupt reduction in the current density J with a dramatic shortening of the pulse duration, indicating the generation of high frequency components. We attribute these observations to the strong carrier intervalley scattering effects driven by the THz pulses with high ponderomotive energy, which lead to an abrupt reduction of the photoconductivity due to the higher effective mass at upper valleys as well as the increased intravalley and intervalley scattering rates. By performing the Monte-Carlo simulations for various incident THz fields used in the experiments, we find that intervalley scattering between Γ and L valleys starts to become significant when the THz field reaches 101 kV/cm, and much stronger scattering effects between Γ, L and X valleys start to dominate at higher fields, leading to an abrupt reduction of photoconductivity and in turn the THz transmission enhancement and the generation of high frequency components and high-order harmonics.

[1] D. Turchinovich, J. M. Hvam and M. C. Hoffmann, "Self-phase modulation of a single-cycle terahertz pulse by nonlinear free- carrier response in a semiconductor", Phys. Rev. B vol. 85, 201304, (2012).

[2] I.-C. Ho and X.-C. Zhang, "Driving intervalley scattering and impact ionization in InAs with intense terahertz pulses", Appl. Phys. Lett. vol. 98, 241908, (2011).

[3] O. Schubert, M. Hohenleutner, F. Langer, B. Urbanek, C. Lange, U. Huttner, D. Golde et al., "Sub-cycle control of terahertz high-harmonic generation by dynamical Bloch oscillations", Nature Photonics vol. 8, 119-123, (2014).

[4] T. Kampfrath, K. Tanaka and K. A. Nelson, "Resonant and nonresonant control over matter and light by intense terahertz transients", Nature Photonics vol. 7, 680-690 (2013).

[5] A. P Long, P. H. Beton and M. J. Kelly, "Hot-electron transport in $In_{0.53}Ga_{0.47}As$", J. Appl. Phys. vol. 62, 1842-1849, (1987).

[6] M. Mohamed, A. Bharthuar and U. Ravaioli (2015), "Bulk GaAs Ensemble Monte Carlo," https://nanohub.org/resources/moca-ensemble. (DOI: 10.4231/D38C9R505).

Enhanced Crystaliozation of Polymer by High-Power THz Radiation

C. Otani[1], H. Hoshina[1], H. Suzuki[1], M. Nagai[2], K. Kawase[3], A. Irizawa[3], G. Isoyama[3]

1- Terahertz Sensing and Imaging Research Team, RIKEN Center for Advanced Photonics, RIKEN, 519-1399 Aramaki-Aoba, Aoba-ku, Sendai, Miyagi 980-0845, Japan.
2- Graduate School of Engineer Science, Osaka University, 1-3 Machikaneyama, Toyonaka 560-8531, Japan..
3- Institute of Scientific and Industrial Research, Osaka University, 8-1 Mihogaoka, Ibaraki, Osaka, 567- 0047, Japan.
E-mail: otani@riken.jp

In terahertz (THz) frequency region, high-power sources have been developped remarkably, opening the possibility of the active uses to change macromolecular structures. Because such molecular structures are closely connected with their functions, this leads to the development of new functions of macromolecules. In this presentation, we will show our recent results related to this topic.

We have irradiated the strong THz radiation into poly-hydroxybutyrate (PHB) and chloroform solution during solvent casting crystallization. We have utilized the free electron laser (FEL) of Institute of Scientific and Industrial Research (ISIR) of Osaka University with the peak power density of 40 MW/cm^2 [1]. Fig. 1(a) and (b) show transmission microscope images of non-irradiated and THz-irradiated PHB using confocal laser microscope, respectively. Thus, the morphological change by the irradiation has been clearly observed. Fig. 1(c) shows IR absorption spectra at the sample center region. The sharper (red) and wider (blue) peaks correspond to the crystal amorphous, respectively. Fig. 1(d) shows 2D plots of absorbance intensity ratios of the crystal and amorphous peaks, showing the crystallinity distribution of non-irradiated and THz-irradiated PHB. Thus, 10−20% increase in crystallinity has been found and we have succeeded to demonstrate the THz-induced intermolecular rearrangement of polymer macromolecules for the first time.

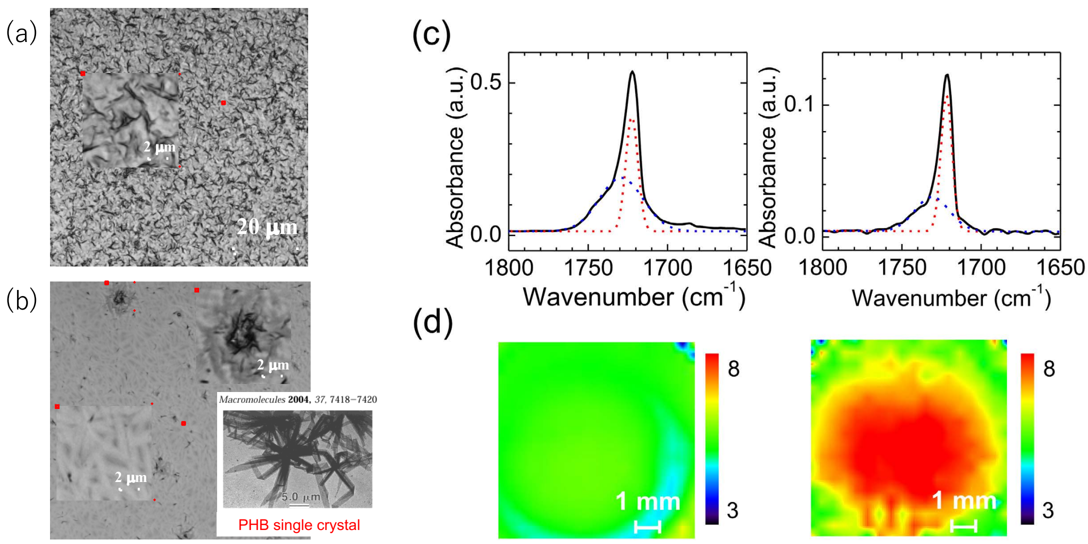

Fig. 1. Transmission microscope images of (a) non-irradiated and (b) THz-irradiated PHB using confocal laser microscope. (c) IR absorption spectra at the central regions. The sharper (red) and wider (blue) peaks correspond to the crystal and amorphous, respectively. (d) 2D plots of absorbance ratios of the crystal and amorphous peaks, showing the crystallinity distribution of non-irradiated and THz-irradiated PHB.

[1] H. Hoshina *et al.*, "Polymer morphological change induced by terahertz irradiation," *Scientific Reports*, vol. **6**, pp. 27180-1-6 (2016).

Optical study of the interaction of Fe2O3 nanoparticles with human erythrocytes and their effect on blood microrheology

A.E. Lugovtsov[1], E.A Shirshin[2], V.I. Kochubey[3,4], V.V. Tuchin[3,4,5], A.V. Priezzhev[1,2]

1 - International Laser Center and 2 - Faculty of physics of M.V. Lomonosov Moscow State University, Leninskiye Gory, 1-2, 119991, Moscow, Russian Federation
3 - Institute of Optics and Biophotonics, Saratov National Research State University, Astrakhanskaya 83, 410012 Saratov, Russian Federation
4 - Interdisciplinary Laboratory of Biophotonics, National Research Tomsk State University, Lenin's av. 36, 634050 Tomsk, Russian Federation
5 - Laboratory of Laser Diagnostics of Technical and Living Systems, Institute of Precision Mechanics and Control RAS,
Rabochaya 24, 410028 Saratov, Russian Federation

anlug@bmp.ilc.edu.ru

Nanoparticles (NP) of Iron (iii) oxide nanoparticles (Fe2O3) have been proposed for various biological and bio-medical applications. These particles are promising, e.g., for biomedical imaging and photodynamic therapy (PDT) of oncology diseases. Recently, the NP with surface functionalization by porphyrins (Fe2O3-POR) were proposed as more efficient for PDT since they strongly absorb light, which is then converted into energy and heat in the illuminated areas. It is presumed that in order to reach the target these particles would be administered into blood. Although NPs Fe2O3 are considered as biocompatible and non-toxic, so far there is little information on the interaction of the particles with major blood components. The aim of this work was to estimate the *in vitro* effect of Fe2O3 particles on blood microrheologic properties.
In this work, all measurements were performed by means of the laser diffractometry and aggregometry techniques by using the commercially available Rheoscan system (Rheomeditech, Korea). The blood samples drawn from seven healthy volunteers were incubated with suspensions of iron oxide porphyrin functionalized (Fe2O3-POR) and none functionalized (Fe2O3) NPs in PBS solution in concentrations of 33, 100 and 1000 μg/ml during 45 minutes.
We found that 45 minutes-long incubation of RBCs with the porphyrin functionalized and non-functionalized Fe2O3 NPs results in significant alterations of the aggregation kinetics and negligible changes in deformability of RBCs. The ability of RBC to aggregate is further impaired with increasing the NP concentration. It was shown, that the characteristic time of aggregates formation increases by 13 ± 4 %, 80 ± 11% and 115 ± 19% in the cases of 33 μg/ml, 100 μg/ml and 1000 μg/ml concentrations of Fe2O3-POR NPs accordingly in comparison with the control group (without nanoparticles, pure blood). Similar results for the non-functionalized particles are 5 ± 3%, 19 ± 8%, and 159 ± 18%. The amplitude of aggregation decreases by 3 ± 2%, 11 ± 8%, and 23 ± 11% for the Fe2O3-POR NPs and 2 ± 1%, 7 ± 4%, and 30 ± 14% for the Fe2O3 NPs in the cases of 33 μg/ml, 100 μg/ml and 1000 μg/ml concentrations respectively. The alterations in the aggregation are seen to be more significant for the higher nanoparticle concentrations and more pronounced for non-functionalized particles. The hydrodynamic strength was reducedby15-42% depending on the type and concentrations of the particles.
To further investigate the interaction between the NPs and RBCs, namely, to study sorption onto the membrane and cellular penetration, we performed experiments using the fluorescence laser confocal microscopy technique. For this, the Nikon A1R (Japan) system was employed, and the fluorescence signal was detected both from the porphyrin-functionalized particles and endogenous RBC fluorophores.
Basing on these results one can conclude that the Fe2O3 particles can be administrated into blood in ambient conditions at low concentrations (33 μg/ml), without significant complicating the blood's rheological conditions. However, controlling the RBCs microrheological properties is necessary during treatment. Further measurements are needed to estimate the effect of the NPs on blood at their *in vivo* incubation.
The work was supported by the RFBR grants № 16-32-50128 and 16-52-51050.

Time-Dependent Analysis and Noise Suppression of Surface Enhanced Raman Spectroscopy Using Optical Code Modulation

Wonkyoung Lee[1,2], Bong Kyu Kim[1], and Ki-Hun Jeong[2]

Bio-Medical IT Convergence Research Division, ETRI, 218 Gajeong-ro, Yuseong-gu, Daejeon, 34129, Korea
Bio and Brain Engineering Department, KAIST, 291 Daehak-ro, Yuseong-gu, Daejeon, 34141, Korea

Main author email address: wklee@etri.re.kr

Surface enhanced Raman spectroscopy (SERS) has been received much attention in the last decade for biological and medical clinic applications due to its excellent molecular specificity and high sensitivity [1, 2]. SERS has considerable potential as a diagnostic tool for tumour identification and in-vivo cancer detection, and even ultrasensitive single molecule detection [3, 4]. SERS is a surface-sensitive technique that improves the intensity of the Raman scattering by enhancing the electric field using excitation of localized surface plasmon on metallic nanoparticles with dimensions much smaller than the wavelength and provides enhancement factors between 10^4 and 10^{14}. Despite the excellent intrinsic properties of SERS, it has been limited in its applicability by strong autofluorescence signals and its spectral fluctuations due to variation of laser intensity and motion of the adsorbed molecule on the surface. In order to overcome this limitation, many methods such as principal component analysis (PCA), time-resolved Raman spectroscopy, and wavelength modulated Raman spectroscopy have been developed [5, 6]. Though many technologies have been suggested, it still remains an important issue how to filter out Raman signals from the autofluorescence signals and system noise.

In this paper, we analyze characteristics of Raman signals and autofluorescence signals in the time domain. Also we study a method which removes background noise such as broad autofluorescence, system noise, external interference, and non-target scattering and improve the signal-to-noise ratio (SNR) of Raman signals. From the time-dependent analysis, we confirm that Raman signals can closely follow the high-frequency modulation of the excited light, while the autofluorescence cannot follow high-frequency modulation owing to its long lifetime. Using the difference in frequency response of the Raman signals and the background fluorescence, and good correlation property of pseudorandom noise (PN) codes, the method effectively extracts the Raman signals from the broad and intense background noise. We verify the feasibility of the proposed method for the SNR enhancement by comparing with results from the normal SERS. The enhanced SNR could contribute to reducing the measurement time and increasing the diagnostic sensitivity for detection of target analytes. Furthermore, the method can serve as a diagnostic tool for ultrasensitive detection at the single molecule level.

[1] Samuel S. R. Dasary et al., Gold Nanoparticle Based Label-Free Probe for Ultrasensitive and Selective Detection of Trinitrotoluence, American Chemical Society, vol. 131, pp. 13806-13812, (2009).
[2] Katherine A. Willets, Super-resolution imaging of SERS hot spots, The Royal Society of Chemistry, vol. 43, pp. 3854-3864, (2014).
[3] Jian Wu et al., Trace cancer biomaker quantification using polystyrene-functionalized gold nanorods, Biomedical Optics Express, vol. 5(12), pp. 4101-4107, (2014).
[4] Natalie L. Gruenke et al., Ultrafast and nonlinear surface-enhanced Raman spectroscopy, The Royal Society of Chemistry, vol. 45, pp. 2263-2290, (2016).
[5] Tatu Rojalin et al., Fluorescence-suppressed time-resolved Raman spectroscopy of pharmaceuticals using complementary metal-oxide semiconductor (CMOS) single-photon avalanche diode (SPAD) detector, Analytical and Bioanalytical Chemistry, vol. 408, pp. 761-774, (2016).
[6] Bavishna B. Praveen et al., Wavelength modulated surface enhanced (resonance) Raman scattering for background-free detection, The Royal Society of Chemistry, vol. 138, pp. 2816-2820, (2013).

Optical clearing of costal cartilage on λ=532 nm and 1.56 µm

Yu. Alexandrovskaya[1,2], **K. Sadovnikov**[3], **E. Sobol**[1,2]

1- Institute of Applied Physics of the Russian Academy of Sciences, Ul'yanov St. 46, 603950 Nizhny Novgorod, Russia
2- Institute of Photon Technologies, Federal Scientific Research Centre "Crystallography and Photonics" of the Russian Academy of Sciences, Pionerskaya St. 2, 142190 Troitsk, Moscow, Russia
3- M.V. Lomonosov Moscow State University, Leninskiye Gory 3, 119991 Moscow, Russia

Main author email address: yu.alexandrovskaya@gmail.com

Near infrared laser with the wavelength λ=1.56 µm is used for the reshaping of costal cartilage grafts to serve as implants in trachea stenosis surgery [1]. Laser-assisted cartilage reshaping can be performed due to the heat-induced relaxation of the internal mechanical stress in tissue when the local temperature reaches 65-70ºC [2]. The absorption of the near infrared radiation by cartilage tissue is determined by water spectrum and on 1.56 µm the absorption coefficient is about 11 cm^{-1} [3] that corresponds to about 0.7 mm depth of radiation absorption. For the safety requirements the time of irradiation usually does not exceed 6 seconds [1]: so, it determines the maximal depth of heating as $\sim\sqrt{at}$ = 1 mm, where a is the tissue thermoconductivity (0.002 cm^2/s) and t – the duration of irradiation (s). Thus, the thickness of an implant that can be effectively heated by the 1.56 µm laser does not exceed 2 mm. For the implants of 3 mm in thickness the residual stress should be taken into account [4]. Consequently, for the thicker implants (up to 3.0-3.5 mm) the problem of effective heating arises along with avoiding the thermal damage of the upper tissue layers. In the present work we offer to use the optical clearing technique well known in optical diagnostics of tissues [5] to enable the deeper penetration of the infrared radiation to costal cartilage. The basic mechanism of the tissue optical clearing is supposed to be the matching of refractive indices of the major tissue components with subsequent decrease of the scattering [5]. The several optical clearing agents (OCAs) were applied to cartilage: glycerin, tartaric acid, fructose and omnipaque. The transmittance of laser radiation was measured for the untreated and immersed in OCAs tissue. The results for 1.56 µm we compared with those for 532 nm to evaluate the OCAs ability to reduce high scattering in the tissue. Different concentrations of the OCAs and kinetics of their diffusion into cartilage were studied. The maximal achieved clearing ability of the used OCAs for the both wavelengths is shown in Fig.1. The maximal clearing in the infrared range was achieved by immersion in fructose, while omnipaque and tartaric acid almost did not changed the tissue transparency. However omnipaque showed the high clearing ability in the visible range. The omnipaque stability under infrared radiation was studied by Raman spectroscopy. Immersion in glycerin solution resulted in the pronounced tissue shrinkage and mass loss and the tissue transparency on λ=1.56 µm was enhanced up to 2.5 times.

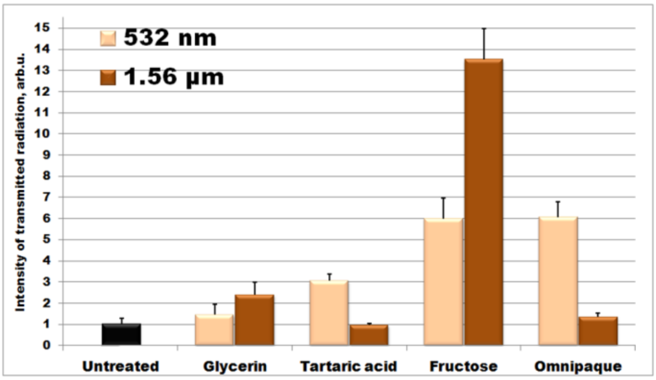

Figure 1. The diagrams of transmitted laser radiation intensity for λ=532 nm and 1.56 µm for cartilage of 1 mm in thickness immersed in different OCAs compared to untreated cartilage.

The work was supported by the Russian Science Foundation grant 16-15-10274.

[1] O. Baum, Yu. Soshnikova, E. Sobol, A. Korneychuk, M. Obrezkova, V. Svistushkin, O. Timofeeva, V. Lunin, Laser reshaping of costal cartilage for transplantation, Lasers Surg. Med., vol. 43(6), pp. 511-515, (2011).
[2] E. Sobol, T. Milner, A. Shekhter, O. Baum, A. Guller, N. Ignatieva, A. Omelchenko, O. Zakharkina, Laser reshaping and regeneration of cartilage, Las. Phys. Lett. vol. 4(7), pp. 488-502, (2007).
[3] M. Chaplin, Water Structure and Science, http://www1.lsbu.ac.uk/water/water_vibrational_spectrum.html#k.
[4] Yu. Soshnikova, M. Keselman, O. Baum, E. Shults, M. Obrezkova, V. Lunin, E. Sobol, Effect of Anisotropy and Drying of Costal Cartilage on Its Optical Transmittance in Laser Reshaping of Implants With 1, 2 and 3 mm in Thickness, Lasers Surg. Med. vol. 48(9), pp. 887-892 (2016).
[5] E. Genina, A. Bashkatov, V. Tuchin, Tissue optical immersion clearing, Expert Rev. Med. Devices, vol. 7(6), pp. 825–842 (2010).

The Changes of Cerebral Hemodynamics during Dexmedetomidine Induced Sedation in a Rat Model

Seonghyun Kim[1], **Jayyoung Bae**[1], **Teo Jeon Shin**[2], **Jae Gwan Kim**[1]

[1]*Department of Biomedical Science and Engineering, Gwangu Institute of Science and Technology (GIST),*
[2]*School of Dentistry, Seoul National University*

jaekim@gist.ac.kr

Dexmedetomidine has been used for sedation in clinics and it becomes more popular since it does not cause a respiratory depression. However, even with high doses of the drug, it does not cause a burst suppressed EEG pattern, which is one of the important parameters of anesthesia depth monitoring device.[1] In this study, we employed a near-infrared spectroscopy(NIRS) to observe cerebral hemodynamic changes induced by dexmedetomidine in rats to see if NIRS can be used to monitor the depth of sedation noninvasively in a real-time.

Our NIRS system consists of a tungsten-halogen lamp, a NIR range spectrometer, a computer and a pair of fiber-optic patch cables. A spectrum in the range of 730-850 nm were acquired at 4Hz. In order to measure the NIR signals and EEG signals from the brain, we implanted optodes into two positions (Right/Left frontal cortex) and EEG electrodes on multiple positions (Right/Left frontal cortex, parietal cortex) on the skull of the rat. EEG depth electrodes were also implanted for the measurement from the thalamus.

We acquired EEG and NIRS signals 30 minutes from freely moving rats as a baseline. Afterwards rats were administered dexmedetomidine by intravenous route, and the acquisition of EEG and NIRS signals were continued during the sedation and until the rat awakes.The acquired intensity values at 5 wavelengths (730, 750, 800, 830, 850 nm) were used to estimate the concentration changes of deoxy- (RHb), oxy- (OHb) and total- (THb) hemoglobin in rat brain by using the modified Beer-Lambert's law. These hemodynamic changes were compared with the EEG signals. From this study, cerebral hemodynamic changes in rats were shown during the dexmedetomidine infusion. Our results are well matched with existing physiological effects of dexmedetomidine. Further investigations are needed to characterize the factors that affect hemodynamics.

[1] Eriksson, Lars I. Miller's Anesthesia: Vol. 1. Elsevier Health Sciences, 2009.

Radio-over-fiber for future mobile and advanced imaging

Tetsuya Kawanishi[1,2], **Atsushi Kanno**[2] **and Naokatsu Yamamoto**[2]

1- Faculty of Science and Engineering, Waseda University, Shinjuku, Tokyo, Japan
2- National Institute of Information and Communications Technology, Koganei, Tokyo, Japan

kawanishi@waseda.jp

This presentation outlines recent radio-over-fiber (RoF) technologies which transfer waveforms for mobile services, advanced imaging, etc.RoF systems consist of electric-to-optical (EO) and optical-to-electric (OE) conversion devices connected by optical fibers where propagation loss would be much smaller than in metallic cables. Future mobile services, such as 5G, would have many base stations and antennas connected by mobile backhaul (MBH) and mobile fronthaul (MFH), in order to achieve broadband data transmission with limited bandwidth radio frequency resources. RoF would provide low-cost and high-performance MFH, while digital transmission based MFHrequires large bandwidth to transfer waveforms for high-speed radio-wave links [1, 2].Wireless sensor networks (WSN) would play very important roles in the Internet of Things (IoT), where information generated at many small sensors is transferred to servers for big data analysis [3]. For applications, such as safety for public transportation, high resolution imaging would be required to detect foreign-object-debris (FOD) by using millimetre-wave radars [4, 5]. Recently, a radar system consisting of many radar heads connected by an optical network has been developed to achieve a few centimetres range resolution in a liner shape area. As with WSN, the optical network dedicated for sensing transfer information for sensing. However, the network would carry waveform generated at the radar heads to compile information from sensor heads coherently at central signal processing units. The optical network and radar heads form a high-performance sensor, so that we call such configuration sensor over fiber (SoF). WSN transmits digital information digitized at sensors in the same way as in MBH, while the network for SoF transfers waveforms as with MFH. SoF can compile information from sensor heads coherently at central signal processing units.

The research work reviewed in this presentation was partially supported by Electronics and Telecommunications Research Institute, South Korea, and by the Japanese Government funding for "R&D to Expand Radio Frequency Resources" from the Ministry of Internal Affairs and Communications.

[1] APT Report on "Wired and Wireless Seamless Connections using Millimeter-Wave Radio over Fiber Technology for Resilient Access Networks," APT/ASTAP/REPT-11
[2] T. Kawanishi, A. Kanno, T. Kuri and N. Yamamoto, "Transparent waveform transfer for resilient and low-latency links," IEEE Photonics Society Newsletter, 28 (2014) 4
[3] T. Kawanishi, A. Kanno, and N. Yamamoto, Concept of sensor over fibers and its application to high resolution millimeter-wave radar, We B6.3, ICTON 2017, Girona Spain
[4] T. Kawanishi, N. Yonemoto, N. Shibagaki, K. Kashima, R. Haramoto, Y. Sato A. Kanno, K. Inagaki, T. Angkaew and P. Janpugdee, "Field trial of radio-over-fiber based high-resolution radar," 2015 Thailand-Japan Microwave (TJMW2015), Bangkok, Thailand, Aug. 2015
[5]T. Kawanishi, A. Kanno, N. Yamamoto, N. Yonemoto, N. Shibagaki and K. Kashima, "Optical fiber network-connected distributed mm-wave radar system,", to be presented in 2017 IEEE Photonics Society Summer Topicals, July 2017. San Juan, Puerto Rico.

Defective WTe_2 Microflakes for Femtosecond Fiber Laser Mode-locking

J. H. Lee [1*], J. Koo[1], J. Lee[1], Y. I. Jhon[2], J. Park[3], Y. M. Jhon[2]

1. School of Electrical and Computer Engineering, University of Seoul, Seoul 02504, South Korea
2. Sensor System Research Center, Korea Institute of Science and Technology, Seoul 02792, South Korea
3. Ultra-Precision Optics Research Sector, Korea Photonics Technology Institute,Gwangju 61007, South Korea
j.h.lee@ieee.org

Femtosecond fibre lasers have attracted huge technical attention in many applications such as fundamental scientific research, material processing, medicine, and sensing in recent years. One commonly used approach for the implementation of femtosecond fibre lasers is to use a mode-locking technique based on a passive nonlinear optical device, called a "saturable absorber (SA)". Most of commercial saturable absorbers have so far been made of III-V semiconductors, other materials including carbon nanotubes, graphene, black phosphorus, gold nanoparticles, and topological insulators etc. have recently been investigated as novel saturable absorption materials [1-4]. Very recently, saturable absorption has also been observed in transition metal dichalcogenides (TMDCs) such as MoS_2, $MoSe_2$, $MoTe_2$, WS_2, WSe_2, and WTe_2, in which mono- and/or few-layer structures of TMDCs were prepared for use as SA materials [5-7]. Since the preparation and/or extraction of mono- and few-layer TMDCs needs considerable effort and time when compared to that of bulk or micro-sized TMDCs, an investigation on the possible use of micro-sized TMDCs as SA materials is very important both for wider application of TMDCs in laser technology as well as for an in-depth understanding of their photonic properties.

In this presentation we review our recent investigation results on defective WTe_2 microflakes composited with polyvinyl alcohol (PVA) as an effective saturable absorption medium that can generate femtosecond fiber laser pulses at a wavelength of 1.55 μm [8]. Our WTe_2 samples are shown to be structurally close to microflakes, which had an average depth of ~300 nm (definitely beyond the 2D regime) and a lateral size of 1–2 μm, while the composition ratio of W and Te atoms changed from 1:2.13 to 1:1.64 or to 1:2.51, according to whether or not PVA was included. These results indicate that our WTe_2 microflakes are defective and bulk-structured. We carried out density functional theory (DFT) calculations of the electronic band structures of a pristine bulk WTe_2 and six monolayer (1L) WTe_2 systems with different chemical compositions and/or oxidation states, conforming to experimental observations. small but distinct band gaps were observed in tellurium-deficient 1L WTe_2 (~0.033 eV for W:Te = 1:1.875 and 1:1.625). Meanwhile, oxidized 1L WTe_2 systems have rather large electronic band gaps ranging from 0.1 to 0.2 eV. Depositing the prepared WTe_2/PVA composite onto a side-polished fiber a saturable absorber was implemented. The saturation power and modulation depth were estimated to be ~64.6 W and ~2.85%, respectively. By incorporating the fabricated saturable absorber into a erbium fiber ring cavity, mode-locked pulses with a temporal width of 770 fs were readily produced. Our work strongly suggests that the saturable absorption performance of TMDCs does not critically depend on their structural dimensionality, indicating the great potential of non-2D-structured TMDCs in the development of passively mode-locked ultrafast lasers in the future

Acknowledgements : This work was supported by the National Research Foundation of Korea (NRF) grant funded by the Korea government (MSIP) (NRF-2015R1A2A2A11000907), Republic of Korea, and the Industrial Strategic Technology Development Program (10048690) funded by the Ministry of Trade, Industry & Energy, Republic of Korea.

[1] S. Y. Set *et al*., "Laser mode locking using a saturable absorber incorporating carbon nanotubes," J. Lightwave Technol., v.22, pp.51-56 (2004).
[2] Q. Bao *et al*., "Atomic-layer graphene as a saturable absorber for ultrafast pulsed lasers," Adv. Funct. Mater., v.19, pp.3077-3083 (2009).
[3] J. Lee *et al*., "A femtosecond pulse erbium fiber laser incorporating a saturable absorber based on a bulk-structured Bi_2Te_3 topological insulator," Opt. Express 22(5), 6165-6173 (2014).
[4] J. Sotor *et al*., "Ultrafast thulium-doped fiber laser mode locked with black phosphorus," Opt. Lett., v.40, pp.3885-3888 (2015).
[5] H. Zhang *et al*., "Molybdenum disulfide (MoS2) as a broadband saturable absorber for ultra-fast photonics," Opt. Express v.22, pp.7249–7260 (2014).
[6] R. I. Woodward *et al*., "Wideband saturable absorption in few-layer molybdenum diselenide ($MoSe_2$) for Q-switching Yb-, Er- and Tm-doped fiber lasers," Opt. Express v.23, pp.20051–20061 (2015).
[7] D. Mao *et al*., "Nonlinear saturable absorption of liquid-exfoliated molybdenum/tungsten ditelluride nanosheets," Small v.12, pp.1489-97 (2016).
[8] J. Koo, Y. I. Jhon, J. Park, J. Lee, Y. M. Jhon, and Ju Han Lee "Near-infrared saturable absorption of defective bulk-structured WTe_2 for femtosecond laser mode-locking" Advanced Functional Materials, v.26, pp.7454-7461 (2016).

High-Speed Transmission Using Directly Modulated Lasers

Hoon Kim, S. H. Bae, M. Kim, and Y. Chung

School of Electrical Engineering, KAIST, 291 Daehak-ro, Yuseong-gu, Daejeon, Korea
Author email address: hoonkim@kaist.ac.kr

The simplest and most economical form of optical transmission systemcan be realized by using a directly modulated laser (DML) and a direct-detection (DD) receiver [1]. However, it is commonly believed that, in comparison withthe externally modulated transmission system, the transmission distance of DML/DDsystem is seriously limited by the waveform distortions caused by the interplay betweenthe large frequency chirp of DML and fiber chromatic dispersion. In this talk, we present the small-signal frequency response of DML/DD system and show that theoptical signal generated from a DML ismoretolerant to fiber chromatic dispersion than one from an external modulator when the extinction ratio of the signal is optimized and an electrical equalizer is employed at the receiver.

The small-signal frequency response of the dispersive single-mode fiber used in a DML/DD system can be expressed as [1]-[3]

$$H_{Fiber} = \sqrt{\alpha^2+1}\cos\left(\theta+\tan^{-1}\alpha\right)+j\frac{\alpha\kappa P_0}{\omega}\sin\theta \tag{1}$$

where α is the linewidth enhancement factor, κ is the adiabatic chirp coefficient, P_0 is theoutput power of the laser, and ω is the angular frequency of the modulated signal. Also, θ isgiven as $D\lambda^2\omega^2 z/(4\pi c)$, where D is the fiber dispersion parameter, λ is the wavelength of theoptical signal, z is the transmission distance, and c is the speed of light in vacuum.It has been recently shown that the interplay between the DML's chirp and fiber's chromatic dispersion creates deep V-shaped dips in the frequency response, but they could not be effectively compensated by an electrical equalizer at the receiver [1]. This implies that the first frequency dip determines the dispersion tolerance of the DML/DD system. From (1), we can express the first null bandwidth of DML/DD system as [1]

$$BW_{DML} \cong \sqrt{c/\left(D\lambda^2 z\right)} \tag{2}$$

We can also write the first null bandwidth of externally modulated transmission systemas

$$BW_{External} = \sqrt{\frac{c}{2D\lambda^2 z}\left(1-\frac{\tan^{-1}\alpha}{\pi}\right)} \tag{3}$$

It is obvious from (3) that

$$\sqrt{c/\left(4D\lambda^2 z\right)} < BW_{External} < \sqrt{3c/\left(4D\lambda^2 z\right)} \tag{4}$$

Equation (4) shows that DML/DD systems are more tolerant to fiber chromatic dispersion than externally modulated transmission systems, regardless of α of the external modulator.

Also presented in this talk is the transmission of 56-Gb/s 4-level pulse amplitude modulation signals generated by using a 1.55-µm DML over 20 km of standard single-mode fiber. A linear feedforward equalizer is employed at the receiver to compensate for the waveform distortions caused by non-flat frequency response of DML and fiber chromatic dispersion. The performance behavior of this system with respect to the transmissiondistance is explained in detail by using equation (1).

This work is supported by Institute for Information & Communications Technology Promotion (IITP) grant funded by Korea government (B0717-16-0035, research on optical transceiver technology based on directly modulated laser for 100G transmission).

[1] S. H. Bae, H. Kim, and Y. Chung, "Transmission of 51.56-Gb/s OOK signal using 1.55-µm directly modulated laser and duobinary electrical equalizer," Optics Express, vol. 24, no. 20, pp. 22555-22562, 2016.
[2] L. Bjerkan, A. Royset, L. Hafskjaer, and D. Myhre, "Measurement of laser parameters for simulation of highspeedfiberoptic systems," J. Lightwave Technol.,vol. 14, no. 5, pp. 839–850, 1996.
[3] E. Peral, W. Marshall, and A. Yariv, "Precise measurement of semiconductor laser chirp using effect ofpropagation in dispersive fiber and application to simulation of transmission through fiber gratings," J.Lightwave Technol., vol. 16, no. 10, pp. 1874–1880, 1998.

Pulsed sodium guide star laser based on Raman fiber amplifiers

Yan Feng, Lei Zhang, and Xuezong Yang

Shanghai Institute of Optics and Fine Mechanics, Chinese Academy of Sciences, Shanghai, China

feng@siom.ac.cn

Astronomers use laser guide star adaptive optics to solve the image blurring due to atmosphere turbulence. It requires a high power narrow linewidth 589 nm laser to excite a layer of sodium atoms at 90 km high in atmosphere, to generate an artificial "guide star". The laser guide star technology is essential for large aperture telescopes to approach the designed angle resolution. Many works had been done to develop robust guide star laser to excite the sodium layer and generate guide star efficiently.

Pulsed guide star lasers are preferred in many circumstances. Pulsed laser with kHz repetition is used to gate out atmospheric Rayleigh scattering noise and avoid fratricide effect in multiple LGS systems. In other hand, guide star laser pulsed at the Larmor frequency, several hundreds of kHz, was proposed to solve a problem caused by geomagnetic field. The presence of geomagnetic field reduces the brightness of sodium guide star, because the sodium atoms precess along the magnetic field. Guide star laser pulsed at Larmor frequency can interact with the atoms at a fixed point in the precession cycle. Sodium guide star lasers pulsed at this frequency range with enough output power are technically challenging to develop.

In this talk, we will report our works on development of Raman fiber amplifier based guide star lasers pulsed at kHz and 100 kHz region. In the kHz case, we had reported a laser producing square-shaped pulses with tunable repetition rate (500 Hz to 10 kHz) and duration (1 ms to 30 μs), while the peak power remain constant as high as 84 W [1]. More recently, we have developed guide star laser pulsing at 100 kHz level Larmor frequency [2]. A continuous wave 1064 nm and 1120 nm double wavelength laser is modulated at 200 ~ 350 kHz repetition rate with an AOM, and seeds an Yb-Raman integrated fiber amplifier to generate high power pulsed linearly polarized 1120 nm laser. By pulse shaping of the seed laser, the amplifier emits close-to-rectangular pulses at 1120 nm. The high power pulsed 1120 nm fiber laser pumps an 1178 nm narrow linewidth Raman fiber amplifier at backward direction. The generated high power 1178 nm laser is then coupled into a frequency doubling resonator locked with the PDH method. Up to 17 W 589 nm laser is obtained. The pulse repetition rate is adjustable from 200 to 350 kHz, and the pulse duty cycle is also adjustable.

[1] L. Zhang, H. Jiang, S. Cui, J. Hu, and Y. Feng, “Versatile Raman fiber laser for sodium laser guide star,” Laser Photon. Rev. 8, 889–895 (2014).
[2] X. Yang, L. Zhang, S. Cui, T. Fan, H. Jiang, J. Dong, Y. Feng, “ Sodium guide star laser pulsed at Larmor frequency,” CLEO PR (2017).

Efficient 810-nm LED-side-pumped Nd:YAG laser

Chun-Yu Cho, Kuan-Wei Su, and Yung-Fu Chen

Department of Electrophysics, National Chiao Tung University, 1001 Ta Hsueh Road, Hsinchu, Taiwan.

sukuanwei@mail.nctu.edu.tw, yfchen@cc.nctu.edu.tw

With the recent development of high-luminescence light-emitting-diode (LED), solid-state lasers pumped by LED have been revisited in past few years [1-3]. However, the optical-to-optical conversion efficiency of the LED-pumped solid-state laser was still much inferior to solid-state lasers obtained by diode or lamp pumping. As a result, investigation to the enhancement of optical conversion efficiency for the LED-pumped solid-state laser is a novel topic nowadays. In this work, we demonstrated a highly efficient LED-pumped Nd:YAG laser by using a specially designed LED array. The spectral absorption efficiency of the Nd:YAG crystal can be up to 50% by using LED dies with a central wavelength of 810 nm and a full-width-half-maximum of 30 nm. The LED array (EPISTAR) was further arranged with area fill factor up to 50% to realize an average pump density of 151.8 W/cm^2. Experimentally, the Nd:YAG laser was first demonstrated by placing the LED array as close as possible to the gain medium with a usual concave-plane resonator. At the total pump energy of 43.2 mJ in a pump duration of 300 μs, the output energy of the LED-pumped Nd:YAG laser was found to be 8.71 mJ, corresponding to an optical conversion efficiency up to 20.2%. We further verified the dependence of output pulse energy on the spacing between LED array and the Nd:YAG crystal. The result indicated that because of the large divergence of pump LED, the optical conversion efficiency strongly depended on the spacing. Consequently, it is crucial to design an efficient LED-pumped laser by placing the pump array as close as possible to the gain medium. With the efficient pump scheme, we further demonstrated the passively Q-switched output by using a Cr^{4+}:YAG saturable absorber. Pulse energy of 1.42 mJ with pulse width of 170 ns and a peak power of 8 kW can be realized. It is highly feasible to further develop LED-pumped lasers for practical applications by scaling the output energy.

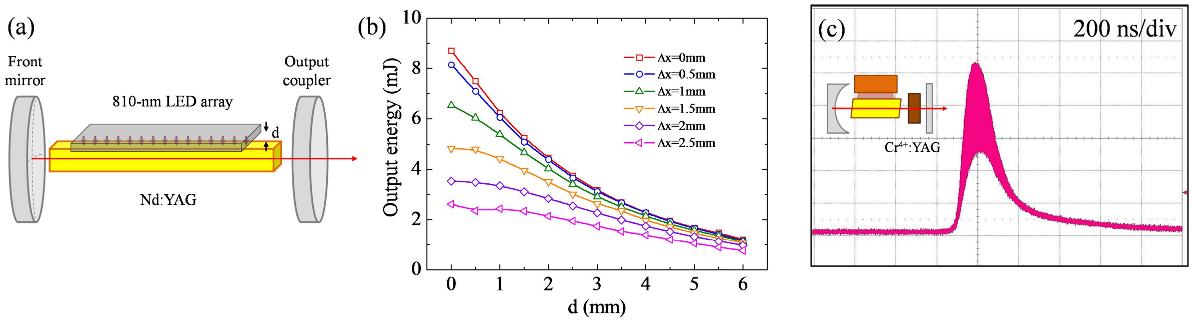

Fig. 1 (a) The experimental setup of the LED-pumped Nd:YAG laser; (b) the dependence of Nd:YAG laser output energy on spacing between LED array and gain medium in various horizontal position; (c) the temporal pulse shape of the passively Q-switched Nd:YAG laser.

[1] A. Barbet, F. Balembois, A. Paul, J. Blanchot, A. L. Viotti, J. Sabater, F. Druon, and P. Georges, Revisiting of LED pumped bulk laser: first demonstration of Nd:YVO_4 LED pumped laser, Opt. Lett., vol. 39, pp. 6731-6734, (2014).
[2] B. Villars, E. S. Hill, and C. G. Durfee, Design and development of a high-power LED-pumped Ce:Nd:YAG laser, Opt. Lett., vol. 40, pp. 3049-3052, (2015).
[3] K. Y. Huang, C. K. Su, M. W. Lin, Y. C. Chiu, and Y. C. Huang, Efficient 750-nm LED-pumped Nd:YAG laser, Opt. Express, vol. 24, pp. 12043-12054, (2016).

Room-temperature-bonding technique for developing new laser and wavelength-conversion devices

Ichiro Shoji

Department of Electrical, Electronic, and Communication Engineering, Chuo University
1-13-27 Kasuga, Bunkyo-ku, Tokyo 112-8551, Japan

ishoji@elect.chuo-u.ac.jp

The room-temperature bonding (RTB) is a versatile method to bond a variety of materials without any degradation of crystal qualities in a vacuum ($\sim 10^{-5}$ Pa) at room temperature [1]. We applied the RTB technique to fabricate some composite lasers and frequency-conversion devices [2,3]. Especially we have recently developed a Nd:YAG/diamond composite laser with an anti-reflection (AR) coating at the bonded interface, and multiple-plate-stacked GaAs quasi-phase-matching (QPM) wavelength-conversion devices [4].

We first fabricated a directly bonded composite of 1 at.% Nd:YAG and diamond. Figure 1 shows the laser characteristics. Although the composite could be pumped at much higher power at which the non-composite Nd:YAG was broken, its slope efficiency was smaller than that of the non-composite due to the Fresnel reflection at the bonded interface caused by the difference of the refractive indices between Nd:YAG and diamond. Then we newly fabricated a Nd:YAG/diamond composite which has an AR-coating layer at the bonded interface, as shown in the inset of Fig. 1. It has achieved almost the same efficiency with that of the non-composite, and still higher output power than that of the directly bonded composite.

QPM stacks of 106 μm-thick GaAs plates have been fabricated for high-power second-harmonic generation (SHG) of CO_2 lasers with the wavelength of 10.6 μm. We developed a consecutive plate-supplying system which used a translation stage to effectively fabricate multiple-plate stacks. The inset of Fig. 2 shows a 30 plate-stacked GaAs. Although the previous process caused inclusion of small particles at the bonded interface, the improved process which covered the translation stage with elastomer sheets minimized the scattering loss, and we succeeded in observing SHG of a CO_2 laser as shown in Fig. 2.

[1] T. Suga, Y. Takagi, B. Gibbesch, and G. Elssner, "Structure of AL-AL and Al-Si3N4 interfaces bonded at room temperature by means of the surface activation method," Acta Metall. Master. **40,** S133–S137 (1992).

[2] I. Shoji, T. Ishikawa, T. Yamauchi, K. Hara, and S. Matsumoto, "Fabrication and characterization of room-temperature-bonded composite lasers," *Conference on Lasers and Electro-Optics Europe* (European Physical Society, Mulhouse, 2013), Technical Digest, paper CE-6.4.

[3] K. Hara, S. Matsumoto, T. Onda, W. Nagashima, and I. Shoji, "Efficient ultraviolet second-harmonic generation from a walk-off-compensating β-BaB_2O_4 device with a new structure fabricated by room-temperature bonding," Appl. Phys. Express **5,** 052201 (2012).

[4] T. Kubota, H. Atarashi, and I. Shoji, "Fabrication of quasi-phase-matching stacks of GaAs plates using a new technique: room-temperature bonding," Opt. Mater. Express **7,** 932–938 (2017).

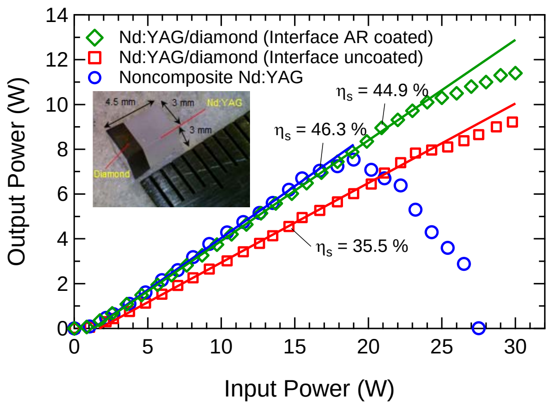

Fig. 1. Laser characteristics of the non-composite Nd:YAG (circle), the directly bonded Nd:YAG/diamond (squares), and the Nd:YAG/diamond with AR coating at the bonded interface (diamonds). Inset: fabricated Nd:YAG/diamond composite with AR coating at the bonded interface.

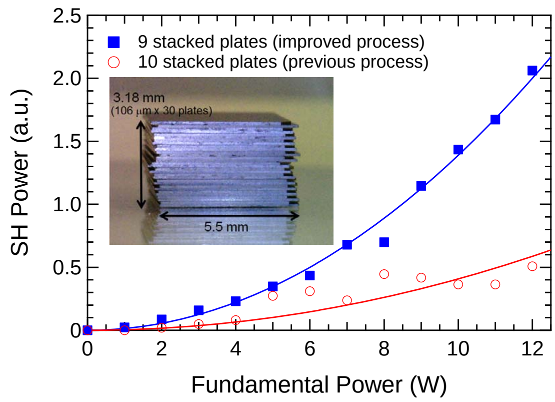

Fig. 2. Second-harmonic power as a function of the fundamental power for the 9 stacked QPM-GaAs plates fabricated with the improved process (squares) and the 10 stacked plates with the previous process (circles). Inset: fabricated 30-plate stack of QPM-GaAs.

Broad expansion of optical frequency combs by self-Raman scattering in coupled-cavity self-mode-locked monolithic lasers

Y. F. Chen[1], M. T. Chang[1], H. C. Liang[2] and K. W. Su[1]
[1]*Department of Electrophysics, National Chiao Tung University, 1001 Ta-Hsueh Rd. Hsinchu 300, Taiwan*
[2]*Institute of Optoelectronic Science, National Taiwan Ocean University, Keelung 20224, Taiwan*

Main author email address: yfchen@cc.nctu.edu.tw

In this work we numerically analyze and experimentally accomplish the broad expansion the optical frequency comb (OFC) by the self-Raman scattering in a coupled-cavity self-mode-locked (SML) monolithic Yb:KGW laser [1,2]. We firstly design a coated Yb:KGW crystal to generate the OFC in the SML operation. The crystal length shorter than 3.00 mm is used to avoid significant re-absorption losses. With a crystal length of 2.93 mm, the SML repetition rate of 25.78 GHz is obtained. We then employ a partially reflective mirror to form a coupled cavity that was set to multiply the repetition rate to reach 128.9 GHz. Furthermore, the critical value of the coupled reflectivity for the generation of self-Raman scattering is systematically explored and found to be approximately 90%. Experimental results reveal that a coupled reflectivity of 95% can lead to the generation of the first- and second-order SRS in the gain medium at the lowest frequency mode. As a result, the OFC can be expanded up to 8.4 THz with the pulse width down to 53 fs, as shown in Fig. 1. The total output power for the fundamental and the Stokes waves can achieve 1.6 W at a pump power of 8.7 W. Previously, several groups demonstrated sub-100 fs Yb:KGW mode-locked lasers with the action of a semiconductor saturable absorber mirror (SESAM) or Kerr-lens. The repetition rates in these earlier works were in the range of 30-80 MHz, whereas the present method can generate the repetition rate greater than 100 GHz. Our exploration confirms that the optical spectra generated by the SML and SRS process can be linked together to obtain an ultrahigh-repetition-rate broadband OFC.

[1] Y. F. Chen, M. T. Chang, W. Z. Zhang, K. W. Su, K. F. Huang, and H. C. Liang, "Generation of sub-terahertz repetition rates from a monolithic self-mode-locked laser coupled with an external Fabry-Perot cavity," Laser Photonics Rev. **9**, 91−97 (2015).
[2] C. Y. Lee, C. C. Chang, H. C. Liang and Y. F. Chen, "Frequency comb expansion in a monolithic self-mode-locked laser concurrent with stimulated Raman scattering," Laser Photonics Rev. **8**, 750−755 (2014).

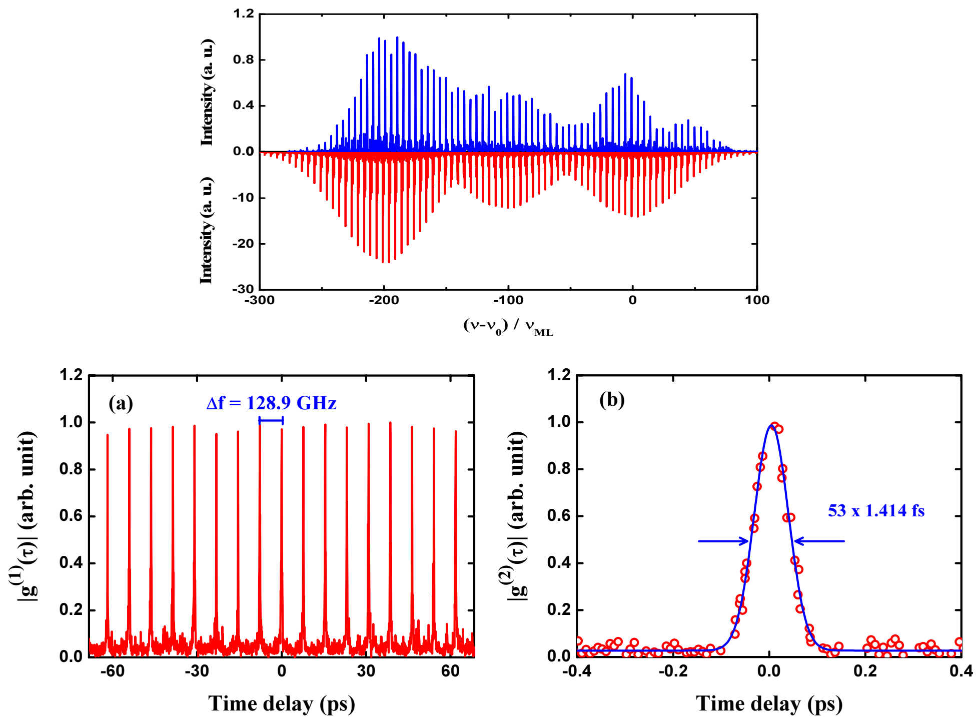

Tailoring laser beam profiles from a dual-cavity laser configuration

J. W. Kim, D. J. Kim, S. H. Noh

Department of Photonics and Nanoelectronics, Hanyang University ERICA, Ansan,Gyunggi-do, Republic of Korea
jwk7417@hanyang.ac.kr

Dual-cavity configuration, which the primary and the secondary cavities share a common gain medium and pump-in-coupling mirror (see Fig. 1), allows us to achieve selective excitation of one or multiple resonating modes in a simple way. Also it is possible to tailor the beam intensity distribution of the laser output by adjusting simply the round-trip loss of the secondary cavity. After it was first reported by our group [1], this laser configuration has successfully demonstrated selective excitation of the TEM_{00} and LG_{01} modes, generation of the laser beam with adaptive beam profiles, and a high-order LG mode beam [1-3]. Moreover, we also succeeded efficient power scaling of the tailored laser beam from the dual-cavity oscillator via a MOPA and dynamic modulation of the laser beam profiles. Therefore, tailored laser beams from the dual-cavity laser resonator should benefit to improve efficient laser operation and generate the optimized beams for various applications, particularly precision micro-machining profiles.

In this paper, we will review the principle of a dual-cavity laser configuration and its achievements in detail. Also we will report a recent work of the pulsed operation in the MOPA yielding >1 mJ of the pulse output with a selected beam profile.

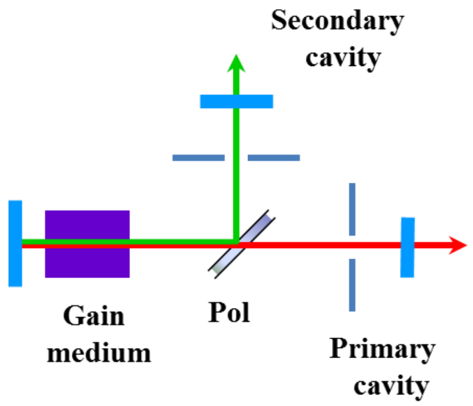

Figure 1. Schematic of a dual cavity configuration.

[1] D. J. Kim, J. W. Kim, "High-power LG_{00} and Laguerre–Gaussian mode generation in double resonator configuration," Appl. Phys. B **121**, 401 (2015).
[2] D. J. Kim, J. I. Mackenzie, J. W. Kim, "Adaptable beam profiles from a dual-cavity Nd:YAG laser," Opt. Lett. **41**, 1740 (2016).
[3] D. J. Kim, and J. W. Kim, "Dual-cavity Nd:YAG laser with Laguerre-Gaussian (LG_{0n}) mode output," Appl. Phys. B 383, 26 (2017).

High Power Fiber Lasers and Beam Combining Technology

B. He[1], Y. Qi[1], Y. Yang[1], H. Shen[1], Z. Quan[1], X. Chen[1], K. Liu[1] and J. Zhou[1]

1- Shanghai Key Laboratory of All Solid-State Laser and Applied Techniques, Shanghai Institute of Optics and Fine Mechanics, Chinese Academy of Sciences, Shanghai, China

Main author email address: bryanho@siom.ac.cn

Fiber amplifier has been established as reliable and promising high-power laser architecture owing to its advantages like compactness, high conversion efficiency and excellent heat dissipation [1]. The increasing demand for high power laser sources with diffraction-limited beam quality has led to a significant scaling in output power [2]. Spectral beam combining (SBC) and coherent beam combining (CBC) technology has been developed to upgrade the power level while maintaining excellent beam quality, at the same time, avoid some limitation of monolithic fiber amplifier, such as thermal damage, nonlinear effects, and modal instability [3]. SIOM have been working for more than 15 years committing to build narrow linewidth single mode fiber laser and high brightness beam combining system. A record of 50 GHz linewidth 2.5 kW fiber amplifier with integration design is achieved lately. An 8 channel 11.27 kW SBC system is established by 1.5 kW-level all-fiber superfluorescent sources. A 4 channel 5.4 kW passive CBC system is established by an all-optical feedback loop.

[1] A. Tünnermann, T. Schreiber, F. Röser, A. Liem, S. Höfer, H. Zellmer, S. Nolte, J. Limpert, J. Phys. B 38, S681-S693 (2005).
[2] J. Limpert, F. Röser, S. Klingebiel, T. Schreiber, C. Wirth, T. Peschel, R. Eberhardt, and A. Tünnermann, IEEE J. Sel. Top. Quantum Electron. 13(3), 537-545 (2007).
[3] T. Y. Fan, IEEE J. Sel. Top. Quantum Electron. 11(3), 567-577 (2005).

Optical fiber methods for deep brain calcium signal measurements in behaving mice

Zhongyang Qi,[1,2] Jingfeng Zhou,[3,4]Qiru Feng,[4]Rui Lin,[4],QingchunGuo[1,2]Hui Gong,[1,2] Qingming Luo,[1,2]Shaoqun Zeng,[1,2]Minmin Luo,[4,5] Ling Fu[1,2,*]

[1]Britton Chance Center for Biomedical Photonics, Wuhan National Laboratory for Optoelectronics-Huazhong University of Science and Technology, Wuhan 430074, China
[2]MoE Key Laboratory for Biomedical Photonics, Department of Biomedical Engineering, Huazhong University of Science and Technology, Wuhan 430074, China
[3]PTN Graduate Program, School of Life Sciences, Peking University, Beijing 100081, China
[4]National Institute of Biological Sciences, Beijing 102206, China
[5]School of Life Sciences, Tsinghua University, Beijing 100084, China
**Correspondence: lfu@mail.hust.edu.cn*

Dysfunctions of many nuclei in the brain (striatum, thalamus, amygdala etc.) are associated with highly prevalent mental diseases such as Parkinson‘s disease and Alzheimer’s disease. It is of prime importance to uncover the fundamental behavioral functions and mechanisms of these nuclei that underlie conditions of both health and disease in model animals. Optical calcium imaging is a powerful tool to record neural activity indicated by calcium transients both *in vitro* and *in vivo*, but its imaging depth is restricted within 1 mm due to the high scattering and absorption of biological tissues. Deep brain function researches requires modification of existed optical detection method. Relaying the deep brain calcium signals to the surface with optical fibers is an efficient approach to extend the *in vivo* optical detection methods. Here, we implemented two optical fiber based methods for deep brain calcium signal measurements in behaving mice: a multichannel fiber photometry and a GRIN lens based confocal microscope [1,2].

1. Q.Guo, J. Zhou, Q. Feng, R. Lin, H. Gong, Q. Luo, S. Zeng, M. Luo, L. Fu, Multi-channel fiber photometry for population neuronal activity recording, Biomedical Optics Express, 6(10): 3919-3931 (2015).
2. Yi Li, W.Zhong, D. Wang, Q. Feng, Z. Liu, J. Zhou, C.Jia, F. Hu, J. Zeng, Q.Guo, L. Fu, M. Luo, Serotonin neurons in the dorsal raphe nucleus encode reward signals, Nature Communications, 7: 10503(2016).

Monitoring of Anesthesia Depth by Near-Infrared Spectroscopy

D. Choi[1*], J. Bae[1*], S. Kim[1*], J. G. Kim[1]

1-Department of Biomedical Science and Engineering, Institute of Integrated Technology, Gwangju Institute of Science and Technology, 123 Cheomdan-gwagiro, Buk-gu, Gwangju, 61005 The Republic of Korea

** These authors contributed equally in this study*

jaekim@gist.ac.kr

Anesthesia level during a general surgery must be maintained properly to prevent an awakening during surgical performance. Currently, bispectral index (BIS) is the most popular device to monitor the depth of anesthesia by processing electroencephalogram (EEG) signals. However, there are cases that BIS may not provide an accurate level of anesthesia depth when patients show abnormal EEG signals [1]. Near-infrared spectroscopy (NIRS) provides concentrations of oxy- (OHb), deoxy- (RHb), total (THb) hemoglobin in tissue, which are surrogates of neuronal activities [2]. This study employs NIRS to see its potential as an anesthesia depth monitoring device by collecting cerebral hemodynamic signals during anesthesia.

Our near-infrared spectroscopy system consists of a tungsten-halogen lamp, a NIR range spectrometer and a pair of fiber-optic patch cables. A spectrum in the range of 730-850 nm were acquired at 3 Hz and a modified Beer-Lambert's law was used to calculate the changes of OHb, RHb and THb concentration. In order to measure the NIR signals from the brain, we established a surgical rat model [3]. Two hand made optodes were implanted onto the rat's skull. Each position of optode corresponds to right and left frontal cortex.

Two anesthetic agents, isoflurane and ketamine, were administered to animals (Sprague-Dawley rat, ~500g). For those animals with isoflurane anesthesia underwent the variation of isoflurane concentration from 2.5% to 0% with a step of 0.5% after 20min of baseline measurement (awake). Anesthesia of other animals was induced by 10 min of ketamine administration (10mg/kg/min) via common jugular vein and was maintained by additional 10 min of ketamine infusion (4mg/kg/min).

The results from isoflurane anesthesia showed that OHb and THb initially increased at the time of anesthesia induction (3% isoflurane). As the isoflurane concentration drops, OHb and THb also decreased accordingly. Ketamine administration caused a rapid increase of OHb and decrease of RHb followed by opposite changes of both OHb and RHb during 10 min of 10mg/kg/min ketamine infusion. The level of OHb and RHb were maintained during 4mg/kg/min of ketamin infusion. OHb then increased once ketamine infusion stopped and decreased as animals awake.

NIRS measurements showed that cerebral hemodynamic signals change depending on anesthesia level. Isoflurane anesthesia depth can be potentially correlated with OHb signal, but there is no clear correlation between the anesthesia depth from ketamine and hemodynamic signals. One common thing that has been found from both anesthetic agents studies is an increase of OHb before animals start to awake. This has a potential of NIRS in early prediction of awakening from anesthesia and further studies are required to concrete the use of NIRS in anesthesia depth monitoring.

[1] L. T. D. Duarte and R. Â. Saraiva, "When the bispectral index (bis) can give false results," Revista brasileira de anestesiologia, 59, 99-109 (2009).

[2] A. T. Lovell, H. Owen-Reece, C. E. Elwell, M. Smith, and J. C. Goldstone, "Continuous measurement of cerebral oxygenation by near infrared spectroscopy during induction of anesthesia," Anesthesia & Analgesia, 88, 554-558 (1999).

[3] D. Choi, T. J. Shin, S. Kim, J. Bae, D. Cho, J. Ham, J, Park, H. Kim, S. Jeong, B. Lee, J. G. Kim, " The monitoring of cerebral oxygenation and local field potential with a variation of isoflurane concentration in a rat model," Biomedical Optics Express, 7(10), 4114-24 (2016).

Functional Near Infrared Spectroscopy as a Clinical Diagnostic Tool

Beop-Min Kim, Ph.D.
School of Biomedical Engineering, Korea University

Abstract

In recent years, optical technologies have grown in importance for their role as a clinical diagnostic tool. Functional near-infrared spectroscopy (fNIRS) is an example of one optical technique that utilizes non-ionizing near infrared light to detect hemodynamic changes (i.e. oxygenated, deoxygenated, and total hemoglobin changes) noninvasively. The parameter of hemodynamic changes has value in understanding the functional behavior of the brain by way of neurovascular coupling. For this purpose, our work has largely focused on applying high density fNIRS probes in order to detect hemodynamic changes in healthy subjects and patients, and also visualizing the hemodynamic changes in real time. Our high density fNIRS probe have been used in clinical studies to understand the impairment of cerebral autoregulation for patients with orthostatic intolerance as they perform the Valsalva Maneuver and Tilt Table task. In addition, we have explored the use of fNIRS for the diagnosis of ADHD and also as an intraoperative monitoring tool for cerebral diseases such as Moyamoya.Finally, we have worked on building a real-time hemodynamic visualization method based on the probabilistic path of light propagation within the tissue to accurately model a volumetric image of cerebral hemodynamic changes.

Brain Activations Associated with Online Video Game Playing: A Functional Near Infrared Spectroscopy Study

Yue Li[1,2], Lei Zhang[1], Ke-hong Long[2], Hui Gong[1], Hao Lei[1,2]

1- Wuhan National Laboratory for Optoelectronics, Huazhong University of Science and Technology;
2- State Key Laboratory of Magnetic Resonance and Atomic and Molecular Physics, Wuhan Institute of Physics and Mathematics, Chinese Academy of Sciences
leihao@wipm.ac.cn

Video games are played for recreation, entertainment, training and rehabilitation purposes, and even as a sport. Appropriate video game playing can improve a broad range of brain functions [1], while excessive video game playing or exposure to improper game content may have serious negative effects such as online game addiction (OGA) [2,3]. Neuroimaging studies have demonstrated that video game playing induces functional and structural plasticity of the brain, especially in the rewarding network and fronto-parietal executive network (FPEN)[4, 5].The mechanisms underlying video game playing-inducedplastic brain changes remain unclear, and might be related to the tonic/phasic activation or inhibition of the affected brain regions during playing, such as the nucleus of accumbens and dorsolateral prefrontal cortex(DLPFC) [6].

Functional near infrared spectroscopy (fNIRs) has been used to monitor hemodynamic changes in the prefrontal cortex (PFC) andtemporal gyrus associated with video game playing [7]. In this study, fNIRs was used to record real-time hemodynamic changes in the PFC of subjects playing a massively multiplayer online battle arena (MOBA) video game, League of Legends (LOL), under naturalistic conditions.Twenty four experienced LOL players were recruited. The subjects played one round of matching mode LOL game, wearing a home-made fNIRS device[8]. An event-related analysis approach [9] was used to track the time-locked hemodynamic responses specific to variousgame events, such as slaying an enemy, being slain and destroying a turret.

The game onset was found to be associated with activations in the ventral lateral prefrontal cortex(VLPFC), and concomitant deactivations in the DLPFC and prefrontal pole. On top of such tonic responses, the VLPFC and DLPFC also showed time-locked hemodynamic changes specific to the game events. It appeared that the VLPFC activities were associated with processing of multi-sensory stimuli from the game, while the dynamic activities of the DLPFC might have reflected the constant shifts of attention and affection states during playing. The results of this study demonstrated the feasibility of using fNIRs as a toolto monitor real time PFC activities associated with immersive interactivity during video game playing under naturalistic settings.

[1] Shams, T.A., Foussias, G., Zawadzki, J.A., Marshe, V.S., Siddiqui, I., Muller, D.J., Wong, A.H., The effects of video games on cognition and brain structure: Potential implications for neuropsychiatric disorders, Curr Psychiatry Rep, 17, 71, (2015).
[2] Lin, F., Zhou, Y., Du, Y., Qin, L., Zhao, Z., Xu, J., Lei, H., Abnormal white matter integrity in adolescents with internet addiction disorder: a tract-based spatial statistics study, PLoS One , 7, e30253, (2012).
[3] Pujol, J., Fenoll, R., Forns, J., Harrison, B.J., Martinez-Vilavella, G., Macia, D., Alvarez-Pedrerol, M., Blanco-Hinojo, L., Gonzalez-Ortiz, S., Deus, J., Sunyer, J., 2016. Video gaming in school children: How much is enough? Ann Neurol, 80, 424-433, (2016).
[4] Kuhn, S., Lorenz, R., Banaschewski, T., Barker, G.J., Buchel, C., Conrod, P.J., Flor, H., Garavan, H., Ittermann, B., Loth, E., Mann, K., Nees, F., Artiges, E., Paus, T., Rietschel, M., Smolka, M.N., Strohle, A., Walaszek, B., Schumann, G., Heinz, A., Gallinat, J., Consortium, I., Positive association of video game playing with left frontal cortical thickness in adolescents, PLoS One,9, e91506, (2014).
[5] Takeuchi, H., Taki, Y., Hashizume, H., Asano, K., Asano, M., Sassa, Y., Yokota, S., Kotozaki, Y., Nouchi, R., Kawashima, R., Impact of videogame play on the brain's microstructural properties: cross-sectional and longitudinal analyses, Mol Psychiatry, 21, 1781-1789, (2016).
[6] Steven W. Cole, D.J.Y., Brian Knutson, Interactivity and reward-related neural activation during a serious videogame, PLoS One, 7, e33909-e33909, (2012).
[7] Ono, Y., Nomoto, Y., Tanaka, S., Sato, K., Shimada, S., Tachibana, A., Bronner, S., Noah, J.A., Frontotemporaloxyhemoglobin dynamics predict performance accuracy of dance simulation gameplay: Temporal characteristics of top-down and bottom-up cortical activities, Neuroimage, 85, 461-470, (2014).
[8] Zhang, Z., Sun, B., Gong, H., Zhang, L., Sun, J., Wang, B., Luo, Q., A fast neuronal signal-sensitive continuous-wave near-infrared imaging system, Rev SciInstrum, 83, 094301, (2012).
[9] Cavanagh, J.F., Castellanos, J., Identification of canonical neural events during continuous gameplay of an 8-bit style video game, Neuroimage, 133, 1-13, (2016).

Skull optical clearing for accessing to cerebral hemodynamics

Dan Zhu

Britton Chance Center for Biomedical Photonics, Wuhan National Laboratory for Optoelectronics
Key Laboratory of Biomedical Photonics of Ministry of Education, Department of Biomedical Engineering, Huazhong University of Science and Technology, Wuhan 430074, China

Email:dawnzh@mail.hust.edu.cn

The tissue optical clearing technique could significantly enhance the biomedical optical imaging depth, but current investigations are mainly limited to in vitro studies. *In vivo* tissue optical clearing method should be enough rapid, transparent and safe, which makes it more difficult, especially, for hard tissue. During the past years, we developed skull optical clearing methods for *in vivo* cortical imaging. This presentation will report recent progress in skull optical clearing method. The skull optical clearing method is proved to be effective for adult mice in different ages and permit various imaging techniques to monitor cortical blood flow, blood oxygen, and vascular with high resolution and contrast, not only for local cortex, but also for whole cortex. The long-term and short-term observation show that there is no obvious effect on cortical vascular function when laser speckle contrast imaging and hyperspectral imaging are used to repeatedly image the cortical blood flow, blood oxygen. Finally, we will demonstrate some applications for physiological or pathological situation, including monitoring the anoxia, drug-induced cortical response, et al.

[1] Xiaoquan Yang, ang Zhang, Kai Zhao, Yanjie Zhao, Yanyan Liu, Hui Gong, Qingming Luo*, and Dan Zhu*, Skull optical clearing solution for enhancing ultrasonic and photoacoustic imaging, IEEE Transactions on Medical Imaging, 35(8): 1093-1096 2016

[2] Jing Wang, Yang Zhang, Pengcheng Li, Qingming Luo, Dan Zhu*, Review: Tissue Optical Clearing Window for Blood Flow Monitoring, IEEE Journal of Selected Topics in Quantum Electronics, 20(2): 6801112, 2014

[3] Dan Zhu, Kirill V. Larin, Qingming Luo, and Valery V Tuchin, Recent progress in Tissue optical clearing, Laser & Photonics Reviews, 7(5), 732-757, 2013.

[4] Jing Wang， Yang Zhang，Tonghui Xu，Qingming Luo，Dan Zhu*，An innovative transparent cranial window based on skull optical clearing，Laser Physics Letters 9(6), 469-473, 2012

Laser-assisted deposition of colloidal nanoparticles forcreation fractal bimetallic structures

A.O. Kucherik[1], D.N. Bukharov[1], S.M. Arakelyan[1], S.V. Kutrovskaya[1,2], A.V. Osipov[1], A.V. Istratov[1], T.A. Vartanyan[3], T.E. Itina[4] andA.V. Kavokin[2,5,6,7]

[1] Stoletovs Vladimir State University, Vladimir, Russia, 600000,
[2]Russian Quantum Center, Novaya 100, 143025 Skolkovo, Moscow Region, Russia
[3]ITMO University,St. Petersburg, Russia, 197101,
[4]Université de Lyon, UJM-Saint-Etienne, CNRS, UMR5516, Laboratoire Hubert Curien, F-42023, Saint-Etienne, France
[5]School of Physics and Astronomy, University of Southampton, SO17 1 BJ, Southampton, United Kingdom
[6]Spin Optics Laboratory, St. Petersburg State University, St. Petersburg 198504, Russia
[7]CNR-SPIN, Viale del Politecnico 1, I-00133, Rome, Italy
[a)]Corresponding author:kucherik@vlsu.ru

E-mail: kucherik@vlsu.ru

Efficient synthesis of thin films with controlled optical and electrical properties is a key issue in modern laser nanotechnologies. Laser-assisted deposition of the colloidal particles on glass substrate represents, furthermore, a promising solution to this challenging problem. The optical and electronic properties of these films strongly depend not only on the composition of the film but also on its morphology. In the case of the structures composed of nanoparticles, such parameters as spacing and ordering of nanoparticles govern the local field enhancement in various discrete modes or even in a wide spectral rang. Furthermore, if the spacing between nanoparticles is comparable with their sizes, optical properties of the random structures can considerably differ from those of the ordered ones. In the case of the thin bimetallic films, one can expect even richer properties.

In our experiment, gold and silver particles were formed as a result of CW laser irradiation of a target in water [1]. We have used the pump power of 30 W, the laser spot diameter was of 100 µm. The target was scanned by a laser beam with a velocity of 100 µm/s; the total exposure time was 30 min. After laser irradiation, the solution was exposed to an ultrasound for 10 min and then separated on a CM-6M centrifuge. The particle sizes in the colloidal solution was investigated by the dynamic light scattering method with a Horiba LB-550 particle-size analyzer. The nanoparticles realized in this way appear to have sizes in the range from 5 to 10 nm. A mixture of silver and gold colloidal solution with the weight ratio of 1:1 was prepared by vigorous stirring.

For the deposition of nanoparticles from the obtained solutions, Ytterbium fiber laser with the wavelength of 1.06 µm, the pulse duration of 100 ns, the repetition rate of 20 kHz, and laser pulse energy up to 1mJwas then used. The diameter of the laser beam at the focal plane was 5 µm. KV8 glass substrate was placed in a cuvette with the nanoparticle solution. Typically, the nanoparticle deposition was realized by scanning the laser beam along the same direction 5 to 25 times. The scanning speed varied from 0.3 mm/s to 1.2 mm/s. We have used KV8 glass substrates (Fig. 1).

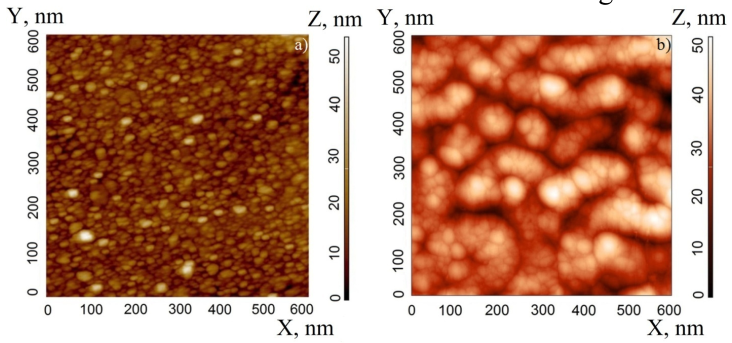

FIGURE 1. AFM images of bimetallic nanostructures deposited at the laser power of 2.5W (a) after 25 passages with the scanning speed of 1.2mm/s; and (b) after 18 passages with a scanning speed of 0.6 mm/s.

[1] S. M. Arakelyan, V. P. Veiko, S. V. Kutrovskaya, A. O. Kucherik, A. V. Osipov, T. A Vartanyan., T. E. Itina J Nanopart Res (2016) 18:155. DOI 10.1007/s11051-016-3468-0.

Milligram-per-Second Femtosecond Laser Production of Se Nanoparticle Inks and Ink-Jet Printing of Anti-Bacterial and Sensing Nanophotonic 2D-Patterns

Andrey Ionin,[1] Anastasia Ivanova,[1,2] Roman Khmel'nitskii[1], Yury Klevkov,[1] Sergey Kudryashov,[1,2,3] Alexey Levchenko,[1] Nikolay Mel'nik,[1] Alena Nastulyavichus,[1] Andrey Rudenko,[1] Irina Saraeva,[1] Nikita Smirnov,[1] Dmitry Zayarny,[1] Sergey Gonchukov,[2] Eteri Tolordava,[4] Anatoly Baranov[5]

1- Lebedev Physical Institute, Leninsky prospect 53, 119991 Moscow, Russia
2 - National research nuclear university MEPhI (Moscow Engineering Physics Institute), Kashirskoe shosse 31, 115409 Moscow, Russia
3 - ITMO University, Kronverkskiy prospect 49, 197101 St. Peterburg, Russia
4 - N.F. Gamaleya Federal Research Centre of Epidemiology and Microbiology, Gamalei street 18, 123098, Moscow, Russia
5 - M.V. Lomonosov Moscow State University, Universitetskaya ploschad' 1, 119899 Moscow, Russia

e-mail: *aion@sci.lebedev.ru*

Milligram-per-second production of selenium nanoparticles in water sols was realized through 6-W, MHz-rate femtosecond laser ablation of a solid selenium pellet. High-yield particle formation mechanism and ultimate mass-removal yield were elucidated by optical profilometry and scanning electron microscopy characterization of crater depths and topographies. Deposited particles were inspected by scanning electron microscopy, while their hydrosols (nanoinks) were characterized by optical transmission, Raman and dynamic light scattering spectroscopy. Anti-bacterial selenium patterns and coatings were ink-jet printed on thin supported silver films and their bare silica glass substrates, characterized by electron microscopy and energy-dispersive x-ray spectroscopy, and were successfully tested regarding viability of antibiotic-resistant *Staphylococcus aureus* and *Pseudomonas aeruginosa* bacteria in their biofilms (Fig. 1). Selenium nanoparticles with their high refractive index in the visible/near-IR ranges were demonstrated as promising all-dielectric sensing building nanoblocks in nanophotonics.

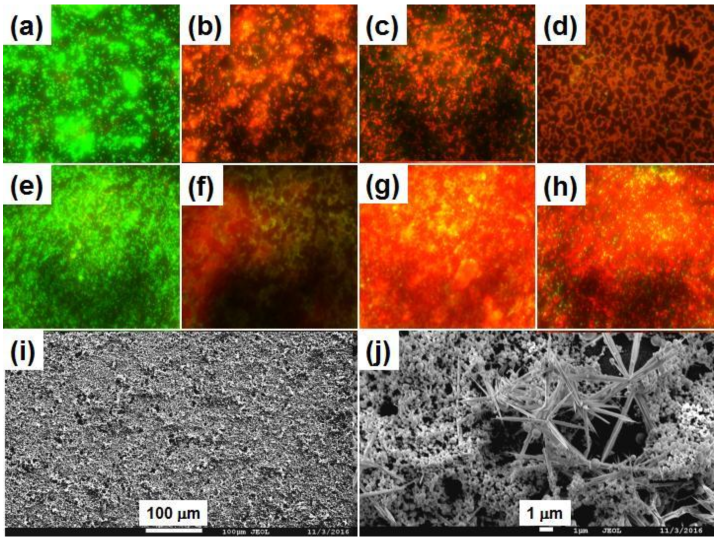

Fig. 1. Optical images of assays of live (a,e) and dead (b-d,f-h) cells in biofilms of *Staphylococcus aureus* (a-d) and *Pseudomonas aeruginosa* (e-h): (a,e) bare silica-glass slide; (b,f) silver film on the glass slide; (c,g) Se-coated silver film on the glass slide; (d,h) Se-coated glass slide (the instrumental magnification – 600x). (i,j) Typical topographies of the ink-jet Se-NP coatings on the supported silver films at low and high FESEM magnification with trace amounts of re-crystallized t-Se nanowires.

This research was supported by the Russian Science Foundation (Project no. 15-19-00208).

Photolytic formation of NV centers in diamond

V.V. Kononenko, V.M. Gololobov, T.V. Kononenko, T.A. Semenov, I.I. Vlasov, A.A. Khomich, V.A. Shershulin and V.I. Konov

General Physics Institute of RAS, 38 Vavilova str., Moscow, Russia

vitali.kononenko@nsc.gpi.ru

Laser-induced formation of nitrogen-vacancy defects in a chemical vapor deposition (CVD)-grown diamond monocrystal is reported in the preablation regime, when slow surface etching (< 10-4 nm/pulse), typically called nanoablation, occurs. The experiments prove that besides the well-known process of graphitization, which leads to a complete collapse of diamond lattice, laser-induced electronic excitation enables the photolytic formation of defects - a bond rearrangement of the point type.

Luminescence measurements confirm that during irradiation by 266-nm femtosecond pulses, the nitrogen-vacancy concentration grows logarithmically and can increase tenfold until it reaches saturation. This process is shown to be accompanied by a progressive decrease in surface reflectance attributed to Frenkel pair generation. Neither surface ablation nor diamond graphitization in the irradiated zone are found. The relationship between the coloration of the diamond and the nanoablation of its surface as well as the possible mechanisms of the photolytic reconfiguration of bonds in the diamond are discussed.

The results indicate femtosecond laser nanoablation to be a promising tool for a precise control of the number of produced vacancies in the lattice and, hence, for managing the probability of formation of an individual NV center in the desired place of a crystal. Besides practical significance, this study gives new insight into laser-induced processes in diamond, considering the point defect creation as a preliminary stage of accumulative graphitization and nanoablation.

Pulsed Laser Nanofabrication of Advanced Nanophotonic Structures

Yu.Kulchin[1], O. Vitrik[1,2], A. Kuchmizhak[1,2]

1- Institute of Automation and Control Processes (IACP), Far Eastern Branch of Russian Academy of Science (FEB RAS), 5 Radio Str., Vladivostok 690041, Russia

2- School of Natural Sciences, Far Eastern Federal University (FEFU), 8 Sukhanova str., Vladivostok 690041, Russia

kulchin@iacp.dvo.ru

Direct ablative laser nanofabrication using tightly focused short and ultrashort laser pulses emerges as a versatile, high-performing, inexpensive, scalable and green technology for designing and fabricating different functional nanotextures readily applied for various applications ranging from chemo- and biosensing to nonlinear optics. In this presentation, we overview our resent finding concerning fabrication of various functional nanostructures on the surface of noble metal films covering heat-insulating substrates. In particular, formation of parabola-shaped surface nanovoids was demonstrated under precise ablation of 50-nm thick Au of Ag films on a glass substrate at pulse energies below the film ablation threshold, with the geometrical shape and dimensions being well controlled by the only parameter, applied pulse energy. The comprehensive 3D molecular dynamic calculations were performed to model the evolution of the molten material via translative hydrodynamic flows [1]. Moreover, such structures were shown to generate structural colors in the polarization-resolved dark-field observation mode via tunable size-dependent plasmon-mediated scattering [2], making the direct laser-based approach promising for plasmonic color painting at lateral resolution reaching *20000 dpi*.
Similarly, single-shot ablation of thermally thin noble-metal films with nanosecond laser pulses followed by subsequent polishing with accelerated Ar-ion beam was shown to provide formation of various isolated plasmonic structures as nanorings, nanorods and nanoring-nanorod ensembles [3]. Furthermore, by controlling the nitrogen doping level of the metal film during its magnetron deposition in the appropriate gaseous environment,we recently demonstrated the formation of similar nanotextures having porous internal structure. The porosity of the fabricated nanotextures was shown to be controlled by the nitrogen doping level of the metal film as well as by the pulse energy applied.
Nanotexturing of *thermally thick* silver films with the femtosecond laser pulses was shown to provide a versatile way for designing surface nanotopography at nano- and microscale level [4]. At pulse energies slightly exceeding the film spallation threshold, the laser pulses appear to produce a nanotextured crater, while at higher energies, the single micro-sized jet appears at the crater center. The spalling nanotextured craters provide significant plasmon-mediated enhancement of the incident optical radiation, emerging as a cheap substrate for routine biosensing and bioidentification tasks utilizing surface-enhanced photoluminescence and surface-enhanced Raman scattering approaches.
Finally, ablation of silver films with nanosecond vortex pulses, generated by passing circular-polarized Gaussian-shape pulses through an*s-waveplate*, was shown to twist transiently molten material producing chiral nanoneedles of various shape and size [5]. We explained the chiral shape of the nanoneedles by the characteristic spiral-shape intensity distribution appeared as a result of interference of the incident donut-shape vortex beam with its distorted reflected replica, which drive spiral thermocapillary flow of the molten film. Such direct laser technique provides the unique opportunity to fabricate plasmonic chiral needles promising for nonlinear photonic applications.

[1] X.W. Wang, A.A. Kuchmizhak, X. Li, S. Juodkazis, O.B. Vitrik, Yu. N. Kulchin, V.V.Zhakhovsky, P.A. Danilov, A.A. Ionin, S.I. Kudryashov, A.A. Rudenko, N.A.Inogamov, Laser-induced Translative Hydrodynamic Mass Snapshots: mapping at nanoscale, arXiv preprint arXiv:1703.06758 (2017).
[2] A. Kuchmizhak, O. Vitrik, Yu. Kulchin, D.Storozhenko, A. Mayor, A.Mirochnik, S. Makarov, V. Milichko, S. Kudryashov, V.Zhakhovsky, N.Inogamov, Laser printing of resonant plasmonic nanovoids, Nanoscale 8 (24), 12352-12361 (2016).
[3] A. Kuchmizhak, S. Gurbatov, O. Vitrik, Y. Kulchin, V. Milichko, S. Makarov, S. Kudryashov, Ion-beam assisted laser fabrication of sensing plasmonic nanostructures, Scientific Reports 6, 19410 (2016).
[4] A. Kuchmizhak, E. Pustovalov, S.Syubaev, O. Vitrik, Y. Kulchin, A. Porfirev, S.Khonina, S. Kudryashov, P. Danilov, A. Ionin, On-fly femtosecond-laser fabrication of self-organized plasmonic nanotextures for chemo-and biosensing applications, ACS Applied Materials & Interfaces 8, 24946-24955 (2016).
[5] S.Syubaev, A.Zhizhchenko, A. Kuchmizhak, A.Porfirev, E.Pustovalov, O. Vitrik, Yu. Kulchin, S.Khonina, S. Kudryashov, Direct laser printing of chiral plasmonic nanojets by vortex beams, Optics Express 25(9), 10214-10223 (2017).

Periodically poled MgO doped $LiNbO_3$ and $LiTaO_3$ for coherent light frequency conversion

V.Ya. Shur[1,2], A.R. Akhmatkhanov[1,2], I.S. Baturin[1,2], D.S. Chezganov[1,2], M.A. Chuvakova[1], A.A. Esin[1]

1-School of Natural Sciencesand Mathematics, Ural Federal University, Ekaterinburg, Russia
2-Labfer Ltd., Ekaterinburg, Russia

shur@labfer.ru

The lithiumniobate$LiNbO_3$(LN)and lithium tantalate$LiTaO_3$(LT) crystals with tailored periodically poled domain structures (PPLN and PPLT) produced with nanoscale period reproducibility have been used for second harmonic generation (SHG) and optical parametric oscillation (OPO) based on quasi-phase-matched nonlinear optical wavelength conversion [1]. The domain patterning in MgO:LN and MgO:LT is realized at elevated temperature by electric field pulses using metal electrodes. The study of the relaxation of abnormally high conductivity of charged domain walls allowed us to optimize the poling process [2]. The important role of the domain-domain interaction has been investigated in details [3].

The global domain kinetics during the poling process at elevated temperatures studied by *in situ* optical observation, allowed us to reveal the main characteristics of the poling process in MgO:LN at elevated temperature. The domain images revealed by chemical etching were visualized by optical and scanning probe microscopy. The optimized design of the electrode pattern was based on experimental results and computer simulation.The deep knowledge of the domain structure evolution at elevated temperatures and relaxation of the bulk conductivity of the charged domain walls in MgO:LN and MgO:LT allowed us to optimize the periodical poling technique and to produce high-fidelity domain patterns: (1) PPLN:MgO with period from 6.95 to 4.3 μm corresponding to green (532 nm) and blue (488 nm) light generation by first order SHG at the temperatures below 60°C. (2) The 1% MgO doped stoichiometric LT with period from 10.75 to 7.99 μm corresponding to green and yellow (589 nm) by first order SHG. The output power above 14 W has been achieved for CW generation of the yellow light. (3) The fan-out periodical domain structures in 3 mm thick MgO:LN wafers allowed to realize the widely tunable OPO generation in wavelength range from 2.5 to 4.5 μm for 1.053 μm pump and real aperture 2.5 mm.

2D distribution of SHG intensity, SHG efficiency, and quasi-phase-matching temperature have been evaluated by the automated testing setup. The good efficiency and uniformity was demonstrated. The comparison of the 2D distribution of SHG efficiency with domain structure revealed by selective chemicaletching on cross-section allowed us to reconstruct the domain kinetics in the bulk and to optimize the pulse parameters thus achieving working aperture > 0.4 mm for MgO:LN and > 0.8 mm for MgO:LT in 1 mm thick crystals.

The electron beam poling technique has been developed [4]. The creation of through periodical domain structure with period near 6.95μm and outstanding uniformity for green light generation was demonstrated. Formation of domain structures of arbitrary orientation by e-beam polingwas achieved. The successive periodical poling realized in soft proton exchange waveguides in LN allowed to obtain high SHG efficiency.

The equipment of the Ural Center for Shared Use “Modern nanotechnology” UrFU was used. The work was supported by Government of the RF (Act 211, Agreement 02.A03.21.0006).

[1] V.Ya. Shur, A.R. Akhmatkhanov, I.S. Baturin, Micro- and nano-domain engineering in lithium niobate, Appl. Phys. Rev., vol.2, p. 040604, (2015).
[2] V.Ya. Shur, I.S. Baturin, A.R. Akhmatkhanov, D.S. Chezganov, A.A. Esin, Time-dependent conduction current in lithium niobate crystals with charged domain walls, Appl. Phys. Lett., vol.103, p. 102905, (2013).
[3] A.V. Ievlev, S. Jesse, A.N. Morozovska, E. Strelcov, E.A. Eliseev, Y.V. Pershin, A. Kumar, V.Ya. Shur, S.V. Kalinin,Intermittency, quasiperiodicity and chaos in probe-induced ferroelectric domain switching, Nature Physics, vol.10, pp.59-66, (2014).
[4] V.Ya. Shur, D.S. Chezganov, A.R. Akhmatkhanov, D.K. Kuznetsov, Domain patterning by electron beam of MgO doped lithium niobate covered by resist, Appl. Phys. Lett., vol.106, p. 232902, (2015).

Disk lasers with multi-beam pumping

I.A. Shcherbakov, V.B. Tsvetkov

A.M. Prokhorov General Physics Institute RAS, 119991, Vavilov str., 38, Moscow, Russia.
e-mail: tsvetkov@lsk.gpi.ru

Application of active disks reduces thermally induced optical effects in powerful solid-state lasers significantly. The next step to improve the quality of output laser emission together with increasing of the output power may be done while using multi beam pumping. At this way we may choose two quite different directions. The first is the use of degenerate laser cavity configuration. In this case the cavity should be designed to cover in series of all the pumped areas in the active disk with intracavity beam and possesses a single channel for the output laser emission. The second way consists in the realization of phase synchronization of several laser channels with a cavity utilizing Talbot effect. In this case bright far-field pattern of a phase-locked microchip laser array may be obtained.

Experimental data concerning both ways of multi-beam pumping realization enables to discuss the possibility of application.

Current status of Kumgang laser: coherent 2 beam combination using pre-pulsed SBS-PCM at high power laser system

Hong Jin Kong[1], **Sangwoo Park**[1], **Sangwoo Park**[1], **Seongwoo Cha**[1], **Hwihyeong Lee**[1], **Seong Woong Choi**[2], **Jumsool Kim**[2], **and Bong Ju lee**[3]

1- Department of Physics, KAIST, 291 Daehak-ro, Yuseong-gu, Daejeon, Republic of Korea
2- Laser spectronix, Byucksan 6-406, Gasan-dong, Gumcheon-gu, Seoul 153-704, Republic of Korea
3-Department of AGEE, Handong Global University, 558 Handong-ro, Buk-gu, Pohang, Gyeongbuk 37554, Republic of Korea

Main author email address: hjkong@kaist.ac.kr

A high average power laser with high repetition rate and high output energy has various applications in the field of laser machining [1] and extreme ultraviolet (EUV) light generation for lithography [2]. However, it is difficult to achieve high average power with high repetition rate and high output energy for a bulk laser [3]. Coherent beam combining using stimulated Brillouin scattering phase conjugate mirror (SBS-PCM) is one of the most promising technique to realize the high average power laser with high energy and high repetition rate [3].
In the presentation, the authors will report a current status of the Kumgang laser system. Kumgang laser system is designed to create 4 kW (0.4 J @ 10 kHz / 10 ns) laser beam using SBS-PCM.

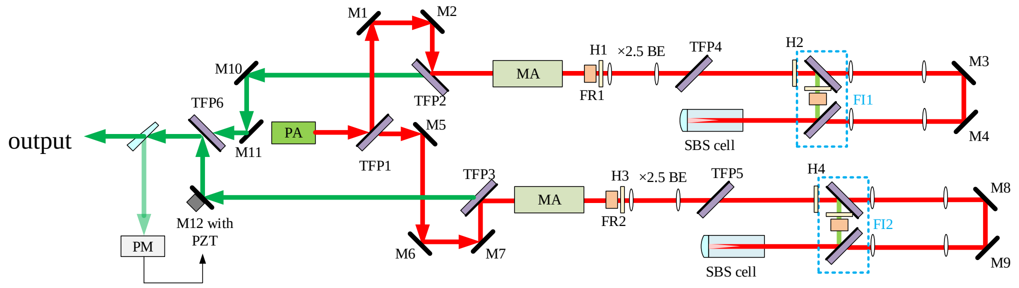

Figure 1. A schematic diagram of the coherent 2-beam combination system of the Kumgang laser using self-phase-controlled SBS-PCM. PA: Pre-amplifier, M1~M12: mirrors, TFP1~TFP6: thin film polarizer, FR1~FR2: Faraday rotator, H1~H4: half wave plate, FI1~FI2: Faraday isolator, PM, phase measurement equipment, PZT: piezoelectric transducer

Figure 1 shows a schematic diagram of the coherent 2-beam combination system of the Kumgang laser using self-phase-controlled (SPC) SBS-PCM.
The beam from the PA is split by thin film polarizer (TFP) 1. The sub-beams are reflected by mirrors and a TFP, and is amplified by MA. A Faraday rotator (FR) and a half wave plates (H) rotates the polarization of the beam from S-polarization to P-polarization. A beam expander (BE) expands the beam 2.5 times, and the beam passes through thin film polarizer to remove depolarization part. An H and a TFP are used to divide a pre-pulse and a main-pulse. The pre-pulse beam is reflected by TFP and passes through an H and a FR, and is reflected by a TFP. The main pulse beam is passes through TFP, mage relay lenses, and TFP sequentially. The pre-pulse makes an acoustic grating in the SBS cell and the main pulse is reflected by the acoustic grating. After the SBS reflection, the main pulse is returns back to MA and amplified once again. The polarization of the output beam is P-polarization, due to the double-pass of FR. The pre-pulse is blocked by FI therefore the pre-pulse does not amplified by MA. After the amplification, the main pulse transmits the TFP. The double-pass output beams are reflected by mirrors and combined at TFP6. The relative phase is measured by small signal divided from the combined beam and control piezoelectric transducer (PZT) to minimize long-term phase fluctuation. The detail of the experimental result will be presented at the conference.

[1] G. Raciukaitis, M. Brikas, P. Gecys, and M. Gedvilas, "Accumulation effects in laser ablation of metals with high-repetition-rate lasers," Proc. SPIE 7005, 70052L (2008).
[2] I.-Y. Park, S. Kim, J. Choi, D.-H. Lee, Y.-J. Kim, M. F. Kling, M. I. Stockman, and S.-W. Kim, "Plasmonic generation of ultrashort extreme-ultraviolet light pulses," Nat. Photonics 5, 677–681 (2011).
[3] H. J. Kong, S. Park, S. Cha, and M. Kalal, "Coherent beam combination laser system using SBS-PCM for high repetition rate solid-state lasers," Opt. Mater. (Amst). 35, 807–811 (2013).

Picosecond diode pumped lasers of high peak and average power

N.G. Mikheev, V.B. Morozov, A.N. Olenin, I.V. Tulin, D.I. Ustinov, D.V. Yakovlev

International Laser Center and Physics Faculty of M.V. Lomonosov Moscow State University, Moscow 119991, Leninskiye Gory

morozov@phys.msu.ru

Compact and energy effective picosecond lasers providing single pulse output of a few millijoules at reasonably high repetition rates within kilohertz, are claimed by a number of applications. Such as satellite and lunar laser ranging, material processing, driving photocathode of electronic accelerators, OPO pumping, time-resolved laser spectroscopy, etc. Most common approaches to designing picosecond laser systems imply stages of pulse generation and regenerative amplification. Dynamical operation control scheme utilizing pulsed repetitive pumping, active and passive mode-locking, negative feedback, adjustable loss level in the oscillator cavity and switching to regenerative amplification regime [1,2], provides laser pulse formation in each laser shot. It takes several microseconds on the end of pump pulse. This approach actually allows shortest way to obtain, just at the laser output, near Fourier transform limited picosecond pulses of more than one millijoule energy with good pulse-to-pulse stability and low optical jitter value [3]. Both oscillator and regenerative amplifier can be based on the same single active crystal. Using Fabry-Perot etalons inside oscillator cavity allows significant varying output pulse width which can take values from 15 (with Nd:YLF) or 25 ps (with Nd:YAG) and up to 300 ps.

Evolution of pulse energy, spectrum and time profile during a single generation cycle can be well illustrated using universal numerical calculation model [2] which describes pulse formation governed by the operation control and also taking into account the pulse profile modifying due to amplification.

Utilizing diode end-pump geometry allows maximal overlapping of resonator mode and pumped volume, whereby providing optimal pump conversion efficiency into output radiation. As a result, using the described picosecond Nd:YAG laser scheme with one addition amplifying stage provides 25 ps pulses of up to 4,2 mJ at fundamental wavelength and 20 ps pulses of up to 2,5 mJ at second harmonic with repetition rates within ~400Hz. Both laser and amplifier use diode end-pumping by means of fiber coupled laser diode arrays of 70 and 120 W maximum peak powers respectively. Owing to pulse regime and end-pump geometry, thermal loading is not high and the system does not require liquid cooling and can be easily power scalable by means of an additional amplification stage.

Further increase of output peak power and, respectively, single pulse energy by means of additional amplification stages implies operating near the saturation regime. However, saturation fluence value for Nd:YAG at pulse length of 20-30 ps is close to the damage threshold. Whereas, increase of the pump beam and laser mode diameter will result in reducing single pulse amplification, need for additional amplification trips and, finally, growth of reflective and diffraction losses and output falling.

At high repetition rates and, respectively, average power values, operation conditions strongly depend on thermal lens induced in the laser crystal [4]. Increase of average pump power at longitudinal geometry principally results in aberrational lens formation. Spherical part of the thermal lens may be compensated using usual spherical optics, whereas aberrational part action is more complex. Along with the irretrievable aberrational losses such a lens exhibits a certain adaptive effect that may maintain, to some extent, operation steadiness. An adequate analysis is required for system developing with laser generation mode of acceptable quality and, at the same time, supporting mode locking regime. Detailed experimental and modeling results will be presented.

[1] M.V.Gorbunkov, A.V.Konyashkin, P.V.Kostryukov, V.B.Morozov, A.N.Olenin, V.A.Rusov, L.S.Telegin, V.G.Tunkin, Yu.V.Shabalin, D.V.Yakovlev. Pulsed-diode-pumped, all-solid-state, electro-optically controlled picosecond Nd:YAG lasers. *Quantum Electron.*, **35** (1), 2-6 (2005).

[2] A.A.Karnaukhov, V.B.Morozov, A.N.Olenin and D.V.Yakovlev. *J. Phys.: Conf. Ser.* **414,** 012027 (2013).

[3] N.G.Mikheev, V.B.Morozov, A.N.Olenin, D.V.Yakovlev. Picosecond lasers with the dynamical operation control. *Proc.of SPIE*, **9917**, 99170A1-9 (2016).

[4] V.B.Morozov, A.N.Olenin, V.G.Tunkin, D.V.Yakovlev. Operation conditions for a picosecond laser with an aberration thermal lens under longitudinal pulsed diode pumping. *Quantum Electron.*, **41** (6), 508–514 (2011).

Technology and applications of kilowatt average power DPSSLs

T. Mocek

HiLASE Centre of Excellence, Institute of Physics, Za Radnici 828, 25241 Dolni Brezany, Czech Republic

mocek@fzu.cz

HiLASE is a new technological infrastructure in the field of application-oriented laser research and development, commissioned in 2015. The main mission of HiLASE is to serve as a bridge between the academic world and hi-tech industry. The Centre provides access to "next generation" laser technology in the form of fully diode pumped, solid state laser (DPSSL) architecture, much of it developed jointly with our strategic partner - Science & Technology Facilities Council (STFC) in UK. Our technology incorporates highly efficient laser emitting diodes to generate the intense light pulses that drive the laser amplifiers based on thin-disk and multi-slab architecture. This DPSSL technology brings a unique combination of high average power, high pulse repetition rate and high efficiency. It makes HiLASE the perfect facility "engine" for the new Centre of Excellence, bringing an unmatched opportunity for research excellence, technological innovation and industrial exploitation. Current status and prospects for major upgrades of the HiLASE facility will be presented.

PERLA-C is an in-house developed thin-disk laser platform generating pulses at 1030 nm with a width of <2 ps (FWHM) after compression, at a repetition rate of 50-100 kHz, and with pulse energies of up to 9 mJ. The average power of high quality (M^2 <1.7) and stable beam reached 500 W. Laser pulses are stretched and compressed by Chirped Volume Bragg Gratings. In addition, a picosecond parametric mid-IR source pumped by the thin-disk laser delivers up to 9 W signal and 5 W idler beam. The signal and idler tuning ranges are 1.7 – 1.95 μm and 2.2 – 2.6 μm, respectively. The output of PERLA-C was also successfully converted to 2nd, 3rd, 4th, and 5th harmonic frequency, respectively, with high conversion efficiency [1]. Recently, we demonstrated Yb:YGAG ceramic slab regenerative amplifier delivering 400 fs pulses at 1030 nm with spectral bandwidth of 4 nm at a repetition rate of 100 kHz.

"Bivoj" is a 100 J-level, diode-pumped solid-state laser system based on cryogenic gas-cooled, multi-slab ceramic Yb:YAG amplifier technology, installed at HiLASE. The system is a scaled-up version of DIPOLE (Diode Pumped Optical Laser for Experiments) laser, and has been developed at the Centre for Advanced Laser Technology and Applications (CALTA) of the STFC's Rutherford Appleton Laboratory in close collaboration with the HiLASE team. In December 2016, we demonstrated efficient and stable operation of the very first multi-joule DPSSL delivering 1 kW average power in 105 J, 10 ns pulses at 10 Hz, confirming the power scalability of multi-slab cryogenic gas-cooled amplifier technology [2].

DPSSL systems deployed at the HiLASE facility are available for external users for testing and/or prototyping of various laser technologies, joint projects, contract research and development, including laser induced damage threshold measurements, laser shock peening, mid-IR generation, micro-nanostructuring and processing of various materials. Examples of application experiments and recent results will be presented.

[1] O. Novák, H. Turčičová, M. Smrž, T. Miura, A. Endo, and T. Mocek, "Picosecond green and deep ultraviolet pulses generated by a high-power 100 kHz thin-disk laser," Opt. Lett. **41**, 5210-5213 (2016).

[2] P. Mason, M. Divoky, K. Ertel, J. Pilar, T. Butcher, M. Hanus, S. Banerjee, J. Phillips, J. Smith, M. De Vido, A. Lucianetti, C. Hernandez-Gomez, C. Edwards, T. Mocek, and J. Collier, "Kilowatt average power 100 J-level diode pumped solid state laser," Optica **4**, 438-439 (2017).

Exploring antiphase dynamics of an orthogonally-polarized dual-wavelength passively Q-switched Nd:YLF laser

<u>Hsing-Chih Liang</u> and Shun-An Gu

Institute of Optoelectronic Science, National Taiwan Ocean University, Keelung 20224, Taiwan

hcliang@email.ntou.edu.tw

Passively Q-switched (PQS) technique has been widely exploited to achieve compact diode-pump solid-state lasers due to high stability, inherent compactness, and low cost [1]. The laser medium with long fluorescence lifetime is highly desirable for continuously pumped passively Q-switched lasers to generate large-energy pulses. As the consequence, Nd:YLF crystal with long upper-state lifetime is appropriate for developing a high-pulse-energy pulsed laser. On the other hands, orthogonally polarized dual-wavelength lasers have attracted much attention for applications such as material process, precision measurement, biomedical instrumentation, optical navigation, and laser interferometry [2]. Recently, we have reported a dual-wavelength self-mode-locked (SML) Nd:YLF laser with orthogonally polarized simultaneous emission at 1047 nm and 1053 nm in a simple concave-plano cavity without any additional optical element [3]. In this work, we extend this technique to demonstrate an orthogonally-polarized dual-wavelength passively Q-switched Nd:YLF laser. At the optimizing PQS operation, the maximum average output power of 0.97 W is achieved under a pump power of 14 W. The total pulse energy was calculated to be 115 μJ and the peak power was 8.2 KW. Furthermore, we have experimentally observed that the stable output pulse trains exhibited complex antiphase dynamics which was attributed to the mode coupling of the two spectral modes. In addition, the ratio between repetition rates at 1053 nm and 1047 nm was experimentally found to be a fraction depending on the pump power. With the modified multimode rate equations, the phenomenon of complex antiphase dynamics was theoretically analyzed.

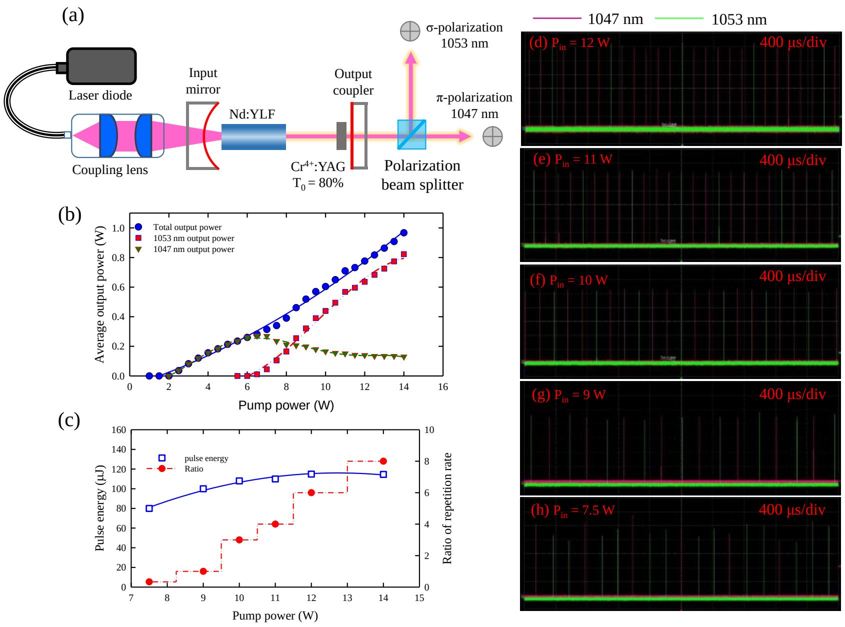

Fig. 1 (a) The experimental setup of the orthogonally polarized dual-wavelength passively Q-switched Nd:YLF laser; (b) the average output power for π- and σ-polarization states and the total output power versus the pump power; (c) dependence of ratio of repetition rate and pulse energy; (d) – (h) oscilloscope trace of π- and σ-polarization states for different pump power.

[1] A. Agnesi, S. Dell's Acqua, C.Morello, G. Piccinno, G. C. Reali, Z. Sun, Diode-pumped neodymium lasers repetitively Q-switched by Cr^{4+} :YAG solid-state saturable absorbers, IEEE J. Sel. Top. Quantum Electron., vol. 3, pp. 45-52, (1997).
[2] S. L. Zhang, Y. D. Tan, and Y. Li, Orthogonally polarized dual frequency lasers and applications in self-sensing metrology, Meas. Sci. Technol. 21, 054016, (2010).
[3] H. C. Liang and C. S. Wu, Diode-pumped orthogonally polarized self-mode-locked Nd:YLF lasers subject to gain competition and thermal lensing effect, Opt. Express, vol. 25, pp. 13697-13704, (2017).

Creation and improvement of tissue optical windows for laser probing and treatment using immersion optical clearing

Valery V. Tuchin

Saratov National Research State University

Institute of Precision Mechanics and Control RAS, Saratov

National Research Tomsk State University, Russia

Immersion optical clearing method is developed to enhance laser probing and treatment of living tissues and organs by creation of new and modifying well identified tissue optical windows [1-5]. The method is based on controllable and reversible modification of tissue optical properties by their impregnation with biocompatible optical clearing agents (OCAs). The enhancement of laser probing depth and image contrast for different human and animal tissues will be demonstrated using collimated transmittance of tissue layers, OCT, photoacoustic microscopy, two-photon autofluorescence, SHG and Raman microscopies, polarization and speckle imaging. Experimental data on diffusivity and permeability of glucose, glycerol, PEG, Omnipaque™ (x-ray contrast) and other optical clearing agents applied to normal and pathological tissues will be presented. Water transport and modification of tissue elastic properties under OCA action such as reversible dehydration and shrinkage, balance of free and bound water will be analyzed. Perspectives of application of immersion optical clearing method to improve weak luminescence from upconversion nanoparticles deeply inserted into living tissue and to detect Cherenkov's fluorescence excited by free electrons or protons in tissue depth will be also discussed.

References:

1. D. Zhu, K. V. Larin, Q. Luo, and V. V. Tuchin, "Recent progress in tissue optical clearing," *Laser Photonics Rev*. **7**(5), 732–757 (2013).
2. V.V. Tuchin, "*In vivo* optical flow cytometry and cell imaging," *Rivista Del Nuovo Cimento*, **37**(7), 375–416 (2014).
3. E. A. Genina, A. N. Bashkatov, Yu. P. Sinichkin, I. Yu. Yanina, V.V. Tuchin, "Optical clearing of biological tissues: prospects of application in medical diagnostics and phototherapy [Review]," *J. Biomed. Photonics & Eng*. **1**(1), 22–58, 2015.
4. V.V. Tuchin, "Tissue optical clearing: New prospects in optical imaging and therapy," in *BioPhotonics, IEEE International Conference,* pp.1-10, 20-22 May 2015; doi: 10.1109/BioPhotonics.2015.7304023.
5. V. V. Tuchin, "Polarized light interaction with tissues," *J. Biomed. Opt*. **21**(7), 071114-1-37 (2016).

Detection of circulating tumor DNA with closed-loop PCR-based Surface Plasmonic Resonance Sensor

W. Na[1], J. Kim[1], D. Jang[2], C. H. Lee[1], C. Seo, S. Shin[1,2]

1- Department of Mechanical Engineering, Korea University, Seoul, Republic of Korea
2- nano-Biofluignostic Engineering Researcg Center, Korea University, Seoul, Republic of Korea

lexerdshin@korea.ac.kr

Circulating tumor DNA (ctDNA) has been demonstrated as the most promising biomarker for non-invasive assessment of cancer as well as the most accurate predictor of cancer treatment responses. However, there are several hundreds of tumor DNAs even for one organ cancer (i.e., Lung cancer) and thus multiplexing is highly required for cancer detection from blood. The conventional techniques have been faced critical limits including multiplexing and cost and innovative technologies are highly required. Here, we present a stable and selective assay for detecting epidermal growth factor receptor (EGFR) mutations in plasma (or liquid biopsy) using DNA-DNA hybridization and Au nanoparticle probe with a lab-made surface plasmon resonance (SPR) sensometry. Target DNAs are amplified in a closed-loop microfluidic PCR module consisting of three different temperature regions. We prepared wild type EGFR, EGFR mutants including point mutation and deletion. Linker DNAs coated on a sensor surface of SPR captured different DNA types. Due to characteristics of SPRi, the whole assay process was monitored in real-time and completed within an hour. This study as a proof of concept can be further expanded into high degree of multiplexing detection of major and known ctDNAs, which could provide a solution for clinical unmet needs in cancer treatment and early detection.

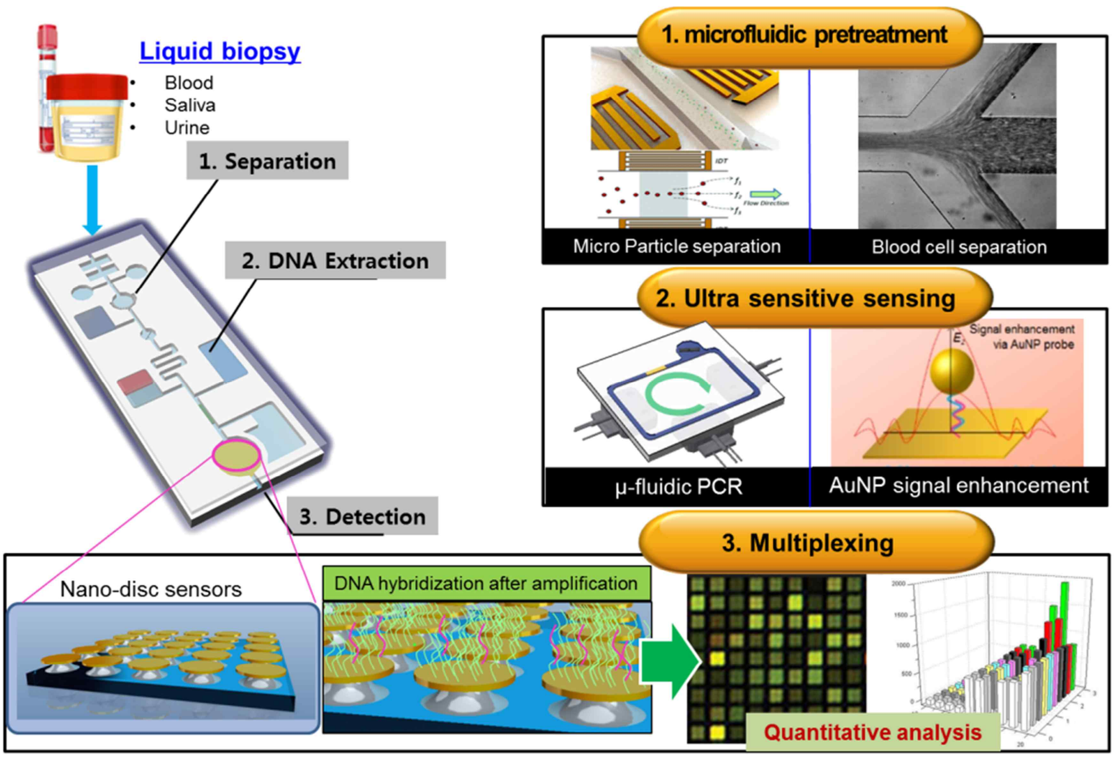

Two-photon tomography of the nail fold: novel insights into the relevance of perivascular tissue parameters for cardiovascular disease diagnosis

E. Shirshin[1], Y. Gurfinkel[2], N. Omelyanenko[3], D. Lysukhin[1], B. Yakimov[1], J. Lademann[4], M. Darvin[4], A. Priezzhev[1]

1- Lomonosov Moscow State University, Faculty of Physics, 119991, Leninski gory 1/62, Moscow, Russia
2- Lomonosov Moscow State University, Moscow University Clinic, 119991, Lomonosovsky prospect 27/10, Moscow, Russia
3- Priorov Central institute of traumatology and orthopedics, 127299, Priorova str. 10, Moscow, Russia
4- Center of Experimental and Applied Cutaneous Physiology, Charité –Universitätsmedizin, 10117, Charitéplatz *1, Berlin, Berlin, Germany*

shirshin@lid.phys.msu.ru

Heart failure (HF) is among the socially significant diseases, involving over 2% of the adult population in the developed countries. According to the data of the European Society of Cardiology, patients with moderate or even minor manifestations of HF may have an increased risk of hospitalization and mortality. However, diagnostics of the early stages of HF remains complicated due to the absence of specific symptoms and objective criteria. We have suggested an indicator of the HF severity based on the perivascular tissue parameters (the perivascular zone (PZ) size) obtained by common digital capillaroscopy, which allows for fast non-invasive measurements. Light area around nail fold capillaries, which is referred to as PZ, is a standard feature of nail fold video capillaroscopy images. Though it is observed in the majority of capillaroscopic studies, it has been rarely used as a clinically significant parameter: the origin of PZ and the reasons underlying its sensitivity to pathological processes accompanying cardiovascular disease has not been discussed up to date and are unknown.

In this work, we present a detailed investigation of the nail fold tissues using two-photon tomography. This method is based on the possibility of tissue imaging using short pulse excitation of nonlinear optical signals such as second optical harmonics (SHG, second harmonic generation) and two-photon excited autofluorescence (TPAEF). Also, fluorescence lifetime imaging (FLIM) can be applied to investigate molecular species in tissue when performing two-photon tomography. Recently, we have demonstrated the possibilities of this approach in studying the papillary dermis blood vessels and localization of structural proteins [1]. Here, we demonstrate a detailed 3D structure of the nail fold tissues on the molecular and cellular levels aimed at the explanation of capillaroscopy-derived parameters to impairments in blood microcirculation.

[1] E. Shirshin, Y. Gurfinkel and B. Author, Two-photon autofluorescence lifetime imaging of human skin papillary dermis in vivo: assessment of blood capillaries and structural proteins localization, Scientific Reports, 7:1171, (2017).

Laser trapping and manipulation of live cells

A.V. Priezzhev[1,2,*], Kisung Lee[2,3], A.N. Semenov[1,2], F. Yaya[3], C. Wagner[3]
1 - International Laser Center and 2 - Faculty of physics of M.V. Lomonosov Moscow State University, Leninskiye Gory, 1-2, 119991, Moscow, Russian Federation
3 – Experimental Physics, Saarland University, Saarbrucken, Germany

avp2@mail.ru

With implication of laser tweezers (LT), laser trapping and manipulation of live cells without mechanical contact have become feasible. LT open up new horizons for scientific and technological achievements and developments as they offer new possibilities for studying multiple phenomena at molecular-cellular interface that make the basis of living matter. However the absence of mechanical contact does not ensure the intactness of the live cell trapped with a high power laser beam even though the laser wavelength is out of the cell absorption spectrum.

The operation principle of laser tweezers is based on the property of strongly focused laser beam to act on the dielectric microparticles located in the vicinity of the beam waist with a force that drives the particle to the equilibrium location and holds it there. If the beam waist position is manipulated, so is the position of the particle. The displacement of the particle from the equilibrium position by external forces can be calibrated so that these forces can be precisely measured in the range ca. 0.1 – 100 pN. This is the range of forces of elastic deformation of live cells and of their interaction with each other. Being able to measure these forces without mechanical contact allows for studying on single cell level the mechanisms of cells interactions, in particular, those of red blood cells (RBC), which make the basis of their aggregation. Such measurements were impossible earlier [1-4].

In this work, we focus on studying with LT the phenomena underlying the interactions of individual RBCs suspended in autologous plasma or in pure proteins solutions. We investigate the effect of laser trapping on RBC dependent on the beam power and duration on trapping. A detailed study of protein synergy shows that it plays a significant role in RBC aggregation: in plasma the role of albumin in aggregation is fibrinogen dependent and changes from agonist at normal concentration range of fibrinogen (2-6 mg/ml) to inhibitor at high concentration of fibrinogen (8 mg/ml). In pure solution of fibrinogen, the addition of albumin leads to significant enhancement of the cells interaction, but spontaneous aggregation is nearly absent. These results show that a complex synergy takes place in plasma, and more components than just fibrinogen and albumin may be essential for RBC spontaneous aggregation.

The work was supported by the grant of Russian Foundation of Basic Research № 17-02-01200.

[1] K. Lee, M. Kinnunen, A.V. Danilina, V.D. Ustinov, S. Shin, I. Meglinski, and A.V. Priezzhev. Characterization at the individual cell level and in whole blood samples of shear stress preventing red blood cells aggregation, *J. Biomech.* 49(7) pp. 1021-1026 (2016).

[2] K. Lee, A.V. Danilina, M. Kinnunen, A.V. Priezzhev, and I. Meglinski. Probing the red blood cells aggregating force with optical tweezers. *IEEE J. Sel. Topics in Quant. Electron.* 22(3), p. 7000106 (2016).

[3] K. Lee, A. Muravyov, A. Semenov, C. Wagner, A. Priezzhev, E. Lyubin, and A. Fedyanin. Gamma globulins-induced interaction between two red blood cells: forces measurement with optical tweezers. Proc SPIE. 10336, Saratov Fall Meeting 2016: *Optical Technologies in Biophysics & Medicine XVII*, p.1033606 (2017).

[4] K. Lee, A. Muravyov, A. Semenov, C. Wagner, and A. Priezzhev. Optical tweezers for measuring the interaction of the two single red blood cells in flow condition, Proc SPIE. 10336, Saratov Fall Meeting 2016: *Optical Technologies in Biophysics & Medicine XVII*, p.1033605 (2017).

Laser tweezers combined with microfluidics and fluorescence microscopy for detecting macromolecule adsorption on single red blood cells

F. Yaya[1,2], K. Lee[1], E. Shirshin[3], A. V. Priezzhev[3], T. Podgorski[2], C. Wagner[1]

[1]*Experimentalphysik (Experimental Physics, University of Saarland, E2.6 Campus, Saarbrücken, Germany)*
[2]*LIPhy (Laboratoire de Physique Interdisciplinaire, University of Grenoble Alpes, 140 Avenue de la Physique, Grenoble, France)*
[3] *MSU (International Laser Center, Lomonosov Moscow State University, Leninskie gory 1/62, Moscow, Russia)*

francois.yaya@uni-saarland.de

Laser tweezers combined with microfluidics and fluorescence microscopy were implemented for assessing single live cells properties. The technique is capable of manipulating single cells and quickly change their suspending medium. Microfluidic techniques were used for achieving a high contrast between media, allowing a very sensitive detection of macromolecule adsorption on single cells.
The technique developed was implemented for accessing the mechanism of the reversible aggregation of red blood cells (RBCs). It is well known that macromolecules are inducing the RBC aggregation, however their exact role in this process is still being investigated. By using our novel technique, we aim to figure out, if macromolecules are adsorbed on RBCs.
The brief experimental procedure was the following: we used a microfluidic chip with two chambers connected with a small interface. A single RBC was trapped inside the larger chamber containing a phosphate buffered saline (PBS, pH = 7.4, 280-315 mOsm/kg) medium of a defined fluorescent dye conjugated with macromolecules (Alexa-488 conjugated fibrinogen or FITC conjugated dextran) at different concentrations and moved into a channel towards the other smaller chamber containing macromolecule-free medium (PBS). A macromolecule-free medium was achieved by constantly “washing” the chamber and by applying a flow using a microfluidic device. It allowed us to achieve a concentration ratio of fluorescent macromolecules over 1:10000, enabling us to detect even a slight amount of adsorbed macromolecules. The results of our experiments prove that both fibrinogens and Dextran 70 kDa are adsorbed on RBCs.

Laser–assisted periodic nanostructure formation in dielectric materials: formation mechanisms

Tatiana E. Itina[1,2], Hongfeng Ma[1], Anton Rudenko[1], Stephane Mottin[1], Vadim. P. Veiko[2], Maksim M. Sergeev[2], and Roman A. Zakoldaev[2]
[1]*Laboratoire Hubert Curien, UMR CNRS 5516/University of Lyon, UJM-Saint-Etienne, France*
[2]*ITMO University, Kronversky pr. 49, 197101, St. Petersburg, Russia*

Numerous promising laser applications are based on their capacity to locally modify dielectric materials with different initial porosity [1]. In particular, various modifications can be performed in volume of different glasses paving a way toward a reliable inscription of numerous nano-structures that can be used as embedded optical components, sensors, and other devises. In particular, the use of ultra-short laser pulses has opened new possibilities in the fabrication of waveguides, volume nanograting, periodic photochromic nanoparticle arrays and many other components [2-3].

Despite a high technological interest, the formation mechanisms of these structures are still puzzling. A better understanding of the involved physical and chemical processes is, however, crucial for the optimization of the laser treatment procedure through a careful identification of the required operating regimes, and, importantly, the optimum laser parameters. For this, we have performed a detailed numerical modeling. The developed model involves such processes as laser propagation, non-linear material ionization, heating of the created free carriers and the following thermal and mechanical effects.

A series of calculations are performed for the cases of both single pulse and multi-pulse femtosecond laser interactions with fused silica. The induced material modifications are correlated with the experimental results demonstrating the model capacities to predict parameter windows associated with several material modification regimes ranging from the densification to the nanocavities formation, shrink or growth. The mechanisms of auto-organized periodic structure formation [4] are then discussed and the required laser irradiation parameters are identified. These regimes are explained based on several thresholds identified in terms of laser pulse energy, wavelength and number of pulses.

The obtained results pave the way toward a better control over ultra-fast laser micro-machining of glass in volume. The proposed modeling is, thus, of interest for the further development of the related laser applications.

References

[1] A. Cerkauskaite et al., Ultrafast laser-induced birefringence in various porosity silica glasses: from fused silica to aerogels, Opt. Express, 25(7) 8011-8021 (2017)
[2] M. Royon et al., X-rays preconditioning effects on the induced refractive index change in femtosecond laser fabrication of embedded waveguides in silica glass, 11th International Symposium on SiO2, Advanced Dielectrics and Related Materials, 2016
[3] L. Bois et al. Chemical growth and photochromism of silver nanoparticles into mesoporous titania template, Langmir 26(2), 1199-1206 (2009)
[4] A. Rudenko et al., From random inhomogeneities to periodic nanostructures induced in bulk silica by ultrashort laser, Phys. Rev. B, 93(7), 075427 (2016)

Role of Laser-Induced Thermal Stresses in Material Modification: Comparative Analysis for Lasers of Different Pulse Duration

N. M. Bulgakova[1], M. V. Shugaev[2], Y. P. Meshcheryakov[3], V. P. Zhukov[4,5]

1- HiLASE Centre, Institute of Physics ASCR, Za Radnicí 828, 25241 Dolní Břežany, Czech Republic
2- Department of Materials Science and Engineering, University of Virginia, 395 McCormick Road, Charlottesville, VA, USA
3- Design and Technology Branch of Lavrentyev Institute of Hydrodynamics SB RAS, Tereshkovoi str. 29, 630090 Novosibirsk, Russia
4- Institute of Computational Technologies SB RAS, 6 Lavrentyev Ave., 630090 Novosibirsk, Russia
5- Novosibirsk State Technical University, 20 Karl Marx ave., 630073, Novosibirsk, Russia

bulgakova@fzu.cz

More than 55 years passed from the creation of first lasers, one of the most impressive inventions of 20th century. During this time, lasers have become an instrument without which it is not possible to imagine both everyday life and many fields of scientific research and industrial applications. However, a great variety of existing and emerging lasers with different irradiation parameters and much greater variety of materials, which can be treated by lasers for improving/modifying their properties or for processing for industrial needs (cutting, drilling, cleaning, etc.), imply a wealth of processes contributing to the laser-matter interaction phenomenon that makes it to be still a hot topic of research. Laser-solid interaction starts from light absorption by material after which the irradiated matter evolves thermodynamically through a sequence of non-equilibrium and quasi-equilibrium states to its final (laser processed) structure. Heating, melting, ablation, resolidification, even of the same sample occur differently depending on laser irradiation parameters (wavelength, pulse duration, energy density, repetition rate). At short and ultrashort laser pulses, when laser-induced heating of materials in a surface layer or in the bulk is highly localized, strong temperature (and hence pressure) gradients are created which affect post-irradiation evolution of matter via generation of stressed states and stress waves. In the cases of layered structures (laser-processed solar elements, laser-induced forward transfer techniques, etc.), stresses play determining role in material ejection from the laser-irradiated samples.

In this talk we will discuss on the role of stresses in material evolution during and after laser irradiation at different pulse duration (femtosecond, nanosecond, and even cw lasers) and different wavelengths from UV to mid-IR. The examples of numerical simulations for metals, semiconductors, and dielectrics, based on specific models, will be demonstrated in both surface ablation and volumetric confinement regimes. It will be shown that, in many cases, for producing the desired material modification/ablation/deposition, the control over laser-induced stresses is necessary that can be achieved via tailoring of the laser energy coupling.

Laser ultrasonic mediated crystalline phase formation in a thin film

J. Wuenschell, H. Helvajian

Physical Sciences Laboratories, The Aerospace Corporation, Los Angeles, California, USA

henry.helvajian@aero.org

We have developed an experimental apparatus that explores the effect of small perturbations of applied energy on a phase transformation process. Our initial experiments focus on the utility of laser ultrasonic excitation to affect the phase transformation of thin (<10 nm) amorphous MoS_2 film into the crystalline form. In our experiment, the pulsed laser source, that generates the ultrasonic excitation, is spatially removed from the focused CW heating laser which drives the crystallization process. The configuration allows time-separation and better control in inducing the energy perturbation. The experimental apparatus is based on a direct write laser processing system and can pattern over a large area (15 cm). Moreover, it has the capability to amplitude modulate the lasers and synchronize the timing between the ultrasonic pulses (i.e. energy perturbation) and the heating source for each and every focal spot that is phase transformed.

It is a well-established fact that a pulsed laser striking a surface produces a wave packet of ultrasonic waves having a wide frequency bandwidth (BW) (i.e. BW ~ $1/\tau$ where τ is laser pulse width). The wave packet travels both along the surface (e.g. Rayleigh waves) and in the bulk and is regulated by the elastic properties of the material. Reproducible excitation is possible if the pulsed laser amplitude is metered to not ablate the surface. In a prior set of experiments in our laboratory, we have demonstrated that the ultrasonic surface excitation modes enhance the mobility of molecular adsorbates [1,2]: enhanced mobility of Au_8 (in air) and deuterated ethylene (in UHV) on crystalline silicon were observed. These results suggested that the inclusion of controlled laser ultrasonic energy could lower the processing temperature of a materials growth process (e.g. CVD). As a test, we explore in this experiment the inclusion of ultrasonic energy to affect crystalline formation from amorphous MoS_2.

At a few monolayers, MoS_2 is a semiconducting analog to graphene with 2D electronics applications. MoS_2 is an indirect bandgap semiconductor in bulk but becomes a direct bandgap system as the thickness approaches 1-2 monolayers. A large body of recent work shows a number of unique properties that could enable electronic/photonic applications on stretchable substrates [3]. Historically, MoS_2 is known for its tribological properties and is extensively used in spacecraft as a dry lubricant. Aerospace, research in the tribology of MoS_2 extends over 20 years (see for example [4]). Borrowing from this expertise we have deposited thin films of amorphous MoS_2 on various substrates (yttrium stabilized zirconia crystal, Willow™ glass, PDMS, crystalline silicon). We will present our results on the efficacy of laser ultrasonic excitation to enhance the phase transformation of amorphous MoS2 to the crystalline form, our current understanding of the underlying physics and the implications with regards to material processing applications

[1] A. J. Manzo, H. Helvajian, *Demonstration of enhanced surface mobility of adsorbate cluster species by surface acoustic wave excitation induced by a pulsed laser*, Proc. SPIE, Vol. 8969, pp. 896908:1-8 (2014).
[2] M. V. Shugaev, A. J. Manzo, C. Wu, V. Yu. Zaitsev, H. Helvajian, and L. V. Zhigilei, *Strong enhancement of surface diffusion by nonlinear surface acoustic waves*, PRB, vol. 91, pp., 235450:1-11, (2015).
[3] R. Ganatra, Q. Zhang, Few-layer MoS2: A promising layered semiconductor, ACS Nano, Vol. 8(5), pp. 4074-4099 (2014).
[4] J. R. Lince, C. S. Clark and S. H. Loewenthal, "Degradation of Sputter-Deposited Nanocomposite MoS2 Coatings for NIRCam during Storage in Air," Proceedings of the 43rd Aerospace Mechanisms Symposium; NASA Conf. Publ. NASA/CP-2016-219090, May 2016.

Rapid electronic and sub-ps structural transitions in ultrafast laser irradiated transition metals

H. Zhang[1], C. Li[1,2], E. Bévillon[1], J. P. Colombier[1], R. Stoian[1]

1- Laboratoire Hubert Curien, UMR 5516 CNRS, Université de Lyon, Université Jean Monnet, 42000 St. Etienne, France

2- State Key Laboratory of Transient Optics and Photonics, Xi'an Institute of Optics and Precision Mechanics, CAS, 710119 Xi'an, China

razvan.stoian@univ-st-etienne.fr

The time needed for a metal to structurally respond to electronic excitation is key in defining material behaviors under extreme conditions. In current views it is usually set by electron-phonon coupling and defines the limitations in the achievement of non-thermal rapid structural phases. Employing time-resolved optical techniques we show that ultrashort laser excitation of metallic tungsten determines unexpectedly fast optical and structural transformations, almost on the timescale of the laser pulse. Driven by Fermi redistribution of carriers around a d-band pseudogap in the vicinity of the damage threshold, quasi-resonant optical excursions occur upon pumping with near-infrared photons, initiating a transient plasmonic state for the initial non-plasmonic metal [1] We discuss the potential impact of this transition in the generation of laser-induced periodic structures [2]. Beyond this range, sub-ps ablation occurs, challenging current thermally-driven scenarios relying on vibrational coupling and phase transformations. We indicate a correlated action towards structure destabilization involving charge depletion and electronic pressure. If, at low excitation, primarily localized states are populated due to Fermi smearing, screening the electron-ion potential, the transfer reverses between low-lying bands to delocalized states with increasing electronic temperature, and a strong charge deficit appears on bonding orbitals [3]. In the presence of pressure gradients, this is prone to rapidly destabilize the structure even in a metallic environment. Using time-resolved ellipsometry, first principle molecular dynamics and hydrodynamic calculations we demonstrate that various mechanisms concur in a correlated way [4]. They include mutual effects of charge-induced bond-softening, swift mechanical pressure drives, or thermodynamic supercritical trajectories. An ultrafast competition between non-classical charge distortions, electron-driven mechanical stress, and classical electron-phonon dynamics appears, with coexistence of thermal and non-thermal effects on scales believed prohibitive for the former.

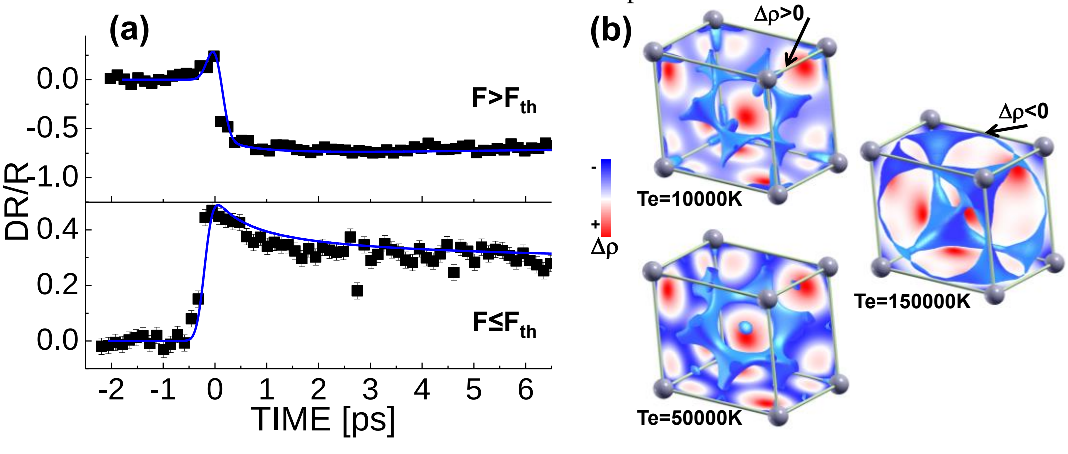

Figure 1: (a) Time-resolved reflectivity measurements on W surfaces close and above the ablation threshold. (b) Iso-surface normalized charts of charge redistribution (loss and gain Δρ domains) in W relative to the unexcited material for a range of electronic temperatures.

[1] E. Bevillon, J. P. Colombier, V. Recoules, H. Zhang, C. Li, and R Stoian, Ultrafast switching of surface plasmonic conditions in nonplasmonic metals Phys. Rev. B 93, 165416 (2016).
[2] H. Zhang, J. P. Colombier, C; Li, N; Faure, G; Cheng, and R; Stoian, Coherence in ultrafast laser-induced periodic surface structures, Phys. Rev. B 92, 174109 (2015).
[3] S. T. Murphy, S. L. Daraszewicz, Y. Giret, M. Watkins, A. L. Shluger, K. Tanimura, and D. M. Duffy, Dynamical simulations of an electronically induced solid-solid phase transformation in tungsten, Phys. Rev. B 92 134110 (2015).
[4] H. Zhang, C. Li, E. Bevillon, G. Cheng, J. P. Colombier, and R Stoian, Ultrafast destructuring of laser-irradiated tungsten: Thermal or nonthermal process, Phys. Rev. B, 94, 224103 (2016).

Pulsed laser synthesis of bioactive thin layers with antimicrobial properties

Carmen Ristoscu[1], Laura Floroian[2], Natalia Mihailescu[1], Anita Visan[1], Ana Janković[3], Mariana Carmen Chifiriuc[4], Ion N. Mihailescu[1]

1- National Institute for Lasers, Plasma and Radiation Physics, 409 Atomistilor street, 077125 Măgurele, Ilfov, Romania, e-mail: carmen.ristoscu@inflpr.ro

2- Transilvania University of Brasov, 29 Eroilor Blvd, 500036, Brasov, Romania

3- Innovation Center, Faculty of Technology and Metallurgy, University of Belgrade, 11000 Belgrade, Serbia
4 - Department of Microbiology, Faculty of Biology, University of Bucharest, 060101 Bucharest, Romania

Titanium and stainless steel are widely used as an implantable biomaterial for medical devices like dental implants, fracture fixations and joint replacements. However, they require an appropriate surface biofunctionalization to increase hard and/or soft tissue compatibility and to exhibit antimicrobial properties for the inhibition of biofilm formation. Biofilm represents a microbial community that irreversibly attaches to a host surface, being protected by a self-secreted extracellular polymeric matrix and other complex mechanisms from the action of antibiotics, disinfectants and host immune effectors.

We report on thin film deposition by Matrix-assisted pulsed laser evaporation (MAPLE) of simple hydroxyapatite (HA) or silver (Ag) doped HA combined with the natural biopolymer organosolv lignin (Lig) (Ag:HA–Lig) [1] and the transfer and printing of novel bioactive glass-polymer-antibiotic composites into uniform thin films onto 316 L stainless steel substrates of the type used in implants [2]. The microbiological evaluation showed that the newly Ag:HA–Lig assembled surfaces exhibited an inhibitory activity both on the initial steps of biofilm forming, and on mature bacterial and fungal biofilm development. The intensity of the antibiofilm activity was positively influenced by the presence of the Lig and/or Ag, in the case of *Staphylococcus aureus, Pseudomonas aeruginosa* and *Candida famata* biofilms.

The obtained surfaces exhibited a low cytotoxicity toward human mesenchymal stem cells, being therefore promising candidates for fabricating implantable biomaterials with increased biocompatibility and resistance to microbial colonization and further biofilm development [1].

On the other hand, it was showed that the incorporated antibiotic in the bioglass matrix underwent a gradually dissolution in physiological fluids thus supporting a high local treatment efficiency. Electrochemical measurements including linear sweep voltammetry and impedance spectroscopy studies were carried out to investigate the corrosion resistance of the coatings in physiological environments. The *in vitro* biocompatibility assay using the MG63 mammalian cell line revealed that the obtained nanostructured composite films are non-cytotoxic. The antimicrobial effect of the coatings was tested against *Staphylococcus aureus* and *Escherichia coli* strains, usually present in implant-associated infections. An anti-biofilm activity was evidenced, stronger against *E. coli* than the *S. aureus* strain. The results proved that the applied method allows for the fabrication of implantable biomaterials which shield metal ion release and possess increased biocompatibility and resistance to microbial colonization and biofilm growth [2].

[1] A. Janković, S. Eraković, C. Ristoscu, N. Mihailescu (Serban), L. Duta, A. Visan, G.E. Stan, A.C. Popa, M.A. Husanu, C.R. Luculescu, V.V. Srdić, Dj. Janaćković, V. Mišković-Stanković, C. Bleotu, M.C. Chifiriuc, I.N. Mihailescu, "Structural and biological evaluation of lignin addition to simple and silver doped hydroxyapatite thin films synthesized by matrix-assisted pulsed laser evaporation", Journal of Materials Science: Materials in Medicine, 26 (1) (2015) 5333

[2] Laura Floroian, Carmen Ristoscu, Natalia Mihailescu, Irina Negut, Mihaela Badea, Doru Ursutiu, Mariana Carmen Chifiriuc, Iuliana Urzica, Hussien Mohammed Dyia, Coralia Bleotu, Ion N. Mihailescu, "Functionalized antimicrobial composite thin films printing for stainless steel implant coatings", Molecules 21 (2016) 740

Laser-diode pumped pulsed visible praseodymium lasers

Haohai Yu

State Key Laboratory of Crystal Materials and Institute of crystal Materials, Shandong University, 27 Shanda Nanlu, Jinan 250100, China

haohaiyu@sdu.edu.cn

Visible lasers have been considered as a significant and fascinating regime owing to the fact that they have widely applications and requirements in various of topical ranges including the medicine, biomedical images, scientific research and our daily life. With the development of blue laser diodes (LDs), the all-solid-state visible lasers with praseodymium (Pr^{3+}) ions doped crystals as the gain materials have attracted more and more attentions with the advantages of simple design and compact structure[1]. Pulsed lasers in the visible range are playing important roles in our daily life and modern technology[2]. However, constrained by the rarity of practical optical modulators in visible ranges, pulse visible lasers are still under development. Therefore, the discovery of optical modulators applied in the visible range is foremost.

In this paper, we mainly demonstrated the passive Q-switched Pr3+ ions pulse visible lasers based on two-dimensional materials molybdenum sulfide (MoS_2)and black phosphorus(BP) and one-dimensional material Au nanorods (NRs) as the saturable absorbers. The novel self-mode-locking technique with the repetition rate of multi-GHz was developed at the wavelengths of 522 nm, 607 nm, 639 nm, and 720 nm. A design criteria for novel 2D optical modulators was also summarized. Based on the design criteria, less than 8 layered the proper MoS_2 samples have been selected as the proposed optical modulators and broadband mode-locked ultrafast lasers from 522 to 639 nm are originally realized in the solid-state praseodymium lasers.

[1] C. Kränkel, D. T. Marzahl, F. Moglia, G. Huber, and P. W. Metz, "Out of the blue: semiconductor laser pumped visible rare-earth doped lasers," Laser & Photonics Rev. 10, 548-569 (2016).

[2] Y. Zhang, S. Wang, H. Yu, H. Zhang, Y. Chen, L. Mei, A. Di Lieto, M. Tonelli, and J. Wang, "Atomic-layer molybdenum sulfide optical modulator for visible coherent light," Sci. Rep. 5, 5:11342-7 (2015).

Monoclinic Double Tungstate Thin-Disk lasers at 2 microns

X. Mateos[1,2,3], P. Loiko[4], S. Lamrini[3], K. Scholle[3], P. Fuhrberg[3], S. Vatnik[5], I. Vedin[5], M. Aguiló[2], F. Díaz[2], U. Griebner[1], V. Petrov[1]

1- Max Born Institute for Nonlinear Optics and Short Pulse Spectroscopy, Max-Born-Str. 2a, D-12489 Berlin, Germany

2- Física i Cristal·lografia de Materials i Nanomaterials (FiCMA-FiCNA)-EMaS, Dept. Química Física i Inòrganica, Universitat Rovira i Virgili (URV), Campus Sescelades, E-43007 Tarragona, Spain

3- LISA laser products OHG, Albert-Einstein-Str. 1-9, D-37191 Katlenburg-Lindau, Germany

4- ITMO University, 49 Kronverkskiy pr., 197101 St. Petersburg, Russia

5- Institute of Laser Physics, Siberian Branch of Russian Academy of Sciences, 13/3 Lavrentyev Ave, 630090 Novosibirsk, Russia

Main author email address: xavier.mateos@urv.cat

The thin-disk laser concept is attractive for both continuous-wave (CW) and pulsed (mode-locked, ML) operation. Such a laser is based on a disk-shaped active element with its thickness being smaller than the size of the laser beam [1]. One surface of the disk is attached to the heat sink providing unidirectional heat flow and, conveniently coated, serving as a cavity mirror. Thin-disk lasers offer reduced thermo-optic effects and good potential for power scaling. Moreover, high slope efficiencies have been demonstrated. In addition, they are attractive for ML lasers due to the diffraction-limited beam and the reduction of the nonlinear effects in the active medium.

CW and ML thin-disk lasers have been extensively studied at ~1 µm utilizing Yb^{3+} ions in hosts such as YAG, Lu_2O_3, $KY(WO_4)_2$, $CaGdAlO_4$, etc. Concerning, the 2 µm spectral range, the research focused mostly on Tm^{3+} ions in YAG [2], Lu_2O_3 or $LiLuF_4$. So far, Ho^{3+} thin-disk lasers have been realized only with Ho:YAG [3], where a 2 at.% Ho:YAG thin-disk operated with a rather complex pump geometry consisting of 24 pump passes (as typical for Yb:YAG thin-disks) using a Tm-fiber laser as pump source, generating 9.4 W in CW at ~2090 nm with a slope efficiency η of ~50% (with respect to the absorbed pump power). Even higher output power, 22 W with η ~27% was achieved in a similar mutipass-pumped Ho:YAG laser using an InP diode.

Monoclinic double tungstates (MDTs), $KRE(WO_4)_2$ where RE = Gd, Y or Lu (shortly KREW), are suitable hosts for Ln^{3+} [4]. They offer the possibility to be doped with relatively high Tm^{3+} or Ho^{3+} concentrations suitable for efficient lasing, high transition cross-sections in polarized light and long lifetime of the upper laser levels. These characteristics make the Tm^{3+} or Ho^{3+}-doped MDTs very promising for thin-disk lasers with ultimately reduced number of pump passes.

MDTs offer an additional benefit which may facilitate their use in 2 µm thin-disk lasers. Thin epitaxial layers of high optical quality, despite the low symmetry of this material, can be grown. Such a concept was used to demonstrate the first Yb MDT thin-disk laser [5].

In this work, we report on Tm^{3+} and Ho^{3+} monoclinic double tungstate thin-disk lasers based on a 250 µm-thick 5 at.%Tm:KLuW grown on a KLuW substrate and a 250 µm-thick 3 at.% Ho:KYW grown on a KYW substrate, respectively. The former thin-disk laser was pumped by an AlGaAs laser diode generating 5.9 W at 1855 nm with η = 47% when using a double-bounce (4 pump passes) pump geometry. The latter, was pumped by a Tm-fiber laser at 1960 nm achieving a maximum output power of 1,57 W at 2056-2059 nm with η of 60%. The two MDT epitaxial structures are promising for multi-watt mode-locked thin-disk lasers at ~2.06 µm.

[1] A. Giesen, H. Hügel, A. Voss, K. Wittig, U. Brauch, and H. Opower, Scalable concept for diode-pumped high-power solid-state lasers, Appl. Phys. B vol. 58, pp. 365-372, (1994).

[2] A. Giesen, and J. Speiser, Fifteen years of work on thin-disk lasers: results and scaling laws, IEEE J. Select. Top. Quantum Electron. vol. 13, pp. 598-609 (2007).

[3] M. Schellhorn, Performance of a Ho:YAG thin-disc laser pumped by a diode-pumped 1.9 µm thulium laser, Appl. Phys. B vol. 85, pp. 549-552 (2006).

[4] V. Petrov, M. C. Pujol, X. Mateos, Ò. Silvestre, S. Rivier, M. Aguiló, R. M. Solé, J. H. Liu, U. Griebner, and F. Díaz, Growth and properties of $KLu(WO_4)_2$, and novel ytterbium and thulium lasers based on this monoclinic crystalline host, Laser Photon. Rev. vol. 1, pp. 179–212 (2007).

[5] S. Rivier, X. Mateos, Ò. Silvestre, V. Petrov, U. Griebner, M.C. Pujol, M. Aguiló, F. Díaz, S. Vernay, and D. Rytz, Thin-disk $Yb:KLu(WO_4)_2$ laser with single-pass pumping Opt. Lett., vol. 33, pp. 735-737 (2008).

Power Scaling of in-band pumped Holmium doped solid-state lasers at ~ 2 µm

D. Y. Shen[1,2], Y. G. Zhao[2,3], W. C. Yao[1], Z. H. Shao[3]

1- Department of Optical Science and Engineering, Fudan University, Shanghai 200433, China
2- Jiangsu Key Laboratory of Advanced Laser Materials and Devices, School of Physics and Electronic Engineering, Jiangsu Normal University, Xuzhou 221116, China
3- Jiangsu Collaborative Innovation center of Advanced Laser Technology and Emerging Industry, Jiangsu Normal University, Xuzhou 221116, China

Email address: shendy@fudan.edu.cn

Laser sources operating in the 2 µm spectral region have numerous applications, including remote sensing, material processing and mid-infrared light generation via pumping of optical parametric oscillators. In this report, thulium doped high power all fiber laser systems with >500 W of output power at ~ 1907 nm and 1941 nm are respectively constructed. The beam quality factor, M^2, of both laser sources are < 3. Based on these home-constructed high power and high brightness fiber pump sources, lasing characteristics and power scaling ability of Ho:YAG, Ho:LuAG in-band pumped at 1907 nm and holmium doped polycrystalline sesquioxide in-band pumped at 1941 nm are investigated. Prospects for high energy/peak-power pulsed operation of fiber laser in-band pumped holmium doped single-crystal and ceramic lasers at ~2 µm are discussed.

Distributed fiber-optic sensing with ultra-high spatial resolution by using linear optical sampling technique

Xinyu Fan[1*], Shuai Wang[1], Qingwen Liu[1], Zuyuan He[1]

1- State Key Laboratory of Advanced Optical Communication Systems and Networks, Department of Electronic Engineering, Shanghai Jiao Tong University, Shanghai 200240, China
**fan.xinyu@sjtu.edu.cn*

Distributed fiber sensing technologies have been used to characterize optical links via backscattered signals. For some high-end applications such as the structural health monitoring of aircrafts [1], and the reading technique of optical identification devices (OID) which use spatially multiplexed fiber Bragg gratings (FBGs) inside fiber connectors as "0" and "1" for access network management [2], it is of great significance to precisely locate the reflections with a very strict requirement for high spatial resolution. In this invited talk, we demonstrate two different kinds of optical reflectometry with ultra-high spatial resolution by using linear optical sampling (LOS) technique [3-5]. The first one is based on optical time domain reflectometry (OTDR), and the second one is based on pulse compression technique.

LOS technique is known for the capability of observing the complex amplitude response of ultrashort optical pulses using slow electronics with a low bandwidth, and its shot-noise limited sensitivity, has been used in many fields for monitoring the waveform in high speed transmission systems. It can also be used to break the limitations of achieving an ultra-high spatial resolution together with a long measurement range. The signal under detection (SUT) interferes with the sampling signal launched from the mode-locked laser (MLL) and is then detected by the ordinary photo-detectors. Because the timing jitter of the MLL is several femtoseconds, the sampling rate can be up to 100 TS/s, and this makes it possible to measure ultrashort pulse launched from pulsed lasers and its reflected lightwave from optical fibers. Therefore, the adopting of LOS in reflectometry system has the potential to realize an ultra-high spatial resolution with a long measurement range.

We firstly demonstrate an OTDR system by using a MLL as the pulse source and use the LOS technique to detect the reflected signals. Taking advantage of the ultrashort input pulse, the large detection-bandwidth, as well as the low timing jitter of linear optical sampling system, a sub-mm spatial resolution is achieved. As the pulse-width is broadened with the increase of distance due to chromatic dispersion and large bandwidth of the ultrashort pulse, by adopting digital chromatic dispersion compensation, we achieved a spatial resolution of 340 microns with a measurement range of 10 km. This technique helps OTDR find new foreground in long-range and ultra-high-resolution distributed applications such as remote optical identification device detection for diagnosing passive optical network links, or precisely detecting fault positions in aircrafts.

Pulse compression technique is another particularly competitive method that enables both high spatial resolution and dynamic range in coherent radar and distributed fiber sensing systems. In this talk, we propose an all-optic sub-THz-range linearly chirped optical source and a large-bandwidth detection system to characterize it. Taking advantage of the chromatic dispersion effect, ultrashort optical pulses are stretched to be ~10 ns linearly chirped pulses with sub-THz range, which yields a large time-bandwidth product of 4500, a high compression ratio of 4167 and a chirp rate of 45 GHz/ns. The generated waveform is characterized with high precision thanks to the large detection bandwidth of LOS technique. A spatial resolution of 120 microns and an extinction ratio of 20.4 dB is demonstrated by using this technique, which paves the way for ultra-high spatial resolution and long range sensing applications such as LIDAR and optical reflectometry.

References

[1] C.-Y. Chong and S. P. Kumar, "Sensor networks: evolution, opportunities, and challenges," Proc. IEEE 91, pp. 1247–1256, 2003.
[2] Y. Koshikiya, N. Araki, C. Kito and F. Ito, "Compact and large capacity identification device for uniquely addressing optical components," in Proc. National Fiber Optic Engineers Conference, 2012, pp. JTh2A-69.
[3] K. Okamoto, F. Ito, "Ultrafast measurement of optical DPSK signals using 1-symbol delayed dual-channel linear optical sampling," IEEE Photon. Technol. Lett., vol. 20, pp. 948-950, 2008.
[4] K. Okamoto, F. Ito, "Dual-channel linear optical sampling for simultaneously monitoring ultrafast intensity and phase modulation," J. Lightw. Technol., vol. 27, pp. 2169-2175, 2009.
[5] C. Dorrer, D. C. Kilper, H. R. Stuart, G. Raybon and M. G. Raymer, "Linear optical sampling", IEEE Photon. Technol. Lett., vol. 15, pp. 1746-1748, 2003.

The Statistical Properties of Distributed Acoustic Sensing

A. Eyal, H. Gabai and I. Shpatz

School of EE, Tel-Aviv University, Tel-Aviv, Israel

avishay@eng.tau.ac.il

Distributed Acoustic Sensing (DAS) has been drawing considerable attention in recent years. In DAS a telecom-type fiber is transformed into an array of thousands of virtual microphones. Commonly DAS systems rely on Rayleigh backscattering to enable dynamic strain sensing. A well-known characteristic of Rayleigh backscattering is coherent fading noise (CFN) or speckle noise [1]. While in traditional reflectometry techniques, such as Optical Time Domain Reflectometry (OTDR), CFN is considered a drawback, in DAS techniques, such as Φ-OTDR, coherent interference between backscattered light from different scatterers is essential for proper operation [2]. Hence, the presence of CFN cannot be avoided. This means that the Signal to Noise Ratio (SNR) with which a dynamical event is sensed and the sensitivity of the system are random processes of position and time [3]. Clearly, it is possible to improve the SNR at the expense of spatial resolution. In Φ-OTDR, for example, the use of longer interrogation pulses will increase the mean SNR. It should be noted, however, that the randomness of the SNR will not be diminished. In fact, as will be described in the talk, the normalized Standard Deviation (STD) (namely, the ratio between the STD and the mean value) of the SNR will be ~1 regardless of the duration of the interrogation pulse. This is a manifestation of a well-known property of speckles: filtering a signal, with 'fully developed' speckles, in the field domain, using a moving window, yields a lower resolution signal but with 'fully developed' speckles as well [4]. In the talk these statistical properties of DAS will be elaborated. In addition, it will be shown that in coherent DAS systems (which collect complex Rayleigh profiles of the sensing fiber) it is possible to trade SNR for resolution while substantially reducing the randomness of the SNR. This result is facilitated by, first, acquiring the complex backscatter profiles with high spatial resolution, calculating unique complex power profiles which retain phase variation information and then low-pass filtering the complex power profiles with a moving window.

[1] R. Goldman, A. Agmon, and M. Nazarathy, "Direct Detection and Coherent Optical Time-Domain Reflectometry With Golay Complementary Codes," Journal of Lightwave Technology, vol. 31, pp. 2207-2222, Jul 2013.

[2] J. C. Juarez, E. W. Maier, K. N. Choi, and H. F. Taylor, "Distributed fiber-optic intrusion sensor system," Journal of Lightwave Technology, vol. 23, pp. 2081-2087, Jun 2005.

[3] H. Gabai and A. Eyal, "On the sensitivity of distributed acoustic sensing," Optics Letters, vol. 41, pp. 5648-5651, Dec 2016.

[4] J. W. Goodman, Speckle Phenomena in Optics: Theory and Applications: Roberts & Company, 2007.

Development and Evaluation of Resonator Fiber Optic Gyroscopes

H. Ma, H. Li, Y. Lin, and Z. Jin

School of Aeronautics and Astronautics, Zhejiang University, Hangzhou 310027

E-mail: mahl@zju.edu.cn

Optical gyroscopes making use of the Sagnac effect are attractive sensors for inertial navigation systems [1]. The first configuration of a passive resonator gyroscope was proposed and demonstrated by Ezekiel and Balsamo in 1977 and the fiber optic resonator version (Resonator Fiber Optic Gyroscope, RFOG) was demonstrated in 1983 [2, 3]. It has been studied extensively over the past three decades. The RFOG uses the frequency shift between the clockwise (CW) and counterclockwise (CCW) resonances in a fiber ring resonator to measure rotation rate. Lightwaves circulate multiple turns in the resonator, thus, theoretically, the RFOG can achieve the same precision as that of the IFOG with much less optical fiber. Actual performance observations in RFOGs, however, are below expectation due to noises resulted from various effects.

The ultimate sensitivity of the RFOG is determined by the shot noise of the photodetector. However, many other factors, including backscattering, polarization fluctuation, nonlinear Kerr effect, and laser frequency noise, etc., exert negative influences. These parasitic effects deteriorate the performance of the RFOG and make it far beyond the shot-noise limited theoretical sensitivity.

In this paper, we describe the four main parasitic effects encountered in the RFOG and their countermeasures [4-8]. The new progress in a feasible RFOG is shown. In addition, the advanced and complex digital signal processing in the RFOG is also addressed [9]. Figure 1 shows the experimetal setup of the closed-loop RFOG and the closed-loop output of the rotation rate. The experimental result shows that it can be used in the tactical-grade applications.

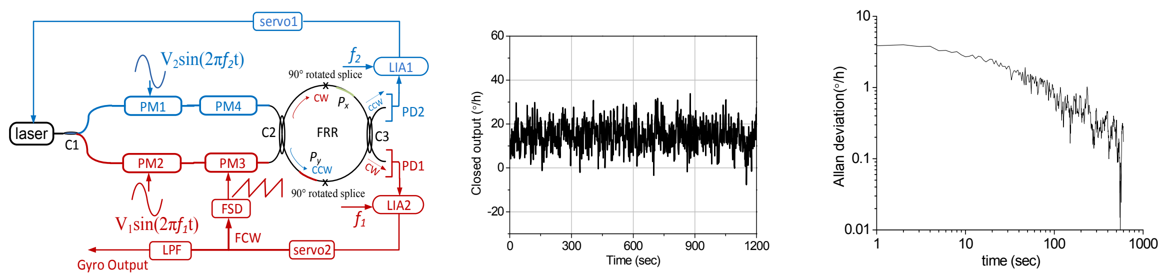

(a) (b) (c)

Fig.1 Experimental setup of the closed-loop RFOG and the closed-loop output of the rotation rate (turntable stationary). (a) Setup of the closed-loop RFOG. (b) RFOG rate output versus running time. (c) Rate uncertainty versus running time

Funding and acknowledgments. The authors would like to acknowledge financial support from the National Natural Science Foundation of China (No. 61675181, 61377101).

[1] G. Sagnac, L'ether lumineux demontre par l'effet du vent relatif d'ether dans un interferometer en rotation uniforme, C. R. Acad Sci. vol.95, pp, 708-710 (1913)

[2] S. Ezekiel and S. R. Balsamo, Passive ring resonator laser gyroscope, Appl. Phys. Lett. vol.30, pp. 478-480 (1977).

[3] R. E. Meyer, S. Ezekiel, D. W. Stowe, and V. J. Tekippe, Passive fiber-optic ring resonator for rotation sensing, Opt. Lett. Vol.8, pp.644–646 (1983).

[4] H. Ma, Z. He, and K. Hotate, Reduction of backscattering induced noise by carrier suppression in waveguide-type optical ring resonator gyro, J. Lightwave Technol., vol. 29, pp. 85-90 (2011).

[5] H. Ma, X. Yu, and Z. Jin, Reduction of polarization-fluctuation induced drift in resonator fiber optic gyro by a resonator integrating in-line polarizers," Opt. Lett., vol. 37, no. 16, pp. 3342-3344 (2012).

[6] H. Ma, X. Li, G. Zhang, and Z. Jin, Reduction of optical Kerr-effect induced error in a resonant micro-optic gyro by light-intensity feedback technique, Appl. Optics, vol. 53, pp. 3465-3472 (2014).

[7] Y. Yan, H. Ma, and Z. Jin, Reducing polarization-fluctuation induced drift in resonant fiber optic gyro by using single-polarization fiber, Opt. Express, vol. 23, pp. 2002-2009 (2015).

[8] H. Ma, Y. Yan, L. Wang, X. Chang, and Z. Jin, Laser frequency noise induced error in resonant fiber optic gyro due to an intermodulation effect, Opt. Express, vol. 23, pp. 25474-25486 (2015).

[9] Z. Jin, X. Yu, and H. Ma, Closed-loop resonant fiber optic gyro with an improved digital serrodyne modulation, Opt. Express, vol. 21, pp. 26578-26588 (2013).

Fiber-optic guided acoustic-wave Brillouin scattering properties and sensing application

Neisei Hayashi,[1,]* Yosuke Mizuno,[2] Kentaro Nakamura,[2] Sze Yun Set[1] and Shinji Yamashita[1]

1-*Research Center for Advanced Science and Technology, The University of Tokyo, 4-6-1, Komaba, Meguro-ku, Tokyo 153-8904, Japan*

2-*Institute of Innovative Research, Tokyo Institute of Technology, 4259, Nagatsuta-cho, Midori-ku, Yokohama 226-8503, Japan*

*[*hayashi@cntp.t.u-tokyo.ac.jp](mailto:hayashi@cntp.t.u-tokyo.ac.jp)*

Guided acoustic-wave Brillouin scattering (GAWBS) is one of the nonlinear optical phenomena that occur in optical fibers, and is generated by the interaction between the incident light and the acoustic wave propagated through the cross-sectional area of the fiber. The GAWBS is forward scattering and it categorized into two: one is the depolarized GAWBS and the other is the polarized GAWBS. The depolarized GAWBS is generated by the polarization modulation by torsional-radial mode acoustic waves ($TR_{2,m}$, m = 1,2,3…), but on the other hand, the polarized GAWBS is generated by the phase modulation by radial mode acoustic waves ($R_{0,m}$, m = 1,2,3…) and the radial component of $TR_{2,m}$. GAWBS can be divided into the spontaneous scattering and stimulated scattering as well as that of backward Brillouin scattering [2]. GAWBS has been studied for sensing application such as temperature sensors [3] and strain sensors [4]. Recently, the optomechanical sensing field has been added to GAWBS-based applications because GAWBS signals are affected by the transverse acoustic waves reflected between cladding and external materials [5]. In the near future, GAWBS will be applicable to the distributed multi-parameter sensors for cancer detection in the human body [6], underground oil layer detection [7] and the quality inspection of the bioethanol [8].

In this paper, we present fundamental properties of GAWBS and sensing properties of GAWBS. As for the fundamental properties, first, we observed the spontaneous depolarized GAWBS in an uncoated standard multi-core fiber (MCF). The GAWBS in the MCF was observed. We clarified that the frequency bandwidth of GAWBS in the side core was ~0.5 times larger than that in center core and the maximum GAWBS peak of the side core was 8 dB smaller than that of the center core [9]. This finding supports the understanding of fundamental physical properties of GAWBS in the standard MCF. Next, we observed the spontaneous depolarized GAWBS in a silica single-mode fiber (SMF) as backward scattering with the conventional pump-probe technique. The backward GAWBS was successfully observed [10]. This observation method could be basic principle of distributed sensing based on GAWBS. As for the sensing properties, first, we measured the external acoustic impedance dependence of depolarized GAWBS spectrum in silica SMF. The acoustic impedance dependence of linewidth of GAWBS was linear with a coefficient of 0.16 MHz/kg/s·mm^2 (Fig. 1), which is applicable to the chemical sensing [11]. Next, we measured temperature dependence of polarized GAWBS in a highly nonlinear fiber (HNLF) by the conversion of phase modulation to intensity modulation based on the dispersion shift property of HNLF [2]. The dependence was linear with a coefficient of 168 kHz/K, which is 1.7 times larger than that of small-core photonic crystal fibers [12]. We expect that this information will be a useful guideline for improving temperature sensing performance based on GAWBS.

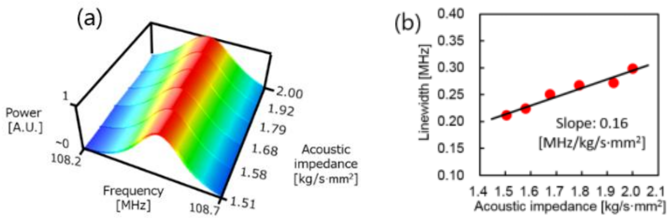

Fig. 1. Measured acoustic impedance dependences of (a) depolarized GAWBS spectrum, (b) its linewidth.

[1] R. M. Shelby, M. D. Levenson, and P. W. Bayer, Phys. Rev. B, **31** 5244–5252 (1985).
[2] C.Wolff, B. Stiller, B. J. Eggleton, M. J. Steel, and C. G. Poulton, New J. Phys. **19**, 023021 (2017).
[3] Y. Tanaka and K. Ogusu, IEEE Photon. Technol. Lett. **10**, 1769–1771 (1998).
[4] Y. Tanaka and K. Ogusu, IEEE Photon. Technol. Lett. **11**, 865–867 (1999).
[5] Y. Antman, A. Clain, Y. London, and A. Zadok, Optica **3**, 510–516 (2016).
[6] Y. Kato, Y. Wada, Y. Mizuno, and K. Nakamura, Jpn. J. Appl. Phys. **53**, 07KF05 (2014).
[7] Schlumberger Limited., *Log Interpretation Principles/ Applications* (Schlumberger Educational Services, Texas, 1991).
[8] S. K. Srivastava, R. Verma, and B. D. Gupta, Sensors and Actuators B: Chemical, **153**, 194–198 (2011).
[9] N. Hayashi, S. Y. Set, and Y. Yamashita, "Observation of spontaneous depolarized GAWBS in multi-core fibers," the 24th Congress of the International Commission for Optics, paper Th3G-03, Tokyo, Japan, August 21-25, (2017).
[10] N. Hayashi, H. Lee, Y. Mizuno, and K. Nakamura, IEEE Photon. J. **8**, 7100707 (2016).
[11] N. Hayashi, Y. Mizuno, K. Nakamura, S. Y. Set, and S. Yamashita, Opt. Exp. **25**, 2239–2244 (2017).
[12] N. Hayashi, K. Suzuki, S. Y. Set, and S. Yamashita, "Temperature dependence of polarized GAWBS spectrum in high nonlinear fibers," Conference on Lasers and Electro-Optics (CLEO) 2017, paper STh1K, San Jose, USA, May 24-28 (2017).

Non-enzymatic sensors based on in situ laser-induced synthesis of copper and copper-gold nano-sized microstructures

I.I. Tumkin, M.S. Panov, E.M. Khairullina, and V.A. Kochemirovsky

1 Saint Petersburg State University, Institute chemistry, Laser chemistry and laser materials department, Saint Petersburg, Russia

Main author email address i.i.tumkin@spbu.ru.

The development of fast, simple and reliable methods for analytical determination of hydrogen peroxide and glucose is important for many areas of medicine, science and industry. In particular, in clinical treatment and diagnostics of diabetes, cancer, atherosclerosis and many other diseases such innovative detection of the aforementioned markers is vital. The synthesis of conductive gold and copper-gold micro structures with high developed surface based on the method of laser-induced metal deposition from solution was developed.

Laser-induced chemical liquid-phase deposition (LCLD) is based on localized deposition of metal from a solution via chemical reduction of the metal or decomposition of its salt (complex) induced by laser radiation. Laser metal deposition from electrolyte solutions can be used to fabricate micro and nano sized metal structures on the surface of dielectrics and semiconductors of different types.

The electrochemical properties of the synthesized materials were investigated using cyclic voltamperometry and amperometry. According to the obtained results, it was found out that copper-gold microstructures demonstrate a linear dependence of Faraday current vs. concentration from 0.025 to 5 μM for D-glucose and from 0.025 to 10 μM for hydrogen peroxide.

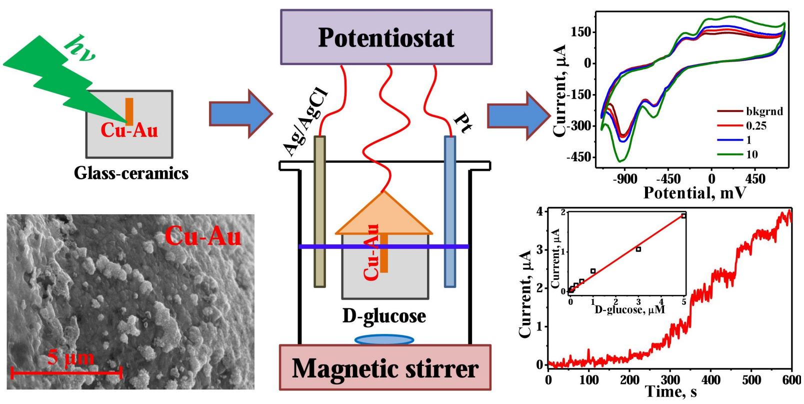

Fig.1. Illustration of the process of laser deposition of metal and the study of electrochemical properties

Acknowledgement

This work was supported by the Russian Fund for Basic Research (grants 16-33-00644 and 17-03-01266). The authors also express their gratitude to the SPbSU Nanotechnology Interdisciplinary Centre, Centre for Optical and Laser Materials Research and Center for Nanophotonics Research.

Reference

1) [21]V.A. Kochemirovsky, M.Yu. Skripkin, Yu.S. Tveryanovich, A.S. Mereshchenko, A.O. Gorbunov, M.S. Panov, I.I. Tumkin, S.V. Safonov, Russ. Chem. Rev. 84 (2015) 1059.

2) K. Lin, Y. Chen, S. Chen, Int. J. Electrochem. Sci. 10 (2015) 9205.

Phase-mode Holographic Three-dimensional Display by Optimized Binary Phase Modulation

O. Matoba[1], S. Harada[1], T. Uemae[1]

1- Graduate School of System Informatics, Kobe University, Rokkodai 1-1, Nada, Kobe 657-8501, Japan

matoba@kobe-u.ac.jp

Holographic three-dimensional (3D) display is one of the promising ways to present an ideal view of the 3D object. In the holographic 3D display, the key component is a spatial light modulator (SLM) to display the amplitude or the phase hologram. There are several types of SLMs such as MEMS (Micro-Electro-Mechanical Systems) mirror, liquid crystal, and magneto-optical effect device. Those SLM have several technical issues such as small number of pixels, large period of the pixel pitch, and amount of modulation. When a fast-operated SLM is available, the time-division multiplexing is used to enlarge the volume of the reconstructed 3D object or the viewing zone. In the fast-operated SLM, binary amplitude or phase modulation is easily implemented.

We have been developing the 3D display systems using phase modulation [1,2]. Especially, when the binary phase modulation is used, the image quality of the reconstructed object from the single binary phase hologram is degraded because of the loss of the amplitude distribution and the binarization of the phase. However, it can be improved by the optimization of the binary phase distribution and the spatial averaging of the speckle patterns [2].

In this invited presentation, we present the numerical results of the improved image quality by optimizing the binary phase distribution by using the modified Fresnel ping-pong algorithm and error diffusion technique. Further improvement can be achieved by spatially averaging the speckle patterns of the reconstructed images when random phase patterns are attached to the original image change. The experimental results are presented by using a fast-operated SLM with ferroelectric liquid crystal. Color reproduction of the reconstructed image is also improved by the proposed method.

(a) (b) (c) (d)

Figure 1 Numerically reconstructed images when the number of accumulation are (a) 1, (b), 10, (c) 30, and (d) 50.

[1] M. Tanaka, K. Nitta, and O. Matoba, "Wide-angle wavefront reconstruction near display plane in three-dimensional display system," Journal of Display Technology, Vol. 6, pp.517-521 (2010).

[2] K. Masuda, Y. Saita, R. Toritani, P. Xia, K. Nitta, and O. Matoba,"Improvement of image quality of 3D display by using optimized binary phase modulation and intensity accumulation," Journal of Display Technology, Vol. 12, pp. 472-477 (2016).

Recent progress on mesh-based computer generated hologram

Jae-Hyeung Park

1- School of Information and Communication Engineering, INHA University, Inha-ro 100, Nam-gu, Incheon, Korea, 22212

jh.park@inha.ac.kr

Computer generated holography (CGH) is a technique to synthesize the complex amplitude that corresponds to three-dimensional objects in space. Three-dimensional objects are divided into a set of primitives and the complex amplitude for every primitive is calculated and added to result in the complex amplitude for the entire three-dimensional object. Depending on the types of the primitives, the CGH techniques can be classified into point cloud method, triangular mesh method, layer method, and light ray field method. Among these methods, the triangular mesh based CGH technique has advantages in terms of the calculation efficiency and the compatibility with current computer graphics techniques. The fully-analytic mesh based CGH which uses analytic formula of the angular spectrum of the reference triangle has an additional advantage that the generated hologram is exact at the given sampling grid in the hologram plane. In this presentation, we present our recent results on the fully-analytic mesh based CGH. The presentation will include dark line artifact removal [1], realization of continuous shading and its fast update without hologram recalculation [2], realization of arbitrary directional reflectance distribution of each triangular mesh surface [3], efficient texture mapping [4], speckle reduction using time multiplexing and occlusion processing with sub-mesh occlusion.

Acknowledgememt

This research was supported by the MSIP(Ministry of Science, ICT and Future Planning), Korea, under the ITRC(Information Technology Research Center) support program (IITP-2017-2015-0-00448) supervised by the IITP(Institute for Information & communications Technology Promotion)"

[1] J.-H. Park, H.-J. Yeom, H.-J. Kim, H. Zhang, B. Li, Y.-M. Ji, and S.-H. Kim, "Removal of line artifacts on mesh boundary in computer generated hologram by mesh phase matching," Optics Express, vol. 23, pp. 8006-8013 (2015)

[2] J.-H. Park, S.-B. Kim, H.-J. Yeom, H.-J. Kim, H. Zhang, B. Li, Y.-M. Ji, S.-H. Kim, and S.-B. Ko, "Continuous shading and its fast update in fully analytic triangular-mesh-based computer generated hologram," Optics Express, vol. 23, pp. 33893-33901 (2015)

[3] H.-J. Yeom, and J.-H. Park, "Calculation of reflectance distribution using angular spectrum convolution in mesh-based computer generated hologram," Optics Express, vol. 24, pp. 19801-19813 (2016).

[4] Y.-M. Ji, H.-J. Yeom, and J.-H. Park, "Efficient texture mapping by adaptive mesh division in mesh-based computer generated hologram," Optics Express, vol. 24, pp. 28154-28169, (2016).

Viewing-zone Scanning Holographic Display Empolying MEMS-SLM

Y. Takaki

Institute of Engineering, Tokyo University of Agriculture and Technology
2-24-16, Nakacho, Koganei, Tokyo 184-8588, Japan

ytakaki@cc.tuat.ac.jp

Holography is an ideal three-dimensional display technique. Because the pixel pitch of spatil light modulators (SLMs), which display hologram patterns, should be reduced to increase the viewing zone and the resolution should be increased to enlarge the screen size, SLMs with a micron order pixel pitch and an ultra-high resolution are required to realize electronic holographic displays.

The viewing-zone scanning holography [1] has been developed to enlarge both the viewing zone and the screen size. As shown in Fig. 1, it consists of a MEMS-SLM, a magnifying imaging system, and a horizontal scanner. The MEMS-SLM generates hologram patterns at a high frame rate. The magnifying imaging system enlarges the hologram patterns so that the screen size increases. In this case, the pixel pitch also increases, thus, the viewing zone reduces. The reduced viewing zone is scanned by the horizontal scanner to enlarge the viewing zone. Therefore, both the viewing zone and the screen size are enlarged. A digital micro-mirror device (DMD) is used as the MEMS-SLM and a galvano scanner is used as the horizontal scanner. The display system having a screen size of 2.0 in. and a viewing zone angle of 40° was demonstrated. In this system, the enlargement of the screen size was limited by the mirror size of the galvano scanner.

The 360-degree holographic display [2] has also been developed based on the viewing-zone scanning holorgraphy. The rotating flat screen is used in stead of the horizontal scanner to scan the reduced viewing zone circularly around a flat screen. Because the screen size of the rotating flat screen can be made larger than that of the galvano scanner. The display system having a flat screen with a diameter of 100 mm was demonstrated.

The multi-channel display system [3] has also been developed in order to further enlarge the screen size. It consists of multiple hologram projectors and a planar scanner as shown in Fig. 2. The images produced by the multiple hologram projectors are tiled seamlessly on the planar scanner. The planar scanner consists of a rotating off-axis Fresnel lens and a vertical diffuser. The two-channel system having a screen size of 7.4 in. and a viewing zone angle of 43° was demonstrated.

The viewing-zone scanning holographic displays have been developed including the 360-degree display system and the multi-channel display system.

This study was partly supported by Japan Society for the Promotion of Science (JSPS) KAKENHI Grant Number 15H03987.

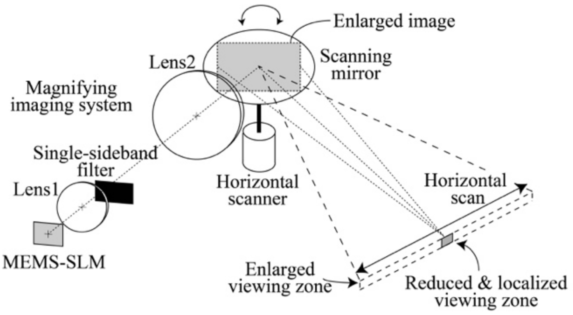

Fig. 1 Viewing-zone scanning holography.

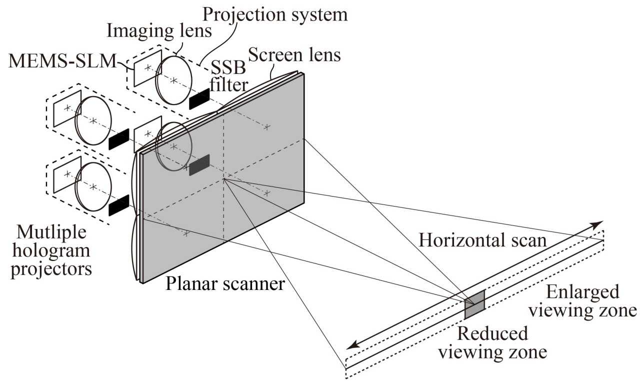

Fig. 2 Multi-channel viewing-zone scanning holography.

[1] Y. Takaki and K. Fujii, "Viewing-zone scanning holographic display using a MEMS spatial light modulator," Opt. Express, vol. 22, no. 20, 24713-24721 (2014).
[2] T. Inoue and Y. Takaki, "Table screen 360-degree holographic display using circular viewing-zone scanning," Opt. Express, vol. 23, no. 5, 6533-6542 (2015).
[3] Y. Takaki and M. Nakaoka, "Scalable screen-size enlargement by multi-channel viewing-zone scanning holography," Opt. Express, vol. 24, no. 16, 18772-18781 (2016).

Implementation of spatially-expanded 360 degree viewable holographic display (Invited)

Yongjun Lim, Keehoon Hong, Eun-Young Chang, Hayan Kim, Minsik Park and Jinwoong Kim

5G Giga Communication Research Laboratory, Electronics and Telecommunications Research Institute (ETRI), South Korea

yongjun@etri.re.kr

To overcome a low space-bandwidth product problem in conventional digital holography, it is necessary to use additional techniques such as spatial multiplexing and temporal multiplexing. Recently, implementation of those two techniques was applied to achieve 360-degree viewable holographic display system [1]. In this previously-reported work, spatial light modulators (SLMs) are arranged to increase the resultant image size of reconstructed holograms, and four digital micro-mirror devices (DMDs) are used as SLMs, and the active region of each DMD is optically stitched by the use of 4-*f* optics. In this talk, to increase the image size of 360-degree viewable color holographic display system, optical configuration for displaying color holograms is to be treated. The optical configuration for generating color holograms and the method for tiling DMDs are shown in Fig. 1. In this figure, three lasers and three DMDs for red, green and blue colors are respectively used as light sources and SLMs, and they are combined to retrieve color digital holograms. Lenses with the focal length of 180 mm and one spatial filter are used to filter out unwanted signals, and the beam splitter shown in Fig. 1 plays a role as a beam combiner. Each DMD has a pixel pitch of 13.68 μm and the pixel number of 1024 (horizontal) × 768 (vertical).

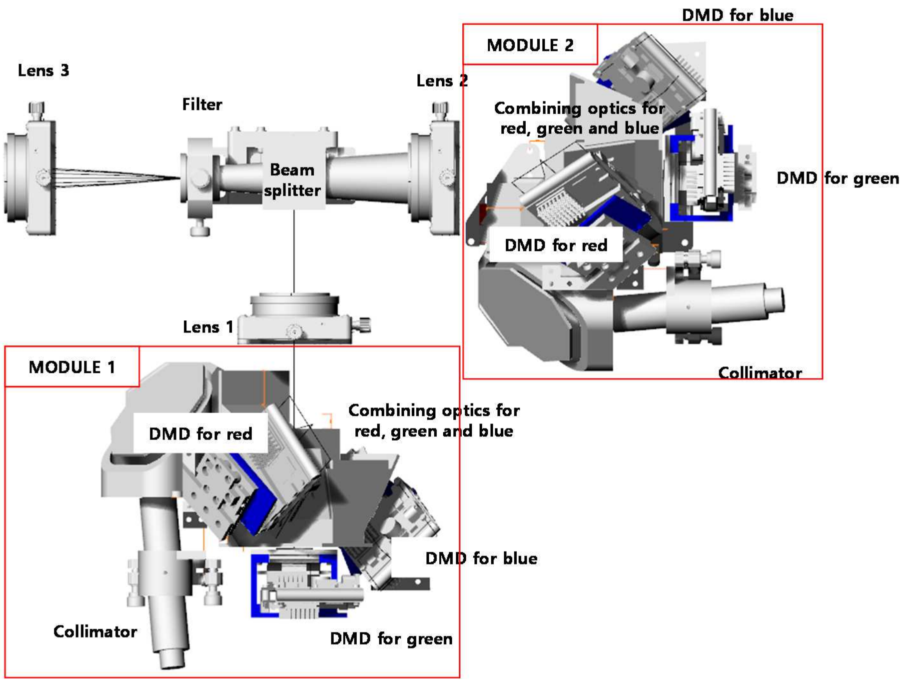

Figure 1. Schematic diagram of spatially-tiled DMDs for reconstructing color digital holograms.

Acknowledgment

This research was supported by GigaKOREA project, (GK17D0100, Development of Telecommunications Terminal with Digital Holographic Table-top Display).

[1] Y. Lim, K. Hong, H. Kim, H. Kim, E. Chang, S. Lee, T. Kim, J. Nam, H. Choo, J. Kim, and J. Hahn, Opt. Express 24, pp. 24999-25009 (2016).

Polarization-encoded multi-focal 3D display

Soon-gi Park

5 Hwarang-ro, 14-gil, Seongbuk-gu, Seoul 02792, Republic of Korea

soongi@kist.re.kr

Recent technical development of augmented reality (AR) and virtual reality (VR) is getting a lot of attention as they can provide realistic and immersive virtual experience combined with the real world. Three-dimensional (3D) displays plays an important role in AR/VR techniques. Most of the AR and VR devices in the market adopted the stereoscopic 3D display method. It is the simple but very effective method to provide 3D perception. However, lack of depth cues in this method results in a visual fatigue which reduces the comfortability of AR/VR devices. In order to increase the usability of AR/VR devices, providing accommodation cue is very important, which can alleviate the accommodation-vergence conflict.

There have been many attempts to realize accommodation cues in 3D displays. A multi-focal method is one of the solutions that can provide accommodation cues by optical techniques. By providing multiple focal planes, a multi-focal display can express 3D objects in a specific volume. However, the expanded volume of 3D images requires tremendous amount of data which is approximately hundreds times higher than that of conventional two-dimensional (2D) images. For this reason, various kinds of multiplexing technique has been adopted including mechanical sweeping, optical switching, or tiling of images. However, these kind of method entails additional devices which increases system complexity.

A new method has been proposed to solve this problem, which can deliver 3D information by the polarization state of 2D images [1]. Polarization-encoded depth map is an image which contains depth information as a state of polarization for each pixel as shown in Fig. 1.

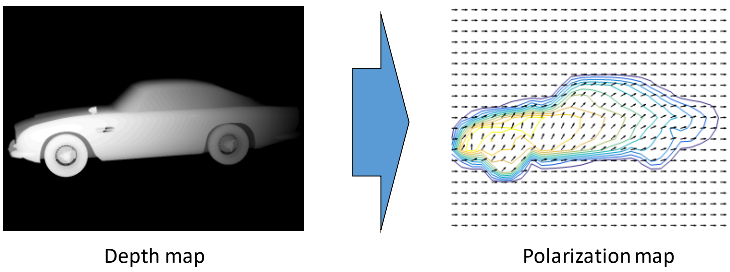

Fig. 1 Concept of the polarization-encoded depth map

As human can not recognize the polarization state, it needs to be decoded into 3D images. In order to reconstruct 3D images from the polarization-encoded depth map, polarization-selective optical devices are required such as polarizers, scattering polarizers, or birefringent materials [2, 3]. Those differences result in slicing of 3D images into the longitudinal direction. If those sliced images are distributed over a specific volume, observers can perceive 3D objects by after image effect and depth-fusing effects [4]. The proposed method can be applied to various display platforms from micro 3D displays for AR/VR application to projection-type immersive large scale glasses-free 3D applications. We believe that it can be a promising method which will widen the 3D display applications in industrial, educational, medical, or entertainment fields.

[1] S.-g. Park, J. Kim, and S.-W. Min, "Polarization distributed depth map for depth-fused three-dimensional display," Opt. Express 19, 4316-4323 (2011).

[2] S.-g. Park, S. Yoon, J. Yeom, H. Baek, S.-W. Min, and B. Lee, "Lamina 3D display: projection-type depth-fused display using polarization-encoded depth information," Opt. Express 22, 26162-26172 (2014).

[3] S. Yoon, H. Baek, S.-W. Min, S.-g. Park, M.-K. Park, S.-H. Yoo, H.-R. Kim, and B. Lee, "Implementation of active-type Lamina 3D display system," Opt. Express 23, 15848-15856 (2015).

[4] S. Suyama, S. Ohtsuka, H. Takada, K. Uehira, and S. Sakai, "Apparent 3-D image perceived from luminance-modulated two 2-D images displayed at different depths," Vision Res. 44(8), 785–793 (2004).

Diffraction microgratings as a novel optical biosensing platform

T. T. H. Nguyen[2,4]**, T. V. Baikova**[1]**, P. N. Danilov**[2,3]**, S. A. Gonchukov**[1]**, V. M. Yermachenko**[1]**, A. A. Ionin**[2]**, R. A. Khmelnitskii**[2]**, S. I. Kudryashov**[2,3]**, A. A. Rudenko**[2]**, I. N. Saraeva**[2,3]**, T. S. Svistunova**[5]**, D. A. Zayarny**[2]**.**

1 - National Research Nuclear University MEPhI (Moscow Engineering Physics Institute), Kashirskoeshosse 31, 115409 Moscow, Russia

2 - Lebedev Physical Institute, Leninskiy prospect 53, 119991 Moscow, Russia; email: sikudr@sci.lebedev.ru

3 - ITMO University, Kronverkskiy prospect 49, 197101 St. Peterburg, Russia, Russia

***4** - Moscow Institute of Physics and Technology, Institutskiypereulok 9, 141701 Dolgoprudny, Moscow Region, Russia*

5 - Infectious Clinical Hospital No 2, 8-thSokolinaya Gora street 15, 105275 Moscow, Russia

Email: trang.nguyenthihuyen@htu.edu.vn

We used a 30-nm thick silver (Ag) film with a optical-quality surface, deposited onto a 1-mm thick CaF_2 substrate by magnetron sputtering of a commercial Ag plate (99.99%) in argon. The diffraction micrograting with diameter ≈ 4 μm and period ≈ 6 μm as a SEIRA sensor (Fig. 1a) was produced via single-shot ablation of the film by moderately (NA ≈ 0.25) focused 515 nm, 220 fs TEM_{00}-mode laser pulses with the energy of 85 nJ (the peak fluence ≈ 0.27 J/cm^2, the threshold fluence for hole formation F_{hole} ≈ 0.14 J/cm^2) (Fig. 1a), and characterized by means of scanning electron microscopy (SEM, JEOL 7001F). IR unpolarized transmittance of the sensor (both – clean and with an effective, on average, monolayer of Staphylococcus aureus (SA) bacteria deposited, was measured in vacuum in the near-mid IR range of spectral wavenumbers υ = 400-5000 cm^{-1}, using a FT-IR spectrometer V-70 (Bruker) [1].

Using a micro-hole grating in a supported silver film as a laser-fabricated novel optical platform for surface-enhanced IR absoprtion/reflection spectroscopy, characteristic absorption bands of Staphylococcus aureus, especially – its buried carotenoid fragments – were detected in FT-IR spectra with 10-fold analytical enhancement, paving the way to spectral express-identification of the pathogenic microorganisms (Fig. 1b, c) [2].

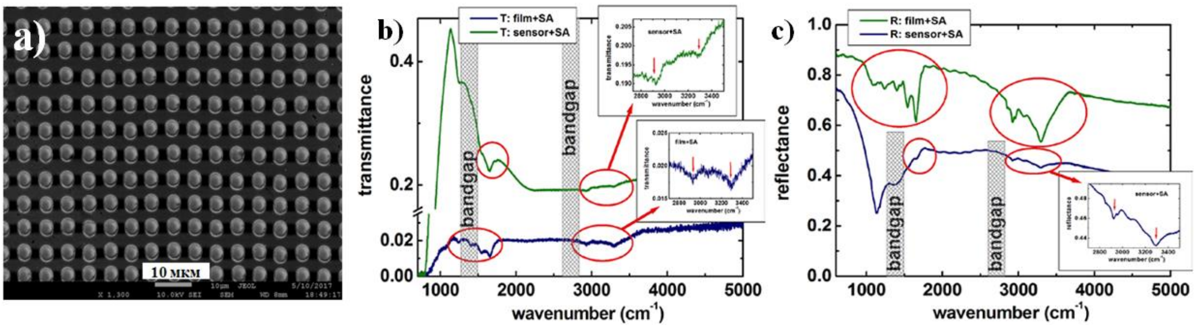

Figure 1: a) SEM-images of diffraction micrograting. b) IR transmission (T) spectra of the film (bottom curve) and the sensor (upper curve) with the SA-layer. c) IR reflection (R) spectra of the film (upper curve) and the sensor (bottom curve) with the SA layer. The red ellipses highlight the characteristic SA absorption bands and their high-frequency overtones. The red arrows point to the insets, presenting the magnified views of the overtone amplitudes for the internal calibration.

[1] P. N. Danilov, S. A. Gonchukov, A. A. Ionin, R. A. Khmelnitskii1, S. I Kudryashov, T. T. H. Nguyen, A. A. Rudenko, I. N Saraeva and D. A. Zayarny, Background-free, highly sensitive surface-enhanced IR absorption of rhodamine 6G molecules deposited onto an array of microholes in thin silver film. Laser Phys. Lett., 13, 055602 (5pp) (2016).

[2] T. V. Baikova, P. A. Danilov, S. A. Gonchukov, V. M. Yermachenko, A. A. Ionin, R. A. Khmelnitskii, S. I. Kudryashov, T. T.H. Nguyen, A. A. Rudenko, I. N. Saraeva, T. S. Svistunova, D. A. Zayarny, Diffraction microgratings as a novel optical biosensing platform, Las. Phys. Lett., 13 (7), 070602 (2016).

Temperature dependent behavior of $Zn_{0.7}Co_{0.3}O$-based memristors

A.A. Lotin[1], O.A. Novodvorsky[1], L.S. Parshina[1], V.A. Mikhalevsky[1], O.D. Khramova[1], E.A. Cherebilo[1]

1- Federal Scientific Research Center "Crystallography and Photonics" RAS, 1 Svyatoozerskaya St., Shatura, 140700, Russia

lotin_82@mail.ru

The memristors based on ZnCoO magnetic semiconductor have been created by pulsed laser deposition method and the temperature dependence of the I-V characteristic of these structures has been studied for the first time. The active area of the memristor thickness ~50 nm consists of two equal on thickness layers - the isolating $Zn_{0.7}Co_{0.3}O$ and the conductive $Zn_{0.7}Co_{0.3}O_y$ synthesized in the oxygen atmosphere and high vacuum conditions, respectively (Fig. 1a, b). The I-V characteristic of such structure demonstrated memristive effect at room temperature. It was established that the current magnitude, the loop area and memristive effect considerably increased at increasing of temperature.

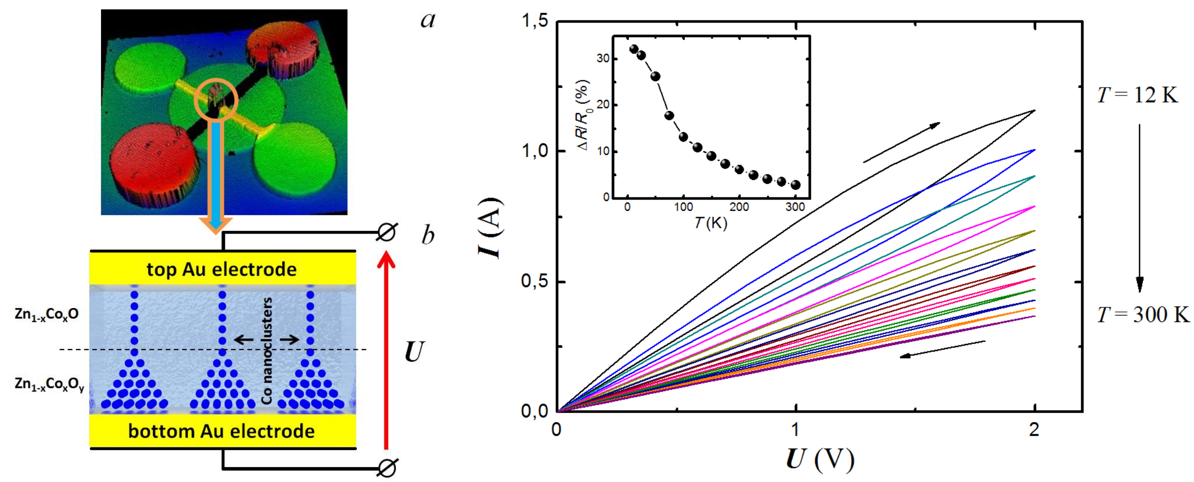

Fig.1. 3d-image (*a*), a cross direction profile (*b*) and the I-V characteristic in dependence on temperature (*c*) of $Zn_{0.7}Co_{0.3}O$-based two-layer memristor. An insert – the resistance change as function of temperature.

It should be noted that the same temperature behavior of conductivity is typical for metals. Earlier we shown [1] that the cobalt nanoclusters are formed in $Zn_{0.7}Co_{0.3}O_y$ films synthesized in the oxygen depleted conditions. At rather high Co concentration (> 16%) nanoclusters can form the carrying-out filaments [2] which provide metallic conductivity in the temperature dependence of I-V characteristic. The cut-off chemical bonds of metal nanoclusters under the influence of external electric field form avalanches and this effect is stronger appeared at low temperature.

This research was supported by the Russian Foundation for Basic Research projects 15-07-03331, 15-29-01171, 15-07-03580, 16-29-05385, 16-07-00842, 17-07-00615.

[1] A.A. Lotin, O.A. Novodvorsky, V.V. Rylkov, et al., Properties of $Zn_{1-x}Co_xO$ films produced by pulsed laser deposition method with speed separation of particles. Semiconductors, vol. 48, pp. 556-563 (2014).
[2] K.M. Kim, G.H. Kim, S.J. Song, et al., Electrically configurable electroforming and bipolar resistive switching in Pt/TiO2/Pt structures, Nanotechnology, vol. 21, pp. 305203-305210 (2010).

Polarization diversity scheme in phase-OTDR based on coherent detection

Gukbeen Ryu[1,2], Gyu-Tae Kim[2], Kwang Yong Song[3], Sang Bae Lee[1], Kwanil Lee[1]

1- Nanophotonics Research Center, Korea Institute of Science and Technology (KIST), Seoul 02792, Korea
2- School of Electrical Engineering, Korea University, Seoul 02841, Korea
3- Dept. of physics, Chung-Ang University, Seoul 06974, Korea

klee21@kist.re.kr

Recently, as one of the distributed optical fiber sensing technique, phase-optical time domain reflectometry (OTDR) that can detect the external vibration by measuring the interference signal between the Rayleigh scattered lights has been widely studied, where the light source with a narrow linewidth is modulated as a pulse and launched into the fiber under test [1]. Also the coherent detection scheme has been introduced to compensate the weak Rayleigh scattering in optical fiber in order for the increased signal to noise ratio (SNR) [2]. However, since the backscattered light is mixed with a local oscillator (LO) and the polarization state between the two lights can be mismatched, the fading phenomenon of the signal occurs, which can cause the deteriorated interference signal at some positions and the decreased SNR.
In this paper, we utilize a polarization diversity scheme to solve this problem [3]. To reduce the fading effect by the polarization mismatch in the coherent detection, the polarization states of the backscattered light and the LO is divided into two orthogonal polarization states respectively by a polarization beam splitter and then the lights with the same states were combined with each other. The two combined signal with the each orthogonal state are detected by two balanced photodetector and the figures 1(a) and 1(b) show examples of the respective results. By additionally combining the two results as shown in Fig. 1(c), the polarization dependence could be lowered and the polarization fading of the signal is also reduced, which could make a more reliable vibration detection.

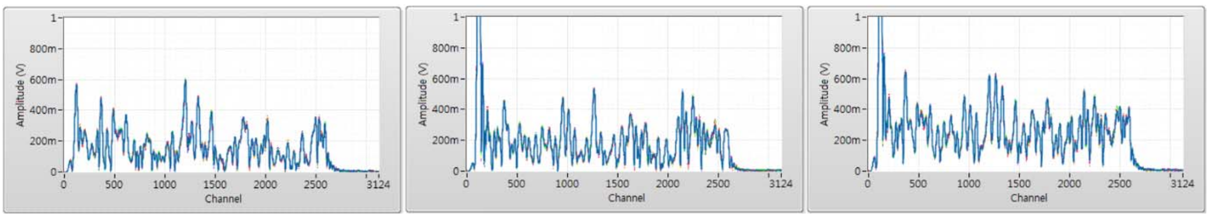

(a) (b) (c)

Fig. 1(a), (b) Phase-OTDR traces divided into two orthogonal polarization states and (c) the combined trace.

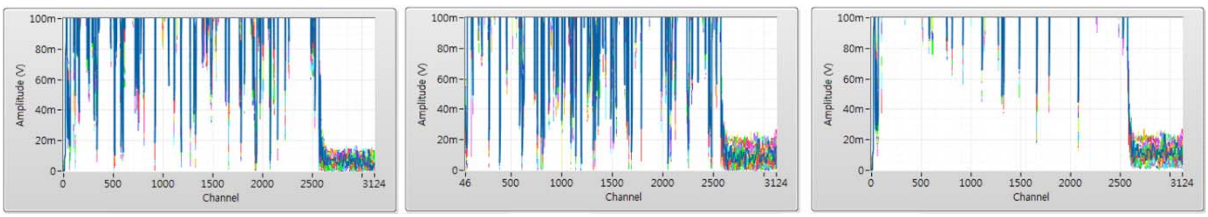

Fig. 2 An enlargement of the Fig. 1 in a low-intensity section, which shows the reduced signal fading induced by the polarization mismatch.

[1] H. F. Tarlor, C. E. Lee, Apparatus and method for fiber optic intrusion sensing, U. S. Patent, 5194847, (1993).
[2] Y. Lu, T. Zhu, L. Chen, X. Bao, Distributed vibration sensor based on coherent detection of phase-OTDR, J. Lightw. Technol., vol. 28, pp. 3243-3249, (2010).
[3] M. Ren, P. Lu, L. Chen, and X. Bao, Theoretical and experimental analysis of phase-OTDR based on polarization diversity detection, IEEE Photonics Technology Letters, vol. 28(6), pp. 697-700, (2016).

Fiber optic pressure sensor based on Sagnac polarization interferometer with tapered birefringent fiber

Sungwook Choi[1], Jihoon Kim[2], Seul-Lee Lee[1], Jun Hyeok Jeong[1], Sun Jae Jeong[1], Min Seok Kim[1], Dokyeong Kim[1], and Yong Wook Lee[1,2,*]

1- *Interdisciplinary Program of Biomedical, Mechanical & Electrical Engineering, Pukyong National University, 45 Yongso-ro, Nam-gu, Busan 48513, Korea*

2- *School of Electrical Engineering, Pukyong National University, 45 Yongso-ro, Nam-gu, Busan 48513, Korea*

yongwook@pknu.ac.kr

In recent years, optical fibers used mainly as optical communication lines can be applied to sensors. Such optical fiber sensors are widely used in a variety of industrial fields because they have advantages such as small size, light weight, and independence from electromagnetic interference as compared with electronic sensors. Most of the fiber-optic pressure sensors are based on interferometers. Among them, Fabry-Perot interferometer based optical fiber pressure sensors based on optical intensity variations from diaphragm are widely studied [1]. However, the Fabry-Perot interferometer based optical fiber pressure sensors have problems such as a change in the light intensity generated on the surface of the film, a change in the power of the input light source, and a micro banding loss in the sensor head. To solve these problems, many researchers are currently studying a wavelength dependent optical fiber pressure sensor based on interferometer [2]. In this paper, we propose a highly sensitive optical fiber pressure sensor based on polarization-diversity loop Sagnac interferometer composed of a polarization beam splitter, a wave plate combination composed of a half-wave plate and a quarter-wave plate, and a sensor head. The sensor head is composed of a tapered panda-type high birefringent fiber (HBF) of 8 cm in length and a fiber Bragg grating (FBG). The center portion of the HBF was tapered to a length of 350 μm using a fusion splicer, and an FBG is used for temperature compensation. The pressure sensitivity of the sensor was measured as approximately –13.229 nm/MPa, and a R^2 value representing the linearity was measured as ~0.9789 in a measurement range of 0–0.3 MPa. The proposed sensor has the pressure sensitivity higher than other polarimetric fiber pressure sensors.

[Acknowledgements]
This research was supported by a grant from Marine Biotechnology Program(20150220) funded by Ministry of Oceans and Fisheries, Korea.

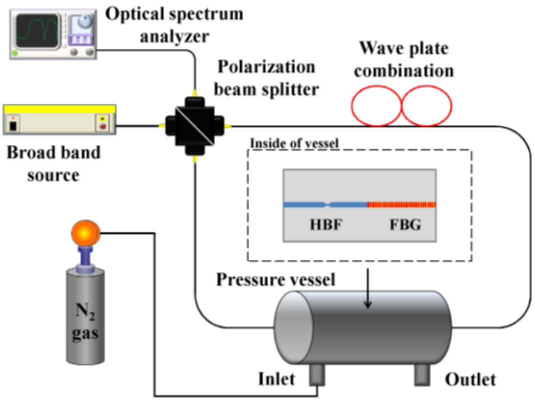

Fig. 1. A schematic diagram of the proposed optical fiber pressure sensor system

[1] E. Cibula and D. Donlagic, "Miniature fiber-optic pressure sensor with a polymer diaphragm," *Appl. Opt*., vol. 44, pp. 2736-2744, (2005).
[2] Z. Li, C. Liao, Y. Wang, L. Xu, D. Wang, X. Dong, S. Liu, Q. Wang, K. Yang, and J. Zhou, "Highly-sensitive gas pressure sensor using twincore fiber based in-line Mach-Zehnder interferometer," Opt. Express 23, pp.6673,(2015).

Temperature Sensitivity of Optical Fibers in Optical Frequency Domain Reflectometry

Yong-seok Kwon[1,2], Khurram Naeem[1], Min Yong Jeon[2*], Il-bum Kwon[1+]

1. *Korea Research Institute of Standards and Science, Yuseong-gu Daejeon, Republic of Korea,*
2. *Department of Physics, Chungnam National University, Daejeon, Korea*

**myjeon@cnu.ac.kr* +*ibkwon@kriss.re.kr*

Optical Frequency Domain Reflectometry (OFDR) is a distributed optical fiber sensor that measures temperature, vibration, and strain in the direction of light propagating through the optical fiber [1],[2]. The spatial resolution of the OFDR depends on the sweeping frequency bandwidth of the optical source. Therefore, a high spatial resolution can be obtained by using a laser having a wide frequency sweeping range. In general, OFDR is divided into small segments and measures the frequency variation in the segment, so strain and temperature according to spatial distribution are measured. However, the use of a laser with a wide frequency sweeping range can increase the spatial resolution, but the temperature resolution is degraded due to their narrow segment setting. This means that there is a trade-off relationship between spatial resolution and temperature resolution.

In order to solve this problem, we propose a method to realize OFDR using optical fiber with high temperature sensitivity. One way to increase the temperature sensitivity of a fiber is to use an optical fiber coated with a material having high temperature sensitivity. Aluminum (Al) has good volume expansion efficiency due to temperature change and is well attached to silica because it is a metal, so temperature change is well transferred to the strain change. Therefore, if OFDR is implemented using an optical fiber coated with Al, the sensing efficiency can be increased with respect to changes in temperature. In this paper, we can achieve the temperature sensitivity is about 1.43 GHz/K by using single mode fiber without jacket for OFDR. On the other hand, the temperature sensitivity of 1.89 GHz/K is obtained for the optical fiber coated with Al. Therefore, by using an optical fiber coated with Al in OFDR, the temperature sensitivity can be improved as the amount of about 30%.

[1] W. Eickhoff and R. Ulrich, Optical frequency domain reflectometry in single-mode fiber, Applied Physics Letters, Volume 39, Issue 9, August 1998.

[2] Jia Song, Wenhai Li, Ping Lu, Yanping Xu, Liang Chen, Xiaoyi Bao, Long-Range High Spatial Resolution Distributed Temperature and Strain Sensing Based on Optical Frequency-Domain Reflectometry, IEEE Photonics Journal, Volume: 6, Issue: 3, June 2014.

Temperature sensitivity of Ge-doped core PCF interrogated by optical frequency domain reflectometer

Khurram Naeem[1], Yong-seok Kwon[1, 2], and Il-Bum Kwon[1*]

1- Korea Research Institute of Standards and Science (KRISS), Daejeon 34113, Republic of Korea.
2- Department of Physics, Chungnam National University, Daejeon 34134, Republic of Korea
**Email address: ibkwon@kriss.re.kr*

Optical frequency domain reflectometer (OFDR) is well-known technique for distributed sensing applications [1] due to its simple configuration. OFDR uses spectral shift of Rayleigh backscattering (RBS) in optical fiber to measure the local change in the refractive index and fiber length with high spatial resolution and high sensitivity. The local spectral shift in the RBS signal caused by the sensing variation can be obtained by computing the cross-correlation between the sensing RBS and reference RBS. Distributed temperature measurement is important for various practical applications in structural health monitoring and other safety purposes. Usually, the OFDR employ conventional optical fibers for temperature sensing. However, the conventional optical fiber exhibit high bending losses, which limits the use of OFDR in practical sensing applications requiring sharp bending turns of the fiber.

Photonic crystal fiber (PCF) is a new kind of optical fiber with air holes around the core running all along the fiber length [2]. It is usually made of single material silica. The surrounding air holes acts like a trench around a core, thus light travel in the fiber core with strong confinement, and experience low or negligible loss of light-power in the event of fiber bending [2]. All-silica PCF cannot be used for temperature sensing as the thermo-optic (TO) mismatch between the solid-silica core and air-silica cladding (both have similar TO properties) is negligible. However, a large thermo-optic mismatch can be introduced in the PCF either by doping the core during fabrication or filling the air holes in cladding after fabrication with temperature-sensitive material.

In this work, we demonstrate a distributed measurement of temperature by using home-made PCF with Ge-doped core in the OFDR setup. The section of Ge-doped core PCF [3] is sandwiched between two single-mode fibers (SMFs). The diameters of core and air hole on average are ~5.1μm and ~1 μm, respectively. The air-filling fraction is measured to be 0.34, which means that our PCF is endlessly single-mode. Temperature measurement was performed by placing an uncoated PCF in the mini-oven (~6 cm) and the measurement range was 26-120 ^{o}C. During OFDR measurement, the laser sweeping-range was 0.5THz which yielded a spatial resolution of 0.2 mm. A linear response was observed between the temperature-change and the spectral shift of RBS, and temperature sensitivity was measured to be 1.46 GHz/ ^{o}C which is almost similar to that of standard SMF.

[1] J. Song, W. Li, P. Lu, Y. Xu, L. Chen and X. Bao, "Long-range high spatial resolution distributed temperature and strain sensing based on optical frequency-domain reflectometry," IEEE Photonics Journal, vol. 6, no. 3, pp. 1-8, (2014)

[2] H-M. Kim, T-H. Kim, B Kim, and Y. Chung, "Enhanced transverse load sensitivity by using a highly birefringent photonic crystal fiber with larger air holes on one axis," Appl. Opt. vol. 49, no. 20, pp. 3841-3845, (2010)

[3] K.Naeem, and Y.Chung, "Strain and temperature discrimination using PCF Bragg-gratings filled with different liquids", OptoElectronics and Communication Conference (OECC) and Australian Conference on Optical Fibre Technology (ACOFT), pp. 795-796, Melbourne, Australia, 6-10 Jul. (2014)

Investigated on weak value amplification for sensitivity improvement of fiber Bragg grating sensors

Kwang-Wook Yoo, Ju Il Hwang, and Young-Geun Han*

*Department of Physics, Hanyang University, Seoul, Republic of Korea, *yghan@hanyang.ac.kr*

Fiber gratings classified by fiber Bragg gratings (FBGs) and long-period fiber gratings (LPFGs) have been attracting much attention in optical sensors because of their many advantages, such as wavelength-selective nature, easy adaptability, low loss, etc. External perturbations essentially change the center wavelength of fiber gratings [1-3]. The weak value amplification (WVA) technique was proposed to improve the sensitivity of the fiber grating sensor to external perturbation. Recently, the polarization-based WVA was investigated to enhance the temperature sensitivity of the FBG sensor. The previous method, however, has many drawbacks, such as complicated structure, instability of experimental setup, and experimental inconvenience due to polarization. In this paper, we propose a new method of the WVA based on the optical attenuation to improve the performance of the FBG sensor, which has a simple structure compared to the polarization-based WVA. The strain sensitivity of the FBG sensor using the proposed attenuation-based WVA is successfully enhanced.

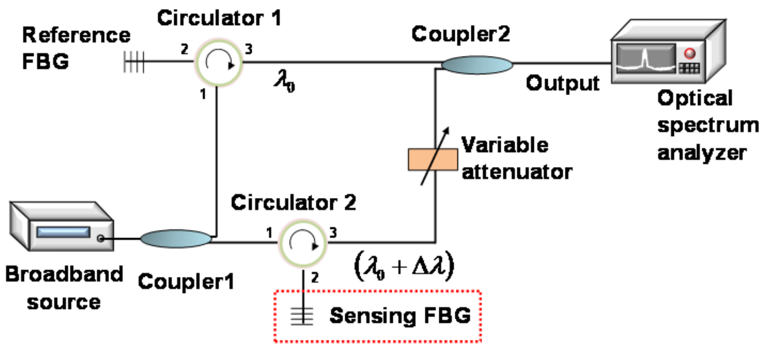

Figure 1. Experimental scheme for the optical attenuation-based WVA.

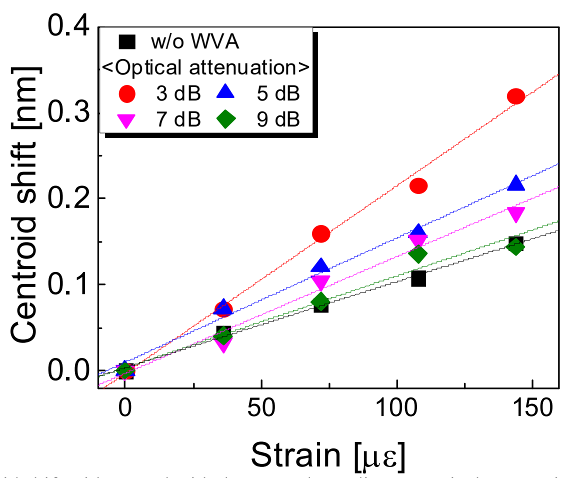

Figure 2. Centroid shift without and with the WVA depending on optical attenuation as a function of strain

[1] Kersey, A. D., Davis, M. A., Patrick, H. J., LeBlanc, M., Koo, K. P, Askins, C. G., Putnam, M. A. and Friebele, E. J., "Fiber grating sensors," J. Lightwave Technol., vol. 15, pp. 1442 – 1463 (1997).
[2] Han, Y. G., Lee, S. B., Kim, C. S., Kang, Jin U., Park, U. C. and Chung, Y., "Simultaneous measurement of temperature and strain using dual long-period fiber gratings with controlled temperature and strain sensitivity," Opt. Express, vol. 11, pp. 476 – 481 (2003).
[3] Aharonov, Y., Albert, D. Z. and Vaidman, L., "How the result of a measurement of a component of the spin of a spin half particle can turn out to be 100," Phys. Rev. Lett., vol. 60, pp. 1351 – 1354 (1988).

Sensitivity improvement of relative humidity sensor with few-mode microfiber knot resonator by alleviating group index difference

Duy Duong Anh Le and Young-Geun Han*

*Department of Physics, Hanyang University, Seoul, South Korea, *yghan@hanyang.ac.kr*

Optical fiber sensing techniques have been attractive in various applications to mechanical, chemical, biological, and environmental industries for measurement of temperature, strain, ambient index, liquid level, and so on [1-3]. Fiber-optic relative humidity (RH) sensors have been widely investigated in a variety of applications in meteorology, medicine, agriculture, and architectural engineering fields [1-3]. In this paper, a few-mode microfiber knot resonator (FM-MKR) is presented for measurement of RH. The proposed FM-MKR includes two optical phenomena, such as optical modal interference in the few mode microfiber and optical coupling in the FM-MKR. When the waist diameter of the microfiber is 4 μm, two modes, such as HE_{11} and HE_{12}, should be excited and interfered together in the nonadiabatically tapered region of the SMF. After making a tie with the few-mode microfiber with a diameter of 4 μm, the FM-MKR can be fabricated. In the FM-MKR, two modes must be circulated within the optical knot and cross-coupled independently with a phase delay. To detect RH, the FM-MKR is coated by using the PVA which effectively absorbs humidity in the external environment. For the microfiber with a diameter of 4 μm, the difference of group effective refractive indices between HE_{11} and HE_{12} modes becomes nearly zero and the sensitivity of the FM-MKR to RH can be successfully improved.

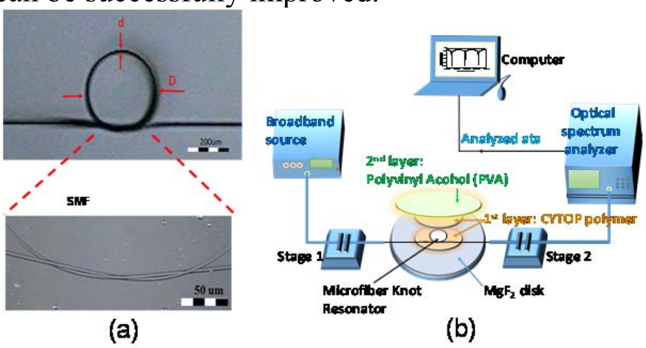

Figure 1. (a) Microscopic images of the fabricated FM-MKR and (b) experimental setup for the proposed RH sensor based on the FM-MKR.

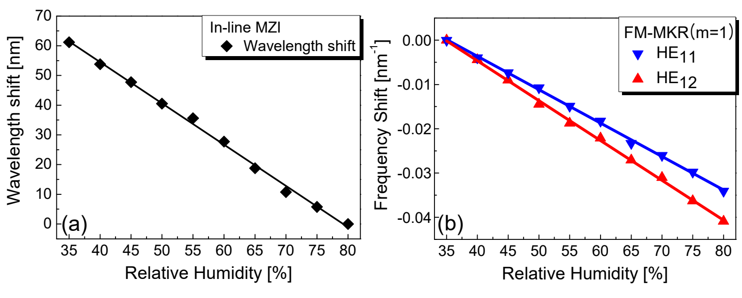

Figure 2. Resonant wavelength and (b) frequency shifts with variations in RH.

[1] W. C. Wong, C. C. Chan, L. H. Chen, T. Li, K. X. Lee, and K. C. Leong, "Polyvinyl alcohol coated photonic crystal optical fiber sensor for umidity measurement," Sens. Actuators B, vol. 174, pp. 563-569, 2012.
[2] D. Su, X. Qiao, Q. Rong, H. Sun, J. Zhang, Z. Bai, Y. Du, D. Feng, Y. Wang, M. Hu, and Z. Feng, "A fiber Fabry–Perot interferometer based on a PVA coating for humidity measurement," Opt. Commun., vol. 311, no. 194, pp. 107–110, 2013.
[3] P. Hu, X. Dong, K. Ni, L. H. Chen, W. C. Wong, and C. C. Chan, "Sensitivity-enhanced Michelson interferometric humidity sensor with waist-enlarged fiber bitaper," Sens. Actuators B Chem., vol. 194, pp. 180–184, 2014

Laser Micromachining Processes in Formation of Blade Ring-Shaped Emitting Structures out of Glassy Carbon

T. Sokolova[1], E. Surmenko[1], D. Bessonov[1], I. Popov[1], Yu. Chebotarevsky[1], V. Shesterkin[2]

1- Saratov State Technical University, 77 Polytechnicheskaya st., 410054, Saratov, Russia
2- JSC "SPE "Almaz", 1 Panfilova st., 410033, Saratov, Russia
sokolova@pribor-t.ru

Paper describes the method of creating the sharp emitting blades on the surface of a glassy carbon field-emission cathode (FEC). The blade ring-shaped structures on the glass-carbon plate are produced by means of nanosecond laser micromachining.
The operations of laser cutting, milling and cleaning were applied for fabrication of the blade FEC with four grooves. The special technique of laser rough and fine milling provided high blades with sharp and smooth apexes (Figure 1). The tests of cathodes showed that high density of current emission and a shorter technological route of production to be reached.

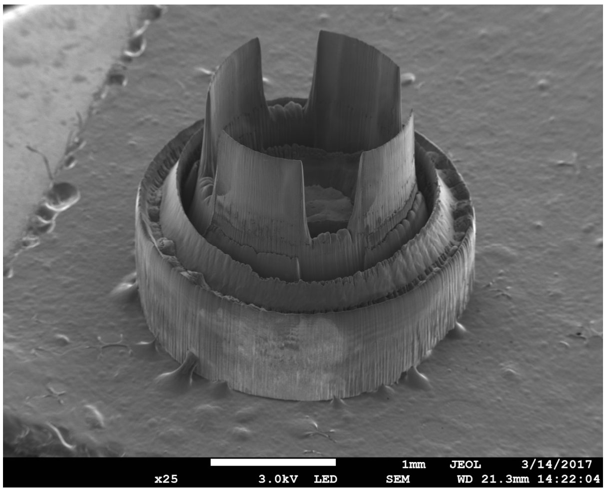

Figure 1 Blade ring-shaped field emission cathode

Laser cutting, milling and cleaning were performed with D-Mark laser commercial installation with parameters: Q-switched Nd:YAG diode-pumped laser, λ=1.06 μm, mean power P=6.7 W, pulse duration 70 ns. Visual investigationwas carried out with MIRA/TESCAN electron microscope. Fabrication of FEC includes several stages, each of which used a separate driving computer program.
The proposed solution results to increase the density of the electron beam current by more than 10 times compared to the previous model with a flat surface [1].
Acknowledgements: The work was implemented on the equipment of the regional branch of CCU "Laser and Optical Technologies",contract 02.552.11.7021 (08.05.2007) in the framework of the basic part of the State Task № 732.

[1] T. N. Sokolova, E.L. Surmenko et al, Laser structuring of glass-carbon for improvement of its emitting properties, Bern Open Publishing / ALT Proceedings, vol.1, https://bop.unibe.ch/ALT-Proceedings/article/view/44, (2012).

The production by PLD of iron nanoparticles used for the growth of carbon nanotubes

O. Novodvorsky[1] , E. Cherebylo[1], F. Putilin[2], A. Egorov[2], S. Savilov[2], O. Khramova[1], V. Mikhalevskiy[1], L. Parshina[1], A.Lotin[1]

1-ILIT RAS – Branch of FSRC "Crystallography and Photonics" of RAS, 1, Svyatoozerskaya str., Shatura, 140700, Moscow Region, Russia
2- Faculty of Chemistry, M.V. Lomonosov Moscow State University, 1 Leninskie Gory, Moscow 119991, Russia

Main author E-mail address:onov@mail.ru

The iron nanoparticles were synthesized by laser deposition method, this particles serve as nucleation centers for the growth of carbon nanotubes. The PLD method makes it possible to obtain continuous films of various materials in uniform with respect to thickness in the droplet free regime [1]. We obtained iron films from 0.5 to 4 nm in thickness at room temperature deposition on silicon (100) and c-sapphire substrates in vacuum. After deposition without depressurization of the chamber, the films were annealed at 500 ° C for 10 minutes followed by vacuum cooling. This led to the formation of iron nanoparticles on the surface of the substrate. The iron films were examined on an electron microscope both before and after annealing. The dimensions of the nanoparticles increased with increasing film thickness. Nanoparticles with a lateral size of 10 to 30 nm are formed from films 0.5 nm thick. X-ray phase analysis of the films was also performed, which showed the presence of α-iron. On the surface of a substrate containing iron nanoparticles, carbon nanotubes were formed by chemical vapor deposition. The synthesis of CNTs was carried out at a substrate temperature of 850 °C and at a reaction gas consumption of C_2H_2 - 50 ml / min, H_2 - 200 ml / min. As a result of the synthesis, carbon nanotubes about 50-60 nm in diameter were formed. The CNT image obtained in an electron microscope is shown in Fig.1.

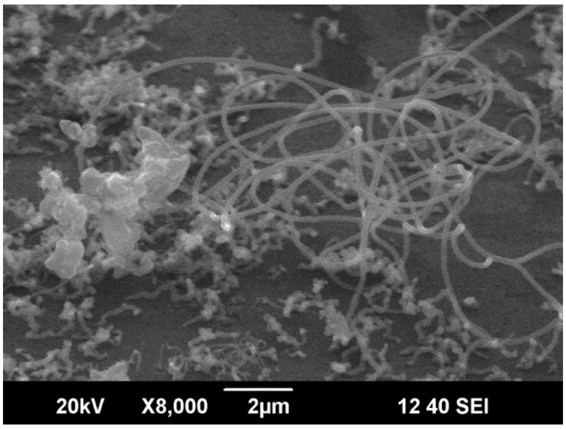

Fig.1. Carbon nanotubes synthesized on iron nanoparticles.

Acknowledgements
The work is supported by RFBR projects No 15-29-01171, 16-07-00657, 16-07-00842, as well as projects of ONIT RAS (program code IV.3.3) and PRESIDIUM of the RAS (Code I.III).

[1]. L. S. Parshina, O. D. Khramova, O. A. Novodvorsky, A. A. Lotin, I. A. Petukhov, F. N. Putilin, K. D. Shcherbachev. Effect of energy density on the target on SnO2:Sb film properties when using a high-speed particle separator/ Semiconductors, Volume 51, Issue 3, pp. 407–411, (2017).

TiO_2 thin films for memristors

O. Novodvorsky[1] , L. Parshina[1], A. Lotin[1], V. Rylkov[2], O. Khramova[1], V. Mikhalevskiy[1], E. Cherebylo[1], V. Panchenko[1]

1-ILIT RAS – Branch of FSRC "Crystallography and Photonics" of RAS, 1, Svyatoozerskaya str., Shatura, 140700, Moscow Region, Russia
2-National Research Centre «Kurchatov Institute», Akademika Kurchatova pl., 1, Moscow, 123182 Russia

Main author E-mail address:onov@mail.ru

The memristive structures of Au/TiO_{2-x}/Au with various contents of oxygen vacancies have been created by the droplet-free PLD method on c-sapphire substrates using mask technologies with a different content of oxygen vacancies or a TiO_{2-x} layer with a smooth or abrupt change in the value of x and their properties have been studied. The films with different oxygen contents were deposited by changing the oxygen pressure in the chamber. To measure the I-V characteristics a voltage pulse was applied on a sample and the current was measured. Then the voltage value was set to 0, and with a certain delay the following pulse was applied. The amplitudes of the pulses changed under the preset law with a certain step. The pulse duration and filling factor could be adjusted. Further the I-V curves were plotted by the resulting pairs of voltage and current values.
The sharp change of concentration of oxygen vacancies (the pressure in the chamber is $2\cdot10^{-3}$ Topp at the first stage of TiO_{2-x} film growth and $3\cdot10^{-3}$ Torr at the second stage) results in the specific resistance of the memristor in the switched-off condition equal to 2000 Ohm·cm. Fig. 1 represents the I-V curve of the memristor at the first positive bipolar switching.

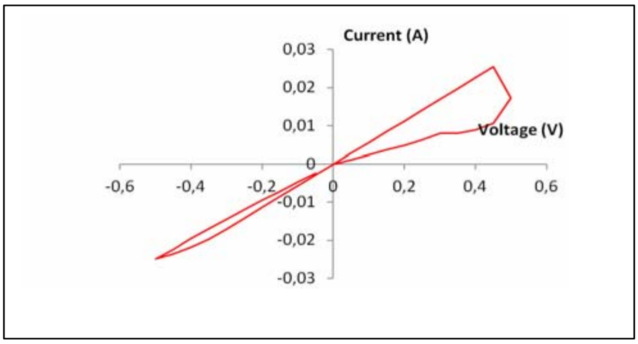

Fig. 1. The I-V curve of the memristor with a sharp boundary of oxygen vacancy concentration in a TiO2-x film (the oxygen pressure in the chamber is 2*10-3 Torr and 3*10-3 Torr) at the first bipolar switching.

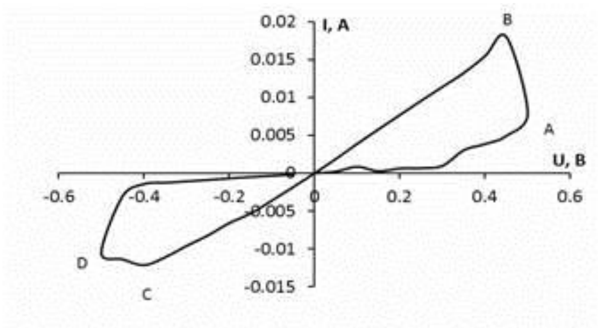

Fig.2. The Au/TiO2-x/TiO2/Au memristor the *I-V* characteristic form at bipolar switching. The cyclic voltage moved according to the scheme 0 *V* → + 0,5 *V* → 0 *V* → - 0,5 *V* → 0 *V*. Sites of A-B and C-D to *I-V* curve are areas of the negative differential resistance.

Fig. 2 represents the I-V curve of the memristor synthesized at the oxygen pressure in the chamber $2\cdot10^{-3}$ Topp at the first stage of TiO_{2-x} film growth and $5\cdot10^{-3}$ Torr at the second stage (x=0). The thickness of a dielectric layer of TiO_2 titanium dioxide was about 5 nanometers. The cyclic voltage moved according to the scheme 0V → + 0,5 V → 0 V → - 0,5 V → 0 V. Sites of A-B and C-D to I-V curve are areas of the negative differential resistance. Existence of pronounced sites with the negative differential resistance between points on a curve of A-B and C-D and the ohmic nature of conduction of the memristor in the "*on*" state between points B and C attracts attention.

Thus the memristive structures Au/TiO2-x /Au, synthesized at the oxygen pressure from $2\cdot10^{-3}$ Torr to $5\cdot10^{-3}$ Torr in the chamber, exhibit a hysteresis of the I-V curves in both the positive and negative branches of the applied voltage, which indicates the ability of these structures to change their electrical resistance when the current flows.

Acknowledgements
The work is supported by RFBR projects No 15-29-01171, 16-07-00657, 16-07-00842, as well as projects of ONIT RAS (program code IV.3.3) and PRESIDIUM of the RAS (Code I.III).

The memristors based on vanadium dioxide

L. Parshina, O. Novodvorsky, A. Lotin, O. Khramova, V. Michalevsky, E. Cherebilo

ILIT RAS, Branch of the Federal Scientific Center "Crystallography and Photonics" RAS, 1 Svyatoozerskaya St., 140700, Shatura, Moscow Region, RUSSIA

ParshinaLiubov@mail.ru

New prospects in creation of computer systems are opened by the use of analog architecture of artificial neural networks [1]. The basis of the proposed neuromorphic systems is made by the memristors – the bipolar devices in which electrical resistance changes in proportion to the charge flowing through them. For the first time the existence of memristive effect in the metal-dielectric-metal nanostructures in the film of titanium dioxide TiO_2 ~5 nm thick was experimentally demonstrated [2]. So far the memristive effect is found in many binary oxides and nitrides of metals [3]. However, instability and bad reproducibility of memristors parameters, such as switching voltage, resistance in the low- resistance and in the high-resistance states keeps currency of new materials search for the memristive devices and new methods of formation of an active layer and electrodes of the memristor.

In our work the VO_2 thin films and the $Au/VO_2/VO_{2-x}/Au$ multilayer structures on their basis were obtained by the droplet-free pulsed laser deposition method on the c-sapphire substrates with the use of mask technologies at room temperature. The memristive effect in the vertical geometry of the $Au/VO_2/VO_{2-x}/Au$ structures was developed during obtaining of which the x value varied during the growth of the structures by changing of the oxygen pressure in the vacuum chamber, which provided the required conductivity in the depleted injection layer of VO_{2-x}. Ablation of the metal targets of vanadium and gold was carried out by an excimer KrF laser radiation at the wavelength of 248 nm with energy density on the target of 3 J/cm^2. The oxygen pressure in the vacuum chamber during the growth of the films varied from 0.1 mTorr to 40 mTorr. The thicknesses of the VO_{2-x} and VO_2 layers ranged from 10 to 100 nm. The I-V characteristic dependence of the memristive structures was investigated in case of unipolar and bipolar scanning of applied voltage. The typical I-V characteristic of such structure is presented in Fig. 1. The memristive properties dependence on thickness of the semiconductor layer and the concentration of the x oxygen vacancies was established.

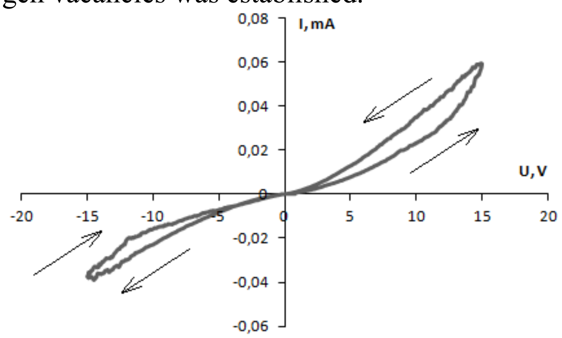

Fig. 1.The I-V characteristic of the $Au/VO_2/VO_{2-x}/Au$ memristor at bipolar switching. The shooters specified the direction of cyclic switching of the voltage on the memristor.

The research was supported by the Russian Foundation for Basic Research projects № 15-29-01171, 16-29-05385, 16-07-00842, 16-07-00657, 16-29-11800, as well as projects of ONIT RAS (program code IV.3.3) and PRESIDIUM of the RAS (Code I.III).

[1] I. Gupta, A. Serb, A. Khiat, R. Zeitler, S. Vassanelli, T. Prodromakis, Real-time encoding and compression of neuronal spikes by metal-oxide memristors, Nature communications, vol. 7, pp. 1-9, (2016).
[2] D.B. Strukov, G.S. Snider, D.R. Stewart, R.S. Williams, The missing memristor found, Nature, vol. 453, pp. 80-83, (2008).
[3] J.J. Yang, D.B. Strukov, D.R. Stewart, Memristive devices for computing, Nature nanotechnology, vol. 8, pp. 13-24, (2013).

Proton beams from an ion layer embedded foil target irradiated by an ultraintense laser pulse

Ha-Na Kim[1,2], Kitae Lee[2], Kyung Nam Kim[3], Woo-Je Ryu[2,4], Shin-Yeong Lee[2,5], Kee Hwan Yi[2,6], Manoj Kumar[2], SeongHee Park[6], Min Yong Jeon[1], Young Uk Jeong[2]

1- Department of physics, Chungnam National University,Daejeon, Korea
2-Radiation center for ultrafast science, Korea Atomic Energy ResearchInstitute,Daejeon, Korea
3-Korea Electrotechnology Research Institute, Ansan, Korea
4- Department of physics, Hannam University, Daejeon, Korea
5- Accelerator and nuclear fusion physical engineering, University of Science and Technology, Korea
6- Department of accelerator science, Korea University,Sejong, Korea

Main author email address : klee@kaeri.re.kr

Proton acceleration induced by laser-plasma interaction has advantages which could be obtained the acceleration field of more than 100 GV/m. However, the energy spectra of the proton beam has very broad distribution and the limitation of the energy which was proportioned by the induced laser intensity of 1/2 squared. So, it is important to find a new acceleration scheme can generate proton beam with narrow energy spread in more efficient way. The Korea Atomic Energy Research Institute investigated the brand new ion acceleration target model, ion layer embedded foil(ILEF) [1]. ILEF is composed of the double layer metal target which has an ion layer inside the two metal layers. Figure 1(a) shows the 2D PIC simulation results of the proton energy spectra from the ILEF target. The proton energy spectra were depended on the position of the ion layer, between the two metal layers, and the quasi-mono energetic distribution could be possible.

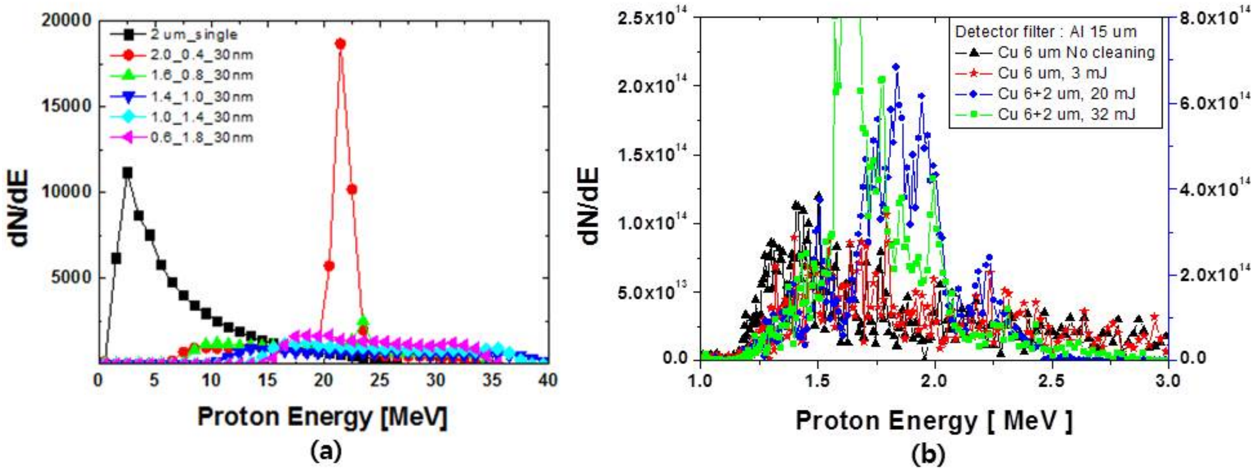

Figure 1. Proton energy spectra of the laser-plasma acceleration with ILEF target. (a) 2D-PIC simulation results. (b) Experimental results.

Figure 1 (b) shows proton energy spectra from a single layer metal target and ILEF target.For these results, a 30 TW Ti:Sapphire laser was focused with an intensity of $2x10^{19}$ W/cm^2 and additional 532 nm laser was used to remove the other ion layer which was naturally overlaid the rare side of second metal layer [2, 3]. As shown in figure 1 (b), some peaks were come out for the high energy region (circles and squares line), when the proton was accelerated from the ILEF target.

[1]Kyung Nam Kim, Kitae Lee, Manoj Kumar, Ha-Na Kim, SeongHee Park, Young UkJeong, NikolayVinokurov, and Yong Gi Kim, “Quasi-monoenergetic proton beam from a proton-layer embedded metal foil irradiated by an intense laser pulse”, Phys. Plasmas **23**, 033119 (2016).
[2] J. M. Lee, and K. G. Watkins, “Laser removal of oxides and particles from copper surfaces for microelectronic fabrication”, Optics Express **7**, 68-76 (2000).
[3] Y. F. Lu, M. Takai, S. Komuro, T. Shiokawa, and Y. Aoyagi, “Surface cleaning of metals by pulsed-laser irradiation in air”, Appl. Phys.A **59**, 281-288 (1994).

Tooth whitening effects by Blue laser

Ryun Kyung Kim[1], Sung-Ho Lee[2], Jong-Ho Lee[2], Kee-Yeon Kum[3], Hyoung Won Baac[1], Kyung Shik Lee[1]

1- 2066 Seobu-Ro, Jangan-Gu, Suwon-Si, College of Information and Communication Engineering, Sungkyunkwan University, Gyeonggi-Do, Republic of Korea
2- 25-9 Jongro-Gu, Yungeon-Dong, Department of Oral and Maxillofacial Surgery, Clinical Trial Center and Oral Cancer Center, Seoul National University Dental Hospital, Seoul, Republic of Korea
3- 25-9 Jongro-Gu, Yungeon Dong, Department of Conservative Dentistry, Dental Research Institute, Seoul National University Dental Hospital, Seoul, Republic of Korea

Ryun Kyung Kim: rkkim@skku.edu

Recently, with a growth of an aesthetic medicine tooth whitening is a very popular treatment in dentistry [1]. Aesthetics of the body including the tooth have been enhanced tremendously to people. Tooth color can be improved by a number of approaches such as whitening toothpastes, scaling, polishing, and bleaching for vital teeth [2, 3]. An in office or power bleaching as the bleaching of vital teeth is a popular treatment method in current. It is based on a relatively high level of whitening gel containing a 35% hydrogen peroxide. Since this can reduce a treatment time and also obtain the immediate results, it can improve satisfaction to the patients with a minimal side effect and a damage by dentist caring. In the treatment by the bleaching, after the whitening gel applied to the teeth, a light source is usually applied to the teeth covered by whitening gel to enhance the effect of tooth whitening. This causes the activations of a bleaching material, which the hydrogen peroxide can be activated by heat or light energy through the light source, such as LEDs, plasma arc lights, and lasers [4]. The hydrogen peroxide oxidizes a variety of organic and inorganic compounds. The bleaching by hydrogen peroxide can form some types of different active oxygen depending on reaction-conditions including temperature, pH, light and presence of transition metals [5]. Using with light sources, it can cause the formation of free radicals according to the effect of heat or light energy on hydrogen peroxide, and consequently increasing the rate of decomposition of oxygen and enhancing the release of stain molecules [6]. However, there are some research results that the light sources cannot give more whitening efficacy [7, 8]. The mechanism and the effect about the bleaching with lights are not fully understood currently.

In this research, a blue visible laser was fabricated and investigated as a medical device for treatments of tooth whitening. The blue laser of 450nm based on a laser diode was applied for activating of a bleaching material with a middle output power. The laser outputs can be adjusted and selected to more effective treatments. The fabricated semiconductor diode laser has the advantage of a good equipment in medical treatment, because it is a compact, safe on using, and a very short warm-up time for laser operation. The extracted human teeth were divided to three groups to test the efficacy for tooth whitening. The 15% hydrogen peroxide containing colorants, which was a product being marketed, was used as a 35% hydrogen peroxide solution for in office bleaching (Trinity white gel, Samil, Korea). The newly developed blue laser was applied to the coffee-colored teeth with two output conditions, and its effectiveness on teeth whitening was investigated by measuring the teeth's color immediately after treatments, after one week, and after four weeks by using a spectrophotometer.

[1] G. Burmahl, Bleaching business is booming: in-office, at home, and over the counter, AGD Impact., 4, 20-24, (1998).
[2] DC. Sarrett, Tooth whitening today, J. American Dental Association, 133, 1535-1538, (2002).
[3] HO. Heymann, Tooth whitening: facts and fallacies, British Dental J., 198, 5-14, (2005).
[4] M. Sulieman, An overview of bleaching techniques. 1. History, chemistry, safety, and legal aspects, Dental Update, 31, 608-616, (2004).
[5] S. Rosenstiel, A. Gegauff, W. Johnston, Duration of tooth color change after bleaching, J. American Dental Association, 122, 54-59, (1991).
[6] M. Kashima-Tanaka, Y. Tsujimoto, K. Kawamoto, N. Senda, K. Ito, M. Yamazaki, Generation of free radicals and/or active oxygen by light or laser irradiation of hydrogen peroxide or sodium hypochlorite, J. Endodontics, 29, 141-143, (2003).
[7] JC. Ontiveros, RD. Paravina, Color change of vital teeth exposed to bleaching performed with and without supplementary light, J. Dent., 37, 840-847, (2009).
[8] DK Hein, BJ. Ploeger, JK. Hartup, RS. Wagstaff, TM. Palmer, LD. Hansen, In-office vital tooth bleaching what do they add?, Compend. Contin. Educ. Dent., 24, 340-352, (2003).

Acknowledgment: This research was supported by Basic Science Research Program through the National Research Foundation of Korea(NRF) funded by the Ministry of Education(NRF-2016R1A6A3A11932897)

Analysis of Laser induced Plasma Density with Hankel-Fourier method

Woo-Je Ryu[1, 2], Ha-Na Kim[1, 4], Shin-Yeong Lee[1, 5], Kee-Hwan Yi[1, 3], Jae Heung Jo[2], Young Uk Jeong[1], Seong Hee Park[3], Kitae Lee[1, †]

1- Radiation Center for Ultrafast Science, Korea Atomic Energy Research Institute
2- Department of Physics, Hannam University
3- Department of Accelerator Physics, Korea University Sejong Campus
4- Department of Physics, Chungnam National University
5- Accelerator and nuclear fusion physical engineering, University of Science & Technology

rwj4292@kaeri.re.kr

When a high power laser beam focuses onto an appropriate density gas target, it generates a high energy electron beam by the acceleration of the wake-field. Plasma density distribution that determines the characteristics of accelerated electron beam is a critical value of charged particle acceleration by laser-plasma interaction. Therefore, it is important to measure the spatial distribution of accelerated electron beam and plasma density accurately. In this study, the plasma density was calculated from the fringe shift moved by the phase change due to the internal refractive index of the plasma. The phase difference of the interference fringe due to the internal refractive index of the plasma is calculated by using Continuous Wavelet Transform (CWT). From calculated phase difference, the spatial distribution of the plasma density with near cylindrical symmetry can be obtained from Abel inverse transformation formula. It was calculated by applying Hankel-Fourier transformation to the Abel inverse transformation formula and converting it to an integral equation without singularity. We modeled the cylindrical symmetric plasma channel density distribution so as to have a parabola (or Gaussian form) in the y direction and a uniform rectangular or trapezoidal shape in the z direction, and calculate the interference fringe distribution by this. Then, the reliability and experimental conditions of the calculation of plasma density distribution using Hankel-Fourier transformation were analyzed.

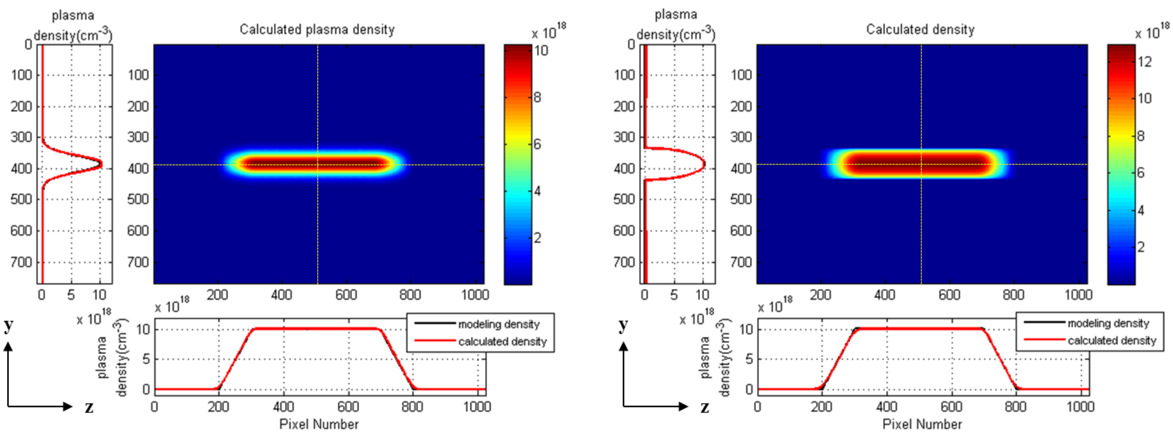

Figure 1. Hankel-Fourier transform simulation for plasma density analysis

The error range of the simulation calculation result applying the Hankel-Fourier transform has been estimated within about <1%. By optimizing the calculated conditions based on measured data and analyzing the plasma density distribution, generation and stabilization condition according to plasma electron density could be obtained.

[1] Ma. SL, Gao. HM, Wu. L, Modified Fourier–Hankel method based on analysis of errors in Abel inversion using Fourier transform techniques, APPLIED OPTIS, **Vol. 47**, No. 9 (2008)
[2] S. L. Jackson, and U. Shumlak, Increasing plasma parameters using sheared flow stabilization of a Z-pinch , Rev. Sci. Instrum. **77**, 083502 (2006).

Development of current sensor based on a microfiber loop resonator

Duy Duong Anh Le, Seungmin Lee, Kwang-Wook Yoo, Ngoc Tuyen Tran, and Young-Geun Han*

*Department of Physics, Hanyang University, Seoul, South Korea, *yghan@hanyang.ac.kr*

The optical resonators based on microfiber are very sensitive to a change in the surrounding environment due to the large evanescent field in the microfiber [1-3]. Recently, the current sensor based on microfiber knot resonator (MKR) has been reported. The current sensor based on MKR was able to overcome the limitation of previous optical current sensor such as, requirement of very long length of fiber due to extremely a small Verdet constant of silica and the complex manufacturing techniques to coat the fiber. However, it is not easy to improve the current sensitivity of the MKR-based current sensor with a copper support rod because of the low the low value of thermal-expansion coefficient and electric resistivity of the copper wire and an undesirable insertion loss in the interface between the copper rod and the MKR. In this paper, we propose a highly sensitive current sensor based on a microfiber loop resonator (MLR) incorporating low index polymer. A microfiber with a diameter of 1 μm is coiled around a nichrome wire with low index polymer coating to make a MLR around the nichrome wire. The electric current in the nichrome wire increases temperature around the nichrome wire and accordingly changes thermal properties of the MRL and low index polymer. Therefore, the proposed MLR-based current sensing probe incorporating low index polymer has a high current sensitivity of 437.9 pm/A2, which is ~10 time higher than the previous result.

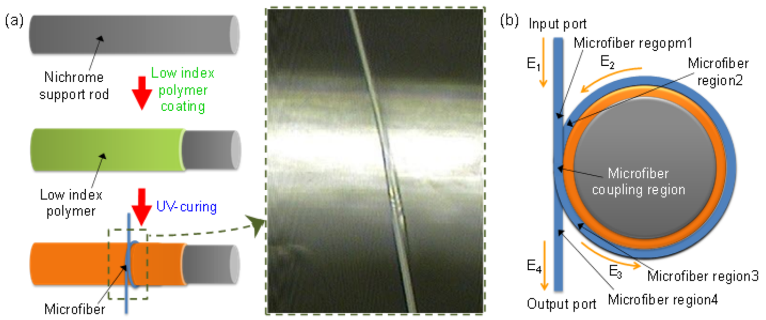

Figure 1. (a) Experimental scheme for the fabrication of the MLR and (b) the operating principle of the MLR.

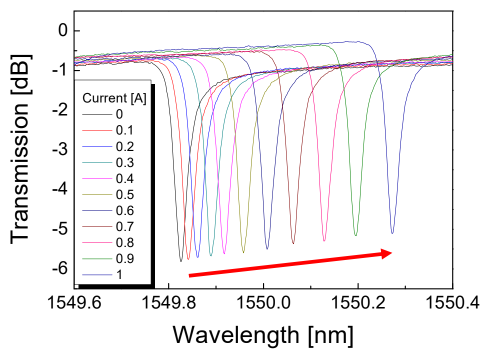

Figure 2. Transmission spectra of the MLR with variations in the electric current.

[1] Y. Chen, Z. Ma, Q. Yang, and L. Tong, "Compact optical short-pass filters based on microfibers," Opt. Lett. 33(21), 2565-2567 (2008).
[2] Brambilla, "Optical fibre nanowires and microwires: a review," J. Opt. 12(4), 1-19 (2010).
[3] X. Zeng, Y. Wu, C. Hou, J. Bai, and G. Yang, "A temperature sensor based on optical microfiber knot resonator," Opt. commun. 282(18), 3817–3819 (2009).

Multi-level information writing in nanoporous glass by single sub-microsecond burst of femtosecond laser pulses.

Fedotov S.S.[1], Okhrimchuk A.G. [1], Glebov I.S. [1], Lipatiev A.S. [1], Lotarev S.V. [1], Stepko A.A. [1], Piyanzina K.I. [1], Sigaev V.N. [1]

1 – D. Mendeleev University of Chemical Technology of Russia, Russia, Moscow, Miusskaya sq. 9

Main author email address: sergey.fedotov.91@gmail.com

The volume of information circulating in the world annually increases exponentially, that creates a request of reliable and long-term data storage. Available storage technologies require periodic rewriting to avoid data loss during long-term storage. In this concern there are strong demand of new solutions for data recording, which would permit to exclude the need for rewriting at all. To increase the durability of optical memory, it is promising to use technology of the direct laser writing by ultrashort pulses in the volume of glass. Due transparency, manufacturability, resistance to elevated temperatures, glass is considered as a potential material of an optical carrier of information that should have a record durability. Up to now there are two formats of recording information in the glass. They are 3D format, which was performed by forming of micron sized pits with a modified refractive index [1], 5D format [2], which is based on the formation of nanogratings in a pit. The nanogratings possess a form birefringence. Parameters of this birefringence, retardance and orientation of optical axis are controlled by direction of the laser beam polarization and number of pulses, whereby several bits of information can be encoded in one pit containing the nanograting. This paves the way for increase of density of information recording and, correspondingly, the capacity of the optical carrier. However, up to now, at least 10 pulses was required for formation of nanogratings in the pit, which imposes serious limitations on the recording speed of information, in particular, in paper [2] the writing speed was 6 KB/sec.

In this paper, we demonstrate for the first time to our knowledge formation of birefringent pits in a nanoporous glass, using a single laser pulse, splitted into a burst of 4 pulses separated by 100 ns in a cavity resembled a Fabry-Perot resonator. The envelope of the pulses amplitudes in such a burst has form of a damped exponential. We assume that the birefringence is due to the formation of the nanogratings, as in silica glass, and this paves the way for multi-bit data recording with speed of 1 MHz in one optical channel. This result was achieved due to use of nanoporous glass, in which small number of pulses (2-3 pulses) is required for nanograting formation, in contrast to silica glass, for which 10 pulses are required at least. The dependence of the retardance and root-mean-square deviation of the angle of the slow birefringence axis on the number of pulses in the burst were studied (Fig.1). In order to demonstrate feasibility of the proposed approach, the information was recorded in the form of an array of birefringent pits, which was then read and restored. The obtained results testify the possibility of increasing the speed of multilevel recording in nanoporous glass up to 10 Mbit/s.

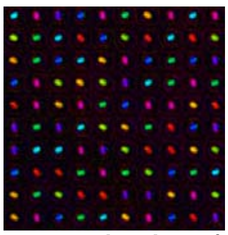

Fig. 1 Array of birefringent pits in the volume of nanoporous glass.

[1] R. Imai, M. Shiozawa, T. Shintani, T. Watanabe, S. Mori, Y. Shimotsuma, M. Sakakura, K. Miura, K. Watanabe. 100-Layer recording in fused silica for semi permanent data storage. Japanese Journal of Applied Physics, 54, 09MC02, 2015.
[2] J. Zhang, M. Gecevicius, M. Beresna, P.G. Kazansky. Seemingly unlimited lifetime data storage in nanostructured glass. Physical Review Letters, 112, 003901, 2014.

Efficient Optical-to-THz Conversion in Organic Crystals by Modifying the Space-filling Characteristics

B. J. Kang[1], S.-J. Lee[2], O-P. Kwon[2], F. Rotermund[1]

[1]*Department of Physics, Korea Advanced Institute of Science and Technology (KAIST), Daejeon 34141, Korea*
[2]*Department of Molecular Science and Technology, Ajou University, Suwon 443-749, Korea*

rotermund@kaist.ac.kr

As table-top intense coherent terahertz (THz) sources are getting more important for advanced THz science, nonlinear organic crystals have been proposed as efficient materials for generation of broadband THz waves thanks to large nonlinear coefficient and excellent phase matching condition [1,2]. Compared with inorganic crystals, organic crystals are regarded as a cost-effective solution, and it is easy to fine-tune the nonlinear optical characteristics by modifying its chemical structures. However, intrinsic phonon mode absorption of organic crystals lead to undesirable dimples in the THz spectrum and limited the THz efficiency [3].

In this work, we report on a novel quinolinium crystals by modifying the space-filling characteristics by introducing various π-conjugated aromatic anions possessing a different spatial volume. New OHQ-CBS (2-(4-hydroxystyryl)-1-methylquinolinium 4-chlorobenzenesulfonate) crystals exhibit an enhanced macroscopic optical nonlinearity and a relatively small absorption coefficient in the range of 0.5-4 THz. This is attributed to suppressed molecular vibrations due to strong hydrogen-bonds. To investigate THz generation characteristics in OHQ-CBS crystal, we used as-grown samples by slow-cooling method in solvent mixture. The temporal and spectral shapes of the THz waves generated by optical rectification with 1300 nm pumping are measured by electro-optic sampling. Based on the large optical nonlinearity and the low intensity of THz phonon modes, 0.39-mm-thick OHQ-CBS crystal exhibits about 30 times higher THz generation efficiency with 3 times broader spectral bandwidth compared to the well-known 1.0-mm-thick standard inorganic ZnTe crystal. Moreover, compared with state-of-the-art analogous OHQ-T crystals, OHQ-CBS crystal exhibits 1.8 times higher field amplitude.

High nonlinearity realized by perfect molecular ordering for optimizing the diagonal second-order nonlinear optical response leads the as-grown OHQ-CBS crystal to an outstanding candidate for intense and broadband THz wave generation. In molecular design of ionic organic nonlinear optical crystals, controlling space-filling characteristics with introducing substituents having simultaneous electron-withdrawing inductive and electron-donating resonance effects is a promising way for enhancement of the macroscopic nonlinearity and suppression of phonon vibrations for efficient THz wave generation.

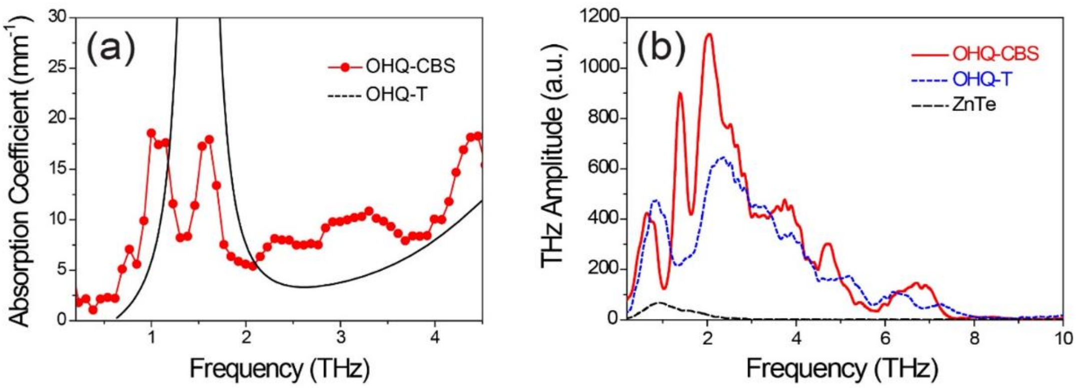

Figure 1. (a) THz absorption coefficient along the polar axis of OHQ-CBS and OHQ-T crystal. (b) THz spectra generated from 0.39-mm-thick OHQ-CBS, 0.35-mm-thick OHQ-T and 1.0-mm-thick ZnTe crystals.

[1] T. Kampfrath et al., Resonant and nonresonant control over matter and light by intense terahertz transients, Nat. Photon. 7, 680-690 (2013).
[2] J.-H. Jeong et al., High-power Broadband Organic THz Generator, Sci. Rep. 3, 3200 (2013).
[3] S.-H. Lee et al., Terahertz phonon mode engineering of highly efficient organic terahertz generators, Adv. Funct. Mater. 42, 1605583 (2017).

Temperature dependence of the terahertz radiation generation in the vanadium dioxide thin films

M. Esaulkov[1], K. Lazareva[2], P. Solyankin[1,2], A.Shkurinov[1,2]

1- ILIT RAS - Branch of FSRC "Crystallography and Photonics" RAS, 140700, 1 Svyatoozerskaya St., Shatura, Russia

2- Faculty of Physics, M.V. Lomonosov Moscow State University, 119992, 1 Leninskie Gory St., Moscow, Russia

solyankin@physics.msu.ru

In this report, we present our studies of terahertz (THz) pulse generation in thin (~150 nm) films of vanadium dioxide (VO_2) under irradiation of optical pulses with duration near 150 fs and central wavelength 795 nm. Measurements were carried out in the wide temperature range (100-373 K) and for different optical power and polarization.

Vanadium dioxide is the material with the sharp change of conductivity during the first order metal-insulator phase transition. Upon the phase transition, electronic structure and crystalline lattice of the material changes. For the bulk samples, transition occurs near 340 K and conductivity changes up to 5 orders of magnitude. For the thin films, these results can vary depending on the substrate type, film thickness and growth parameters. THz properties also change: for our films THz transmission (measured for amplitude of the field) in conductive state decreases to 20% of initial value.

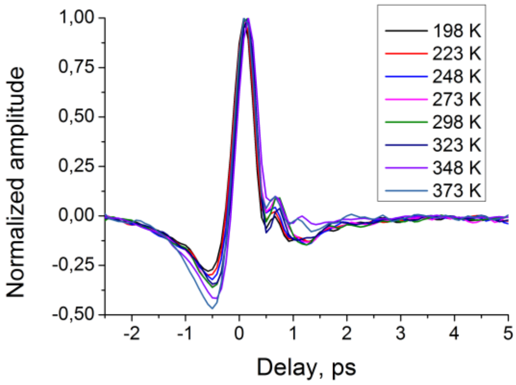

Figure 1. Normalized time profiles of the THz signal at different sample temperatures

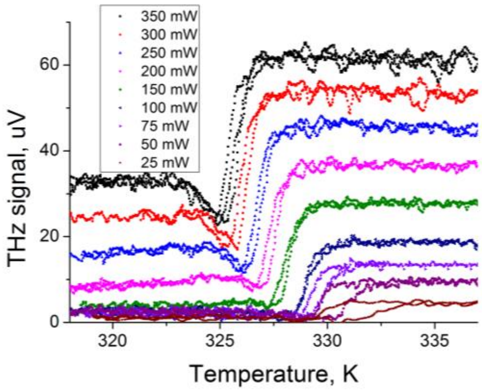

Figure 2. Temperature dependence of the THz generation amplitude near the phase transition temperature

In our recent work [1] we have studied the THz generation properties at two fixed temperatures below and above the phase transition. Different polarization properties and optical power dependences for these two temperatures were shown, so distinct generation mechanisms could be proposed. However, the THz generation in vicinity of the phase transition temperature was not studied yet. In this work, we control the temperature of the film during the THz generation process to see the change in the generation mechanism.

For this we use a THz time-domain spectroscopy (TDS) setup, which is fed by a Ti:Sa regenerative amplifier. Samples were grown on the R-cut sapphire substrates by the PLD method, sample thickness was around 150 nm. Typical measured waveforms for fixed optical power and different temperatures are shown at Fig. 1. The change in TDS waveforms with temperature is negligible. Temperature dependence of THz signal amplitude at different optical power is presented at Fig. 2. There is an increase in generation efficiency in conductive state, but near the phase transition curves have complex behavior. We compare these graphs with the optical transmission at the same optical power and with the results of optical pump – THz probe experiments to reveal the nature of the hysteresis width change and the local minimum of the THz generation amplitude prior to phase transition.

This work was supported by RFBR Grants № 16-29-11800 and № 17-02-01217.

[1] M. Esaulkov et al., Emission of Terahertz pulses from vanadium dioxide films undergoing metal-insulator phase transition, Optica, 2 (9), pp. 790-796 (2015).

Terahertz and X-Ray emission during interaction of high-intense ultrashort laser pulses with gas cluster beam.

A.V. Balakin[1], M.S. Dzhidzhoev[1], V.M. Gordienko[1], M.N. Esaulkov[2], I.A. Zhvaniya[1], N.A. Kuzechkin[2], P.M. Solyankin[1,2], A.P. Shkurinov[1,2]

1- Faculty of Physics and International Laser Center, M. V. Lomonosov Moscow State University, Moscow 119991, Russia
2- Institute on Laser and Information Technologies of the Russian Academy of Sciencies — Branch of the Federal Scientific Research Centre «Crystallography and Photonics» of Russian Academy of Science, Shatura, 140700, Russia

ashkurinov@physics.msu.ru

Cluster beam, produced by the technique of adiabatic gas condensation [1], combines advantages of solid-state and gaseous target: clusters inherit high local density and this implies high value of nonlinear response; at the same time the cluster beam does not expose to ablation and renews its properties before each act of interaction with the laser pulse. Intense terahertz generation in argon clusters under excitation with ultrashort laser pulses was reported in some resent articles [2]-[4]. Authors of [2]-[4] observed more than 2 orders of magnitude enlargement of THz pulse intensity in Ar cluster jet compared that in gaseous Ar with equal average atomic density. Cluster target seems suitable to improve laser-plasma technique of THz generation and obtain efficient source of coherent pulsed THz radiation. Moreover, understanding of physics of laser-cluster interaction is an actual problem and studies of THz and X-Ray emission allow to obtain new information about this phenomena. The aim of the present work is an experimental study of the simultaneous generation terahertz and X-Ray pulses produced by the laser-cluster interaction in both the single-color and dual-color regimes of excitation.

In our experiments cluster beam was produced by partial condensation of pure Ar and mixture CF_2Cl_2+He during their expansion through a conical nozzle into vacuum. We have found that amplitude of THz signal strongly decreases in the region of minimum durations of the pump laser pulse whereas X-Ray signal demonstrates maximum values under these conditions. We observed similar scaling of THz yield with pulse duration in atomic (Ar) and molecular (CF_2Cl_2) cluster beams both in single- and two color excitation schemes. We observed that usage of two color excitation scheme results in ~5-fold enhancement of THz pulse energy emission from clustered plasma. Both in single- and two color excitation regimes THz yield growth without saturation with increasing of laser pulse energy. We have found that THz signal generated at forward direction under two-color excitation of cluster jet strongly depends on average density of Ar atoms in the jet and presence of clusters does not affect on its value. This allows to suppose that THz emission at forward direction originates from non-clustered gas phase in the jet.

[1] O. F. Hagena and W. Obert, "Cluster formation in expanding supersonic jets: Effect of pressure, temperature, nozzle size, and test gas," J. Chem. Phys., vol. 56, p. 1793–1802 (1972)
[2] T. Nagashima, H. Hirayama, K. Shibuya, M. Hangyo, M. Hashida, S. Tokita and S. Sakabe, "Terahertz pulse radiation from argon clusters irradiated with intense femtosecond laser pulses," Opt. Exp., vol. 17, p. 8907–8912 (2009).
[3] F. Jahangiri, M. Hashida, T. Nagashima, S. Tokita, M. Hangyo and S. Sakabe, "Intense terahertz emission from atomic cluster plasma produced by intense femtosecond laser pulses," Appl. Phys. Lett., vol. 99, p. 261503-1–261503-3, (2011)
[4] F. Jahangiri, M. Hashida, S. Tokita, T. Nagashima, M. Hangyo, and S. Sakabe, "Enhancing the energy of terahertz radiation from plasma produced by intense femtosecond laser pulses," Appl. Phys. Lett., vol. 102, 191106-1-191106-4 (2013)

Determination of biologically safe energy threshold for terahertz radiation

O. Cherkasova[1], A. Gapeyev[2], M. Nazarov[3], A. Angeluts[4], M. Esaulkov[5], P. Solyankin[4,5], A. Shkurinov[4,5]

1-Institute of Laser Physics of SB RAS, pr. Lavrentyeva, 13/3, Novosibirsk, 630090 Russia
2- Institute of Cell Biophysics of RAS, st. Institutskaya 3, 142290, Pushchino, Russia
3 - Kurchatov Institute National Research Center, Moscow, 123182, Russia,
4 - Lomonosov Moscow State University, Moscow, 119991, Russia
5 - Crystallography and Photonics Federal Research Center RAS, Moscow, Russia

e-mail: o.p.cherkasova@gmail.com

The recent progress of techniques for generation and detection of terahertz radiation as well as the unique properties of this electromagnetic radiation (EMR) within the frequency range 0.1 – 10.0 THz offer the challenge of its wide application in security, communication, medical diagnostics and therapy systems. Thereby a question arises about the relation between biological effects and the physical parameters of the EMR in the terahertz range. Safety limits of its use should be estimated. However, the presently existing hygienic standards regulating the use of electromagnetic radiation sources are restricted to the frequency range below 0.3 THz [1].

The aim of the present work was to determine the limits of biologically safe energy threshold for terahertz radiation by estimating its damaging effect on DNA of human blood leukocytes. The studies were performed using three experimental setups, differing in the terahertz radiation parameters, namely, the spectral range, the spectral intensity and the mean and peak powers. This allowed implementation of the experimental conditions routinely used in THz spectroscopic studies.

The simplest and operative method that allows detection of damage and modification of cellular DNA structure is the express method of molecular genotoxicology known as the comet assay (method of DNA comets or single cell gel electrophoresis). This method is recommended by the WHO for performing genotoxicity analyses, is certified and widely used in many countries [2].

The experiments were carried out using the general fraction of whole blood leukocytes from healthy donors. The analysis of the DNA damage in cells was carried out using the alkaline version of the comet assay with certain modifications [3]. The method is based on analysing the electrophoresis pattern of individual cells, whose DNA is stained with a fluorescent dye. The DNA damage was estimated by the percentage of the DNA in the “comet tail”. As an indicator of condensation/decondensation of chromatin the nucleoid radius was used.

Our studies have shown that the influence of picosecond pulsed of terahertz radiation in the frequency range of 0.1 – 6.5 THz on human blood leukocytes does not induce DNA damage during the 20 min exposure with the mean intensity up to 200 μW/cm^2 and peak intensity of 7.8 kW/cm^2. In this case the heating of the irradiated sample does not exceed 1 °C [4]. Thus, acting on leukocytes of peripheral blood of healthy donors, the above energy parameters of the pulsed terahertz radiation can be accepted as safe for the exposure durations no greater than 20 min. However, one should keep in mind that an increase in the pulsed radiation intensity can lead to inducing DNA damage [5]. Special thorough studies should be devoted to investigate the dependences of terahertz EMR biological effect upon other parameters, such as the exposure duration, the carrier and modulation frequency spectrum.

[1] IEEE Standard for Safety Levels with Respect to Human Exposure to Radio Frequency Electromagnetic Fields, 3 kHz to 300 GHz. IEEE Std C95.1 (2005).
[2] Gun-Sik Park et al. Convergence of Terahertz Sciences in Biomedical Systems (Dordrecht: Springer, 2012).
[3] A.B. Gapeyev, N.A. Romanova, N.K. Cheremis, Changes in the chromatin structure of lymphoid cells under the influence of low-intensity extremely high-frequency electromagnetic radiation against the background of inflammatory process, Biophysics, vol. 56 (4), pp.672-678 (2011).
[4] A.A. Angeluts, A.B. Gapeyev, M.N. Esaulkov et al, Study of terahertz-radiation-induced DNA damage in human blood leukocytes, Quantum Electronics, vol. 44 (3), pp. 247 – 251 (2014).
[5] Doria A., Gallerano G.P., Giovenale E., et al., THz radiation studies on biological systems at the ENEA FEL facility, Infrared Physics &Technology, vol. 45, pp. 339-347 (2004).

Terahertz Nondestructive evaluation System for Industrial Applications

E. S. Lee, K. Moon, I.-M. Lee, H.-S. Kim, D. W. Park, J.-W. Park, D. H. Lee, S.-P. Han, and K. H. Park

THz Basic Research Section, Electronics and Telecommunications Research Institute, Daejeon 3-5-700, Korea
euisu@etri.re.kr

Recently, the continuous-wave (CW) terahertz (THz) technologies are attracting attentions for their various industrial applications such as wireless communications, spectroscopy, sensing and imaging. Toward the widespread industrial application of THz technology, highly-efficient and compact THz modules should be supplied with a reasonable cost. In the past, we have developed key components for the photonics-based CW THz technologies as well as modules to implement high-performance THz platforms as the main building blocks of a THz system [1-4]. Here, we report on our recent achievements in CW THz devices and systems with an illustrative example of THz real-time imaging for nondestructive evaluation (NDE). In addition to the typical technical specifications for an imaging system, such as resolution, signal-to-noise ratio, and image quality, the imaging area and time are critical to the NDE applications, should be considered in the design. We resolved the imaging time and area issue by adopting a specially designed high-density polyethylene (HDPE) THz telecentric f-theta lens with a two-dimensional Galvano scanning mirror system (Cambridge Technology, 6240H-25mm). An experimental imaging setup is shown in Fig. 1. After preliminary imaging experiments, we have developed a prototype imaging system to find human errors that may occur in various industrial fields, which is expected to find many intriguing industrial applications in the near future.

Fig1. Fabricated telecentric f-theta lens with an experimental imaging system.

[1] N. Kim, J. Shin, E. Sim, C. W. Lee, D.-S. Yee, M. Y. Jeon, Y. Jang, and K. H. Park, "Monolithic dual-mode distributed feedback semiconductor laser for tunable continuous-wave terahertz generation," Opt. Express, vol. 17, no. 16, pp. 13851–13859, (2009).

[2] K. Moon, D. W. Park, I. -M. Lee, N. Kim, H. Ko, S. -P. Han, D. Lee, J. -W. Park, S. K. Noh, and K. H. Park, "Low-temperature-grown InGaAs terahertz photomixer embedded in InP thermal spreading layer regrown by metalorganic chemical vapor deposition," Opt. Lett., vol. 38, no. 24, pp. 5466–5469,(2013).

[3] T Il-Min Lee, Namje Kim, Eui Su Lee, Sang-Pil Han, Kiwon Moon, and Kyung Hyun Park, "Frequency modulation based continuous-wave terahertz homodyne system", Optics Express, 23(2), pp. 846-858, (2015).
Author and B. Author, Title of paper, Journal Name, vol., pp. startpage-endpage, (year).

[4] Sang-Pil Han, Hyunsung Ko, Namje Kim, Won-Hui Lee, Kiwon Moon, Il-Min Lee, Eui Su Lee, Dong Hun Lee, Wangjoo Lee, Seong-Tae Han, Sung-Wook Choi, and Kyung Hyun Park, "Real-time continuous-wave terahertz line scanner based on a compact 1 × 240 InGaAs Schottky barrier diode array detector ", Optics Express, 22(23), pp. 28977-28983, (2014).

THz square-loop metamaterial based on tungsten-doped vanadium dioxide thin films

Jun-Hwan Shin[1], Kyung Hyun Park[1], Han-Cheol Ryu[2]

1- Terahertz Basic Research Section, Electronics and Telecommunications Research Institute (ETRI), Daejeon 34129, Korea

2- Division of Computer-Mechatronics, Sahmyook University, Seoul 01795, Korea

Email address: jh-shin@etri.re.kr

An electrically controllable terahertz (THz) square-loop metamaterial structure was designed and evaluated on tungsten-doped vanadium dioxide (W-doped VO_2) thin films. This closed-loop shaped metamaterial allows to simultaneously functions both the highly selective bandpass filter and micro-heater [1]. In addition, VO_2 thin films with various W concentrations were successfully deposited on Al_2O_3 substrates by using sol-gel method. With increasing W concentration, the transition temperature is considerably decreased by room temperature and the conductivity-temperature hysteresis curve was broadened [2]. The THz wave amplitude was precisely and continuously tuned in the frequency range between 0.4 and 0.7 THz through the proposed metamaterial fabricated onto 1.2 at% W doped VO_2 thin film by applying a bias voltage. These experimental results can be utilized for analog and digital modulator and filter applications in THz frequency range.

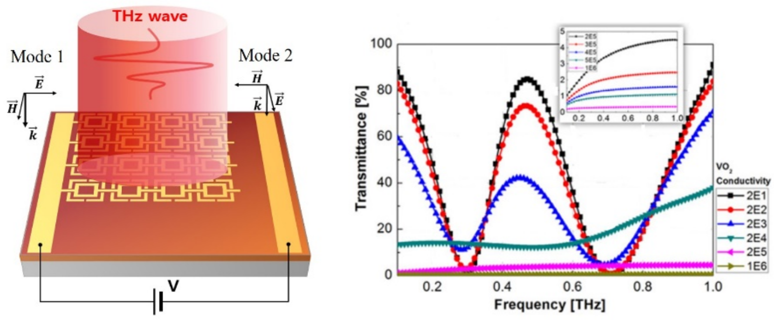

Figure 1. (a) Schematic of the measured device and (b) transmittance in mode 2. (Inset of fig. 1 (b): the results of the conductivity in the ran ge of $2\cdot10^5$-$1\cdot10^6$ S/m)

[1] Jun-Hwan Shin, Kyung Hyun Park, and Han-Cheol Ryu, Electrically controllable terahertz square-loop metamaterial based on VO_2 thin film, Nanotechnology, 27, 195202 (8pp), (2016).

[2] G. Karaoglan-Bebek, M. N. F. Hoque, M. Holtz, Z. Fan, and A. A. Bernussi, Continuous tuning of W-doped VO_2 optical properties for terahertz analog applications, Appl. Phys. Lett., 105, 201902 (5pp), (2014).

CIGS thin-film solar cell patterning at different wavelengths

P. Gečys, E. Markauskas, G. Račiukaitis

Center for Physical Sciences and Technology, Savanoriu Ave. 231, LT-02300, Vilnius, Lithuania

p.gecys@ftmc.lt

Over the past few years, CIGS thin-film technology experienced considerable increase in power conversion efficiency [1]. High CIGS thin-film solar cell efficiency, flexibility and light weight make this technology attractive for future developments. In order to preserve small cell efficiency over the large area, structuring of large-scale devices is needed. Module patterning is obtained by implementation of free step laser scribing process [2]. P1 laser process patterns the back-contact forming the stripe-shaped molybdenum grid. P2 is used for the series interconnect formation between the adjacent cells after the TCO deposition. The P3 process is used for isolation of neighboring cells by removing the top TCO layer or entire CIGS structure to expose the molybdenum back-contact. One of the factors responsible for the efficiency losses are the laser induced shunts during the P3 scribing process. The use of ultra-short lasers can notably increase the scribing quality. However, CIGS thin-film solar cell is a multilayer structure with different layer optical properties. Wavelength optimization for P3 laser patterning is crucial to obtain damage free laser scribing.

In this work, we will present wavelength dependent laser processing of the CIGS thin-film solar cells. Modern picosecond and nanosecond lasers covering wavelength range from 355 nm to 2.5 μm were used for solar cell processing. Two main P3 scribing approaches were investigated – ablation of the full layer stack to expose the molybdenum back-contact (P3 “type 1”), and removal of the front-contact only (P3 “type 2). The scribing was evaluated visually followed by electrical testing. We used a linear laser scribing technique to validate the scribe conductivity [3]. Laser wavelength played important role in the case of damage free laser scribing. The lowest scribe conductivity values were obtained either for UV or infrared wavelength processing. The results are shown in the figure 1. Furthermore, we simulated full size module operation in respect to scribing conditions. Processing with 355 nm and 2.5 μm laser wavelengths showed the best results. Absolute efficiency losses were negligible - below 0.1 % absolute efficiency in both cases (0.02 % for 2.5 μm and 0.08 % for 355 nm laser wavelengths).

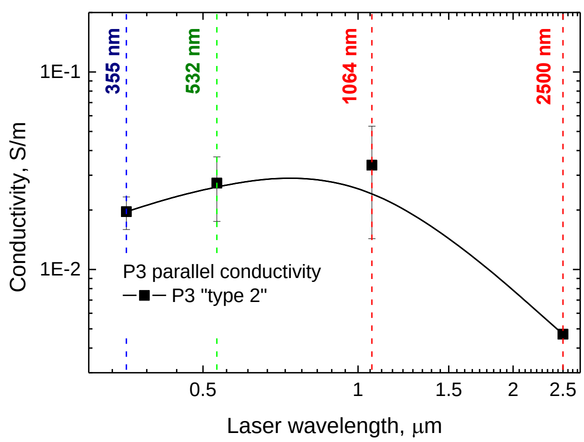

Fig. 1 P3 “type 2” scribe parallel conductivity vs laser wavelength.

[1] P. Gečys, E. Markauskas, S. Nishiwaki, S. Buecheler, R. De Loor, A. Burn, et al., CIGS thin-film solar module processing: case of high-speed laser scribing, Sci. Rep., 7., pp. 40502, (2017).
[2] C. Dunsky, F. Colville, Solid state laser applications in photovoltaics manufacturing, Proc. SPIE, 6871., (2008).
[3] E. Markauskas, P. Gečys, A. Žemaitis, M. Gedvilas, G. Račiukaitis, Validation of monolithic interconnection conductivity in laser scribed CIGS thin-film solar cells, Sol. Energy, 120., pp. 35–43, (2015).

Ytterbium fiber-based High-power chirped pulse amplification

Seolwon Park, Duchang Heo*, Chur Kim, Jun Wan Kim, Byunghak Lee, Sergey Chizhov, Elena Sall, Guang-Hoon Kim

Advanced Medical Device Research Division, Korea Electrotechnology Research Institute, Ansan-city, 15588, Korea

*dcheo@keri.re.kr**

Recently, High-power femtosecond fiber lasers have attracted considerable attentions in the industrial applications as well as medical applications, because the femtosecond fiber lasers have significant advantages over bulk solid-state lasers such as lower cost, average power scaling, compact size, high beam quality, efficient heat dissipation and alignment free system [1].
Amplification of femtosecond laser has the restriction of nonlinear effects, which destroy the shape of compressed pulse such as pedestal and degrade pulse duration [2]. Therefore, the chirped pulse amplification (CPA) system was introduced to avoid the nonlinear effects and self-phase modulation effects for amplification [3]. The CPA systems consist of a femtosecond laser, a stretcher, a chain of amplifiers and compressor [4]. In the case of amplifier with fiber, large mode area (LMA) fibers are commonly used. The use of LMA fiber reduces nonlinear effect due to the reduction of propagating intensity along the fiber [5].
We report the high-power all fiber chirped pulse amplification system for medical applications. The system consists of an ytterbium-doped mode-locked fiber laser, a long fiber stretcher, a series of ytterbium-doped fiber amplifiers using LMA fiber and compressor. In addition, we insert an acousto-optic modulator (AOM), to adjust the repetition rate of few megahertz for medical applications.
The seed is an ytterbium-doped mode-locked fiber ring cavity oscillator with transmission type saturable absorber (SA), producing pulses with central wavelength of 1040 nm and a bandwidth of 3.7 nm at the 3dB and repetition rate of 22.6 MHz. The stretcher consists a few km HI1060 fibers. The pulse width is stretched to few hundred ps. With four stages of ytterbium-doped amplification, the average output power is scale up to 1 W. The amplified pulses are compressed using a conventional diffraction grating pair. By optimizing the spectrum shape and power efficiency, a high power CPA system is achieved.

[1] M. E. Fermann and Ingmar Hartl, Ultrafast fiber laser technology, IEEE J. Sel. Top. Quantum Electron., vol. 15, pp. 191-204, (2009).
[2] Zhi-Guo Lv, Hao Teng, Li-Na Wang, Jun-Li Wang and Zhi-Yi Wei, High-energy femtosecond Yb-doped all-fiber monolithic chirped-pulse amplifier at retetition rate of 1 MHz, Chin. Phys. B., vol. 25, no. 9, pp. 094208 , (2016).
[3] M. D. Perry, T. Ditmire and B. C. Stuart, Self-Phase modulation in chirped-pulse amplification, Opt. Lett., vol. 19, pp. 2149-2151, (1994).
[4] D. Strickland and G. Mourou, Compression of amplified chirped optical pulse, Opt. Commun., vol. 56, no. 3, pp. 219-221, (1985).
[5] Oleg G. Okhotnikov, Fiber lasers (Wiley), Chapter 2.2.2, (2012).

Cavity dumped optical parametric oscillator for near-infrared femtosecond pulses

Ji-Eon Park[1], Tae-Young Jeong[1], Ki-Ju Yee[1]

1- Department of Physics, Chungnam National University, Daejeon 34134, Republic of Korea

pjeon1124@gmail.com

We report on a cavity-dumped optical parametric oscillator (OPO) operating in near-infrared region. The near-infrared OPOs with broadly tunable wavelength region almost 500 nm or more were reported. However, these OPOs have low pulse energy [1]. In order to improve the pulse energy, the cavity dumping method can be applied.

We fabricated a linear resonator, as shown in figure 1. In order to solve the efficiency drop by phase mismatch in gain medium, we used a periodically poled lithium niobate (PPLN) with a period of 21.2 μm as gain medium for the quasi phase matching [2]. The OPO is synchronously pumped by Ti:sapphire pulsed laser that produces 1.9 W at 807 nm with 10 nm FWHM and a repetition rate of 76 MHz. To compensate for positive group velocity dispersion caused in gain medium, we used a SF10 prism pair the negative group velocity dispersion [3]. For the tunning of wavelength, the mirrors (M_5) is adjusted. In the cavity dumping components, we used a bragg cell (BC) made from fused silica.

The OPO is broadly tunable from 1050 nm to 1600 nm. The output pulse has almost 50 nJ pulse energy at a repitition rate of 400 kHz, with a pulse duration almost 200 fs. As the cavity-dumped OPO produces higher pulse energy, it can be applied to experiments such as observing nonlinear optical phenomena of materials in the near infrared region.

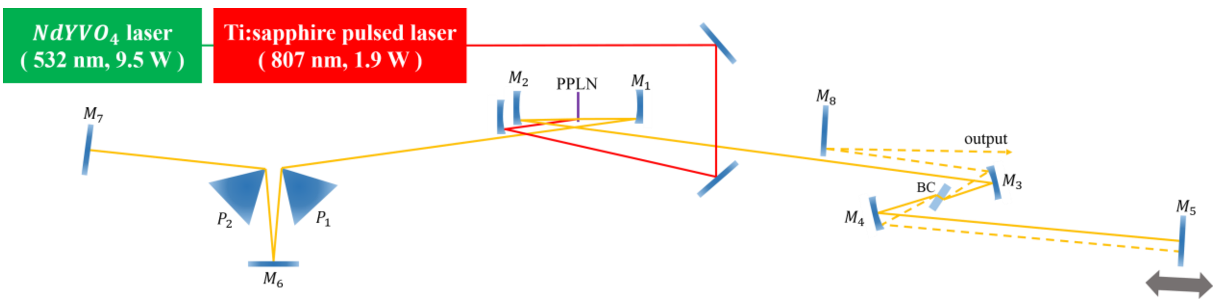

Fig. 1. Schematic of near-infrared cavity dumped optical parametric oscillator.

[1] Kang-Jeon Han, et al., "Synchronously pumped optical parametric oscillator based on periodically poled MgO doped lithium niobate", Optics Express, 16, 8, 5299-5304, (2008)

[2] L. E. Myers, et al., "Quasi-phase-matched optical parametric oscillators in bulk periodically poled LiNbO3", J. Opt. Soc. Am. B, 12, 11 (1995).

[3] R. L. Fork, et al., "Negative dispersion using pairs of prisms", Opt. Lett. 9, 5, (1984).

Cavity-Dumped Mode-locked Picosecond Alexandrite Single Pulse Laser

Hee Dong Yang[1, 2], **Byung Hyuck Moon**[1], **Ju Han Lee**[2] **and Young Min Jhon**[1]*

1 Sensor System Research Center, Korea Institute of Science and Technology, Seoul 136-791, South Korea

2 School of Electrical and Computer Engineering, University of Seoul, 163 Seoulsiripdae-ro, Dongdaemun-gu, Seoul 130-743, Korea

**ymjhon@kist.re.kr*

Cavity-dumped and mode-locked(CDML) single pulse laser has been developed for many fields such as medical science, bio engineering, material science, etc, because it has extremely short pulse width and can make high peak power [1, 2]. Alexandrite as a laser medium has 700-800 nm range of oscillation wavelength [3]. For these characteristics, Alexandrite has also been researched for wavelength tunable laser, because of its wide wavelength range [4] and its characteristics of gain tunability for temperature change [5].

In this study, CDML Alexandrite single pulse laser was developed, and the output characteristics were measured for various conditions.

Q-switching and cavity dumping were achieved by a Pockels cell to obtain high peak power output of single pulse laser as shown in Figure 1. Photons traveling back and forth between Mirror 1 and Mirror 2 get accumulated in resonator until they are dumped out of the resonator when their polarzation is changed by the EOM (Pockels cell). Figure 2 shows a pulse width of 555ps of the CDML picosecond Alexandrite single pulse laser.

The pulse energy and pulse width were measured for various pumping energy and the maximum pulse energy was obtained to be 113 mJ.

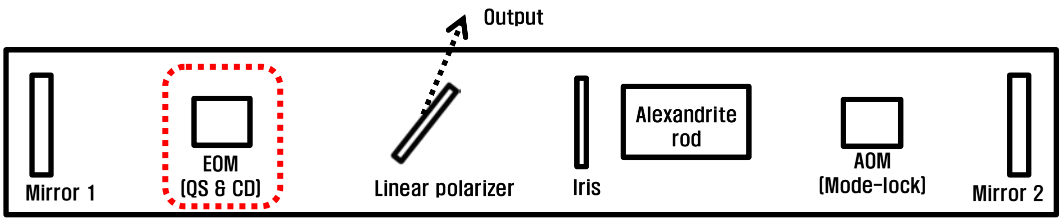

Figure 1. Schematic diagram of CDML Picosecond Alexandrite Single Pulse laser

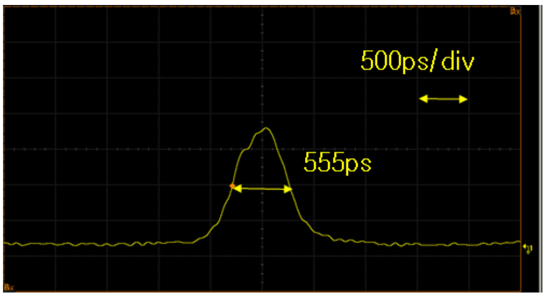

Figure 2. Pulse width of QSML Alexandrite laser

[1] M Glotz and H-J Eichler, "Cavity dumping of a mode-locked pulsed Nd:YAG laser" , *J. Phys. E: Sci. Instrum.* ***20,*** *1493-1496 (1987).*
[2] H. Hitotsuya, M. Takama, M. Inoue, S. Matsubara, Y. Sasatani, N. Shimojo, S. Kawato, "CAVITY-DUMPED MODE-LOCKED YT-TERBIUMDOPED $Y_3Al_5O_{12}$ LASER", International Journal of Latest Research in Science and Technology, **2**, 434-436 (2013).
[3] C. L. Sam, J. C. Walling, H. P. Jenssen *, R. C. Morris * *, E. W. O'Dell, " Characteristics of alexandrite lasers in Q- switched and tuned operations ", Advances in Laser Engineering and Applications, SPIE Vol 247, pp. 130-136, (1980).
[4] John C. Walling, Donald F. Heller, H. Samelson, D.J. Harter, Joseph A. Pete, and R. C. Morris, "Tunable Alexandrite Lasers: Development and Performance", IEEE Journal of Quantum Electronics, vol. QE-21, pp. 1568-1581, (1985).
[5] Steve Guch, Jr., and Carl E. Jones, "Alexandrite-laser performance at high temperature," Optics Letters, vol. 7, pp. 608-610, (1982).

Passively Mode-Locked Laser Pulse Generation by Nonlinear Polarization Rotation in Alexandrite Rod

Byunghyuck Moon[1,2], Yohan Kim[1,2], Byeong-kwon Ju[2] and Young Min Jhon[1*]

1- Sensor System Research Center, Korea Institute of Science and Technology, Seoul 136-791, Rep. of Korea
2- Display and Nanosystem Laboratory, College of Engineering, Korea Univ., Seoul 136-713, Rep. of Korea

**ymjhon@kist.re.kr*

Ultrashort pulses in solid-state lasers can be generated by active or passive mode locking. Active mode locking is mainly achieved by active optical modulators to generate pulses, which has high pulse stability but requires expensive electrical and electronic components [1]. Passive mode locking can be achieved by using SESAM (SEmiconductor Saturable Absorber Mirror), SHG (Second harmonic generation) crystal or Kerr lens effect [2-4], which has the advantage of not requiring expensive optical modulators or electronic circuits. NPR (Nonlinear Polarization Rotation) mode locking is a powerful and well-known method for generation of short pulses from fiber lasers [5] but has not been achieved in solid-state lasers.

In this paper, we propose a new NPR mode-locked solid-state laser in Alexandrite rod, which is achieved by using the high nonlinear coefficient, polarization dependency of gain, and the birefringence in Alexandrite rod [6].

The experimental setup consists of a linear resonator as shown in Figure 1 and optically pumped with a Xenon lamp [7]. The Pockels cell was used to obtain Q-switching and control laser output. The Alexandrite rod was rotated by ~30 degrees for anisotropic amplification and polarization control. The vertical polarization component in the resonator was used as the output by using the linear polarizer. Polarization inside the resonator changes due to anisotropic absorption efficiency, birefringence, and nonlinearity due to rotation of the Alexandrite Rod. This polarization change can create resonator losses within the resonator, which can be used to generate mode-locked pulses. The mode-locked pulses have a repetition rate of 80 MHz and has a pulse width of 83 ps.

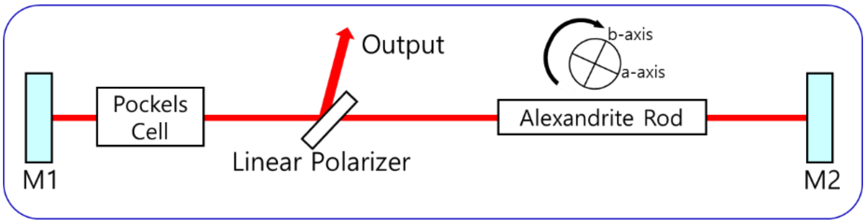

Figure 1. Schematic diagram of NPR Alexandrite laser

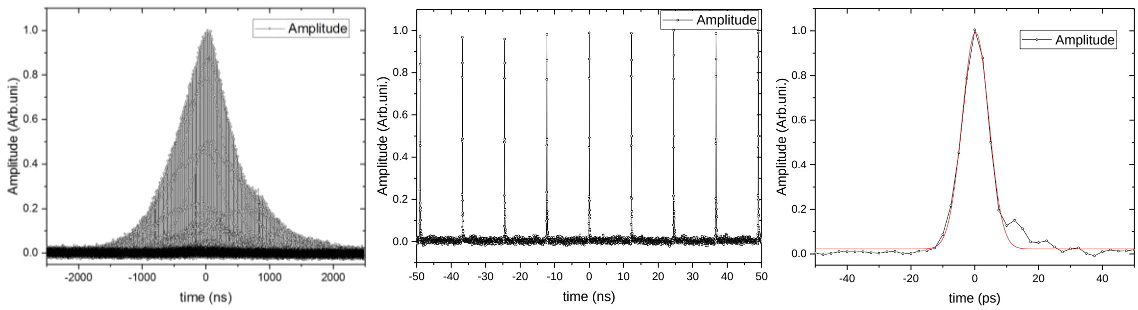

Figure 2. Mode-locked pulse train

[1] C. Antoncini, Ultrashort Laser Pulses, Department of Physics University of Reading, pp. 1-35 (2014)
[2] U.Keller, Ultrafast solid-state laser oscillators, Appl. Phys. B **100,** pp. 15-28 (2010)
[3] V. Couderc, F. Louradour, A. Barthelemy, 2.8 ps pulses from a mode-locked diode pumped Nd:YVO4 laser using quadratic polarization switching, Opt. Commun. **166**, pp. 103-111 (1999)
[4] Shirin Ghanbari, Reza Akbari, Arkady Major, Femtosecond Kerr-lens mode-locked Alexandrite laser, Opt. Express **24**, pp. 14836 (2016)
[5] H. A. Haus, E. P. Ippen, and K. Tamura, Additive-pulse modelocking in fiber lasers, IEEE J. Quantum Electron. **30**, 200–208 (1994)
[6] http://www.northropgrumman.com/BusinessVentures/SYNOPTICS/Products/LaserCrystals/Documents/pageDocs/Alexandrite.pdf
[7] J. Ahn, M. K. Jung, M. Seo, S. Lee and Y. M. Jhon, Q-switched mode-locked alexandrite laser for picosecond pulses, 2015 11th CLEO-PR, Busan, pp. 1-2 (2015)

Femtosecond Laser Rapid Prototyping of Glass Microfluidic Chips for Application of Optical Analysis

Sung-il Kim [1, 2], Chiwan Koo[2], Yeun-Ho Joung[2], and Jiyeon Choi[1]

1- Dept. of Electronics and Control Engineering, Hanbat National University, Daejeon, Korea
2- Dept. of Laser and Electron Beam Application, Korea Institute of Machinery and Materials, Daejeon, Korea

Main author email address: jchoi@kimm.re.kr

Microfluidic technology that allows small samples of fluids to be controlled and analyzed within micro-scale channels has been widely used in various aspects of biology experiments including synthesis, analysis, detection, separation, sensing, catalysis, and therapy. Over the last decade most of microfluidic devices are fabricated with a polymer material, polydimethylsiloxane (PDMS). However, the PDMS has shortcomings such as low gas hermeticity, poor chemical compatibility with solvents, low thermal conductivity, and low pressure resistance. While glass has many potentials in microfluidics over PDMS due to its stronger stiffness, easy integration with electrodes, excellent optical transparency and chemical properties. But glass micromachining using semiconductor processes requires many steps such as patterning, protection layering, etching, and bonding so it is hard to reduce long fabrication time, high cost, and complexity in processing [1]. For this reason, we propose a simple and rapid glass micromachining method using a ultrafast laser process as shown in figure 1. The ultrafast laser process having high peak power and ultra short pulse width minimizes heat-affected zones (HAZ). First step, micro channels are fabricated on a glass laser direct writing such as multi trench structuring. After then, the glass was immersed in hydrofluoric acid (HF) for about 30 minutes to obtain the single channel of 50 μm wide. Laser assisted selective etching (LASE) are LASE which induces higher etch rate of the substrate by changing of material density and generation of nano-size cracks. For this reason, minimize debris, cracks and good roughness better than ablation process [2]. Second step to make inlets and outlets, four holes of 500 μm diameter were drilled on a glass sheet using a galvano scanner. Third step the glass sheet with the channel was bonded to another glass sheet by laser welding. Laser welding process is able to give particularly reliable sealing without any adhesive layer or material because it melts only the interface of two sheets by locally heating them using nonlinear absorption that is induced by the femtosecond pulse laser. In result, the total fabrication process for a simple T-junction microchannel was done within one hour. To show perfect sealing of the channels, a flow test with three color dyes was conducted and a laminar flow was created without any leak around the microfluidic channel. The channels roughness and flatness are as good as the channel that is fabricated by photolithography-based MEMS. In addition we were able to multi width channel fabricated for droplet generation as shown in figure 2. For the future work, we will develop a glass microfluidic device for specific small cell analysis using spectroscopy or fluorescence and a glass implantable medical sensor using the hermetic seal of glass packages.

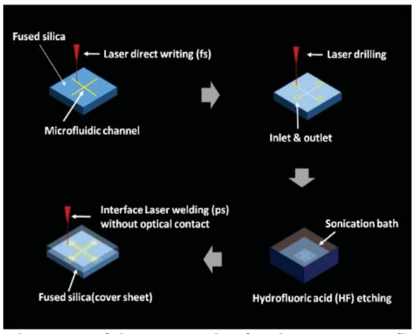

Figure 1 A schematic of three-step ultrafast laser process flow chart.

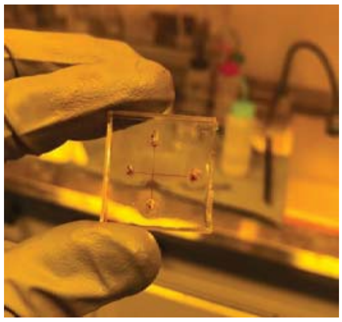

Figure 2. Fabricated droplet generator

[1] Qiang C, et al. "A Rapid and Low-Cost Procedure for Fabrication of Glass Microfluidic Devices", IEEE J.MEMS, Vol.16, pp.1193-1200 (2007)
[2] Y.Cheng, "Internal Laser Writing of High-Aspect-Ratio Microfluidic Structures in Silicate Glasses for Lab-on-a-Chip Applications," Micromachines, vol.8, pp.59-73 (2017)

Output Characteristics of CW laser using Multi-Pass Pumping Yb:YAG Thin-Disk Module

DH Jin, TJ Kang, YS Kim, DJ Shin, SH Kim, J.Ku

EO Technics

91 Dongpyeonro, Anyang, 13930, South Korea

dhjin@eotechnics.com

We present our recent studies regarding the characteristics of CW laser generated with multi and single mode using Yb:YAG thin disk module. In the multi mode, 260W signal output power was obtained at 430W pumping power. In the single mode, 122W signal output power was achieved at 380W pumping power with M2 <1.1. The multi pass pumping alignment in the thin disk module was optimized to form a single spot even over a tens of round trips, at this time, the maximum pumping power density at the applied pump spot diameter was calculated and the thin disk endurance test at the corresponding power density was also performed. A multi mode CW setup consisted of an output coupler and a few mirrors with very high reflectance for the signal beam, and showed pump-signal conversion efficiency of about 60% and M2 with 1.7~1.8. A single mode test was performed using concave, convex and flat mirrors, in this case, we observed that pump-signal conversion efficiency of 32% and M2 were founded to be 1.1 or less. Since the Yb:YAG thin disk is a very thin laser medium with a thickness of 100 to 300 um or less, single pass gain is so small that a tens of times multi pass pumping has been applied and a tens of pumping spots have to form the same spot, therefore an optimization method capable of forming a single spot was applied as very precise pumping alignment.

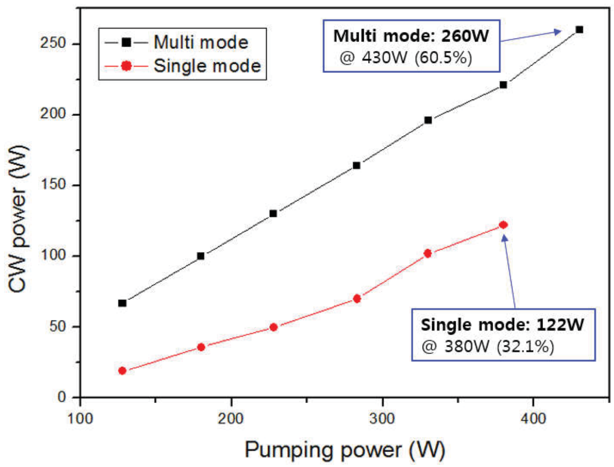

Figure 1. CW output characteristics of multi mode and single mode operations.

Acknowledgement

This work was supported by the Technological R&D Program funded by the Small and Medium Business Administration (SMBA).(No.S2367864)

References

[1] A. Giesen, et al. "Scalable Concept for Diode-Pumped High-Power Solid-State Lasers", Appl. Phys. B 58, 365-372 (1994)
[2] A. Giesen, et al. "Fifteen Years of Work on Thin-Disk Lasers: Results and Scaling Laws", IEEE, Vol.13, No.3, pp.598-609 (2007)
[3] U. Keller, "The Ultrafast Future", Laser & Photonics Marketplace Seminar 2015.

Wide and flat optical spectrum in a mode-locked laser diode with Bragg grating reflector on an active waveguide region

Young Ahn Leem[1], Namje Kim[1]

1- Photonics/Wireless Convergence Components Department, ETRI, Daejeon, Korea

leem@etri.re.kr

Recently, optical comb sources have a great attention as compact WDM source because it is hard to reduce the size of the laser diode array. Although there are several ways to construct optical comb source, optical comb sources based on pulsating laser diode have the advantage due to the small size and PIC (Photonic Integrated Circuit). Mode-locked laser diode (MLLD) and gain switching laser diode (GSLD) are used to construct the comb. [1, 2] As the optical bandwidth in the case of GSLD is limited, electro-optical modulator or nonlinear fiber are used to expand the bandwidth. In the case of MLLD, the wide optical bandwidth is achieved when the cavity is formed by facet reflections. However, the optical bandwidth is limited less than 1nm in MLLD with DBR (Distributed Bragg Reflector). [3] In considering PIC (Photonic Integrated Circuit), reflectors such as DBR that act like facet reflection are needed. Although the grating of a large coupling coefficient was realized to extend the bandwidth, the dispersion of DBR limited the optical bandwidth. When applying the chirped grating to compensate the dispersion, the wide optical bandwidth was realized. [3] However, the spectrum was not flat.

In the DBR configuration, it is difficult to simultaneously achieve a wide reflection bandwidth and a low dispersion. To decrease the dispersion, the length of DBR should be minimized, but the 3dB bandwidth of the reflection is reduced. To solve this problem, we use the InGaAs grating layer to realize a high coupling coefficient of ~150cm^{-1} in the planar buried heterostructure with p-n-p current blocking and the waveguide of DBR region is the active waveguide to flatten the reflection profile of DBR. In this way, we achieve the wide optical bandwidth of ~4nm and the spectrum has a flat top as shown in figure 1. The RF linewidth of 1.2MHz and the optical modulation depth of larger than 30dB confirm passive mode locking.

This work was supported by Electronics and Telecommunications Research Institute (ETRI) grant funded by the Korean government. [17ZB1500, Development of key material and device technologies for next generation semiconductor devices with extreme performance]

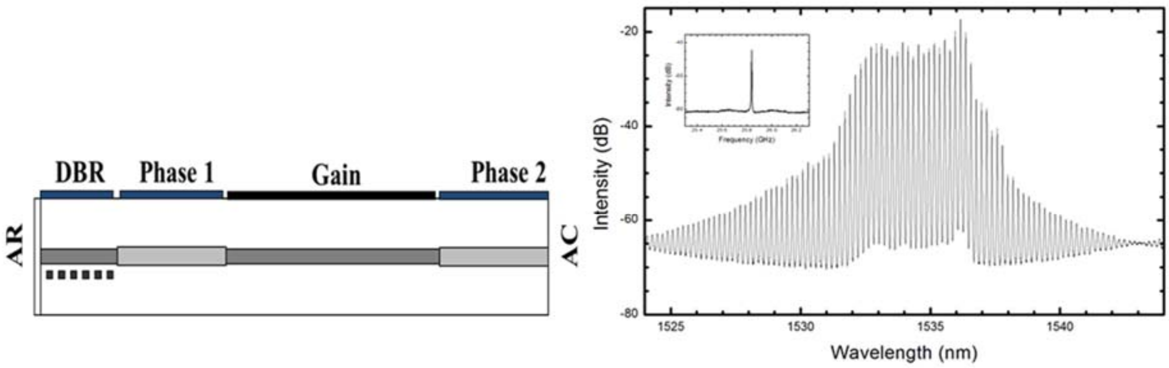

Figure 1.
Left: the schematic diagram of the device, Right: the optical spectrum and the RF spectrum (inset)

[1] V. Vujicic, P. M. Anandarajah, R. Zhou, C. Browning, and L. P. Barry, Performance investigation of IM/DD compatible SSB-OFDM systems based on optical multicarrier sources, IEEE Photon. J. , vol.6 , no. 7903110, (2014).
[2] V. Vujicic et al. , Quantum dash mode-locked lasers for data centre applications, IEEE J. Sel. Topics Quantum Electron., vol.21, no.1101508, (2015)
[3] M. J. Strain, P. M. Stolarz, and M. Sorel, Passively mode-locked lasers with integrated chirped Bragg grating reflectors, IEEE J. Quantum Electron., vol.47 , pp. 492-498, (2011).

Laser assisted selective copper plating on polymers

Karolis Ratautas[1], Mindaugas Gedvilas[1], Ina Stankevičiene[1], Aldona Jagminienė[1], Eugenijus Norkus[1], Nello Li Pira[2], Stefano Sinopoli[3], Gediminas Račiukaitis[1]

[1] *Center for Physical Sciences and Technology, Savanoriu Ave. 231, Vilnius, LT-02300, Lithuania*
[2] *Centro Ricerche Fiat, Strada Torino 50, Orbassano (TO), 10043, Italy*
[3] *BioAge Srl, Via Dei Glicini 25, Lamezia Terme (CZ), 88046, Italy*

E-mail: karolis.ratautas@ftmc.lt

Laser writing for selective plating of electro-conductive traces for electronics has several significant advantages, compared to conventional printed circuit board technology. Firstly, this method is faster and cheaper for prototyping. Secondly, material consumption is reduced, because it works selectively. However, the biggest merit of this approach is potentiality to produce moulded interconnect device (MID), enabling creation of electronic circuits on 3D surfaces, thus saving space, materials and cost of production.

Moulded interconnect devices (MID) offer the material, weight and cost saving by integration electronic circuits directly into polymeric components used in automotive and other consumer products. Lasers are used to write circuits directly by modifying the surface of polymers followed by an electroless metal plating.

Fabrication of circuit traces is the most challenging task in the Molded Interconnection Device (MID) technology. The technical difficulties which can be met when producing conductive traces are spatial selectiveness and adhesion of a plated metal. On the other hand, the technique used to manufacture circuit should be cost-effective as well. Considering this background, two methods of selective plating induced by a laser are presented here. This presentation consists of two parts. In the first part, we describe new PP and PC/ABS masterbatch with carbon-based additives for the laser direct structuring (LDS) approach. The second part presents a new technology for MID: Selective Surface Activation Induced by Laser (SSAIL). This new technique for selective surface plating enables to use standard plastics without any LDS additives. In both cases, metal deposition was performed by electroless plating. Nanosecond and picosecond lasers were applied for polymer surface treatment. The narrowest width of a copper-plated line was less than 23 μm. The Scotch tape test was applied to measure the adhesion of a plated metal.

There are several techniques of laser writing for selective plating of polymers: metal nano-ink printing, laser-induced forward transfer (LIFT) [1], laser-induced selective activation (LISA) [2] and laser direct structuring (LDS). However, all of them, except LDS, have a limitation when it is being applied on a curved surface.

For our investigation, we used LDS [3] and our new method: selective surface activation induced by laser (SSAIL). The main difference between LISA and SSAIL is that the second one is performed in atmospheric ambient. That simplifies the processing of 3D surface.

In the SSAIL method, pure plastics without any dopant (filler) can be used. SSAIL is a 3 step process. The first step is surface modification by laser, second – chemical activation of modified areas and the last step is electroless plating. In LDS method, special fillers are mixed in the polymer matrix. These fillers are activated during laser writing process and in the next processing step scanned area can be selectively plated with metals. There are some commercial materials available on the market for LDS; however, mostly they are based on expensive fillers, usually palladium. Considering the need of MID market, we are looking for the way to reduce the price of circuit traces manufacturing. Therefore, for LDS approach, we suggest new material: polypropylene with carbon-based additives, which increases the price of masterbatch much less than alternative additives used in polymers for LDS. While for the SSAIL method we used just commercial PC/ABS blend at all. Tests were performed using picosecond and nanosecond laser pulses. Different processing parameters (laser energy, scanning speed, the number of scans, pulse durations, wavelength and overlapping of scanned lines) were applied. A sheet resistance of selectively plated samples manufactured with different laser processing parameters and the same chemical bath conditions has been measured in order to determine the optimal regime of activation. Spatial selectivity tests showed high plating resolution. The narrowest width of plated line was less than 23 μm. The activation process was also investigated using Raman spectroscopy analysis. In Raman experiments, two spectra of treated and untreated plastic surfaces were compared. Finally, a prototype of the electronic circuit board was performed using both methods.

[1] S. H. Ko, J. Chung, Y. Choi, C. P. Grigoropoulos, N. R. Bieri, T.-y. Choi, C. Dockendorf, and D. Poulikakos, "Laser-based hybrid inkjet printing of nanoink for flexible electronics," Proc. SPIE, **5713**, 97-104, (2005).

[2] Y. Zhang, H. Hansen, A. De Grave, P. Tang, and J. Nielsen, "Selective metallization of polymers using laser induced surface activation (LISA)—characterization and optimization of porous surface topography," Int. J. Adv. Manuf. Technol., vol. 55, pp. 573-580, 2011.

[3] J. K. M. Huske, J. Mller, G. Esser, "Laser Supported Activation and Additive Metallization of Thermoplastics for 3D-MIDs," Proc. LANE, (2001).

Investigation of Pitch Variationsin Cholesteric Liquid Crystal Cell using Wavelength-Swept Laser

MyeongOck Ko[1], Sung-Jo Kim[2],Jong-Hyun Kim[1], and Min Yong Jeon[1]*

1- *Department of Physics, Chungnam National University, Daejeon 34134, Korea*

2- *Center for Soft and Living Matter, Institute for Basic Science, Ulsan 44919, Korea*

**myjeon@cnu.ac.kr*

A cholesteric liquid crystal (CLC) is a liquid crystal mixture in which a chiral dopant is added to a nematic liquid crystal (NLC) to induce a periodic spiral structure.It has a helical structure along the twisting direction of the NLC.Moreover, it isvery sensitive to external environmental conditions. Therefore,the pitch of the helical structure is changed when the external physical state surrounding the CLC is changed. When a horizontal electric field is applied to a horizontally aligned thin CLC cell, the pitch length is changed discontinuously.The measurement of the instantaneous change in bandgap structure when an electric field is applied to the CLC is very important for characterizing the CLC. Recently, J. Yoshioka have been reported that the director fluctuations in CLC by using a method of dynamic light scattering measurement [1]. However,it is difficult to directly observe the dynamic variation of the bandgap movement, since the measurement setup is very bulky and the optical alignment is difficult [2].To solve this problem, a wavelength-swept laser can be used to measure the variation of the dynamic bandgap structure [3].Because the wavelength signal in the spectral domain corresponds to the pulse signal in the temporal domain, the change in the pulse signal can be measured instead of the change in the wavelength signal.In this paper, instantaneous bandgap shift was confirmed by measuring the transmission spectrum variationof CLC in real time.The use of wavelength-swept lasers is expected to be useful for the researches of fast electro-optic devices and dynamic physical sensors based on CLC devices [4,5].

[1] J. Yoshioka, Y. Takanishi and J. Yamamoto, "Dispersion relations of director fluctuations along the direction perpendicular to the helical axis in cholesteric liquid crystals," EPL 98, 16006 (2012).
[2] M.S. Giridhar and K.A. Suresh, "A dynamic light scattering study of the viscoelastic twist mode in cholesteric liquid crystals," Eur. Phys. J. E 7, 167-173 (2002).
[3] Myeongo Ock Ko, Sung-Jo Kim, Jong-Hyun Kim, Bong Wan Lee, and Min Yong Jeon, "Dynamic measurement for electric field sensor based on wavelength-swept laser," Opt. Express 22,16139-16147 (2014)
[4] Ho Hyun Lee, Jeong-Seon Yu, Jong-Hyun Kim, "Fast electro-optic device controlled by dielectric response of planarly alighned cholesteric liquid crystals," J. Appl. Phys. 106, 014503 (2009)
[5] Chin-Kai Chang, Shih-Wen Chiu, Hui-Lung Kuo, and Kea-Tiong Tang, "Cholesteric liquid crystal-carbon nanotube hybrid architectures for gas detection," Appl. Phys. Lett. 100, 043501 (2012)

Low-cost compact tunable wavelength filters based on polymeric waveguide Bragg grating

Tae-Hyun Park, Eon-Tae Kim, Sung-Moon Kim, Min-Cheol Oh*

Dept. of Electronics Engineering, Pusan National University, 2, Busandaehak-ro 63beon-gil, Geumjeong-gu, Busan (Pusan) 609-735, Republic of Korea

Main author email address: taehyun@pusan.ac.kr

Tunable wavelength filters are necessary component for selecting a certain wavelength from a WDM signal arrived at the subscriber of the WDM optical communication network. Various tunable wavelength filters have been demonstrated based on thin film filters [1], Fabry-Perot cavity devices [2], fiber Bragg gratings [3], etc. Among them, Bragg reflector is the most suitable device for dense WDM optical communication because of its unlimited free spectral range (FSR), narrow bandwidth, and flat-top passband [4]. Polymeric wavelength filters with a Bragg reflector has the advantages of a simple structure and a wide tuning range. For an ordinary Bragg reflector, to separate the reflected signal from the input signal, an external circulator device is indispensable. However, in this work, a tilted Bragg grating along with an asymmetric Y-branch are incorporated to direct the reflected light into another separated port as shown in Fig. 1 [5].

The asymmetric Y-branch exhibits good mode sorting efficiency and tilted Bragg reflector operates as a mode converter for a specific wavelength satisfying the Bragg condition. The wavelength filter was fabricated using a LFR polymer material produced by ChemOptics Inc. Broadband light source covering the C-band was used to characterize the device. The reflected signal at the output port was directly monitored with an optical spectrum analyzer, and the signal returning to the input port was measured using an optical circulator. The side mode suppression ratio (SMSR) of the output signal was -24.71 dB because of the NEEW reflection peak as shown in Fig. 2. The polarization dependence measured by the reflection peak was less than 0.1 nm. By applying an electrical power on the thin film heater, the reflected wavelength was tuned, as shown in Fig. 3. The tuning range was increased over 41.39 nm for an applied thermal power of 352 mW. The manufacturing tolerances of the device was quite large as we observed by the production yield, and the device is suitable for mass production with the high-yield.

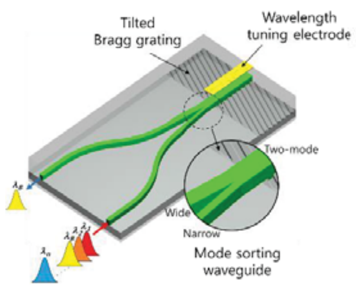

Figure 1. Schematic of a channel-drop filter

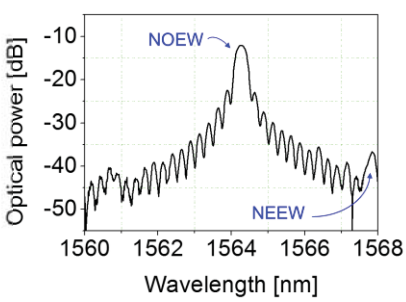

Figure 2. Measured reflection spectra

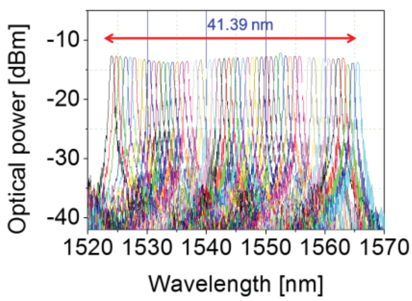

Figure 3. Tuned reflection spectra

[1] L. Domash, M. Wu, N. Nemchuk, E. Ma, Tunable and switchable multiple-cavity thin film filters, J. Lightwave Technol. 22(1), 126-135 (2004).
[2] B. Yu, G. Pickrell, and A. Wang, Thermally tunable extrinsic Fabry-Perot filter, IEEE Photon. Technol. Lett. 16(10), 2296-2298 (2004).
[3] A. D. Kersey, M. A. Davis, H. J. Patrick, M. LeBlanc, K. P. Koo, G. G. Askins, M. A. Putnam, E. J. Friebele, Fiber grating sensors, J. Lightwave Technol. 15(8), 1442-1463 (1997).
[4] M.-C. Oh, H.-J. Lee, M.-H. Lee, J.-H. Ahn, S. G. Han, H.-G. Kim, Tunable wavelength filters with Bragg gratings in polymer waveguides, Appl. Phy. Lett. 73(18), 2543-2545 (1998).
[5] J.-S. Shin, T.–H. Park, W.–S. Chu, C.-H. Lee, S.-Y. Shin, M.-C. Oh, Tunable channel-drop filters consisting of polymeric Bragg reflectors and a mode sorting asymmetric X-junction, Opt. Express 23(13), 17223-17228 (2015).

Mode-locked Yb-doped Fiber Laser based on Birefringent Spectral Filter

Hyun Moon Yang, Ji Su Kim, and Min Yong Jeon*

Department of Physics, Chungnam National University, Daejeon, Korea

**myjeon@cnu.ac.kr*

Over the past decade, ultrafast fiber lasers have been developed for many applications in the fields of material processing, optical communications, bio-photonics, THz science, and so on. In particular, mode-locked Yb-doped fiber lasers have advantages of wide gain bandwidth and good quantum efficiency. Therefore, many researches on mode-locked Yb-doped fiber lasers have been reported [1-3]. In this paper, we report a mode-locked Yb-doped fiber lasers in a normal dispersion region using a birefringent spectral filter. The center wavelength and the full width at half maximum (FWHM) of the mode-locked fiber laser depend on angle of the optical axis and the azimuthal angle of the birefringent plate. The repetition rate and the FWHM of the mode-locked fiber laser were ~104.2 MHz and 18.09 nm, respectively. The direct pulse width was measured with 1.71 ps, assuming a Gaussian pulse shape. The total dispersion value has a positive at a center wavelength of 1.03 μm and thus the output short pulse has a large amount of chirp. A pulse compressor was constructed to compensate for chirp using a pair of diffraction gratings, and a dechirped pulse of 148 fs was finally obtained. The peak power of the pulse was ~ 7.14 kW. The dechirped pulse has a time-bandwidth product of 0.75. The center wavelength of the mode-locked fiber laser could be changed from 1026.9 nm to 1045.6 nm according to the angle of the optical axis of the birefringent plate.

[1] A. Chong, J. Buckley, W. Renninger, and F. Wise, “All-normal-dispersion femtosecond fiber laser,” Opt. Express **14**, 10095–10100 (2006).

[2] A. Chong, W. H. Renninger, and F. W. Wise, “All-normal-dispersion femtosecond fiber laser with pulse energy above 20 nJ,” Opt. Lett**.** **32**, 2408–2410 (2007).

[3] M. S. Kong, J. S. Kim, S.-P. Han, N. Kim, K. Moon, K. H. Park, and M. Y. Jeon, "Terahertz radiation using log-spiral-based low-temperature-grown InGaAs photoconductive antenna pumped by mode-locked Yb-doped fiber laser," Opt. Express **24**, 7037-7045 (2016)

Wavelength-switchable operation of the erbium-doped fiber laser with orthogonal polarization

Seul-Lee Lee[1], Jihoon Kim[2], Sungwook Choi[1], Jun Hyeok Jeong[1], Sun Jae Jeong[1], Min Seok Kim[1], Dokyeong Kim[1], and Yong Wook Lee[1,2,*]

1- *Interdisciplinary Program of Biomedical, Mechanical & Electrical Engineering, Pukyong National University, 45 Yongso-ro, Nam-gu, Busan 48513, Korea*

2- *School of Electrical Engineering, Pukyong National University, 45 Yongso-ro, Nam-gu, Busan 48513, Korea*

yongwook@pknu.ac.kr

We propose a wavelength-switchable erbium-doped fiber (EDF) ring laser with orthogonal polarization by incorporating a cavity filter based on a polarization-diversified loop (PDL) using two fiber Bragg gratings (FBGs) with different resonances. FBG, which has a reflection spectrum of narrow band characteristics at a special resonance wavelength, has been used as ideal wavelength selection elements for fiber lasers [1]. However, there are some problems to use FBGs as cavity filters that an additional component is necessarily required including an optical coupler or an optical circulator, and one of reflection spectra of serially connected FBGs cannot be individually selected. To solve these problems, an inline switching filter based on a PDL was suggested using a polarization beam splitter and three quarter-wave plates (QWPs), and two FBGs (FBG 1 and FBG 2) with different Bragg wavelengths [2]. The proposed laser is composed of EDF, a 980 nm laser diode, a wavelength-division-multiplexing coupler, a rotatable linear polarizer, an optical isolator, a 3 dB optical coupler, and the inline switching filter. At a special combination of the orientation angles of the three QWPs, the inline filter based on PDL can offer a different transmittance according to input polarization realizing the polarization-dependent band-pass operation at each Bragg wavelength. In other words, reflection spectrum of FBG 1 or FBG 2 can be selected for horizontally or vertically polarized input light, respectively. Consequently, switching operation between two laser lines with orthogonal polarization at the two FBG resonance wavelengths can be achieved by varying the orientation angle of the linear polarizer. In the fabricated laser, it was demonstrated that lasing operation at a resonance of FBG 1 or FBG 2, that is 1550.05 nm or 1555.14 nm, respectively, could be implemented by properly controlling cavity polarization, with a signal-to-ratio (SNR) of ~56.24 dB or ~57.31 dB, indicated as a red or blue solid line, respectively, as shown in Figure 1.

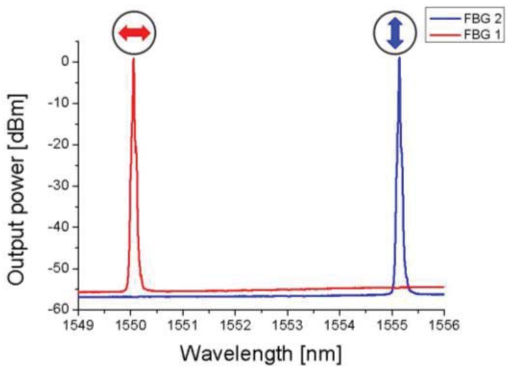

Fig. 1. Measured lasing spectra of proposed fiber laser with orthogonal polarization

[1] Q. Mao and J. W. Y. Lit, "Switchable multiwavelength erbium-doped fiber laser with cascaded fiber grating cavities," *IEEE Photon. Technol. Lett.*, vol. 14, pp. 612-614, **(2002)**.
[2] J. Kim, H. W. Kang, S. Y. Nam, J. Oh, and Y. W. Lee, "Inline selection of transmission or reflection spectra of different fiber Bragg gratings using polarization-diversity loop," *J. Opt.*, vol. 18, 015702, **(2016)**.

A Highly-Junction-Capacitance-Isolated 10-Gb/s CMOS Optoelectronics Receiver IC for Short Reach Applications

Jae-Sung Kim[1], Ki-Yong Kim[1], Kangyeob Park[2], and Won-Seok Oh[2]

1-Seil Technology Co., Ltd., 166 Gosan-ro, Gunpo-si, Gyeonggi-do, Korea 15850
2- Korea Electronics Technology Institute, 25 Saenari-ro, Seongnam-si, Gyeonggi-do, Korea 13509

jskim@seiltnn.com

This paper describes a 10-Gb/s CMOS optoelectronics receiver IC for short reach applications with a second-order LC-ladder network to highly isolate an inherent junction capacitance of p-i-n photodiode. The second-order LC-ladder network is adopted as an input configuration which can compensate the large junction capacitance for high-speed operation. The receiver IC is implemented in 65-nm standard CMOS technology and includes trans-impedance amplifier and limiting amplifier. By using the LC-ladder network, the receiver IC can detect 10-Gb/s optical NRZ data against 5.5 pF of junction capacitance. Additionally capacitive degeneration, inductive peaking, active feedback amplifier, and negative capacitance compensation techniques are exploited to enhance 3-dB bandwidth.

In optical receiver IC design, the p-i-n photodiode (PD) can be simply modeled to be a dependent current source with a parallel junction capacitance (C_{PD}) and a series resistor. Many studies have been reported that can reduce the junction capacitance by using various physical methods [1, 2]. These efforts unfortunately increase the PD costs, thus a circuit technique that can provide high-speed operation even with a large C_{PD} is desired for short-reach applications, such as chip-to-chip interconnect, display interconnect, 40GBASE-SR4, and 100GBASE-SR10.

Figure 1 describes a block diagram of the proposed receiver IC. The receiver consists of LC-ladder network, trans-impedance amplifier (TIA), limiting amplifier (LA), and output buffer. We exploit passive LC-ladder network in the input of optical receiver IC to use the low-cost PD having large C_{PD}. The proposed receiver achieves 7.9 GHz of 3-dB bandwidth with 5.5 pF of junction capacitance for 10-Gb/s operation. -17-dBm of the measured sensitivity is achieved for less than 10^{-12} BER.

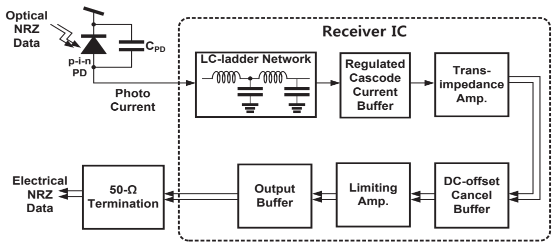

(a)

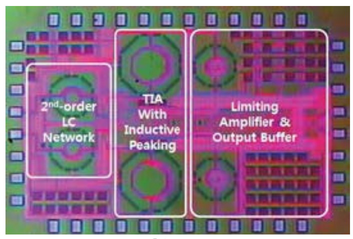

(b)

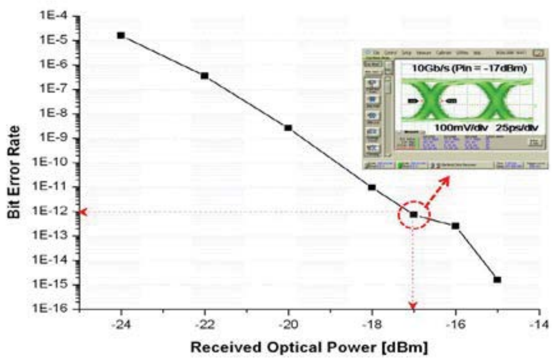

(c)

Figure 1. (a) Block diagram, (b) microphotograph, and (c) measured sensitivity & 10Gb/s eye diagram of the proposed receiver IC

[1] Zuon-Min Chuang, et al., Low Capacitance, Front-Illuminated Planar InGaAs PIN Photodiode on Semi-insulating InP Substrate, Electron Device and Materials Symposium, pp. 25-28 (1994).

[2] H. Zimmermann and B. Muller, Ultralow-Capacitance Lateral P-I-N Photodiode in a Thin c-Si Film, IEEE Transactions on Nuclear Science, vol. 49, pp. 2032-2036 (2012).

Continuously tunable microwave photonic filter with a wavelength-spacing tunable multiwavelength fiber laser

Seungmin Lee, Ngoc Tuyen Tran, and Young-Geun Han*

*Department of Physics, Hanyang University, Seoul, Republic of Korea, *yghan@hanyang.ac.kr*

Microwave photonic filters have great potential in the application to Radio-over-Fiber (RoF) systems because they can provide by using microwave photonic filters the limitation of the traditional filters, e.g., the electric bottleneck problem and other sources of degradation [1-3]. The wavelength spacing of the multiwavelength laser or the dispersion of the dispersive medium should be adjusted in order to control the free spectral range (FSR) of the microwave photonic filter. For the realization of multiwavelength laser with tunable wavelength spacing, tunable laser array was exploited. The FSR of the microwave photonic filter was tuned discretely by switching on and off the laser source. To realize multiwavelength in the single laser with the tunability of the wavelength spacing, tunable high birefringent Sagnac loop was used as a comb filter [1-3]. In this manuscript, we demonstrate a novel continuously tunable microwave photonic filter based on a polarization differential delay line (PDDL). The continuously tunable multiwavelength laser was realized by using the Saganc loop mirror with the PDDL. By controlling the PDDL, the wavelength spacing of the multiwavelength laser was continuously controlled while the stable lasing output was maintained. As the wavelength spacing was adjusted from 1.2 to 6.8 nm with the extinction ratio of ~ 40 nm, the FSR of the microwave photonic filter was continuously controlled from 1.84 to 0.33 GHz.

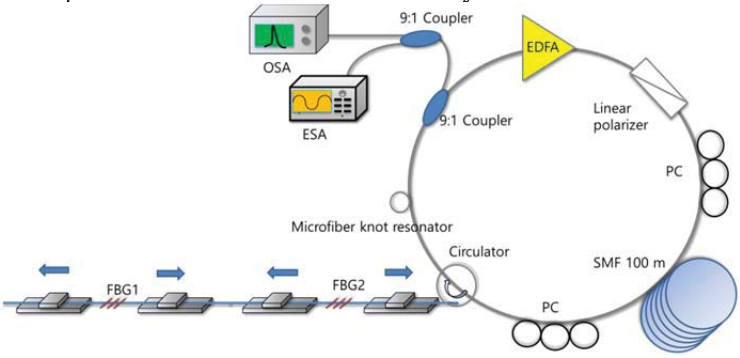

Figure 1. Experimental scheme for the optical attenuation-based WVA.

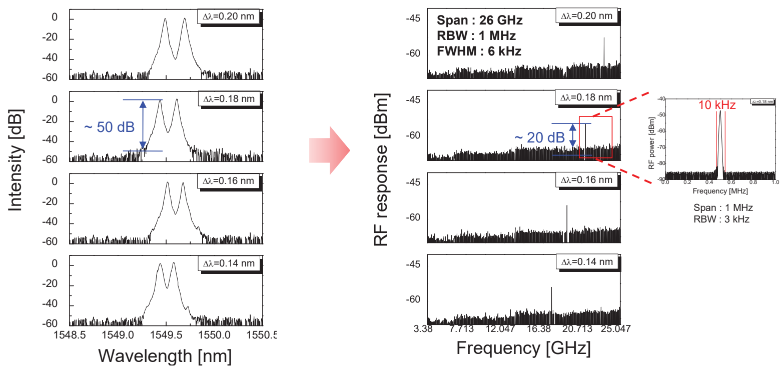

Figure 2. Measurement of microwave frequency using the proposed wavelength-spacing tunable multiwavelength fiber laser

[1] K. Zhu, H. Ou, H. Fu, E. Remb, and S. He, A simple and tunable single-bandpass microwave photonic filter of adjustable shape, IEEE Photon. Technol. Lett., vol. 23, pp. 1917-1919 (2008).
[2] S. Chun, B. Lee, Variable wavelength-spacing tunable filter using polarization differential delay line, Optical Engineering, vol. 44.2, pp. 020501 – 02051(2005) .
[3] Z. Zhang, L. Zhan, K. Xu, J. Wu, Y. Xia, and J. Lin, Multiwavelength fiber laser with fine adjustment, based on nonlinear polarization rotation and birefringence fiber filter, Opt. Lett., vol. 33, pp. 324 – 326 (2008).

100G Integrated Coherent Receiver Development and Performance Evaluation

H.-D. Jung, C.-J. Yoon, Y.-T. Han, S.-Y. Lee, J.-S. Choe, Y.-H. Ko, J.-H. Kim, Y.-S. Baek

Photonic Wireless Convergence Research Division, ETRI, Daejeon, 34129, Korea

hdjung@etri.re.kr

The abrupt adaptation of smart devices combined with the demands for seamless connections and high quality multimedia services gave rise to today's explosion of data traffic. To handle enormous data traffic properly and ensure QoS communications, optical backbone networks with coherent communications based on advanced modulation are essential. Among the elements of optical coherent system, an integrated coherent receiver (ICR) is the key component, enabling 100G and above flexible-grid software-defined optical networks.

In this paper, we reports the research activities to develop 100G ICR and long-haul transmission experiment results for the performance evalution of the developed ICR. The coherent receiver module shown in Fig.1 is composed of a silica PLC heterogeneous assembly, which uses a 2% Δ silica waveguide, high-speed waveguide type photodetectors, a printed circuit board, and a CuW block. To increase the cost-effectiveness, the ICR is fabricated based on simple chip-to-chip butt coupling method with waveguide PD. Additionally, low-cost PCB is used with CuW block, which allows low packaging cost.

To evaluate the performance of the developed ICR, the long-haul optical transmission was conducted with network nodes. 4 channel 112Gbps DP-QPSK coherent signals with different wavelengths were generated and transmitted through a re-circulating setup which cosists of 100km optical spool, wavelength selective switch as a network node, and EDFAs to compensate optical losses. As shown in Fig. 2, the signals were successfully delivered up to 1800km with the developed 100G ICR.

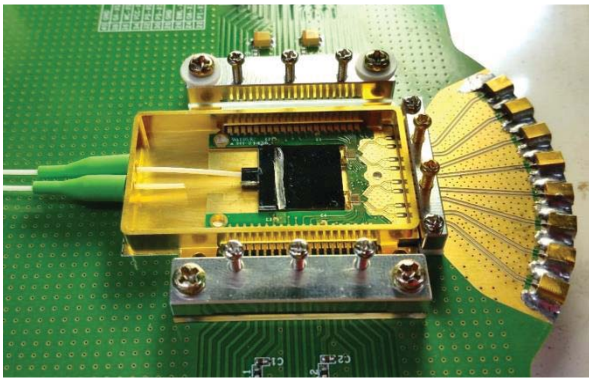

Fig.1 the developed 100G coherent receiver

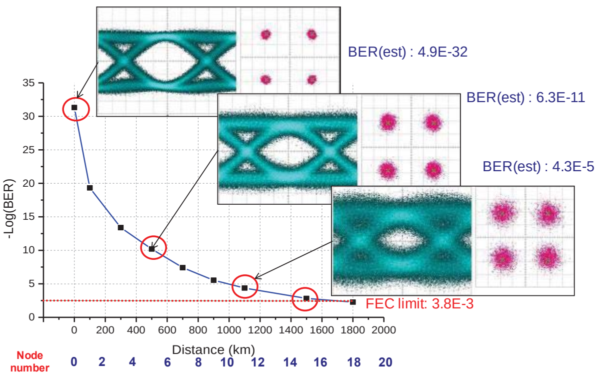

Fig.2 Transmission performance (BER vs. Distance)

[1] T. Ohyama, and et.al. 'All-in-one 112-Gb/s DP-QPSK Optical Receiver Front-End Module Using Hybrid Integration of Silica-based Planar Lightwave Circuit and Photodiode Arrays', IEEE Photon. Technol. Lett., vol. 24, pp.646-648 (2012)
[2] C. Xie, and et.al. 'Transmission of Mixed 224-Gb/s and 112-Gb/s PDM-QPSK at 50GHz Channel Spacing Over 1200km Dispersion-Managed LEAF Spans and Three ROADMs', J. of Light. Technol., vol. 30, pp.547-552 (2012)
[3] S.-Y. Lee, et.al. 'A cost effective silica-based 100G DP-QPSK Coherent Receiver', ETRI Journal, vol.38, pp.981-987 (2016)

Polarization singularities nucleation in the self-focusing of an elliptically polarized laser beam in Kerr medium and isotropic phase of nematic liquid crystal

V.A. Makarov[1,2], K.S. Grigoriev[1], N.A. Panov[2], O.G. Kosareva[1], G.M. Shishkov[1]

1- Faculty of Physics M.V. Lomonosov Moscow State University Leninskie Gory, 1, str. 2 Moscow, 119991, Russia
2- International Laser Center M.V. Lomonosov Moscow State University Leninskie Gory, 1, str. 62 Moscow, 119991, Russia

vamakarov@phys.msu.ru

The possibility of the formation of light polarization singularities (C-points) in the elliptically polarized laser beam, focused into nonlinear isotropic medium are of special interest [1-4]. In [2] the singularities did not appear because of the specific range of the nonlinear medium's parameters considered. In the present paper we study [3,4] the possibility of C-points formation during the self-focusing of an initially homogeneously elliptically polarized Gaussian beam, which propagates in an isotropic medium with cubic nonlinearity without spatial and frequency dispersion and in isotropic phase of nematic liquid crystal, the temperature of which is close to the temperature of nematic-isotropic phase transition.

We have numerically and analytically shown [3] that in the case of axially symmetric beam the emerging C-lines have the shape of circumference with the center at the beam's axis and they are located in the separate transversal planes in the medium. If the axial symmetry of the incident beam is broken then the even number of C-points with opposite topological charges are nucleated in the medium. They exist in a certain range of propagation coordinate z and then they collide and annihilate each other.

Numerical simulations of initially homogenously polarized Gaussian light beam self-focusing in isotropic phase of nematic liquid crystal were carried out. We show [4] that C-lines of both polarization handednesses are nucleated near these transversal cross-sections of the beam, in which local extrema of peak intensities of corresponding circularly polarized components of the beam are attained. These lines are closed loops, surrounding the beam axis. They appear in wide range of beam and nonlinear medium parameters. Minor fluctuations of beam parameters do not destroy these singularities.

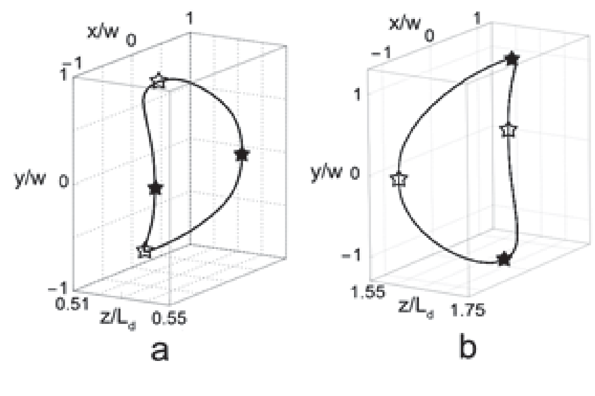

The typical example of three-dimensional right-hand (a) and left-hand (b) C-lines. White stars show the points of singularities nucleation and black stars show the points of their annihilation.

[1] S. Shiffler, P. Polynkin, J. Moloney, "Self-focusing of femtosecond diffraction-resistant vortex beams in water", Opt. Lett., v. 36, 3834-3837, (2013).
[2] V.A. Makarov, A.A. Golubkov, I.A. Perezhogin, S.S. Savvina, "Polarization transformation during beam focusing in chiral liquid", Proc. SPIE, v. 5333, 290-296, (2004).
[3] N.A. Panov, V.A. Makarov, K.S. Grigoriev, M.S. Yatskevitch, O.G. Kosareva, "Generation of polarization singularities in the self-focusing of an elliptically polarized laser beam in an isotropic Kerr medium", Physica D, v. 332, 73–78, (2016).
[4] K.S. Grigoriev, V.A. Makarov, G.M. Shishkov, "Polarization singularities in the self-focusing of an elliptically polarized laser beam in an isotropic phase of nematic liquid crystal close to the temperature of phase transition", Molecular crystals and liquid crystals, v. 647, 000, (2017), *in press*.

Efficient second and third harmonic generations in magnetic metamaterials

Iman Sajedian[1], Inki Kim[1] and Junsuk Rho[1,2*]

[1]*Department of Mechanical Engineering, Pohang University of Science and Technology (POSTECH), Pohang 37673, Republic of Korea*
[2]*Department of Chemical Engineering, Pohang University of Science and Technology (POSTECH), Pohang 37673, Republic of Korea*
*[*jsrho@postech.ac.kr](mailto:jsrho@postech.ac.kr)*

Here we study the linear and nonlinear behavior of magnetic metamaterials in their magnetic resonance. We show that the current loop formed in the magnetic resonant frequency acts as a source for nonlinear effects. This current loop is induced in the metallic regions, and the electric field in this loop is much stronger than the background electric field. Considering the fact that the nonlinear behavior of metamaterials is originated from the nonlinear behavior of metals, therefore this current loop acts as source for nonlinear behavior.

We will show that due to the circular shape of the current loop, two orthogonalnonlinear effects will occur in metamaterials. Then we will discuss howthe symmetrical properties of metamaterial determine the type of generatednonlinear harmonic effects. Based on these results we will propose a method foramplifying the nonlinear behavior in metamaterials. We will show that adding agrating under the metamaterial leads to the amplification of absorption. In fact, the grating and the metamaterial will form a Fabry-Perot like cavity which leadsto the amplification of fields in the metamaterial. This increase in the absorption isequivalent to an increase in the induced currents in the current loop, which leads tostronger nonlinear effects.

[1] I. Sajedian, A. Zachary and J. Rho, Optics Communications 397, 17-21 (2017)
[2] I. Sajedian, I. Kim, A. Zachary and J. Rho, Optics Communications , 401, 66-70 (2017)

Slowdown of Light in Free Space via Rayleigh Anomaly

Kyoung-Youm Kim[1] and Alan X. Wang[2]

[1]*Department of Electrical Engineering, Sejong University, Seoul 05006, Korea*
[2]*School of Electrical Engineering and Computer Science, Oregon State University, Corvallis, Oregon 97331, USA*

Main author email address: kykim@sejong.ac.kr

Light interacting with diffraction gratings changes its direction of propagation. When a grating has a certain period, the incoming light can be diffracted perpendicular to the surface normal of the grating, which we call Rayleigh anomaly (RA) [1–4]. Recently, we showed that RA can slow down the transmitted light in free space over a very long effective range [5]. Especially, we found out that the velocity reduction effect becomes more significant as the relative amount of diffracted light increases. Therefore, RA with efficient gratings can inspire a new mechanism for the optical sensing and photo-detection which requires a long interaction path as in near-infrared gas absorption. There remain, however, several issues that should be taken into consideration for the actual application of RA. The effect of finite grating size [5] and group velocity dispersion (see Fig. 1) are among them. We will discuss these subjects in the presentation.

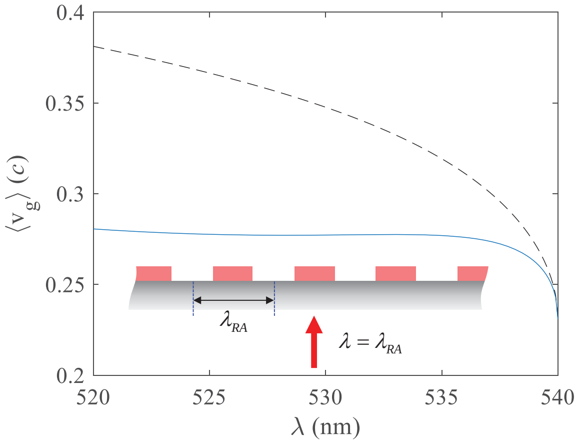

Fig. 1. Group velocity of the transmitted light in free space. We can reduce the group velocity dispersion (dashed to solid) by the appropriate design of the grating structure.

This work was supported by the Basic Science Research Program through the National Research Foundation of Korea funded by the Korean government (MSIP)(NRF-2016R1D1A1B03931510).

[1] R. W. Wood, "Anomalous diffraction gratings," Phys. Rev., vol. 48, pp. 928-936 (1935).
[2] J. W. S. Rayleigh, "Note on the remarkable case of diffraction spectra discovered by Prof. Wood," Philos. Mag., vol. 14, pp. 60-65 (1907).
[3] U. Fano, "The theory of anomalous diffraction gratings and of quasi-stationary waves on metallic surfaces (Sommerfeld's waves)," J. Opt. Soc. Am., vol. 31, pp. 213-222 (1941).
[4] F. Ren, K.-Y. Kim, X. Chong, and A. X. Wang, "Effect of finite metallic grating size on Rayleigh anomaly-surface plasmon polariton resonances," Opt. Express, vol. 23, pp. 28868-28873 (2015).
[5] K.-Y. Kim, X. Chong, F. Ren, and A. X. Wang, "Slow-light effect via Rayleigh anomaly and the effect of finite gratings," Opt. Lett., vol. 40, pp. 5339-5342 (2015).

Kerr soliton combs in crystalline microresonators with a regular multifrequency diode lasers

N. G. Pavlov [1,2], G. Lihachev[2,3], S. Koptyaev [4], A. S. Voloshin [2], and M. L. Gorodetsky [2,3]

1. Moscow Institute of Physics and Technology, 141700 Dolgoprudny, Russia

2. Russian Quantum Center, 143025 Skolkovo, Russia

3. Faculty of Physics, M. V. Lomonosov Moscow State University, 119991 Moscow, Russia

4. Samsung R&D Institute Russia, SAIT-Russia Laboratory, Moscow, 127018, Russia

Kerr optical frequency combs in high-Q microresonators [1] are attracting growing interest, especially after mode-locking via dissipative Kerr solitons (DKS) has been demonstrated on a variety of platforms [2,3]. Such combs have promising applications due to low power consumption and possibility of chip integration. A traditional approach to obtaining DKS in microresonators relies on narrow-linewidth tunable lasers for pumping. Independently the same type of microresonators could be used for significant line narrowing of diode lasers exploiting resonant Rayleigh backscattering [4] for self-injection locking [5]. Kerr soliton frequency combs have also been demonstrated with self-injection locked diode lasers [6]. Previously for self-injection locking only single frequency stabilized diode lasers were used with either Bragg-grating or distributed feedback configuration, having narrow linewidth comparable to the resonance linewidth of the high-Q microresonator. Surprisingly, we found that the initial stabilization is not required for soliton comb generation, and simpler but more powerful diode lasers may be used, and demonstrate a technique to stabilize, generate and control coherent low-noise soliton Kerr combs using commercial broad spectrum multi-frequency CW laser diodes, self-injection-locked to an ultra- high-Q crystalline whispering-gallery-mode microresonator. In this configuration the role of the microresonator is twofold: 1) it selects and narrows the linewidth of the laser via self-injection locking, and 2) soliton Kerr comb is generated in the microresonator. We manufactured a MgF_2 resonator, 5 mm in diameter with computer controlled single-point diamond turning machine and polished it with diamond slurries, achieving $Q > 10^9$. For pumping, we used free-space laser diodes (Seminex, λ~1535, 1550 and 1650 nm, spectrum width ~10 nm, P~200 mW) coupled to the resonator with a total internal reflection prism. Generation of self-injection locking soliton combs stable for hours (beat note linewidth <1kHz) was observed when the laser current was adjusted [Fig.1]. By changing current it was possible to select the pumped mode of the resonator thus gradually changing the central frequency of the soliton by 10 nm. In several cases, we observed simultaneous excitation of two solitons with different central frequencies. In this case beat note spectrum demonstrated two narrow lines separated by ~ 10 MHz distance, corresponding to FSR difference at central frequencies. The diode multimode spectrum (10 nm) was narrowed to single mode line with FWHM of only 5 kHz, comparable to the results achieved with self-injection-locked DFB lasers. The work was supported by the Russian Science Foundation project #17-12-01413

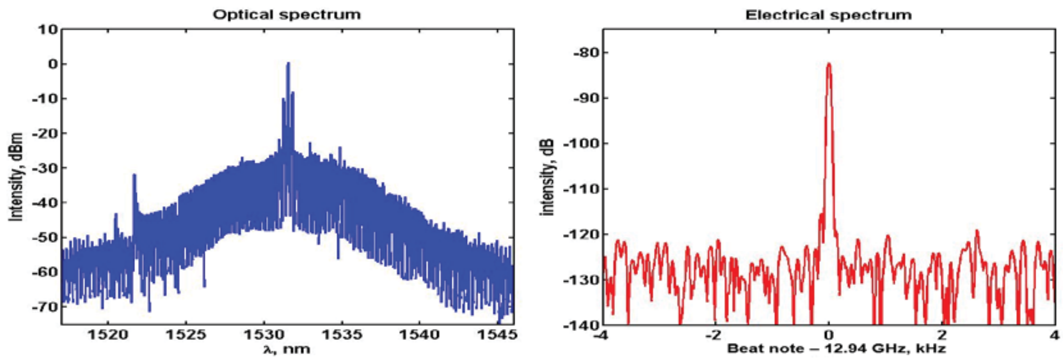

Fig. 2. Soliton comb in a microresonator injection locked to a broad spectrum diode laser (left), and beat note spectrum of a single soliton state (right) in the vicinity of the repetition rate frequency 12.94 GHz.

References

[1]. P. Del'Haye, A. Schliesser, O. Arcizet, T. Wilken, R. Holzwarth, and T. J. Kippenberg, "Optical frequency comb generation from a monolithic microresonator", Nature 450, 1214 (2007).

[2] T. Herr, V. Brasch, J. D. Jost, C. Wang, M. Kondratiev, M. L. Gorodetsky, and T. J. Kippenberg, "Temporal solitons in optical microresonators", Nat. Photonics 8, 145 (2014).

[3] V. Brasch, M. Geiselmann, T. Herr, G. Lihachev, M. Pfeiffer, M. L. Gorodetsky, and T. J. Kippenberg, "Photonic chip–based optical frequency comb using soliton Cherenkov radiation", Science 351, 357 (2016).

[4] M. L. Gorodetsky, A. D. Pryamikov, and V. S. Ilchenko, "Rayleigh scattering in high-Q microspheres" J. Opt. Soc. Am., B17, 1051 (2000).

[5] V. V. Vassiliev, V. L. Velichansky, V. S. Ilchenko, M. L. Gorodetsky, L. Hollberg, and A. V. Yarovitsky, "Narrow-line-width diode laser with a high-Q microsphere resonator", Opt. Comm. 158, 305 (1998).

[6] W. Liang, D. Eliyahu, V.S. Ilchenko, A.A. Savchenkov, A.B. Matsko, D. Seidel, and L. Maleki,, "High spectral purity Kerr frequency comb radio frequency photonic oscillator", Nat. Commun. 6, 7957 (2015).

Broadband Nonlinear Photonics in Graphene

F. Rotermund

Department of Physics, Korea Advanced Institute of Science and Technology (KAIST), Daejeon 34141, Korea
e-mail address: rotermund@kaist.ac.kr

Graphene, a two-dimensional lattice of sp^2-hybridized carbon atoms in a hexagonal structure, has been widely investigated for a variety of applications in electronics and photonics. In the present talk, universal use of graphene-based saturable absorbers applicable for mode-locking and Q-switching bulk, fiber and waveguide lasers in a wide spectral range will be discussed [1-5]. Experimental results achieved with various types of lasers in steady-state regimes are reviewed with essential linear and nonlinear optical carracteristics. In addition, interesting results on enhanced terahertz nonlinearities of graphene and graphene-based materials will be shown [6,7].

[1] W. B. Cho, J. W. Kim, H. W. Lee, S. Bae, B. H. Hong, S. Y. Choi, I. H. Baek, K. Kim, D.-I. Yeom, and F. Rotermund, "High-quality, large-area monolayer graphene for efficient bulk laser mode-locking near 1.25 μm," Opt. Lett. 36, 4089 (2011).
[2]] I. H. Baek, H. W. Lee, S. Bae, B. H. Hong, Y. H. Ahn, D.-I. Yeom, and F. Rotermund, "Efficient mode-locking of sub-70-fs Ti:sapphire laser by graphene saturable absorber," Appl. Phys. Express 5, 032701 (2012).
[3] M. N. Cizmeciyan, J. W. Kim, S. Bae, B. H. Hong, F. Rotermund, and A. Sennaroglu, "Graphene mode-locked femtosecond Cr:ZnSe laser at 2500 nm," Opt. Lett. 38, 341 (2013).
[4] W. B. Cho, S. Y. Choi, C. Zhu, M. H. Kim, J. W. Kim, J. S. Kim, H. J. Park, D. H. Shin, M. Y. Jung, F. Wang, and F. Rotermund, "Graphene mode-locked femtosecond Cr^{2+}:ZnS laser with ~300 nm tuning range," Opt. Express 24, 20774 (2016).
[5] M. H. Kim, T. Calmano, S. Y. Choi, B. J. Lee, I. H. Baek, K. J. Ahn, D.-I. Yeom, C. Kränkel, and F. Rotermund, "Monolayer graphene coated Yb:YAG channel waveguides for Q-switched laser operation," Opt. Mater. Express 6, 2468 (2016).
[6]] I. H. Baek, J. M. Hamm, K. J. Ahn, B. J. Kang, S. S. Oh, S. Bae, S. Y. Choi, B. H. Hong, D.-I. Yeom, B. Min, O. Hess, Y. U. Jeong, and F. Rotermund, "Boosting the terahertz nonlinearity of graphene by orientation disorder," 2D Mater. 4, 025035 (2017).
[7] H. J. Choi, I.-H. Baek, B. J. Kang, H.-D. Kim, S. S. Oh, J. Hamm, A. Pusch, J. Park, K. Lee, J. Son, Y. U. Jeong, O. Hess, F. Rotermund, and B. Min, "Control of terahertz nonlinear transmission with electrically gated graphene metadevices," Sci. Rep. 7, 42833 (2017).

Self-referenced waveform measurement of ultrashort mid-infrared pulses

T. Fuji, H. Shirai, Y. Nomura

Institute for Molecular Science, 38 Nishigonaka Myodaiji Okazaki, 444-8585, Japan

email address: fuji@ims.ac.jp

Development of intense mid-infrared (MIR) femtosecond lasers has been in rapid progress for a past decade. The cutoff extension of high harmonic generation driven by a long wavelength few-cycle pulse has been realized [1], and generation of shorter attosecond pulses is predicted. In such an experiment, field-revolved detection of few-cycle MIR pulses becomes very important since the cutoff of high harmonic generation is sensitive to the field strength of the driver laser pulse.

Electro-optic sampling (EOS) is one of the methods to measure electric field evolution. It is routinely used for measurement of terahertz (THz) waves. Very recently, the scheme was applied for electric field measurement of a near-infrared pulse [2]. However, it is necessary to prepare a much shorter reference pulse than the period of the field oscillations. The preparation of such a reference pulse is sometimes difficult. Self-referenced waveform measurement gives us significant benefits when the wavelength of the target pulse is rather short.

In 2013, we proposed a new scheme of waveform characterization, frequency-resolved optical gating capable of carrier-envelope phase determination (FROG-CEP) [3], which is based on a combination of frequency-resolved optical gating (FROG) with a carrier-envelope phase (CEP) sensitive time-domain nonlinear interferometer. The intensity and relative spectral phase of the target pulse are obtained from the FROG measurement, and the CEP is obtained from the nonlinear interferometer. Combining these data sets, we are able to retrieve a complete waveform of the target pulse. In this method, it is possible to measure a waveform with a reference pulse that has a longer duration than the period of the target pulse. The fact suggests that self-referenced waveform characterization is possible by using FROG-CEP.

In this invited talk, we report the experimental demonstration of self-referenced FROG-CEP for few-cycle MIR pulses. We have characterized the waveforms of ∼20-fs MIR pulses without any reference pulses. We simultaneously measured a trace of second harmonic generation FROG (SHG-FROG) and interferogram between second harmonic (SH) and self diffraction (SD) signals. The intensity and relative spectral phase of the target pulse are obtained from SHG-FROG, and the CEP is obtained from the interferogram. The retrieved waveform is shown in Fig. 1. The method can immediately be applied for waveform characterization of few-cycle near-infrared or mid-infrared pulses for high harmonic generation.

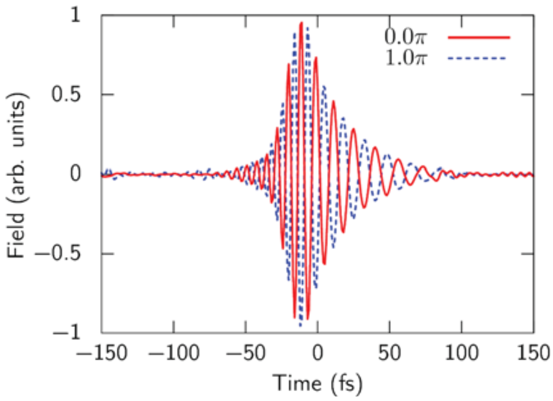

Figure 1: Retrieved electric-field in time domain. The solid line is the electric-field reconstructed with the method describedin the text. The dotted line is the electric field where the CEP of the pulse is experimentally changed by π .

[1] T. Popmintchev, M.-C. Chen, D. Popmintchev, P. Arpin, S. Brown, S. Alisauskas, G. Andriukaitis, T. Balciunas, O. D. Muecke, A. Pugzlys, A. Baltuska, B. Shim, S. E. Schrauth, A. Gaeta, C. Hernandez-Garcia, L. Plaja, A. Becker, A. Jaron-Becker, M. M. Murnane, and H. C. Kapteyn, "Bright coherent ultrahigh harmonics in the kev x-ray regime from mid-infrared femtosecond lasers," Science 336, 1287–1291 (2012).

[2] S. Keiber, S. Sederberg, A. Schwarz, M. Trubetskov, V. Pervak, F. Krausz, and N. Karpowicz, "Electro-optic sampling of near-infrared waveforms," Nat. Photon. (2016).

[3] Y. Nomura, H. Shirai, and T. Fuji, "Frequency-resolved optical gating capable of carrier-envelope phase determination," Nat. Commun. 4, 2820 (2013).

Optical tracing and tailoring phase of acoustic phonons

H. Jeong[1], A.J. Minnich[2], C.J. Stanton[3], Y.D. Jho[1]

1- School of Electrical Engineering and Computer Science, Gwangju Institute of Science and Technology, Korea

2- Division of Engineering and Applied Science, California Institute of Technology, United States

3- Department of Physics, University of Florida, United States

jho@gist.ac.kr

The development of precisely controllable thermal materials requires the manipulations of phonon wave properties [1], where the ability to measure and understand the phase could enable a wide range of applications. The relationship between phonon generation mechanisms and phase has been known for decades; the screening of the strain by ultrafast charge carrier generations or displasive excitation of coherent phonons (DECP) and impulsive stimulated Raman or Brillouin scattering (ISRS or ISBS) are responsible for initiating phonons. In the context of phase, the DECP mechanism induces "cosinelike" oscillations while ISRS (or ISBS) has "sinelike" oscillation.

In the case of acoustic phonons under DECP generations, the existing tensile and compressive strains at the nanoscale heterointerfaces are both compensated by imposing charge carriers, initiating descending and ascending waves from the two-dimensional epicenters. Here, we note that the displacements at the descending wavefronts and oscillate "cosinelike" but with additional phase shift π between them, considering the strain signs. Such acoustic phonon phase flipping could be optically detected, resulting the phonon-phase-sensitive dynamic Fabry-Perot (DFP) oscillations in differential reflectivity spectra, representatively in LEDs under applied bias.

From the time-dependent phase analysis, we further note that the phase information of the quantum well phonons was lost prior to that of the barrier phonons when the acoustic waves are reflected and propagate in doped layers, possibly due to the faster anharmonic phonon decay with broad phonon spectral bandwidth. This work in combination with our previous works on thermal transports [2] and electrical manipulations of phonons [3] could be useful in understanding detailed pictures of heat carriers during thermal transport.

[1] See, e.g., Madovan, M., "Phonon wave interference and thermal bandgap materials" Nature Mater., 14, 667-673, (2015).

[2] Hang Zhang, Xiangwen Chen, Young-Dahl Jho, Austin J. Minnich, "Temperature Dependent Mean Free Path Spectra of Thermal Phonons Along the c-axis of Graphite", Nano Letters, 16, 1643-1649 (2016); . Taeyong Kimy,Ding Dingy, Jong-Hyuk Yim, Young-Dahl Jho, Austin J. Minnich, "Measurement of In-plane Elastic and thermal properties in Free-standing Molybdenum Disulfide Membranes", submitted (2017).

[3] H. Jeong, Y.D. Jho, C.J Stanton., "Electrical manipulation of crystal symmetry for switching transverse acoustic phonons" Phys. Rev. Lett., 114, 043603-043607,(2015); H. Jeong, Y.D. Jho *et al.*, "Electrical Modulation and Switching of Acoustic Phonons", Phys. Rev. B 94, 024307-024315 (2016).

Low-noise mode-locked fiber lasers and their high-precision applications

Jungwon Kim

School of Mechanical and Aerospace Engineering, Korea Advanced Institute of Science and Technology (KAIST), Daejeon 34141, South Korea
jungwon.kim@kaist.ac.kr

We present our most recent progress in low-noise mode-locked fiber lasers [1] and their high-precision applications [2]. Our research has put special emphasis on the reduction of timing jitter and intensity noise of mode-locked fiber lasers. Using balanced optical cross-correlation [3] and fiber interferometer-based methods [4], we could characterize timing jitter spectral densities of free-running mode-locked laser oscillators with sub-femtosecond resolution. We identified that intra-cavity dispersion engineering enables the optimization of timing jitter to the sub-100-attosecond regime [5,6]. We further show that proper intra-cavity filtering can significantly reduce timing jitter of large-dispersion fiber lasers as well [7]. Regarding intensity noise, we recently identified that intensity noise can be greatly suppressed to 0.005% rms (integrated from 1-Hz to 1-MHz) by proper use of intra- and extra-cavity filtering. We have applied such low-noise mode-locked fiber lasers for various high-precision applications. I will show some of the applications that we have demonstrated, such as laser-microwave synchronization [8], low-noise microwave generation [9], fiber-based repetition-rate stabilization [10], RF phase detection and synchronization of ultrafast electron diffraction (UED) systems [11,12], remote RF phase transfer over fiber and free-space links [13,14], and sensitive time-of-flight-based strain sensors.

[1] J. Kim and Y. Song, Ultralow-noise mode-locked fiber lasers and frequency combs: principles, status and applications, Adv. Opt. Photon., vol. 8, pp. 465-540 (2016).
[2] J. Kim, K. Jung, J. Shin, C. Jeon, D. Kwon, Femtosecond laser-based microwave signal generation and distribution, J. Lightw. Tech., vol. 34, pp. 4631-4638 (2016).
[3] Y. Song, K. Jung, and J. Kim, Impact of pulse dynamics on timing jitter in mode-locked fiber lasers, Opt. Lett., vol. 36, pp. 1761-1763 (2011).
[4] D. Kwon, C. Jeon, J. Shin, M. Heo, S. Park, Y. Song, and J. Kim, Reference-free, high-resolution measurement method of timing jitter spectra of optical frequency combs, Sci. Rep., vol. 7, pp. 40917 (2017).
[5] Y. Song, C. Kim, K. Jung, H. Kim, and J. Kim, Timing jitter optimization of mode-locked Yb-fiber lasers toward the attosecond regime, Opt. Express, vol. 19, pp. 14518-14525 (2011).
[6] T. K. Kim, Y. Song, K. Jung, C. Kim, H. Kim, C. H. Nam, and J. Kim, Sub-100-as timing jitter optical pulse trains from mode-locked Er-fiber lasers, Opt. Lett., vol. 36, pp. 4443-4445 (2011).
[7] P. Qin, Y. Song, H. Kim, J. Shin, D. Kwon, M. Hu, C. Wang, and J. Kim, Reduction of timing jitter and intensity noise in normal-dispersion passively mode-locked fiber lasers by narrow bandpass filtering, Opt. Express, vol. 22, pp. 28276-28283 (2014).
[8] K. Jung and J. Kim, Subfemtosecond synchronization of microwave oscillators with mode-locked Er-fiber lasers, Opt. Lett., vol. 37, pp. 2958-2960 (2012).
[9] K. Jung, J. Shin, and J. Kim, Ultralow phase noise microwave generation from mode-locked Er-fiber lasers with subfemtosecond integrated timing jitter, IEEE Photon. J., vol. 5, pp. 5500906 (2013).
[10] K. Jung and J. Kim, All-fibre photonic signal generator for attosecond timing and ultralow-noise microwave, Sci. Rep., vol. 5, pp. 16250 (2015).
[11] M. Walbran, A. Gliserin, K. Jung, J. Kim, and P. Baum, 5-fs laser-electron synchronization for pump-probe crystallography and diffraction, Phys. Rev. Appl., vol. 4, pp. 044013 (2015).
[12] H. Yang, B. Han, J. Shin, D. Hou, H. Chung, I. Baek, Y. Jeong, and J. Kim, 10-fs-level synchronization of photocathode laser with RF-oscillator for ultrafast electron and X-ray sources, Sci. Rep., vol. 7, pp. 39966 (2017).
[13] K. Jung, J. Shin, J. Kang, S. Hunziker, C. Min, and J. Kim, Frequency comb-based microwave transfer over fiber with $7x10^{-19}$ instability using fiber-loop optical-microwave phase detectors, Opt. Lett., vol. 39, pp. 1577-1580 (2014).
[14] J. Kang, J. Shin, C. Kim, K. Jung, S. Park, and J. Kim, Few-femtosecond-resolution characterization and suppression of excess timing jitter and drift in indoor atmospheric frequency comb transfer, Opt. Express, vol. 22, pp. 26023-26031 (2014).

High power femtosecond fiber laser and its nonlinear frequency conversion

Minglie Hu

Ultrafast Laser Laboratory, College of Precision Instrument and Optoelectronics Engineering, Key Laboratory of Optelectronic Information Technology (Ministry of Education),Tianjin University, Tianjin 300072, China

Main author email address: huminglie@tju.edu.cn

It has been shown by intensive research activities in the laser and photonics fields that many novel properties unimaginable with conventional optical fibers can result from the photonic crystal fibers (PCFs). Recently, based on some of these properties, photonic crystal fibers have been successfully applied in femtosecond laser technology and greatly improve the performance of femtosecond laser. A brief review of recent work on high power femtosecond laser based on PCF is demonstrated. Furthermore, harmonic generation and optical parametric process based on the high power femtosecond fiber laser can generate new wavelengths of femtosecond pulses from the ultraviolet to mid-infrared. And the wavelength tunable femtosecond lasers devices have a tremendous impact on physics in subwavelength Optics, Chemistry and Biology.

[1] Wu Liu, Jintao Fan, Chen Xie, Youjian Song, Chenlin Gu, Lu Chai, Chingyue Wang, and Minglie Hu, "Programmable controlled mode-locked fiber laser using a digital micromirror device," Opt. Lett. 42, 1923-1926 (2017)
[2] Sijia Wang, Wei Chen, Peng Qin, Youjian Song, Minglie Hu, and Bowen Liu, "Spectral and temporal breathing self-similar evolution in a fiber amplifier for low-noise transform-limited pulse generation," Opt. Lett. 41, 5286-5289 (2016)
[3] Haochen Tian, Youjian Song, Fei Meng, Zhanjun Fang, Minglie Hu, and Chingyue Wang, "Long-term stable coherent beam combination of independent femtosecond Yb-fiber lasers," Opt. Lett. 41, 5142-5145 (2016)
[4] Huanyu Song, Bowen Liu, Yang Li, Youjian Song, Hao He, Lu Chai, Minglie Hu, and Chingyue Wang, "Practical 24-fs, 1-μJ, 1-MHz Yb-fiber laser amplification system," Opt. Express 25, 7559-7566 (2017)
[5] Haosen Shi, Youjian Song, JiaHe Yu, Runmin Li, Minglie Hu, and Chingyue Wang, "Quantum-limited timing jitter characterization of mode-locked lasers by asynchronous optical sampling," Opt. Express 25, 10-19 (2017)
[6] Jintao Fan, Chenglin Gu, Chingyue Wang, and Minglie Hu, "Extended femtosecond laser wavelength range to 330 nm in a high power LBO based optical parametric oscillator," Opt. Express 24, 13250-13257 (2016)
[7] Shutong He, Jijil JJ Nivas, Antonio Vecchione, Minglie Hu, and Salvatore Amoruso, "On the generation of grooves on crystalline silicon irradiated by femtosecond laser pulses," Opt. Express 24, 3238-3247 (2016)
[8] Wei Chen, Youjian Song, Kwangyun Jung, Minglie Hu, Chingyue Wang, and Jungwon Kim, "Few-femtosecond timing jitter from a picosecond all-polarization-maintaining Yb-fiber laser," Opt. Express 24, 1347-1357 (2016)

Low-dimensional material-based in-line saturable absorbers for ultrafast fiber laser applications

Nam Hun Park, and Dong-Il Yeom

Department of Physics & Department of Energy Systems Research, Ajou University, 16499, Suwon, Republic of Korea

diyeom@ajou.ac.kr

Low-dimensional carbon materials such as carbon nanotube (CNT) and graphene have shown promising electrical and optical properties in the past decade, demonstrating novel photonic devices such as broadband electro-optic modulators, optical limiters, photo detectors, and saturable absorbers [1, 2]. Particularly, their huge Kerr-nonlinearity with ultrafast nonlinear response over broad spectral range facilitated its applications to the nonlinear optic fields. One of the successful applications of the carbon-nano materials is a saturable absorber (SA), i.e., an optical element used for initiating and stabilizing the pulsed laser operation. Recently, other two-dimensional (2D) layered materials such as molybdenum disulfide (MoS_2) and tungsten disulfide (WS_2) have received great attention due to their potentials in electro-optic and photonic applications [3, 4]. The reduced dimensionality and symmetry of 2D material films led to unique opportunities very different from those of their bulk states. These emerging 2D materials also show high third-order nonlinearity and pulse shaping effects when incorporated into mode-locked lasers [5, 6].

In the presentation, we review our recent works on in-line saturable absorbers based on various low-dimensional materials including single-walled CNTs, graphene, MoS_2 and WS_2. Particularly we made effort for the improvement of light-2D material interaction through the evanescent wave. A side polished fiber (SPF) has offered an efficient fiber optic template to maximize the evanescent wave interaction between the light and the overlaid nano sheet materials, which enabled robust and stable in-line SAs in various fiber lasers operating at high power. By integrating the fabricated in-line SAs into the fiber laser cavity, we report high power passively mode-locked fiber lasers operating at various spectral ranges and diverse intra-cavity dispersions. We also show that deoxyribonucleic acid (DNA) can be used as an SA because of its large optical nonlinearity and ultrafast response time. Finally, we will compared the performance of emerging SAs based on low-dimensional materials and discuss future perspective.

[1] T. Hasan, Z. Sun, F. Wang, F. Bonaccorso, P. H. Tan, A. G. Rozhin, and A. C. Ferrari, "Nanotube–Polymer Composites for Ultrafast Photonics," Adv. Mater., vol.21, pp.3874-3899, (2009).

[2] F. Bonabboroso, Z. Sun, T. Hasan, and A. C. Ferrari, "Graphene photonics and optoelectronics," Nat. Photonics vol. 4, pp. 611-622, (2010)

[3] K. F. Mak, C. Lee, J. Hone, J. Shan, and T. F. Heinz, "Atomically Thin MoS_2: A New Direct-Gap Semiconductor." Phys. Rev. Lett., vol.105, pp. 136805, (2010)

[4] W. Zhao, Z. Ghorannevis, L. Chu, M. Toh, C. Kloc, P.-H. Tan, and G. Eda, "Evolution of Electronic Structure in Atomically Thin Sheets of WS_2 and WSe_2," ACS Nano, vol.7, pp. 791-797, (2013).

[5] R. Khazaeizhad, S. Hosseinzadeh Kassani, H. Jeong, D.-I. Yeom, and K. Oh, "Mode-locking of Er-doped fiber laser using a multilayer MoS_2 thin film as a saturable absorber in both anomalous and normal dispersion regimes," Opt. Express, vol.22, pp. 23732-23742, (2014).

[6] S. Wang, H. Yu, H. Zhang, A. Wang, M. Zhao, Y. Chen, L. Mei, and J. Wang, "Broadband Few-Layer MoS2 Saturable Absorbers," Ad v. Mater., vol. 26, pp. 3538-3544, (2014).

A multi-wavelength λ/4-shifted distibuted feedback laser diode array for WDM-based datacenter networks.

Su Hwan Oh, **Oh Kee Kwon, Ki Soo Kim, Chul Wook Lee,**

Young Ahn Leem, and Eun Soo Nam

Optical/Wireless Convergence Component Research Department,
Electronics and Telecommunication Research Institute, 218 Gajeongro, Daejeon, korea
osh@etri.re.kr

A multi-waveelgnth laser diode(LD) is an attractive solution as a light source for a 100 Gb/s datacenter communication network [1]. The laser diode array is a promising approach to meet a number of requirements of datacenter such as low power consumption, high energy efficiency and good channel uniformity. Specification for a datacenter network were recently proposed and revised for a 100b/s transmission of Ethernet signals over single mode fiber (SMF) with a distance of 2 m to 2 km, 10 km, or 40 km [2]. In previous reports[3, 4], we studied a multi-channel 10 Gb/s distributed feedback laser diode array (DFB-LDA) satisfying the above specifications by using selective area growth (SAG), E-beam lithography, and planner buried heterostructure (PBH) LD growth techniques.

A schematic configurations of the 8-channel λ/4-shifted PBH DFB-LDA is shown in figure 1 (a). The cavity length of the DFB laser array was 300 μm, and the spacing between adjacent DFB lasers was 500 μm. The wavelength interval of each channel was designed to be 8 nm. The λ/4-shifted gratings were applied to the DFB laser array for single-mode operation of all channels. The active section of the DFB-LDA was fabricated using a PBH for a low operating current and a better output beam quality. To obtain a high speed operation of over 10 Gb/s, we used the Etched Mesa(EM) PBH structure and the polyimide island structure. The outer part of the EM PBH region, including the active layer, was etched out to reduce the parasitic capacitance of the DFB-LDs. The width and depth of the EM PBH were fabricated to be 8 or 5μm, respectively. A polyimide island region was formed on one sides of the EM PBH region though the selective wet etching and polyimide process to reduce the parasitic effect of the pad-metal region for a over 10 Gb/s operation. A SEM photograph of the fabricated DFB-LD is shown in figure 1 (b)

In this Letter, we report the performance of a multi-channel PBH DFB-LDA. The threshold currents of the fabricated LDs were 10 mA, ±1.5 mA, for all channels. The module shows clear eye patterns before and after a 2-km transmission with an ER of over 4.5 dB at a low operating current of 50 mA for all channels. After the 2-km SMF transmission, the power penalty of each channel was less than 2 dB.

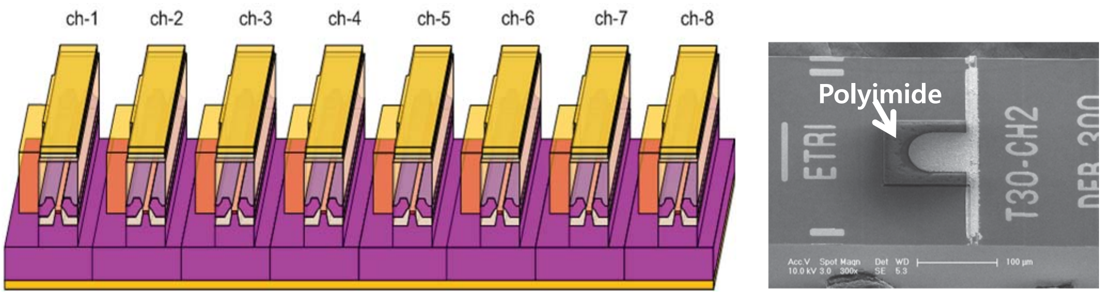

(a) (b)

Figure 1. (a) A schematic configuration of the 8-channel DFB-LDA, (b) SEM photograph of DFB-LD

[1] IEEE 802.3ba 40 Gb/s and 100 Gb/s Ethernet Task Force Public Area. [Online]. Available: http://www.ieee802.org/3/ba/index.html, (2010)

[2] 10 × 10 Low Cost 100Gb/s Pluggable Optical Transceiver. [Online]. Available: http://10x10msa.org/documents.htm, (2012)

[3] O. K. Kwon, Y.-T. Han, Y. A. Leem, J.-U. Shin, C. W. Lee, and K. S. Kim, "A 10 ×10 Gb/s DFB-LD array integrated with PLC-based AWG for 100-Gb/s transmission," IEEE Photon. Technol. Lett., vol. 26, pp. 2177–2180, (2014).

[4] S. H. Oh, O. K. Kwon, K. S. Kim, Y. T. Han, C. W. Lee, Y. A. Leam, J. W. Shin, and E. S. Nam, "A multi-channel etched-mesa PBH DFB laser array using a SAG technique," IEEE Photon. Technol. Lett., vol. 27, pp. 2567–2570, (2015).

Tunable External Cavity Laser Using InP Gain-Chip and Polymer Waveguide Grating for Coherent Optical Communications

Dong Churl Kim[1], Young-Tak Han[1], Dong-Hoon Lee[1], Byung-Seok Choi[1], Sang-Ho Park[1], Jang-Uk Shin[1], Won Seok Han[1], Yong Hwan Kwon[1], Jong-Hoi Kim[1], Ho-Sung Cho[2] and Yongsoon Baek[1]

1- Electronics and Telecommunications Research Institute, Yuseong-Gu, Daejeon 34129, KOREA
2- ELDIS, Inc., Buk-Gu, Gwangju 61008, KOREA

dchankim@etri.re.kr

Tunable laser is an important component in optical communications because it can resolve the inventory problem of laser didoes (LDs) with an allocated emission wavelength in wavelength division multiplexing (WDM) optical networks. In coherent optical communications that is recently deployed to cope with increasing information and data traffic, the tunable laser is still one of the key devices [1]. There have been many types of the tunable lasers. Monolithically integrated tunable lasers such as sampled-grating distributed Bragg reflector LDs and array of distributed feedback LDs are the representative types of the tunable lasers. External cavity laser type showed very good performances as well [2].

Fig. 1 shows the tunable external cavity laser that we have developed for coherent optical communications. Using an InP gain-chip and a polymer waveguide grating, we assembled a tunable laser. In our scheme, the emission wavelength can be tune by locally heating the polymer waveguide grating to change the refractive index of the polymer material. The gain-chip in our tunable laser was a ridge type LD with a multi-layered asymmetric broad waveguide structure to provide low loss and high gain. The output facet was coated with an anti-reflection dielectrics and a high-reflection film was deposited on the opposite facet. The polymer waveguide grating was made by conventional lithography. After curing the polymer material, a dry etching was applied to etch the side wall to make periodic grating structure and an electrode used as the heater was formed. The module also has a wavelength locker and a flexible PCB as Fig. 1.

The measured spectra for several wavelengths are shown in Fig. 2. As shown in this figure, the tuning range and the side-mode suppression ratio were about 35nm and 43 dB, respectively. The output power was larger than 10 mW and the linewidth was less than 0.6 MHz.

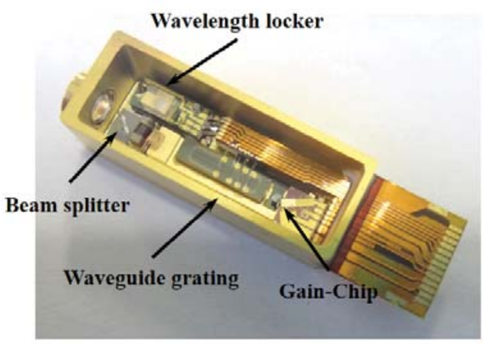

Fig. 1 Assembled tunable external cavity laser module.

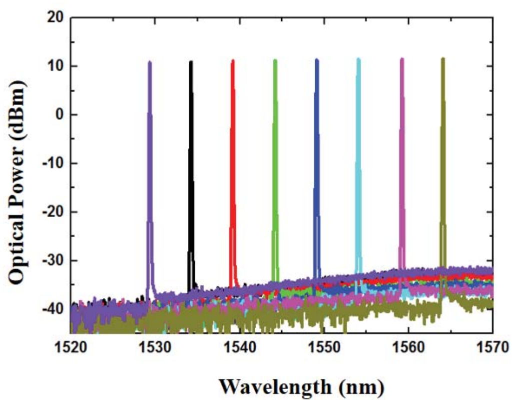

Fig. 2 Measured optical spectra.

[1] Kazuro Kikuchi "Fundamentals of Coherent Optical Fiber Communications", J. Lightwave Technol., Vol. 34, no. 1, p.157 (2016).
[2] J. Buus et al., "Tunable Lasers in Optical Networks," J. Lightwave Technol., Vol. 24, no. 1, p.5 (2006).

RoF technologies for mobile fronthaul and indoor DAS applications

Seung-Hyun Cho[1], Hwan Seok Chung[1], Minkyu Sung[1], Joonyoung Kim[1], Joon Ki Lee[1], and Jong Hyun Lee[1]

1- Electronics and Telecommunications Research Institute, 218, Gajeong-ro, Yuseong-gu, Daejeon, Korea

shc@etri.re.kr

Recently, the rapid evolution of mobile telecommunication technologies has enabled subscribers to experience various services requiring high bandwidth traffic. In addition, in order to commercialize 5G mobile communication systems capable of providing a user with a few Gb/s services in the near future, we need to consider the change of mobile fronthaul and indoor distributed antenna system (DAS) based on digitalized fibre-optic transmission system using current common public radio interface (CPRI) or open base station archiotecture initiative (OBSAI) protocol. Currently, excessive data traffic is generated and transmitted compared to the required effective bandwidth due to the procedures such as analog-to-digital conversion and digital framing for existing mobile fronthaul and indoor DAS netowrk. The RoF technologies, which directly transmit analog waveforms through the optical fiber without analog to digitalization process, is an alternative technique for solving the above-mentioned traffic explosion problem, and many works have been undergoing worldwide for several years [1]. Moreover, international standardization activities on RoF technologies utilizing optical access network infrastructure is also underway [2]. When employing RoF technologies for mobile fronthaul and indoor DAS network, it is possible to reduce the amount of data traffic and realize the low delay infrastructure. However, it has also disadvantages such as degrdations of transmission performance due to nonlinear distortion and limitations of link budget [3].
Fig. 1 shows the schematic diagram of mobile fronthaul or indoor DAS netowrk utilizing RoF technologies. As shown in the Fig. 1, when the RoF technologies are used for the mobile fronthall, the mobile baseband signals having the analog waveform from the baseband modem unit are frequency upconverted to a specific frequency band suitable for bandwidth efficient optical transmission without digital conversion process. Besides, since multiple mobile baseband signals can also be multiplexed and transmitted in the frequency domain, it is possible to simultaneously transmit a lot of mobile baseband signals within a single optical wavelength with the help of well-known intermediate frequency over fibre (IFoF) method.

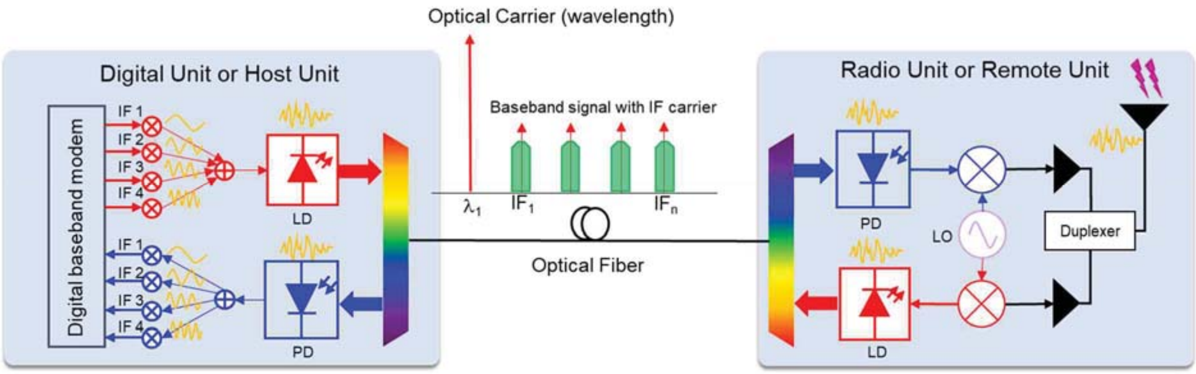

Fig. 1. Schematic diagram of mobile fronthaul or indoor DAS network utilizing RoF technologies.

In this paper, we introduce the system demonstrations for mobile fronthall and Indoor DAS based on RoF technologies. We also measure and analyze their transmission performances by utilizing RoF technologies. Several mobile internet servicces using commercial mobile terminals like smartphones and tablet computers are also demonstrated to confirm their technical feasibility.

[1] Seung-Hyun Cho et al., “Cost-effective next generation mobile fronthaul architecture with multi-IF carrier transmission scheme, Opt. Fiber Commun. Conf., San Francisco, CA, USA, Tu2.B6 (2014)
[2] Recommendations ITU-T G.RoF “RoF (radio over fiber) systems” (2015-)
[3] Seung-Hyun Cho et al., “Demonstration of mobile fronthaul testbed based on RoF technology supporting two frequency assignments and 2 × 2 MIMO Antennas”, ETRI Journal, vol. 37, no. 6, 1055-1064e, (2015).

O-band Optical Transmission Technologies for 100G Ethernet Passive Optical Networks

H. H. Lee, K. H. Doo, K. O. Kim, S. G. Mun, S. H. Kim, J. Y. Oh, H. Park, D. Y. Kim, H. S. Chung

Electronics and Telecommunications Research Institute, Daejeon, Korea

hanhyub@etri.re.kr

A passive optical network (PON) is well known as a promising technology to deploy optical access networks. PON has a simple link configuration which consists of an optical fiber and a passive optical splitter between an optical line terminal (OLT) at the central office and an optical network unit (ONU) at the subscriber. Since passive optical network (PON) has performance, maintenance and operational benefits large numbers of PON are deploying by network operators. Time division multiplexed-PON such as Ethernet PON (EPON) or Gigabit capable PON (G-PON) used bidirectional wavelength division multiplexing (WDM) transmission for the downstream and the upstream signals. O-band (Original band, 1260 nm – 1360nm) is allocated to the upstream signal since a wideband low-cost F-P LD can be employed to ONU optical transmitter due to low fiber chromatic dispersion in O-band. Recently, a transmission speed of PON has been gradually increasing to support various types of internet service offerings up to 1 Gb/s and mobile data service offerings towards multi-Gb/s speeds as well [1]. ITU-T XG-PON and IEEE 10G-EPON have provided 10 Gb/s transmission capacity. However, 10 Gb/s capacity will be not enough to support the services considering that 100-Gb/s capacity will be needed around 2020 and beyond [1]. For supporting 100 Gb/s PON, IEEE 802.3ca TF has studied 100G-EPON standardization and selected $4\lambda\times25$ Gb/s a wavelength and time division multiplexing passive optical network (WDM/TDM-PON) as a solution of 100G-EPON to enable the bandwidth capacities of 100 Gbit/s [2]. Various modulation formats included NRZ in O-band, optical duo-binary (ODB) and electrical duo-binary (EDB) in C-band, and pulse-amplitude modulation (PAM)-4 in C-band were proposed to 25 Gb/s signal in order to provide a simple and cost effective solution of 100G-EPON standardization. Finally, IEEE 802.3ca TF decided NRZ modulation format for downstream and upstream in O-band. In our previous work, we demonstrated a real-time 25-Gb/s PON prototype with NRZ modulation format in O-band[3].

In this paper, we review O-band transmission technologies for 100G-EPON and 2×25 Gb/s WDM/TDM PON. The WDM/TDM-PON consists of O-band transceiver based on a cost-effective 25 Gb/s APD, and MAC/PHY including forward error correction (FEC) function. 50 Gb/s downstream and 20 Gb/s upstream Ethernet traffics are successfully transmitted through 20-km SMF and 1×64 splitter without packet loss. In addition, we present link budget extended WDM/TDM-PON by using an O-band SOA with assist light. The link budget can be increased to 35.7 dB (splitting ratio of 256 and transmission length of 20 km) by using the O-band SOA.

Acknowledgements
This work was supported by ICT R&D program of MSIP/IITP [B0132-17-1004, SDN based wired and wireless converged optical access networking].

[1] IEEE 802.3 Industry Connections Feasibility Assessment for the Next Generation of EPON (2015)
[2] IEEE P802.3ca 100G-EPON Task Force, Physical layer specifications and management parameters for 25 Gb/s, 50 Gb/s, and 100 Gb/s passive optical networks, (http://www.ieee802.org/3/ca/)
[3] Han Hyub Lee, et al., Real-time demonstration of QoS guaranteed 25-Gb/s PON prototype with Ethernet-PON MAC/PHY and cost-effective APD receivers for 100-Gb/s access networks, Opt. Express, vol. 24, pp.13984 (2016)

Broadband compact polarization splitters based on a mode extracting polymer waveguide

Guanghao Huang, Tae-Hyun Park, and Min-Cheol Oh

Dept. of Electronics Engineering, Pusan National University, 2, Busandaehak-ro 63beon-gil, Geumjeong-gu, Busan (Pusan) 609-735, Republic of Korea

Main author email address: mincheoloh@pusan.ac.kr

As the data traffic capacity over the internet is daily growing and the trend of internet services is diversifying, the need for quantum encrypted communication arises. For the Bell state measurement in quantum key distribution, compact integrated-optic polarization splitters are highly anticipated [1, 2]. In this work, we propose a compact polarization mode extracting device utilizing highly birefringent polymer. It has a tiny mode converter with a taper that is effective only for TE polarized light, and then the TE polarized mode is extracted by another path. The polarization splitter proposed in this work incorporates a crosslinkable liquid crystal material, Reactive Mesogen (RM), which is inserted within the Y-branch optical waveguide to extract TE polarized light. As shown in Fig. 1, in the case of TM polarized light, the CO-polymer waveguide has a relatively higher refractive index than the RM waveguide, so that the light follows the CO-polymer waveguide. However, for TE polarization, RM has the higher refractive index, then the TE polarized light is coupled into the RM waveguide through the taper structure. The RM waveguide is positioned to connect the gap of the CO-polymer Y-branch so that the TE polarized light can pass through the disconnected branch. RM is a liquid crystal that forms an optically uniaxial thin film with an optical axis in the plane direction. According to the prism coupling refractive index measurement, the RM film exhibited refractive index values of 1.6457 and 1.5205 for TE and TM polarized light, respectively. However, we found the RM could have TM refractive index of 1.536 during the experiment of the polarization splitter device based on total internal reflection interface [3]. To confirm the broadband operation, we measured the device characteristics over the wavelength range of 1500 ~ 1600 nm. The crosstalk of the device was maintained to be less than -25 dB, and the insertion loss change was negligible.

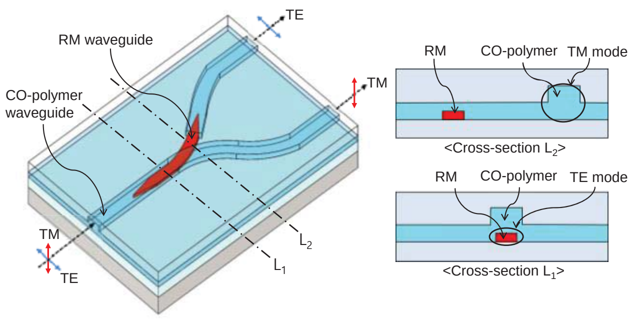

Figure 1. Schematic diagram of the polarization splitter

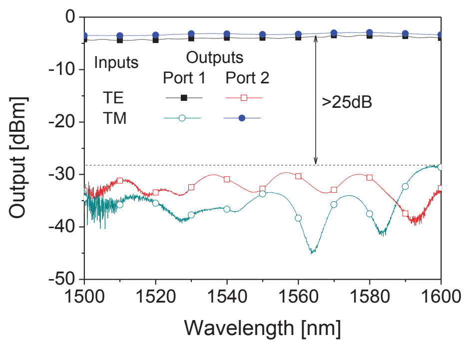

Figure 2. Measured wavelength dependence over 1500 ~ 1600 nm

[1] Ekert, A. K. Quantum cryptography based on Bell's theorem. Phys. Rev. Lett. 67, 661-663 (1991).
[2] Bennett, C. H. & Brassard, G. Quantum cryptography: Public key distribution and coin tossing. Theor. Comput. Sci. 560, 7–11 (2014).
[3] Huang, G., Park, T.-H., Chu, W.-S., & Oh, M.-C. Integrated optic polarization splitter based on total internal reflection from a birefringent polymer. Opt. Express 24, 21012-21019 (2016).

Time-variant metasurface as a frequency converting platform

Bumki Min[1]

1- Department of Mechanical Engineering, Korea Advanced Institute of Science and Technology (KAIST)

bmin@kaist.ac.kr

A few years before the experimental demonstration of coherent nonlinear optical effect, Morgenthaler contemplated an alternate route towards the conversion of light frequency via velocity modulation of the wave, i.e. temporal variations of permittivity and/or permeability of the media [1]. Afterwards, continual theoretical efforts have been made to understand this linear frequency conversion. Experimental verifications followed then in the field of plasma physics; notable examples were the observation of frequency shift in rapidly growing plasma from laser ionization of gases and semiconductors. However, it was not until a group of researchers proposed chip-scale dynamic photonic structures, such as photonic crystals [2-5], micro-ring resonators [6], and waveguides [7] for the observation of wavelength conversion that the phenomena became the subject of engineering. Active resonant metamaterials, in which the resonating meta-atoms are hybridized with electrically or optically reconfigurable natural materials, can be thought of as an optimal platform that can be spatiotemporally rearranged. Here, we propose rapidly time-varying metasurfaces as a frequency converting platform and demonstrate their efficacy experimentally at terahertz frequencies. Since our proposed conversion scheme does not rely on a nonlinearity of comprising materials, the conversion efficiency is invariant with respect to the intensity of an input wave. Therefore, this method would be beneficial especially for the frequency conversion of waves with weak intensities. Furthermore, the frequency of a converted wave and its efficiency is tailorable to a large degree as the conversion process does not require energy conservation between participating waves.

[1] Morgenthaler, F. R. “Velocity modulation of electromagnetic waves,” IRE Trans. Microwave Theory Tech. Vol. 6, 167-171, 1958.
[2] Yacomitti, A. M. et al. “Nonadiabatic dynamics of the electromagnetic field and charge carriers in high-Q photonic crystal resonators,” Phys. Rev. Lett. Vol. 96, 093901, 2006.
[3] Notomi, M. and Mitsugi, S. “Wavelength conversion via dynamic refractive index tuning of a cavity,” Phys. Rev. A. Vol.73, 05180, 2006.
[4] Tanabe, T., Notomi, M., Taniyama, H., and Kuramochi, E. “Dynamic release of trapped light from an ultrahigh-Q nanocavity via adiabatic frequency tuning,” Phys. Rev. Lett. Vol. 102, 043907, 2009.
[5] Kampfrath, T. et al. “Ultrafast adiabatic manipulation of slow light in a photonic crystal,” Phys. Rev. A. Vol. 81, 043837, 2010.
[6] Preble, S. F., Xu, Q. and Lipson, M. “Changing the colour of light in a silicon resonator,” Nat. Photon. Vol. 1, 293-296, 2007.
[7] Fan, L. et al. “Integrated optomechanical single-photon frequency shifte,” Nat. Photon. Vol. 10, 766-770, 2016.

Ultrafast Photoexcited Carrier Dynamics and Photo Response of 3D Dirac Semimetallic Cd_3As_2

Dong Sun

1- International Center for Quantum Materials, School of Physics, Peking University, Beijing 100871, P. R. China

Dong Sun: sundong@pku.edu.cn

Three dimensional (3D) Dirac semimetals which can be seen as 3D analogues of graphene have attracted enormous interests in research recently. In order to apply these ultrahigh-mobility materials in future electronic/optoelectronic devices, it is crucial to understand the relaxation dynamics of photoexcited carriers. In this talk, we would first introduce our work of using ultrafast transient reflection measurements to study the photoexcited carrier dynamics in cadmium arsenide (Cd_3As_2). By using low energy probe photon of 0.3 eV, we probed the dynamics of the photoexcited carriers that are Dirac-Fermi-like approaching the Dirac points. We systematically studied the transient reflection on bulk and nanoplate samples that have different doping intensities by tuning the probe wavelength, pump power and lattice temperature, and find that the dynamical evolution of carrier distributions can be retrieved qualitatively by using a two-temperature model. This result is similar to that of graphene, but the carrier cooling through the optical phonon couplings is slower and lasts over larger electron temperature range because the optical phonon energies are much lower than those in graphene.

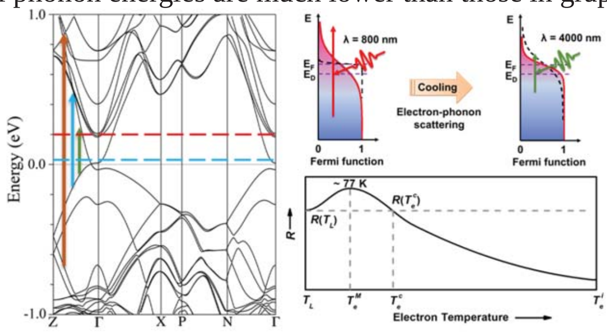

Figure 1. Photoexcited carrier dynamics: (a) Band diagram of Cd_3As_2 and pump/probe photon transition configuration. (b) Schematic diagrams of the dynamical carrier distribution around the Fermi level. (c) Transient reflectivity of bulk at 4 μm as function of instantaneous electron temperature.

Furthermore, based on the fast carrier transient time, we report the realization of an ultrafast broadband photodetector based on Cd_3As_2. The prototype metal-Cd_3As_2-metal photodetector exhibits a responsivity of 5.9 mA/W with response time of about 6.9 ps without any special device optimization. Broadband responses from 532 nm to 10.6 μm are measured with potential detection range extendable to far infrared and terahertz. Systematical studies indicate that the photo-thermoelectric effect plays important roles in photocurrent generation. Our results suggest Cd_3As_2 can be harnessed for photodetection with high sensitivity and high speed (~145 GHz) over broad wavelength range.

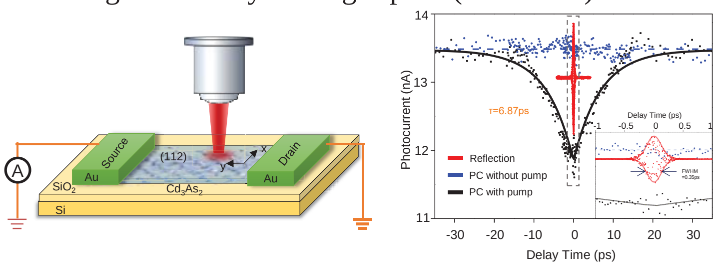

Figure 2. Schematic of scanning and time-resolved photocurrent measurements of Cd_3As_2 photodetectors.

[1]. Wei Lu, Shaofeng Ge, Xuefeng Liu, Hong Lu, Caizhen Li, Jiawei Lai, Chuan Zhao, Zhimin Liao, Shuang Jia, D. Sun, "Ultrafast Relaxation Dynamics of Photo-excited Dirac Fermion in Three Dimensional Dirac Semimetal Cadmium Arsenide" Phys. Rev. B 26, 037801 (2016)
[2]. Q. S. Wang, C.-Z. Li, S. F. Ge, J.-G. Li, W. Lu, J. W. Lai, X. F. Liu, J. C. Ma, D.-P. Yu, Z.-M. Liao, D. Sun, "Ultrafast Broadband Photodetectors Based on Three-dimensional Dirac Semimetal Cd3As2" Nano Letters 17,834 (2017)

Twenty years of Doppler OCT and OCT angiography: past, present, and future

Zhongping Chen, Ph.D.

Department of Biomedical Engineering, Beckman Laser Institute, University of California, Irvine, Irvine, CA

z2chen@uci.edu

Noninvasive techniques for imaging *in vivo* blood flow and tissue biomechanical property are of great value to biomedical research and clinical diagnostics where many diseases have a vascular etiology or elastic component. In ophthalmology, many ophthalmic diseases may involve disturbances in ocular blood flow, including diabetic retinopathy, low tension glaucoma, anterior ischemic optic neuritis, and macular degeneration. For example, in diabetic retinopathy, retinal blood flow is reduced and the normal autoregulatory capacity is deficient. Ocular hemodynamics is altered in patients with glaucoma, and severe loss of visual function has been associated with reduced macular blood flow. Simultaneous imaging of tissue structure and blood flow could provide critical information for early diagnosis of ocular diseases.

In this presentation, I will review the advances in Doppler OCT over the last 20 years. Several Doppler OCT techniques, including phase variation and intensity variation methods, will be compared. The recent applications of Doppler OCT for quantifying the ocular flow velocity, mapping retinal and choroidal microcirculation, detection of ciliary beating pattern and frequency, and evaluating mechanical properties with optical coherence elastography will be discussed.

Functional Fourier Domain Optical Coherence Tomography and its Applications

Zhihua Ding, Jianrong Qiu, Ziwei Shangguan, Shanshan Yan, Wen Bao, Pei Li, Peng Li

State Key Lab of Modern Optical Instrumentation, College of Optical Science and Engineering, Zhejiang University, Hangzhou 310027, China

Zhihua Ding: zh_ding@zju.edu.cn

Novel optical coherence tomography (OCT) systems with ultralong depth range, ultrawide lateral field, and ultrahigh axial resolution are developed, which envision new medical applications. Typical applications of structural and functional OCT are presented. As a depth-resolved optical imaging modality with the merits of non-destruction, high-resolution, and high-speed, OCT is promising for applications in variety areas.

Most recently, our group has made a step forward in instrumentations of the Fourier Domain OCT systems. The depth range is extended to be over 200 mm [1-3], the lateral field of view is increased to be 35 mm [4-6], and the axial resolution is improved to be 0.9 μm. Angio-OCT with enhanced contrast is developed for vasculature mapping [7, 8]. Pump-probe OCT with molecular contrast is also developed. Novel OCT systems with enhanced parameters and novel contrasts will definitely open new OCT applications [9, 10].

[1]C. Wang, Z. Ding, S. Mei, H. Yu, W. Hong, Y. Yan, W. Shen, Ultralong-range phase imaging with orthogonal dispersive spectral domain optical coherence tomography, Optics Letters, 37, 4555-4557, (2012).

[2]W. Bao, Z. Ding, P. Li, Z. Chen, Y. Shen, C. Wang, Orthogonal dispersive spectral-domain optical coherence tomography, Optics Express, 22, 10081-10090, (2014).

[3]W. Bao, Y. Shen, T. Chen, P. Li, Z. Ding, High-speed high-precision and ultralong-range complex spectral domain dimensional metrology, Optics Express, 23, 11013-11022, (2015).

[4]Z. Chen, C. Zhao, Y. Shen, P. Li, X. Wang, Z. Ding, Ultrawide-field parallel spectral domain optical coherence tomography for nondestructive inspection of glass, Optics Communications, 341, 122-130, (2015).

[5]Z. Chen, Y. Shen, W. Bao, P. Li, X. Wang, Z. Ding, Identification of surface defects on glass by parallel spectral domain optical coherence tomography, Optics Express, 23, 23634-23646, (2015).

[6]Z. Chen, Y. Shen, W. Bao, P. Li, X. Wang, Z. Ding, Motion correction using overlapped data correlation based on a spatial-spectral encoded parallel optical coherence tomography, Optics Express, 25, 7069-7083, (2017).

[7]P. Li, Y. Cheng, P. Li, L. Zhou, Z. Ding, Y. Ni, C. Pan, Hybrid averaging offers high-flow contrast by cost apportionment among imaging time, axial, and lateral resolution in optical coherence tomography angiography, Optics Letters 41, 3944-3947, (2016).

[8]P. Li, Y. Cheng, L. Zhou, C. Pan, Z. Ding, P. Li, Single-shot angular compounded optical coherence tomography angiography by splitting full-space B-scan modulation spectrum for flow contrast enhancement, Optics Letters, 41, 1058-1061, (2016).

[9]W. Bao, Z. Ding, J. Qiu, Y. Shen, P. Li, Z. Chen, Quasi-needle-like focus synthesized by optical coherence tomography, Optics Letters, 42, 1385-1388, (2017).

[10]L. Guo, R. Shi, C. Zhang, D. Zhu, Z. Ding, P. Li, Optical coherence tomography angiography offers comprehensive evaluation of skin optical clearing in vivo by quantifying optical properties and blood flow imaging simultaneously, Journal of Biomedical Optics, 21, 081202, (2016).

3D intraoral scanning system for structure/diagnosis in dentistry

Joo Beom Eom, Anjin Park, Jaesung Ahn, Honglyel Jung, and Jong hyun Eom

1- Bio-medical photonics research center, Korea Photonics Technology Institute, Gwangju 61007, South Korea

We report fabrication and performance of the three-dimensional intraoral scanner based on optical coherence tomography (OCT). The OCT system was configured the swept source OCT (SS-OCT), that is based on the swept source with center wavelength of 1310 nm, the scanner was built using MEMs mirror and optical collimator. The implemented SS-OCT based on MEMs scanner show axial resolution of 14 μm, scan length of 10 mm. By equipping the implemented OCT system, the intraoral scanner was constructed and used to demonstrate the fesibility of intraoral scanner that is able to acquire the structure and functional images of the human tooth, for intraoral scanner 3D image in dentistry.

Motion-free and true-shape three-dimensional retinal imaging by Lissajous optical coherence tomography

Yoshiaki Yasuno

Computational Optics Group, University of Tsukuba, Tsukuba, Ibaraki, Japan

yasuno@optlab2.bk.tsukuba.ac.jp

Ocular diseases are frequently associated with slow longitudinal alternation of posterior eye's morphology. For example, age-related macular degeneration is characterized by choroidal neovascularization (CNV) and evaluation of its morphological development in days and weeks are important for its treatment. Glaucoma development is also associated with very slow morphological alteration of optic nerve-head in years. Time-course evaluation of such morphological alteration is important for monitoring disease progression and optimal intervention.

Optical coherence tomography (OCT) is widely used for three-dimensional (3-D) morphological investigation of posterior eye. However, the 3-D tomography obtained by OCT is significantly distorted by inevitable eye motion. It makes it difficult to use the OCT for time-course evaluation of the small and slow morphological alteration.

This paper presents a new OCT scanning technique which enables motion-free true-morphological imaging of the eye. In this method, the posterior eye is scanned with a Lissajous pattern as shown in Figure 1 rather than a conventional raster scan. The Lissajous scan pattern covers a 6-mm × 6-mm region on the retinal with multiple elliptic trajectories.

In our Lissajous method, the OCT signals obtained by the Lissajous scan were then image-processed to generate motion-free retinal OCT as follows. For each elliptic cycle, its ellipticity is altered. So, each arbitrary pair of subsets of Lissajous scan have four overlapping regions. See overlaps among three-representative elliptic trajectories in Fig. 1 for example. As far as the subset is obtained in short in time, it can be treated as nearly not being suffered by the eye motion. These nearly motion-free subset scans are mutually co-registered to form a motion-free OCT volume. Some residual motions are further corrected by using fine image registration technique. More detailed and comprehensive descriptions of this method is found elsewhere [1].

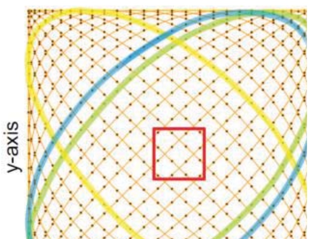

Fig. 1: An example of Lissajous OCT can pattern.

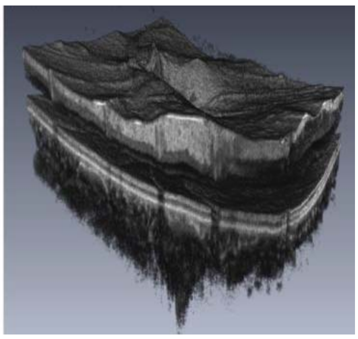

Fig. 2: 3-D motion-free optic hearvehead obtained by Lissajous scan.

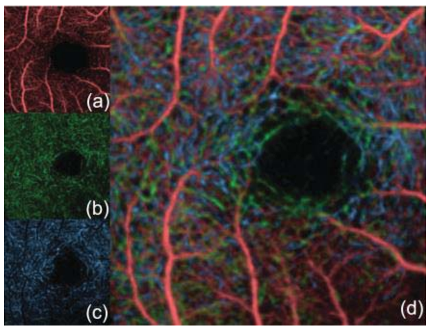

Fig. 3: Motion-free OCTA obtained by Lissajous scan.

Figure 2 shows and example of 3-D motion-free human optic nerve head image. Not as like conventional rater scan OCT, this image represents true 3-D morphology of an *in vivo* human eye. In the presentation, further modification of the Lissajous OCT for motion-free OCT angiography (OCTA) is presented [2]. An example of the motion-free OCTA is shown in Fig. 3.

[1] Y. Chen, Y.-J. Hong, S. Makita, and Y. Yasuno, "Three-dimensional eye motion correction by Lissajous scan optical coherence tomography," *Biomed. Opt. Express* **8**, 1783-1802 (2017).

[2] Y. Chen, Y.-J. Hong, S. Makita, and Y. Yasuno, "Motion-corrected en face optical coherence tomography angiography imaging based on the modified Lissajous scanning pattern," *Proc. of SPIE* **10045**, 100450U (2017).

New Ba-Based Nonlinear Crystals for Frequency Conversion of Near-IR Lasers into the Mid-IR

V. Petrov[1], V. Badikov[2], D. Badikov[2], V. Laptev[3], K. Mitin[4], G. Shevyrdyaeva[2], N. Kostyukova[1,5,6], A. Boyko[1,5,6], E. Boursier[7,8], V. Panyutin[1], N. Shchebetova[4], A. Tyazhev[1], G. Marchev[1], A. Kwasniewski[9], D. Kolker[5], P. Segonds[7,8], B. Boulanger[7,8]

1- Max-Born-Institute for Nonlinear Optics and Ultrafast Spectroscopy, 2A Max-Born-Str., D-12489 Berlin, Germany
2- High Technologies Laboratory, Kuban State University, Stavropolskaya Str. 149, 350040 Krasnodar, Russia
3- Institute of Spectroscopy, Russian Academy of Sciences, Fizicheskaya Str. 5, 142190 Troitsk, Russia
4- Astrophysika National Laser Centre, Volokolamskoe sh. 95, 125424 Moscow, Russia
5- Research Laboratory of Quantum Optics Technology, Novosibirsk State University, 2 Pirogova Str., 630090 Novosibirsk, Russia
6- Special Technologies, Ltd., 1/3 Zeljonaja gorka Str., 630060 Novosibirsk, Russia
7- Universite Grenoble Alpes, Institut NEEL, F-38042 Grenoble, France
8- CNRS, Institut NEEL, F-38042 Grenoble, France
9- Leibniz Institute for Crystal Growth, Max-Born-Str. 2, 12489 Berlin, Germany
e-mail: petrov@mbi-berlin.de

The ongoing search for new highly efficient non-oxide nonlinear crystals for the mid-IR part of the spectrum in recent years targets mainly frequency down-conversion of advanced all-solid-state laser sources operating in the near-IR [1]. Only few such crystals are commercially available and widely spread. On the first place, these are the I-III-VI_2 chalcopyrites $AgGaS_2$ (AGS) and $AgGaSe_2$ (AGSe) which represent the benchmarks for pumping near 1 µm (Nd- or Yb-laser systems) and near 1.5 µm (Er-laser systems). In addition, AGSe is the primary choice for frequency doubling of CO_2 lasers at 10.6 µm. Both of them show, however, a number of limitations which hinder their application in practice, on the first place the chemical instability of the polished surface in air. In addition, the optical damage thresholds are one of the lowest, especially for down-conversion. Moreover, to obtain optically uniform samples, annealing at high temperature is necessary for long periods.

Here we present four Ba compounds that can be now added to this short list: the orthorhombic $BaGa_4S_7$ (BGS), the monoclinic $BaGa_4Se_7$ (BGSe), as well as the trigonal $BaGa_2GeS_6$ (BGGS) and $BaGa_2GeSe_6$ (BGGSe). They all possess the phase-matching capability to cover the mid-IR spectral range by down-conversion of 1.064 µm laser radiation. We summarize their main properties (transmission, dispersion, birefringence, nonlinearity), measured using large size single crystals of high optical quality, and review some of the phase-matched nonlinear frequency down-conversion processes already realized.

We have applied BGS and BGSe in few experiments converting 1.064 µm laser radiation into the mid-IR. BGS was employed in an optical parametric oscillator (OPO) generating <6 ns long idler pulses with energies as high as 0.5 mJ at ~6.2 µm (tuning range from ~5.5 to ~7.3 µm) and average power of ~50 mW at 100 Hz. Notwithstanding the relatively low nonlinearity, ~3 times above threshold operation was achieved at pump intensities more than 5 times below the crystal surface damage limit. A BGSe ns OPO provided extremely wide idler tunability (2.7-17 µm), with an energy of 3.7 mJ at ~7.2 µm in ~10-ns pulses at 10 Hz. The pump to idler conversion efficiency for this wavelength reached 5.9% with a slope of 6.5% corresponding to a quantum conversion efficiency or pump depletion of 40%. By intracavity mixing the signal and idler of a 1.064-µm pumped Rb:PPKTP OPO in BGSe we achieved an overall quantum conversion efficiency of 7.8% or pump efficiency of ~1.2%. In this way, a pulse energy ~0.71 mJ was generated at ~7 µm and 100 Hz. Tuning of the mid-IR radiation up to ~8.2 µm was possible in this case by heating of the Rb:PPKTP crystal.

[1] V. Petrov, "Frequency down-conversion of solid-state laser sources to the mid-infrared spectral range using non-oxide nonlinear crystals," Progress Quantum Electron. **42**, 1-106 (2015).

Laser-nonlinear oxide media doped with Tm^{3+} ions

L.I.Ivleva, M.E.Doroshenko

A.M. Prokhorov General Physics Institute Russian Academy of Sciences,
Vavilov str., 38, Moscow 119991, Russia

ivleva@lst.gpi.ru

Last time a special attention is directed to creation of compact solid-state lasers in which one active crystal serves both as lasing and nonlinear-active medium. There are several oxide crystals with such unique properties— Raman -active media (tungstates, molybdates, and vanadates with cubic nonlinearity) and SHG-active media (lithium niobate, strontium-barium niobate with quadratic nonlinearity) doped with rare earth ions for effective lasing with self-conversion of laser radiation. In this paper we consider structural, spectroscopic and laser properties of two oxide crystals doped with Tm^{3+} ions: SRS -active SrMoO4 and SRS/SHG-active SBN:61.

SrMoO4 is well-known effective crystalline Raman medium due to the progress in stimulated Raman scattering (SRS) in the crystal under nano- and picosecond laser pumping. Tm:SrMoO4 material has several advantages: it is simultaneously a good laser medium (the laser emission cross-sections at $^3F_4$-$^3H_6$ (2 μm) and $^3H_4$-$^3F_4$ (1.5 μm) transitions are quite similar being about $1x10^{-20}$ cm^2 in maximum; the upper level $^3F_4$ and $^3H_4$ lifetime is 1.5 ms and 0.235 ms, respectively), and a SRS medium (the SRS gain g = 5.7 cm GW^{-1}, the Raman frequency _R = 887.8 cm^{-1}). According to our data its refined composition is supposed to be $0 \rightarrow Tm_i^{n\bullet} + V_{Sr}^{m'} + Nb_i^{p\bullet} + V_{Mo}^{q'}{}'$, what can be explained by the strong difference of 21.4 % for ionic radii Sr^{2+} and Tm^{3+} (r_{Sr2+} =1.26 Å, r_{Tm3+} =0.99 Å). The presence of Nb^{5+}ions-compensators at tetrahedral positions which have a larger ionic radius as compared to the ionic radius of Mo^{6+} (r_{Mo6+} = 0.41 Å, r_{Nb5+} = 0.48 Å) could lead to an increase in the size of the tetrahedron. At the same time vacancies were found in Sr and Mo positions and some Tm and Nb ions occupy interstitial positions close to V_{Sr} and $V_{Mo,}$ respectively. Such structural peculiarities cause the specific spectroscopic properties of the material. Efficient room temperature lasing under 1700 nm laser diode pumping was obtained in the Tm^{3+}:$SrMoO_4$ concentration ($C=4.8x10^{19}$ cm^{-3}) crystal with slope efficiency up to 18%. Broad oscillation wavelength tuning within 1840-1980 nm spectral range was obtained. First time to our best knowledge lasing of thulium ions in $SrMoO_4$ crystal at $^3H_4$-$^3F_4$ transition with oscillation wavelength near 1500 nm under 793 nm laser diode pumping was realized. Self-terminated oscillations at two 1452 and 1492 nm lines corresponding to fluorescence maxima of $E \perp c$ and $E||c$ fluorescence spectra respectively were obtained with slope efficiency up to 0.3%.

Strontium barium niobate $Sr_xBa_{1-x}Nb_2O_6$ (SBN-x) belongs to tungsten bronze type crystals. Change of strontium and barium contents ($0.25 \le x \le 0.75$), and also doping by various impurities lead to wide possibilities of the crystal property control. The crystal with low content of strontium has the highest nonlinear characteristics. In the case of fixed concentrations of strontium and barium in $(Sr,Ba)Nb_2O_6$ crystals, their doping with RE elements leads to decreasing of nonlinear susceptibility of the SBN materials. Nonlinear media with a random distribution of domains can be used as effective laser frequency converters. The diffuse noncollinear second harmonic generation (SHG) emitted by a random domain pattern was observed in $Sr_{0.61}Ba_{0.39}Nb_2O_6$ crystals. This noncollinear optical frequency doubling is provoked by the specific needlelike form of the domain structure in SBN. Raman spectra show the typical behavior of tungsten bronze type crystals with broad bands and complicated spectral shapes. Stimulated Raman scattering in the SBN-61 crystal under18 ps laser pumping at 1064 nm was observed. Effective Raman oscillation was achieved at the first Stokes Raman component (at the wavelength of 1143 nm) and also at the second Stokes component (at the wavelength of 1230 nm) corresponding to the frequency shift of 640 cm^{-1}. The steady-state Raman gain coefficient was calculated to be 0.42 cm/GW. For SBN:Tm^{3+} (lasing at 2000nm) effective Raman oscillation can be achieved at the first Stokes Raman component (at the wavelength of 2294 nm) and also at the second Stokes component (at the wavelength of 2689 nm) corresponding to the frequency shift of 640 cm^{-1}; calculated the first Anti-Stokes at the wavelength of 1773 nm; the second Anti-Stokes at the wavelength of 1592 nm.

Disordered perovskite crystals for CW and ultrafast laser sources

Stefano Veronesi[1], **Quiangqiang Hu**[2], **Zhitai Jia**[2], **Jian Zhang**[2], **Xutang Tao**[2]

1- NEST- Istituto Nanoscienze – CNR, Piazza S. Silvestro 12, Pisa, 56127, Italy,
2- State Key Laboratory of Crystal Materials & Shandong University, Jinan, 250100, China

Layered Perovskites represent an important class of laser material owing to their disordered members, which produce broad emissions, ideal for ultrafast and tunable laser applications. Particularly relevant is a wide family of isomorph tetragonal materials having the form $ABCO_4$, where A is usually an alkali earth element, B is a rare earth element and C is Al or Ga. Mixed crystals are also utilized in order to increase the structure disorder and consequently broaden emission further. Maybe the most known material belonging to this family is CALGO, widely utilized for infrared pulsed laser sources mainly based on Yb and Tm. Moreover their phonon energy (about 600-650 cm-1) is close to the lower bound of oxides materials, which reduces the detrimental non-radiative contributions opening perspectives in the visible region too.

The spectral characteristic of such hosts are very well exploited in mode locking (ML) laser sources. In fact sub 50 fs pulse duration, widely tunable sources has been achieved with Yb:CALGO and Yb:CALYO laser media utilizing SESAM technology. The spectroscopic characterization and few laser results in ML regime, obtained with Yb:CALGO and Yb:CALYO will be presented. Pulses as short as 36 fs and 43 fs has been achieved for CALGO and CALYO respectively with a tuning range of 40 nm for both hosts. Recently this crystal family has been enlarged by growing mixed crystals, where the rare earth Gd has been substituted by a mix of Gd and Lu, namely a material in the stoichiometric form $Yb{:}CaLu_xGd_{(1-x)}AlO_4$ [2,3]. Moreover, a spectroscopic analysis of $Yb{:}CaLu_xGd_{(1-x)}AlO_4$ mixed host will be reported in comparison with Yb:CALGO. As expected emission band broaden with respect to CALGO, confirming the potentiality of mixed hosts for ultrafast laser application. An interesting perspective of this host family is represented by visible sources. In this frame a Pr doped CALGO has been investigated. Polarized emission spectra show an interesting green band, whose yield is remarkably high, while the lattice disorder is exploited in broad emission bands. Room temperature absorption spectra of ^3P_j manifold, in the usual GAN diodes pumping range, show maxima located at 452.6 nm in π polarization and at 451.6 nm in σ polarization. Highest absorption cross section value occurs in π polarization, resulting $\sigma_{abs} = 6.06*10^{-20}$ cm^2. $^3P_0$ lifetime is shorter than usual fluorides hosts but remains in the ten microsecond range.

[1] D. Zhou, X. Xu, X. Chen3, Haomiao Zhu, D. Li, J. Di, C. Xia, F. Wu, and J. Xu, "*Crystal growth and spectroscopic properties of Er^{3+} doped $CaYAlO_4$*" Phys. Status Solidi A 4, 730 (2012).
[2] Q. Hu, Z. Jia, A Volpi, S. Veronesi, M. Tonelli and X. Tao, "*Crystal growth and spectral broadening of a promising $Yb{:}CaLu_xGd_{1-x}AlO_4$ disordered crystal for ultrafast laser application*" Cryst. Eng. Comm. 19(12), 1643 (2017).
[3] F. Pirzio, S. Cafiso, M. Kemnitzer, A. Guandalini, F. Kienle, S. Veronesi, M. Tonelli, J. Aus der Au, and A. Agnesi, "*Sub-50-fs widely tunable Yb:CaYAlO4 laser pumped by 400-mW single-mode fiber-coupled laser diode*" Opt. Express 23(8), 9790-9795 (2015).
[4] F. Pirzio, M. Kemnitzer, A. Guandalini, F. Kienle, S. Veronesi, M. Tonelli, J. Aus der Au, and A. Agnesi "*Ultrafast, solid-state oscillators based on broadband, multisite Yb-doped crystals*" Opt. Express 24, 11782, (2016).

Efficient generation and modulation of THz waves by using nanostructures

Chul Kang[1], Hyung Keun Yoo[2], Jung Woo Leem[3], Youngwoon Yoon[4], Jae Su Yu[4], Kiejin Lee[3], Myong Kyu Oh[1], In-Wook Hwang[1], Joong Wook Lee[5], Chul-Sik Kee[1]

1- Advanced Photonics Research Institute, GIST, Gwangju 61005, Korea
2-S. LSI Metrology & Inspection, Samsung Electronics, Yongin 17113, Korea
3-Department of Physics, Sogang University, Seoul 121-742, South Korea
4-Department of Electronics and Radio Engineering, Kyung Hee University, Gyeonggi-do 446-701, South Korea
5-Department of Physics, Chonnam National University, Gwangju, Korea
cskee@gist.ac.kr

Terahertz (THz) radiation has attracted considerable interest in recent years because it could be useful in non-destructive diagnosis, home security, and medical imaging. To realize the potential applications, an efficient and practical THz radiation source and THz devices such as modulators are necessary [1-2].

Recently, several investigators have examined modulation and switching of THz wave transmission in semiconductor heterostructures or structured metal-semiconductor hybrid systems. For example, carriers excited within semiconductor substrates have attenuated THz transmission on substrates at structured metal film resonant frequencies. Further, long-living electron-hole pairs in quantum wells have enabled optically controllable THz attenuators. However, for practical application, materials suitable for efficient modulation across a wide frequency range of an initial THz pulse are required. Further, material processing is simple and cheap for device fabrication. Since sharing properties with semiconductors, as well as including simple and cheap fabrication, organic semiconducting polymers have been widely used in optoelectronic devices such as solar cells and flexible display panels.

Although semiconducting polymers are practically suited for THz optoelectronic devices, employing semiconducting polymer film in THz optoelectronic devices has not been carried out because most polymers are considered transparent within the THz range.

In this presentation, we propose a simple and efficient broadband terahertz wave modulator based on an organic conjugated material thin film on Si substrate. Terahertz modulators can exhibit very high modulation efficiencies under lower optical excitation. Our results suggest that introducing properly designed nanostructures should be efficient ways to generate and modulate terahertz radiation [3-4].

When semiconductors are illuminated by a femtosecond laser pulse, photo-carriers excited by the laser cause transient currents that generate THz radiation. Therefore, direct-gap semiconductors such as GaAs and InAs wafers are more efficient than indirect-gap semiconductors such as Ge and Si wafers in generating THz radiation. We also report strong emission of terahertz radiation from germanium wafers with nanostructured surfaces. The power of the terahertz radiation from a Ge wafer with an array of nano-bullets is comparable to that from n-GaAs wafers, which have been widely used as a terahertz source [5].

[1] Y.-S Lee, Principles of Terahertz Science and Technology, (Springer, New York, 2009).
[2] K. Sakai, Terahertz Optoelectronics, (Topics Appl. Phys. 97, Springer-Verlag, Berlin Heidelberg, 2005).
[3] H. K. Yoo, C. Kang, Y. Yoon, H. Lee, J. W. Lee, K Lee, and C.-S. Kee, Appl. Phys. Lett. 99, 061108 (2011).
[4] H. K. Yoo, Y. Yoon, K Lee, C. Kang, C.-S. Kee, I.- W. Hwang, and J. W. Lee, Appl. Phys. Lett. 105, 011115 (2014).
[5] C. Kang, J. W. Leem, I. Maeng, T. H. Kim, J. S. Lee, J. S. Yu, and C.-S. Kee, , Appl. Phys. Lett. 106, 261106 (2015).

THz Metamaterials for Sensing and Communication Application

Seongsin Margaret Kim

Electrical and Computer Engineering, The University of Alabama, Alabama, Tuscaloosa, 35487 USA
seonsgin@eng.ua.edu

Terahertz (THz) spectral region remains a scientifically rich but technologically underdeveloped research area. Since many molecules possess THz spectral fingerprints (ranging from 0.1THz up to 10 THz), and a large variety of non-conductive materials are transparent to THz radiation, THz radiation promises various potential applications. Nonetheless, there exists a shortage of natural materials capable of interacting with THz radiation from which useful THz detectors, emitters, switches, and other devices may be manufactured. Metamaterials, artificially designable structures that render desired optical properties at a given wavelength, could be alternative candidates to design THz devices. They are made by assembling sub-wavelength unit cells called meta-atoms. Metamaterials are well-known for their interesting electromagnetic characteristics. They exhibit extraordinary and unusual responses such as negative refractive index, subwavelength imaging, and invisibility cloak. But, metamaterials can also imitate some of the renowned condensed matter and atomic phenomena e.g. orbital hybridization, Fano resonances, and electromagnetically induced transparency (EIT). In this paper, we will report our recent works on perfect metamaterial absorbers and EIT- metamaterials. In perfect metamaterial absorber, we will present design, simulation, and characterization of polarization independent metamaterial absorber and the dynamic circuit model to interpret its underlying absorption mechanism [1]. Then, inspired by stereoisomers in chemistry we will exhibit our stereometamaterial absorber with polarization controllable response [2]. The stereometamaterial absorber is composed of a two layer frequency selective surface (FSS), dielectric spacer and metal backplane. The FSS is composed of two ring tightly close to each other where the positioning of the rings relative to each results in distinct and multifunctional THz response of the device such as single band, broadband absorption, and absorption/reflection switching controllable by the polarization of the incident THz radiation. In EIT-metamaterials, we will represent our approach called hybrid double split ring resonators (DSRRs) to achieve reduced group velocity of light at a transparency window [3]. Finally liquid crystal based THz absorber shows promising approach to obtain electrically controlled tunablity [4].

[1] M.P. Hokmabadi, D.S. Wilbert, P. Kung, and S, M. Kim, "Design and analysis of perfect terahertz metamaterial absorber by a novel dynamic circuit model," Optics express, 21(14), 16455-16465(2013).
[2] M.P.Hokmabadi, D.S. Wilbert, P. Kung, and S.M. Kim, "Polarization-dependent, frequency-selective THz stereometamaterial perfect absorber" Physical Review Applied, 1(4), 044003(2014).
[3] M.P. Hokmabadi, E. Philip, E. Rivera, P. Kung, and S.M. Kim, "Plasmon-Induced Transparency by Hybridizing Concentric-Twisted Double Split Ring Resonators" Scientific reports, 5, 15735 (2015).
[4] M.P. Hokmabadi, A. Tareki, E. Rivera, P. Kung, R.G. Lindquist, S.M. Kim, "Investigation of tunable terahertz metamaterials perfect absorber with anisotropic dielectric liquid crystal," AIP Advances, 7 (1) 015102 (2017)

Development of Microbial Sensors Using Terahertz Split-ring Resonator Arrays

Y. H. Ahn and S. J. Park
Department of Physics and Department of Energy Systems Research, Suwon 16499, Korea

Department of Physics and Department of Energy Systems Research, Suwon 16499, Korea

ahny@ajou.ac.kr

Detections of biological substances such as fungi, bacteria, and virus in the terahertz (THz) frequency range have been of particular interests; however, there has been hardly any progress since they are mostly transparent against THz waves. On the other hand, metamaterials have been studied extensively to develop effective biosensors. In particular, THz metamaterials have micro-gap structures that are compatible with the sizes of the microorganisms. Here we present that metamaterials operating in the THz frequency range shows promising potential for use in fabricating the highly sensitive and selective microbial sensors that are capable of high-speed on-site detection of microorganisms [1].

We fabricated THz metamaterials such as split-ring resonator (SRR) arrays by using a photolithography techniques. A clear shift in the resonant frequency is observed following the deposition of microorganisms, which arises due to the change in the effective dielectric constant in a gap area of the SRR structures. Strong field localization and enhancement in the gap area enables us to detect the microorganisms with high sensitivity. We were able to detect extremely small amounts of fungi, bacteria, and viruses, enabling us to count the number of low-density microorganisms.

In particular, the resonant frequency shift is higher for the microorganisms with larger dielectric constants, which was successfully interpreted by the dielectric constant measurements of the individual fungi and bacteria [1, 2]. In addition, our THz SRR sensors can be applied in aqueous conditions as easily as in ambient conditions. This is because the THz metamaterial is extremely sensitive to the substances located near the surface, allowing us to use a thin water layer without suffering from the poor transmission in conventional THz spectroscopies. THz metamaterial sensing is a universal method because it is based on the dielectric sensing, while a selective detection is also possible by functionalizing the substrates with antibodies specific to the target substances [1].

To design optimized microbial sensor, the sensitivity of THz SRR sensors has been studied as a function of the substrate dielectric constant, gap size and the metal film thickness [3]. For instance, we were able to increase the sensitivity by about 6 times by exploiting the extremely thin polyimide substrate (4 μm) which has a very low effective index [4]. In addition, we found that the shape of the individual target material was a crucial factor in determining metamaterial sensor sensitivity [5]. We are currently developing hybrid structures based on the split-ring resonators combined with nanomaterials for the enhanced field localization effects.

Our work shows promising potential for use in the fabrication of highly sensitive microbial detectors that are capable of high-speed on-site detection of hazardous microorganisms in various environments.

[1] S. J. Park, J. T. Hong, S. J. Choi, H. S. Kim, W. K. Park, S. T. Han, J. Y. Park, S. Lee, D. S. Kim, and Y. H. Ahn, Detection of microorganisms using terahertz metamaterials. Scientific Reports vol. 4, pp. 4988, (2014).
[2] S. J. Park, S. A. N. Yoon, Y. H. Ahn, "Dielectric constant measurements of thin films and liquids using terahertz metamaterials", RSC Advances vol. 6, pp. 69381-69386, (2016).
[3] S. J. Park, B. H. Son, S. J. Choi, H. S. Kim, and Y. H. Ahn, "Sensitive detection of yeast using terahertz slot antennas", Optics Express vol. 22, pp. 30467-30472, (2014).
[4] A. Tenggara, S. Park, H. Yudistira, Y. H. Ahn, D. Byun, "Fabrication of terahertz metamaterials using electrohydrodynamic jet printing for sensitive detection of yeast", Journal of Micromechanics and Microengineering vol. 27, pp. 035009, (2017).
[5] S. J. Park, S. W. Jun, A. R. Kim, Y. H. Ahn, "Terahertz metamaterial sensing on polystyrene microbeads: shape dependence", Optical Materials Express vol. 5, pp. 2150-2155, (2015).

Spectroscopic study of NP influence on *in vitro* development of preimplantation mouse embryos

A. Karmenyan[1], A. Krivokharchenko[2], H. H. Chang[3], E. Perevedentseva[1,4], L.C. Liu[1], M. Kormacheva[1], Ashek-I-Ahmed[1], C. L. Cheng[1]

1- National Dong Hwa University, Hualien, Taiwan
2- N.N.Semenov Institute of Chemical Physics, RAS, Moscow, Russia
3- Department of Molecular Biology and Human Genetics, Tzu Chi University, Hualien, Taiwan
4- P.N.Lebedev Physics Institute of RAS, Moscow, Russia

artashes@gms.ndhu.edu.tw

Recently nanotechnologies comprising bio-nanotechnologies and the applications of nanoparticles (NP) in biomedical research, diagnosis and treatment are intense developed. As a result, the nanotechnology products can enter into living organism and interact with the organism structures, including reproductive system. Simultaneously, development of assisted artificial reproductive technologies for animals and humans involving in-vitro manipulations with mammalian gametes and early embryos and new technologies for the embryo analysis and treatment dramatically increases the probability of the direct interaction between NP and the ova. It makes actual the problem of embryo-nanosafety. Therefore, study of processes, mechanisms and effects of NP interaction with gametes and embryos becomes extremely important. At the same time, such investigations can lead to better understanding of fundamental mechanics of preimplantation mammalian development. The present work is aimed to study the impact of various NP on early mouse embryos to estimate their potential for researches and toxicity for embryo.
The NP examined were nanodiamonds (ND) of different size and surface properties, TiO_2 NP of different structure, using at various concentrations. These kinds of NP have been selected due to previously demonstrated non-toxicity for cellular models and optical-spectroscopic properties promising for imaging applications and some bio-optical treatments, as well as for drug- and gen-delivery facilities [1, 2].
The study was carried out on mice provided by National Applied Research Laboratories of National Laboratory Animal Center of Taiwan (Taipei, Taiwan). The 2-cell stage embryos have been recovered from female mice of C57BL/6 strain. NP have been added into culture medium and development of the in vitro cultivated embryos was evaluated during 72 h. All embryos were cultivated in 4-well plates with culture medium in incubator at 37°C with 5% of carbon dioxide. The developmental rate has been estimated and compared with control embryos.
The interaction of the NP with the embryos was observed using the confocal fluorescence microscopy (TCS SP5, Leica) and fluorescence lifetime imaging (FLIM), performed at 2-photon excitation with tunable Ti-Sapphire laser (Coherent); pulse duration 150 fs; repetition rate 80 MHz; equipped with single photon counting system, with cooled PMT and two-dimensional scanner. No well-observable penetration of the NP into the embryos has been detected. However, drastically differences in the visible interaction of embryos zona pellucid (ZP) with various NP, depending also on the NP concentrations, and in the effects on the embryo development were founded.
In conclusion, we have demonstrated correlation between interaction of NP with ZP and detrimental effect on embryo early development in-vitro. Influence of NP on embryo development depends on their surface properties. Application of FLIM and Raman spectroscopic analysis for estimation of the embryo state at the treatments; and the mechanisms of NP effect and safe conditions of NP treatment are discussed.
Work was supported by the MoST, Taiwan, projects numbers 104-2811-M-259-012, 104-2811-M-259-013, 105-2811-M-013, 105-2923-B-320-001-MY3, and RFBR, Russia 16-53-52046.

[1] V. Kumar, A. Kumari, P. Guleria, S. K. Yadav. Evaluating the Toxicity of Selected Types of Nanochemicals. D.M. Whitacre (ed.), Reviews of Environmental Contamination and Toxicology, 215, Springer Science+Business Media, LLC, pp. 39-121 (2012).
[2] E. Perevedentseva, Y.-C. Lin, Mona Jani, C.-L. Cheng, Biomedical Applications of Nanodiamond in Imaging and Therapy, Future Medicine. Nanomedicine 8(12) 2041 (2013).

Optical-Spectroscopic Studies for Nanoparticles-Mediated Drug Delivery

E. Perevedentseva[1,2], Y.C. Lin[1,3], A. Karmenyan[1], Z.R. Lin[1], C.H. Liu[1], C.C. Chang[1], C.Y. Song[1], N.N. Melnik[2], C.L. Cheng[1]

1- National Dong Hwa University, Hualien, Taiwan
2- P.N.Lebedev Physics Institute of Rus Acad Sci, Moscow, Russia
3- Institute of Physics, Academia Sinica, Taipei, Taiwan

elena@gms.ndhu.edu.tw

Development of different kinds of nanocarriers for drug delivery is now widely discussed [1]. Together with increasing the efficiency of the delivery the application of nanoparticles (NP) for this purpose opens ways for new methods of delivery control, monitoring, and for integration of several functionalities in one NP-drug complex. Sensitive and non-invasive optical-spectroscopic methods are used to observe and analyze the delivery, to provide the information about the cell (or multicellular target), including chemical, structural, and, in result, metabolic and physiological conditions at the interaction with the used NP, drug or at other treatments [2], as well as for monitoring the process of NP-drug system synthesis and the product characterization [3].

In this presentation like drug carrier we are considering nanodiamonds (ND). During last years ND has been demonstrated as a biocompatible and feasible platform to increase efficiency of anticancer drug delivery [4, 5]. The delivery tracing and biodistribution visualization based on ND optical-spectroscopic properties can be realized via fluorescence confocal imaging, Raman mapping, FLIM and other methods or their combinations. Together with development of the optical-spectroscopic methods and their using for detection, observation, investigation of processes and interactions in the targets, and treatments, wide variability of ND properties and size opens new possibilities for multifunctional applications.

In our work the interaction of nanodiamond-drug complex with cells and multicellular 3D systems is analyzed using plant alkaloid berberine and anticancer drug doxorubicin for the conjugation. The fluorescence properties of these drugs allow use of spectroscopic methods for comparison of effects of ND, the drug solution and ND-drug complex and to analyze the difference in terms of control of delivery.

To discuss the methods of controlled and spectroscopically-observable delivery using multifunctional NP we consider also the magnetic-modified ND. The strong magnetic susceptibility of this ND has been demonstrated (however the origin of magnetism is unclear) [6]. It is important, that simultaneously the magnetic ND reveals strong fluorescence especially at two-photon excitation and also strong distinguishable signal at fluorescence lifetime analysis.

The mechanisms of the changes of fluorescence properties of nanostructured carbons in result of the modification of other physical and structural characteristics (e.g. magnetic properties or surface termination) are discussed. Possible applications of this effect for bio-imaging and bio-sensing with spectroscopic detection are considered.

Acknowledgements. The authors appreciate the financial support of this research by the Ministry of Science and Technology of Taiwan, Grant No. MOST 103-2112-M-259-001-MY3, and "Ray Techniques", Israel, for provided magnetic ND.

[1] E. Blanco, H. Shen, M. Ferrari, Principles of nanoparticle design for overcoming biological barriers to drug delivery. Nature Biotechnology 33, 941-951 (2015).
[2] S. Kalinina, J. Breymayer, P. Schäfer, E. Calzia, V. Shcheslavskiy, W. Becker, A. Rück, Correlative NAD(P)H-FLIM and Oxygen Sensing-Plim for Metabolic Mapping. J Biophotonics. 9(8), 800-811 (2016).
[3] A. Paudel, D. Raijada, J. Rantanen. Raman spectroscopy in pharmaceutical product design. Adv Drug Delivery Rev 89, 3-20 (2015).
[4] E.K. Chow, X.-Q. Zhang, M. Chen, R. Lam, E. Robinson, H. Huang. Nanodiamond Therapeutic Delivery Agents Mediate Enhanced Chemoresistant Tumor Treatment. Sci. Transl. Med. 3(73), 73ra21 (2011).
[5] X. Wang, X. C. Low, W. Hou, L. N. Abdullah, T. B. Toh, M. M. A. Rashid, D. Ho, E. K.-H. Chow. Epirubicin-Adsorbed Nanodiamonds Kill Chemoresistant Hepatic Cancer Stem Cells. ACS Nano 8 (12), 12151-12166 (2014).
[6] C.Y. Song, N. Perov, V. Samsonova, S. Norina, L.C. Liu, Z.R. Lin, Y.C. Lin, A.-I-Ahmed, A. Karmenyan, O. Levinson, B. Zousman, E. Perevedentseva, C.L. Cheng. Magnetic-modified nanodiamond for bio-applications. Proc. of 10th International Conference on New Diamond & Nano Carbons; Xi'an, China, 118 (2016).

Microstructural alterations in cornea under thermo-mechanical effect of 1.56μm laser radiation. Towards a new refractive technology

O. Baum[1], A. Yuzhakov[1,2], A. Omelchenko[1,2], V. Zaitsev[2], A. Bolshunov[3], V. Siplivy[3], E. Sobol[1,2].

1- Institute Photonic Technologies of Federal Scientific Research Centre "Crystallography and Photonics" of RAS, Moscow (Troitsk), Russia.
2- Institute of Applied Physics Russian Academy of Sciences, Nizhniy Novgorod, Russia.
3- Federal State Scientific Institute "Research Institute of Eye Diseases", Moscow, Russia.

baumolga@gmail.com

This work continues a series of investigations of a new approach to the eye refraction correction by nondestructive laser action on the cornea [1]. Our previous in vivo studies in experiments on rabbit eyes have shown that sequential laser irradiation of the sclera and cornea yields a significant alteration in the eye refraction [2], which in particular can be used in treatment of astigmatism. If there is no astigmatism, it is convenient to use a similar approach to correction of eye refraction with ring-shaped laser beam for obtaining controllable alterations of the eye refraction with axial symmetry. This approach allows one to obtain axial symmetry of alteration in the eye refraction depending on the ring diameter without any pathological changes in central part of cornea. Such a configuration provides axial symmetry of the effect and excludes the occurrence of astigmatism. At ring-shaped distribution of intensity of laser radiation, the temperature of cornea surface and tension also have ring-shaped distributions, which results in deformation of cornea in the central part and heating only on the periphery.

In more detail, we discuss here micro-alterations in the cornea structure of excised rabbit and mini-pig eyes that were produced by IR laser irradiation at 1.56 μm wavelength and were investigated with phase-sensitive optical coherence tomography for visualizing dynamic and cumulative strains [3, 4], as well as using atomic force microscopy with nanoindentation. The results obtained demonstrated, that the collagen structure of the cornea was not destroyed and the treatment did not cause worsening of tissue mechanical and optical properties [5].

Acknowledgements

The study was supported by the Russian Science Foundation grant number 16-15-10274 and the Russian Foundation of Basic Research grant numbers 15-02-06078 and 15-29-03811.

[1] Bolshunov A., Sobol E., Avetisov S., Baum O., Siplivy V., Omelchenko A., Fedorov A., "A new method of the eye refraction correction under non-ablative laser radiation". Acta Ophthalmologica. - 2011. - V89. P.0. [doi: 10.1111/j.1755-3768.2011.2172.x].
[2] EN Sobol', OI Baum, AV Bol'shunov, VI Sipliviy, N Yu Ignat'eva, OL Zakharkina, VV Lunin, AI Omel'chenko, VA Kamenskiy, AV Myakov "Eye tissue structure and refraction alterations upon nondestructive laser action". Laser physics 16 (5), 735-740.
[3] Vladimir Y Zaitsev, Alexander L Matveyev, Lev A Matveev,Grigory V Gelikonov, Alexander I Omelchenko, Dmitry V Shabanov, Olga I Baum, Valery M Svistushkin and Emil N Sobol. "Optical coherence tomography for visualizing transient strains and measuring large deformations in laser-induced tissue reshaping". 2016 Laser Phys. Lett. 13 115603.
[4] Vladimir Y Zaitsev, Alexander L Matveyev, Lev A Matveev, Grigory V Gelikonov, Alexander I Omelchenko, Olga I Baum, Sergey E Avetisov, Andrey V Bolshunov, Vladimir I Siplivy, Dmitry V Shabanov, Alex Vitkin, Emil N Sobol "Optical coherence elastography for strain dynamics measurements in laser correction of cornea shape". Journal of Biophotonics 1–14 (2017) / DOI 10.1002/jbio.201600291
[5] Yuzhakov A.V, Sviridov A.P., Baum O.I., Shcherbakov E.M., Sobol E. N., Optical Characteristics of the Cornea and Sclera and their Alterations under the Effect of Nondestructive 1.56-mkm Laser Radiation, Journal of Biomedical Optics 18(5), 058003, 2013.

Optical trapping and diffuse light scattering techniques for *in vitro* assessing the effect of albumin and fibrinogen synergy on red cells aggregation in blood plasma

A.N. Semenov[1,2], K. Lee[1,3], H. Lee[4], A.E. Lugovtsov[2], F. Yaya[3], C. Wagner[3], S. Shin[4], A.V. Priezzhev[1,2]

1 - Faculty of physics and 2 - International Laser Center of M.V. Lomonosov Moscow State University, Leninskiye Gory, 1-2, 119991, Moscow, Russia
3 - Experimental Physics, Saarland University, Campus building E2 6, Saarbrücken, Germany D-66041
4 - School of Mechanical Engineering, Korea University, Seoul, 145, Korea

semenov@physics.msu.ru

At the cellular level, the blood flow regulation is mostly conducted via red blood cell (RBC) spontaneous aggregation and shear forced disaggregation. The mechanisms of RBC aggregation are presumed to be connected with protein content in blood plasma. However so far they are not completely understood as, in the experiments, the roles of different proteins often seem controversial [1]. In this work, we aimed for assessing the roles of albumin and fibrinogen affecting RBC aggregation in plasma with optical techniques.

Holographic multiple laser tweezer (LT) allows for effective measuring of the interaction forces between RBCs on the single cell level [2]. The aggregating force (F_A), the force leading to overlapping of two adjacent RBCs, was measured by comparing it with the minimum optical trapping force required for holding the trapped cells from aggregate formation. The RBC interaction at disaggregation was estimated by measuring the probability of cells separation with LT – a ratio of successfully dispersed RBC doublets to the total number of separation attempts at defined trapping force. Force measurements were performed in diluted suspensions of RBCs (~0.05%) in plasma with varied concentrations of fibrinogen and albumin.

Diffuse light scattering technique is based on measuring the intensity of light scattered from a whole blood sample. Further analysis of the obtained data allows for estimating the RBC interaction via the aggregometry parameters. In this work, the aggregation index (A.I., %), aggregation time ($T_{1/2}$, s) and critical shear stress (CSS, mPa) were measured using the aggregometer RheoScan AnD-300. Blood samples were prepared by mixing the RBCs with platelet poor plasma at 40% hematocrit level with EDTA as anti-coagulant agent.

F_A measurements showed that increasing the albumin concentration from 40 to 80 mg/ml led to the significant growth of the aggregating force at 4 – 8 mg/ml fibrinogen concentration. For fibrinogen concentration of 2 - 6 mg/ml the same growth of albumin concentration led to a decrease in the separation probability. However at 8 mg/ml fibrinogen concentration the separation probability was increasing with addition of albumin.

Aggregometry measurements showed A.I. and $T_{1/2}$ highly depended on fibrinogen concentration and were less sensitive to a possible synergetic effect of albumin. CSS measurements showed that at 2 – 4 mg/ml of fibrinogen concentration adding albumin either didn't affect or led to non-significant growth of the RBC interaction strength. But at high fibrinogen concentrations (>4 mg/ml) CSS was decreasing when albumin concentration changed from 40 to 80 mg/ml indicating that RBCs aggregates became less strong.

We conclude that fibrinogen and albumin have a complex synergetic effect on RBC aggregation in plasma. CSS and disaggregation forces measurements showed correlation revealing a change in albumin role in RBC aggregate strength regulation from agonist to inhibitor. Possible underlying mechanisms of the observed synergetic effects could be due to a change in the RBC membrane potential or formation of albumin-fibrinogen complexes preventing strong RBC aggregation. These ideas require further studies.

[1] Lee K., Kinnunen M., Danilina A.V., Ustinov V.D., Shin S., Meglinski I., Priezzhev A.V, Characterization at the individual cell level and in whole blood samples of shear stress preventing red blood cells aggregation, Journal of Biomechanics, vol. 49(7), pp. 1021-1026 (2016).
[2] Lee K., Wagner C., Priezzhev A.V., Assessment of the "cross-bridge"-induced interaction of red blood cells by optical trapping combined with microfluidics, Journal of Biomedical Optics, vol. 22(9), pp. 091516-1 – 091516-6 (2017)

Applications of inverse scattering principles with digital holography

Y.K. Park[1]

1- Department of Physics, KAIST, Daejeon, Republic of Korea
**E-mail: yk.park@kaist.ac.kr*

In this talk, we will present the applications of inverse scattering principles with digital holography [1-4]. First, I will present the recently developed 3-D holotomography setup using a dynamic mirror device, which is an optical analogous to X-ray computed tomography. In particular, I will discuss the visualization of 3D refractive index distributions of biological cells and tissues measured with the 3-D holotomography using the transfer function method. For a weakly scattering sample, such as biological cells and tissues, a three-dimensional refractive index tomogram of the sample can be reconstructed with the inverse scattering principle from multiple measurements of two-dimensional holograms. The outcome demonstrates outstanding visualization of 3D refractive index maps of live. In addition, we also discuss the applications of inverse scattering principle for highy scattering layers. With wavefront shaping techniques using digital holography, we demonstrate ultra-high-definition dynamic holographic display exploiting large space-bandwidth in volume speckle. Exploiting light scattering in diffusers, we also demonstrate the holographic image sensor which does not require for the use of a reference beam [5]

[1] H. Yu et al., Ultrahigh-definition dynamic 3D holographic display by active control of volume speckle fields, Nature Photonics, 11:186–192 (2017)
[2] K. Kim et al., Tomographic active optical trapping of arbitrarily shaped objects by exploiting 3-D refractive index maps, Nature Communications, 8:15340 (2017)
[3] Y. Jo et al., Holographic deep learning for rapid optical screening of anthrax spores, bioRxiv preprint, doi: 10.1101/109108
[4] J. Yoon, Label-free identification of non-activated lymphocytes using three-dimensional refractive index tomography and machine learning, Scientific Reports, (in press)
[5] K. Lee and Y. Park, Exploiting the speckle-correlation scattering matrix for a compact reference-free holographic image sensor, Nature Communications, 7:13359 (2016)

Wideband Ultrashort Pulse Fiber Lasers and Their Applications

Norihiko Nishizawa, Jin Lei, and Masahito Yamanaka

Department of Electronics, Nagoya University, Furo-cho, Chikusa-ku, Nagoya 464-8603, Japan
nishizawa@nuee.nagoya-u.ac.jp

Passively mode-locked fiber lasers are stable and practical ultrashort pulse laser sources. Recently, nano-carbon materials absorb a lot of attentions as a useful mode-locker. So far, we have been investigating the highly functional ultrashort pulse fiber laser sources and their applications to ultrahigh resolution (UHR) optical coherence tomography (OCT) [1,2]. In this talk, we present our recent progress about our research.

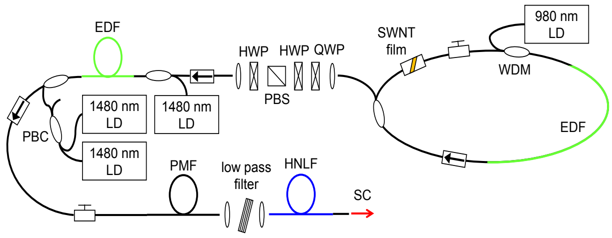

Fig. 1. Supercontinuum generation system

Figure 1 show the configuration of high power supercontinuum generation based on single wall carbon nanotube (SWNT) fiber lasers. The ultrashort pulses from fiber lasers were amplified in Er-doped fiber amplifier. The Raman shifted ultrashort pulse was coupled into highly nonlinear fiber, and Gaussian shaped supercontinuum (SC) was generated at 1.7 um wavelength region, as shown in Fig. 2 [3]. Figure 3 shows the observed 3D OCT image of mouse brain with generated SC. Owing to the lower scattering coefficient, the precise structures were observed at deeper part with ultrahigh resolution. Recently, we also developed optical coherence microscopy (OCM) at wavelength of 1.7 um [4]. The coherent SC also works as the wideband optical frequency comb.

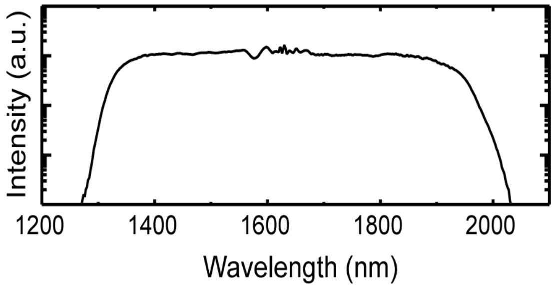

Fig. 2. Optical spectrum of coherent SC

Using the nonlinear fiber technologies, we generated rapid, wideband wavelength tunable, narrow linewidth sources, as shown in Fig. 4. The wavelegnth shift was increased as the fiber input power was increased due to soliton self-frequency shift. Using the electro-optical modulator, the wavelength can be shifted shot by shot. For the spectral compression, we desinged the quasi-dispersion increasing fiber using the comb profiled fiber technique. The pulse spectrum was comressed through the adiabatic soliton spectral compression[5]. The large, and ideal spectral compression was achieved in the wide wavelength range. To the best of our knowledge, this is the fastest wavelength tunable pulse sources.

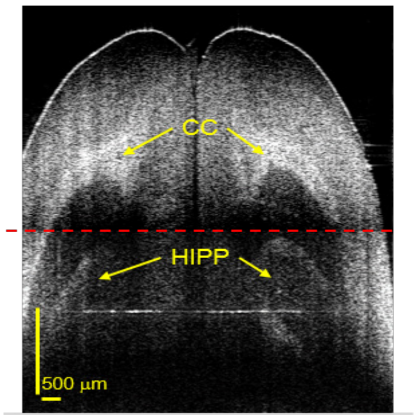

Fig. 3. UHR-OCT image of mouse brain

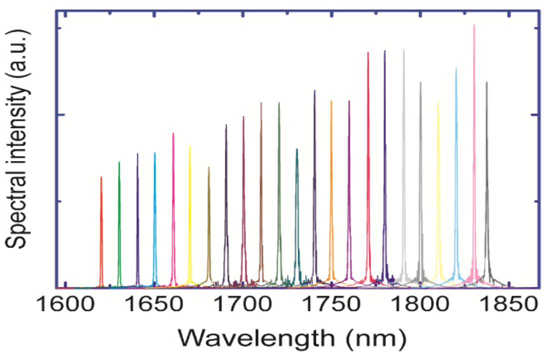

Fig. 4. Spectra of wavelength tunable source

[1] N. Nishizawa, Ultrashort pulse fiber lasers and their applications, Jpn. J. Appl. Phys. vol.53, 090101 (2014) (invited review paper)
[2] N. Nishizawa, Wideband ultrafast fiber laser sources for OCT and metrology, J. Phys. B, vol.49, 182003 (2016) (topical review paper)
[3] H. Kawagoe, S. Ishida, M. Aramaki, Y. Sakakibara, E. Omoda, H. Kataura, and N. Nishizawa, Biomed. Opt. Express, vol. 5, pp.932-943 (2014)
[4] M. Yamanaka, T. Teranishi, H. Kawagoe, and N. Nishizawa, Optical coherence microscopy in 1700 nm spectral band for high-resolution label-free deep-tissue imagind, Sci. Rep. vol.6, 31715 (2016)
[5] N. Nishizawa, Y. Andou, E. Omoda, H. Kataura, and Y. Sakakibara, Characterisitics and improvement of wideband wavelength tunable narrow-linewidth source by spectral compression in quasi-increasing comb-profiled fiber, Opt. Express, vol.24, 23403 (2016)

Yb^{3+}-doped CaF_2-LaF_3 ceramics for high power ultrashort pulse lasers

Akira Shirakawa[1], Shotaro Kitajima[1], Kentaro Yamakado[1], Ken-ichi Ueda[1], Hitoshi Ishizawa[2]

1- Institute for Laser Science, University of Electro-Communications, 1-5-1 Chofugaoka, Chofu, Tokyo 182-8585, Japan

2- NIKON Corporation, 1-10-1 Asamizodai, Minami-ku, Sagamihara, Kanagawa 228-0828, Japan

akira@ils.uec.ac.jp

Today Yb^{3+}-doped calcium fluoride ($Yb:CaF_2$) attracts growing attention. It has many advantages suitable for ultrashort pulse lasers: the broad and smooth fluorescence spectrum, the favorite thermal property, and the long fluorescence lifetime. Recently fabrication of rare-earth doped CaF_2 ceramics have been investigated extensively [1-3]. Here we report the laser operation of Yb^{3+}-doped CaF_2-LaF_3 ceramics fabricated from nanocrystals [1,4].

Our fabrication process is based on the hot isostatic pressing (HIP) method. Three type of fluoride nanocrystals which are CaF_2 and two kinds of rare-earth fluoride particles synthesized by a chemically process are mixed. In this work, we choose the Yb-ions and La-ions. Incorporation of small amount of lanthanum fluoride modified the lattice structure of CaF_2 and suppresses the formation of Yb^{2+} ions. The fluorescence spectrum changes by the doping concentration of Yb^{3+} ions. As the Yb ion doping concentration increases, the fluorescence spectrum becomes broader and smoother.

The CW operation of $Yb:CaF_2$-LaF_3 ceramics was demonstrated with the simple two-mirror cavity setup. A 3%La1%Yb sample marked the highest slope efficiency of 69.5% and a 2%La3%Yb sample marked the highest maximum output power of 4.36 W (Fig.1) [4]. We are also challenging mode-locked laser operation of those ceramics.

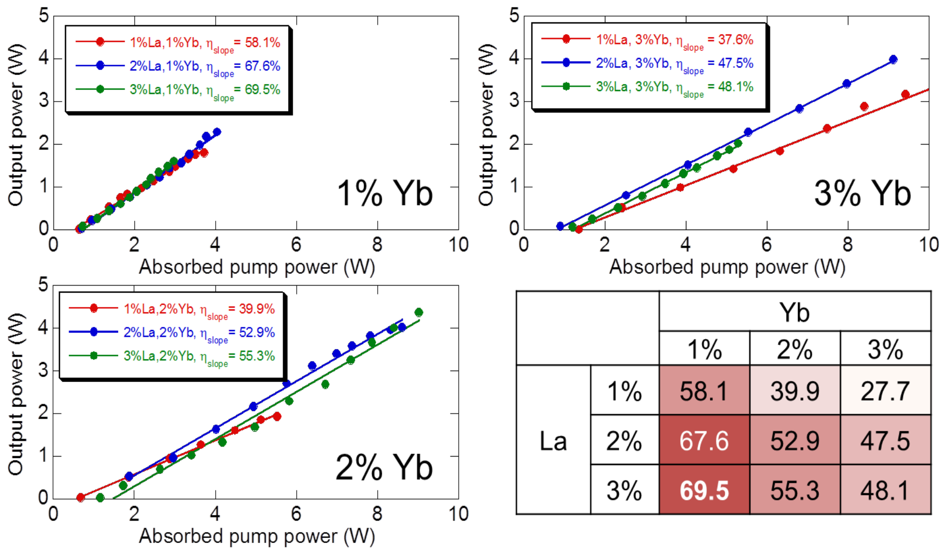

		Yb		
		1%	2%	3%
La	1%	58.1	39.9	27.7
	2%	67.6	52.9	47.5
	3%	69.5	55.3	48.1

Fig. 1. Output power of 1 at.% Yb doped, 2 at.% Yb doped and 3 at.% Yb doped CaF_2-LaF_3 ceramic laser versus absorbed pump power with different La concentration. The lower right table shows the summary of the slope efficiencies.

[1] A. Shirakawa, H. Nakao, Y. Higashi, K. Ueda, Y. Ezura, and H. Ishizawa, "Yb^{3+}-doped CaF_2-LaF_3 Ceramic Laser," Advanced Solid-State Lasers Congress 2013 Technical Digest, JTh5A. (postdeadline paper)

[2] M. E. Doroshenko, V. A. Konyushkin, A. Ya. Karasik, P. P. Fedorov, V. V. Osiko, H. Jelinkova and J. Sulc, "Fluoride ceramics for mid IR lasing (2 -3 μm) and planar waveguides," Advanced Solid-State Lasers Congress 2013 Technical Digest, AM1A.6.

[3] P. Aballera, A. Suganuma, F. Druon, J. Hostalrich, P. Georges, P. Gredin, M. Mortier, "Laser performance of diode-pumped $Yb:CaF_2$ optical ceramics synthesized using an energy-efficient process," Optica vol.2, 288-291 (2015).

[4] S. Kitajima, K. Yamakado, A. Shirakawa, K. Ueda, Y. Ezura, H. Ishizawa, "Yb^{3+}-doped CaF_2-LaF_3 ceramics laser," Optics Letters vol. 42, 1724-1727 (2017).

High-power ultrafast MOPA laser system based on Yb:YAG elements of advanced geometries

I. Kuznetsov, I. Mukhin, E. Perevezentsev, M. Volkov, O. Palashov

Institute of Applied Physics of the Russian Academy of Science, 46 Ul'yanova str., Nizhny Novgorod, Russia, 603950

kuznetsov@ipfran.ru

Picosecond lasers with high average and high peak power become an indispensable tool in science and industry. Such devices should combine high power, high efficiency, good stability and reliability. We propose the advanced concept of the high-power picosecond laser that is based on successive amplification of the signal from the sub-picosecond fiber master oscillator in the set of laser amplifiers based on Yb:YAG elements of different geometries. At the preamplifier stage we apply thin-rod Yb:YAG active elements with high-brightness diode pumping [1]. It provides very high gain coefficient and it is able to work at average power of some tens of watts and pulse energy >1 mJ. At the power amplifier stage we use the Yb:YAG thin-disk multipass amplifier that is able to provide very high average power and pulse energy but it is limited in terms of gain coefficient. The scheme of the laser and the photos of the gain modules are shown in Fig. 1.

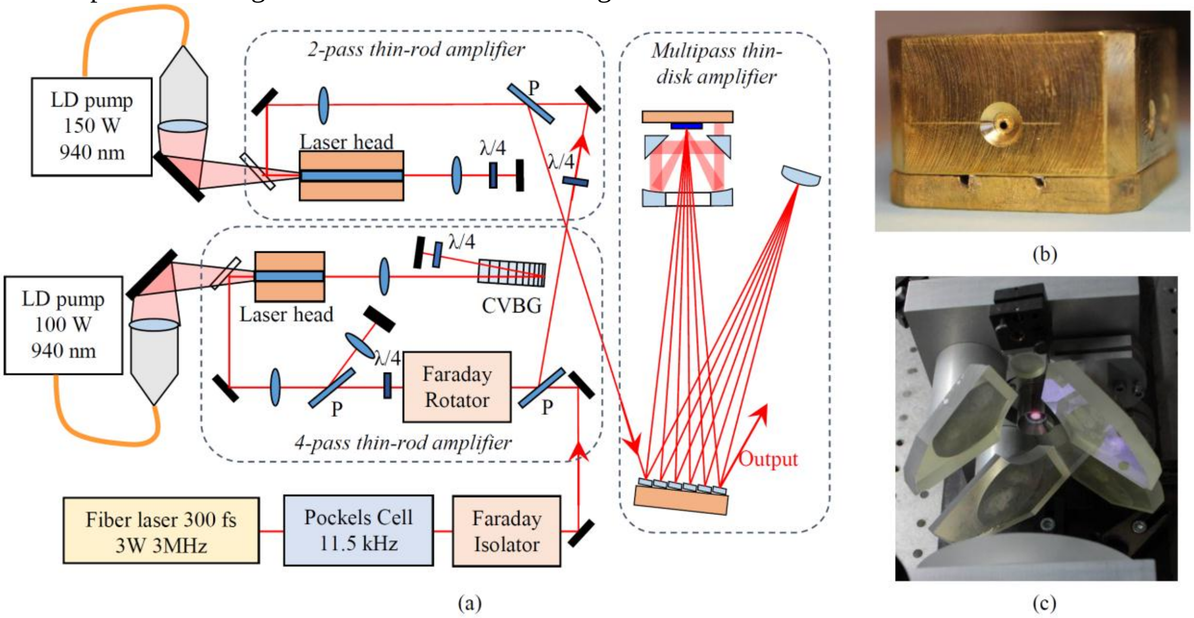

Fig. 1. The scheme of the laser system (a), the photo of the gain module with the thin-rod active element (b) and with the thin-disk active element (c).

The laser system consists of 4-pass thin-rod preamplifier, which includes the chirped volume Bragg gratings (CVBG) for pulse stretching, 2-pass thin-rod preamplifier and multipass thin-disk amplifier. In the multipass amplifier we tested two types of optical schemes including the telescopic scheme and the scheme based on the stack of the plane mirrors [2]. The scheme with the stack of the plane mirrors in comparison with the telescopic scheme allows improving the beam quality of the laser due to the spatial filtering of the mode in the scheme. However, at the same time it leads to the decreasing of the output power of the amplifier. Today after two preamplifier stages we achieved 12 W average power that corresponds to >1 mJ pulse energy. In the thin-disk stage it was amplified up to 80 W average power and 7 mJ pulse energy. In the nearest future output power of the laser will be further increased.

[1] I. Kuznetsov, I. Mukhin, O. Palashov, Yb: YAG thin-rod laser amplifier with a high pulse energy for a fibre oscillator, Quantum Electronics 46 (4), pp. 375-378 (2016).

[2] K. Schuhmann, M.A. Ahmed, A. Antognini, T. Graf, T.W. Hänsch, K. Kirch, F. Kottmann, R. Pohl, D. Taqqu, A. Voss, B. Weichelt, Thin-disk laser multi-pass amplifier, SPIE LASE, pp. 93420U-93420U (2015).

Comparative analysis of evanescent field interaction with carbon nanotubes in the Q-switched Yb:KYW planar waveguide laser

Jun Wan Kim[1], Sun Young Choi[2], Jieun Bae[3], Xavier Mateos[4], Francesc Díaz[4], Uwe Griebner[5], Valentin Petrov[5], Guang-Hoon Kim[1], and Fabian Rotermund[3]

1- *Advanced Medical Device Research Division, Korea Electrotechnology Research Institute (KERI), 15588 Ansan, Republic of Korea*

2- *Institut für Laser-Physik, Universität Hamburg, 22761 Hamburg, Germany*

3- *Department of Physics, Korea Advanced Institute Science and Technology (KAIST), 34141 Daejeon, Republic of Korea*

4- *Física i Cristal·lografia de Materials i Nanomaterials (FiCMA-FiCNA), Universitat Rovira i Virgili (URV), 43007 Tarragona, Spain*

5- *Max Born Institute for Nonlinear Optics and Short Pulse Spectroscopy, 12489 Berlin, Germany*

rotermund@kaist.ac.kr

Waveguide laser which adopt waveguide structure in the gain medium have been intensively investigated as the compact pulsed laser thanks to the simple and small cavity configuration, low lasing threshold operation, and cost-effectiveness of laser systems [1, 2]. For the pulsed operation of waveguide laser, saturable absorber is essential and lots of demonstrations have been reported. But in case of waveguide laser, damage issue of saturable absorber (SA) is easily occurred due to small beamsize corresponding to the waveguide size. To avoid this problem, evanescent field interaction is proposed and widely researched for various SA of BDN dye, carbon nanotubes (CNT), and graphene which don't have to consider the lattice mismatch between gain medium and SA [2-6]. But most demonstrations have been only focused to the evanescent field interaction itself, and the comparative analysis of the evanescent field interaction has not yet been investigated.

In this study, we conduct comparative analysis between direct and evanescent field interaction in the Q-switched Yb:KYW planar waveguide lasers for the first time. While maintaining same cavity configuration, Q-switched operations of Yb:KYW planar waveguide laser are achieved for the different positions of CNT-SA. The CNT-SAs are placed on an end mirror (M-coating), on an output coupler (OC-coating), and top side of Yb:KYW planar waveguide (WG-coating). In case of OC-coating, maximum output powers, maximum repetition rate, and minimum pulse durations are 61 mW, 1103 kHz, 215 ns. In case of WG-coating and M-coating, maximum output powers, maximum repetition rate, and minimum pulse durations are 39 mW, 1052 kHz, 275 ns, and 26 mW, 1119 kHz, 217 ns, respectively. Each case exhibits stable Q-switched operations with spatial single-mode and follows the tendencies of the general SA Q-switched lasers. For the comparative analysis of evanescent field interaction, we calculate intracavity beam size and E-field distribution in our Yb:KYW planar waveguide laser. From the E-field distribution calculation, it is confirmed that maximum intensity at the CNT-SA is about 0.079% of that in the Yb:KYW planar waveguide. From this value, it is found that the maximum intensity at SA of WG-coating is about 1000 times lower than that of M-coating. These large difference is originated from large refractive index difference between gain medium and SA.

[1] M. Pollnau, Y. E. Romanyuk, F. Gardillou, C. N. Borca, U. Griebner, S. Rivier, and V. Petrov, "Double Tungstate Lasers: From Bulk Toward On-Chip Integrated Waveguide Devices," IEEE J. Sel. Top. Quant. vol. 13, pp. 661-671 (2007).

[2] J. I. Mackenzie, "Dielectric Solid-State Planar Waveguide Lasers: A Review," IEEE J. Sel. Top. Quantum Electron. vol. 13, pp. 626-637 (2007).

[3] B. Charlet, L. Bastard, and J. E. Broquin, "1 kW peak power passively Q-switched Nd^{3+}-doped glass integrated waveguide laser," Opt. Lett. vol. 36, pp. 1987-1989 (2011).

[4] J. W. Kim, S. Y. Choi, D.-I. Yeom, S. Aravazhi, M. Pollnau, U. Griebner, V. Petrov, and F. Rotermund, "Yb:KYW planar waveguide laser Q-switched by evanescent-field interaction with carbon nanotubes," Opt. Lett. vol. 38, pp. 5090-5093 (2013).

[5] Y. Tan, C. Cheng, S. Akhmadaliev, S. Zhou, and F. Chen, "Nd:YAG waveguide laser Q-switched by evanescent-field interaction with graphene," Opt. Express vol. 22, pp. 9101-9106 (2014).

[6] J. W. Kim, S. Y. Choi, S. Aravazhi, M. Pollnau, U. Griebner, V. Petrov, S. Bae, K. J. Ahn, D.-I. Yeom, and F. Rotermund, "Graphene Q-switched Yb:KYW planar waveguide laser," AIP Adv. vol. 5, pp. 017110 (2015).

[7] A. Choudhary, S. J. Beecher, S. Dhingra, B. D. Urso, T. L. Parsonage, J. A. G.-Jacob, P. Hua, J. I. Mackenzie, R. W. Eason, and D. P. Shepherd, "456-mW graphene Q-switched Yb:yttria waveguide laser by evanescent-field interaction," Opt. Lett. vol. 40, pp. 1912-1915 (2015).

Characterization of thermal effect in quasi-phase-matched nonlinear crystal

Sunao Kurimura[1] and Hwan Hong Lim[2]

1- National Institute for Materials Science, 1-1 Namiki, Tsukuba, 305-0044 Japan
2- Institute for Molecular Science, 38 Nishigonaka, Myodaiji, Okazaki, 444-8585 Japan

Kurimura.sunao@nims.go.jp

Thermal effect in a nonlinear optical crystal is amajor obstacle for power scaling [1, 2], and could be reduced by an effective heat removal structure. We developed a quantitative technique to characterize heat dissipation from a nonlinear crystal, which is a significant tool for improving the heat dissipation quality. The technique named as "Phase-Matched Calorimetry (PMC)" provides characteristic index of *heat capacity*$C\alpha$as a measure of heat removal performance [3].

The PMC measuresa temperature increase in the nonlinear crystal by observing phase matching temperature-tuning curve. By fitting input-power dependence of the temperature increase,$C\alpha$ in the unit of W/deg.C, $C\alpha$ an affordable power for unit temperature increase. We here perform single-pass cw SHG in quasi-phase-matched (QPM) Mg-doped stoichiometric lithium tantalate (Mg:SLT)surrounded by soft metal.

The index$C\alpha$ depends on the geometry of the device and thermal contact between the QPM crystal and a metal holder. For higher heat removal the device aperture should be as small as possible in the range three times larger than the beam diameter. The aperture width of 0.3 mm produces 30% higher $C\alpha$than 0.5 mm in the case of 10 mm device length. $C\alpha$ also depends on the focusing parameter ξ of the input beam [4]. We found a trade-off relationship between $C\alpha$ andη_{norm} –normalized SHG conversion efficiency. Tight focusing at high ξyields high efficiency and low $C\alpha$, where the thermal effect limits the maximum output power. Weak focusing at low ξ reduces the thermal effect at the cost of the efficiency. According to Fig.1 we can choose an appropriate focusing parameter for the required output power. The $C\alpha$ attractsresearchers in Moscow State University as reported in the recent paper[5].

The authors appreciate Prof. Ichiro Shoji of Chuo University (Japan)and his students for their contribution to thermal characterization.

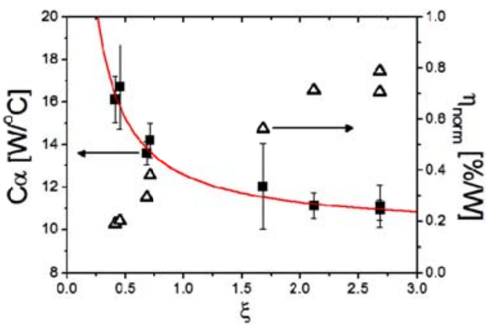

Fig.1 Focusing parameter dependence of Cα and η_{norm} in cw SHG withQPM Mg:SLT

[1] N. E. Yu, S. Kurimura, Y. Nomura, and K. Kitamura, "Stable high-power green light generation with thermally conductive periodically poled stoichiometric lithium tantalate," Jpn. J. Appl. Phys. **43**, pp. L1265–L1267 (2004).
[2] S. V. Tovstonog, S. Kurimura, I. Suzuki, K. Takeno, S. Moriwaki, N. Ohmae, N. Mio, and T. Katagai, "Thermal effects in high-power CW second harmonic generation in Mg-doped stoichiometric lithium tantalate," Opt. Express **16**, pp. 11294–11299 (2008).
[3]H. H. Lim, T. Katagai, S. Kurimura, T. Shimizu, K. Noguchi, N. Ohmae, N. Mio, and I. Shoji, "Thermal Performance in High Power SHG Characterized by Phase-Matched Calorimetry," Opt. Express**19**, pp. 22588-22593 (2011).
[4] H. H. Lim, S. Kurimura, K. Noguchi, and I. Shoji,"Thermal characteristics of second harmonic generation byphase matchedcalorimetry," Opt. Express**22**, pp. 18268-18277 (2014).
[5] A. A. Surin, T. E. Borisenko, and S. V. Larin, "Generation of 14 W at 589 nm by frequency doubling of high-power CW linearly polarized Raman fiber laser radiation in MgO:sPPLT crystal," Opt. Lett. **41**, pp. 2644-2647 (2016).

The Talbot effect revisited: Studies in the terahertz range

B. Knyazev[1,2], V. Cherkassky[2], Yu. Choporova[1,2], B. Goldenberg,[1] Kameshkov[1,2], V. Pavelyev[4,5]

1- Budker Institute of Nuclear Physics SB RAS, 11, Lavrentieva Ave, Novosibirsk 630090, Russian Federation
2- Novosibirsk State University, 2, Pirogova St,, Novosibirsk 630090, Russian Federation
4- Samara University, 34, Moskovskoe shosse, Samara 443086, Russian Federation
5- Image Processing Systems Institute of the Russian Academy of Sciences, 151, Molodogvardejskaya St, Samara 443001, Russian Federation

ba_knyazev@phys.nsu.ru

Due to the long wavelength of terahertz radiation equal to fractions of a millimeter, different diffraction effects in this range can be investigated with greater detail than in the visible range. First, the characteristic dimensions of the diffraction structures can be two orders of magnitude larger, which facilitates their production. Second, the characteristic dimensions of the sensitive elements of the microbolometric or pyroelectric matrices used for imaging are smaller than the wavelength, which allows one to record diffraction patterns with a resolution close to the wavelength limit. Both of these properties were used in this paper. The Talbot effect [1] is a well-known diffraction phenomenon. In the terahertz range, this effect was demonstrated in [2]. In this paper we present the results of two studies: (1) the study of Talbot images with hole diameters (slit widths) close to the radiation wavelength, and (2) beam diffraction studies with orbital angular momentum on periodic structures (analogue of the Talbot effect). As far as we know, such experiments, at least in the terahertz range, have not yet been carried out. Since both experiments require a high intensity of radiation, the Novosibirsk free electron laser [3] with an average beam power of several tens of Watts was used as a source of monochromatic radiation. In different experiments, the radiation was tuned to wavelengths of 121, 130 or 141 μm.

Periodic structures of different aspect ratio in metallic or dielectric plates of different thickness, used in the experiments, were fabricated using x-ray LIGA technology, laser drilling, or ion beam lithography. Both amplitude and phase gratings were studied.

In the experiments on recording Talbot images in fundamental and fractional planes, we investigated shapes of self-images of gratings openings at fundamental and higher spatial frequencies. We were able to obtain images even for gratings with a hole diameter of about 3/4 wavelength. Using a 320x240 microbolometer array, moved along the optical axis by a linear translator with a stepper motor, we recorded terahertz video films, which allowed us, after processing the video, to reconstruct Talbot carpets.

Diffraction of beams with an orbital angular momentum on periodic structures was investigated using first and second order vortex Bessel beams formed by binary phase axicons with spiral zones [4]. Experiments and numerical calculations showed that the gratings self-imaging, which observed in the case of the classic Talbot effect, is not observed in the case of vortex beams. Nevertheless, in the planes corresponding to the Talbot planes, some periodic patterns are observed. They are not repeated when moving from closer planes to distant ones. These patterns depend on grating period, insident Bessel beam diameter, openings diameter, and value and sign of beam topological charge. The most characteristic structure is a lattice of rings with a phase structure that repeats the phase of the incident vortex beam. Thus, a macroscopic vortex beam after passing a periodic two-dimensional grating can be transformed into a system of helicoidal microbeams with an annular amplitude distribution and a phase increasing in azimuth. Such beams can be used, for example, to create a lattice of optical traps and other applications.

1.F. Talbot, Philos. Mag, 9. 401-407, (1836).
2. B. A. Knyazev, V. S. Cherkassky, Yu. Yu. Choporova, V. V. Gerasimov, M. G. Vlasenko, 35th Internat. Conf. Infrared, Millimeter and Terahertz Waves. Rome, 2010, Paper Tu.-B1.5.
3. G. N. Kulipanov, et al., IEEE Trans. THz Sci. Technol. 5, 798-809, (2010).
4. Yu. Yu. Choporova, B. A. Knyazev, M. S. Mitkov, V. S. Pavelyev, B O. Volodkin, Phys. Rev. Lett., 115, 163901, (2015).

Sub-THz Vacuum Devices Based on Grating and CW Imaging

Jung-Il Kim, Geun-Ju Kim, Jeong-Hun Lee, Sang-Hoon Kim, Yong-Seok Lee, and Insoo S. Kim

Korea Electrotechnology Research Institute, Ansan, Gyeonggi-do 15588, Korea

sky@keri.re.kr

There have been considerable demands on the terahertz (THz) technology for various applications in bio-medical imaging, quality control, material sciences, and high-speed communications. Among the THz radiation sources, the vacuum electronic devices based on the metallic grating are investigated. And, for the continuous-wave (CW) THz imaging, the THz slit probe is employed to enhance the spatial resolution.

Backward wave oscillator (BWO) consists of the rectangular waveguide grating and the sheet electron beam to increase the output power. As for the metallic grating of the 0.1 THz BWO, the groove period is 310 μm and the groove thickness is 150 μm. And, the 0.1 THz metallic grating is fabricated by the wire electric discharge machining (EDM). The sheet electron beam of the 2.5 x 0.14 mm^2 is propagated near to the surface of grating with the tilt angle to maximize the interaction with the surface modes. The generated 0.1 THz wave is coupled into the output coupler which is expanded into the WR-10 waveguide. To focus the sheet electron beam along the grating, the magnetic circuit of about 0.4 T fabricated by the Sm-Co magnet is applied. When the beam current of 200 mA is emitted from the cathode, the output power of about 10 W at the frequency of 0.1 THz is measured. To increase the output power and efficiency, the two stage waveguide grating is proposed. From the 3D particle-in-cell (PIC) simulation, the output power is enhanced more than 2 times due to the enhancement of the normalized 1st beam harmonics. As for the 0.2 THz metallic grating, the groove period of 145 μm and the groove thickness of 65 μm are calculated. And, to fabricate the 0.2 THz grating, the fabrication process using the MEMS techniques based on the deep reactive ion etching (DRIE) is examined.

The THz slit probe is applied in the CW 0.2 THz imaging system to enhance the spatial resolution with the reduction of power loss inside the THz probe. For the 0.2 THz system, the WR-5 waveguide based slit probe is designed and fabricated by using the electroforming method. And, to improve the responsivity reducing the reflection from the surface, the CW THz imaging system is compared by using the patterned Si wafer. The responsivity in the amplitude and phase information is enhanced up to 90 times using the pattern of the diameter of 0.5 mm and the depth of 50 μm.

0.1 THz BWO using the rectangular waveguide grating and the sheet electron beam is developed for the sub-THz radiation source. And, the CW 0.2 THz imaging system using the THz slit probe is developed for the high-resolution THz imaging system.

[1] John H. Booske, Richard J. Dobbs, Colin D. Joye, Carol L. Kory, George R. Neil, Gun-Sik Park, Jaehun Park, and Richard J. Temkin, “Vacuum Electronic High Power Terahertz Sources”, IEEE Tran. Terahertz Sci. and Tech., Vol. 1, pp. 54-75 (2011).
[2] K. Schunemann and D. M. Vavriv, “Theory of Grating: A Grating Backward-Wave Oscillator with Inclined Electron Beam,” IEEE Tran. Elec. Dev., 46, 2245 (1999).
[3] Wai Lam Chan, Jason Deibel, and Daniel M Mittleman, “Imaging with Terahertz Radiation”, Rep. Prog. Phys., Vol. 70, pp. 1325-1379 (2007).
[4] Jung-Il Kim, Seok-Gy Jeon, Geun-Ju Kim, and Jaehong Kim, “Enhancement of Terahertz Radiation in a Smith-Purcell Backward Wave Oscillator by an Inverse Wet-Etched Grating”, Phys. Lett., Vol. 375, pp. 589-592 (2011).
[5] Geun-Ju Kim, Jung-Il Kim, Seok-Gy Jeon, Jaehong Kim, Kyung-Kook Park, Chang-Hyun Oh, “Enhanced Continuous-Wave Terahertz Imaging with a Horn Antenna for Food Inspection”, J. Infrared Milli. Terahz. Waves, Vol. 33, pp. 657-664, 2012.

Long Distance Propagation by THz Pulse

T.-I. Jeon

Korea Maritime and Ocean University, Busan, 49112, South Korea

jeon@kmou.ac.kr

I present experimental studies of terahertz (THz) pulse propagation by metal-wire lines [1,2]. Because most of THz electric field concentrates in between air spaced two-wire lines, the wire have very small group velocity dispersion (GVD), and relatively low attenuation. However, when the wire is bent, most of THz field radiate into the air because of very small skin depth. In this study, I demonstrate that the bending loss of two-wire lines with rough dielectric-coated surface is considerably lower than that of two-wire lines with smooth uncoated surface [3]. In addition, the characteristics of the guiding properties are analyzed and compared using a Computer Simulation Technology (CST) Microwave Studio software.

Meanwhile, Fig. 1. shows the THz pulse propagation through 186 m and 910 m distance which are approximately equal to 52 and 255 round-trips of the circulating 50 fs optical pulse within the mode-locked ring laser, respectively [4]. Thereby, giving sampling pulses delayed by 52 and 255 pulses down the pulse train from the excitation pulses. The time shift depends on water vapor densities (WVD) by comparing the 186-m- and 910-m-long path measurement.The time shifts of the THz pulses for different WVD are 1.80 and 12.56 ps/(g/m^3) for 186-m and 910-m distances, respectively.

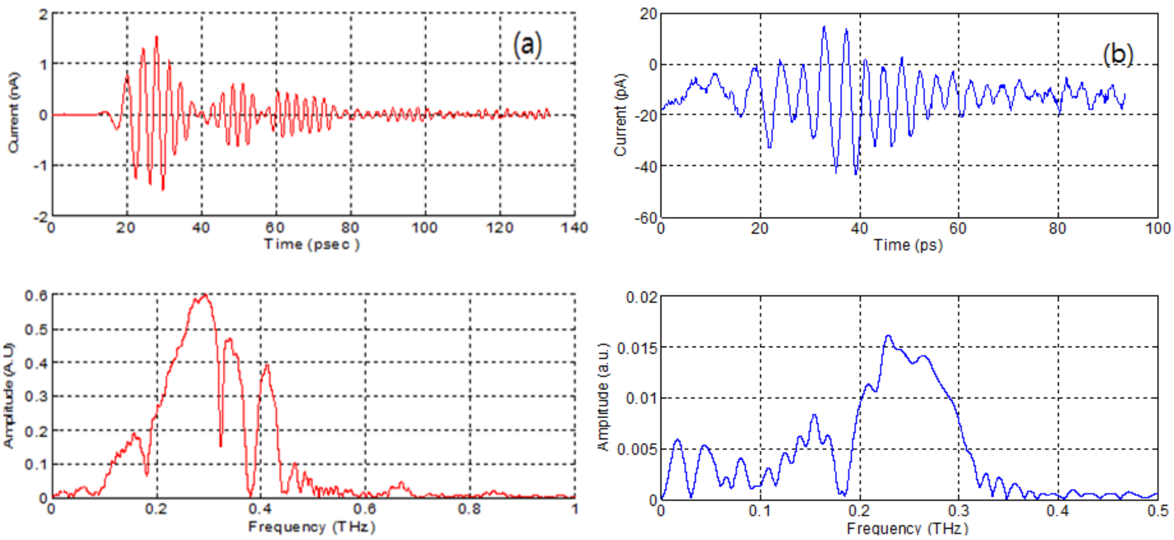

Fig. 1. Measured THz pulses and corresponding amplitude spectra for the pulses.
(a) 186-m long path. (b) 910-m path.

[1] T.-I. Jeon, J. Zhang, and D. Grischkowsky, “THz Sommerfeld wave propagation on a single metal wire,” Appl. Phys. Lett., vol. 86, pp. 161904, (2005).
[2] J. S. Jo, T.-I. Jeon, and D. Grischkowsky, “Prototype 250 GHz Bandwidth Chip to Chip Electrical Interconnect, Characterized With Ultrafast Optoelectronics,” IEEE Trans. Terahertz. Sci. and Tech., vol. 3, pp 453-460 (2013).
[3] J. Zha, G. J. Kim, and T. -I. Jeon, “Enhanced THz guiding properties of curved two wire lines Optics Express, vol. 24, 6136 (2016).
[4] E.-B Moon, T.-I. Jeon, and D. Grischkowsky, “Long-Path THz-TDS Atmospheric Measurements Between Buildings,” IEEE Trans. Terahertz Sci. and Tech., vol. 5, 742-750 (2015).

Accelerator based THz sources and its applications in Japan

H. Ohgaki[1]

1- Institute of Advanced Energy. Kyoto University, Gokasho, Uji, Kyoto 6110011, Japan

ohgaki.hideaki.2w@kyoto-u.ac.jp

In the THz region, there have been significant progress in solid state laser based sources. However, a high peak power THz radiation sources are still required in some applications. Accelerator based THz sources, e.g., free electron lasers and coherent THz radiations, can be the one of option for generation of high-power and tunable THz radiations. In Japan, linear accelerator based THz sources are developed and available in AIST[1,2,3], KEK[4,5,6], KURRI[7,8,9], KU-FEL[10,11,12], LEBRA[13,14,15], t-ACTS[16,17], and Waseda University [18,19] where they use the coherent radiation from short electron bunches. FEL-TUS[20] and ISIR[21,22,23] are using FEL system. There is one SR based coherent THz radiation source is available in UVSOR[24,25,26]. Each facility has different specifications. These accelerator based THz sources and their typical application research will be introduced in this talk.

[1] R. Kuroda et al., Generation of 0.1 THz coherent synchrotron radiation with compact S-band linac at AIST, Infrared Physics & Technology, vol. 51, pp. 390-393 (2008).
[2] N. Sei et al., Measurement of intense coherent synchrotron radiation at frequencies around 0.1 THz using the compact S-band linac, Journal of Applied Physics, 104, 114908 (2008).
[3] R. Kuroda et al., Development of a coherent THz radiation source based on the ultra-short electron beam and its applications. Nuclear Instruments and Methods in Physics Research A, 637, pp. S30-S32 (2011).
[4] G. Naumenko et al., Monochromatic coherent grating transition radiation in sub-THz frequency range, Nuclear Instruments and Methods in Physics Research Section B, vol.402, pp. 153-156 (2017).
[5] Y. Honda et al., Terahertz Source Utilizing Resonant Coherent Diffraction Radiation at KEK ERL Test Accelerator, Proceedings of FEL2015, pp.547-549 (2015).
[6] Y. Honda et al., Resonant Coherent Diffraction Radiation System at ERL Test Accelerator in KEK, Proceedings of IPAC2017, pp.887-889 (2017).
[7] Y. Shibata et al., Observation of coherent synchrotron, Čerenkov, and wake-field radiation at millimeter wavelengths using an L-band linear accelerator, Physical Review A, vol.44, R3449(R) (1991).
[8] T. Takahashi et al., Utilization of coherent transition radiation from a linear accelerator as a source of millimeter-wave spectroscopy, Review of Scientific Instruments, vol. 69, 3770 (1998).
[9] T. Takahashi et al., Development of a Scanning Near-Field Sub-THz-Wave Microscopy with Coherent Transition Radiation. Journal of Physics: Conference Series 359, 012016 (2012).
[10] N. Sei et al., Development of intense terahertz coherent synchrotron radiation at KU-FEL, Nuclear Instruments and Methods in Physics Research Section A, vol.832, 208-213 (2016).
[11] H. Zen et al., Present Status and Perspectives of Long Wavelength Free Electron Lasers at Kyoto University, Physics Procedia, vol.84, pp.47-53 (2016).
[12] S. Suphakul et al., Beam Dynamics Investigation for the Compact Seeded THz-FEL Amplifier, Energy Procedia, vol.89, pp.373-381 (2016).
[13] N. Sei et al., Observation of intense terahertz-wave coherent synchrotron radiation at LEBRA. Journal of Physics D: Applied Physics 46, 045104 (2013).
[14] N. Sei et al., Millijoule terahertz coherent transition radiation at LEBRA, Japanese Journal of Applied Physics, vol.56, 032401 (2017).
[15] Y. Hayakawa et al., Project on the superposition of beamlines for parametric X-ray radiation and coherent transition radiation in the THz region at LEBRA, Journal of Physics: Conference Series, vol.732, 012013 (2016).
[16] H. Hama et al., Test-accelerators as coherent terahertz source program (t-ACTS) at Tohoku University, Energy Procedia, vol.9, pp.391-397 (2011).
[17] S. Kashiwagi et al., Proof-of-Principle Experiment of Velocity Bunching for Ultra-Short Electron Pulse Production, Energy Procedia, vol.9, pp.346-352 (2016).
[18] Y. Koshiba et al., Characterization of THz Radiation Generated by Ultra-Short Bunch from Energy Chirping Cell attached RF Electron Gun, Vibrational Spectroscopy, vol.75, pp.184-189 (2014).
[19] K. Sakaue et al., Ultrashort electron bunch generation by an energy chirping cell attached rf gun, Physical Review Special Topics – Accelerators and Beams, vol.17, 023401 (2014).
[20] H. Koike et al., Design and study of FIR FEL device using S-band linac at FEL-SUT, Nuclear Instruments and Methods in Physics Research A, vol.507, pp.242-245 (2003).
[21] K. Kawase et al. The high-power operation of a terahertz free-electron laser based on a normal conducting RF linac using beam conditioning, Nuclear Instruments and Methods in Physics Research A, vol.726, pp.96–103 (2013).
[22] H. Hoshina et al., Polymer Morphological Change Induced by Terahertz Irradiation, Scientific Reports, vol.6, 27180 (2016).
[23] M. Nagai et al., Luminescence induced by electrons outside zinc oxide nanoparticles driven by intense terahertz pulse trains, New Journal of Physics, vol.19, 053017 (2017).
[24] S. Bielawski et al., Tunable narrowband terahertz emission from mastered laser–electron beam interaction, Nature Physics, vol.4, 390-393 (2008).
[25] N. Yamamoto et al., Ultra-short coherent terahertz radiation from ultra-short dips in electron bunches circulating in a storage ring, Nuclear Instruments and Methods in Physics Research A, 637, S112-S115 (2011).
[26] M. Hosaka et al., Saturation of the laser-induced narrowband coherent synchrotron radiation process: Experimental observation at a storage ring, Physical Review Special Topics – Accelerators and Beams, vol.16, 020701 (2013).

THz parametric source and its applications

Kodo Kawase, **Kosuke Murate**

Nagoya University, Department of Electronics, Furocho, Nagoya 4648603, Japan

kawase@nuee.nagoya-u.ac.jp

In 2003, we reported the first-ever development of a spectral imaging system using THz-wave parametric oscillator (TPO) [1]. At that time, the TPO had a dynamic range below four orders of magnitude, which enables it to identify reagents only through thin (0.2mm^t) envelopes using spectral imaging.

Recently, we have succeeded in the development of high power and high sensitivity THz wave spectral imaging system using injection-seeded THz parametric generation (is-TPG) and detection [2] as shown in Fig. 1. A dynamic range of 100 dB has been obtained, which is much higher than that of the 2003 TPO. The peak output power of is-TPG approached 50 kW by introducing a microchip YAG laser with shorter pulse width of 420ps. In the detection section of our system, THz-wave was converted back into near infrared beam by nonlinear optical wavelength conversion. We have realized ten orders of dynamic range using commercially available near infrared photo detector. Now we can detect drugs under much thicker obstacles than before using evolved is-TPG spectroscopic imaging system as shown in Fig. 2. Our evolved is-TPG system has potential applications in spectroscopic sensing and imaging of chemicals through obstacles [3] and non-destructive CT imaging of plastic/ceramic products [4]. We have also compared our is-TPG spectrometer and TDS (THz Time Domain Spectroscopy) for the purpose of drug detection through thick envelopes.

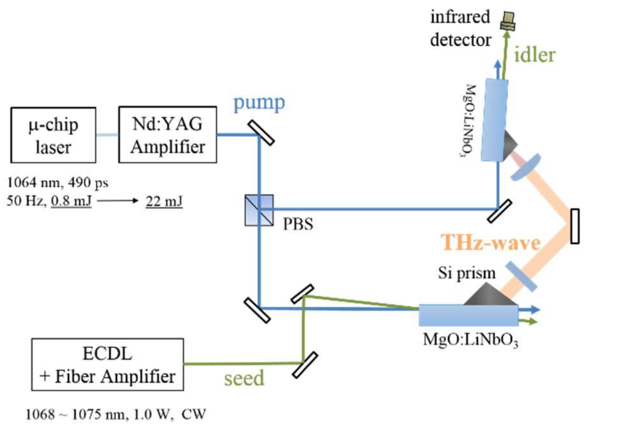

Fig.1. Experimental set up for THz spectrometer using is-TPG

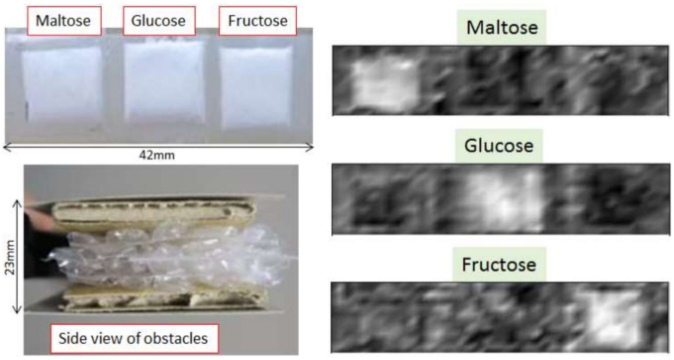

Fig. 2 THz spectroscopic imaging of powder samples in two cardboards + four bubble wraps + two corrugated boards.

The authors thank Mr. M. Yoneda of Nagoya Univ., Dr. S. Hayashi of NICT, Dr. H. Minamide, Dr. K. Nawata of RIKEN, and Prof. T. Taira of IMS for helpful discussions and advices. This work was supported by KAKENHI 25220606 and 15J04444.

[1] K. Kawase, Y. Ogawa, Y. Watanabe and H. Inoue, “Non-destructive terahertz imaging of illicit drugs using spectral fingerprints,” Optics Express, vol. 11, no. 20, pp. 2549-2554 (2003).

[2] S. Hayashi, K. Nawata, T. Taira, J. Shikata, K. Kawase, H. Minamide "Ultrabright continuously tunable terahertz-wave generation at room temperature," Scientific Reports, Vol. 4, Article number 5045 (2014).

[3] M. Kato, S. R. Tripathi, K. Murate, K. Imayama and K. Kawase, “Non-destructive drug inspection in covering materials using a terahertz spectral imaging system with injection-seeded terahertz parametric generation and detection,” Optics Express, 24(6), 6425-6432 (2016).

[4] S. Tripathi, Y. Sugiyama, K. Murate, K. Imayama, K. Kawase, “Terahertz wave three-dimensional computed tomography based on injection-seeded terahertz wave parametric emitter and detector,” Optics Express, 24(6), 6433-6440 (2016).

Laser-induced porous glass densification – the way for integral sensors fabrication

Veiko V.P.[1], Zakoldaev R.A.[1], Segeev M.M.[1], Sivers A.N.[1], Antropova T.V.[2], Itina T.E. [1,3]

1- 1ITMO University, Kronverkskiy Pr. 49, St. Petersburg 197101, Russia
2- Institute of Silicate Chemistry, Russian Academy of Sciences, Russia, Saint-Petersburg, nab. Makarova, 2
3-Laboratoire Hubert Curien, UMR CNRS 5516/UJM/University of Lyon, 42000, Saint-Etienne, France
Main author email address: vadim.veiko@mail.ru

In recent years, numerous studies have been carried out for the fabrication of optical sensors based on porous materials to monitor changes in the environment. The function of these sensors is based on a change in the transmissive or reflective capacity of the reagent located in the porous matrix due to its response to the surrounding medium [1]. One of the suitable material is a porous glass (PG) [2]. At present, there is an interest in its local processing for the creation of microsystems based on PG. A local control of porosity allows us to create the molecular barriers with controlled permeability along the thickness of the PG plate. The organisation of such inner elements can allow us to design an integral devices like a gas analyzer.

The purpose of this work is laser-induced control of the PG density during the formation of molecular barriers with full and selective permeability.

The end-to-end densification of the PG plate was carried out in the following way:

1. Inscription of the extended densified regions inside of PG plates by using ultrashort laser pulses (λ = 515 nm, E_p = 1 - 2 μJ, τ = 200 fs, ν = 500 kHz). Applying different number of pulses with varied pulse energy, it is possible to achieve a local densification of PG structure [3]. A set of similar regions along the thickness of the sample represents a molecular barrier inside of PG. The permeability of the barrier is determined by the relative distance between the regions.
2. The molecular barrier was densified from the surface by the action of CO_2 laser radiation. As a result of the strong absorption of CO_2 laser radiation, local densification along the barrier occurs, which ensures a complete cell impenetrability. Thus, the PG plate was divided into a few barriers (Fig. 1 «a»).

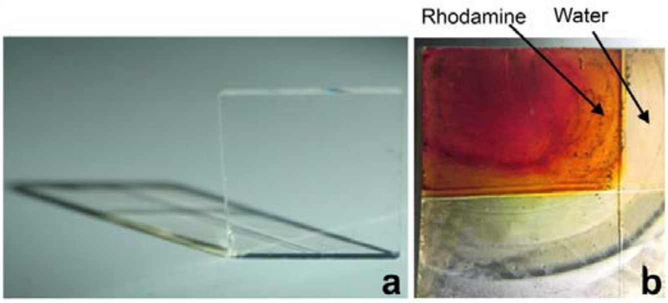

Figure 1 Molecular barriers inside of porous glass: general view (a) and testing during its impregnation with water solution of rhodamine.

A set of molecular barriers were created inside of the PG plate. The impermeability of these molecular barriers to rhodamine molecules is experimentally proven (Fig. 1 «b»). It is shown that the rhodamine molecules are too large to cross the fabricated barrier. At the same time, water molecules are able to penetrate thought the barrier. In addition, the formation mechanisms of the barrier are discussed based on the calculation results allowing the quantitative prediction of the laser parameters required for the corresponding PG modifications.

Acknowledgements

The reported study was financially supported by the Ministry of Education and Science of the Russian Federation, research agreement №14.587.21.0037 (RFMEFI58717X0037).

[1] Jerónimo P. C. A., Araújo A. N., Montenegro M. C. B. S. M. Optical sensors and biosensors based on sol–gel films //Talanta V.72(1), pp. 13-27 (2007).
[2] Maruo Y. Y. et al. Measurement of local variations in atmospheric nitrogen dioxide levels in Sapporo, Japan, using a new method with high spatial and high temporal resolution //Atmospheric Environment. V.37(8) pp. 1065-1074 (2003).
[3] Veiko V. P. et al. Femtosecond laser-induced stress-free ultra-densification inside porous glass //Laser Physics Letters. 2016. V13(5), pp. 055901 (2016).

Laser created functional microstructures

E. Stankevičius, **M. Garliauskas, E. Daugnoraitė, G. Račiukaitis**

1- Center for Physical Sciences and Technology, Savanoriu Av. 231, LT-02300 Vilnius, Lithuania

estankevicius@ftmc.lt

At the ripe age of 60 years, the laser has become a mature technological device with many applications. This was not always true, of course. For many years, the laser was viewed as ‘an answer in search of a question’. That is, it was seen as an elegant device, but one with no real useful application outside of fundamental scientific research. In the last two to three decades however, numerous laser applications have moved from the laboratory to the industrial workplace or the commercial market. Lasers are unique energy sources characterized by their spectral purity, spatial and temporal coherence, and high peak intensity. [1]

In recent years, techniques based on photo-polymerization has been demonstrated the fabrication of complex 3D and 2D objects of dimensions required for practical applications in photonics, micro-optics, micro-fluidics and biomedicine. Usually, such structures were fabricated using ultra-short laser pulses, but some investigations have been performed by employing low-cost lasers emitting picosecond or nanosecond laser pulses including continuous wave (CW)-laser.

The fabrication technique based on the laser interference lithography (LIL) is among the most practical and elegant approaches to the fabrication of the extended polymeric periodic microstructures. LIL is based on the multi-beam interference phenomenon. By recording the multi-beam interference pattern into photopolymer it is possible to fabricate 1D, 2D and 3D periodic structures by a single laser exposure. Depending on the laser wavelength, the exposure can be achieved via linear or nonlinear absorption. LIL allows fabricating periodic structures over a large area relatively fast and that makes this technique attractive and promising for mass-fabrication of the functional devices such as microoptical and microfluidics elements or scaffolds (shown in Fig. 1).

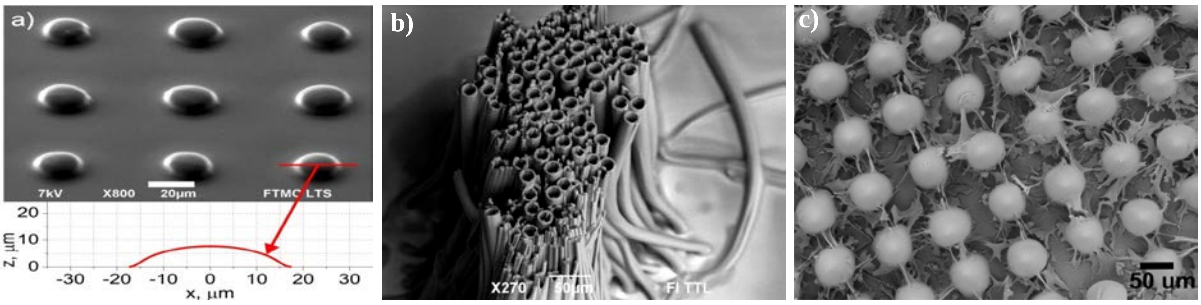

Fig. 1. SEM images of functional structures fabricated via the four-beam interference lithography: a) microaxicon-like structures [2]; b) microtubes [3]; c) scaffolds. [4]

In this presentation, the fabrication of various periodic structures by using laser interference lithography will be demonstrated. The shape of the fabricated microstructures depends on many factors of the interfering beams such as the polarization, the number of the interfering beams, the phase shift, the laser irradiation dose, the angle between interfering beams, the wavelength, etc. The fabricated periodic structures using LIL have the potential to be used for various applications such as photonics - for light localization, microoptics – for light guiding or Bessel-like beam generation, biomedical - for the investigation of stem cell behavior, microfluidic – for controlling the flow of fluids on small length scale or in tissue engineering by creating an artificial vessels.

[1] T. Lippert and A. Wokaun, "Laser Processing of Novel Functional Materials," CHIMIA International Journal for Chemistry **55**, 783-786 (2001).

[2] E. Stankevičius, M. Garliauskas, M. Gedvilas, and G. Račiukaitis, "Bessel-like beam array formation by periodical arrangement of the polymeric round-tip microstructures," Opt. Express **23**, 28557-28566 (2015).

[3] E. Stankevicius, T. Gertus, M. Rutkauskas, M. Gedvilas, G. Raciukaitis, R. Gadonas, V. Smilgevicius, and M. Malinauskas, "Fabrication of micro-tube arrays in photopolymer SZ2080 by using three different methods of a direct laser polymerization technique," J. Micromech. Microeng. **22**, 065022 (2012).

[4] E. Stankevicius, E. Balciunas, M. Malinauskas, G. Raciukaitis, D. Baltriukiene, and V. Bukelskiene, "Holographic lithography for biomedical applications," Proc. of SPIE **8433**, 843312-843317 (2012).

Abstract for ALT 2017

Fabrication of mechanical traps for atomic force microscopy investigations of living cells by ultrashort pulse laser ablation

Inam Mirza[1], Jan Pokorny[2], Yoann Levy[1], Radek Machulka [3], Ondrej Haderka[4], Nadezhda M. Bulgakova[1], Tomas Mocek[1]

1- HiLASE Centre, Institute of Physics CAS, Dolní Břežany, Czech Republic
2-Institute of Physics CAS, Prague, Czech Republic
3-Joint Laboratory of Optics of Palacky University and Institute of Physics CAS, Olomouc, Czech Republic
4-Regional Centre of Advanced Technologies and Materials, Joint Laboratory of Optics of Palacký University and Institute of Physics CAS, Palacký University, Olomouc, Czech Republic

mirza@fzu.cz

Nanomechanical properties of cell membranes exhibit characteristics of many biological processes undergoing inside living cells. Nanoscale membrane fluctuations are considered as a signature of life. [1]. They are correlated with cellular activities, physiology and metastatic potential and, hence, can be used for diagnostics. In particular, cell walls exhibit temperature-dependent nanomechanical motion at characteristic frequencies [2] which can be used to monitor cellular response to changes in physiological conditions or exposure to certain drugs. For nanoscale measurements of fluctuations using atomic force microscopy (AFM), living cells must be immobilized. This is usually done via mechanical trapping, e.g. in polycarbonate membranes [2].

In this work, based on the results of ultrafast-laser processing of Corning Willow glass [3], we present a laser-ablation method of microwell fabrication to immobilize living cells for AFM measurements of their nanomechanical motions. For microwell fabrication, single- and multi-shot laser ablation of surfaces of glass bottom dishes (100-µm-thick borosilicate glass) was performed by a Ti:Sapphire laser operating at λ = 800 nm with a pulse width of 130 fs. A range of techniques such as space-and-time resolved spectroscopy and optical profilometry were used to study laser ablation dynamics and crater (microwell) quality. The produced microwells have diameters in the range of 10–15 um and a depth of ~5–8 um. First testing results of AFM measurements of nanomechanical motion of living cells trapped in the laser-produced mechanical traps will also be reported.

[1] S. Kasas. et al, Detecting nanoscale vibrations as signature of life, Proceedings of the National Academy of Sciences of the United States of America (PNAS), 112., pp. 378-381, (2015).
[2] A.E. Pelling, S. Sehati, E.B. Gralla, J.K. Ginzewski, Time dependence of the frequency and amplitude of the local nanomechanical motion of yeast, Nanomedicine, 1., pp.178-183, (2005).
[3] I. Mirza. et al, Ultrashort pulse laser ablation of dielectrics: Thresholds, mechanisms, role of breakdown, Scientific Reports, 6., pp. 39133 1-11, (2016).

The Laser-Induced Synthesis of Linear Carbon Chains Stabilized by Noble Metal Particles

A.V. Osipov[1], A.O. Kucherik[1], S.V. Kutrovskaya[1] and S.M. Arakelian[1]

[1] *Stoletovs Vladimir State University, Vladimir, Russia, 600000,*

E-mail: osipov@vlsu.ru

Metal-carbon materials realize surface-enhanced Raman scattering. Such structures were synthesized using the laser irradiation of colloidal systems consisting of carbon and noble metal nanoparticles. Synthesis of new carbon form is an actual task of modern nanotechnology. Laser methods for the synthesis of nanostructured carbon allows to vary the composition and morphology of the structures obtained according to the experiments conditions. In our experiments, we demonstrate the synthesis of carbyne with the irradiation of the colloidal system obtained during laser ablation of a schungite target in water. Also, adding nanoparticles of noble metals in obtained colloidal system and extra laser irradiation of in results in the producing of metal-carbyne particles (carbon chains anchored by metal nanoparticles). Our experiments suggest that a change in the conditions of exposure (the exposure time and the energy of the impact) by YAG:Nd laser with a pulse duration of 10 ns leads to the controlled formation of metal-carbyne structures.

In our experiments, the proposed method is based on the laser irradiation of colloidal systems consisted of shungite and noble metal (Au and Ag) nanoparticles. Such colloidal system is placed under Yb-fiber laser (1.06 μm) with a pulse duration of 100 ns and a pulse energy of up to 1 mJ, and the process results in the fabrication of LLCC in liquid. The mechanism for that realizes because of the homogeneous symmetry interaction in liquid for the carbon system that stabilizes the linear structure. In this study, we have analyzed the possibility of controlling the properties of fabricated composites by changing the irradiation conditions and the particle concentration in colloid. The laser irradiation of the colloidal system was performed by scanning a focused laser beam (focal spot diameter 5 μm) in a cuvette volume with a scanning speed of 50 μm/s; the total irradiation time was about 15 min.

The Raman spectra (fig. 1) shows the difference between carbyne colloidal system without metal particlles (left) and includung them (right). The peak at 2100-2300 cm^{-1} and 1900-2200 cm^{-1} corresponds to the polyyne chains $(–C\equiv C–)_n$ and commulene chains $(=C=C=)_n$ respectively. The peak at 600-900 cm^{-1} is a mechanical stress in chains. The Raman spectra of the colloidal solution which includes noble metals (right) does not have any peaks near the frequency corresponding to the mechanical stress, the carbyne chains became stabilized by noble metal particles.

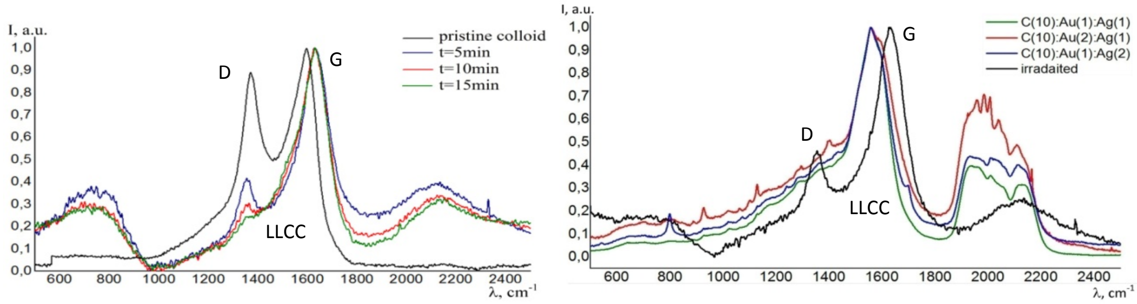

Figure 1. Raman spectra of colloidal system with only carbon chains (left); and colloidal system with carbyne chains stabilized by noble metal particles (right).

The laser with nanosecond pulse duration allows to modify the structure of carbon bonds and creates best conditions for obtaining of linear carbon chains with different hybridization. The obtained structures are planned to be used for the registration of the effect of the SERS with the possibility of the sensitivity control in different areas of the spectra because of the changing of the initial component concentration and morphology

[1] S.M. Arakelyan, V.P. Veiko, S.V. Kutrovskaya, A.O. Kucherik, A.V. Osipov, T.A. Vartanyan., T.E. Itina J Nanopart Res (2016) 18:155. DOI 10.1007/s11051-016-3468-0.

Nanoscale heat transfer in laser interference ablation by ultra-short pulses

Mindaugas Gedvilas, Simonas Indrišiūnas, Bogdan Voisiat, Evaldas Stankevičius, Gediminas Račiukaitis

Center for Physical Sciences and Technology, Savanoriu Ave. 231, LT-02300 Vilnius, Lithuania

mgedvilas@ftmc.lt

Efficient and precise texturing of silicon is a critical process in many applications of modern technologies especially for the fabrication of optoelectronic devices and solar cells. Several techniques are commonly used to pattern the silicon surface such as chemical etching, nano-imprinting, electron beam lithography, reactive ion etching or laser beam patterning. However, all these techniques are time-consuming and hardly acceptable for the real industrial batch production. The patterning speed over large area can be enhanced by using a laser interference ablation (LIA) by ultra-short pulses [1-3]. The principle of LIA is based on the interference of the coherent laser beams which forms a periodically modulated laser intensity pattern which interacts with a material. The laser pulse duration is a critical parameter in the formation of periodic structures with a sub-micron resolution by LIA. The highest spatial resolution of the ultrafine LIA is determined by the nanoscale heat transfer during laser-matter interaction time. However, there is no scientific work dedicated to the fundamental law on how the duration of the laser pulse affects the smallest achievable feature size and spatial resolution of the LIA. The main purpose of this work is to find the analytical equation defining the interference period and laser pulse duration for ultra-fine periodical LIA.

In this research, the simple analytical recipe for choosing duration of the laser pulse for the ultra-fine LIA is presented. A new semi-empirical equation binding the pulse duration, heat diffusion coefficient and thermal modulation depth for a particular structure period was introduced. The equation has been verified by experiments and numerical modelling of LIA (Figure 1).

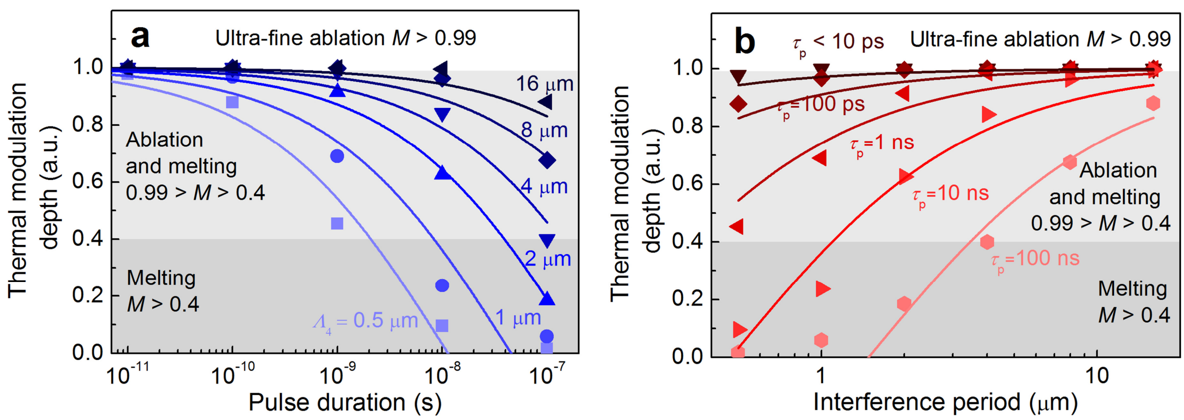

Figure 1: (a) Dependence of the calculated thermal modulation depth M of the periodical thermal field on the silicon surface on laser pulse duration τ_p after the irradiation with the laser interference beam for various interference periods Λ_4. (b) Dependence of the calculated modulation depth M of periodical thermal field on silicon surface on the interference period Λ_4 after irradiation with the laser interference beam for the various pulse durations τ_p. The regions marked with different grey colours represent qualities of LIA: ultra-fine ablation; ablation and melting; melting. Solid lines - fit of the data points by the new semi-empirical equation.

The derived equation is in good agreement with the numerical simulations and experimental results. The developed new method can be used for selecting a laser source with the proper pulse duration for periodical interference structuring with the required spatial resolution.

[1] M. Gedvilas, B. Voisiat, S. Indrišiūnas, G. Račiukaitis, V. Veiko, R. Zakoldaev, D. Sinev, E. Shakhno, Thermo-chemical microstructuring of thin metal films using multi-beam interference by short (nano- & picosecond) laser pulses, Thin Solid Films, vol. 634, pp. 134–140, (2017).

[2] V. Veiko, M. Yarchuk, R. Zakoldaev, M. Gedvilas, G. Raciukaitis, M. Kuzivanov, A. Baranov, Picosecond laser registration of interference pattern by oxidation of thin Cr films, Appl. Surf. Sci., vol. 404, pp. 63–66, (2017).

[3] S. Indrišiūnas, B. Voisiat, M. Gedvilas, G. Račiukaitis, New opportunities for custom-shape patterning using polarization control in confocal laser beam interference setup, J. Laser Appl., vol. 29, pp. 011501, (2017).

Laser manipulation of single-wall carbon nanotubes

Satoru SHOJI
Department of Engineering Science, The University of Electro-Communications
JST, ERATO MINOSHIMA Intelligent Optical Synthesizer (IOS)

1-5-1 Chofugaoka, Chofu, Tokyo 182-8585 Japan
Satoru.Shoji@uec.ac.jp / http://www.phomat.es.uec.ac.jp

We found a phenomenon that, when laser light is tightly focused into aqueous suspension of single-wall carbon nanotubes (SWCNT), SWCNT with a specific diameter could be accumulated into the laser spot [1]. We built a confocal Raman microscopy system to measure the temporal change of Raman spectrum of the suspension from only within the focal volume. We observed a clear increase in one peak of radial breathing mode during laser irradiation at 632.8 nm. This phenomenon can be understood by optical gradient force resonantly generated onto SWCNT exhibiting strong dispersion in dielectric constant to the frequency of the laser. In this presentation we show the result of chirality analysis of our experimental result by Lorentz curve fitting, which implies the possibility that only one specific chirality of SWCNT is preferentially accumulated by a laser light of 632.8 nm. We also show the temporal behavior of Raman spectrum of SWCNT in different circumstances during laser irradiation. According to this result, we developed another configuration using microscale glass capillary to efficiently condense SWCNTs with having a specific chirality [2]. By careful tuning of the wavelength by means of a CW tunable Ti:Sapphire laser, we achieved chirality dependent accumulation of SWCNTs in the capillary. Both methods are based on resonant optical forces acting on SWCNTs. Similar approach was also reported in other nanomaterials such as plasmonic metal particles [3,4]. In the presentation, we also introduce a method to fix SWCNTs into 3D architectures with controlling orientation of SWCNTs[5-7]

This work was supported by JST ERATO Grant Number JPMJER1304, JSPS KAKENHI Grant Nunber JP16H06505 in Scientific Research on Innovative Areas “Nano-Material Optical Manipulation”, and JSPS KAKENHI Grant Number JP16K04972, Japan.

References

1) T. Rodgers, S. Shoji, Z. Sekkat, and S. Kawata, ***Phys. Rev. lett.,*** **101,** 127402 (2008).
2) S. E. Skelton Apesyvtseva, S. Shoji, and S. Kawata, ***Phys. Rev. Appl.,*** **3,** 044003 (2015).
3) S. Ito, H. Yamauchi, M. Tamura, S. Hidaka, H. Hattori, T. Hamada, K. Nishida, S. Tokonami, T. Itoh, H. Miyasaka, and T. Iida, ***Sci. Rep.,*** **3,** 3047 (2013).
4) K. Masui, S. Shoji, K. Asaba, T. Rodgers, F. Jin, X.-M. Duan, and S. Kawata, ***Opt. Express,*** **19,** 22786-22796 (2013).
5) S. Ushiba, S. Shoji, K. Masui, P. Kuray, J. Kono, and S. Kawata, Carbon, **59,** 283-288 (2013).
6) S. Shoji, H. Suzuki, R. P. Zaccaria, Z. Sekkat, and S. Kawata, Phys. Rev. B, **77,** 153407(2008).
7) K. Masui, S. Shoji, K. Asaba, T. Rodgers, F. Jin, X.-M. Duan, and S. Kawata, Opt. Express, **19,** 22786-22796(2011).

Highly transparent and conductive glass electrodes using nanoscale conducting channels

T. H. Lee, B. R. Lee, K. R. Son, J. H. Park, T. G. Kim

School of Electrical Engineering, Korea University, Seoul 136-701, Republic of Korea
tgkim1@korea.ac.kr

There have been considerable efforts to achive highly conductive and transparent electrodes in a wide spectral region from visible to deep-UV (DUV) [1, 2]. However, nobody has provided a solution to this matter bucasue these two properties are mutually exclusive. In this stdudy, we proposed highly transparent and conductive glass electrodes using SiO_2 or AlN thin films with nanoscale conducting channels [3], formed by either DC or AC bias application as a solution, which exhibited high transmittance in the DUV region (over 95 % at 230 nm) and low contact resistance even with a highly resistive p-$Al_{0.4}Ga_{0.6}N$ layer ($\rho_c = 3.2 \times 10^{-2}\ \Omega\cdot cm^2$).

These methods have been applied to various types of materials and photonic devices such as wide-bandgap oxide/metal/oxide multilayers, visible-to-deep UV light-emitting diodes (LEDs), and even micro-LED pixel arrays to verify their usefulness at the device level. Details on the experimental and silulation results in these devices will be presented at the conference.

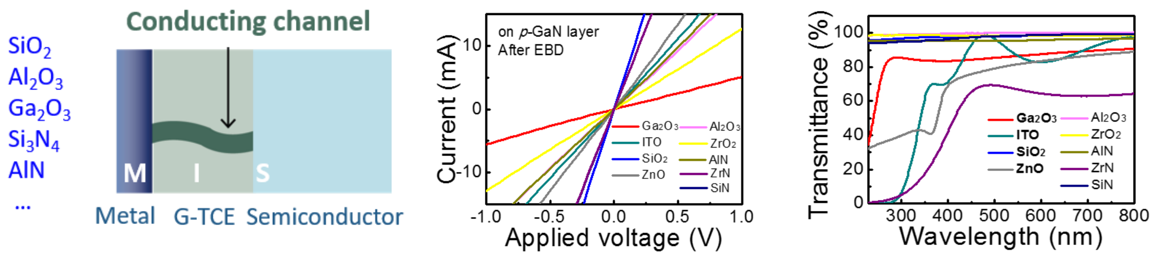

Fig. 1 Conceptual drawing of highly transparent and conductive glass-based transparent electrode (G-TCE) with conducting challel (left). Ohmic behaviors (middle) and optical transmittnace (right) of nine different G-TCE films on p-GaN and quartz substrates, respectively.

[1] B.-J. Kim, M. A. Mastro, J. Hite, C. R. Eddy, J. Kim, *Opt. Express*, 18, 23030 (2010).
[2] H. Wu, D. Kong, Z. Ruan, P.-C. Hsu, S. Wang, Z. Yu, T. J. Carney, L. Hu, S. Fan, Y. Cui, *Nat. Nanotechnol.*, 8, 421 (2013)
[3] T. H. Lee, K. H. Kim, B. R. Lee, J. H. Park, E. F. Schubert, T. G. Kim, *ACS Appl. Mater. Interfaces*, 8, 35668 (2016).

Design of graphene-integrated silicon electro-optic modulators based on isotropic and anisotropic graphene models

Jin-Soo Shin[1], Kwang Hyo Chung[2], Bong Kyu Kim[2], and Jin Tae Kim[2]

1- Department of Electrical Engineering, KAIST, Daejeon 34141, Korea
2-Bio-Medical IT Convergence Research Division, Electronics and Telecommunications Research Institute (ETRI), Daejeon 34129, Korea

jintae@etri.re.kr

Rigorous experimental investigations of graphene-based silicon optical modulators have been performed over the years [1–4]. Moreover, numerous theoretical investigations have been conducted to explain the previous experimental data and to design better devices with an improved performance [5–10]. However, numerical and experimental studies have disagreed, owing to the disagreement over whether graphene is an isotropic or anisotropic material.

In this study, we designed graphene-integrated silicon electro-optic modulators and theoretically investigated their optical characteristics in both isotropic and anisotropic graphene models. Regardless of the graphene model, the optical transmission increases with the chemical potential of graphene because of the Pauli blocking principle. However, we found that the modulator based on the isotropic graphene exhibits an abrupt decrease in transmission for the transverse-magnetic (TM) polarization mode due to the epsilon-near-zero effect in the isotropic graphene at a certain chemical potential. Conversely, the anisotropic graphene-based modulator exhibits no such transmission dip [11].

To further enhance the transmission dip in the isotropic graphene model, we suggest a simply modified modulator structure that increases the transmission depth for the TM polarization mode. To enhance the feasible realization of compact nanoscale photonics-electronics integrated circuits, a silicon electro-optic modulator was designed, based on a graphene-hBN heterostructure. The graphene-hBN structure, with a metal gating cap, is integrated on a silicon optical waveguide. We performed optimization of the key structural parameters to achieve satisfactory modulation characteristics [11].

[1] M. Liu, X. Yin, E. Ulin-Avila, B. Geng, T. Zentgraf, L. Ju, F. Wang, and X. Zhang, Nature, vol. 474, pp. 64–67 (2011).
[2] N. Youngblood, Y. Anugrah, R. Ma, S. J. Koester, and M. Li, Nano Lett., vol. 14, pp. 2741–2746 (2014).
[3] Y. Ding, X. Zhu, S. Xiao, H. Hu, L. H. Frandsen, N. A. Mortensen, and K. Yvind, Nano Lett., vol. 15, pp. 4393–4400 (2015).
[4] Z. Sun, A. Martinez, and F. Wang, Nat. Photonics, vol. 10, pp. 227–238 (2016).
[5] Z. Lu and W. Zhao, J. Opt. Soc. Am. B, vol. 29, pp. 1490–1496 (2012).
[6] J. Gosciniak and D. T. H. Tan, Nanotechnol., vol. 24, p. 185202 (2013).
[7] S. J. Koester and M. Li, IEEE J. Sel. Top. Quantum Electron., vol. 20, p. 6000211 (2014).
[8] J.-S. Shin and J. T. Kim, Nanotechnol., vol. 26, p. 365201 (2015).
[9] J.-S. Shin, J.-S. Kim, and J. T. Kim, J. Opt., vol. 17, p. 125801 (2015).
[10] J. -S. Kim and J. T. Kim, J. Lightwave Technology, vol. 34, pp. 5293-5299 (2016).
[11] B J. Park M. -K. Kim, and J. T. Kim, , J. Korean Phys. Soc. (2017) Accepted.

Exciton-polaritons in nanostructured semiconductors

Chang-Hee Cho

Department of Emerging Materials Science, DGIST, Daegu 42988, South Korea

Semiconductor nanostructures are promising building blocks for coherent light-emitters at the nanoscale, which can be exploited in the fields of nanophotonics, nano-optics and nanobiotechnology. Light-matter interaction between the excitons and the cavity photons could be enhanced in nanostructure geometry because of the enhanced oscillator strength and the reduced mode volume compared to conventional micro-cavities. One of fascinating effects of the light-matter interaction is the low-threshold polariton lasing without the population inversion, resulting from Bose-Einstein condensation of polaritons. Therefore, the polaritons in nanowire cavity could be a key to achieve the low-threshold coherent light-emitters at the nanoscale. The lasing mechanism for various material systems, such as GaAs, CdS, and GaN, has been widely investigated to achieve the polariton lasing from nanowire systems. ZnO nanostructures are one of the best materials for room temperature polariton lasing because of the strong oscillator strength and the large exciton binding energy (60 meV). However, it is still not clear whether the lasing mechanism in ZnO nanostructure at room temperature is attributed to the condensation of polaritons. Also, it is quite difficult to achieve the room temperature polariton lasing in ZnO nanostructures because of several limitations such as the low cavity quality factor and thermal broadening of the exciton resonance at room temperature. In this work, the radial ZnO/MgZnO quantum wells, which could provide the larger oscillator strength and more stable exciton at room temperature, was introduced to achieve the room temperature polariton lasing in ZnO nanorods. The radial quantum well nanorods exhibited the outstanding features, including the thermal stability of polaritons up to the room temperature, ultra-low lasing threshold, and high spectral coherence. The characteristic features of room temperature polariton lasing will be presented.

Laser cataract extraction. Physical aspects and 20 years of clinical experience.

Valentina G. Kopayeva[1], Sergey Yu. Kopayev[1], A V Belikov[2]

1 - *The S. Fyodorov Eye Microsurgery Federal State Institution, Moscow, Russia*
2 - *Saint-Petersburg National Research University of Information Technologies, Mechanics and Optics, St. Petersburg, Russia*

Main author email address: meddv@grv.ifmo.ru

Background: A unique laser cataract extraction (LCE) technology with a high-intensity Nd:YAG laser with wavelength 1.44 μm was developed in IRTC "Eye Microsurgery" (Russia) under supervision of Academician S.N. Fyodorov [1,2]. At present report the results of the analysis of LCE technology on the safety and efficiency parameters was presented. The biological response of highly sensitive cells of the eye and on postoperative clinical and functional data was shown. The criteria for the confirmation of the high level of efficiency and safety of the LCE technology was discussed.
Methods: The laser of "Rakot" complex (Nela Ltd., Russia) as a source of radiation with a wavelength of 1.44 μm (laser-endodissector) was used. Laser radiation was delivered to the eye lens via laser tip - a fragment of a quartz optical fiber with a 450±10 μm core. The laser pulses repetition rate was 20-30 Hz, average laser power - 4±0.5 W, laser pulse duration - 250±50 μs, laser pulse energy was 100-400 mJ. The surgery method - bimanually through two punctures in the cornea. Effective aspiration-irrigation system is of original construction was used. More than 25,000 surgeries in IRTC "Eye Microsurgery" (Moscow, Russia) for the last 20 years were performed.
Results: The experimental data indicate that the surgeon should activate the laser-endodissector only when the distal end of laser tip is in contact with the eye lens surface. The water environment of anterior chamber significantly attenuate the laser energy, so it does not extend beyond the soft part of the epinucleus and the lens capsule ensuring the safe use of this type of radiation in cataract surgery. During clinical application, the negative impact on ocular structures adjacent to the lens (cornea, iris, ciliary body) was not observed. The laser energy does not reach posterior pole. The LCE technology excludes mechanical pressure on the nucleus and zonula stretch either therefore. The LCE technology is effective, safe for treatment of any nucleus density, and preferable when operating patients of elder age and lens subluxation, in complicated cases. There are no restrictions for LCE technology. Post–op clinical and functional outcomes surpass those after ultrasound phacoemulsification. The endothelial cell loss after LCE is twice less in compare with ultrasound phacoemulsification.
Conclusion: 20 years of clinical experience demonstrate that: the Nd:YAG laser with wavelength λ=1.44 μm can be used for safe and efficient extraction of cataract of any density. Ultrasonic and femtolaser analogues available in the world destroy only soft nucleus of the lenses. LCE technology is the "purely" energetic technology enabling to operate on any nucleus density without manual fragmentation. Indications for LCE applications: hard nucleus and complicated cataracts (diabetes mellitus, high myopia, pseudoexfoliative syndrome, lens subluxation, intumescent cataracts etc.).

[1] Fedorov S N, Kopaeva V G, Belikov A V, Erofeev A V, Andreev Yu V 1997 Device for ophthalmic operations *Patent RU 2130762*
[2] Fedorov S N, Kopaeva V G, Belikov A V, Erofeev A V, Andreev Yu V 1998 Device for ophthalmic operations *Patent RU 2157158*

PHOTODITHAZINE - AMPHIPHILIC POLYMER COMPLEXES IN ANTIMICROBIAL PHOTODYNAMIC THERAPY OF MODEL WOUNDS IN RATS

Anna B. Solovieva[1], Tatiana G. Rudenko[2], Anatoly B.Shehter[2], Nadezda N. Aksenova[1], Nicolai N. Glagolev[1], Aleksandr L. Spokoiny[3], Serge F. Timashev[1]

1- N.N. Semenov Institute of Chemical Physics RAS, Moscow, Russia
2 - First Moscow State Medical University, Moscow, Russia
3 – State Research and Clinical Center of Laser Medicine, Moscow, Russia

ann.solovieva@gmail.com

Photodynamic therapy is one of effective methods for treating a number of malignant tumors, used since the 60-ies. In recent years, PDT was successfully used in the treatment of inflammatory processes in purulent surgery as well as in stomatology, ophthalmology, etc [1].
Evolution PDT methods associated with the creation of new types of photosensitizers with improved bioavailability and reduced non-specific toxicity.
Previously, the authors of this work for the first time used the complexes of photosensitizer with amphiphilic polymers (AP) at PDT of tumors in rats [2].
It has been found that in the presence of AP the activity of photosensitizers in PDT of tumors and gunshot wounds in laboratory animals is increased several times.
The creation of new types of antimicrobial photosensitizers for photodynamic therapy is impossible without elucidating the mechanisms of action their influence on the process of wound healing. However, despite the growing interest in the issue and the appearance of first positive clinical experience reports, there is practically no morphological and pathophysiological substantiation for the PDT of wounds and burns using photosensitizers modified with amphiphilic polymers.
The objective of this work was an experimental morphological study of the specific features of the early stage of the wound healing process in the case of laser PDT with use the photosensitizer Photoditazin (chlorin e6 diglutamic salt) and its complexes with amphiphilic polymers of different nature. In the present work, we analyze effects of Photoditazin, an e6 chlorine derivative, and its complexes with amphiphilic polymers on the early stage of wound healing in a rat model. A skin excision wound model with prevented contraction was developed in male albino rats divided into groups according to the treatment mode. All animals received injections of one of the studied compositions into their wound beds and underwent low intensity laser irradiation. The clinical monitoring and histological examination of the wounds were performed. It has been found that all the Photoditazin formulations have significant effects on the early stage of wound healing. The superposition of the inflammation and/or regeneration is the main difference between groups. The aqueous solution of Photoditazin alone induced a significant capillary hemorrhage, while its combinations with amphiphilic polymers did not. The best clinical and morphological results were obtained for the Photoditazin-Pluronic F127 composition. Compositions of Photoditazin and amphiphilic polymers, especially Pluronic F127, probably have a great potential for therapy of wounds. Their effects can be attributed to the increased regeneration and suppressed inflammatory changes at the early stages of repair. In particular, to attain these objectives, it has been suggested that complexes composed of photosensitizers and amphiphilic polymers differing in nature, such as polyoxyethylene, polyvinylpyrrolidone, Pluronic F127 and polyvinyl alcohol, should be used for the PDT purposes. In experiments with other polymers forming complexes with photosensitizers, positive biological effects were also noted.

1. Hamblin, M.R. and Hasan, T. (2004) Photodynamic therapy: a new antimicrobial approach to infectious disease? Photochem. Photobiol. Sci. **3**, 436–450.
2. RF Patent 2314606, 2008.

The work is kindly supported by Russian Scientific Foundation (grant 16-13-10295).

Optical-Spectroscopic Investigation of Nanoparticles Interaction with Animal Skin *In-Vitro*

N. Ali[1], M. Kinnunen[2], E. Perevedentseva[3,4], A. Karmenyan[3], A.-I-Ahmed[3], S. Vainio[1], I. Meglinski[2], C.-L. Cheng[3]

1- Biocenter Oulu, Oulu, Finland
2- Opto-Electronics and Measurement Techniques Research Unit, University of Oulu, Oulu, Finland
3- Physics Department, National Dong Hwa University, Hualien, Taiwan
4- P.N. Lebedev Physics Institute of Rus Acad Sci, Moscow, Russia

elena@gms.ndhu.edu.tw

Resent development of nanoparticles' (NPs) bio-applications implies the NPs interaction with living organism and its parts and needs in corresponding investigations [1, 2]. NPs can enter the body by various ways, particularly, transdermal one. NPs' interaction with skin can involve different mechanisms on tissue- and cellular levels. Non-invasive optical-spectroscopic methods are developed for use in bio-medical studies to obtain comprehensive information about NP interaction with animal skin [3].

Among the other NPs, nanodiamonds (NDs) attract interests in bio-medical research due to their physical and chemical properties. The effects of NDs on cells, tissues, organs, and organisms are widely studied using different methods in terms of nano-safety and bio-medical applications [4]: ND's optical-spectroscopic properties are demonstrated applicable for different methods of bio-imaging [4]; surface properties can be used for controlled drug delivery; as for interaction with skin, NDs have been shown attenuating UV radiation through absorption and scattering [5] and can be considered as potential sunscreen candidate. Our main focus is to analyze the penetration, distribution, and effects of NDs with different size and surface properties (carboxylated [6], hydrogenated [7]) and NDs complex (combined with bovine serum albumin (BSA), prepared accordingly [6]), on the murine skin. The methods of optical coherence tomography (spectral-domain OCT, Thorlabs Inc., USA), fluorescence confocal imaging with microscope TCS SP5 (Leica, Germany) and two-photon imaging and fluorescence lifetime imaging (FLIM) at excitation by Ti-sapphire laser (Coherent, USA) with wavelength 800 nm, at pulse duration 140 fs, repetition rate 80 MHz are used for the analysis. The skin samples have been prepared accordingly [8]. All the mice experiments were conducted in accordance with the Finnish national legislation, the European Convention (ETS 123), and the EU Directive 86/609/EEC.

The detecting NDs fluorescence and alteration of scattering properties of the skin significant ND penetration into skin has been observed. ND's applicability for imaging and delivery tracing as fluorescent marker and as OCT contrast agent is demonstrated. Used methods allow analyzing the influence of surface properties and modification. ND with adsorbed BSA is demonstrated like model system for further studies of intradermal drug delivery.

Acknowledgements: The authors appreciate the financial support of this research by grant of Academy of Finland (297542) and the Ministry of Science and Technology of Taiwan, Grant No. MOST 103-2112-M-259-001-MY3

[1] W.J. Stark, Nanoparticles in biological systems, Angew.Chem. 50, 1242-1258 (2011).
[2] S. Barua, S. Mitragotri, Challenges associated with penetration of nanoparticles across cell and tissue barriers: A review of current status and future prospects, Nano Today 9, 223-243 (2014).
[3] M. Schneider, F. Stracke, S. Hansen, U. F Schaefer. Nanoparticles and their interactions with the dermal barrier. Dermatoendocrinol. 1(4), 197-206 (2009).
[4] V.N. Mochalin, O. Shenderova, D. Ho, Y. Gogotsi, The properties and applications of nanodiamonds, Nat. Nanotech. 7, 11-23 (2012).
[5] O.Shenderova, V.Grichko, S. Hens, J.Walch, Detonation nanodiamonds as UV radiation filter, Diam. Relat.Mater. 16, 2003-2008 (2007).
[6] P.H. Chung, E. Perevedentseva, J.S. Tu, C.C. Chang, C.L. Cheng, Spectroscopic study of bio-functionalized nanodiamonds, Diam. Relat. Mater. 15, 622-625 (2006).
[7] A.-I- Ahmed, S. Mandal, L. Gines, O. A. Williams, C.-L. Cheng. Low temperature catalytic reactivity of nanodiamond in molecular hydrogen. Carbon 110, 438-442 (2016).
[8] K.B. Jensen, R.R. Driskell, F.M. Watt, Assaying proliferation and differentiation capacity of stem cells using disaggregated adult mouse epidermis, Nat. Protocols 5, 898-911 (2010).

PHOTON DENSITY NORMALIZED MAXIMUM MOVEMENT IN SOFT BIOLOGICAL TISSUE CONSIDERING TURBID MEDIA DEFORMATION

A.Yu. Potlov, S.V. Frolov, S.G. Proskurin

Biomedical Engineering, Tambov State Technical University
Sovetskaya 106, Tambov, Russia
zerner@yandex.ru

Near infrared optical irradiation which is used in Diffuse Optical Tomography (DOT) is diffusely transmitted through a biomedical object. It carries useful information about the object's optical properties and spatial distribution of them. Quantification and mapping of tissue optical properties based on this information requires solving forward and inverse problems of light propagation in highly scattering objects.

Source and detection fibers of a DOT system should be in a tight contact with investigated area to provide an accurate detection of diffusely transmitted photons, and reduce the loss of the signal. At the same time, compression plates or, in our case, elastic bracelet, lead to deformations of the tissue [1]. As the mechanical properties of the tissue can significantly affect the quality of image reconstruction in DOT [2], the image artifacts, caused by the discrepancy between the actual boundaries of the investigated object and its mathematical model can occur [1, 2]. This problem usually appears when the investigated object consists mainly of a soft tissue [2].

In this study, the influence of deformations on the optical properties and photon density distribution is numerically simulated using diffusion approximation to the radiative transfer equation. Biological tissue also is simulated as a linear isotropic pseudo-incompressible medium [1, 2].

There are few regularities of the Photon Density Normalized Maximum (PDNM) movement in a conical object have been found out based on the computer simulations (Fig. 1). This let us to evaluate the influence of deformation along with optical properties change inside the object on the photon density distribution and attenuation, and will be useful for solving DOT inverse problem [3]:

1) Independently on the values of the absorption and scattering, PDNM moves toward to the geometric center of the object in the deformed and undeformed states;

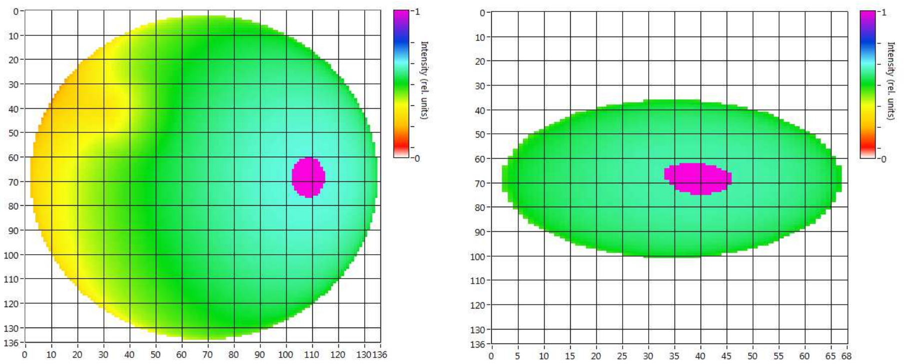

(a) (b)

Figure 1 Photon density distributions in the slice of the undeformed (a) and the deformed (b) conical inhomogeneous object with a spherical scattering inhomogeneity inside of it after the injection of the light pulse (t=0.7 ns).

2) In presence of a scattering inhomogeneity, PDNM moves to the center of it regardless of the deformation;

3) In the undeformed object radiation intensity decay is about 8-10% higher than in the deformed one.

[1] H. Dehghani, S. Srinivasan, B. Pogue, A. Gibson, Numerical Modelling and Image Reconstruction in Diffuse Optical Tomography, Phil. Trans. R. Soc. A, Vol. 367, pp. 3073-3093 (2009).

[2] A.Yu. Potlov, T.I. Avsievich, S.V. Frolov, S.G. Proskurin, Computational Biomechanics for Medicine (Springer International Publishing, editors G. Joldes, B. Doyle, A. Wittek, P. M. F. Nielsen, K. Miller), Forward Problem of Time-Resolved Diffuse Optical Tomography Considering Biological Tissue Deformation (2016).

[3] A. Yu. Potlov, S. V. Frolov, S. G. Proskurin, Localization of Inhomogeneities in Diffuse Optical Tomography Based on Late Arriving Photons, Optics and Spectroscopy, Vol. 120, pp. 9 – 19 (2016).

NIR fluorescence imaging methods to evaluate blood flow state in the skin lesions

P.V. Grachev[1], Z.N. Abdulvapova[2], V.I. Makarov[1], G.R. Galstyan[2], V.B. Loschenov[1]

[1]General Physics Institute of RAS, Moscow, 119991, Russian Federation
[2]Endocrinology Research Centre, Moscow, 117036, Russian Federation
p.v.grachev@gmail.com

Introduction.
NIR fluorescence imaging methods have great advantages. They are fast and noninvasive. Using NIR photosensitizers, such as indocyanine green (ICG), it is possible to evaluate blood flow in real time. These methods find their application in problems of engraftment of skin grafts [1] and in the evaluation of the severity of peripheral arterial disease during indocyanine green fluorescence angiography procedure (ICGA) [2].

Materials and Methods.
Irradiation and registration of fluorescent images and video was performed using video system that consists of a 785-nm laser diode, a broadband source diode, a beam splitter with a dichroic mirror and two digital CMOS cameras for recording color and luminescence images.
The principle of fluorescence imaging used in ICGA is simple: illuminate the tissue of interest with laser and broadband light, and observing it at longer emission wavelengths (810-850nm) with cameras.
Condition of blood flow in the autografts was assessed by analysing the recorded fluorescent images fluorescent dyes that absorb in the red and near-infrared spectral range for deeper penetration of light into the skin.
ICGA was performed in 4 diabetic patients with limb ischemia and foot ulcers. To evaluate the soft tissue perfusion of the foot diabetic patients via FAG the following parameters have been used T_{0m} - time to reach maximum intensity after intravenous administration of the ICGA; T_{Im}- the onset of maximum intensity with the appearance of the ICGA in the area of interest; I_m - the level of the maximum intensity. Region of interest: near wound area of the foot.

Results.
Fluorescence images show the spread of ICG in skin tissue. The degree of the formation of new blood vessels can be evaluated by intensity of fluorescence.
There were not any adverse reactions during ICGA procedure. Data from all ROI with different ICGA parameters was collected. There were difference in T_{0m} and T_{Im} in different ROI more than 10 sec.

Acknowledgement. This work was supported by a grant RFBR # 15-29-04869-ofi-m

References.

[1] Washington Y. Sanchez , Michael Pastore, Isha N. Haridass, Karsten König, Wolfgang Becker, Michael S. Roberts, *Chemical Physics* Vol.111(2015) p.457
[2] Terasaki H. et al, *Annals of vascular surgery* Vol.27 (2013) p.1154

Experimental modeling of local laser hyperthermia using thermosensitive nanoparticles absorbing in NIR

Grachev P.V.[1], Romanishkin I.D.[1], Pominova D.V.[1], Burmistrov I.A.[1], Kaldvee K.[2], Sildos I.[2], Vanetsev A.S.[1], Orlovskaya E.O.[1], Orlovskii Yu.V.[1], Loschenov V.B.[1], Ryabova A.V.[1]

1- Prokhorov General Physics Institute, Russian Academy of Sciences, Vavilov Str., 38, Moscow, 119991, Russia
2- Institute of Physics, University of Tartu, Ravila 14c, Tartu 50411, Estonia

nastya.ryabova@gmail.com

Until now, the method of local laser hyperthermia has not been introduced into clinical practice because of the difficulty to control the uniformity of volumetric warming of the tumor, the lack of a technical solution that allows the hyperthermia procedure to be performed automatically without complicated calculations of temperature fields and attracting the support of highly qualified technical personnel [1]. The paper presents a complex approach to precise controlled laser hyperthermia, which minimizes the risk of insufficient exposure and overheating in the volume of the tumor, and, accordingly, continued malignant growth and necrotic lesions.
The theoretical modeling of the excitation radiation parameters for the effective hyperthermia in biological tissue using a thermosensitive nanoparticles LaF_3:Nd(1%)@$DyPO_4$ (NPs) [2] is performed. When irradiating with a continuous laser irradiation at 805 nm even at power density of 1 W/cm^2 without cooling a superheat of the surface (T=50˚C) is observed. The solution to the problem of surface overheating is the use of a cooling device. At a power density of laser irradiation at 3 W/cm^2 the cooling with the temperature of cooler 10°C is enough to avoid overheating.
The experimental modeling was performed on phantoms of biological tissues. The part of the phantom simulating the neoplasm was a cylinder 0.5 cm in height and 1 cm in diameter and contained NPs (at a concentration from 0 to 10 mg/l). Experimental dependences of backward diffuse scattering and a luminescent signal were obtained upon excitation by a continuous laser at 805 nm with a power from 0.8 to 4 W, and with an area of the illuminated surface of 0.8 cm^2. For spectra detection Raman-HR-TEC (StellarNet, USA) spectrometer was used. Additionally, the monitoring of the heating of phantoms was performed by a thermometric infrared camera JADE MWIR SC7300M (CEDIP, France). The luminescence spectra of NPs were obtained at 800-1000 nm spectral range with 805 nm laser excitation ($^4F_{5/2}$ Nd^{3+} level) at different temperatures fixed by a thermostat. Local heating of NPs calculated from spectral data were compared with a simultaneous infrared camera measurement.
The maximum relative change in the average heating temperature of the phantom containing the investigated NPs (1 cm depth from the surface) recorded by the IR thermocamera was 7˚C at a power density of 1.7 W/cm^2. The heating of phantoms that do not contain NPs is negligible, the maximal value is 2˚C. The maximum relative change in the NPs temperature in the phantom, calculated from the Nd^{3+} luminescence spectra, was 17˚C for a depth of 5 mm and 9˚C for a depth of 7 mm at a laser power density of 1.3 W/cm^2.
Comparing the results obtained with the IR thermocamera and the spectroscopic method, it can be concluded that the temperature values obtained by the former are significantly underestimated and can be used only to estimate the heating temperature of the medium as a whole. The spectroscopic method makes possible to estimate the immediate heating temperature of the NPs and their nearest microenvironment.
This work was supported by MES RF: RFMEFI61615X0064.

[1] P. Saccomandi, E. Schena, S. Silvestri, Techniques for temperature monitoring during laser-induced thermotherapy: An overview, International Journal of Hyperthermia, vol. 29, issue 7, pp. 609-619 (2013).
[2] K. Kaldvee, A. Nefedova, S. Fedorenko, A.S. Vanetsev, E.O. Orlovskaya, L. Puust, M. Pärs, I. Sildos, A.V. Ryabova, Yu.V. Orlovskii, Approaches to contactless optical thermometer in the NIR spectral range based on Nd^{3+} doped crystalline nanoparticles, J. Lumin vol. 183, pp. 478-485, (2016).

Multifunctional imaging with polarization-sensitive optical coherence tomography for monitoring wound healing

Kwan Seob Park[1], Woo June Choi[2], Shaozhen Song[2], Jingjiang Xu[2], Ruikang J. Wang[2], and Tae Joong Eom[1]

1- Advanced Photonics Research Institute, Gwangju Institute of Science and Technology, 123 Cheomdan-gwagiro, Gwangju 61005, South Korea
2- Department of Bioengineering, University of Washington, Seattle 98195, WA, USA

E-mail: ganseobi@gist.ac.kr

We demonstrate multifunctional in vivo imaging for monitoring wound healing using a swept-source based polarization-sensitive optical coherence tomography (SS-PS-OCT). First, a 1-mm-diameter wound is generated in the mouse pinna using a complete biopsy punch and the wound site is monitored at intervals of one week over a month. Three complementary images indicating the changes in anatomical, vascular, and birefringent information of tissue around the wound are simultaneously provided from a 3D PS-OCT data set during the wound healing. Specifically, inflammatory and proliferative phases of wound healing process are characterized by thickened epidermal tissues (from OCT images) and angiogenesis (from OCT angiography images) around wound, respectively. Also, it is observed that the regenerating tissues have highly realigned birefringent structures (from PS-OCT images). Our initial finding suggests that this versatile imaging modality has great potential for understanding vascular and tissue responses to injury.

This work was supported by the GIST Research Institute (GRI) in 2016, the industrial technology innovation program (10063062), and the industrial strategic technology development program (10063364) of the Ministry of Trade, Industry & Energy of Korea.

Application of laser scanning confocal fluorescent microscopy for visualization of erythropoietin receptors in mouse local cerebral ischemia

M. Glyavina[1,2], P. Loginov[2], V. Dudenkova[1,2], M. Muraveva[1], E. Klyuev[2], N. Prodanets[2], A. Dyagtereva[2] and I. Mukhina[2]

1- Department of neurotechnology, Institute of biology and biomedicine, Nizhny Novgorod State University, Russia, Nizhny Novgorod, Gagarin Avenue 23-1
2- Central Scientific Research Laboratory of the Nizhny Novgorod State Medical Academy, Russia, Nizhny Novgorod, Gagarin Avenue 70-2

mariyannov@gmail.com

Ischemic stroke is one of the most frequent causes of death and disability of patients. At present, drugs mainly aimed at minimizing the consequences of a stroke are intensely developed. The objective of this work is to study the effect of erythropoietin receptor activation (EPOR) for promising ischemic therapy. At the moment, one of the new lines in the development of neuroprotection methods in a stroke is to use a β- common receptor subunit (β-cR) with EPOR as a therapeutic target. Laser radiation is used to image the receptors for heterodimer erythropoietin (EPOR). EPOR locate in erythropoietic cells and also in brain cells. When the receptor is connected to erythropoietin, this triggers two types of reactions, namely, a positive one, which activates the protective mechanisms of damaged neurons, and a negative one, which is caused by the increasing number of erythrocytes, resulting in re-formation of a thrombus and a rise in blood pressure [1]. Therefore, some erythropoietin derivatives are able to protect neurons from ischemic damage, ignoring hemopoiesis, which prevents the increase in hematocrit. Approximately 80% of the thrombotic or thromboembolic strokes occur in the middle cerebral artery. Thus, a model of transient occlusion of the middle cerebral artery (tOCMA) [2] was used to study the stroke pathogenesis mechanism The report presents the results of studying the EPOR distribution in the somatosensory cortex of the mouse brain in the postischemic period based on the tOCMA model.

For this experiment, we use C57BL/6 mice. Surgery has been made using a binocular microscope and under isoflurane anesthesia. One-hour exposure was proceeded by a 7-0 microfilament from Doccol Corporation. The localization and volume of the damage is determined through an Agilent Technologies DD2-400 9.4 T (400 MHz) tomograph. Brain is fixed in 4% paraformaldehyde (PFA). EPOR are marked by primary antibodies to the Anti-EPO Receptor Rabbit polyclonal and by secondary fluorescent antibody AlexaFluor 555. Nucleus are marked by DAPI (4′,6-Diamidine-2′-phenylindole dihydrochloride). Visualization is carried out by a ZEISS LSM 880 laser scanning confocal fluorescents microscope with an 40x immersion objective and a yellow-green spectrum filter. Paraffin coronal sections of the brain are studied at a depth of 1.7 mm from the Bregma suture. The sections are 5 μm thick. The images are processed using ImageJ software.

The mouse brain is studied in the 10th day after the ischemia. Long-term memory in the "conditioned reflex of passive avoidance" test is restored for the group with active EPORs. Simultaneously, associative learning in the "study of a new object" test improves the results. However, the volume of ischemic damage in the groups with active EPORs remained almost the same. Activation of EPORs result a trend towards increasing the amount of EPOR in the hemisphere with ischemic damage. The situation was opposite in the healthy hemisphere and at the same site in the brain of the intact mouse.

Thus, the results demonstrate the possibility of using the heterodimer EPORs activation as a promising strategy for the treatment of an ischemic stroke.Visualization of the EPOR at the cellular level (for example, neurons, astrocytes, and microglia) can be provided with Stochastic optical reconstruction microscopy (STORM). Visualization in vivo experiments with two-photon microscopy showed the distribution of EPOR in depth also. It can help understand the role of the erythropoietin receptors in restoring the central nervous system after ischemia.

[1] R.T.Mallet, M.G.Ryou. Erythropoietin: Endogenous Protection of Ischemic Brain. Vitam Horm.,105, 197-232, (2017),

[2] J.Koizumi, Y.Yoshida, T.Nakazawa. Experimental studies of ischemic brain edema: a new experimental model of cerebral embolism in rats in which recirculation can be introduced in the ischemic area. Stroke Jpn J., 8, 1-8, (1986).

On the Possibility of Developing a Quasi-CW High-Power High-Pressure Laser on 4p–4s Transition of ArI with Electron-Optical Pumping

A.A. Ionin, **I.V. Kholin, A.Yu. L'dov, L.V. Seleznev, N.N. Ustinovskii, and D.A. Zayarnyi**

Lebedev Physical Institute, Leninsky prospect 53, 119991 Moscow, Russia
e-mail: aion@sci.lebedev.ru

Quite recently a high-pressure He–Ar laser on Ar atomic transition $4p[1/2]_1 - 4s[3/2]_2^o$ with wavelength of 912.3 nm with combined pumping was launched [1]. In such a laser, pumping of the upper laser level is performed in a two-step process. At the first stage, a sufficient density of $4s[3/2]_2^o$ metastable Ar states is produced by conduction electrons in high-current electric discharge plasma. In the second stage, a population inversion on the laser transition is formed in accordance with the classical three-level scheme due to optical excitation of higher-lying $4p[5/2]_3$ level by a semiconductor laser at wavelength of 811.5 nm and subsequent collisional quenching to $4p[1/2]_1$ upper laser level.

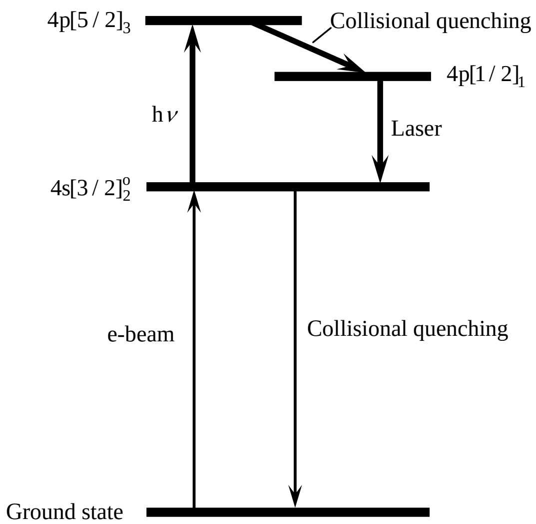

Fig. 1. Schematic of combined e-beam (thin arrow) and optical pumping (thick arrow).

In paper [1], application of a pulsed electric discharge was a principal matter for lasing, since $4s[3/2]_2^o$ metastable state of argon is collisionally quenched in the active medium with formation of excimer molecules, whereas long lasting pumping of these states from the ground state by the electric discharge is limited by the development of ionization instability leading to rapid discharge contraction. To bring into action a quasi-cw operation, in this presentation we propose to create and maintain the necessary density of excited metastable atoms in the active medium during a required time by a fast electron beam (Fig. 1) in the way similar to the electro-ionization pumping [2]) but applying the optical pumping instead of an electrical field. Our estimates demonstrate that such an electron-optical pumping can increase both the lasing duration and active laser volume and, consequently, substantially elevate the laser output.

This research was supported by the Russian Foundation for Basic Research (Project 17-02-00241).

1. J. Han and M. Heaven. Kinetics of optically pumped Ar metastables. *Opt. Lett.* **39**, 6541–6544 (2014).
2. N.G. Basov, V.V. Baranov, A.Yu. Chugunov, V.A. Danilychev, A.Yu. Dudin, I.V. Kholin, N.N. Ustinovskii, D.A. Zayarnyi. 60 J quasistationary electroionization laser on Xe atomic metastables. *IEEE J. Quant. Electron.*, **QE-21** (11), 1756–1760 (1985).

Quenching of 4s ($^3P_2$) Lower Laser Level of the Laser on 4p–4s Transition of ArI with Electron-Optical Pumping

A.A. Ionin, I.V. Kholin, A.Yu. L'dov, N.N. Ustinovskii, D.A. Zayarnyi

Lebedev Physical Institute, Leninsky prospect 53, 119991 Moscow, Russia
e-mail: aion@sci.lebedev.ru

A new approach of the development of a quasi-cw high-pressure He-Ar laser on argon atom transition $4p[1/2]_1 - 4s[3/2]_2^o$ at wavelength of 912.3 nm with combined pumping was proposed in [1]. The new approach consists in accomplishment of two-stage electron-optical pumping, firstly, in applying fast electron beam to produce and maintain a necessary density of excited metastable states $4s[3/2]_2^o$ of argon; secondly, in employment of a laser diode pump radiation to form population inversion on the laser transition using a classical three-level scheme, namely, by optically pumping from $4s[3/2]_2^o$ level to higher-lying level $4p[5/2]_3$ and subsequent collisional quenching to $4p[1/2]_1$ upper laser level.

To estimate an efficiency of the proposed scheme before carrying out a complicated experiment, it is necessary to know, in particular, rate constants of the collisional plasma-chemical reactions in He-Ar mixtures, but relevant literature data are currently practically absent. This presentation is the first step in this direction and deals with the collisional quenching of the $4s[3/2]_2^o$ lower laser level in reactions:

$$\mathrm{Ar}(4s[3/2]_2^o) + \mathrm{He} + \mathrm{Ar} \rightarrow \mathrm{Ar}_2^* + \mathrm{He}, \quad (1)$$

$$\mathrm{Ar}(4s[3/2]_2^o) + 2\mathrm{He} \rightarrow \mathrm{HeAr}^* + \mathrm{He}, \quad (2)$$

$$\mathrm{Ar}(4s[3/2]_2^o) + \mathrm{He} \rightarrow \mathrm{Products} + \mathrm{He}. \quad (3)$$

He–Ar mixtures excited by a beam of fast electrons were studied. Measurements of the reaction rate constants were performed by the method of absorption probing based on the dependences of the decay rate of $4s[3/2]_2^o$ state on the total pressure and concentration ratio between the working and buffer gas. For this purpose, in the afterglow arising under an action of a high-power beam of fast electrons, the absorption time behavior of a probing light pulse at the wavelength of 912.3 nm (the lasing wavelength of the discussed He–Ar laser) was recorded. A unique broadband light source served as a source of probe signal with a pulse duration of ~30 μs in conjunction with high-aperture monochromator. In detail, this measurement procedure was described in [2].

Reaction	Measured rate constant
(1)	$(3.6 \pm 0.4)\times10^{-33}$ cm^6/s
(2)	$(4.4 \pm 0.9)\times10^{-36}$ cm^6/s
(3)	$(2.4 \pm 0.3)\times10^{-15}$ cm^3/s

The measurements demonstrated for the rates of collisional quenching of the state under study to be low being considerably inferior to the rates of similar processes in the mixtures of other inert gases measured in [2]. This circumstance does indicate that production and maintenance of the necessary amount of argon atoms in $4s[3/2]_2^o$ state is feasible at very moderate current densities of pumping electron beam.

This research was supported by the Russian Foundation for Basic Research (Project 17-02-00241).

1. A.A. Ionin, I.V. Kholin, A.Yu. L'dov, L.V.Seleznev, N.N. Ustinovskii, D.A. Zayarnyi. On the possibility of development of a quasi-cw high-power high-pressure laser on 4p–4s transition of ArI with electron-optical pumping, *ALT'17 Conference, Book of Abstracts, 10-15 Sept 2017, Busan, Korea.*
2. I.V. Kholin, A.Yu. L'dov, N.N. Ustinovskii, D.A. Zayarnyi. Quenching of metastable 5s'($^3P_0$) krypton atoms in collisions with krypton and argon atoms in high-pressure laser mixtures. *Journal of Russian Laser Research*, **36** (1), 74–80 (2015).

Eco-friendly reduction of graphene oxide by polyphenol extracts

Su Hyeon Go[1], Young-Kwan Kim[1*]
(List of authors in 11point, centred and bold: the presenting author underlined)

1- Carbon Composite Materials Research Center, Institute of Advanced Composite Materials, Korea Institute of Science and Technolgy, San 101, Eunha-ri, Bongdong-eup, Wanju-gun, Jeollabuk-do, 565-905, Korea

youngkwan@kist.re.kr

Graphene is a two-dimensional (2D) honeycomb lattice material consisting of single layer of sp^2carbon atoms. The graphene's unique structure and properties have attracted a great deal of interest. Graphene has superior electrical, mechanical, thermal and optical properties. There are various methods to make graphene such as mechanical exfoliation, liquid phase exfoliation, chemical vapor deposition (CVD) and thermal decomposition on SiC.Although these methods provide high quality graphene, they are expensive and not compatible with large-scale production. In this regard, the chemical oxidation and exfoliation of graphite is promising strategy to synthesize graphene oxide (GO) and the GO can be readily reduced by chemical reductants to convert GO into reduced GO (RGO), graphene analogue.[1]Therefore, it is an urgent issue to devise an eco-friendly reduction strategy for the synthesis of water dispersible RGO because the general reducing agents such as hydrazine and sodium borohydrate are toxic and harmful, and lead to immediate aggregation of RGO due to strong π-π interaction.[2] Herein, we investigated the eco-friendly reduction of GO to synthesize water dispersible RGO by using polyphenolswhich are known as natural anti-oxidants. The reduction process was confirmed by using UV-visible, X-ray photoelectron, Fourier-transform infrared (FT-IR) and Raman spectroscopies.

[1] Songfeng Pei, Hui-Ming Cheng , The reduction of graphene oxide , Carbon,50,93210-3228, (2012)
[2] Young-Kwan Kim, Mi-Hee Kim and Dal-Hee Min, Biocompatible reduced graphene oxide prepared by using dextran as amultifunctional reducing agent, Chem.Commun, 47, 3195-3197, (2011).

Adaptive interferometer based on spectral multiplexing of dynamic holograms in PRC

R.V. Romashko[1,2], **M.A. Asalkhanova**[2]

1- School of Natural Sciences, Far Eastern Federal University, 10 Ajax Bay, Russky Island, Vladivostok, Russia, 690091

2- Laboratory of Precision Optical Measurement Techniques of Institute of Automation and Control Processes FEB RAS, 5 Radio St., Vladivostok, Russia, 690041

romashko@iacp.dvo ru

An adaptive holographic interferometer using laser radiation with two and more spectral components is presented. Multicomponent laser radiation records a set of dynamic holograms in photorefractive CdTe:V crystal (the number of holograms corresponds to the number of spectral components). Adaptive interferometer based on a theoretical model describing the process of dynamic holograms recording by multispectral radiation [1]. Interaction of the reference and signal waves of the interferometer on each recorded holograms provides the phase demodulation [2]. Presented interferometer is attractive for monitoring dynamic strains because it is adaptive and spectral multiplexable. Adaptivity implies that interferometer could selectively monitor dynamic strains without active compensation of large quasi-static strains and large temperature drifts that otherwise would leads to the drift of interferometer operating point. At the same time, spectral multiplexability allows using several sensors without crosstalk.

As the multispectral source the radiation of three Fiber Bragg Grating laser diodes with wavelength 1050, 1060 and 1070 nm mixed by fiber couplers is used. The set of dynamic holograms were recorded in CdTe:V crystal in orthogonal geometry. Figure 1 demonstrates the oscillograms illustrated the simultaneous operation of 2 channels at wavelength of 1060 and 1070 nm.

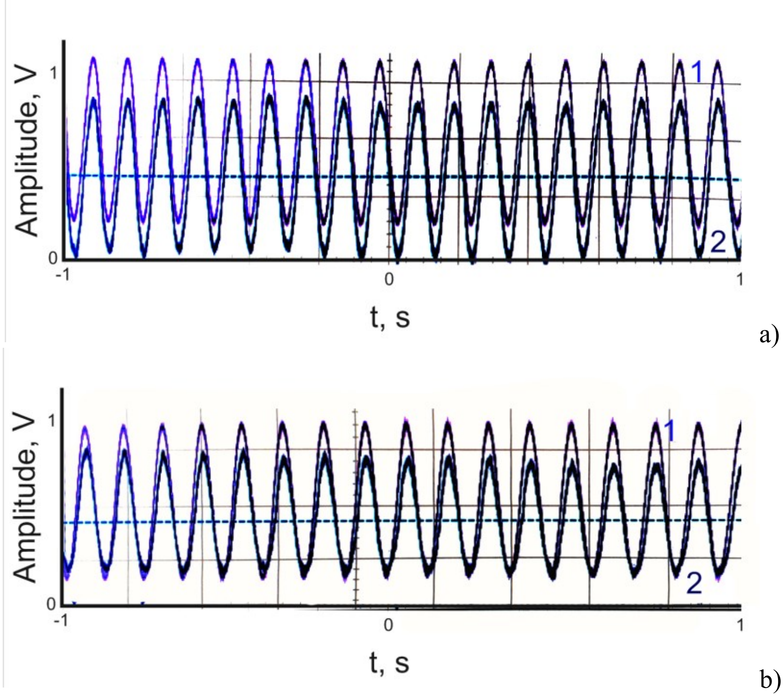

Figure 1. The oscillograms illustrated the simultaneous operation of 1st channel (at wavelength 1060 nm) and 2nd channel (at wavelength 1070 nm): 1 – drive voltage, 2 – output signal in the adaptive interferometer channels

[1] R. V. Romashko, M. A. Asalkhanova, Y. N. Kulchin. “Polychromatic Two-wave Mixing in a Cubic Photorefractive Crystal” Physics Procedia, vol. 86, pp. 155-159 (2017)

[2] A. A.Kamshilin, R. V. Romashko, Y. N. Kulchin. “Adaptive interferometry with photorefractive crystals,” J.Appl. Phys., vol.105, No.3, pp.031101 (2009)

Calculation of the Wide-band Laser Beams Amplification in the Yb:YAG Thin-Rod Active Elements

I.I. Kuznetsov[1], I.B. Mukhin[1], O.V. Palashov[1], O.L.Vadimova[1], G.H. Kim[2], B. Lee[2], S.A. Chizhov[2], E.G. Sall[2]

1- Institute of Applied Physics of the Russian Academy of Sciences, 46 Ul'yanov street, 603950, Nizhny Novgorod, Russia

2 – Korea Electrotechnology Research Institute, 12, Bulmosan-ro 10beon-gil, Seongsan-gu, Changwon-si, Gyeongsangnam-do, 51543, Korea

olga.l.vadimova@gmail.com

A combination of a fiber oscillator and a solid-state amplifier is a promising way to developing a laser system emitting ultra-short pulses with high energy (>1 mJ) and high average power (>100 W). Amplifiers in such systems should provide high gain and should not be exposed the thermal effects. One of the most successful technology in this area is the thin-rod Yb:YAG amplifier with waveguide pumping (single-crystal fiber) [1]. Thin-rod geometry provides effective crystal cooling and bright waveguide diode pump allows achieving of high gain. The speciality of this geometry is a strong longitudinal inhomogeneity of the population inversion and laser intensity distributions inside the active element (AE). It limits gain coefficient and power extraction efficiency in the AE and complicates the numerical simulation of the amplification of the laser pulse.

In the present work, the amplification of the laser beams in a thin-rod AE was investigated numerically. For this purpose, the numerical model described in [2] was updated to enable simulations in thin-rods and to take into account spectral properties of amplified laser emission and active medium. The pump density distribution was precalculated separately with the 3D ray-tracing method, the pump absorption was not accounted in the calculations. The laser beam amplification was investigated in thin-rod made of Yb:YAG with 1% doping, 0.8 mm diameter and 30 mm length. One and two passes through the AE were considered. The spectral characteristics of the amplified laser radiation and of the active medium were taken from experimental data.

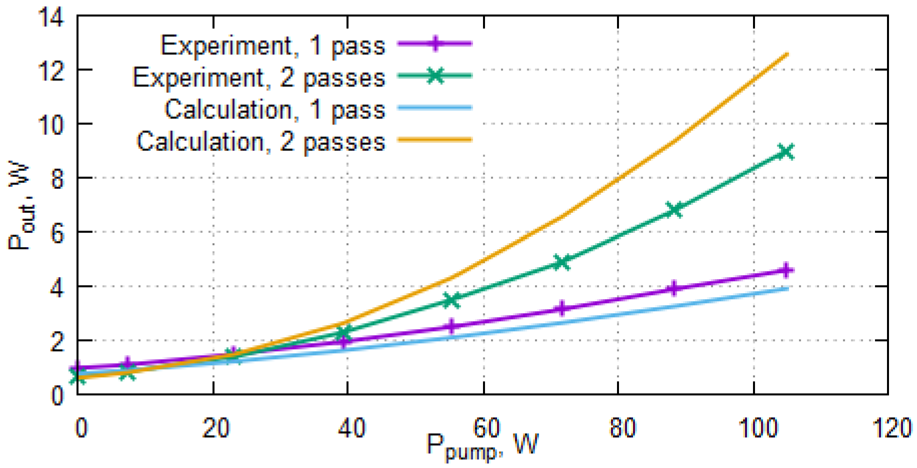

Figure 1. Dependence of the output power on the pump power for 1 and 2 passes through the thin-rod AE.

The amplification of the beam was calculated in AE described above for pump power up to 100 W. The results of the simulation are represented on Figure 1 as well as experimental data for the same AE, it can be seen that the data in agreement with each other. It was shown that the regime of amplification saturation was achieved under conditions used for simulation and the bandwidth of amplification band was 5nm.

[1] X. Délen, Y. Zaouter, I. Martial, N. Aubry, J. Didierjean, C. Hönninger, E. Mottay, F. Balembois, P. Georges, Yb:YAG single crystal fiber power amplifier for femtosecond pulses, Optics Letters, Vol. 38(2), pp. 109-111 (2013).
[2] O.L. Vadimova, I.B. Mukhin, I.I. Kuznetsov, O.V. Palashov, E.A. Perevezentsev, E.A. Khazanov, Calculation of the gain coefficient in cryogenically cooled Yb:YAG disks at high heat generation rates, Quantum Electronic, vol. 43 (3), pp. 201-206 (2013)

R.F. Mutalova[1,2], K.A. Prokhorov[2], G.Yu. Nikolaeva[2], E.A. Sagitova[2], P.P. Pashinin[2], M.A. Guseva[3], B.F. Shklyaruk[3], V.A. Gerasin[3]

[1]Moscow Institute of Physics and Technology (State University), Institutskiy per. 9, 141701 Dolgoprudny, Moscow Region, Russian Federation
[2]Prokhorov General Physics Institute, Russian Academy of Sciences, Vavilov St. 38, 119991 Moscow, Russian Federation
[3]Topchiev Institute of Petrochemical Synthesis, Russian Academy of Sciences, Leninsky Pr. 29, 119991 Moscow, Russian Federation

41615nerenata@gmail.com

Due to excellent physical and chemical properties and relatively low cost polyethylene (PE) and isotactic polypropylene (PP) rank first and second, respectively, in the polymer world output. These polymers are thermodynamically incompatible and immiscible, and their melting and crystallization temperatures and crystallization rates are significantly different. These distinctions provide with possibility to modify structure and, as consequence, properties of melt-mixed PE/PP blends in a wide range by altering conditions of production and processing. Besides, different polymorphs of isotactic PP can be obtained depending on the conditions of the melt cooling.

Due to improved mechanical properties PE/PP blends themselves have a great potential for practical applications. An interesting feature of nanocomposites with matrix of PE/PP blend is preferred localization of nanofiller in the PE domains. This feature opens new ways for development of functional materials, which are in demand from new high-tech applications. The study of PE/PP blends is of significant interest from the point of view of polymer recycling and reprocessing.

In this work we present Raman study of blends of isotactic PP and two grades of PE with very different structural characteristics (the degree of branching, density, the degree of crystallinity, the melting and crystallization temperature, etc.). We analyze dependence of the blend structure on relative content of the blend components and preparation conditions (quenching or annealing). We show that Raman spectroscopy is very informative and convenient tool to evaluate structure of polymer blends in terms of chemical, conformational, and phase compositions, including description of various crystalline modifications and non-crystalline regions.

This work is supported by the Russian Foundation for Basic Research (project code 16-02-00808-a).

Glass composition for 2.3 µm Tm^{3+} bulk and fiber lasers

B. I. Denker[1], V.V. Dorofeev[2*], B. I. Galagan[1], S.E. Motorin[2], S. E. Sverchkov[1]

[1]*A.M.Prokhorov General Physics Institute of RAS, Viviloa str. 38, 119991, Moscow, Russia.*

[2]*G.G. Devyatykh Institute of Chemistry of High-Purity Substances of RAS, Tropinina 49, N. Novgorod, Russia.*

[3]*Center of Laser Technology and Material Science, Vavilova st. 38, Moscow, Russia*

e-mail:denker@lst.gpi.ru

The advantages of TeO_2 – based glasses (TG) are their high solubility of lanthanide ions and high oscillator strengths (see Fig.1) of their electronic transitions. This presentation is devoted to the spectral, kinetic and lasing properties of $^3F_4$ - $^3H_5$ Tm^{3+} transition in ultrapure and highly dehydrated TeO_2–ZnO glass. This laser transition (λ~2.3 µm) lies within the air transparency window and can be used for remote detection of CO, CH_4 and HF gases having absorption lines around this wavelength. The idea behind the present study is that TG phonon spectrum can simultaneously provide the two main demands for the 4-level laser media: high quantum yield of the upper laser level ($^3F_4$) and very short lifetime of the lower laser level ($^3H_5$). We could not find in literature any reliable data about the $^3F_4$ Tm^{3+} luminescence quantum yield in well-dehydrated TGs. Moreover, we have found no data about the lifetimes of the lower laser level $^3H_5$ in any laser materials. And the noticeable lifetimes of the $^3H_5$ lower laser level that can be expected in fluoride glasses may cause sufficient inversion losses in pulsed regimes of laser operation. In order to evaluate the laser potential of TG we had to develop the measurement procedure of these parameters by comparison with Tm-doped ZBLAN. We have found that the total quantum yield of the transitions starting from $^3F_4$ level in TeO_2 – ZnO glass is lower than that in ZBLAN due to multiphonon relaxation but still remains high (~70%). Tm doping level in both samples was low enough to avoid cross-relaxation: (2÷3)x10^{19} ions per cm^3. As for the lower laser level $^3H_5$ lifetime the measurements of 1.8 µm emission buildup gave the values of 130 and 2600 ns for TeO_2 – ZnO and ZBLAN glass respectively. The resulting spectral properties of TG were found to be quite suitable for 2.3 µm laser action. The preliminary laser tests of this bulk glass were held using pulsed ruby laser as a pump source (see Fig.2). The sample of 38 mm length was longitudinally pumped with Ø1.5 mm beam. The resonator was formed by two flat mirrors with 11% outcoupling.

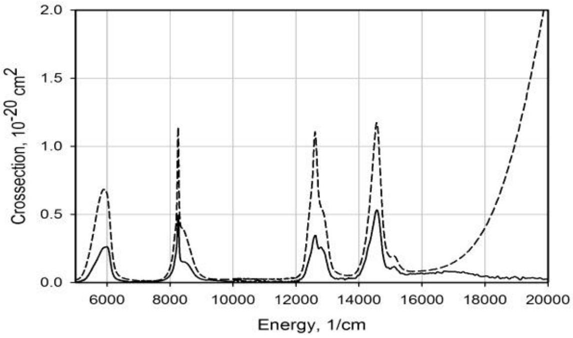

Fig.1 Absorption of Tm-doped TeO_2-ZnO (dashed line) and ZBLAN (solid line) glasses.

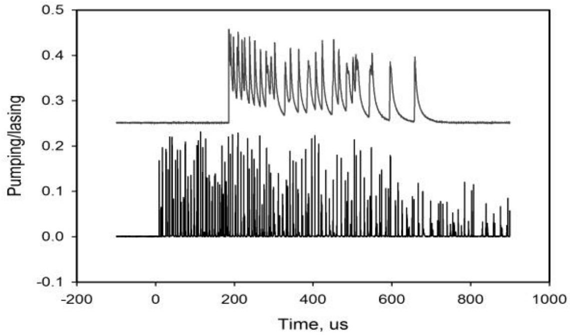

Fig.2 Oscillograms of pump laser pulse (bottom) and 2.3 µm laser pulse (top).

Thus TeO2 – ZnO based glass has shown itself an appropriate host for 2.3 µm Tm3+ lasers. Further experiments with diode pumping and fiber configurations are in progress.

Acknowledgements

This work was supported by Russian Science Foundation (grant 17-12-01324).

Multiplication of pulse energy towards kJ level in Nd:glass laser for pumping PEARL OPCPA stages

A. Kuzmin, O. Kulagin, A. Shaykin, I. Shaykin, E. Khazanov

Institute of Applied Physics of the Russian Academy of Sciences, Nizhny Novgorod, Russia

alexeyhsgap@yandex.ru

Optical breakdown is one of the main restrictions for increasing output power of most laser systems. An Nd:glass laser with 300 J, 1 ns pulses used for pumping OPSPA stages of the petawatt laser facility PEARL [1] is not an exception. As the maximum diameter of Nd:glass rods is 100 mm, this laser operates near the optical breakdown threshold. Larger active rod diameters are not available today. Another specific feature of the OPSPA system is a short pulse duration of 1 ns. In this paper we propose two ways to overcome the breakdown threshold. The first one is amplification in one power channel of several consequently propagating replicas of the input pulse. This method allows not only increasing the total output energy, but also reducing distortions of the sub-pulses during their amplification. In our experiments the output energy of the used Nd:glass laser has been increased from 300 to 500 J by splitting the input nanosecond pulse into two orthogonally polarized sub-pulses. The number of amplifying stages, the total small signal gain and the optical load on the elements of the laser have not been changed. Figure 1 shows the near-field intensity distributions and the oscillogram of the output sub-pulses with energies of 300 and 200 J.

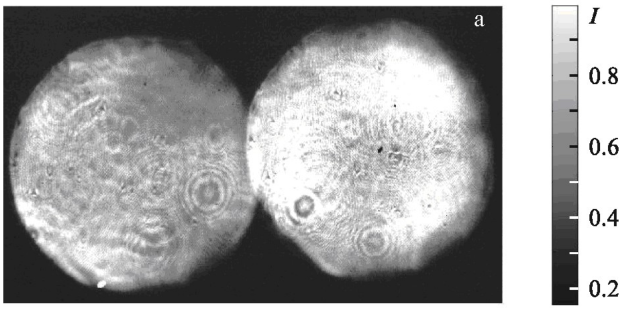

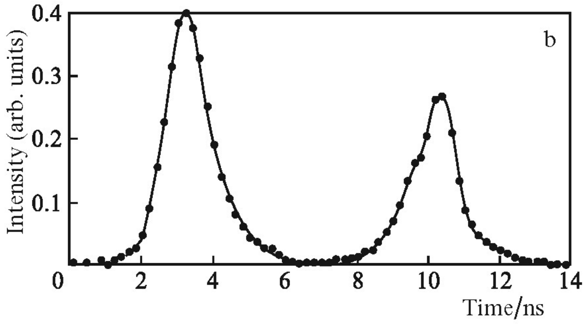

Fig. 1. Output intensity distributions (a) in the near-field zone and (b) in time. The pulse energies are 300 and 200 J; the beam diameter is 100 mm

The second way to multiple output pulse energy is amplification in Nd:glass of long pulses (tens ns in duration) and shortening them at the output by means of some nonlinear compression process. For example, for 16 ns pulses the optical breakdown threshold is 4 times higher than that for 1 ns pulses. That is why 16 ns pulses could be amplified in our Nd:glass laser up to 1200 J. We propose to use stimulated Brillouin scattering (SBS) for pulse compression [2]. The results of our first experiments in that direction will be presented as well.

Acknowledgements. The work was supported by the Russian Foundation for Basic Research (Grant No. 15-02-08099) and the grant program of the President of the Russian Federation for young scientists and postgraduate students engaged in advanced research and development in priority areas of modernization of the Russian economy (Grant No SP-703.2016.2).

[1] V.V. Lozhkarev et. al., Laser Phys. Lett., vol. 4, pp. 421-427 (2007).
[2] Brignon Arnaud and Jean-Pierre Huignard. Phase conjugate laser optics (Publisher John Wiley & Sons), chapter 7 (2004).

Y_2O_3 Passivated Quantum cascade lasers with Double Channel Structure

J. Kang[1], B. Joo[1,2], H. Yang[1], J. Song[3], I. Han[1,*]

1- Nanophotonics Research Center, Korea Institute of Science and Technology, Hwarangno 14-gil 5, Seongbuk-gu, Seoul 02792, Korea
2- Department of Physics, University of Seoul, 163 Seoulsiripdaero, Seoul 02504, Korea
3- Center for Optoelectronic Materials and Devices, Korea Institute of Science and Technology, 14-gil 5 Hwarang-ro, Seongbuk-gu, Seoul 02792, Korea

**hikoel@kist.re.kr*

Quantum cascade lasers (QCLs) are continuously improving their performance in the broad emission range with high power operation at elevated temperatures[1,2]. High performance operation of QCLs leads QCLs to be used in many applications. At the mid IR region, QCLs can be used as effective light source for the laser spectroscopy by utilizing their wide tunability of the emission wavelength[3,4].

As a passivation layer for the metal contact, SiO_2 is commonly used for the QCL fabrication but SiO_2 exhibits relatively high absorbance in the 8 to 10 μm region. In contrast, Y_2O_3 is transparent up to 12 μm and shows good insulating performance. For comparison, the refractive indices and absorption coefficients of SiO_2 and Y_2O_3 are plotted in Fig. 1. We used Y_2O_3 instead of SiO_2 as a passivation layer for the double channel (DC) structure QCL. The DC-QCL is made by etching both side of the mesa and then, the mesa is covered by contact metals with an insulation layer. The fabrication process of the DC-QCL is cost effective since it does not require any regrowth process[5].

Fig. 2 shows the emission spectra of fabricated DC-QCL with Y_2O_3 passivation layer. The peak wavelength was around 8.1 μm at 20ºC and the laser emission was successfully maintained over 50ºC. (200-ns-pulse with 20 kHz repetition ratio). Y_2O_3 shows better thermal conductivity than SiO_2, which means the Y_2O_3 passivated QCLs also have high potential of heat-dissipation performance in CW operation.

[1] J. Faist, Federico Capasso, D. L. Sivco, C. Sirtori, A. L. Hutchinson, A. Y. Cho, "Quantum Cascade Laser," Science, vol. 264, pp. 553-556 (1994).
[2] A. Lyakh, R. Maulini, A. Tsekoun, R. Go, C. Pflügl, L. Diehl, Q. J. Wang, F. Capasso, C. K. N. Patel', "3W continuous-wave room temperature single-facet emission from quantum cascade lasers based on nonresonant extraction design approach," Appl. Phys., Lett. vol. 95, p. 141113, (2009).
[3] R. Maulini, A. Mohan, M. Giovannini, Jerome Faist, E. Gini, "External cavity quantum-cascade laser tunable from 8.2 to 10.4 μm using a gain element with a heterogeneous cascade," Appl. Phys. Lett., vol. 88, p. 201113, (2006).
[4] G. Wysocki, R. Lewicki, R. F. Curl, F. K. Tittel, L. Diehl, F. Capasso, M. Troccoli, G. Hofler, D. Bour, S. Corzine, R. Maulini, M. Giovannini, J. Faist, "Widely tunable mode-hop free external cavity quantum cascade lasers for high resolution spectroscopy and chemical sensing," Appl. Phys. B, vol. 92, pp 305-311, (2008)
[5] W. Metaferia, B. Simozrag, C. Junesand, Y. T. Sun, M. Carras, R. Blanchard, F. Capasso, S. Lourdudoss, "Demonstration of a quick process to achieve buried heterostructure quantum cascade laser leading to high power and wall plug efficiency," Opt. Eng. vol. 53, p. 087104, (2014).

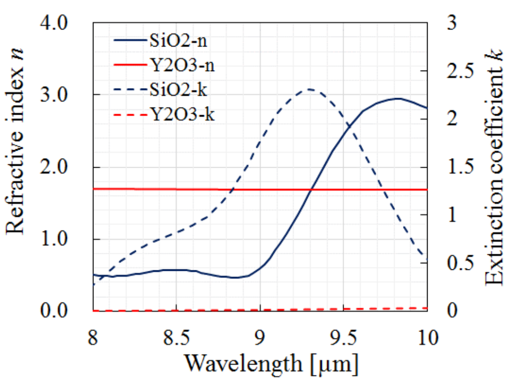

Fig. 1. Refractive index and extinction coeffcient of SiO_2 and Y_2O_3

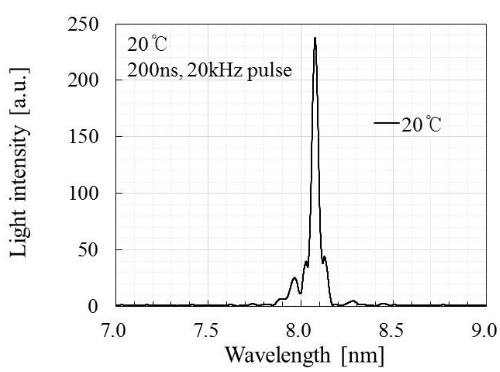

Fig. 2. Emission spectra of Y_2O_3 passivated QCL

The spectroscopic study of a Tm:Ho:$Yb_3Al_5O_{12}$ crystal

Yu.D. Zavartsev, A.I. Zagumennyi, Yu.L. Kalachev, S.A. Kutovoi, V.A. Mikhailov, I.A. Scherbakov

A.M. Prokhorov General Physics Institute, RAS, Moscow, Russia

kalachev@kapella.gpi.ru

The laser crystal Tm:Ho:YbAG (Tm^{3+}:Ho^{3+}:$Yb_3Al_5O_{12}$) demonstrates high laser efficiency in 2 um spectral range [1]. In this report spectroscopic properties and luminescent lifetime of this crystal are studied.

The Tm:Ho:YbAG crystal was grown by the Czochralski method from an iridium crucible. The concentration of Tm^3+ and Ho^{3+} ions in the active elements was 6,4% and 0,8%, respectively. Luminescence spectra in IR-region under 794 nm pumping were recorded. Pump power density was varied from 0,3 to 9,5 kW/cm^2. Pump beam was modulated by mechanical chopper with frequency from 2 to 200 Hz. IR-region of luminescent spectrum is shown in Fig.1.

For luminescent lines located at 1634 nm, 1750 nm, 2096 nm, 2126 nm and 1034 nm the phase-frequency response was analyzed to calculate decay times of tested lines. Line wavelengths were chosen to assure not overlapping of luminescence of different type of ions. At 1634 and 1750 nm only Tm^{3+} ions radiate, at 2096 and 2126 nm - only Ho^{3+} ions, at 1034 nm - Yb^{3+} ions. Phase-frequency response of Tm and Ho luminescence indicate 2-poles of transfer functions which is correspond to cascade excitation of Ho ions and equilibrium between Tm an Ho due to sharing of excitation energy [2]. Decay times depends on pumping power density and have typical values near 1,5 ms for fast component and 2,5-4,5 ms for slow component as it is shown in Fig.2. Decay time of Yb^{3+} ions, recorded at 1034 nm, was single-pole and independent on pumping power density and it is equal to 2,1 ms. Decay times were calculated by means of fitting the phase -frequency response by arctan - functions [3]: ϕ=arctan(2π F t_1)+ arctan(2π F t_2) for two -poles transfer function and ϕ=arctan(2π F t_1) - for single pole transfer function. (ϕ - phase shift, F - modulation frequency t $_{1,2}$ - decay times).

There was not detected significant up-conversion radiation in the visible region. Dependencies of luminescent intensities and decay times on pumping power density were obtained.

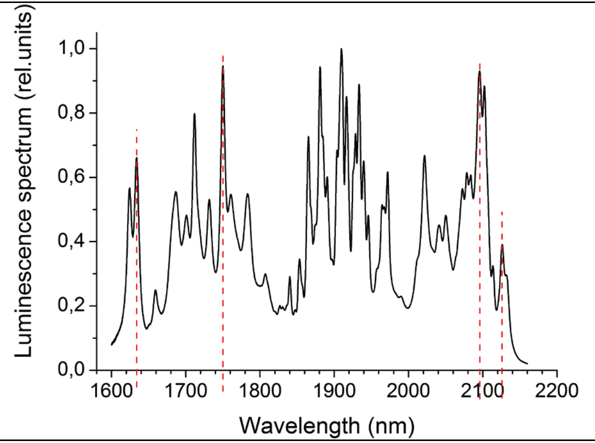

Fig.1 Luminescent spectrum in 2 um region. Red lines indicate wavelengths of analyzed spectral lines.

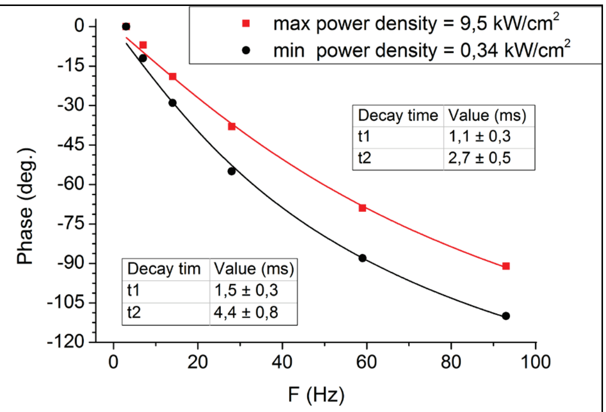

Fig.2 Phase frequency response of 2096 nm luminescent line at different pump density.

This work was supported by the Russian government in the frame of Program of RAS.

[1] Yu.D. Zavartsev, A.I. Zagumennyi, Yu.L. Kalachev, S.A. Kutovoi, V.A. Mikhailov, I.A. Shcherbakov, "Lasing in a Tm:Ho:$Yb_3Al_5O_{12}$ crystal pumped into the $^3H_6$ – $^3F_4$ transition", Quantum Electronics vol. 46 (3), pp. 189 – 192, (2016)
[2] B. M. Walsh, N. P. Barnes, B. Di Bartolo, "The temperature dependence of energy transfer between the Tm $^3F_4$ and Ho $^5I_7$ manifolds of Tm-sensitized Ho luminescence in YAG and YLF", Journal of Luminescence vol. 90, pp. 39-48, (2000).
[3] R.C .Dorf, R.H. Bishop, "Modern control system/Twelth edition", Pearson Education, Inc., Upper Saddle River, New Jersey 07458, chapter 8, (2011)

Optical Properties of $Gd_3Al_2Ga_3O_{12}$:Ce Crystals co-doped with Sc; Sc+Ca ; Mg

O. Buzanov[1], V. Kasimova[2], N. Kozlova[2], A. Kozlova[2], D. Spassky[2,3], E. Zabelina[2]

1- "Fomos-Materials" Ltd.,. Buzheninova street 16, Moscow, 107023 Russia
2- National University of Science and Technology "MISiS", Leninskii pr. 4, Moscow, 119049 Russia
3- D.V. Skobeltsyn Institute of Nuclear Physics, M.V. Lomonosov Moscow State University, Leninskie gory, GSP-1, 119991, Moscow, Russia

Main author email address: kozlova_nina@mail.ru

The purpose of this study was: 1) to determine the optical characteristics of GGAG:Ce crystals co-doped: Sc; Sc+Ca; Mg by optical spectrophotometry on the UV-Vis-NIR spectrophotometer Cary-5000 (Agilent Technologies) with the accessory "UMA" and the luminescent characteristics; 2) to establish the influence of partial substitution of cations Al and Ga cations of Sc, Mg and Ca +Sc on optical and luminescent properties of GAGG:Ce crystals .
These crystals are of the cubic structure, sp. gr. Ia3d. GGAG:Ce is proposed for use in medical visualization equipment as a sensor element in a positron emission tomograph (PET).
Cerium-doped gadolinium–gallium–aluminum garnet ($Gd_3Al_2Ga_3O_{12}$:Ce, GGAG:Ce) is a promising new scintillation material which was synthesized for the first time in 2011 [1].
Optical properties of GGAG:Ce crystals co-doped with Sc; Sc+Ca ; Mg virtually unexplored. These crystals were grown at "Fomos-Materials" Ltd. by the Czochralski method on an upgraded Kristall-3m system. The initial material for growth was a stoichiometric charge prepared by solid-phase synthesis from a mixture of initial oxides with the purity of 99.99%. The crystals were grown from an iridium crucible 80 mm in diameter in a mixture of argon with 1–2% of oxygen.
The spectral dependences of the transmission coefficients of these materials were obtained under normal incidence of naturally polarized light in the wavelength range of 250–800 nm; where three absorption bands can be observed: in the range of $\lambda \sim 420$–460 and near $\lambda \sim 340$ and 270 nm. Co-doping with Sc; Sc+Ca; Mg shows decrease in transmission in the range of $\lambda \sim 275$-375 nm.
The band disappears almost completely for the crystals co-doped with Mg. The half-width of the main transmission band ($\lambda \sim 350$-450 nm) decreases sharply for co-doped crystals. The main band is shifted to the long wave region for crystals co-doped Mg.
We obtained spectra of thermostimulated luminescence upon the UV range energy excitation at temperature range of 77 – 500 K for GAGG:Ce,Ca and GAGG:Ce, Sc + Ca crystals.
The reflectance and transmittance spectra were measured for p-, s-polarized light in the wavelength range of 250–800 nm at the angle of light incidence of 10º– 75° with a step of 5°; based on these data, the spectral dependences of the absorption coefficient were calculated taking into account the reflection. In order to obtain the refractive indices we use two spectrophotometric methods: a) definition the Brewster angles; b) measurement of the reflection spectra from one surface at the angle of incidence close to normal of GGAG:Ce crystals [2].
We calculated the refractive indices, plotted the dispersion dependence, and approximated the experimental data using the Cauchy equation. The refractive indices are listed in Table 1.

Table 1. Refractive indices **n**

Crystals	λ =370 nm	λ =400 nm	λ = 450 nm	λ =589 nm	λ =650 nm
$Gd_3Al_2Ga_3O_{12}$: Ce	1.949	1.915	1.899	1.895	1.891
$Gd_3Al_2Ga_3O_{12}$: Ce Sc	1.923	1.916	1.909	1.905	1.904
$Gd_3Al_2Ga_3O_{12}$: Ce, Sc+ Ca	1.936	1.903	1.897	1.893	1.890
Gd3Al2Ga3O12: Ce, Mg	2.012	1.914	1.904	1.888	1.887

[1] K. Kamada, T. Yanagida, T. Endo, et al., 2-inch size single crystal growth and scintillation properties of new Scintillator; Ce:$Gd_3Al_2Ga_3O_{12}$" IEEE Nuclear Science Symposium Conference Record., pp. 1927 , (2011).
[2] N. S. Kozlova, O. A. Busanov, E. V. Zabelina, A. P. Kozlova, and V. M. Kasimova Optical Properties and Refractive Indices of $Gd_3Al_2Ga_3O_{12}$:Ce^{3+} Crystals, Crystallography Reports, vol. 61, No. 3, pp. 474–478, (2016)

Endoscopic Visualization of Tumors in Gynecology

N. Kalyagina[1,2,*], **A. Borodkin**[1], **M. Loschenov**[1]
1-Prokhorov General Physics Institute, Russian Academy of Sciences, Vavilov Str. 38, 119991 Moscow, Russian Federation
2-National Research Nuclear University MEPhI, Kashirskoye shosse 31, 115409, Moscow, Russian Federation
** Nina.Kalyagina@gmail.com*

Today, many neoplastic lesions are unnoticed due to the lack of effective and minimally invasive methods of detecting early changes in the tissues of internal organs, such as cervical neoplasmes, as well as of the possibility of combining fluorescence imaging of tissue in the red with the usual endoscopic image in white light. A dual-channel laser endoscopic video system for fluorescence monitoring with enhanced depth probing, applicable in the conditions of blood presence and with the function of quantifying the concentration of the photosensitizer has been developed. By using the system extended diagnostic depth and numerical estimation of photosensitizer concentration were achieved. Moreover the overlay mode provides fluorescence visualization right on top of the real-time image in natural colors.

Incorporate assessment of optical coherence tomography and optical diagnostic techniques for the enhanced visualization of industrial resin defects

Ruchire Eranga Wijesinghe, Kibeom Park, Muhammad Faizan Shirazi, Mansik Jeon, and Jeehyun Kim

School of Electronics Engineering, College of IT Engineering, Kyungpook National University, 80 Daehak-ro, Buk-gu, Daegu 41566, Korea

E-mail: msjeon@knu.ac.kr

The liquid crystal display (LCD) panels and mobile phones can become defective as a result of the defective raw materials and industrial liquid resins, since the refractive index of LCD panels can be changed due to internal micrometer range substances, which are formed as a result of defectiveness and the insufficient solidification of industrial liquid resins. Numerous studies have been performed frequently using visual inspection methods and machine vision inspection techniques with charged coupled devices (CCD) for the defect detection of the topography, which suffer from inaccurate detection of internal cross-sections [1]. Hence, a reliable and accurate process inspection method is the most essential requirement to reduce the defects of the final product, which is capable of identifying defective raw materials and industrial resins prior to the manufacturing process. To overcome the diagnostic limitations, alternative non-invasive inspection techniques have gained an enormous attention. In this study, we utilized the non-destructive and high-resolution optical imaging technique called optical coherence tomography (OCT) to demarcate and numerate defects of industrial liquid resins of LCD display production [2, 3]. An incorporate assessment of the resin hardening rate and the stiffness of various liquid resins was performed by integrating a commercially available powerful analytical optical tool called fluorescence detector based UV hardening system to enhance the competence of the proposed inspection protocol. Thus, the incorporated assessment of OCT and fluorescence detector can be considered as a potential method of cost saving in LCD industry to obtain an immediate quality improvement of the final product.

Reference

[1] Kim, S.-H., J.-H. Kim, and S.-W. Kang, Non-destructive defect inspection for LCDs using optical coherence tomography. Displays, 2011. 32(5): p. 325-329.
[2] Prykäri, T., et al., Optical coherence tomography as an accurate inspection and quality evaluation technique in paper industry. Optical review, 2010. 17(3): p. 218-222.
[3] Tsai, M.-T., et al., Optical inspection of solar cells using phase-sensitive optical coherence tomography. Solar Energy Materials and Solar Cells, 2015. 136: p. 193-199.

Anisotropic behavior of refractive index in black phosphorus obtained by transmittance and reflectance measurement

Seong-Yeon Lee, Jeong-Jae Park, Tae-Young Jeong, Ki-Ju Yee

Department of Physics, Chungnam National University, Daejeon 34134, Republic of Korea

lsy929292@naver.com

Black phosphorus (BP), a new promising layered-material, has unique optical properties such as the direct bandgap and layer-dependent energy gap. [1] Particularly, anisotropic characteristics of BP are gaining more interests recently and expected to contribute in future optical device applications. One of the most important and direct works in understanding its anisotropic optical behavior is to specify the polarization dependent refractive index.

In this work, a few-layered BP is produced by mechanical exfoliation method. We confirmed by AFM that the thickness of the BP we studied is ~ 8 nm. To find the precise refractive index, we construct the experimental setup enabling to measure the reflected and transmitted light intensity through sample simultaneously. Transfer matrix theory is chosen for calculation of refractive index because of multi-layer structures of BP/quartz. With this technique, we obtain the complex refractive indices of BP as a function of wavelength at two different light polarizations. The polarization directions are determined as the maximum and minimum transmittance, which are aligned with zigzag and armchair direction of BP, respectively [2].

It is demonstrated that real part of refractive index exhibits no significant change from zigzag to armchair direction. However, the imaginary part of the refractive index in the armchair direction is always larger than the one in the zigzag direction in a range from 500 nm ~ 850 nm. It indicates that the absorption of light in the armchair direction is greater than the one for latter. We also show that relative imaginary refractive change ($\Delta\kappa/\kappa_{zigzag}$) at 550 nm is the largest in the visible region. $\Delta\kappa$ ($\kappa_{armchair}$ - κ_{zigzag}) is difference of the imaginary part of refractive index between armchair and zigzag direction. Such anisotropic absorption characteristics can be utilized in various nonlinear optics fields and technical applications for laser. [3] Moreover, the technique to calculate refractive index obtained from transmittance and reflectance spectroscopy can be applied to the optical analysis of other layered 2D materials as well.

[1] X. Fengnian and W. Han, Two-dimensional material nanophotonics, Nature Photonics, 8, 899-907, (2014).
[2] M. Nannan, T. Jingyi, Optical Anisotropy of Black Phosphorus in the Visible Regime, J.Am.Chem, 138, 300-305, (2016)
[3] Li. D, Juusila. H, Polarization and thickness dependent absorption properties of balck phosphorus: new saturable absorber for ultrafast pulse generation, Scientific Report, 5, 15899 (2015)

Highly Polarization Dependent Coherent Phonon of Black Phosphorus Measured With a Femtosecond Pulse Laser

J.J. Park[1], T.Y. Jeong[1], S.J. Kim[1], K.J. Yee[1]
Department of Physics, Chungnam National University, Daejeon 305-764, Republic of Korea

Pngj90@gmail.com

Black phosphorus (BP) is in the spotlight as a new 2D-material because BP has direct band gap energy varying with the layer number, high carrier mobility, and anisotropic properties. Especially, BP has two in-plane crystal axes, which are called “armchair” and “zigzag” direction and exhibits highly anisotropic properties such as anisotropic optical absorption, carrier mobility, and refractive index.

In this experiment, we used a Ti: shappire laser with a center wavelength of 780 nm, 19 nm FWHM, 61 fs pulse duration and 148 $\mu J/cm^2$ pump power to investigate the optical response of the BP. The direction of crystallization of BP is confirmed by polarization dependent transmittance measurement [1, 2]. We perform one color pump probe measurement and carry out pump and probe polarization dependent experiment using $\lambda/2$ plate to change of the light polarization.

One-color pump probe results show transmittance change with time delay. The periodic lattice vibration with time from the transmittance change data is obtained through smoothing and FFT and We obtained 10.84 and 13.96 Thz phonon frequency corresponding to A^1_g and A^2_g phonon mode.

The phonon mode shows different intensity depending on the polarization of incident light. We change the polarization directions of the pump and the probe and confirm that the A^1_g and A^2_g modes have dependence on the incident lights polarization [3]. We experimented with changing the temperature and found that the phonon frequency decreased and the dephasing rate increased with temperature. We also experimented with increasing pump power and found that the phonon frequency decreased and the dephasing rate increased. As a result, we found that the increase in dephasing rate with pump power were induced due to the phonon-carrier interaction rather than due to the optical heating of the sample.

[1] Diao Li, Henri Jussila, Polarization and Thickness Dependent Absorption Properties of Black Phosphorus: New Saturable Absorber for Ultrafast Pulse Generation, Scientific Reports 5, (2015)
[2] Xi Ling, Anisotropic Electron-Photon and Electron-Phonon Interactions in Black Phosphorus, Nano Lett., 16, 2260–2267, (2016)
[3] Jungcheol Kim, Jae-Ung Lee, Jinhwan Lee, Anomalous polarization dependence of Raman scattering and crystallographic orientation of black phosphorus, Nanoscale, 7, 18708-18715, (2015).

Spectroscopy of laser-induced breakdown spectroscopy under the action of ultrasound

A.V. Bulanov[1,3], I.G. Nagorny[2,3]

1- V.I.Il'ichev Pacific Oceanological Institute, 43, Baltiyskaya Street, Vladivostok, 690041, Russia
2- [2]Institute for automation and control processes, 5, Radio Street, Vladivostok, 690041, Russia
3- Far Eastern Federal University, 8 Suhanova St., Vladivostok, 690950, Russia

Main author email address: a_bulanov@me.com

The method of laser induced breakdown spectroscopy (LIBS) was used to investigate intensive lines of sodium, calcium in the dissolved solutions under the action of ultrasound at two frequencies of 10.7 kHz and 60 kHz. To excite optical breakdown in water the Nd:YAG laser was used. The parameters of laser pulses were so: the wavelength of 532 nm, the pulse duration of 10 ns and pulse energies of up to 180 mJ (in a modulated Q-mode). Acoustic radiation was generated within of cylinder transducers using a digital generator and powerful amplifier with the maximum amplitude of 100 kPa. For synchronization of acoustic and optical radiation, the generator of delays was used and so the problem of synchronization of acoustic and optical radiation was solved successfully. The change of the time delay for the control pulses allows synchronizing the time of maximum expansion or compression of the liquid under the acoustic pulses action which gives rise the optical breakdown.

The additional influence of ultrasonic radiation on the process of laser breakdown was studied. The increasing of the intensity of the line under the influence of ultrasound was observed at all concentrations of the used solutions. It was shown that the phase of the acoustic impact has a great significance for the rate of ultrasound action on the dynamics of the cavity in liquid. To increase the efficiency of combined effects it was important that the process of laser breakdown and ultrasonic tension would be in-phase. As a result, it was shown that under the influence of ultrasound the strong strengthening of the intensity of spectral lines of elements dissolved in aqueous solutions of NaCl, NaHCO3, and CaCl2 was observed.

The obtained results indicate the possibility of increasing the efficiency of laser-induced breakdown spectroscopy of liquid in the ultrasound field and allow you to talk about the possibility of application of ultrasound in technology LIBS - a kind of new combined method for ultrasonic laser-induced breakdown spectroscopy (ULIBS).

This work was supported by the Russian Science Foundation (agreement #14-50-00034) and Russian Foundation for Basic Research (project 16-02-00841 a, project 17-02-00561 a).

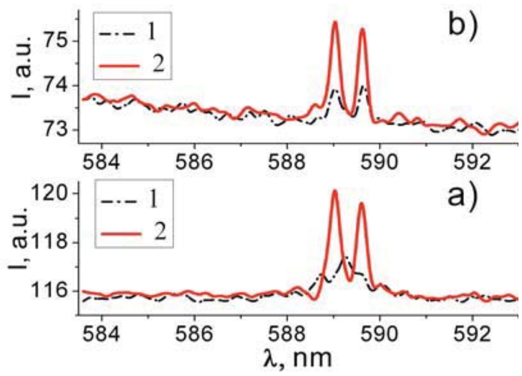

Fig.1. The line intensity I of the sodium without the use of ultrasound (1) and with using (2) for different concentration of NaCl solution: a) 10 % ; b) 3.5 %

[1] A.V. Bulanov, I. G. Nagorny. // Proc. SPIE 10176 (2016); doi: 10.1117/12.2268161;

Linear and Non-Linear Optical Diagnostics of Nano-Bio-Systems for Cancer Theranostic Applications

V. Yu. Timoshenko[1,2,3], A. Yu. Kharin[2], A.F. Alykova[2], T. Yu. Bazylenko[1,2], V. Lysenko[2,4], S. I. Derzhavin[2,5] , S. M. Klimentov[2,5], Ya. Dombrovska[2], I. N. Zavestovskaya[2,3], A. V. Kabashin[2,6]

(1) Lomonosov Moscow State University, Physics Department, 119991 Moscow, Russia; (2) National Research Nuclear University "MEPhI", 115409 Moscow, Russia; (3) Lebedev Physical Institute of RAS, 119333 Moscow, Russia; (4) University of Lyon, Institute of Nanotechnology of Lyon, UMR CNRS 5270, INSA de Lyon, France; (5) Prokhorov General Physics Institute of RAS, 119991 Moscow, Russia; (6) Aix-Marseille University, CNRS, UMR 7341, LP3, Marseille Cedex 9, France

E-mail: vtimoshe@gmail.com

Optical methods are widely used for medical diagnostics and therapy, including their combination, i.e. theranostics [1,2]. Photoluminescence (PL) spectroscopy and microscopy of nanoparticles (NPs) introduced into cancer cells and malignant tumors represent examples of bioimaging diagnostics [3,4]. Recently, different linear and non-linear optical methods such as the PL microscopy, Raman scattering, coherent anti-Stokes scattering, two-photon excited PL etc. were applied to monitor uptake and dissolution of silicon nanoparticles (SiNPs) in cancer cells *in vitro* [4-9]. SiNPs prepared by different physical and chemical methods [4-6] were found to be non-toxic, biodegradable and possess a lot of the physical and biochemical properties, which can be used for biomedical applications [5-12]. In our work SiNPs were formed by (1) laser ablation of c-Si targets at low pressure helium atmosphere and (2) electrochemical etching of c-Si wafers followed by mechanical grinding of the prepared porous Si layers in a ball mill. The prepared nanoparticles and their aqueous suspensions were studied by means of the linear and non-linear optical spectroscopy and were analyzed as active agents for cancer theranostics. The PL properties of microporous and laser-ablated SiNPs were explored for the bioimaging of cancer and normal cells. Porous SiNPs were found to be efficient sensitizers for the phototherapy (photodynamic and photothermal) of cancer. Porous and laser-ablated SiNPs suspended in aqueous media have been tested as sensitizers for radio-frequency electromagnetic hyperthermia [10] and sonodynamic therapy [11] of cancer. The obtained results demonstrate prospects of the optical diagnostics of SiNPs for cancer theranostic applications.

The work was partially supported by the Russian State Programs for Universities (projects 16.2969.2017/ПЧ and 16.7917.2017/БЧ).

[1] S. P. Morgan, F. R. Rose, S. J. Matcher, Optical Techniques in Regenerative Medicine. CRC Press (2013).
[2] S. S. Kelkar, Th.M. Reineke, Theranostics: Combining Imaging and Therapy, Bioconjugate Chem., vol. 22, pp.1879–1903 (2011).
[3] L. A. Osminkina, K. P. Tamarov, A.P. Sviridov, R.A. Galkin, M.B. Gongalsky, V.V. Solovyev, A.A. Kudryavtsev, V.Yu Timoshenko, Photoluminescent biocompatible silicon nanoparticles for cancer theranostic application, J. Biophotonics, vol.5, pp.529–535 (2012).
[4] M. B. Gongalsky, L.A. Osminkina, A. Pereira, A. A. Manankov, A. A. Fedorenko, A.N. Vasiliev, V. V. Solovyev, A. A. Kudryavtsev, M. Sentis, A. V. Kabashin, V.Yu.Timoshenko. Laser-synthesized oxide-passivated bright Si quantum dots for bioimaging, Sci. Rep., vol.6: 24732, pp.1-8 (2016).
[5] A. V. Kabashin, V. Yu. Timoshenko. What theranostic applications could ultrapure laser-synthesized Si nanoparticles have in cancer? Nanomedicine, vol.11(17), pp. 2247-2250 (2016).
[6] L.A. Osminkina, V.Yu. Timoshenko, Porous Silicon as a Sensitizer for Biomedical Applications, Mesopor. Biomat., vol.3, pp.39-48 (2016).
[7] E. Tolstik, L.A. Osminkina, C. Matthäus, M. Burkhardt, K.E. Tsurikov, U.A. Natashina, V.Yu. Timoshenko, R. Heintzmann, J. Popp, V. Sivakov. Studies of Silicon Nanoparticles Uptake and Biodegradation in Cancer Cells by Raman Spectroscopy, Nanomedicine: Nanotechnology, Biology & Medicine, vol.12, pp.1931–1940 (2016).
[8] E. Tolstik , L.A. Osminkina, D. Akimov, M.B. Gongalsky , A.A. Kudryavtsev , V. Yu. Timoshenko, R. Heintzmann , V. Sivakov, J. Popp, Linear and Non-Linear Optical Imaging of Cancer Cells with Silicon Nanoparticles, Int. J. Mol. Sci., vol.17:1536, pp.2-14 (2016).
[9] V. Yu. Timoshenko, Porous Silicon in Photodynamic and Photothermal Therapy, In "Handbook of porous silicon", Ed. L. Canham, Springer Publ., pp. 929-936 (2014).
[10] K.P. Tamarov, L.A. Osminkina, S.V. Zinovyev, K.A. Maximova, J.V. Kargina, M.B.Gongalsky, Yu. Ryabchikov, A.Al-Kattan, A.P. Sviridov, M. Sentis, A.V. Ivanov, V.N. Nikiforov, A. V. Kabashin, V. Yu. Timoshenko. Radio frequency radiation-induced hyperthermia using Si nanoparticle-based sensitizers for mild cancer therapy, Sci. Rep., vol.4 :7034, pp. 1-7 (2014).
[11] L. A. Osminkina, A.L. Nikolaev, A.P. Sviridov, N.V. Andronova, K.P. Tamarov, M.B. Gongalsky, A.A. Kudryavtsev, H.M. Treshalina, V. Yu. Timoshenko. Porous silicon nanoparticles as efficient sensitizers for sonodynamic therapy of cancer, J. Micropor. Mesopor. Mat., vol.210, pp.169-175 (2015).
[12] A. P. Sviridov, L.A. Osminkina, A.Yu. Kharin, M.B.Gongalsky, J.V. Kargina, A.A Kudryavtsev, Yu.I. Bezsudnova, T.S. Perova, A. Geloen, V. Lysenko, V.Yu. Timoshenko, Cytotoxicity control of silicon nanoparticles by biopolymer coating and ultrasound irradiation for cancer theranostic applications, Nanotechnology, vol. 28 (10), pp.105102 (2017).

Growth and Properties of Gallium Selenide Nanoparticles

A.M. Pashayev[1], E.Yu. Salayev[2], M. F. Huseyinoglu[3], K. R. Allakhverdiev[1]

1 - National Aviation Academy, Mardakyan prospect, 30, Az1045 Baku, Azerbaijan
2 - Azerbaijan National Academy of Sciences, Institute of Physics, Az1073 Baku, Azerbaijan
3 - Nature and Environment Research Center, Girne American University, Kyrenia, Cyprus

kerim.allahverdi@gmail.com

An overview of the current state of the literature and research performed by the authors of the present work on the experimental results on the structural-, optical-, nonlinear optical (NLO)- properties of nanoparticles (grown via sonication) of 2-D Gallium Selenide (GaSe) will be presented. Studied properties are important for development of different devices by using these nanoparticles.

Nanoparticles reveal highly effective NLO properties: high transparency range (1.0-20.0 μm); low absorption coefficient in the transparency range (less than 1 cm^{-1}); high NLO coefficient (not less than ≈ 90 pm/V); high power optical damage threshold for different laser lines (λ = 1.06; 2.36; 2.54; 5.3 and 10.6 μm), etc. It is shown that with decreasing the nanoparticles size (starting from 50 nm in diameter): transparency range shifts to blue range of spectra; NLO coefficient and damage threshold for different laser lines slightly increases; threshold power for visualization of λ = 1.06 μm line of Nd:YAG laser decreases; room-temperature exciton position shifts to lower wavelength with decreasing the size of nanoparticles.

Results obtained are discussed by using different models considered in the present research. Perspectives for future research of GaSe nanoparticles are also considered in the present research, which does not pretend to be one summarizing all existing papers on nanoparticles of GaSe and discussed subject.

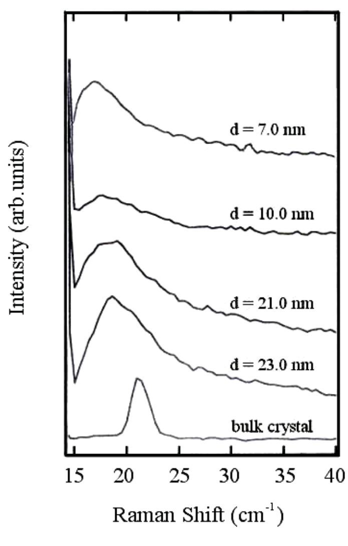

Figure.Room-temperature frequency position of rigid layer mode of GaSe in dependence on particle size. Spectra were excited with 632 nm (30 mW) of HeNe laser line in confocal geometry.

Interplay between Kerr and Raman effects in microcomb generation.

A.V. Cherenkov[1,2,*], **N. M. Kondratiev**[2], **V.E. Lobanov**[2], **G. Lihachev**[1,2] **and M.L. Gorodetsky**[1,2]

1- Faculty of Physics, M. V. Lomonosov Moscow State University, 119991 Moscow, Russia
2- Russian Quantum Center, 143025 Skolkovo, Russia

*av.cherenkov@physics.msu.ru

Kerr frequency combs are generated by coupling a cw laser and High-Q microresonator that converts the initial pump frequency into a broadband frequency comb by cascaded four-wave mixing processes [1]. Microresonator-based frequency combs are widely employed in various applications where high power per comb line and high repetition rate are important, e.g.in precision frequency metrology, highly multiplexed spectroscopy, fiber telecommunications and many others [2]. Pump threshold power is determined by Q-factor and can be reduced to sub-mW level. It was shown that the integrated group velocity dispersion (GVD) of the microresonator plays an important role in the possibility of comb generation, because phase-matching condition for four-wave mixing processes impose severe restrictions on the microresonator dispersion [3]. Generation of frequency combs in the normal GVD region has been actively explored in recent years and has been demonstrated experimentally, but has been less well studied.

New way to comb generation in normal GVD was opened due to the interplay between Kerr and Raman effects [4]. Stimulated Raman scattering and four-wave mixing process are the most important effects associated with the cubic nonlinearity of the resonator. However, the influence of Raman effect on frequency combs characteristics was studied mostly for anomalous GVD. In this work, we offer theoretical approach based on coupled-mode equation to study interaction between Kerr and Raman effects in whispering-gallery mode microresonators and experimentally demonstrated the generation of an optical frequency comb in the Raman scattering band (Fig 1). The proposed approach allows to describe the dynamics of the frequency comb generation in the Raman scattering band and to take the characteristics of the resonator dispersion into account. We demonstrated numerically that stimulated Raman scattering may provide generation of optical frequency comb in normal GVD region. The relevance of the theoretical model is confirmed by the experimental results.

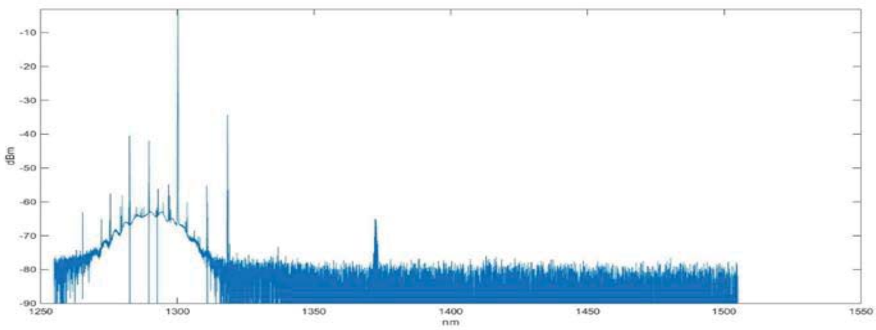

Fig 1. Experimental spectrum for comb generation in magnesium fluoride microresonators pumping at 1300 nm for FSR of 12.1 GHz and Q-factor of $5 * 10^9$.

This work was supported by RFBR grant 17-02-00522.

[1] P. Del'Haye, A. Schliesser, O. Arcizet, T. Wilken, R. Holzwarth, and T. J. Kippenberg. Optical frequency comb generation from a monolithic microresonator. Nature, 450(7173):1214–1217, 2007.
[2] T. J. Kippenberg, R. Holzwarth, and S. A. Diddams. Microresonator-based optical frequency combs. Science, 332(6029):555–559, 2011.
[3] T. Herr, V. Brasch, J. D. Jost, I. Mirgorodskiy, G. Lihachev, M. L. Gorodetsky, and T. J. Kippenberg. Mode spectrum and temporal soliton formation in optical microresonators. Phys. Rev. Lett., 113(12):123901, 2014.
[4] Yanne K. Chembo, Ivan S. Grudinin, and Nan Yu. Spatiotemporal dynamics of Kerr-Raman optical frequency combs. Phys. Rev. A, 92:043818, Oct 2015.

Speckle Noise Reduction Using the Multi-Channel Chirped Quasi-Phase Matching Device

Seong-Jin Son[1], Hsin-Jung Lee[2], Lung-Han Peng[2], Do-Kyeong Ko[1,3], Nan Ei Yu[3,*]

1- Department of Physics and Photon Science, GIST, Gwangju 61005, Republic of Korea

2- Department of Electrical Engineering, National Taiwan University, Taipei 10617, Taiwan, Republic of China

3- Advanced Photonics Research Institute, GIST, Gwangju 61005, Republic of Korea

*Main author email address: *neyu@gist.ac.kr*

The Laser projection display (LPD) system has a lot of merits such as colour gamut, brightness, dynamic range, contrast, light source lifetime, mercury free, and low power consumption compared with traditional display systems [1]. But, highly coherent of the laser light bring about the speckle noise [1,2]. In addition, the spectral bandwidth of the second harmonic generation (SHG) beam is narrower than that of the fundamental beam. The speckle of SH is more seriously than fundamental beam due to the narrow spectral bandwidth. Many scientists have been making an effort to reduce the speckle noise by mechanically moving the screen, inserting the diffractive optical elements(DOE), spectrum broadening etc. [1,2]. In our previous study, we demonstrated that the apodized step-chirped grating quasi-phase matching (QPM) device could reduce the speckle contrast [3]. In this letter, we try to overcome the speckle noise problem by a combination of the spatial distribution and the spectrum broadening using the multi-channel chirped (MCC) QPM devices. In order to generate the spatial distribution of the SHG beam, we designed the multi-channel QPM devices. The MCC QPM channel consisted of two apertures with 10um width and three subchannels of which widths were 100um, 200um, and 100um respectively. The MCC QPM device had chirped period. The QPM period distribution was from 7.69 to 7.96 um with an interaction length of 4.5 mm. We made SHG experiment set-up using the Yb-doped fiber laser. The laser has a center wavelength of 1064 nm, FWHM bandwidth of 10 nm, the repetition rate of 27 MHz and pulse duration of 290 fs. First, we got a reference data of single grating uniform PPLN whose period is 6.7um in the experimental set-up. We measured the spectral bandwidth of 1.1nm with a clear circular beam shape of the SHG green by the reference PPLN. Second, the MCC QPM generated SHG with a center wavelength of 532nm and FWHM bandwidth of 2.8 nm with the far-field patterns shown in figure 1(a). Figure 1(b) show that the far-field pattern was generated by interference of sub QPM channel like the double-slit interference experiment. In addition, we measured the speckle pattern using the CCD camera of reference PPLN and MCC QPM. The experimental condition was set to be as similar as possible to human eyes response. The speckle contrast was calculated by the standard deviation of the SH intensity over the average intensity of SH. The PPLN and MCC QPM had the speckle contrast of 47 % and 16 % respectively. We confirmed by 31 % reduction of speckle contrast due to the MCC structure.

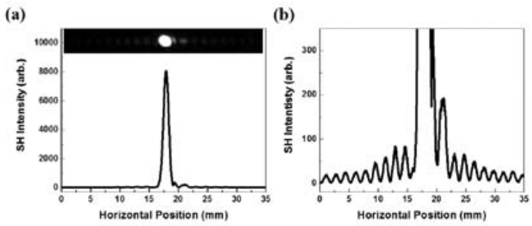

Fig. 1 (a) CCD image of SH beam pattern and its horizontal line profile graph. (b) Magnification graph of horizontal line profile of the SH interference pattern

In summary, we suggested the MCC QPM structures for broadening the spectral bandwidth and spatial distribution. We demonstrated that the MSC QPM generated far-field interference patterns and broadband SH spectrum. Furthermore, we confirmed the reduction of speckle noise.

[1] M. N. Akram and X. Chen, "Speckle reduction methods in laser-based picture projectors," Opt. Rev. 23, 108 (2016)

[2] J. W. Goodman, Speckle Phenomena in Optics: Theory and Applications (Roberts, Colorado, 2007)

[3] N. E. Yu, J. W. Choi, H. Kang, D.-K. Ko, S.-H. Fu, J.-W. Liou, A. H. Kung, H. J. Choi, B. J. Kim, M. Cha, L.-H. Peng, "Speckle noise reduction on laser display via a broadband green light source," Opt. Express, 22(3), 3547 (2014)

Optimization ofelectrical breakdown process forglasselectrodesin blue micro light-emitting diodes

K.R.Son, S. H. Oh, H. T. Kim, D. Y. Kang, B. R. Lee,T. G. Kim

School of Electrical Engineering, Korea University, Seoul 135-701, Republic of Korea

Main author email address: rack0907@naver.com

Indium tin oxide (ITO) is broadly used as transparent conductive electrodes (TCEs) in diverse areas including light-emitting diodes (LEDs), organic LED (OLED) and solar cell due to its excellent electrical and optical properties. But,its pricehas been increasing every year due to a limited supply of indium and increasing cost of mining and refinement. To replace that problem, manyresearch on TCEs have been reported such asoxide/metal/oxide (OMO) structure, conductive polymers andmetal nanowire; however, these approaches still remain challenging due to a trade-off relationship between optical transmittance and electrical conductivity [1, 2].

In order to overcome this problem, our group introduced the so-called 'glass electrodes' which is oxide/nitride-based materials with a high optical transmittanceandelectricalproperty. The electrical property of glass electrodes was obtained by using electrical breakdown (EBD) process, which is a sensitive technique because it may affect the performance of optical devices, even destroy devices. Therefore, the researchonreducing the electrical damages caused by EBD process such as using a buffer layer under the glass electrode layer [3] and rod-shaped (not planar-shaped) glass electrodes for confining the areaof EBD process have beenreported, but there have been few reports on the fundamental solution to this issue.

In this work, we studied the effect of the number of EBD process on electrical and optical properties of blue micro-LEDsdevice using 10-µm-AlNrod-shaped glass electrodes.As the number of EBD process was increased, the leakage current (@ -5 V) was increased while the optical output power was decreased. In addition, the leakage current flowing before turn-on voltage (@ 20 mA) was increased when electrical damages was accumulated, which means that the micro-LED pixel is destroyed and no longer emits light. Therefore, we shown that the best number of EBD process for micro-LEDs with 130 µm x 130 µm pixel is 6-time EBD process and weapplied it to micro-array-LEDs. As a result,the enhanced device performances compared to conventional ITO-based micro-array-LEDs was obtained. More details including the glass electrode's ohmic transport mechanism and real emission profiles of devices will be presented at the conference.

[1] Y. M. Kim, T. I. Ryu, K.H. Ok, M. G. Kwak, S. M. Park, N. G. Park, C. J. Han, B. S. Kim, M. J. Ko, H. J. Son, J. W. Kim, Advanced Functional Materials, 25, 4580-4589, (2015).
[2] D. Y. Cho, Y. H. Shin, H. K. Kim, Y. J. Noh, S. I. Na, K. B. Chung, Troll-to-roll sputtered Si-doped In_2O_3/Ag/Si-doped In_2O_3 multilayer as flexible and transparent anodes for flexible organic solar cells, Journal of Vacuum Science & Technology A: Vacuum, Surfaces, and Films, 33, 021501(1)-021501(11), (2015).
[3] T. H. Lee, K. H. Kim, B. R. Lee, J. H. Park, E. F. Schubert, T. G. Kim, Glass-based transparent conductive electrode: Its application to visible-to-ultraviolet light-emitting diodes, 8, 35668-35677, (2016).

GaN Based Light-Emitting Device Using Resistive Switching Material

H. T. Kim[1], B. R. Lee[1], J. H. Park[1], T. H. Lee[1], K. R. Son[1], S. H. Oh[1], T. G. Kim[1]

1- School of Electrical Engineering, Korea University, Anam-dong 5-ga, Sungbuk-gu, Seoul 136-701, Republic of Korea

ssansiro12@korea.ac.kr

Recently, there have been many research in multifunctional devices which combine two different device functions into a single device. One of them is the light-emitting diode (LED) with resistive random access memory (RRAM), so-called light-emitting memory (LEM). Many progresses have been achieved in LEMs, but non of them could actually manufactured because there are some obstacles on realizing the LEMs in an array in aspects of device complexity and performance. For example, the LEMs with three electrodes, which are for controlling the LED and RRAM unit independently [1], has different structure from the practical LED, so the increase in the device complexity would occur. The recently reported LEMs with defective active layers for emitting light and forming conducting filaments simultaneously [2] have exactly same structure to the practical LEDs, but many intended defects in the active layers unavoidably lead to the performance degradation.

We demonstrate novel type of LEMs using the RRAM structure as an n-type contact electrode of a GaN blue LED. Pt/ZnO/Pt unipolar RRAM structure is deposited on the mesa-etched n-type GaN. The RRAM unit works as an on/off switch of the LED as well as an electrode for current injection. RRAM has a planar structure, so we can easily maintain the entire structure of LEMs same as the practical LEDs without the degradation of device performance. So here, we actually realized the LEM array. The device shows I-V characteristics similar to those of typical RRAM after the forward voltage is over the threshold voltage of the LED. At the high resistance state (HRS), no light is emitted even if the voltage is over the threshold voltage, and at the low resistance state (LRS), the LED works normally. The current level is >1mA at LRS and <0.1uA at HRS at the operating voltage of 4V. The on/off ratio is 10,000:1, which shows great increase from that of previous reported LEMs, 100:1 [1].

[1] C.-W. Chang, W.-C. Tan, M.-L. Lu, T.-C. Pan, Y.-J. Yang, Y.-F. Chen, Electrically and optically readable light emitting memories, Scientific Reports, 4, 5121, 2014

[2] K. Zheng, J. L. Zhao, Z. H. Zhang, Y. Ji, B. B. Zhu, S. T. Tan, H. V. Demir, K. L. Teo, and X. W. Sun, An optically readable InGaN/GaN RRAM, IEEE Tans. Electron Devices, 63, 2328-2333, 2016

Improved Light Extraction Efficiency ofGaN-BasedMicro-LightEmitting Diode Using Al_2O_3/TiO_2 DBR withConductiveFilaments

S. H. Oh,H. T. Kim, B. R. Lee, K. R. Son, S. M. Oh, T. G. Kim

School of Electrical Engineering, Korea University, Seoul 135-701, Republic of Korea

Main author email address:dhtkdgns3212@gmail.com

Recently, there have been many studies onGaN-based micro light emitting diodes(micro LEDs),fabricated with typically square shapesand smaller sizesless than 50µm to achieve high efficiency, excellent heat dissipation, short carrier lifetime, etc.Thses micro LEDs can be applied in various fields such as micro display, visible light communication (VLC), and solid-state lighting and optogenetics.However, lateral micro LEDs have some limitations in terms of extraction efficiencybecause thelight emitting area(p-GaN) is covered by an electrode (typicall as wide 10μm) for current injection. To solve this problem, Ag and Al reflectors that can reflect the light covered by the electrode have been used in some groups at the visible wavelength. However,the reflectance of Agwas drasically decreasedat ultraviolet (UV) wavelengthwhereas Al reflector did not form ohmic contacts to p-GaN because of its low work functon. They are not very suitable for p-type reflective electrodes.[1, 2]

In this study, wereport UV micro LEDs having high extraction efficiency by insertinga distributed bragg reflector(DBR with conductivefilamentsof the same size as p-electrode between light-emitting area(p-GaN) and p-type electrode with a backside reflection scheme.Although the DBR has high reflectance at certain wavelengthdepending on the thickness,it is difficult to inject currents through the DBR because it is not conductive. So, we employed an electrical breakdown (EBD) technique to form conductive filaments (or current paths) for current injection into the DBR structure. The DBRconsisted of three pairs ofAl_2O_3/TiO_2layersunder Cr/Ni/Au electrodes, with which the reflectance was enhanced up to 95 % whereas that of the Ag mirror was as low as 70% [3]. Details on the experimental results containing light output power will be presented at the conference

[1]J. K. Sheu, I-Hsiu Hung, W. C. Lai, S. C. Shei, M. L. Lee, Appl. Phys. Lett. 93, 103507, (2008).

[2] D. R. Lide, Handbook of Chemistry and Physics CRC, New York, 12–114,(2006).

[3]K. Y. Ban, H. G. Hong, D. Y. Noh, T. Y. Seong Materials Science and Engineering B, 133, 26–29,(2006).

Enhancement of AlGaN-based deep-ultraviolet light-emitting diodes with edge graded Al composition electron blocking layer

M. R. Kwon, B. R. Lee, T. H Lee, T. H. Park, Y. W. Kim, C. Y. Kim, T. G. Kim

School of Electrical Engineering, Korea University, Seoul 135-701, Republic of Korea

Main author email address: kwonmiram@naver.com

Recently, AlGaN-based deep-ultraviolet light-emitting diodes (DUV-LEDs) with emission wavelength from 227 nm to 280 nm are having considerable attention for a wide variety of applications, including sterilization, air and water purification, medical and biochemistry, UV curing. However, AlGaN-based DUV-LEDs still suffer from relatively low internal quantum efficiency (IQE) and light output power (LOP). These are attributed to a number of factors such as a severely bent downward conduction band at the last quantum barrier (LQB) /EBL interface due to the spontaneous and piezoelectric polarization field effect, electron leakage and poor hole injection efficiency [1], dislocation density as well as Auger recombination. To overcome such problems, various approaches have been proposed to improve the efficiency of AlGaN-based DUV LEDs. Hirayama et al. reported that varying the carrier confinement structures and characteristics such as multiquantum-barrier (MQB) electron-blocking layer (EBL) could increase the external quantum efficiency of DUV LEDs [2]. However, they reported that the IQE is not changed.

In this study, we propose edge graded Al composition to the conventional MQB EBL of AlGaN-based DUV-LEDs and numerically analyzed using SimuLED simulation program to improve the IQE and LOP. It is important to efficiently confine the carriers in the multiple quantum well (MQW) and mitigate the severely bent downward conduction band at the LQB/EBL interface where electrons can accumulate and jump over or tunnel through the EBL. The IQE and LOP were significantly improved with the proposed structure. The improvements are attributed to field changing in the EBL so that the conduction band of the interface bends upwards, which makes electrons accumulate less, and improves radiative recombination rates resulting from enhanced hole injection and electron confinement within MQW. Details on the simulation results will be presented at the conference.

[1] A. Khan, K. Balakrishnan, and T. Katona, Ultraviolet light-emitting diodes based on group three nitrides, Nature Photonics 2, 77-84, (2008).

[2] H. Hirayama, Y. Tsukada, T. Maeda and N. Kamata, Marked enhancement in the efficiency of deep-ultraviolet AlGaN light-emitting diodes by using a multiquantum-barrier electron blocking layer, Applied Physics Express, 3, 031002, (2010).

Optical measurement of resonant mechanical oscillation of micro glass tubes

Kouhei MATSUMOTO, Taiki YAMAMOTO, and Satoru SHOJI
Department of Engineering Science, The University of Electro-Communications
JST, ERATO MINOSHIMA Intelligent Optical Synthesizer (IOS)

1-5-1 Chofugaoka, Chofu, Tokyo 182-8585 Japan
m1733119@edu.cc.uec.ac.jp / http://www.phomat.es.uec.ac.jp

In this study, we measured vending oscillation of microscale glass tube under optical microscope. We observed that resonant mechanical oscillation frequency of the micro glass tube changed by enclosing material in the micro glass tube. We could evaluate the change of the resonant mechanical oscillation frequency of the micro glass tube containing water or ethanol in micro glass tube respectively. Further, we enclosed UV curable resin (1) in the micro glass tube. Ultraviolet curing resin solidifies by irradiating ultraviolet rays (365nm) to cause photo-polymerization reaction. We observed the change in the resonant mechanical oscillation frequency of the micro glass tube depends on the change of ultraviolet irradiation time.The micro glass tube is made from silica glass. The diameter, wall thickness, and the length of the micro glass tube were 27 µm, 3µm, 1.3cm, respectively. The micro glass tube is hollow. Contacted tip of the micro glass tube with water or ethanol could be enclosed in micro glass tube. We constructed confocal laser microscopic optical system to measure micro glass tube oscillation. In this system, continuous wave laser has wavelength 638nm. Laser beam was spread by beam expander which consists of a plano convex lens having focal lengths of 50mm and 200mm. The laser beam was introduced in an optical microscope. An objective lens focused the laser beam onto the micro glass tube. Reflected light from a micro glass tube was collected by the same objective lens and reflected by beam splitter to photo-detector. The laser beam was detected by a photo-detector. Pinholes were put at the focus spots in the beam expander, and in front of photodetector, to construct a confocal optical system. The micro glass tube was fixed to sample stage of the microscope and sound wave was irradiated from the side of micro glass tube with speaker. We scanned sound wave frequency from 100Hz to 10000Hz and clearly measured the several resonant mechanical oscillation frequency of the micro glass tube.

This work was supported by JST ERATO Grant Number JPMJER1304, JSPS KAKENHI Grant Nunber JP16H06505 in Scientific Research on Innovative Areas “Nano-Material Optical Manipulation”, and JSPS KAKENHI Grant Number JP16K04972, Japan.

References

(1)K Masui, S Shoji, K Asaba, T C. Rodgers, F Jin, X M Duan, and S Kawata.”*Laser fabrication of Au nanorod aggregates microstructures assisted by two-photon polymerization.*” OPTICS EXPRESS Vol. 19, pp. 22786-22796(2011)

Improved Performance of Low-Illuminance Organic Photovoltaics Using Highly Transparent and Conductive Thin Indium Tin Oxide Films via Electrical Doping

Y. W. Kim[1], B. R. Lee[1], T. H Lee[1], M. R. Kwon[1], D. S. Jeon[1], S. C. Shin[2], J. W. Shim[2], T. G. Kim[1]

1- School of Electrical Engineering, Korea University, Seoul 135-701, Republic of Korea

2- Department of Electronic and Electrical Engineering, Dongguk University, Seoul 100715, Korea

Main author email address: woono@nate.com

Nowadays, with the coming of the fourth industrial revolution, internet of things (IoT) focused on indoor devices (smart LED, sensor and switch, etc.) use battery or general electricity as their source of power. However, batteries have some limitations in lifetime and environmental problems. Low-illuminance organic photovoltaics (OPVs) have received an attention as a suitable solution; they have light, flexible, and eco-friendly features. To improve the performance of these devices, it is important to obtain a transparent conductive electrode (TCE) with high transmittance and high conductivity [1]. However, most of the TCEs including conventional ITO, oxide-metal-oxide, conductive polymer, and graphene have a "trade-off" problem between these two exclusive properties [2]. Therefore, we could not help optimizing the two properties (or sacrificing one of the properties). For example, the use of thick ITO films is good for electrical conductivity but bad for optical transmittance.

In this study, we report highly conductive thin ITO (HCTI) films that can overcome such a "trade-off" problem, fabricated using an electrical doping (ED) method. According to the previous report [3], the electrical breakdown (EBD) induced a diffusion of top metal atoms such as Ni and Cr into the films below the metal. To allow such metal dopants to be incorporated in the thin ITO films without optical losses, we prepared an ITO/AlN/Cr/Ni structure and removed AlN/Cr/Ni layers after the ED process under electric fields. As a result, one of the 10-nm-thick ITO films (after the ED process for low illuminance OPVs) exhibited a low sheet resistance of ~200 Ω/sq and a high transmittance (>95%) in the visible region. This result shows the improvement by approximately 350% in electrical conductivity (or sheet resistance) compared to that of the conventional ITO (about 750 Ω/sq) [4]. Consequently, low illuminance OPVs using the proposed HCTI (10 nm) as a cathode exhibited increased a power conversion efficiency as compared to those with conventional ITO (150 nm). Details on the experimental processes and results will be presented at the conference.

[1] M. Kasemann, K. Ruhle, L. M. Reindl, Photovoltaic Energy Harvesting under Low Lighting Condition , AMA conference, 483-485, (2013).
[2] P. Kuang and J.-M. Park, W. Leung, R. C. Mahadevapuram, K. S. Nalwa, T. G. Kim, S. Chaudhary, K. Ho, K. Constant, A New Architecture for Transparent Electrodes: Relieving the Trade-Off between Electrical Conductivity and Optical Transmittance, Adv. Mater., 23, 2469-2473, (2011).
[3] T. H. Lee, K. H. Kim, B. R. Lee, J. H. Park, E. F. Schubert, T. G. Kim, Glass-Based Transparent Conductive Electrode : Its Application to Visible-to-Ultraviolet Light-Emitting Diodes, ACS Appl. Mater. Interface., 8, 35668-35677, (2016).
[4] H. Peng and W. Dang, Topological insulator nanostructures for near-infrared transparent flexible electrode, Nature Chemistry, 4, 281-286, (2012).

Laser interference exposure lithography for fabricating super-hydrophilic pillar arrays made of polymer

Ryusaku HIDA and Satoru SHOJI
Department of Engineering Science, The University of Electro-Communications
JST, ERATO MINOSHIMA Intelligent Optical Synthesizer (IOS)

1-5-1 Chofugaoka, Chofu, Tokyo 182-8585 Japan
h1733104@edu.cc.uec.ac.jp / http://www.phomat.es.uec.ac.jp

The plants and insects of the natural world grow micro-scale fibers/hairs to possess hydrophobic surface on their bodies. Hydrophobic surface is important for small plants and insects in their life. They keep their fragile bodies against surface tension of water droplets and their body surface clean [1,2]. We inspired such natural microstructures and artificially fabricated such periodic pillar arrays made of polymer. For the fabrication of periodic pillar structures, we developed laser interference exposure lithography system. We used a third-harmonic light of Nd:YVO4 ultraviolet laser, with its wavelength of 355nm, as the light source. The laser beam was expanded by a beam expander and was the size of 5 times. The laser beam was divided into four beams by a diffraction type beam splitter. The four laser beams were gathered by a pair of single lenses into one point, so that interference fringe exhibiting square-lattice light hot spots was formed. We put a photoresist film at the position where the laser beams were gathered, and exposed the film under the laser light. The photoresist was cured according to the interference pattern. The material of periodic pillar structures was SU-8(product made in Microchem). The material was ultraviolet rays hardening resin. SU-8 applied it uniformly by the spin coater. After the irradiation of the laser beam, SU-8 which was not irradiated dissolved by developing solution (propylene glycol monomethyl alcohol). After developing procedure, we obtained square-lattice polymeric pillar structures. The distance and tilting angle of the pillars can be tuned by the incident angles of four beams. The thickness and the height of the pillars can be can be tuned by the exposure dose of laser beams, and the diameter of our prepared resist film, respectively. By a single shot laser exposure for 0.3 seconds, we simultaneously fabricated an array of ~ 60,000 pillars with their diameter and the height of ~20 µm, and 3.5 µm, respectively, in a dimension of 4mm2. We obtain contact angle is 26° on the square-lattice polymeric pillar structures and 72° on the flat surface. Hydrophilic is enhanced by the square-lattice polymeric pillar structures.

This work was supported by JST ERATO Grant Number JPMJER1304, JSPS KAKENHI Grant Nunber JP16H06505 in Scientific Research on Innovative Areas "Nano-Material Optical Manipulation", and JSPS KAKENHI Grant Number JP16K04972, Japan.

References

[1] Neelesh A. Patanker, "Mimicking the Lotus Effect: Influence of Double Roughness Structures and Slender Pillars," Langmuir, 2004, pp8209-8213.

[2] Masatsugu Shimomura, "Surface Science and Biomimetics," Journal of The Surface Finishing Society of Japan, 2013, Vol.64 No.1 p2-8.

Improvement of light extraction efficiency in AlN/Al backside reflector in AlGaN-based ultraviolet light emitting diodes

T. H. Park, T. H. Lee, T. G. Kim

School of Electrical Engineering, Korea University, Seoul 135-701, Republic of Korea

Main author email address: polt555@korea.ac.kr

Near-ultraviolet light emitting diodes (NUV LEDs) have potential applications in various industry, including white LEDs, UV curing, sterilization and etc. Many researchers have conducted to improve the overall efficiency of these devices. Increasing light extraction efficiency is important to improve the efficiency of LED. However, general LEDs can be emitting in all directions, so some photons are lost due to downward emission. In addition, NUV LEDs has a low external quantum efficiency (EQE) problem. To solve this problem, in AlGaN-based NUV LEDs, researchers redesigned the LED structure, and fabricated with truncated cone structures, distributed Bragg reflectors, omnidirectional reflectors [1, 2]. In particular, Al and Ag reflector metals have been widely used. The Ag was regarded as a good reflector, but has poor thermal stability and reflectance in the UV region, whereas the Al exhibited higher reflectance than Ag in the UV region.

In this study, we proposed anAlN/Al backside reflector for AlGaN-based NUV LEDs, and continued to examine a light extraction mechanism for the AlN/Al reflector with surface roughness control of Al_2O_3. To enhance the light extraction efficiency, the surface roughness of Al_2O_3 backside should be reduced as much as possible. Moreover, an additional AlN/Al bilayer was deposited on the backside of the lateral LED structure.The light extraction efficiency of the LEDs was enhanced by the reflectance of the backside reflector.The surface roughness treatments with annealing processes may reduce the interface roughness and thusincrease the reflectance of the AlN/Al reflector metals.A simulation of the backside reflector showedlight reflection by the Al layer and the trapping of the scattered light in the AlN layer.Details on the device performance will be presented at the conference.

[1] J. W. Lee, J. H. Park, D. Y. Kim, E. F. Schubert, J. Kim, J. Lee, Y. Kim, Y. Park and J. K. Kim, Arrays of Truncated Cone AlGaN Deep-Ultraviolet Light-Emitting Diodes Facilitating Efficient Outcoupling of in-Plane Emission, ACS Photonics, 3(11), 2030-2034, (2016)

[2] H. Chen, H. Guo, P. Zhang, X. Zhang, H. Liu, S. Wang and Y. Cui, Enhanced Performance of GaN-Based Light-Emitting Diodes by Using Al Mirror and Atomic Layer Deposition-TiO2/Al2O3 Distributed Bragg Reflector Backside Reflector with Patterned Sapphire Substrate, Appl. Phys. Express 6, 022101, (2013)

Ultra-thin ITO Films with High Transmittance and Conductivity Using Electrical Doping Methods: Its Application to both Organic and InorganicLight-Emitting Devices

T. H. Lee[1], B. R. Lee[1], K. R. Son[1], Y. W. Kim[1], J. H. Park[1], M. S. Chae[1], T. G. Kim[1]

1-School of Electrical Engineering, Korea University, Seoul 136-701, Republic of Korea

Main author email address: tgkim1@korea.ac.kr

Achieving highly transparent and conductive electrode (TCE) in a broad spectrum is an ultimate goal for reserchers who are working with optoelectronic devices such as light-emitting diodes (LED), organic LEDs (OLED), and solar cells, etc [1, 2].Until now, several candidates such as indium-dopedtin oxide (ITO), aluminium-doped zinc oxide (AZO) and silver nanowirehave been widely used as TCEs. However, it was difficult to develop such a TCE with high conductivity and transmittance simultaneously because these two properties are mutually exclusive.For example, as the thickness of the TCE film is decrease, the transmittancewould be reduced in a broad spectrum includingthe UV region, but the conductivity (or sheet resistance) would be decreased (or increased).In addition, in the case ofoptoelectronic devicesthat require smooth charge carrier (electron or hole) injection into various organic/inorganic materials, doping on the TCEs is an important factor with regards to work function engineering.

To solve these problems, our group has suggested and developed a novel electric-field-assisted doping treatment method to produce ultra-thin TCE films with both high transmittance owing to thin films and low sheet resistanceowing to electrical doping. The electric-field-assisted doping was performed via wide-bandgap materials such as AlN layersdeposited on the ultra-thin TCE. After the electrical doping process, wide-bandgap sacrificial materials were removed to form conductive filamentsin the ultra-thin TCE films, which improved the current injection and controlled the work function of ultra-thin TCE filmswhile maintaining its high optical transmittance.Finally we applied theseultra-thin TCEs to TCTA/TPBI-based green phosphorescent OLEDs as well as AlGaN-based UV LEDs, and confirmed their outstanding performance. Details on the electrical and optical propertiesof these devices will be presented at the conference.

[1] B.-J. Kim, C.Lee, Y.Jung, K. H.Baik, M. A.Mastro,J. K.Hite,C. R.Eddy Jr., J.Kim, Large-Area Transparent Conductive Few-LayerGraphene Electrode in GaN-Based Ultra-Violet Light-Emitting Diodes, Appl. Phys. Lett. 99., pp. 143101, (2011).
[2] Han, T. H.; Lee, Y.; Choi, M. R.; Woo, S. H.; Bae, S. H.; Hong, B.H.; Ahn, J. H.; Lee, T. W. Extremely Efficient Flexible Organic Light-Emitting Diodes with Modified Graphene Anode, Nat. Photonics, 6., pp. 105−110, (2012).

High-Performance ZnO/Ag/ZnO Transparent Electrodes for Flexible Organic Photovoltaic Cells

B. R. Lee[1], G. E. Park[2], Y. W. Kim[1], H. T. Kim[1], T. H. Lee[1], K. R. Son[1], S. H. Oh[1], M. R. Kwon[1], S. B. Hong[1], D. H. Choi[2], T. G. Kim[1]

1-School of Electrical Engineering, Korea University, Seoul 135-701, Republic of Korea

2-Department of Chemistry, Research Institute for Natural Sciences, Korea University, Seoul 136-701, Republic of Korea

Main author email address: goodboyopen2@daum.net

Organic photovoltaic (OPV) cells have received great attention as renewable energy source due to its advantages including flexibility, low weight, low cost, and suitability for large-scale and mass production. In particular, flexible OPV cells have countless potentials to assemble on diverse products such as clothing, flexible window and backpack. In recent years, many technologies of highly flexible transparent conducting electrodes (TCEs) such as dielectric/metal/dielectric (D/M/D) for opto-electronic devices, including OPV and various display, have been widely investigated. In particular, ZnO/Ag/ZnO multilayers have been extensively researched for OPV cells because ZnO have benefits including flexibility, cheap price and non toxic property. However, hiterto there are no reports having better power conversion efficiency (PCE) of OPV cells with ZnO/Ag/ZnO multilayers than that of indium thin oxide (ITO). For example, Vedraine et al. reported the OPV cells with a ZnO/Ag/ZnO anode having a PCE of 2.58%, while the OPV cells with a ITO anode having a PCE of 2.99%. And, T.-Y. Seong et al. reported the inverted OPV cells with a ZnO/Ag/ZnO cathode having a PCE of 2.63%, while the OPV cells with a conventional ITO anode have a PCE of 2.71% [1, 2]. It is thought to due to low electrical conductivity of ZnO and work function miss match.

In this work, we optimized electrical and optical properties of ZnO/Ag/ZnO cathode using RF-magnetron sputtering system and two-dimensional finite-difference time-domain (FDTD) simulation. According to the optimized results in this work and previous researches of other groups, the thickness of ZnO have to be larger more than 30 nm to obtain high transmittance of ZnO/Ag/ZnO multilayers. However, the 30nm-thick ZnO is too resistive to transport current flow efficiently. Therefore, in order to minimize the resistance of ZnO deposited on Ag electrode, ZnO/Ag/ZnO multilayers were selectively deposited only in the active region, not in the electrode region for mesurement. Finally, we reported superior OPV cells with ZnO/Ag/ZnO cathode having a PCE of 5.20% better than OPV cells with reference ITO having a PCE of 5.09%. Furthermore, we also enhanced a PCE of OPV cells with ZnO/Ag/ZnO multilayers by enhance conductivity of ZnO on active region using electrical break down (EBD) process [3].

[1] S. Vedraine, A. El Hajj, P. Torchio and B. Lucas, Optimized ITO-free tri-layer electrode for organic solar cells, Org. Electron 14, 1122, (2013).
[2] J. H. Kim, T.-W. Kang, S.-I. Na, Y.-Z. Yoo and T.-Y. Seong ITO-free inverted organic solar cells fabricated with transparent and low resistance ZnO/Ag/ZnO multilayer electrode, Current Applied Physics, 15, 829-832, (2015).
[3] T. H. Lee, K. H. Kim, B. R. Lee, J. H. Park, E. F. Schubert and T. G. Kim, Glass-Based Transparent Conductive Electrode: Its Application to Visible-to-Ultraviolet Light-Emitting Diodes, ACS Applied Materials & Interfaces, 8, 35668– 35677, (2016).

A study on the active terahertz asymmetric split loop resonator with an outer square loop based on VO_2 having a high-Q factor

Dae-Jun Park, Han-Cheol Ryu*

Department of Convergence Science, Sahmyook University, Seoul 139-742, Korea

Tel: +82-2-3399-1801; Fax: +82-2-3399-1805; E-mail: hcryu@syu.ac.kr

The development of devices that can be used in the terahertz band is inadequate compared to microwave or optical bands because the electrical and magnetic properties of natural materials are not suitable for use as devices in the terahertz band. Therefore, researches that utilize metamaterial as a device of terahertz waves are attracting much attention [1]. Metamaterials can make negative refractive index or transparent shape, which is a unique property that does not exist in nature, and research has been conducted in various fields [2]. It is important to increase the quality factor of the metamaterial in order to better utilize it as application devices. However, the radiation loss of the metamaterial in the resonance state has been a major limitation in increasing the quality factor, and a lot of research has been conducted on the asymmetric metamaterial to increase the quality factor by suppressing the radiation loss of the metamaterial [3]. In addition, securing the activity of metamaterials is very important to increase utilization of metamaterials.

In this study, we proposed an asymmetric split-loop resonator with an outer square loop (ASLR-OSL) based on VO_2, which can actively control terahertz wave transmission properties while maintaining a high-Q factor of the asymmetric split-loop resonator (ASLR). The VO_2 thin film, which exhibits an insulator-metal phase transition with temperature change, was deposited on the Si substrate for the active control of ASLR. An outer square loop was added to the ASLR for the active control without any degradation of the Q-factor of the ASLR. The added outer square loop can perform both a resonant structure and a micro-heater. The designed ASLR-OSL showed transmission characteristics similar to those of the ASLR. The bias voltage directly applied to the added outer square loop can change the temperature and the conductivity of the VO_2. Accordingly, the transmission characteristics of ASLR-OSL was successfully controlled by simple bias engagement. Based on these results, an electrically controllable terahertz high-Q metamaterial could be achieved simply by adding a square loop to the outside of a well-known high-Q metamaterial.

[1] J. Valentine, S. Zhang, T. Zentgraf, E. Ulin-Avila, D. A. Genov, G. Bartal, and X. Zhang, "Three-dimensional optical metamaterial with negative refractive index," Nature 455, 376-379 (2008).W.-K. Chen, Linear Networks and Systems (Book style). Belmont, CA: Wadsworth, 1993, pp. 123–135.

[2] M. Choi, S. H. Lee, Y. Kim, S. B. Kang, J. Shin, M. H. Kwak, K. Y. Kang, Y. H. Lee, N. Park, and B. Min, "A terahertz metamaterial with unnaturally high refractive index," Nature 470, 369-373 (2011).

[3] C. Jansen, A. I. Al-Naib. Ibraheem, N. Born, and M. Koch, "Terahertz metasurfaces with high Q-factors," Applied. Physics. Letters 98, 051109 (2011).

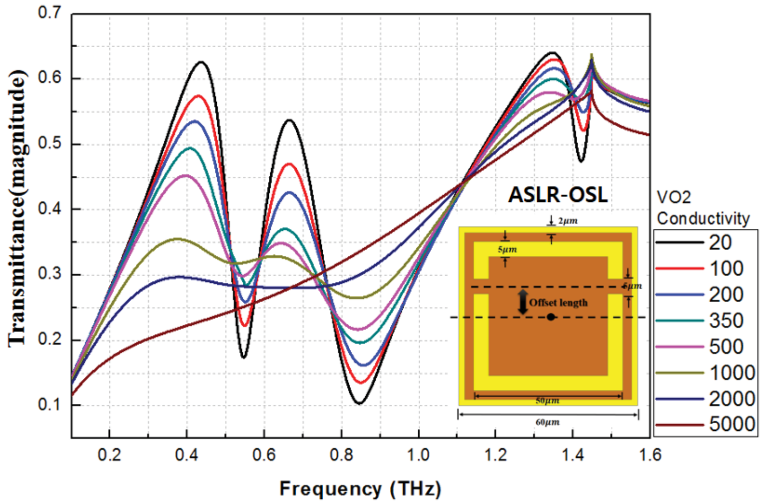

Figure 1. The transmittances of an asymmetric split-loop resonator with an outer square loop (ASLR-OSL) according to the various conductivity of VO_2. The right bottom inset shows the schematic of an ASLR-OSL

Nanoscale mapping of surface and interfacial strain in tapered ZnO nanorods by two-photon confocal laser scanning microscopy

H. Y. Hwang[1], R. Hossen[1], H. J. Baek[2], G. C. Yi[2], and Y. D. Jho[1*]

1- School of Electrical Engineering and Computer Science, Gwangju Institute of Science and Technology, Gwangju 61005, South Korea

2- Department of Physics and Astronomy, and Research Institute of Advanced Materials, Seoul National University, Seoul 08826, South Korea

jho@gist.ac.kr

Most of the studies regarding the size-dependent surface strain have been focused on metallic materials. For example, size-dependence of surface strain for Cu nanorod (NR) have been theoretically reported in the nanoscales[1]. However, surface strain characteristics in the nanoscale semiconductor structures have rarely been reported. Here, we newly report the spatial distributions of strain along the z-axis in an array of tapered ZnO NRs using confocal laser scanning microscopy induced by two-photon excitation. The tapered ZnO NRs were vertically grown on sapphire along c(or z)-axis and consist of three regions: (I) the rapidly tapered tip from z = 0 nm (diameter, d = 3 nm) to z = 10 nm (d = 20 nm), (II) the gradually tapered region from z = 10 nm (d = 20 nm) to z = 200 nm (d = 58 nm), and (III) the pillar with constant diameter of 58 nm above z = 200 nm as displayed in Fig. (a). To quatify the strain-associated parameters in photoluminescence (PL) spectra, we traced the PL peak energy as a function of z at 293K in Fig. (b). Based on the spatial distributions of strain as a function of z derived from the strain Hamiltonian[2], a variation of surface strain in the range of 0 nm to 200 nm in Fig. (b) shows good agreement with theoretical curve of size-dependent surface strain. In addition, interfacial tensile strain up to 0.26% was manifested near the NR/sapphire interface (or at z = 1200 nm) and interfacial strain was exponentially relaxed away from the NR/sapphire interface as shown in Fig. (b). In Fig. (c), surface and interfacial strain with increasing temperature are strongly influenced by size-dependent thermal expansion and difference of thermal expansion between ZnO NRs and sapphire, respectively.

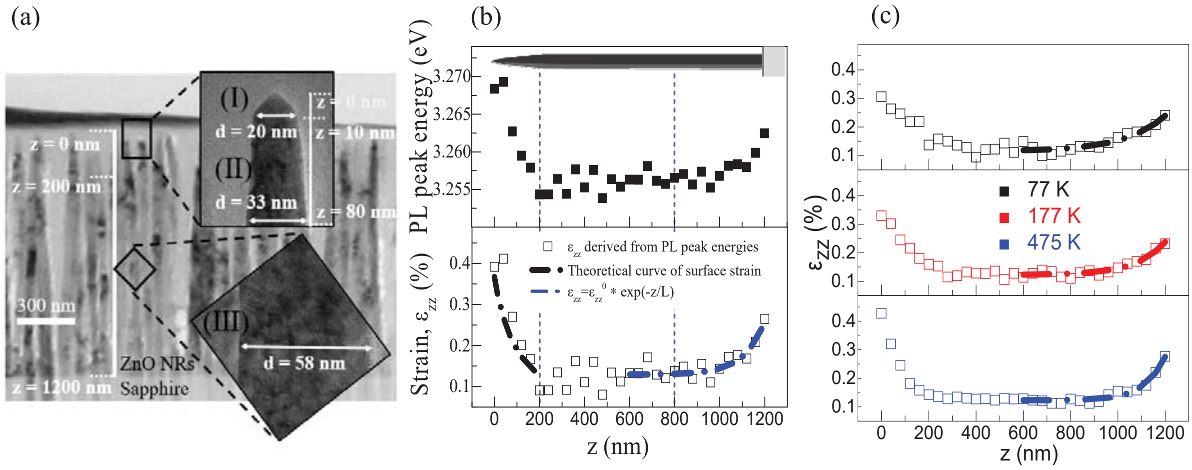

Figure. (a) Side-view TEM images of the tapered ZnO NRs. Upper and lower insets show close-up image of tapered tip below z = 80 nm and that of pillar with constant diameter above z = 200 nm, respectively. (b) PL peak energy and strain at 293K as a function of z. (c) Strains at 77K, 177K, and 475K as a function of z.

[1] R. Dingreville, J. Qu, M. Cherkaoui, Surface free energy and its effect on the elastic behavior of nanosized particles, wires and films, J. of the Mech. and Phys. of Solids, 53, pp. 1827-1854, (2005).
[3] T. Makino, et. al., Strain effects on exciton resonance energies of ZnO epitaxial layers, Appl. Phys. Lett. 79, pp. 1282, (2001).

This work was supported by GIST Research Institute (GRI) in 2017.

Phonon-Assisted Anti-Stokes Photoluminescence in GaN Nanopyramid Structure

Raqibul Hossen[1], Hyeong-Yong Hwang[1], Seung-Hyuk Lim[2], Hyun Gyu Song[2], Kie Young Woo[2], Yong-Hoon Cho[2], Young-Dahl Jho[1*]

1- School of Electrical Engineering and Computer Science, Gwangju Institute of Science and Technology, Gwangju 61005, Republic of Korea.
2- Department of Physics, Korea Advanced Institute of Science and Technology (KAIST), Daejeon 34141, Republic of Korea.
Email: jho@gist.ac.kr

Anti-Stokes photoluminescence (ASPL) has been studied in numerous GaN structures [1], where the mechanism attributing to this phenomena has been mainly divided into two categories. In most of the cases, multi-photon absorption was considered as the dominant mechanism for ASPL in GaN [2], while phonon-assisted absorption was also reported as the dominating mechanism, such as in GaN film at room temperature (RT) [3]. Here we newly considered the structural role of submicron scale pyramids to enhance ASPL. For the first time, we are reporting ASPL detection at RT from hexagonal GaN nanopyramids fabricated on GaN-based LED structure with InGaN/GaN MQWs, as shown in Fig. 1(a).

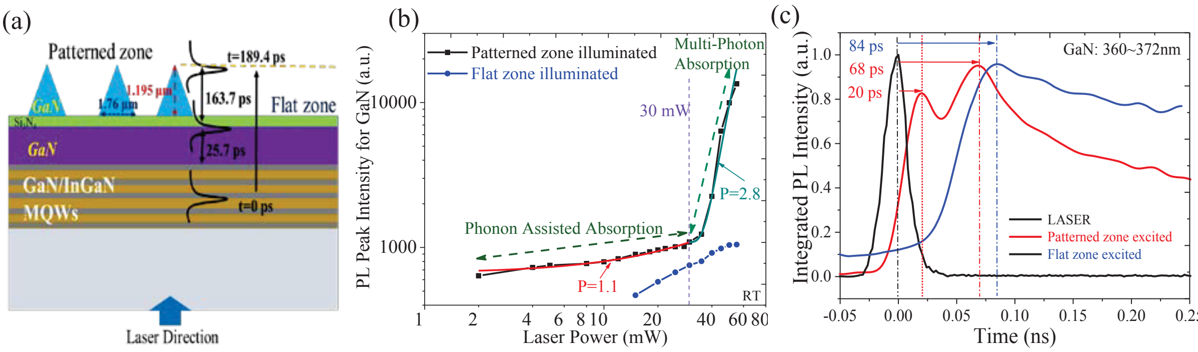

Figure 1. (a) Schematic of GaN-based LED structure with GaN nanopyramids, (b) PL peak intensity for GaN as a function of laser power, where the colored lines resemble power fit to data. (c) Time-resolved photoluminescence spectra at room temperature, where the dotted line depicts the delay of the peak appearance corresponding to the laser.

We first measured PL at RT varying laser power at below bandgap excitation (3.1 eV), illuminating both patterned and flat zone of the sample. Obtained pump power dependence of ASPL intensity for the peak at 370 nm in both cases has been illustrated in Fig. 1(b), from where it's clearly evident that the ASPL intensity have been enhanced in nanopyramids compared to flat zone. Moreover, while patterned zone have been excited ASPL intensity shows almost linear dependence until the pump power reaches 30 mW and changes nonlinearly after that, though the flat zone excitation result don't follow similar trend. Such linear power dependence of ASPL is the characteristic for phonon-assisted absorption [3] and the following case supports multi-photon absorption mechanism [1]. Furthermore, to study phonons' role in ASPL, time-resolved PL has been measured and the results are shown in Fig. 1(c) for both patterned and flat zone excitation. From Fig. 1(c) it is visible that there is a 68 ps of delay in TRPL signal appearance in case of patterned zone excitation, while in case of flat zone excitation the delay is about 84 ps. This delay could be interpreted as the propagation time for phonon to reach focusing point in nanopyramids and consequence in ASPL due to high intensity of phonons at focusing point, though this interpretation is needed to be studied further for precise understanding. Generation and observation of the propagating acoustic phonon dynamics in our sample were confirmed through pump-probe measurement with a frequency doubled Ti:Sapphire laser in the tuning range of 390-420 nm. This work could open up new opportunities for efficient removal of non-equilibrium phonons and optical cooling.

[1] Y.J. Ding and J.B. Khurgin, From anti-Stokes photoluminescence to resonant Raman scattering in GaN single crystals and GaN-based heterostructures, Laser & Photon. Rev., vol. 6, pp. 660-677, (2012).
[2] Y. Toda, et. al., Two-photon absorption and multiphoton-induced photoluminescence of bulk GaN excited below the middle of the band gap, Appl. Phys. Lett., vol. 82, pp. 4714-4716, (2003).
[3] S. K. Tripathy, Y. J. Ding and J. B. Khurgin, Anti-Stokes photoluminescence from n-type free-standing GaN at room temperature based on competition between phonon-assisted and two-photon absorption, Semiconductor Science and Technology, vol. 24 (5), pp. 1-5, (2009).

This work was supported by GIST Research Institute (GRI) in 2017.

Terahertz molecular fingerprintof cancer DNA

Joo-Hiuk Son[1] and Hwayeong Cheon[1]

[1]*Department of Physics, University of Seoul, Seoul 02504, Republic of Korea*

joohiuk@uos.ac.kr

Cancer is defined asa genetic and epigenetic disease involvingthe chemical and structural alteration of DNA. Because optical techniques measure overlappedand synthetic signals of materials, regardless of“ordering” features (such as the nucleotide order of a DNA sequence), it is difficult to sequencea genome to detectcancerous genetic changes using optical techniques.For this reason, previous genome sequencing methods, such as nanopore sequencing, have usually used electronic techniques[1, 2]. This only serves to emphasizethe importance role of detecting cancerous epigenetic changes to DNA, whenthe optical molecular fingerprints of cancer are found.Aberrant DNA methylationisan epigenetic modification, a well-known carcinogenic mechanism [3, 4], and a common chemical and structural modification of DNAthat does not change the DNA sequence. Terahertz wavescan be used to observe modificationstoDNA because the characteristic energiesof biomolecules occur in the terahertz region. We found resonance fingerprints of methylation in cancer DNAs using improved terahertz spectroscopic methods [5]. The terahertz characteristics of methylated cytidine, a nucleoside, were a clue toobserving the resonance fingerprints of DNA methylation. In aqueous solutions,we tracked and monitored the molecular resonances of genomic DNA from two control (293T, M-293T) and five cancer (PC3, A431, A549, MCF-7, SNU-1) cell lines, using freezing techniques and baseline corrections, as shown in Fig. 1 (a). The amplitudes of the resonance signals weredependent on the types of cancer cells the DNA had come from. These signals were quantified to identify cancer cell types,and the results were similar to those of biological quantification methods (Fig. 1 (b)). This research demonstrated that the molecular resonance fingerprints of cancerDNAsexist in the terahertz region,and they can be measured using advancedterahertz time-domain spectroscopy (THz-TDS) techniques. These results can be utilized to diagnoseearly cancer at the molecular level, and provide a potential cancer biomarker.

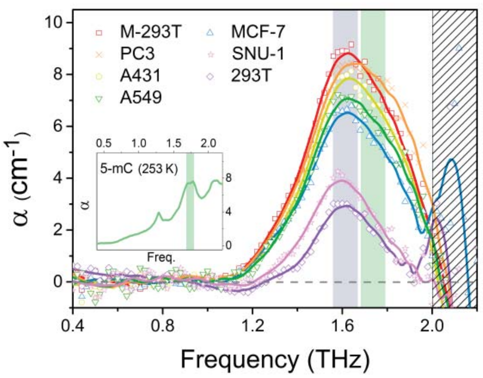

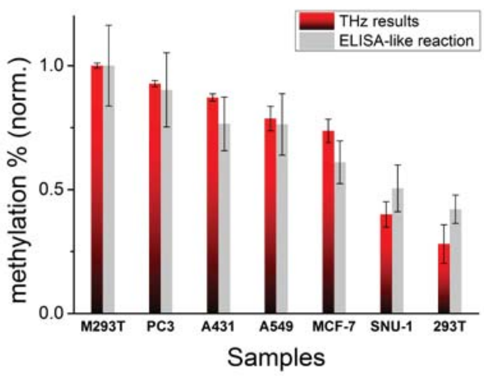

Fig. 1. (a) Resonance of normal and cancerDNA; (b) DNA quantification results.

References

[1] Branton D. et al., The potential and challenges of nanopore sequencing. Nat. Biotechnol. 26 (10), 1146–1153 (2008).
[2] Sadeghi H. et al., Graphene sculpturenenanopores for DNA nucleobase sensing. J. Phys. Chem. B 118, 6908–6914 (2014).
[3] Jones, P. A. DNA methylation and cancer. Oncogene 21, 5358–5360 (2002).
[4] Laird, PW. The power and the promise of DNA methylation markers. Nat. Rev. Cancer 3, 253–266 (2003).
[5] Cheon, H. et al., Terahertz molecular resonance of cancer DNA. Scientific Reports 6, 37103 (2016).

CMOS Biosensor Using Picosecond Dynamics of Water Molecule

Y. Ogawa[1], T. Suzuki[1]

1- Graduate School of Agriculture, Kyoto University, Kitashirakawa-Oiwakecho, Kyoto, Japan

ogawayu@kais.kyoto-u.ac.jp

About 70% of intracellular is dominated by water. Various cellular functions and activities have been revealed by molecular biological approach. Nevertheless, the role of intracellular water is still cloaked in mystery because bulk water dynamics with sub-picosecond and picosecond timescales have never directly probed by conventional experimental techniques. THz time-domain attenuated total reflection (THz TD-ATR) spectroscopy based on femtosecond laser technology enables an understanding of the picosecond dynamics of the hydrogen bond network, giving us detail water molecular dynamics through the complex dielectric constant of solutions in THz region [1]. Recently, we also have succeeded in measuring the complex dielectric constant of the cultured cells on the ATR prism [2]. Since the penetration depth of the evanescent field (sample depth) in this technique is greater than the thickness of the cell monolayer, the contribution of the medium was removed by a two reflection interface model; cell monolayer as first component on the ATR prism and second component as liquid medium (Fig. 1). Fitting Debye-Lorentz function to the spectra enables discussions and characterization of the intracellular water dynamics. Characteristic of dielectric constant in terahertz range originates from slow relaxation in hydrogen bond network of bulk water, fast relaxation of isolated water and intermolecular vibration between water molecules etc. Experimental result demonstrated significant changes of intracellular water dynamics: decrease of hydrogen bond network and increase of isolated water molecule. Such analysis of intracellular water dynamics has potential for classification and quantification of cellular activity.

Such spectra information give us a chance to develop an unique sensor cell science. We have been developing CMOS array sensor working at 60 GHz and 120 GHz as a tool to collect quantitative cellular property in terahertz region [3]. More than 100 number of LC-oscillators designed for sub-THz range to capture change of dielectric constant originated from bulk water, are arranged in 2 dimensions periodically (Fig.2). The resonance frequency shifts by dielectric change just of the surface of the sensor, and is measured rapidly. Integration of the oscillators enables near-field imaging with high spatial resolution. In simulation and experiment, frequency shifts of the CMOS sensor agreed well with dielectric constant change of water and solution on the surface. Difference of dielectric constant between living cell and liquid medium was also demonstrated.

This work was supported by JSPS KAKENHI Grant Numbers 16H05010, 16K18779, and Collaborative Research Based on Industrial Demand Program from Japan. Science and Technology Agency, JST. We are grateful to Mr. Iizuka, Mr. Yamanoue, Mr. Mitsunaka, Mr. Ashida, Mr. Ashida and Mr. Sato, Sharp Corporation for support of the research.

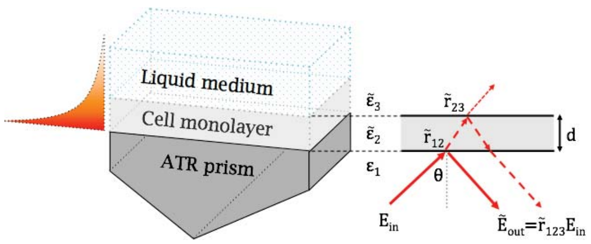

Fig. 1 Schematic illustration of THz TD-ATR spectroscopy with the two-interface model.

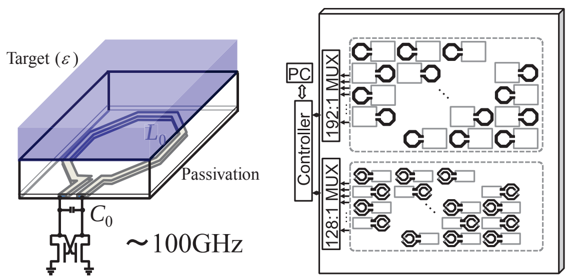

Fig. 2 Schematic structure of CMOS sensor.

[1] H. Hirori, K. Yamashita, M. Nagai and K. Tanaka, Attenuated Total Reflection Spectroscopy in Time Domain Using Terahertz Coherent Pulses, Japanese Journal of Applied Physics, vol. 43, pp. 1287-1289, (2004).

[2] K. Shiraga, Y. Ogawa, T. Suzuki, N. Kondo, A. Irisawa and M. Imamura, Characterization of dielectric responses of human cancer cells in the terahertz region, Journal of Infrared, Millimeter, and Terahertz Waves, vol. 35, pp. 493-502, (2014).

[3] T. Mitsunaka, D. Sato, *et al*., CMOS Biosensor IC Focusing on Dielectric Relaxations of Biological Water With 120 and 60 GHz Oscillator Arrays, IEEE Journal of Solid-State Circuits, vol. 51, no. 11, pp. 2534-2544, (2016).

Biomedical Imaging Technology Using THz Wave

Seung Jae Oh[1], Young Bin Ji[1], Jin Such Suh[1,2]
1-Medical Convergence Research Institute, Yonsei University College of Medicine, Seoul, Korea
2- Department of Radiology, Yonsei University College of Medicine, Seoul, Korea

Main author email address: issac@yuhs.ac

Terahertz (THz) is a new medical technology because of its high sensitivity to water and fat in the living body and its biosafety due to low energy. THz wave technology is being studied to be applied to a variety of biomedical fields such as dentistry, dermatology and oncology to neurology and physiology. Recently, various diseases such as stomach cancer, brain cancer, etc. have been studied for application to the biomedical field. Particularly, research is being conducted to improve target specificity and penetration depth in vivo as a technique required for practical medical field application. This study showed that THz wave can be used for the diagnosis of gastric cancer, brain cancer and otitis media.

[1] J. -H. Son, Terahertz electromagnetic interactions with biological matter and their applications, J. Appl. Phys., vol. 105, no. 10, p. 102033, (2009).
[2] Y. B. Ji et al., Feasibility of terahertz reflectometry for discrimination of human early gastric cancers, Biomedical Optics Express, col. 6, no. 4, pp. 1398-1406, (2015).
[3] S. J. Oh et al., Study of freshly excised brain tissues using terahertz imaging, Biomedical Optics Express, vol. 5, no. 8, pp. 2837-2842, (2014).
[4] Oh, S. J. et al., Measurement depth enhancement in terahertz imaging of biological tissues, Opt. Express 21(18), 21299–21305 (2013).
[5] Ji, Y. B. et al.,Terahertz otoscope and potential for diagnosing otitis media, Biomed. Opt. Express 7(3), 1201-1209 (2015).
[6] Ji, Y. B. et al., Terahertz reflectometry imaging for low and high grade gliomas, Scientific Reports 6, Article number: 36040 (2016)

In-vivo THz Sensing of Tear Film and Corneal Tissue

A. Angeluts[1], A. Balakin[1], M. Mischenko[1], I. Ozheredov[1], M. Prokopchuk[1], T. Saphonova[2], P.Solyankin[1], A. Shkurinov[1]

1- Moscow State University, Leninskie Gory 1, Moscow, 119992 Russia
2- Research Institute of Eye Diseases, Rossolimo Str. 11, Moscow, 119021 Russia

E-mail: ozheredov@physics.msu.ru

The cornea is of the great importance among the other eye refractive structures. The cornea maintains the most eye's refractive power and provides the visual function. The clarity of corneal tissue is vitally important for this function and strongly dependent on its tissue hydration level. This level is regulated by internal eye mechanisms and in the most cases varies from 78% to 80% by volume [1]. The change of hydration level even for a few percents may indicate various possible corneal diseases related to the restructuring and swelling of the various cornea layers, tear film and epithelium / endothelial integrity [2].
The THz radiation has a great potential for development of corneal tissue hydration monitoring techniques. At first, there is very high sensitivity of this radiation to water content in biological tissues. At second, due to non-invasive nature of the THz radiation the technique might be used for in-vivo sensing. And last, but not least, there is high homogeneity of water distribution in the eye cornea and low physiological variability of cornea as compared to other human tissues.
We proposed simple THz frequency-domain apparatus with the smooth tuning within "low frequency" THz range that might be used for in-situ control of tear-film drying and sensing of human corneal tissue hydration level. THz generator was based on the two continuous DFB diode lasers with the generation of narrow (10 kHz) line in the range 1530 – 1608 nm. Radiation from the lasers was combined by X-type fiber optical beam splitter with the ratio 50/50. At the output of the splitter the radiation was modulated by the frequency detuning of two lasers. A semiconductor low-temperature InGaAs bow-tie photoconductive antenna (PCA) was used for converting of this modulated radiation into the THz emission. Such source showed high efficiency at frequencies of 30-300 GHz. For detection the similar InGaAs PCA was used. Both emitter and detector equipped with the focusing lens and were placed on the special ophthalmology stage. This stage allowed placing the patient's eye cornea in the focal plane and provided the detection of the THz radiation reflected from the cornea. The photo of experimental apparatus is shown in fig.1.

Fig.1. Photo of the experimental apparatus for in-vivo human cornea hydration sensing.

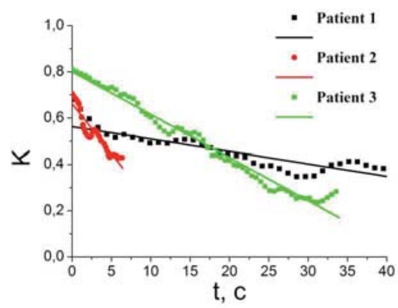

Fig.2. The cornea reflection coefficient versus time after the latest blinking for different patients. Dots-experiment, lines - linear fit.

Using the proposed setup we conducted measurements of the eye cornea reflection coefficient for several patients of different age. Fig.2 shows a few experimental results of in-vivo measuring the dynamics of tear film drying and cornea hydration measurements in case of using for sensing the radiation of 40 GHz. These preliminary measurements clearly showed the high sensitivity of our approach for different states of cornea and tear film.
The authors acknowledge financial support of RFFI under project No.15-29-03900.

[1] I.Fatt, B.A.Weissman, Physiology of the eye: an introduction to the vegetative function (Butterworth-Heinemann) (2013).
[2] W.S.Vanmeter, W.B.Lee, D.G.Katz, Duane's Clinical Ophthalmology. Chapter 16A, Corneal Edema (2006).

THz Spectroscopy and Imaging of Blood

Chi-Kuang Sun

Graduate Institute of Photonics and Optoelectronics, National Taiwan University, Taipei 10617, Taiwan

Blood is the most essential body fluid, containing many kinds of proteins, carbohydrates, hormones, lipids, blood cells, and salts. Blood is responsible for distribution of oxygen and nutrition, core body temperature regulation, and immunological function. Many biochemical variables in blood plasma, such as glucose, thrombus, and total cholesterol, are highly related to diseases such as diabetes, stroke, and heart diseases. Remote sensing of the component content of blood is critical for developing the current wearable devices for daily heath care monitoring as well as for intense care unit for continuous risk factor monitoring. Currently the concentration and molecular properties of most biochemical variables can only be examined *ex-vivo*, while a noninvasive and in vivo method is highly desired.

Recently, THz wave has been proved to have strong interactions with many biochemical molecules such as amino acids, proteins, and DNA. In aqueous solutions composed of water, THz wave has also been found to be a sensitive tool to investigate the collective bending vibration of hydrogen bond of water molecules. Recent studies indicate that the THz absorption of water solution is highly sensitive to the concentration of various solutes since the polarized solute would change the collective bending vibration of hydrogen bond. Blood has around 80% water content and contains many kinds of polarized solutes, representing different risk factors of human. Comparing to existing enzymatic colorimetric examination methods, THz wave could be a potential candidate to monitor the risk factors in human blood in a longitudinal and noninvasive way.

In this presentation, I will review our recent efforts on THz spectroscopy and imaging of blood. Recent THz spectroscopy studies of human and animal blood had indicated the high sensitivity of THz waves to a few critical blood ingredients including triglyceride, red blood cell, and glucose level [1-6]. In our recent clinical study of the sub-THz spectra of *ex-vivo* fresh human whole blood [6], which was taken from 57 patients following 8-hours fasting guideline, a great difference between the sub-THz absorption properties of human blood among different people was observed, while the difference can be >15% of the averaged absorption coefficient. Our pilot clinical study indicates that triglycerides and the number of red blood cells were two dominant factors to have significant correlation to the sub-THz absorption coefficients. A near-field sub-THz transmission-type image system, operating at a frequency close to 300GHz, for vessel imaging *in-vivo* was also demonstrated for noninvasive quantitative imaging of THz absorption constant of blood [7], to demonstrate the capability of THz waves for longitudinal and noninvasive monitoring of blood in vivo.

[1] D.-K. Kim, J.-H. Won, V. V. Meriakri, and E. E. Chigrai, Device for the non-invasive measurement of blood glucose concentration by millimeter waves and method thereof, US Patent 7371217 B2, Samsung Electronics Co., Ltd. (2008).
[2] C.-K. Sun, Y.-F. Tsai, and H. Chen, Method and device for detecting a blood glucose level using an electromagnetic wave, US patent 20130289370 A1, National Taiwan University (2013).
[3] O. P. Cherkasova, M. M. Nazarov, I. N. Smirnova, A. A. Angeluts, and A. P. Shkurinov, Application of timedomain THz spectroscopy for studying blood plasma of rats with experimental diabetes, Phys. Wave Phenom. Vol. 22(3), pp. 185–188 (2014).
[4] K. Jeong, Y. M. Huh, S. H. Kim, Y. Park, J. H. Son, S. J. Oh, and J. S. Suh, Characterization of blood using terahertz waves, J. Biomed. Opt. vol. 18(10), 107008 (2013).
[5] C. B. Reid, G. Reese, A. P. Gibson, and V. P. Wallace, Terahertz time-domain spectroscopy of human blood, IEEE J. Biomed. Health Inform. Vol. 17(4), pp. 774–778 (2013).
[6] T.-F. Tseng, B. You, H.-C. Gao, T.-D. Wang, and C.-K. Sun, Pilot clinical study to investigate the human whole blood spectrum characteristics in the sub-THz region, Optics Express vol. 23 (7), pp. 9440-9451 (2015).
[7] T.-F. Tseng, S.-C. Yang, Y.-T. Shih, Y.-F. Tsai, T.-D. Wang, and C.-K. Sun, A near-field sub-THz transmission-type image system for vessel imaging *in-vivo,*" *Optics Express vol.* 23 (19), pp. 25058-25071 (2015).

Correlative Optical Imaging in the Far-field and Near-field Regimes: Architecture, Applications and Perspectives

S.G. Stanciu[1], D.E. Tranca[1], R. Hristu[1], G.A. Stanciu[1]

1-Center for Microscopy - Microanalysis and Information Processing, University Politehnica of Bucharest, 313 Splaiul Independentei, 060042, Romania

stefan.stanciu@cmmip-upb.org

Modern investigation frameworks used for the characterization of biological matter, advanced materials or devices rely on a wide variety of high- and ultra-high resolution imaging techniques. Among these, optical nanoscopy techniques are gaining increasing interest, as their resolution capabilities can lead to achieving significant breakthroughs in multiple key scientific domains. However, the applicability and popularity of some variants are still biased by data interpretation issues. This is mainly connected to the fact that performing an imaging experiment for the first time using a technique that has not been employed before in similar purposes can be difficult. Initial observations of optical details at nanoscale are at first puzzling for almost any considered sample and leave room for a myriad of questions. Such situations often times lead to contradictory interpretations of the collected data sets, a situation which is especially accentuated in the case of independent experiments.

The situation above described applies also in the case of Apertureless Scanning Near-Field Optical Microscopy (ASNOM), a family of imaging techniques that not until long ago were available only in the form of home-made versions. ASNOM holds significant potential for advancing beyond the state-of-the-art our current understanding on the structural, chemical and optical features of biological samples, materials or devices. However, due to the above mentioned reasons its applicability is not always straightforward. One way to alleviate this situation is to correlate ASNOM data sets with well understood data sets collected with mature imaging techniques. Such cross-correlative studies are nevertheless not always easy to implement as identifying sample regions of interest after switching between imaging systems based on different contrast mechanisms, and working at different scales, is usually cumbersome. For this reason, we have recently developed a multimodal imaging system capable to collect optical data sets on overlapping field-of-views by several ASNOM and far-field Laser Scanning Microscopy (LSM) techniques. Moreover, this system incorporates as well a series of Scanning Probe Microscopy variants, which are useful for placing optical data sets into a topographic context. The contrast mechanisms of the incorporated imaging techniques provide complementary information, which plays an important role in facilitating nanoscale data understanding and interpretation. In our contribution we present this imaging architecture and showcase a series of results collected on nanostructured materials and biological samples in the frame of innovative correlative-imaging assays, e.g. [1]. A special focus of attention is placed on highlighting the capabilities of scattering-type SNOM, an ASNOM variant, to extract information over the real-part and imaginary-part of the dielectric function at spatial resolutions beyond the diffraction barrier [2]. In the frame of correlative ASNOM-LSM studies such dielectric properties can be placed in correspondence with other information categories, e.g. fluorescence or non-linear optical phenomena related. Perspectives for extending this architecture with additional workmodes are also discussed, together with connected potential applications. The presented results demonstrate that correlating far-field and near-field optical data sets can enable new perspectives in many fields of science such as biology, medicine or materials science.

Acknowledgment: The presented work has been supported by LANIR and MICRONANO research grants. LANIR has received funding from the European Community's Seventh Framework Programme (FP7/2012-2015) under grant agreement n°280804. MICRONANO (PN-II-RU-TE-2014-4-1803) is funded by the Romanian Executive Agency for Higher Education, Research, Development and Innovation Funding (UEFISCDI).

[1] S.G. Stanciu, D.E. Tranca, C. Ruggiero, G.A. Stanciu, E. Dellacasa, A. Antipov, R. Hristu, L. Pastorino, Combined far-field, near-field and topographic imaging of nano-engineered polyelectrolyte capsules, Materials Letters, vol. 183, pp. 105-108, (2016)

[2] D.E. Tranca, S.G. Stanciu, R. Hristu, C. Stoichita, S.A.M. Tofail, G.A. Stanciu, High-resolution quantitative determination of dielectric function by using scattering scanning near-field optical microscopy, Scientific Reports, 11876, (2015)

VOCs emitted from seeds germinated with heavy metals measured by optical spectroscopy technique

C. Achim (Popa)[1], D. C. Dumitras[1,2]

1- National Institute for Laser, Plasma and Radiation Physics, Laser Department, 409 Atomistilor St., PO Box MG-36, 077125 Bucharest-Magurele, Romania
2-University "Politehnica" of Bucharest, Faculty of Applied Sciences, Physics Department, 313 Splaiul Independentei, Bucharest – 060042, Romania

email address: dan.dumitras@inflpr.ro, cristina.achim@inflpr.ro

In this research, we report the photoacoustic analysis [1] of volatile organic compunds – VOCs, e.g. ethylene and ammonia, from plantlets (common wheat seeds, Spelt wheat, common corn, alfalfa, and green peas), measured after the germination with five heavy metals (Cd, Hg, Pb, Cu and Zn) in order to analyse the plant growth regulator and degradation of proteins at plant tissue level. The results were compared with the data from seeds germinated with distilled water (used as the control treatment).
The use of these gas molecules in the respiration of plantlets for seeds germinated with heavy metals is theoretically reasonable; metabolic changes occur in plantlets that inevitably lead to the production of abnormal metabolites. These molecules are transported through diffusion and the metabolites will then be discharged into the respiration of plantlets as components of each biological sample [2,3].
Our results support the hypothesis that protein damage and oxidative attack seems to be a key effect in the toxicity and carcinogenicity of heavy metals at plantlets and suggest new markers that may contribute to a better understanding of heavy metals influence.
In the same time, the investigations presented in this work showed that the photoacoustic technology in the detection of VOCs was able also to distinguish between seeds germinated with heavy metals and seeds germinated with distilled water and can play an important role in testing the contaminated biological samples.
The results from this research contribute to the understanding of toxicity and damage of contaminated plants using a sensitive and non-invasive method like laser photoacoustic spectroscopy [4,5].
The technique from this research assure the advantages of health state assessment by monitoring the level of VOCs (from seeds germinated with heavy metals) that can be metabolized inside the organism with adverse effects on human health (e.g. ethylene is metabolized to ethylene oxide and, in accordance with International Agency for Research on Cancer, ethylene oxide is a human carcinogen) [6].

Acknowledgments: This work was funded by CNCS-UEFISCDI, project number PN-II-PT-PCCA-2013-4-0608 (72/2014) and by Space Technology and Advanced Research-ESA, project (C3 2016) no. 603 „Development of a New Instrument for Monitoring of the Astronauts Health" IMAH. We gratefully acknowledge the assistance provided by the Dr. Marian Mogildea from the Institute for Space Sciences (ISS), Bucharest-Magurele, Romania.

References

[1] D.C. Dumitras, S. Banita, A.M. Bratu, R. Cernat, D.C.A. Dutu, C. Matei, M. Patachia, M. Petrus and C. Popa, "Ultrasensitive CO_2 laser photoacoustic system", Infrared Physics & Technology Journal, Vol. 53, No. 5, pp. 308-314 (2010).
[2] C. Popa, D.C. Dumitras, M. Patachia, and S. Banita, "Testing fruits quality by photoacoustic spectroscopy assay", Laser Physics, Vol. 24, No. 10, doi:10.1088/1054-660X/24/10/105702 (2014).
[3] C. Popa, D. C. Dumitras, M. Patachia and S. Banita,"Improvement of a photoacoustic technique for the analysis of non-organic bananas during ripening process" Rom. J. Phys., Vol. 60, No. 7-8, pp 1132-1138 (2015)
[4] C. Popa, M. Petrus, A.M. Bratu, M. Patachia, S. Banita and D.C. Dumitras, "Food safety test by laser photoacoustic spectroscopy assessment", Ed. Univ. Transilvania, Brasov, Ed. Florescu Monica, Chapter in "Biophysics for Biomedical and Evironmental Sciences", ISBN 978-606-19-0768-7 (2016).
[5] C. Popa and M. Petrus, "Spectroscopic analysis of some heavy metals on the contaminated vegetation", Ed. Univ. Transilvania, Brasov, Ed. Florescu Monica, Chapter in "Biophysics for Biomedical and Evironmental Sciences", ISBN 978-606-19-0768-7 (2016).
[6] http://monographs.iarc.fr/ENG/Monographs/vol100F/mono100F-28.pdf.

Control of CdTe quantum dots photostability

A.S. Tsipotan[1], A.S. Aleksandrovsky [2], V.V. Slabko[1]

1- Siberian Federal University, Krasnoyarsk, 660041, Russia.

2- Russian Academy of Sciences, Kirensky Institute of Physics Krasnoyarsk 660036, Russia.

cipotana@mail.ru

Semiconductor nanocrystals (colloid quantum dots (QD)) attract great attention in recent years due to numerous possible applications. The progress in these studies is sometimes hindered by the limitations of chemical stability and photostability of QDs in solution [1]. The latter is especially important in the physical regimes when QDs undergo long-lasting or multiply repeated optical irradiation. Such the regimes occur, for example, when QDs are utilized for cellular labeling and biological imaging [2] or in the processes of self-assembly of QDs into the structures of pre-defined geometry in the field of laser radiation [3].

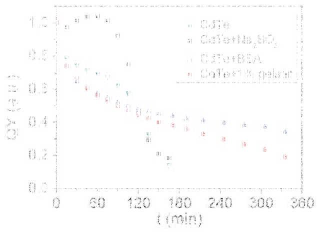

Figure 1. Quantum yield of QDs under UV irradiation for CdTe in the buffer solution; with addition of Na_2SO_3; in 1% gelatin solution; additionally stabilized by BSA.

Additional enhancement of TGA-stabilized CdTe QDs' photostability under UV irradiation is demonstrated. The methods employed are chemical removal of oxygen, solution viscosity increase, and additional passivation of TGA@QD complexes. Introduction of excessive oxygen-binding Na_2SO_3 enables perfect photostability during the time period of order of hours, until the expenditure of this stabilizer. Control of solution viscosity by gelatin addition produces two-fold increase of QDs' photostability. The combined TGA+BSA stabilization of QDs must be considered as the most promising one since it not only enhances the photostability but also makes QDs more biocompatible and extends the possibilities of their applications in biological media.

The reported study was funded by RFBR and Krasnoyarsk Krai according to the research project No. 16-42-240410r_a and RFBR research project No. 16-32-00129.

[1] J. Aldana, Y.A. Wang, X. Peng, Photochemical Instability of CdSe Nanocrystals Coated by Hydrophilic Thiols, J. Am. Chem. Soc., vol. 123 (36), pp. 8844–8850, (2001).

[2] J. Ma, J.Y. Chen, Y. Zhang, et.al. Photochemical Instability of Thiol-Capped CdTe Quantum Dots in Aqueous Solution and Living Cells: Process and Mechanism, J. Phys. Chem. B, vol. 111, pp. 12012-12016, (2007).

[3] A.S. Tsipotan, M.A. Gerasimova, V.V. Slabko, A.S. Aleksandrovsky, Laser-Induced Wavelength-Controlled Self-Assembly of Colloidal Quasi-Resonant Quantum Dots, Opt. Express, vol. 24(10), pp. 11145-11150 (2016).

Non-destructive detection capability of laser diagnostics based optical coherence tomography for agricultural applications

Mansik Jeon

School of Electronics Engineering, College of IT Engineering, Kyungpook National University, 80 Daehak-ro, Buk-gu, Daegu 41566, Korea

E-mail: msjeon@knu.ac.kr

The pathological and physiological defects in various types of agricultural materials lead to an enormous amounts of economical waste. Thus, the interest towards non-destructive and high-resolution optical imaging techniques for the diagnosis of aforementioned defects has been increased during past few decades [1-4]. It is well recognized that pathological infections caused internal defects of plant materials can be effectively visualized at an initial stage of the disease by using a well-known bio-photonic detection method called optical coherence tomography (OCT) and optical coherence microscopy (OCM), which were initially developed for medical applications. The exploitation of high-resolution benefits of OCT and OCM for various agricultural research studies were frequently reported through the obtained exemplary high-resolution two-dimensional, volumetric three-dimensional images, and quantitative evaluations revealing complementary morphological abnormalities between healthy and defected specimens [5-6]. Although several plant-inspection technologies, such as magnetic resonance imaging (MRI), X-rays, positron emission tomography (PET), and confocal microscopy were frequently applied for plant material experiments, the potential applicability of these methods has been limited by factors such as a low resolution, limited penetration, and long acquisition time. Hence, to avoid the aforementioned limitations, OCT and OCM were considered as ideal inspection techniques by various research groups. This paper highlights and briefly introduces the main benefits and the potential ability of optical coherence imaging techniques in various agricultural applications, verifying the capability of characterizing internal microstructures that are useful in agriculture for the initial diagnosis of plant diseases and defects.

Reference

[1] S.-Y. Lee, C. Lee, J. Kim, and H.-Y. Jung, "Application of optical coherence tomography to detect Cucumber green mottle mosaic virus (CGMMV) infected cucumber seed," Horticulture, Environment, and Biotechnology, vol. 53, pp. 428-433, 2012/10/01 2012.
[2] C. Lee, S.-Y. Lee, J.-Y. Kim, H.-Y. Jung, and J. Kim, "Optical sensing method for screening disease in melon seeds by using optical coherence tomography," *Sensors,* vol. 11, pp. 9467-9477, 2011.
[3] R. E. Wijesinghe, S.-Y. Lee, P. Kim, H.-Y. Jung, M. Jeon, and J. Kim, "Optical Inspection and Morphological Analysis of Diospyros kaki Plant Leaves for the Detection of Circular Leaf Spot Disease," *Sensors,* vol. 16, p. 1282, 2016.
[4] R. Wijesinghe, S.-Y. Lee, N. K. Ravichandran, M. F. Shirazi, and P. Kim, "Optical screening of Venturianashicola caused Pyruspyrifolia (Asian pear) scab using optical coherence tomography," International Journal of Applied Engineering Research, vol. 11, pp. 7728-7731, 2016.
[5] N. K. Ravichandran, R. E. Wijesinghe, M. F. Shirazi, K. Park, S.-Y. Lee, H.-Y. Jung, M. Jeon, and J. Kim, "In vivo monitoring on growth and spread of gray leaf spot disease in Capsicum annuum leaf using spectral domain optical coherence tomography," Journal of Spectroscopy, vol. 2016, 2016.
[6] R. E. Wijesinghe, S.-Y. Lee, N. K. Ravichandran, S. Han, H. Jeong, Y. Han, H.-Y. Jung, P. Kim, M. Jeon, and J. Kim, "Optical coherence tomography-integrated, wearable (backpack-type), compact diagnostic imaging modality for in situ leaf quality assessment," Applied Optics, vol. 56, pp. D108-D114, 2017.

Designing microcavity laser diodes by using transformation optics

Muhan Choi[1*], Yushin Kim[2], Jung-Wan Ryu[3], Inbo Kim[1], and Bumki Min[2]

1- School of Electronics Engineering, Kyungpook National University Daegu, 41566, South Korea

2-Department of Mechanical Engineering, Korea Advanced Institute of Science and Technology Daejeon, 34141, South Korea

3-Center for Theoretical Physics of Complex Systems, Institute for Basic Science, Daejeon 34051 South Korea

**E-mail address: mhchoi@ee.knu.ac.kr*

The ultrahigh Q-factor of whispering gallery modes (WGMs) is of great merit in cutting-edge photonic devices, but their isotropic emission due to the rotational symmetry is a serious drawback in applications that require directional light sources[1]. Here, we showed that the optical mode properties of dielectric cavities, such as quality factor and emission directionality, can be tailored at will by using transformation optics[2-3]. The Q-spoiling problem that inevitably is involved with emission directionality is resolved by restoring WGMs in two-dimensional (2-D), deformed, inhomogeneous dielectric cavities. The restored WGMs retain the ultrahigh Q-factor even in considerably deformed cavities and exhibit emission directionality as well. The boundary shape and the refractive index profile are depicted in Fig. 1a and 1c, and its far-field distribution are shown in Figs. 1b and 1d, respectively. The spatially varying refractive index profile can be implemented by drilling subwavelength-scale air holes in a dielectric slab. The proposed design scheme of microcavities based on the transformation optics will open a new horizon of application beyond the conventional microcavity laser diodes.

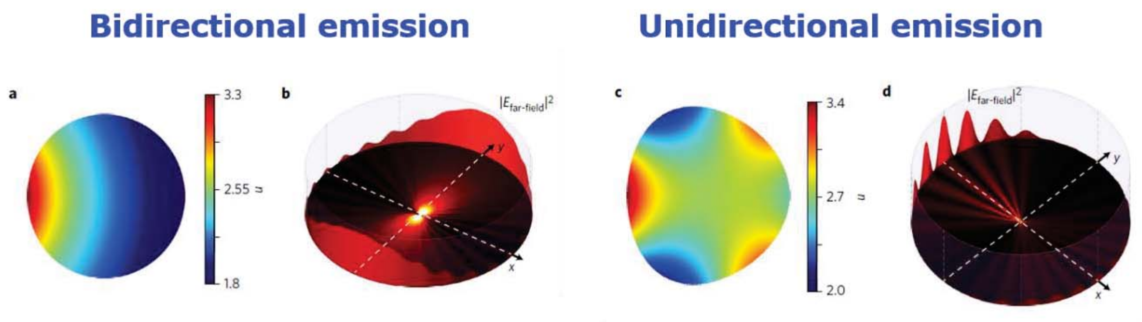

Fig 1. Bi-directional and uni-directional far-field emission of the cWGM of a limaçon-shaped and triangular transformation.

[1] K. J. Vahala, Optical microcavities, Nature, vol.424, pp.839-846, (2003)
[2] J. B. Pendry, D. Schuring, and D. R. Smith, Controlling Electromagnetic Fields, Science, vol.312, pp. 1780-1782, (2006)
[3] Leonhardt, U., Optical conformal mapping, Science, vol.312, pp. 1777-1780, (2006)

First observation of the number-density-dependent growth of plasmonic nanobubbles

Takashi Nakajima

Institute of Advanced Energy, Kyoto University, Gokasho, Kyoto 611-0011, Japan

In recent years lots of studies have been carried out to clarify or apply the light-nanoparticle (NPs) interactions. Very opften the surrounding medium of NPs is a solution, and the plasmonic heating of metallic NPs by the resonant laser leads to the formation of nanobubbles (NBs). They are usually called plasmonic NBs after the plasmonic heating of NPs. The dynamics of NPs and NBs are strongly related not only to the incident laser fluence but also the pulse duration, laser wavelength, etc. We note that very little attention has been paid to the number density of NPs [1] or NP-NP interactions [2] in the solution.

In this paper we discuss the time-dependent dynamics of plasmonic NBs upon irradiation of single nanosecond laser pulses onto the Ag NPs solution with moderate number densities ($3.7 \text{x} 10^7$-$3.7 \text{x} 10^8/\text{cm}^3$), and show that the speed of the growth and the size of plasmonic NBs are strongly dependent on the number density of NPs [1]. Note that our observation cannot be explained by the cnventionally accepted physical picture of plasmonic NBs [3,4]. To explain the experimental results we propose a new model in which the bubble growth is strongly influenced by the pressure waves produced by the surrounding NPs. This interpretation is qualitatively consistent with our experimental observation, and to be more quantitative, we carry out the numerical calculations by solving the Rayleigh-Plesset equation with appropriate modifications to incorporate the time-varying external pressure exterted from the surrounding NPs to find the good agreement with our experimental results. Our findings imply that the number density of NPs in the solution can serve as a new parameter to control laser-NBs/NPs interactions.

[1] T. Nakajima, X. Wang, S. Chatterjee, and T. Sakka, Sci. Rep. **6**, 28667 (2016).
[2] J. Lombard, T. Biben, and S. Merabia, Phys. Rev. E **91**, 043007 (2015).
[3] V. Kotaidis and A. Plech, Appl. Phys. Lett. **87**, 213102 (2005).
[4] D. Werner, A. Furube, T. Okamoto, S. Hashimoto, J. Phys. Chem. C **115**, 8503 (2011).

Holographic manipulation of femtosecond laser pulses for advanced material processing

S. Hasegawa and Y. Hayasaki

Center for Optical Research and Education (CORE), Utsunomiya University, Japan
Main author email address: hasegawa_s@opt.utsunomiya-u.ac.jp

Femtosecond laser processing is a promising tool for fabricating three-dimensional (3D) optical devices in transparent materials. In order to fabricate such optical devices at the millimeter scale, an enormous number of processing points are required, and therefore, the processing throughput must be improved. To address this issue, holographic manipulation of femtosecond laser pulses based on an array of spots has been proposed. Computer-generated holograms (CGHs) enable arbitrary control of the spatial pulse shape and the polarization of the pulse, and spatial light modulators (SLMs) displaying a dynamic CGH have been used to achieve variable spatial shaping of femtosecond pulses. Femtosecond laser processing with a CGH, known as holographic femtosecond laser processing [1], has the advantages of high-throughput pulsed irradiation and highly energy-efficient use of the pulse. In this paper, we demonstrate an arbitrary and variable beam shaping of femtosecond pulses by a CGH displayed on a SLM for high-speed and high light-use efficiency, internal and surface, micro and nano fabrications of materials.

An experimental setup is mainly composed of an amplified femtosecond laser system, liquid-crystal-on-silicon SLMs, laser processing optics, and a personal computer. The femtosecond pulse had a center wavelength of 800 nm, a spectral width of 25 nm FWHM, a pulse width of 40 fs, a repetition frequency of 1 kHz, and linear polarization with a p-component. The pulse was radiated onto the first SLM, which displayed CGH1 for applying a pure phase delay to the p-component, that is, phase modulation. The pulse was also radiated onto the second SLM, which displayed CGH2 for applying a phase delay between the p- and s-components, that is, polarization modulation. The circular or elliptical polarization reflected from SLM2 was converted to linear polarization using a QWP. Consequently, the reconstructed spot array with a desired polarization distribution was obtained and was directed to the laser processing optics, containing a 40× objective lens (OL) with NA = 0.60.

Figure 1 shows an experimental result of a laser processing. Figures 1(a) to 1(c) show the case of radial polarization beam. Figures 1(a) shows CGHs for the phase and polarization modulation, respectively. Figures 1(b) is the optical reconstruction. In the figure, the white arrows mean the polarization direction. The reconstruction had a doughnut-shaped intensity at focus because each focal spot had a phase and polarization singularity at the beam center. Figure 1(c) shows SEM images from top and bird’s eye view of structure fabricated by the vector beam. A pitch of fabricated nanostructure was approximately 180 nm. An orientation of nanostructure was perpendicularly arraigned to the polarization state of vector beam. Figures 1(d) to 1(f) show the case of azimuth polarization beam. Figures 1(g) to 1(i) show the case of windmill polarization beam. From each SEM image, three types of spatially complex nanostructure were fabricated on the sidewall of the hole.

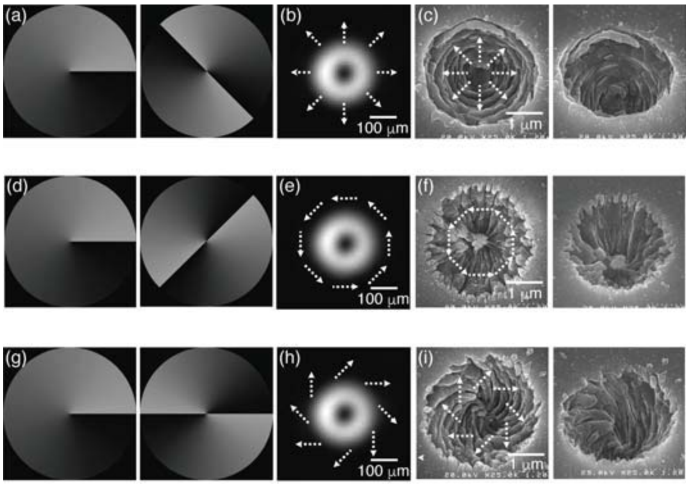

(a)-(c) The case of a radial polarization beam. (a) The CGHs for wavefront modulation, polarization modulation, and (b) their respective optical reconstructions. (c) SEM images from a top and bird's eye view of the fabricated structure. (d)-(f) The case of an azimuth polarization beam. (g)-(i) The case of a windmill polarization beam.

[1] Y. Hayasaki, T. Sugimoto, A. Takita and N. Nishida, Appl. Phys.Lett. vol. 87, pp. 031101 (2005).

Mid-Infrared Active Plasmonics in Graphene

M. S. Jang[1]

1- School of Electrical Engineering, KAIST, Daejeon 34141, Korea

jang.minseok@kaist.ac.kr

Graphene is an interesting material for mid-infrared active nanophotonics. Recent studies have shown that the effective optical index of graphene depends on the local Fermi level, which can be varied greatly via electrostatic gating techniques. More interestingly, the low carrier concentration and the atomic thinness of graphene allows for highly confined plasmonic modes whose properties are also widely tunable as a function of doping density. We showed that these plasmonic modes can play a dominant role in controlling the optical properties of periodically patterned graphene at mid-infrared frequencies. We showed that the energy-momentum dispersion relation of graphene plasmons are fundamentally different from the conventional noble metal surface plasmons and that the wavelength of graphene plasmons is more than 100 times shorter than the free space wavelength. As a consequence of such extreme field confinement, we further demonstrated that graphene plasmons strongly interact with substrate phonons, forming hybrid modes called surface phonon plasmon polaritons. By placing a reflector to block transmission channels and engineering the spacing between the reflector and the graphene resonators, we demonstrated that the absorption in a single layer of graphene resonators can be dynamically tuned from 0 to 25% by electrostatic gating. We also showed that the absorption modulation by graphene resonantors can be 2.67 fold enhanced by incorporating EOT(extra-ordinary transmission) metallic resonant restructures. By further advancing the idea of overlapping various scales of resonances in a narrow spectral and spatial window, we recently demonstrated that it is possible to achieve perfect mid-infrared absorption modulation based on graphene plasmonic metasurfaces. Finally, Kirchhoff's law of thermal radiation, which states the absorptivity and the emissivity of an object are equal, also allows for dynamic control of thermal radiation from heated graphene plasmonic nanoresonators. These tunable plasmonic modes offered by graphene and other 2D materials provide new opportunities to create electo-optically active devices with novel functionalities that have thus far been impossible to be realized by using conventional media.

Simple field enhancement formulation for gold bipyramids for application in two-photon luminescence and scattering

James W. M. Chon and Stuart J. Flanders

Centre for Micro-Photonics, Dept. of Physics, Faculty of Science, Engineering and Technology, Swinburne University of Technology, Hawthorn, 3122, VIC, Australia
jchon@swin.edu.au

Recent advances in two-photon excited photoluminescence of plasmonic gold nanorods have greatly expanded their application. Shape-controlling of nanorods can enhance a particular photophysical process to tailor needs but its application to two-photon luminescence is yet to be fully developed despite its importance in biolabelling. In particular, bipyramidal gold nanorods have received a large amount of interest as a biolabelling due to highly localised field at their tips, which provide enhancement for emission processes. However, no proper evaluation of geometrical properties of bipyramids such as tip shape, curvature, pentagonal cross section or the waist have been conducted on the field enhancement and peak evolution. Numerical simulations using finite element analysis show that small change in tip radius of curvature can change nonlinear process such as two-photon luminescence (TPL) two to four-fold increase. However, such large increase is not observed in experimental measurement of TPL with respect to tip curvature, indicating that there is fundamental limit to how the field enhancement can influence emission processes.

Here we present a full numerical simulation of field enhancement around bipyramidal gold nanorods with variation in geometry. We also present a simple analytical theory based on quasistatic field around prolate spheroids to account for bipyramidal shape with correction factors to approximate the shape difference. Quasistatic theory for a prolate spheroid has been used to approximate various rod structures, but such a theory has not been used for bipyramidal shapes. We solved explicit expressions for electric field around prolate spheroids and the derived equations that are compared to the results from numerical methods (Finite element method) for prolate spheroids (Fig. 1), bipyramids and capsule shapes of multiple sizes and aspect ratios. For bipyramids, the geometric correction factor incorporates the sharpness of the tip curvature, the volume difference between spheroid to the bipyramid with the same length and width as well as a radiative damping correction. The results will be compared with finite element simulations as well as experimental measurement of its action cross-sections. This work will provide an easily accessible and less computational taxing method of predicting plasmonic bipyramid field enhancement and far-field response for future bio-labelling research.

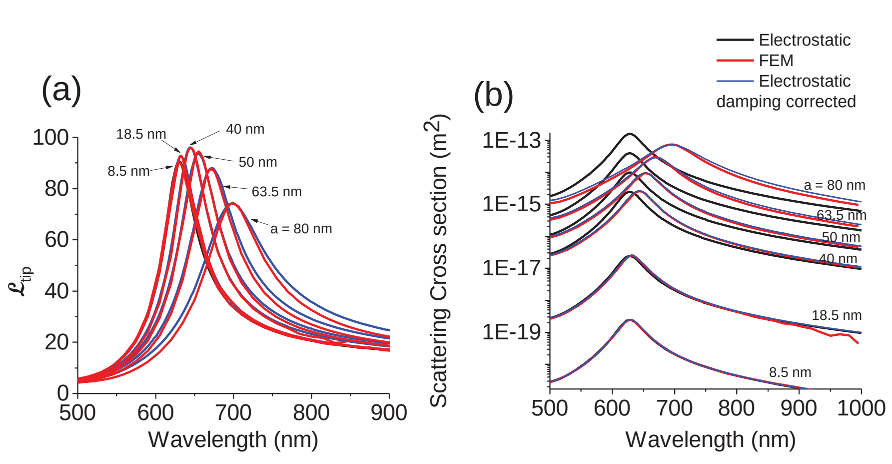

Fig. 1 (a) Field enhancement factor at the tip $\mathcal{L}_{tip}$ for an aspect ratio 3.5 gold rod (prolate spheroid) calculated with quasistatic model with respect to wavelength is shown as black line. Together shown are the numerically simulated electrodynamic field enhancement using FEM technique at different gold rod sizes (red lines), and damping corrected electrostatic model (blue lines). Half length of the rod a = 8.5, 18.5, 40, 50, 63.5, 80 nm are specified. (b) Far-field scattering cross sections are shown for the same rods as (a) using the electrostatic (black) and FEM model (red) and damping corrected electrostatic (blue) are shown.

[1] A. M. Siddiquee, A. B. Taylor, S. Syed, G. H. Lim, B. Lim and J. W. M. Chon, *J. Phys. Chem. C*, 119, 28536-28543, (2015)

Plasmonics and Metamaterials for Imaging and Hologram Applications

Choon-Gi Choi[1,2]

1-Graphene Research Lab.(Emerging Devices Research Group), Electronics and Telecommunications Research Institute (ETRI), Korea
2-School of Engineering, Korea University of Science & Technology, Korea

Plasmonics and metamaterials have attracted considerable attention over the past decade in the fields of superlens, cloaking, absorber, etc. Recently, plasmonics and metamaterials have seen a dramatic increase of novel ideas with combination of new materials and structures. Finding the best set of materials and structures for plasmonics and metamaterials can realize many interesting functionalities in devices from ultraviolet to terahertz wavelength for sensor, imaging, energy harvesting, display, hologram and other nanophotonic applications.

In this talk, we introduce a subwavelength imaging in the visible range by using a metal coated carbon nanotube forest. We demonstrate a nano-imaging system which can resolve two slits separated by 160 nm with visible light of 532 nm wavelength. The metal coated CNT forest, as a wire medium nano-lens, successfully transfer nano-scale spatial information from one side to the other side using surface plasmon polariton modes.

We also report a reflection-type spatial amplitude modulation in the visible region using a pixelated sub-wavelength metamaterial absorber for 3D hologram application. We utilize a pixelated array of absorbing elements based on a two dimensional sub-wavelength metal grating, and the reflectance of each pixel is controlled by simple structural modification. The structure of each absorbing element is appropriately modified to have the designed reflectance utilizing its frequency selective property, and adjacent elements of the same type are combined into a single pixel. This method will be utilized as a basic component for developing future spatial light modulation technologies.

Laser-induced wavelength-controlled self-assembly of colloidal quasiresonant nanoparticles: chance to overcome the diffraction limit

V.V. **Slabko**[1], **A.S. Tsipotan**[1], **A.S. Aleksandrovsky** [2]

1- Siberian Federal University, Krasnoyarsk, 660041, Russia.

2- Russian Academy of Sciences, Kirensky Institute of Physics Krasnoyarsk 660036, Russia.

vslabko49@mail.ru

The problem of formation of the nanostructures with the pre-defined properties is among the most important ones that arise ever-increasing interest of researchers. Employment of photolithography that is traditionally used in microelectronics for the nanoscale meets a number of insurmountable obstacles connected with diffraction limitations. Present talk presents the results of our studies indicating on the possibility, under certain circumstances, to construct nanostructures with pre-defined shape and content from colloid nanoparticles in the field of quasi-resonant laser radiation, the dimentions of these nanostructures being much smaller than laser wavelength.

Under the action of optical radiation onto nanoparticles, the polarization induced by laser field leads to a number of interesting effects. The interaction of polarization with the radiation field leads to optical trapping [1], while field-mediated interparticle interaction leads to optical binding [2]. If the isolated particle possesses resonant transition close to the field frequency then the energy of interparticle interaction increases, and the resonant transition experiences the shift proportional to the interaction energy. Besides, the shift of resonance depends on the spatial arrangement of interacting particles with respect to the polarization plane of inducing radiation. Thus, the potential well is formed in the energy profile, the depth and spectral position of which depends on the optical frequency and particles' arrangement [3,4]. As a rule, colloid particles are stabilized against spontaneous aggregation with a potential barrier with the height higher than the thermal movement energy. If the energy of interparticle interaction exceeds the barrier energy then a group of particles in the state of Brownian movement will aggregate into structure with the dimensions much smaller than the wavelength, the shape and content of which is determined by the frequency of polarization-inducing field.

Different particles can be chosen for the experimental study, namely, metallic particles possessing surface plasmonic resonance, or dielectric nanoparticles doped with transition metal or rare-earth ions, or quantum dots. Present talk reports the results of experiment on the formation of pairs of CdTe nanoparticles under irradiation with nanosecond pulses at wavelengths 555 or 560 nm.[5]. Formation of pairs is justified by corresponding changes of absorption spectra. Conditions of the experiment are in excellent agreement with those predicted by the theory of laser-induced dipole-dipole interaction of QDs. The fraction of QDs assembled into pairs is up to 47%.

The reported study was funded by RFBR and Krasnoyarsk Krai according to the research project No. 16-42-240410r_a and RFBR research project No. 16-32-00129. VVS is grateful for the support from the Ministry of Education and Science of the Russian Federation (Grant № 3.6341.2017/VU).Ё

[1]. P. M. Bendix, L. Jauffred, K. Norregaard, and L. B. Oddershede, “Optical trapping of nanoparticles and quantum dots,” IEEE J. Sel. Top. Quantum Electron. 20, 4800112 (2014)

[2]. K. Dholakia and P. Zemanek, “Gripped by light: Optical binding,” Rev. Mod. Phys. 82(2), 1767–1791 (2010).

[3]. V. V. Slabko, G. G. Khachatryan, and A. S. Aleksandrovsky, “Self-organized aggregation of small metal particles controlled by an external light field,” JETP Lett. 84(6), 300–304 (2006)

[4]. V. V. Slabko, A. S. Tsipotan, A. S. Aleksandrovsky, and E. A. Slyusareva, “Dynamics of self-organized aggregation of resonant nanoparticles in a laser field,” Appl. Phys. B 117(1), 271–278 (2014)

[5]. Aleksey S. Tsipotan, Marina A. Gerasimova, Vitaliy V. Slabkoand Aleksandr S. Aleksandrovsky Laser-induced wavelength-controlled selfassembly of colloidal quasi-resonant quantum dots. OPTICS EXPRESS Vol. 24, No. 10 (2016)

Photoacoustic Spectroscopy Technologies for Non-invasive Detection of Glucose in Human Body

C. G. Ahn, J. Y. Sim, C. Huh, K. H. Chung, E. J. Jeong, B. K. Kim

Bio-Medical IT Convergence Research Department, Electronics and Telecommunications Research Institute, Daejeon, 34129, Korea

cgahn@etri.re.kr

Diabetes mellitus is growing as a global challenge. According to the World Health Organization, an estimated 422 million adults were living with diabetes in 2014 and the number of diabetic people worldwide is expected to double within the next ten years. When diabetes is uncontrolled, it can affect not only the patient’s internal organs, circulation system and eyesight, but also his or her entire life. Therefore, a regular or continuous monitoring and subsequent, immediate control of the glucose level is significant to keep the healthy life of the patients. The most established self-monitoring methods for blood glucose level is based on enzyme reactions and is painful because of the procedure extracting blood invasively from patients by piercing a fingertip with a needle, which often makes diabetics unwilling to check their glucose level as frequently as doctors recommend. There have been many attempts to develop alternative non-invasive procedures for the glucose measurement, comparable to the presently available invasive techniques. Most of the approaches are mainly based on optical methods, since the optical methods utilize the vibrational modes of the glucose molecule that are highly specific and thus selective for glucose-sensing even in a complex matrix like whole blood. The analysis of the received light signal, however, is inherently complex because the glucose signal is often very faint and easily interfered with other signals from a variety of analytes in blood. The variability and the inhomogeneity of the human skin are also big obstacles for the commercial application of the *in vivo* optical monitoring. In recent years, the technique of photoacoustic spectroscopy (PAS) has been used for trace detection of gases due to the higher sensitivity it offers, relative to optical absorption spectroscopy. In this method, a high-energy laser beam irradiated on skin produces a thermal expansion, thereby generating an acoustic wave. Unlike ordinary acoustics, sound waves produced by the PA method carry information about the material properties of the substance in which they are generated [1].

We have extensively studied the non-invasive glucose monitoring method based on PAS technique. Mid-infrared light beam from an external-cavity quantum-cascade laser (EC-QCL) was applied to obtain the clear glucose spectrum using the optical properties of strong energy absorption and vibrational energy relaxation from the energy states of glucose molecules in this region. Using the mid- infrared light source also has another strong advantage of little inference of the glucose signal by probing the interstitial fluid with only several analytes thanks to a shallow penetration depth of mid-infrared in skin. We will present the optical PA system setup and the signal processing developed for the PA measurement of glucose in skin. To amplify the weak photoacoustic signal due to the impedance mismatch of the acoustic medium, a sensitive photoacoustic detector with an acoustic resonance cell was developed by the theoretical analysis and simulation of the resonance mode of the PA cell as well as the extensive experimental optimization of the PA cell. In addition, we matched the resonant characteristics of a photoacoustic cell with that of a microphone in order to enhance the signal-to-noise ratio in the PA detector. A preliminary test with healthy volunteers demonstrates the feasibility of a non-invasive glucose monitoring well, showing that most of data points fall within the critical region of the Clarke error grid, which would be the requirement for the clinical use of this method.

[1] M. A. Pleitez, T. Lieblein, A. Bauer, O. Hertzberg, H. Toal, and W. Mantele, In Vivo Noninvasive Monitoring of Glucose Concentration in Human Epidermis by Mid-Ifrared Pulsed Photoacoustic Spectroscopy, Analytical Chemistry, vol 85. Pp. 1013-1020, (2015)

Effect of Photon Lifetime in Silicon Nanowire Ensembles on Efficiency of Raman Scattering and Third-Harmonic Generation

L.A. Golovan[1], S.V. Zabotnov[1,2,3], N.B. Tkachenko[1], D.E. Presnov[1,4], L.A. Osminkina[1], A.I. Efimova[1]

1- [1] Physics Department, M.V.Lomonosov Moscow State University, Moscow, 119991, Russia
[2] National Research Center 'Kurchatov Institute', Moscow, 123182, Russia
[3] FNBIC, Moscow Institute of Physics and Technology, Moscow, 123098, Russia
[4] Skobeltsyn Institute of Nuclear Physics, M.V.Lomonosov Moscow State University, Moscow, 119991, Russia

golovan@physics.msu.ru

Ensembles of silicon nanowires (SiNWs) of about 100 nm in diameter are of great interest. Typically, SiNWs are aligned pillars with the length controlled by the formation procedure. They are characterized by extremely low reflection and high light absorption in the visible spectral region and high reflection in near-infrared (NIR) region indicating their promising photovoltaic or sensor applications. Enhanced efficiency of such optical processes as Raman scattering, third-harmonic (TH) generation, and photoluminescence are found in SiNWs. These effects are often connected with the light trapping in SiNW arrays caused by effective light scattering, which in its turn depends on length, orientation, and arrangement of the SiNWs. Thus, studying correlation of the SiNW structural parameters and efficiency of the optical processes including nonlinear-optical ones seems to be very instructive for further applications of the SiNW arrays.

To reveal effects of SiNW ensemble structure on efficiency of the optical processes the dependence of the Raman scattering and TH signals on the light polarization and thickness of the sample were found. These processes are sensitive to the light polarization and local field effects. The obtained results were complemented by measurements of cross-correlation function for the laser pulse and radiation scattered by SiNW ensemble, which allows estimation of photon lifetime in SiNW. A quasi-cw Cr:forsterite laser radiation (1250 nm, 80 fs, 150 mW, 80 MHz) was used for these purposes.

Dependences of Raman and TH signals on the thickness of SiNW layer demonstrate rise increase with the layer thickness increase. For the TH signal the rise follows a decrease in the TH intensity for thinner layers (0.2–2 lm), while Raman signal grows monotonously from the thinnest SiNW layers and tends to saturation for the layer thickness above 5 μm. The difference is due to absorption of the TH radiation and coherent nature of the TH generation.

The phton lifetime measurements revealed that for the SiNWs of the thickness above 4 μm the cross-correlation function has an expressed tail, indicating diffusion-like radiative transport in the SiNW array. The typical photon lifetimes were found to be 0.5 and 1.4 ps for the SiNW arrays with thicknesses of 4.5 and 16 μm, respectively. The rise of the TH generation efficiency starts at the same thickness as the increase of the photon lifetime in the SiWNs. Such a correlation let us suppose that the latter one is responsible for the rise of the TH generation efficiency.

The SiNWs formed on (110) Si substrate are tilted at 45° to the surface. In this case, TH signal exceeds one for crystalline Si, in the case of the fundamental radiation incident perpendicular to the SiNWs, whereas in the case of incident wave propagation along the SiNWs it falls several time in comparison with crystalline Si,.

Thus, multiple scattering of near-infrared light in SiNW ensembles leads to photon lifetime enhancement which is manifested by substantial increase of the Raman scattering and TH generation efficiencies. Polarization dependence of the TH signals strongly depends on the incident wave propagation (perpendicular or parallel to the SINW), with the light incidence perpendicular to the SiNWs being more effective than along the SiNWs. The obtained results could be explained by variations of in the local fields in SiNWs and scattering cross-section.

The work was supported by the Russian Foundation for Basic Research Grant no. 15-29-01185, and it was partially performed at the Center of User's Facilities of Moscow State University.

Nanoscale chemical mapping: photo-induced force microscopy and photothermal-induced resonance microscopy

J. Jahng[1], H. Kwon[1], E. S. Lee[1]

1- Nanometrology, Korea Research Institute of Standards and Sciences, Daejeon 34113

phyjjh@kriss.re.kr

The enormous advances made in nanotechnology have also intensified the need for tools that can chemically characterize nanomaterials with high sensitivity and with high spatial resolution. Many existing tools with nanoscale chemical imaging, including scattering scanning optical near-field microscope (s-SNOM) and tip-enhanced Raman spectroscopy (TERS), can generate highly detailed maps of nanoscopic structures. In scattering based nanoscopy such as s-SNOM and TERS, one important challenge is the interpretation of the image separated from the far-field background. The recorded spectral response originates from the near-field and is a rather complex function of sample absorption, tip response and tip-sample coupling under illumination.

To address this issue, a new and emerging far-field free technique in this area is based on non-optical detection mechanism such as photo-induced force microscopy (PiFM) [1-3] and photothermal-induced resonance microscopy (PTIR) [4-6], which enable spectroscopic probing of materials with a few nm spatial resolution. The PiFM is based on the dipole-dipole interaction in the tip-sample junction, enhanced by the plasmonic field, and depends on the local refractive index of the sample which is basically dispersive force. One the other hand, the PTIR is addressed by local heating of the sample based on absorption and thermal expansion. The advantage of these approaches are that any optical transitions linear and nonlinear of molecules can be probed directly as a far-field free manner. However, when the light illuminated on the tip-sample junction, the dipole-dipole interaction and the thermal interaction are simultaneously induced. Here, we present the way to distinguish two different phenomena based on the sample properties and the timescale of light source. The ability for nanometer scale optical microscopic and spectroscopic analysis with far-field free manner will open new opportunities in materials science and biology by investigating the chemical and optical nature of individual molecules.

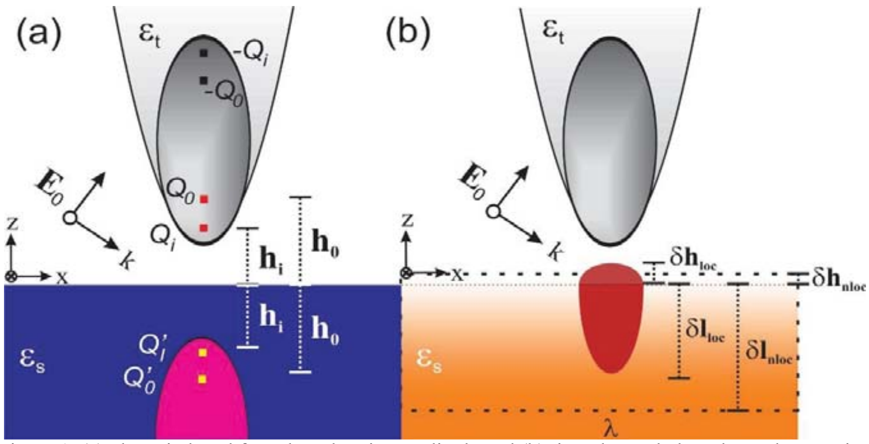

Figure 1. (a) photo-induced force based on image dipole and (b) tip-enhanced photothermal expansion

[1] I. Rajapaksa *et al.*, “Image force microscopy of molecular resonance: A microscope principle", Appl. Phys. Lett. 97, 073121 (2010).
[2] J. Jahng *et al.*, “Linear and nonlinear optical spectroscopy at the nanoscale with photo-induced force microscopy”, Acc. Chem. Res. 48 (10), 2671-2679 (2015).
[3] D. Nowak *et al.*, "Nanoscale chemical imaging by photoinduced force microscopy," Sci. Adv. 2, e1501571 (2016).
[4] A. Dazzi *et al.*, “Theory of infrared nanospectroscopy by photothermal induced resonance”, J. Appl. Phys. 107, 124519 (2010).
[5] A. Centrone *et al.*,“Nanoscale Infrared Spectroscopy: Improving the Spectral Range of the Photothermal Induced Resonance Technique”, Anal. Chem. 85, 1972−1979 (2013).
[6] F. Lu *et al*, “Tip-enhanced infrared nanospectroscopy via molecular expansion force detection”, Nat. Photo. 8, 307-312 (2014)

High Resolution Imaging with Electron Beam Assisted (EXA) Micrscopy for Bio Technology

Yoshimasa Kawata[1,2], Masahiro Fukuta[1], Wataru Inami[1,2]

1- Faculty of Engineering, Shizuoka University, Johoku, Naka, Hamamatsu 432-8561, Japan
2- Research Institute of Electronics, Shizuoka University, Johoku, Naka, Hamamatsu 432-8561, Japan
kawata@eng.shizuoka.ac.jp

High-resolution imaging of cellular structures, such as actin filaments, mitochondria, and nuclei, is key tools for analyzing cellular activities, including movement, organelle transportation, and energy generation. Since the spatial resolution of conventional optical microscopes is bounded by the diffraction limit, it is difficult to observe a cell's detailed structures. To reveal new mechanisms of cellular function, improved optical microscopes are needed for achieving greater spatial resolution.

We have developed an electron-beam excitation-assisted optical (EXA) microscope, which can observe label-free cells with high spatial resolution. The cathodoluminescent (CL) light source is excited in the luminescent thin film by the irradiation of an electron beam. The EXA microscope observes the specimen beyond the diffraction limit by raster scanning the CL light source, where the CL spot is a few tens nm of nanometers in diameter. Using the EXA microscope, we demonstrated label-free biological cell imaging with 82 nm spatial resolution.

We present label-free and high spatial-resolution imaging for specific cellular structures using an electron-beam excitation-assisted optical microscope (EXA microscope). Images of the actin filament and mitochondria of stained HeLa cells, obtained by fluorescence and EXA microscopy, were compared to identify cellular structures. Based on these results, we demonstrated the feasibility of identifying cellular structures at a spatial resolution of 82 nm.

Figure 1 shows the result of high spatial-resolution imaging of the HeLa cell and (b) shows the intensity profile in the vicinity of the intracellular granules, highlighted by arrows in Fig. 1(a). The full width at half maximum (FWHM) of the intracellular granules is 82 nm and the signal-to-noise ratio (SNR) is 10.5.

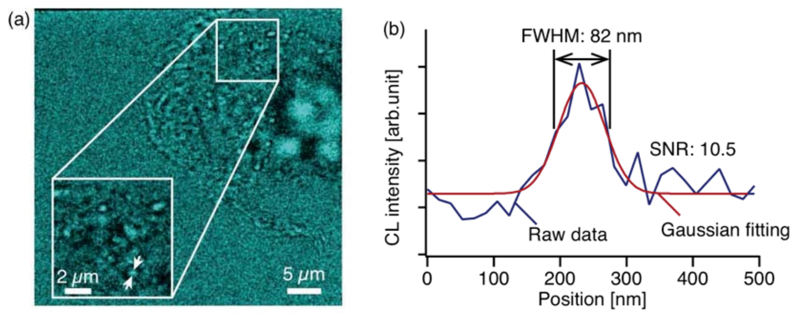

Figure 1. (a) High resolution EXA imaging and (b) Intensity profile of the cellular granules

[1] M. Fukuta. S. Kawamori, T. Furukawa, Y. Nawa, et. al., Sci. Rep. **5**, 16068 (2015).
[2] W. Inami, K. Nakajima, et.al., *Opt. Exp*. **18**, 12897 (2010).
[3] Y. Nawa, W. Inami, A. Ono, et. al., *Opt. Exp*.**20**, 5629 (2012).
[4] Y. Nawa, W. Inami, S. Lin, et. al., *ChemPhysChem*, **2014**, 721 (2014).

Terahertz nanophotonics and its sensing applications

H. -R. Park[1], **D. S. Kim**[2]

1- Department of Physics, Chungbuk National University, Cheongju 28644, South Korea
2- Department of Physics and Astronomy and Center for Atom Scale Electromagnetism, Seoul National University, Seoul 08826, South Korea

hrpark@cbnu.ac.kr

Observation of single nanoparticles, having dimensions in deep sub-wavelength region, has been still a big issue since it requires detection of very weak light absorption or scattering. Recently, the ability to detect individual nanoparticles using sub-wavelength metallic structures, such as plasmonic dipole antennas and microresonator, has been a widely-spread tool for observing optical properties of single metallic nanoparticles and biomolecules [1-4]. Here, we investigate whether single metallic nanoparticles with a dimension of 100 nm fitted into nano-slot can be detected using a terahertz (THz) wave with sub-millimeter wavelength. Strikingly, single gold nanoparticles inside a single THz nano-slot antenna induce a noticeable modulation of the THz transmission through the slot. This ability would pave a new way for detecting nanoparticles in infrared and THz regimes.

We perform THz time-domain spectroscopy for a frequency range of 0.3-1.1 THz (1-0.27 mm) using an 80 MHz repetition rate femtosecond Ti:Sapphire laser oscillator. The p-polarized terahertz pulses with polarization perpendicular to the long axis of the slot are normally incident on the sample, which a single THz nano-slot antenna on the center. When we put gold nanoparticles with the diameter of 100 nm into the THz nano-slot antenna with the length of l=150 μm and the width of w=120 nm, the nanoparticle as an obstacle could disturb a fundamental resonant mode of the slot antenna despite the particle's dimension being smaller than about $\lambda/5000$.

For detecting single nanoparticles as promised by the strong field enhancement inside the slot antenna, we designed a single THz nano slot antenna with a large length/width ratio of about 1250, to have three orders of magnitudes of electric field enhancement. The resonance frequency of the antenna, 0.55 THz, satisfies the condition $f_{res}=c/(2n_{eff}l)$ where n_{eff} is the effective index of refraction of the antenna-substrate composite and l is the length of the slot. When we put the gold nanoparticles with the total number of 5.5×10^7 over the entire area of the sample, only the two nanoparticles are embedded inside the slot antenna (Fig. 1(a)), decreasing the resonant transmission amplitude to 65 %, as shown in Fig. 1(b). Moreover, more nanoparticles of 1.1×10^8 totally blocked the terahertz transmission through the sample. This phenomenon is attributed to the presence of the strong local field inside nano slot, which could increase the scattering or the absorption from particles thereby enabling detection of subwavelength particles beyond the diffraction limit.

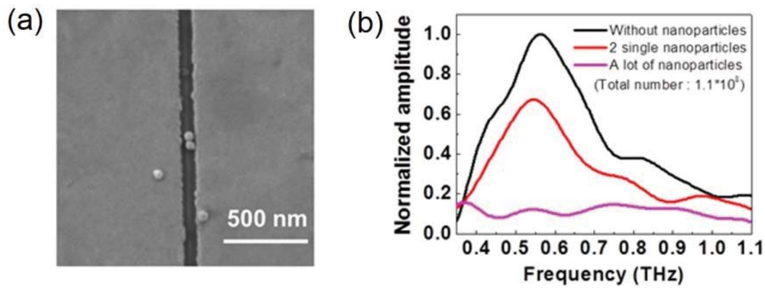

Fig. 1. (a) an SEM image of only two single gold nanoparticles with a size of 100 nm inside the slot. (b) Experimental normalized transmitted (electric field) amplitude spectra through a single THz nano-slot antenna without and with gold nanoparticles

[1] W. H. Zhang, L. N. Huang, C. Santschi, and O. J. F. Martin, Trapping and Sensing 10 nm Metal Nanoparticles Using Plasmonic Dipole Antennas, *Nano Lett.*, vol. 10, pp. 1006-1011, (2010).
[2] M. Righini, P. Ghenuche, S. Cherukulappurath, V. Myroshnychenko, F. J. G. de Abajo, and R. Quidant, Nano-optical Trapping of Rayleigh Particles and Escherichia coli Bacteria with Resonant Optical Antennas, *Nano Lett.*, vol. 9, pp. 3387-3391, (2009).
[3] J. McPhillips, A. Murphy, M. P. Jonsson, W. R. Hendren, R. Atkinson, F. Hook, A. V. Zayats, and R. J. Pollard, High-Performance Biosensing Using Arrays of Plasmonic Nanotubes, *Acs Nano*, vol. 4, pp. 2210-2216, (2010).
[4] K. Lindfors, T. Kalkbrenner, P. Stoller, and V. Sandoghdar, Detection and spectroscopy of gold nanoparticles using supercontinuum white light confocal microscopy, *Phys. Rev. Lett.*, vol. 93, pp. 037401, (2004).

Terahertz vortex generation and its applications

Katsuhiko Miyamoto[1,2], **Fabian Rotermund**[3], **and Takashige Omatsu**[1,2]

1- Department of Materials Science, Chiba University, 1-33, Yayoi-cho, Inage-ku, Chiba, 263-8522, Japan
2-Molecular Chirality Research Center, Chiba University, 1-33, Yayoi-cho, Inage-ku, Chiba, 263-8522, Japan
3- Department of Physics, Korea Advanced Institute of Science and Technology,
291 Daehak-ro, Yuseong-gu, Daejeon 34141, Korea

k-miyamoto@faculty.chiba-u.jp

Imaging systems in a terahertz (THz) region, in which various molecules and clusters exhibit eigen vibration frequencies, have been intensely studiedin biomedicine, security, and non-destructive testing. However, their spatial resolution is mostly limited to a sub-millimeter scale.

An optical vortex with an annular intensity profile and orbital angular momentum (characterized by a topological charge ℓ) provides us a variety of potential research opportunities, such as high speed optical communications, optical manipulations, and chiral materials fabrications [1-3]. It also enables us to develop a 'super-resolution' microscope (with a spatial resolution beyond the diffraction-limit) based on nonlinear fluorescence depletion phenomena.

A 'super resolution' technique based on nonlinear effects induced by a highly intense THz vortexwill bea promising way to achieve a micrometer-scale spatial resolution beyond the diffraction limit.

In this presentation, we propose a Tsurupica spiral phase plate with extremely low dispersion and high transmission in a frequency range of 0.1-6 THz for generation of THz vortex [4]. We also demonstrate the generation of a monochromatic THz vortex output with a topological charge of $\ell = \pm 1$, 2 and a monocycle THz vortex pulse.We also address the 'super-resolution' measurement of nonlinear transmission behaviors of bilayer graphene byemploying the monochromatic 0.6 THz vortex pulse with an average power of 2.3 mW [5].

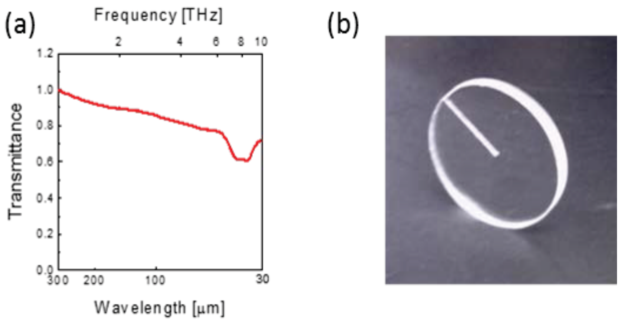

Fig1. (a) Transmittance of the Tsurupica polymer in the THz region. (b) Photo of the Tsurupica SPP.

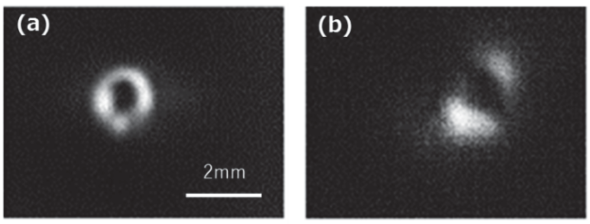

Fig. 2 (a) Spatial profile of the 0.6 THz vortex output. (b)Focused spot of the THz vortex by a tilted lens.

[1] K. Toyoda, K. Miyamoto, N. Aoki, R. Morita, and T. Omatsu, *Nano Lett.*, **12**, 3645-3649 (2012).
[2] F. Takahashi, K. Miyamoto, H. Hidai, K. Yamane, R. Morita, and T. Omatsu, *Scientific Reports***6**: 21738 (2016).
[2] K. Toyoda, F. Takahashi, S. Takizawa, Y. Tokizane, K. Miyamoto R. Morita, T. Omatsu, *Phys. Rev. Lett.*, **110**, 143603-1-5 (2013).
[3] M. Watabe, G. Juman, K. Miyamoto, T. Omatsu, *Scientific Reports*, **4**: 4281, (2014).
[4] K. Miyamoto, K. Suizu, T. Akiba, T. Omatsu, *Appl. Phys. Lett.*, **104**, 261104 (2014).
[5] K. Miyamoto, B-J. Kang, W-T. Kim, Y. Sasaki, H. Niinomi, K. Suizu, F. Rotermund and T. Omatsu, *Scientific Reports*, **6**: 38880 (2016).

Resonant tip enhanced Raman scattering imaging of defects in 2 dimensional WS_2 monolayer

Chanwoo Lee[1], Seung Mi Lee[2], Mun Seok Jeong[1]

1- Department of Energy Science, Sungkyunkwan University, Suwon 16419, Republic of Korea
2- Korea Research Institute of Standards and Science (KRISS), Daejeon 34113, Republic of Korea

Main author email address: mjeong@skku.edu

Monolayer tungsten disulfide (WS_2) has emerged as a material for optoelectronic applications because of its remarkable quantum yield of photoluminescence. However, a simple and easy quality evaluation criterion like the D mode in the Raman spectrum of graphene does not exist in monolayer WS_2. Here, we report that resonant tip-enhanced Raman spectroscopy (TERS) imaging can reveal defect-induced Raman modes, which are the shifted A_{1g} mode with D and D′ modes in monolayer WS_2 with a high spatial resolution beyond the optical diffraction limit. We also find a strong correlation with the structural defects through a scanning tunneling microscope. Furthermore, our density functional theory calculations demonstrate that sulfur vacancies introduce not only the red-shifted A_{1g} mode but also the D and D′ modes. Observed defect-related Raman modes can be utilized to evaluate the quality of monolayer WS_2 and will be helpful to improve the performance of WS_2 optoelectronic devices.

[1] Kyoung-Duck Park, Markus B. Raschke, Joanna M. Atkin, Young Hee Lee, and M.S. Jeong*, "Probing Bilayer Grain Boundaries in Large Area Graphene with Tip-Enhanced Raman Spectroscopy", Advanced Materials, 29, 1603601 (2017).
[2] Chanwoo Lee, Sung Tae Kim, Byeong Geun Jeong, Seok Joon Yun, Young Jae Song, Young Hee Lee, Doo Jae Park*, and M.S. Jeong*, "Tip-Enhanced Raman Scattering Imaging of Two-Dimensional Tungsten Disulfide with Optimized Tip Fabrication Process", Scientific Reports, 7, 40810 (2017).